

VOLUME 80

MAY 20, 1976

NUMBER 11

JPCHAx

THE JOURNAL OF
PHYSICAL
CHEMISTRY



PUBLISHED BIWEEKLY BY THE AMERICAN CHEMICAL SOCIETY

From the borders of organic chemistry . . . To the borders of theoretical physics:

Inorganic Chemistry brings you a broad range of authoritative information presenting both experimental and theoretical studies in all phases of inorganic chemistry.

Each month, this rapidly growing journal brings you the data you need on synthesis and properties of new compounds, quantitative studies regarding structure, and thermodynamics of inorganic reactions.

When you've seen the 50 or more papers offered in each issue, you'll also want to look through the Notes and Correspondence sections for their concise exchange of scientific views and ideas.

To order INORGANIC CHEMISTRY today, just complete and return the form below.



. . . another ACS service

Inorganic Chemistry



Inorganic Chemistry
American Chemical Society
1155 Sixteenth Street, N.W.
Washington, D.C. 20036

1976

Yes, I would like to receive INORGANIC CHEMISTRY at the one-year rate checked below:

	U.S.	Foreign and Canada	Latin America
ACS Member Personal-Use One-Year Rate	<input type="checkbox"/> \$24.00	<input type="checkbox"/> \$30.50	<input type="checkbox"/> \$29.75
Nonmember	<input type="checkbox"/> \$96.00	<input type="checkbox"/> \$102.50	<input type="checkbox"/> \$101.75
Bill me <input type="checkbox"/>	Bill company <input type="checkbox"/>	Payment enclosed <input type="checkbox"/>	

Name _____

Street _____ Home
Business

City _____ State _____ Zip _____

Journal subscriptions start January '76

THE JOURNAL OF PHYSICAL CHEMISTRY

BRYCE CRAWFORD, Jr., *Editor*
STEPHEN PRAGER, *Associate Editor*
ROBERT W. CARR, Jr., **FREDERIC A. VAN-CATLEDGE**, *Assistant Editors*

EDITORIAL BOARD: C. A. ANGELL (1973-1977), F. C. ANSON (1974-1978), V. A. BLOOMFIELD (1974-1978), J. R. BOLTON (1976-1980), L. M. DORFMAN (1974-1978), H. L. FRIEDMAN (1975-1979), H. L. FRISCH (1976-1980), W. A. GODDARD (1976-1980), E. J. HART (1975-1979), W. J. KAUZMANN (1974-1978), R. L. KAY (1972-1976), D. W. McCLURE (1974-1978), R. M. NOYES (1973-1977), W. B. PERSON (1976-1980), J. C. POLANYI (1976-1980), S. A. RICE (1976-1980), F. S. ROWLAND (1973-1977), R. L. SCOTT (1973-1977), W. A. STEELE (1976-1980), J. B. STOTHERS (1974-1978), W. A. ZISMAN (1972-1976)

Published by the
AMERICAN CHEMICAL SOCIETY
BOOKS AND JOURNALS DIVISION
 D. H. Michael Bowen, Director

Editorial Department: Charles R. Bertsch, Head; Marianne C. Brogan, Associate Head; Celia B. McFarland, Joseph E. Yurvati, Assistant Editors

Graphics and Production Department: Bacil Guiley, Head

Research and Development Department: Seldon W. Terrant, Head

Advertising Office: Centcom, Ltd., 50 W. State St., Westport, Conn. 06880.

© Copyright, 1976, by the American Chemical Society. No part of this publication may be reproduced in any form without permission in writing from the American Chemical Society.

Published biweekly by the American Chemical Society at 20th and Northampton Sts., Easton, Pennsylvania 18042. Second class postage paid at Washington, D.C. and at additional mailing offices.

Editorial Information

Instructions for authors are printed in the first issue of each volume. Please conform to these instructions when submitting manuscripts.

Manuscripts for publication should be submitted to *The Journal of Physical Chemistry*, Department of Chemistry, University of Minnesota, Minneapolis, Minn. 55455. Correspondence regarding **accepted papers and proofs** should be directed to the Editorial Department at the ACS Easton address.

Page charges of \$60.00 per page are assessed for papers published in this journal. Ability to pay does not affect acceptance or scheduling of papers.

Bulk reprints or photocopies of individual articles are available. For information write to Business Operations, Books and Journals Division at the ACS Washington address.

Requests for **permission to reprint** should be directed to Permissions, Books and Journals Division at the ACS Washington address. The American Chemical Society and its Editors assume no responsibility for the statements and opinions advanced by contributors.

Subscription and Business Information

1976 Subscription rates—including surface postage

	U.S.	PUAS	Canada, Foreign
Member	\$24.00	\$29.75	\$30.25
Nonmember	96.00	101.75	102.25
Supplementary material	15.00	19.00	20.00

Air mail and air freight rates are available from Membership & Subscription Services, at the ACS Columbus address.

New and renewal subscriptions should be sent with payment to the Office of the Controller at the ACS Washington address. **Changes of address** must include both old and new addresses with ZIP code and a recent mailing label. Send all address changes to the ACS Columbus address. Please allow six weeks for change to become effective. **Claims** for missing numbers will not be allowed if loss was due to failure of notice of change of address to be received in the time specified; if claim is

dated (a) North America—more than 90 days beyond issue date, (b) all other foreign—more than 1 year beyond issue date; or if the reason given is “missing from files”. Hard copy claims are handled at the ACS Columbus address.

Microfiche subscriptions are available at the same rates but are mailed first class to U.S. subscribers, air mail to the rest of the world. Direct all inquiries to Business Operations, Books and Journals Division, at the ACS Washington address or call (202) 872-4444. **Single issues** in hard copy and/or microfiche are available from Special Issues Sales at the ACS Washington address. Current year \$4.75. Back issue rates available from Special Issues Sales. **Back volumes** are available in hard copy and/or microform. Write to Special Issues Sales at the ACS Washington address for further information. **Microfilm** editions of ACS periodical publications are available from volume 1 to the present. For further information, contact Special Issues Sales at the ACS Washington address. **Supplementary material** must be ordered directly from Business Operations, Books and Journals Division, at the ACS Washington address.

	U.S.	PUAS, Canada	Other Foreign
Microfiche Photocopy	\$2.50	\$3.00	\$3.50
1-7 pages	4.00	5.50	7.00
8-20 pages	5.00	6.50	8.00

Orders over 20 pages are available only on microfiche, 4 × 6 in., 24X, negative, silver halide. Orders must state photocopy or microfiche if both are available. Full bibliographic citation including names of all authors and prepayment are required. Prices are subject to change.

American Chemical Society
 1155 16th Street, N.W.
 Washington, D.C. 20036
 (202) 872-4600

Member & Subscription Services
 American Chemical Society
 P.O. Box 3337
 Columbus, Ohio 43210
 (614) 421-7230

Editorial Department
 American Chemical Society
 20th and Northampton Sts.
 Easton, Pennsylvania 18042
 (215) 258-9111



*The Editors join with his former students and
research associates in dedicating this issue of
The Journal of Physical Chemistry to*

Richard C. Lord

*on the occasion of his sixty-fifth year and his
retirement as Director of the Spectroscopy Laboratory
at the Massachusetts Institute of Technology*

“The accomplishments achieved by scientists
through use of the spectroscope form a list
so imposing as to leave no doubt that this
instrument is one of the most powerful now
available for investigating the natural universe.”

From the book "Practical Spectroscopy" by R.
C. Lord, G. R. Harrison, and J. R. Loofbourov, p
1. Copyright 1948 by Prentice-Hall. Reprinted
with the permission of Prentice-Hall.

RICHARD COLLINS LORD

Richard Collins Lord will retire as Director of the Spectroscopy Laboratory at the Massachusetts Institute of Technology on June 30, 1976. For 30 years he has guided the laboratory with distinction and maintained it as one of the world's great centers for research in spectroscopy. Although he will continue to teach at MIT, this event marks a milestone in his illustrious career and provides an opportunity to acknowledge his many contributions to science. It is a privilege to provide this account of the man and his work at the request of the Editor.

Lord was born in Louisville, Kentucky, on October 10, 1910. He came from a family with a strong academic tradition. Dartmouth College has a Lord Hall which is named for a great-great grandfather who was President there for 35 years. There is also a Lord Hall at Ohio State University, named for a relative who was Professor of Geology. During one of the annual Ohio State Symposia on Molecular Structure and Spectroscopy Dick Lord, Bryce Crawford, and one or two others were walking across the campus. New name plaques had been affixed to the buildings, and it was noted that one structure was designated as Lord Hall. This led to some joshing of Dick. He explained that actually two Lord brothers had been on the faculty there concurrently. One was a Professor of Astronomy and the other of Geology, and the students had referred to them as Lord of the Heavens and Lord of the Earth. "Well", said Crawford, "what a shame there wasn't a chair in Vulcanology for your branch of the family, Dick".

His father, also named Richard Collins Lord, was chief chemist for the Louisville and Nashville Railroad, and then worked for several chemical firms. In 1922 he joined the faculty of Kenyon College, Gambier, Ohio where he taught chemistry and served as registrar for the rest of his career. The family lived adjacent to the campus, and a college joke was that the Lord's house was not the chapel—it was next door. The son got his B.S. degree from Kenyon in 1931. After teaching chemistry and physics for a year at Tome School in Maryland, he began graduate work in chemistry at the Johns Hopkins University. His Ph.D. degree was received in 1936 for a thesis entitled "Vibrational Analysis and the Symmetry of the Benzene Molecule" done with the late Professor Donald H. Andrews. During this period he became acquainted with Edward Teller, recently arrived at George Washington University. Teller had more influence on his thinking in molecular spectroscopy than any other single person. The two worked together on a fundamental paper dealing with the theory of the effects of deuterium substitution on infrared and Raman intensities in the benzene spectrum, which was published in 1937.

Next came 2 years as a Fellow in Chemistry of the U.S. National Research Council. The first year was spent at the University of Michigan, which at that time was an outstanding center for infrared spectroscopy under H. M. Randall, E. F. Barker, and D. M. Dennison. Lord was initiated into that field by Norman Wright, then a post-doctoral fellow in Physics at Michigan. At Teller's suggestion the second year was spent at the University of Copenhagen, mainly in Professor Alex Langseth's laboratory but also partly in association with Georg Placzek. It was a wise choice. Andreas Klit had recently prepared the 12 deuterated benzenes there, and Langseth had

just obtained their Raman spectra. Lord and Langseth analyzed the results in a long and masterly paper.

In the fall of 1938 Lord returned to the Johns Hopkins University as Assistant Professor of Chemistry, and proceeded to build a Raman spectrograph designed around a Wood grating with which he began a program on the use of deuterium in the analysis of spectra. In early 1942, shortly after our entry into World War II, he went to MIT to work with George R. Harrison, first as Technical Aide and then as Deputy Chief in the Optics Division of the National Defense Research Committee. The work dealt with military applications of infrared radiation, and included early efforts on guided missiles. Not all of his wartime work was administrative, however. He was the bombardier on the first drop of the prototype of the "Azon" guided missile at Eglin Field in 1942. On another occasion some naval tests of infrared equipment were being made that involved maneuvers of a submarine with surface vessels. Lord was in the submarine, and after a long, wearisome period of work he had an opportunity for a short rest. There was an empty bunk near the bow where he lay down, but he had scarcely dozed off when the submarine collided with a surface vessel. Lord barely escaped from the bow compartment before a water-tight door was automatically slammed shut to seal off that section. Fortunately the submarine ultimately was able to surface with no loss of life.

After the war Lord spent the 1945-1946 academic year at Johns Hopkins, and then returned to MIT in 1946 as Associate Professor of Chemistry and Director of the Spectroscopy Laboratory. He was made full Professor in 1954.

In 1943 Lord married Dr. Wilhelmina Van Dyke, a pediatrician who has continued to practice her specialty throughout their married life. The fact that they share the same birthday (October 10) is symbolic of their happy compatibility. They have four daughters: Diana (Mrs. Scott Adam), Susan (Mrs. Charles Lundt), Margaret (Mrs. John Sacco), and Catherine. When the fourth child was born Lord called the laboratory to give his students the news. The one who took the message asked solicitously whether it was a girl. "Is there any other kind?" was the response.

Lord's father's Ph.D. thesis, earned at Washington and Lee University, was published in this journal in 1907: "An Investigation of the Double Cobalt Malonates", R. C. Lord, *J. Phys. Chem.*, 11, 173-200 (1907). Thirty years later his own thesis from Johns Hopkins was also published here: "Entropy and the Symmetry of the Benzene Molecule", R. C. Lord, Jr., and D. H. Andrews, *J. Phys. Chem.*, 41, 149-158 (1937). It is most appropriate that his daughter Susan has in this present issue a paper describing part of her Ph.D. research at Cornell University Medical College: "ESR Studies of Neurophysin and Its Interaction with Spin-Labeled Peptides", S. L. Lundt and E. Breslow, *J. Phys. Chem.*, this issue.

Richard Lord has had an exceptionally productive career. He has directed 11 masters and 51 doctoral theses, written several books and chapters, and published 133 scientific papers. (See the Publications of Richard C. Lord at the end of this article.) It is difficult to summarize such a large and diverse body of work, but some of the major themes can be indicated. His graduate study began in 1932, an exciting time for a physical chemist. Quantum mechanics was beginning to be applied to chemistry, and statistical mechanics was being

developed. Although infrared spectroscopy was rather quiescent, Raman spectroscopy was an active field. An understanding of vibrational spectra and how they could be used to study molecular structure was developing. The discovery of deuterium was announced that same year, and it slowly became available for research. All of these topics are reflected in the subject matter of his first three papers: "Raman Spectrum of Benzene- d_6 ", "The Entropy of Carbon Tetrachloride", and "Entropy and the Symmetry of the Benzene Molecule". These were the result of his graduate research. His early interest in the use of deuterium in the analysis of vibrational spectra continued throughout his career, and was the subject of a paper as recently as 1975. The preparations of some of the compounds, and of most of the deuterium derivatives, were research problems in themselves. Synthetic methods are the topic of about half a dozen papers, and are an essential part of many more. He and his students were seldom deterred by the necessity of synthesizing the required isotopic derivatives.

Other early interests were the theoretical calculation of the heat capacity of molecular solids (four papers) and the calculation of thermodynamic properties from spectral data (three papers). In 1953 his first paper on the study of hydrogen bonds appeared, to be followed by a dozen more extending into 1975.

Another major contribution was his extensive work in the far-infrared region (200 to 10 cm^{-1}). Perhaps more than any other individual he popularized the use of this region by chemists. A paper with McCubbin in 1957 showed that a small grating spectrometer is very useful from 2000 to 50 cm^{-1} . Further work extended the range and improved the performance. Later, following his design, the Jarrell-Ash Co. built for him a large vacuum instrument which is one of the most powerful far infrared grating spectrometers ever used. With this instrument an extensive series of important studies was made, dealing mainly with (a) pure rotational spectra, (b) the inversion (or puckering) modes of small ring molecules, and (c) pseudorotation in nonplanar rings.

In the last 14 years Lord's attention has turned more and more to large, complex molecules of biochemical interest. His first paper on the subject, a study of the manner in which DNA is affected by the absorption of water, appeared in 1962. Initially infrared spectroscopy was the main tool, and attention centered on hydrogen bonding in these systems. In 1967 came his first paper using Raman spectroscopy in this field, followed by 17 more since then. He and his students have done the basic work on the Raman spectroscopy of nucleic acids and proteins, and these biomolecules have been the major interest in the latter part of his career.

Some of his papers do not fit into any of the above categories. There are half a dozen dealing with spectroscopic apparatus or techniques, while others are concerned with the theory of Coriolis constants of vibration-rotation interaction, rotational fine structure, or barriers to internal rotation. His publications as a whole constitute an impressive body of research—large, diverse, pioneering, and thoroughly dependable. He has always insisted on the highest standards for both his own and his students' work. It is no wonder that his laboratory became a mecca for scientists from many parts of the world.

Several other professional activities deserve comment. In 1950 he founded the MIT summer course on Infrared Spectroscopy. This was the first of the post-graduate courses on applied infrared spectroscopy. It has been held every year since then, although in 1972 it was moved from MIT to Bow-

doin College. This year (1976) will be its 27th year. The course has had a tremendous impact on the practice of infrared spectroscopy, for over 2400 students have attended it. They have come from industrial, government, and academic laboratories in this country and many other parts of the world. In the earliest years most of the American manufacturers of infrared instruments sent engineers and designers to participate. The give and take among staff, students, instrument builders, and instrument users was exhilarating and helpful to all concerned. The author had the good fortune to be present the first year. The lectures were held in a hot, noisy room. There was no air conditioning there in those days, and jackhammers were busy just outside the windows. Van Zandt Williams from the Perkin-Elmer Corporation, William Gallaway from Beckman Instruments, Bruce Billings and David Robinson from Baird Associates, and other very knowledgeable spectroscopists were present. There were vigorous discussions, and it was a highly stimulating week.

Lord, together with Elkan Blout, conceived the idea of a Gordon Conference on Infrared Spectroscopy and organized the first one in 1954. These meetings have been held biennially ever since. From the beginning they were outstanding in quality and drew the leading vibrational spectroscopists. It was through them that many American "infrared-ers" became personally acquainted with prominent foreign spectroscopists.

Another major contribution was his co-authorship of the book "Practical Spectroscopy" with G. R. Harrison and J. R. Loofbourow (1948). This filled a unique role by providing an authoritative account of experimental methods and applications across the whole gamut of optical spectroscopy. No other book on the subject has had quite the same useful mixture of fundamental knowledge and practical advice. It is now out of print, and there has been no adequate replacement.

While serving on the IUPAC Commission on Molecular Structure and Spectroscopy, Lord accepted the task of editing the compilation of "Tables of Wavenumbers for the Calibration of Infrared Spectrometers". Although several other individuals helped greatly by contributing experimental results, it was he who did the detailed, judgmental work of editing. His name is not mentioned as editor (none is), so unfortunately this very useful piece of work has not brought him the credit that is deserved.

No list of his contributions would be complete without mention of one of the most important of all—the influence he has had through his training of people. This has been multifaceted: through formal teaching of undergraduate and graduate classes, by directing graduate studies, by having guest workers in his laboratory, and through his summer infrared courses. He has been eminently successful. Many of his students are having notable careers, and he now has some third-scientific-generation descendants (e.g. Lord-Lippincott-Fateley-Tuazon). His relations with his graduate students were excellent. It was his custom to eat lunch with them regularly at a large round table in the student refectory. This was a splendid educational technique, transferring a great deal of information informally and developing the *esprit de corps* of his group. There was a fine spirit of camaraderie and a genuine pleasure in the work. Lord is a good teacher who strives to give his students understanding and insight in addition to hard facts. It is interesting to watch him work his way out of a temporary difficulty at the blackboard, and to observe his method of reasoning. On at least one occasion when he completed the last lecture of the term in freshman chemistry, the students applauded thunderously to show their appreciation. He follows the careers of his students with keen in-

terest, and often helps them in quiet ways that open new professional opportunities. Many of the beneficiaries are not aware of his aid. His students often seek his advice on important career decisions after they have left school.

These professional achievements have brought many recognitions and honors. After World War II Lord served on the Panel on Infrared of the U.S. Research and Development Board (1947–1953, Chairman 1952–1953). For service to the government he was awarded the Presidential Certificate of Merit by President Truman in 1948. Since 1948 he has been a consultant to the Central Research and Development Department of E. I. du Pont de Nemours and Co. He has participated in the work of international scientific bodies, having served on the U.S. National Committee of the International Commission on Optics (1956–1959), on the Commission on Molecular Structure and Spectroscopy of the International Union of Pure and Applied Chemistry (1957–1971, Chairman 1961–1967), and on the ICSU Inter-Union Commission on Spectroscopy (1967–1971). He has been active in the affairs of the Optical Society of America, and was its President in 1964. He has served on the editorial advisory boards of several periodicals (*Journal of Chemical Physics*, *Journal of Molecular Spectroscopy*, *Journal of the Optical Society of America*, *Journal of Raman Spectroscopy*, and *Spectrochimica Acta*), and as editor in the area of optics for the McGraw-Hill *Encyclopedia of Science and Technology*.

Kenyon College awarded him an honorary Doctor of Science degree in 1957. Other honors include being a Reilly Lecturer at the University of Notre Dame (1958), Guggenheim Fellow at the University of California at San Diego (1960), and Visiting Professor at the University of Georgia (1971). He received the Pittsburgh Spectroscopy Award in 1966, and will be the first recipient of the Ellis R. Lippincott Medal in 1976. He was made an Honorary Member of the Society for Applied Spectroscopy in 1967, and the Coblenz Society in 1976. He is a fellow of the Optical Society of America and of the American Academy of Arts and Sciences, and has been a trustee of Kenyon and Curry Colleges.

The preceding recitation of facts is sadly inadequate because it fails to describe the personality and character, the warmth and likableness, of the man as his friends know him. Although he has no consuming hobbies, he greatly enjoys many interests. Among them are his family and home, friends, good food, good conversation, and travel. Socially R.C. is a captivating personality. Whether he is recounting an unusual

experience, sharing a limerick, or listening attentively to the tales of others, he makes delightful company. He has been a bed-time reader for years, and his diverse reading interests (in more than one language) bring forth some fascinating stories at the dinner table. His presence enlivens every gathering and banishes dullness. His friends, of whom there are legions, would describe him with terms such as warm, sincere, loyal, delightful—just a very fine person.

Each of his graduate students must have a few especially vivid vignettes involving him which they carry through the years. Perhaps the author may be permitted to mention two of the many which he treasures. The first took place one fine May day during the period when I was a graduate student at Johns Hopkins. "Doc" (as we called him then) came into the laboratory and said, "It's too nice to work inside today. Would you like to play golf this afternoon?" How would any graduate student respond to such an excellent suggestion from his professor? Paul Emmett, the well-known authority on catalysis, was enlisted, and a fourth person whom I do not recall, and we had a delightful afternoon on the Clifton Park course. That first round of golf with R.C. has been followed by many other pleasant ones during Gordon Conferences and the Ohio State Symposia, but none is etched as vividly in my memory as that one.

The second vignette concerns the evening before my final oral examination for the Ph.D. degree. Lord and a number of graduate students lived and ate in the student dormitory, and on this fine evening several of us were sitting outside on a bench after dinner. Final orals were quite an ordeal at Johns Hopkins, and I made some remark about hoping that Lady Luck would be on my side the next day. "I don't know about Lady Luck, but there will be a Lord there", was his quick reply. In retrospect I have come to realize how this short response encompasses so many of his fine personal qualities: his humor, his understanding of another's concerns, and his assurance of support. All of us who have been his students and research associates have counted it a very great privilege. To Richard Lord, our admired and beloved teacher, mentor, confidant, and friend, we dedicate this issue.

Foil A. Miller
Department of Chemistry
University of Pittsburgh
6 February 1976

Doctoral Theses Supervised by Richard C. Lord

1941	Foil A. Miller	1955	Dean W. Robinson* Howard D. Stidham George B. Wilmot	1967	George J. Thomas, Jr. Jaan Laane* George O. Neely
1943	Frederick Halverson Alfred L. Marston	1956	Allan P. Gray H. Shreepathi Rao	1969	Lionel A. Carreira Constantin C. Milionis Nai-Teng Yu
1947	Ellis R. Lippincott	1958	Alfred Danti Monroe V. Evans	1970	Warren J. Adams Carl W. Wickstrom
1948	Lester Corrsin	1959	Charles H. Sederholm	1971	C. Scott Blackwell
1949	Maurice A. Lynch, Jr.* Emil J. Slowinski, Jr.	1961	Walter J. Lafferty Robin S. McDowell	1972	Richard Mendelsohn Tatsuya Ikeda Thomas C. Rounds
1950	Alvin W. Baker Betty Jane Fax (Mrs. Walter Daskin) Elmer Nielsen	1962	James R. Durig David W. Ellis* Karl A. Hartman, Jr. Burton Krakow	1973	Charles J. Wurrey Michael C.-C. Chen
1951	William D. Phillips Raymond C. Sangster*	1965	Karl R. Loos L. Claron Hoskins	1974	Mwindace N. Siamwiza
1952	Robert S. McDonald Robert W. Walker	1966	Wallace C. Pringle, Jr.	1975	Christopher S. Liu
1953	Richard E. Merrifield			1976	Gary T. Forrest (expected)
1954	Donald G. Rea			1977	Gilbert D. Lee (expected)

* Jointly with another faculty member.

Master's Theses Supervised by Richard C. Lord

1953	Charles McHenry Steese, Jr.	1964	Albert Bigelow Harvey	1970	Terry L. Berman
1958	Thomas John Porro	1965	Diane M. Meyer (Mrs. Charles)	1971	Victoria Reid Sauer Mwindace Siamwiza
1961	Louis Isaacson	1969	Daniel Chung-Man Luk	1975	Gilbert D. Lee
1963	Karl Rudolf Loos				

Guest and Research Associates with Richard C. Lord

1949	Jean Brossel	1958	James R. Aronson Ichiro Nakagawa	1965	Issei Harada Thomas M. Hard Yoshimasa Kyogoku Mireille Perek de Yagupsky
1951	Henry Cohn Andreas Klit Putcha Venkateswarlu	1959	Andrew R. H. Cole Dana W. Mayo	1966	Heinz Abplanalp
1952	Johan J. Lothe	1960	Michael Falk	1967	Roger F. Lake Soon Ng
1953	R. K. Asundi Cyril G. Cannon Antonio Foffani T. King McCubbin, Jr. Benoit Nolin	1961	Alfred J. Perkins Clive H. Perry	1968	Dennis W. Wertz
1954	Daniel R. J. Boyd Hans H. Günthard	1962	Graham R. Hunt Baij Nath Khanna Samuel Schrage	1969	Anne-Marie Bellocq
1955	C. Ramasastry	1963	Richard Lumley Jones Ian Mark Mills Edward C. Reifenstein III	1970	Thomas B. Malloy Toyotoshi Ueda
1956	René Fritz Zürcher	1964	Chadwick A. Tolman	1972	Robert H. Larkin
1957	Henrik F. Van Woerden Peter C. Von Planta George L. Zimmerman			1973	Evan Bayne Carew Michael C.-C. Chen David F. Eggers, Jr. Noel Relyea Ralf Steudel Hiromu Sugeta

Publications of Richard C. Lord

BOOKS, CHAPTERS, AND ARTICLES PUBLISHED IN BOOK FORM

"Practical Spectroscopy", Prentice-Hall, Englewood Cliffs, N.J., 1948; Tenth Printing, 1968 (with George R. Harrison and John R. Loofbrow). Also published by: (a) Blackie and Son, Ltd., London and Glasgow, 1950; (b) The State Publishing Institute, Moscow, 1950; (c) Naucna-Rujiga, Belgrade, Yugoslavia, 1962.

Articles on "Infrared Radiation", "Infrared Spectroscopy", "Raman Effect", "Physical Optics", "Wave Optics", and others in the fields of optics and spectroscopy. "McGraw-Hill Encyclopedia of Science and Technology", McGraw-Hill, New York, N.Y., 1960, and later editions.

"Tables of Wavenumbers for the Calibration of Infrared Spectrometers", Butterworths, London and Washington, 1961 (with R. N. Jones, E. K. Plyler and others). (Listed also under papers published.)

"Multilingual Dictionary of Important Terms in Molecular Spectroscopy", International Union of Pure and Applied Chemistry, Physical Chemistry Division, Commission on Molecular Structure and Spectroscopy, published by the National Research Council of Canada, Ottawa, 1966 (with G. Herzberg, et al.).

"Far-Infrared Spectra of Four-Membered Ring Compounds", in "Vibrational Spectroscopy and Structure", J. R. Durig, Ed., Marcel Dekker, New York, N.Y., 1972, Chapter 1, pp 1-24 (with C. S. Blackwell).

"Structural Studies of Nucleic Acids and Polynucleotides by Infrared and Raman Spectroscopy", in "Physio-Chemical Properties of Nucleic Acids", J. Duchesne, Ed., Academic Press, London, 1973, Chapter 10, pp 1-89 (with K. A. Hartman and G. J. Thomas, Jr.).

PAPERS

"Raman Spectrum of Benzene- d_6 ", *J. Chem. Phys.*, **4**, 82-83 (1936).

"The Entropy of Carbon Tetrachloride", *J. Chem. Phys.*, **4**, 707-710 (1936) (with E. R. Blanchard).

"Entropy and the Symmetry of the Benzene Molecule", *J. Phys. Chem.*, **41**, 149-158 (1937) (with D. H. Andrews).

"The Infrared Absorption Spectrum of Carbon Suboxide", *J. Chem. Phys.*, **5**, 642-649 (1937) (with N. Wright).

"Structure of Benzene. Part X. Remarks on the Intensities of the Raman Lines in Benzene and Hexadeuterobenzene", *J. Chem. Soc.*, 1728-1737 (1937) (with E. Teller).

"Crystalline Heat Capacities of Benzene and Benzene- d_6 ", *J. Chem. Phys.*, **5**, 649-654 (1937) (with J. E. Ahlberg and D. H. Andrews).

"The Fine Structure of the Totally Symmetrical Raman Lines in Benzene and Benzene- d_6 ", *J. Chem. Phys.*, **6**, 203-204 (1938) (with A. Langseth).

"The Raman Spectra of the Deuterated Benzenes", *K. Dan. Vidensk. Selsk., Mat.-Fys. Medd.*, **16**, 1-85 (1938) (with A. Langseth).

"The Heat Capacities of Molecular Lattices. I. Introduction", *J. Chem. Phys.*, **9**, 693-699 (1941).

"The Heat Capacities of Molecular Lattices. II. The Structure of Metallic Lithium", *J. Chem. Phys.*, **9**, 700-705 (1941).

"The Vibrational Spectra of Pyrrole and Some of Its Deuterium Derivatives", *J. Chem. Phys.*, **10**, 328-341 (1942) (with F. A. Miller).

"The Raman Spectrum of Cyclooctatetraene", *J. Am. Chem. Soc.*, **68**, 1868 (1946) (with E. R. Lippincott).

"The Infrared and Raman Spectra of Heavy Cyclooctatetraene", *J. Chem. Phys.*, **16**, 548-549 (1948) (with E. R. Lippincott and R. S. McDonald).

"The Structure of Cyclooctatetraene", *J. Chim. Phys.*, **45**, 47-49 (1948).

"The Vibrational Spectra and Structures of Iodine Pentafluoride and Heptafluoride", *J. Am. Chem. Soc.*, **72**, 522-527 (1950) (with M. A. Lynch, Jr., W. C. Schumb, and E. J. Slowinski, Jr.).

"Structure of Cyclooctatetraene", *Nature (London)*, **166**, 227 (Aug 5, 1950) (with E. R. Lippincott and R. S. McDonald).

"Apparatus for Low Temperature Study of the Raman Effect", *J. Opt. Soc. Am.*, **40**, 655-657 (1950) (with E. Nielsen).

"The Vibrational Spectra of Diborane and Some of Its Isotopic Derivatives", *J. Chem. Phys.*, **19**, 1-10 (1951) (with E. Nielsen).

"The Raman Spectrum of Allene- d_4 ", *J. Chem. Phys.*, **19**, 260-261 (1951) (with J. Ocampo).

"The Vibrational Spectra and Structure of Cyclooctatetraene", *J. Am. Chem. Soc.*, **73**, 3370-3385 (1951) (with E. R. Lippincott and R. S. McDonald).

"The Thermodynamic Functions of Cyclooctatetraene", *J. Am. Chem. Soc.*, **73**, 3889-3891 (1951) (with E. R. Lippincott).

"Far Infrared Transmission of Silicon and Germanium", *Phys. Rev.*, **85**, 140-141 (1952).

"Notes on the Practice of Infrared Spectroscopy", *J. Opt. Soc. Am.*, **42**, 149-159 (1952) (with R. S. McDonald and F. A. Miller).

"Exchange Reactions of γ -Pyrone and Synthesis of Deuterated Pyrones", *J. Am. Chem. Soc.*, **74**, 2429-2430 (1952) (with W. D. Phillips).

"The Rotation-Vibration Spectra of Allene and Allene- d_4 ", *J. Chem. Phys.*, **20**, 1237-1247 (1952) (with P. Venkateswarlu).

"A Vacuum-Tight Seal between LiF and Silver", *Rev. Sci. Instrum.*, **23**, 442 (1952) (with R. S. McDonald).

"Evaluation of the Zeta Sums for Rotation-Vibration Interaction in Axially Symmetrical Molecules", *J. Chem. Phys.*, **20**, 1348-1350 (1952) (with R. E. Merrifield).

"Strong Hydrogen Bonds in Crystals", *J. Chem. Phys.*, **21**, 166-167 (1953) (with R. E. Merrifield).

"Synthesis of Cyclobutene- d_6 and Cyclobutane- d_8 ", *J. Chem. Phys.*, **21**, 378 (1953).

"Hydrogen Bonding in Crystals and the Nature of the Hydrogen Bond", *Anal. Chem.*, **25**, 527 (1953) (with R. E. Merrifield).

"The Vibrational Spectra of Pyridine and Pyridine- d_5 ", *J. Chem. Phys.*, **21**, 1170-1176 (1953) (with L. Corrsin and B. J. Fax).

"The Infrared Spectra of Propylene and Propylene- d_8 ", *J. Opt. Soc. Am.*, **43**, 1079-1085 (1953) (with P. Venkateswarlu).

"The Infrared Spectra of Monochlorogermane and Monochlorogermane- d_3 ", *J. Chem. Phys.*, **22**, 542-546 (1954) (with C. M. Steese).

"Rotation-Vibration Spectra and Structure of the Allene Molecule", *J. Opt. Soc. Am.*, **44**, 256 (1954).

"Vibrational Spectra and Possible Structures of the Dimers of Cyclooctatetraene", *J. Am. Chem. Soc.*, **76**, 2518-2525

- (1954) (with R. W. Walker).
- "Quantitative Study of the Bonding of Chloroform-*d* in Various Solvents by Infrared Spectrometry", *J. Am. Chem. Soc.*, **77**, 1365-1368 (1955) (with B. Nolin and H. D. Stidham).
- "Vibrational Spectra and Structure of Cyclopropane and Cyclopropane-*d*₆", *J. Chem. Phys.*, **23**, 1636-1643 (1955) (with A. W. Baker).
- "High-resolution Spectroscopy in the 3-5 Micron Region with a Small Grating Spectrometer", *J. Opt. Soc. Am.*, **45**, 441-446 (1955) (with T. K. McCubbin, Jr.).
- "Vibrational Spectra and Structure of Disiloxane and Disiloxane-*d*₆", *J. Am. Chem. Soc.*, **78**, 1327-1332 (1956) (with D. W. Robinson and W. C. Schumb).
- "Vibrational Spectra of Ethylene Oxide and Ethylene Oxide-*d*₄", *J. Chem. Phys.*, **24**, 656-658 (1956) (with B. Nolin).
- "Factors Influencing Characteristic Vibrational Frequencies of Molecules: Intramolecular Effects", *Appl. Spectrosc.*, **10**, 115-123 (1956) (with F. A. Miller).
- "Rotation-Vibration Spectra and the Molecular Constants of Cyclopropane and Cyclopropane-*d*₆", *J. Chem. Phys.*, **25**, 768-774 (1956) (with H. H. Günthard and T. K. McCubbin, Jr.).
- "The Synthesis of Spiropentane-*d*₈", *J. Org. Chem.*, **21**, 1487-1491 (1956) (with H. O. House and H. S. Rao).
- "Vibrational Spectra of 1,3,5-Cyclooctatriene, Bicyclo[4.2.0]octa-2,4-diene, and Their Dichlorides", *J. Am. Chem. Soc.*, **79**, 567-569 (1957) (with E. R. Lippincott).
- "Calculation of the Heat Capacity of α -Quartz and Vitreous Silica from Spectroscopic Data", *J. Chem. Phys.*, **26**, 230-232 (1957) (with J. C. Morrow).
- "Rotation-Vibration Spectra of Methylamine and Its Deuterium Derivatives", *J. Chem. Phys.*, **26**, 690-705 (1957) (with A. P. Gray).
- "The Vibrational Spectra and Structure of Cyclobutene and Cyclobutene-*d*₆", *J. Am. Chem. Soc.*, **79**, 2401-2406 (1957) (with D. G. Rea).
- "Infrared and Raman Spectra of the Diazines", *Spectrochim. Acta*, **9**, 113-125 (1957) (with A. L. Marston and F. A. Miller).
- "Infrared Spectroscopy from 5 to 200 Microns with a Small Grating Spectrometer", *J. Opt. Soc. Am.*, **47**, 689-697 (1957) (with T. K. McCubbin, Jr.).
- "Etudes à Grande Résolution Dans L'Infrarouge Avec Un Petit Spectromètre à Réseau Plan", *Compte Rendus du 18eme Congres, Groupement pour L'Avancement des Methodes Spectrographiques, Paris, 1955*, pp 349-367 (with T. K. McCubbin, Jr.).
- "The Preparation and Vibrational Spectra of Disilylacetylene", *Spectrochim. Acta*, **12**, 147-153 (1958) (with D. W. Mayo, H. E. Opitz, and J. S. Peake).
- "Pure Rotational Absorption of NO₂ in the 50-200 Micron Region", *Spectrochim. Acta*, **12**, 247-252 (1958) (with G. R. Bird and A. Danti).
- "Rotational Analysis and Upper-Stage Transitions of Parallel Absorption Bands in Benzene, *sym*-Benzene-*d*₃, Benzene-*d*₆, and Pyridine", *Spectrochim. Acta*, **13**, 180-191 (1958) (with A. Danti).
- "Pure Rotational Absorption of Ozone and Sulfur Dioxide from 100 to 200 Microns", *J. Chem. Phys.*, **30**, 1310-1313 (1959) (with A. Danti).
- "Infrared Emission Spectra of Ammonia-Oxygen and Hydrazine Flames", *Spectrochim. Acta*, **15**, 605-626 (1959) (with C. H. Sederholm).
- "Vibrational Spectra and Structure of the Tropilidene Molecule", *J. Am. Chem. Soc.*, **82**, 1876-1882 (1960) (with M. V. Evans).
- "Far Infrared Spectrum of Trimethylene Oxide", *J. Chem. Phys.*, **33**, 294-295 (1960) (with A. Danti and W. J. Lafferty).
- "Far Infrared Spectrum and Structure of Disiloxane", *J. Chem. Phys.*, **33**, 1004-1007 (1960) (with J. R. Aronson and D. W. Robinson). Erratum, *ibid.*, **35**, 2245-2246 (1961).
- "Infrared Structural Studies beyond Fifty Microns", *Adv. Mol. Spectrosc., Proc. Int. Meet., 4th, 1959*, 49-59 (1962) (with J. R. Aronson, A. Danti, and W. J. Lafferty). Also printed as "Investigation of Far Infrared Spectra", Wright Air Development Division Technical Report 59-498, Feb, 1960.
- "An Infrared Study of the Dimerization of Caprolactam by Hydrogen Bonding", *Z. Elektrochem.*, **64**, 672-676 (1960) (with T. J. Porro).
- "Tables of Wavenumbers for the Calibration of Infrared Spectrometers", *Pure Appl. Chem.*, **1**, 537-699 (1961) (with R. N. Jones, E. K. Plyler, and others) (Also published in book form).
- "Synthesis and Vibrational Spectrum of Bicyclo[3.2.0]hepta-2,6-diene", *J. Am. Chem. Soc.*, **83**, 3409-3413 (1961) (with M. V. Evans).
- "High Resolution Raman Spectroscopy of Gases. XV. Rotational Spectrum and Structure of Cyclobutane", *Can. J. Phys.*, **40**, 725-731 (1962) (with B. P. Stoicneff).
- "Infrared Transmittance and Reflectance of Beryllium Oxide", *J. Opt. Soc. Am.*, **52**, 1078 (1962) (with J. R. Durig, W. J. Gardner, and L. H. Johnston).
- "Pure Rotational Absorption of Nitrosyl Fluoride and Nitrosyl Chloride in the 80-250 Micron Region", *Spectrochim. Acta*, **19**, 421-429 (1963) (with J. R. Durig).
- "Hydration of Deoxyribonucleic Acid. I. A Gravimetric Study", *J. Am. Chem. Soc.*, **84**, 3842-3846 (1962) (with M. Falk and K. A. Hartman, Jr.).
- "Hydration of Deoxyribonucleic Acid. II. An Infrared Study", *J. Am. Chem. Soc.*, **85**, 387-391 (1963) (with M. Falk and K. A. Hartman, Jr.).
- "Hydration of Deoxyribonucleic Acid. III. A Spectroscopic Study of the Effect of Hydration on the Structure of DNA", *J. Am. Chem. Soc.*, **85**, 391-394 (1963) (with M. Falk and K. A. Hartman, Jr.).
- "Far Infrared Absorption, Vibrational Spectra, and Structure of Tetrafluoro-1,3-dithietane", *Spectrochim. Acta*, **19**, 769-774 (1963) (with J. R. Durig).
- "Infrared Spectrum of Tetrafluorohydrazine", *Spectrochim. Acta*, **19**, 1877-1883 (1963) (with J. R. Durig).
- "Normal Vibrations, Potential Constants, and Rotation-Rotation Interaction Constants in Cyclobutane and Cyclobutane-*d*₈", *J. Chem. Phys.*, **39**, 2951-2965 (1963) (with I. Nakagawa).
- "Exchange Reactions of 4-Pyrone and 4-Pyrone Derivatives", *J. Org. Chem.*, **29**, 2682-2685 (1964) (with D. W. Mayo, P. J. Sapienza, and W. D. Phillips).
- "The Synthesis of Oxetane-*d*₆", *J. Org. Chem.*, **29**, 2799-2800 (1964) (with W. J. Lafferty and D. W. Mayo).
- "Vibrational Spectrum and Barrier to Internal Rotation of CF₃CFO", *Spectrochim. Acta*, **21**, 119-125 (1965) (with K. R. Loos).
- "An Infrared Study of High-Area Metal Films Evaporated in Carbon Monoxide", *J. Phys. Chem.*, **69**, 1188-1195 (1965) (with C. W. Garland and P. F. Troiano).
- "Infrared Spectrum of Carbon Monoxide Chemisorbed on

- Evaporated Nickel Films", *J. Phys. Chem.*, **69**, 1195–1203 (1965) (with C. W. Garland and P. F. Troiano).
- "Hydrogen-Bonded Dimers of Adenine and Uracil Derivatives", *Science*, **148**, 1734–1737 (1965) (with R. M. Hamlin, Jr., and A. Rich).
- "Infrared Spectrum and Vibrational Potential Function of AsF₃", *J. Chem. Phys.*, **43**, 155–158 (1965) (with L. C. Hoskins).
- "Infrared Spectrum of Sulfur Trioxide", *J. Chem. Phys.*, **44**, 3640 (1966) (with B. Krakow).
- "Far-Infrared Spectra of Four-Membered-Ring Compounds. I. Spectra and Structure of Cyclobutanone, Cyclobutanone-*d*₄, Trimethylene Sulfide, and Perfluorocyclobutanone", *J. Chem. Phys.*, **45**, 61–66 (1966) (with J. R. Durig).
- "Hydrogen Bonding Specificity of Nucleic Acid Purines and Pyrimidines in Solution", *Science*, **154**, 518–520 (1966) (with Y. Kyogoku and A. Rich).
- "An Infrared Study of Hydrogen Bonding between Adenine and Uracil Derivatives in Chloroform Solution", *J. Am. Chem. Soc.*, **89**, 496–504 (1967) (with Y. Kyogoku and A. Rich).
- "The Effect of Substituents on the Hydrogen Bonding of Adenine and Uracil Derivatives", *Proc. Natl. Acad. Sci. U.S.A.*, **57**, 250–257 (1967) (with Y. Kyogoku and A. Rich).
- "Vibrational Spectra of PF₅ and AsF₅: Height of the Barrier to Internal Exchange of Fluorine Nuclei", *J. Chem. Phys.*, **46**, 2402–2412 (1967) (with L. C. Hoskins).
- "Two Vibration–Rotation Bands of Cyanogen Fluoride", *J. Mol. Spectrosc.*, **23**, 86–93 (1967) (with A. R. H. Cole and L. Isaacson).
- "Raman Spectral Studies of Nucleic Acids and Related Molecules. I. Ribonucleic Acid Derivatives", *Spectrochim. Acta, Part A*, **23**, 2551–2591 (1967) (with G. J. Thomas, Jr.).
- "Raman Studies of Nucleic Acids. II. Aqueous Purine and Pyrimidine Mixtures", *Biochim. Biophys. Acta*, **142**, 1–11 (1967) (with G. J. Thomas, Jr.).
- "Cyclic Polyolefins. XLV. *cis,trans*-1,5-Cyclooctadiene", *J. Am. Chem. Soc.*, **89**, 4024–4027 (1967) (with A. C. Cope, C. F. Howell, J. Bowers, and G. M. Whitesides).
- "Spectroscopic Studies of Molecular Interaction in DNA Constituents", *Dev. Appl. Spectrosc.*, **6** (1968) (with G. J. Thomas, Jr.).
- "Application of Infrared Spectroscopy to Art Problems", Proceedings of the Seminar on the Application of Science in Examination of Works of Art, Museum of Fine Arts, Boston, Mass., Sept 1965, p 222. (Published by the Museum, Dec 1967.)
- "Recent Studies in High-resolution Far-Infrared Spectroscopy", *Proc. Int. Conf. Spectrosc.*, *1st*, 1967, 173–180 (1967).
- "Far-Infrared Spectra of Ring Compounds. II. The Spectrum and Ring-Puckering Potential Function of Cyclopentene", *J. Chem. Phys.*, **47**, 4941–4945 (1967) (with J. Laane).
- "Far-Infrared Spectra of Ring Compounds. III. Spectrum, Structure, and Ring-Puckering Potential of Silacyclobutane", *J. Chem. Phys.*, **48**, 1508–1513 (1968) (with J. Laane).
- "A Double-beam High-resolution Spectrometer for the Far-Infrared", *Appl. Opt.*, **7**, 589–598 (1968) (with T. M. Hard).
- "Specific Hydrogen Bonding of Barbiturates to Adenine Derivatives", *Nature (London)*, **218**, 69 (1968) (with Y. Kyogoku and A. Rich).
- "A High-resolution Far-infrared Study of Rotation in HN₃, HNCO, HNCS, and Their Deuterium Derivatives", *J. Mol. Spectrosc.*, **27**, 148–176 (1968) (with B. Krakow and G. O. Neely).
- "Search for Pure Rotational Infrared Absorption in Allene", *J. Chem. Phys.*, **50**, 565 (1969) (with W. C. Pringle, Jr.).
- "An Infrared Study of the Hydrogen-bonding Specificity of Hypoxanthine and Other Nucleic Acid Derivatives", *Biochim. Biophys. Acta*, **179**, 10–17 (1969) (with Y. Kyogoku and A. Rich).
- "Far-Infrared Spectra of Ring Compounds. IV. Spectra of Compounds with an Unsymmetrical Potential Function for Ring Inversion", *J. Chem. Phys.*, **51**, 2735–2744 (1969) (with L. A. Carreira).
- "Far-Infrared Spectra of Ring Compounds. V. Ring-Puckering Potential Functions of Some Oxygen-Containing Molecules", *J. Chem. Phys.*, **51**, 3225–3231 (1969) (with L. A. Carreira).
- "Low-Frequency Infrared and Raman Spectra of Some Adenine and Uracil Crystals", *Spectrochim. Acta, Part A*, **26**, 2305–2318 (1970) (with I. Harada).
- "Laser-Excited Raman Spectroscopy of Biomolecules: I. Native Lysozyme and Its Constituent Amino Acids", *J. Mol. Biol.*, **50**, 509–524 (1970) (with Nai-Teng Yu).
- "Laser-Excited Raman Spectroscopy of Biomolecules: II. Native Ribonuclease and α -Chymotrypsin", *J. Mol. Biol.*, **51**, 203–213 (1970) (with Nai-Teng Yu).
- "Far-Infrared Spectra of Ring Compounds. VI. Structure of 1,4-Cyclohexadiene", *J. Mol. Spectrosc.*, **39**, 340–344 (1971) (with J. Laane).
- "Laser Raman Spectroscopy of Biological Macromolecules", Special supplement to *Pure Appl. Chem.* on selected lectures at XXIIIrd International Congress of Pure and Applied Chemistry, Boston, Mass., July, 1971: Vol. VII, 179 (1971). (See *Pure Appl. Chem.*, **28**, XIX (1971).)
- "Far-Infrared Spectra of Ring Compounds. VII. Spectra of Chloro-, Bromo-, and Cyanocyclobutane", *J. Chem. Phys.*, **56**, 1706–1711 (1972) (with C. S. Blackwell, J. R. Durig, and J. M. Karriker).
- "Far-Infrared Spectra of Ring Compounds. VIII. The Effect of a Finite Barrier on Pseudorotation in Five-Membered Rings", *J. Chem. Phys.*, **56**, 1434–1439 (1972) (with T. Ikeda, T. B. Malloy, Jr., and T. Ueda).
- "Laser-Excited Raman Spectroscopy of Biomolecules. III. Bovine Serum Albumin and β -Lactoglobulin", *Biochim. Biophys. Acta*, **257**, 280–287 (1972) (with A. M. Bellocq and R. Mendelsohn).
- "Far-Infrared Spectra of Ring Compounds. IX. Pseudorotation in Cyclopentanone", *J. Chem. Phys.*, **56**, 4450–4466 (1972) (with T. Ikeda).
- "Laser Raman Spectra of Aqueous Lysozyme Denatured by Lithium Bromide", *J. Am. Chem. Soc.*, **94**, 2133–2135 (1972) (with R. Mendelsohn).
- "Infrared and Raman Spectra of Cyclobutane and Cyclobutane-*d*₈", *Spectrochim. Acta, Part A*, **28**, 603–618 (1972) (with R. J. Capwell, F. A. Miller, and D. G. Rea).
- "Far-Infrared Spectra of Ring Compounds. X. Hindered Pseudorotation in Six-Membered Rings: Estimation of the Barrier Height of Half-Chair Inversion in Dioxene and 2,3-Dihydropyran", *J. Chem. Phys.*, **57**, 2572–2580 (1972) (with T. C. Rounds and T. Ueda).
- "Infrared Studies on Selective Hydrogen Bonding of the Nucleic Acid Purine and Pyrimidine Derivatives and Some Other Compounds", *Jerusalem Symp. Quantum Chem. Biochem.*, **4**, 223–240 (1972) (with Y. Kyogoku, B. S. Yu, and A. Rich).
- "Far-Infrared Spectra of Ring Compounds. XII. Analogs of Bicyclo[3.1.0]hexane", *J. Mol. Spectrosc.*, **46**, 358–370 (1973) (with T. B. Malloy, Jr.).
- "Far-Infrared Spectra of Ring Compounds. XIII. The Spec-

- trum and Structure of 1,4-Dioxacyclohexadiene-2,5", *J. Chem. Phys.*, **58**, 4344–4349 (1973) (with T. C. Rounds).
- "Ring Inversion in Dioxene: Comparison of the Barrier Heights by Nuclear Magnetic Resonance and Far-Infrared Measurements", *J. Am. Chem. Soc.*, **95**, 5129–5132 (1973) (with R. H. Larkin). Erratum, *ibid.*, **96**, 1643 (1974).
- "Tables of Wavenumbers for the Calibration of Infrared Spectrometers, Parts III and IV: 600–1 cm⁻¹", *Pure Appl. Chem.*, **33**, 607–651 (1973) (with A. R. H. Cole and R. N. Jones).
- "Far-Infrared and Raman Spectra of Gaseous Carbon Suboxide and the Potential Function of the Low-Frequency Bending Mode", *J. Chem. Phys.*, **59**, 1028–1037 (1973) (with L. A. Carreira, R. O. Carter, J. R. Durig, and C. C. Milionis).
- "Transfer RNA: Change of Conformation Upon Aminoacylation Determined by Raman Spectroscopy", *Biochem. Biophys. Res. Commun.*, **54**, 570–577 (1973) (with G. J. Thomas, Jr., M. C. Chen, P. S. Kotsiopoulos, T. R. Tritton, and S. C. Mohr).
- "Laser-Excited Raman Spectroscopy of Biomolecules. IV. Thermal Denaturation of Aqueous Lysozyme", *Biochim. Biophys. Acta*, **328**, 252–260 (1973) (with M. C. Chen and R. Mendelsohn).
- "Laser-Excited Raman Spectroscopy of Biomolecules. V. Conformational Changes Associated with the Chemical Denaturation of Lysozyme", *J. Am. Chem. Soc.*, **96**, 3038–3042 (1974) (with M. C. Chen and R. Mendelsohn).
- "Reinvestigation of Specific Hydrogen Bonding of Certain Adenine and Uracil Derivatives by Infrared Spectroscopy", *Biochim. Biophys. Acta*, **340**, 90–94 (1974) (with M. C. Chen).
- "Biscyclopropylidene: The Case of the Missing Double-Bond Raman Frequency", *Spectrochim. Acta, Part A*, **30**, 915–928 (1974) (with C. J. Wurrey).
- "Laser Excited Raman Spectroscopy of Biomolecules. VI. Some Polypeptides as Conformational Models", *J. Am. Chem. Soc.*, **96**, 4750–4752 (1974) (with M. C. Chen).
- Contribution on "Studies of Protein Structure by Raman Spectroscopy", Proceeding of the Conference on Critical Evaluation of Chemical and Physical Structural Information, Dartmouth College, June 24–29, 1973. National Academy of Sciences, Washington, D.C., 1974, pp 263–265.
- "The Far-Infrared Spectrum of Collagen", *Macromolecules*, **7**, 954–956 (1974) (with P. L. Gordon, C. Huang, and I. V. Yannas).
- "Hydrogen Bonding by Chloroform-*d* as a Conformational Probe of the Macrobicyclic Amines", *Spectrochim. Acta, Part A*, **31**, 1381–1387 (1975) (with M. N. Siamwiza).
- "Far-Infrared Spectra of Ring Compounds. XIV. The Ring-Puckering Potential Function of Thietanone-3", *J. Mol. Spectrosc.*, **55**, 460–463 (1975) (with C. S. Blackwell).
- "Laser-Excited Raman Spectroscopy of Biomolecules. VII. Yeast Phenylalanine Transfer RNA in the Crystalline State and in Solution", *Biochemistry*, **14**, 4385–4391 (1975) (with M. C. Chen, R. Giegé, and A. Rich).
- "Direct Observation of the Torsional Fundamental of Gaseous C₂F₆ in the Far-Infrared", *J. Mol. Spectrosc.*, **59**, 63–73 (1976) (with D. F. Eggers, Jr., and C. W. Wickstrom).
- "Interpretation of the Doublet at 850 and 830 cm⁻¹ in the Raman Spectra of Tyrosyl Residues in Proteins and Certain Model Compounds", *Biochemistry*, **14**, 4870–4876 (1975) (with M. N. Siamwiza, M. C. Chen, T. Takamatsu, I. Harada, H. Matsuura, and T. Shimanouchi).
- "Laser-Excited Raman Spectroscopy of Biomolecules. VIII. Conformational Study of Bovine Serum Albumin", *J. Am. Chem. Soc.*, **98**, 990–992 (1976) (with M. C. Chen).
- "Laser-Excited Raman Spectroscopy of Biomolecules. IX. Study of Thermal Unfolding of Ribonuclease A", *Biochemistry*, **15**, 1889–1897 (1976) (with M. C. Chen).

THE JOURNAL OF
PHYSICAL CHEMISTRY

Volume 80, Number 11 May 20, 1976

JPCHAx 80(11) 1123-1266 (1976)

ISSN 0022-3654

Electron Spin Resonance Studies of Neurophysin and Its Interaction with Spin-Labeled Peptides	Susan Lord Lundt* and Esther Breslow*	1123
Deuterium Exchange in Pyridine Dinucleotide Coenzymes. Raman Spectroscopic Evidence for a Modified Amide Charge Distribution in β -Dihyronicotinamide Adenine Dinucleotide	G. Forrest	1127
Vibrational Spectra and Normal Coordinate Analysis of Ethyl Cyanides	C. J. Wurrey, W. E. Bucy, and J. R. Durig*	1129 ■
Correlation between the Absorption Spectra and Resonance Raman Excitation Profiles of Astaxanthin	V. R. Salares,* R. Mendelsohn, P. R. Carey, and H. J. Bernstein	1137
Identification and Estimation of the Relative Abundance of Two Conformers of 1,2,3,6-Tetrahydropyridine from the Microwave Spectrum	S. Chao, T. K. Avirah, Robert L. Cook, and Thomas B. Malloy, Jr.*	1141
Raman Spectrum and Torsional Potential Function of Acrolein	L. A. Carreira	1149
Raman Spectra of Some Neurotoxins and Denatured Neurotoxins in Relation to Structures and Toxicities	Issei Harada,* Tadahisa Takamatsu, Takehiko Shimanouchi, Tatsuo Miyazawa, and Nobuo Tamiya	1153
Studies of Virus Structure by Laser-Raman Spectroscopy. 3. Turnip Yellow Mosaic Virus	T. A. Turano, K. A. Hartman,* and G. J. Thomas, Jr.	1157
A Raman Spectroscopic Study of Complexes of Polylysine with Deoxyribonucleic Acid and Polyriboadenylic Acid	B. Prescott, C. H. Chou, and G. J. Thomas, Jr.*	1164
Ring-Puckering Vibrational Spectra of Cyclopentene-1- d_1 and Cyclopentene-1,2,3,3- d_4	J. R. Villarreal, L. E. Bauman, and J. Laane*	1172
Effect of Carbonyl Substitution on the Barrier to Planarity in Cyclobutanes	A. L. Meinzer and W. C. Pringle*	1178
Resonance Raman Spectra of Metallooctaethylporphyrins. Low Frequency Vibrations of Porphyrin and Iron-Axial Ligand Stretching Modes	T. Kitagawa,* M. Abe, Y. Kyogoku, H. Ogoshi, E. Watanabe, and Z. Yoshida	1181
Vibrationally Averaged Interatomic Distances	I. M. Mills	1187
Microwave, Infrared, and Raman Studies of Several Isotopic Species of Vinylidifluoroborane	J. R. Durig,* L. W. Hall, R. O. Carter, C. J. Wurrey, V. F. Kalasinsky, and J. D. Odom	1188 ■
Infrared Spectral Behavior of Fine Particulate Solids	Graham R. Hunt	1195
Spectra and Structure of Small-Ring Molecules. 33. Microwave Spectrum of Silacyclopentane	J. R. Durig,* W. J. Lafferty, and V. F. Kalasinsky	1199
Vibrational Constants and Force Field of Sulfur Hexafluoride	Robin S. McDowell,* Jack P. Aldridge, and Redus F. Holland	1203

WHAT'S HAPPENING IN CHEMISTRY?

Send for This Concise, Information-Packed Summary and Find Out!

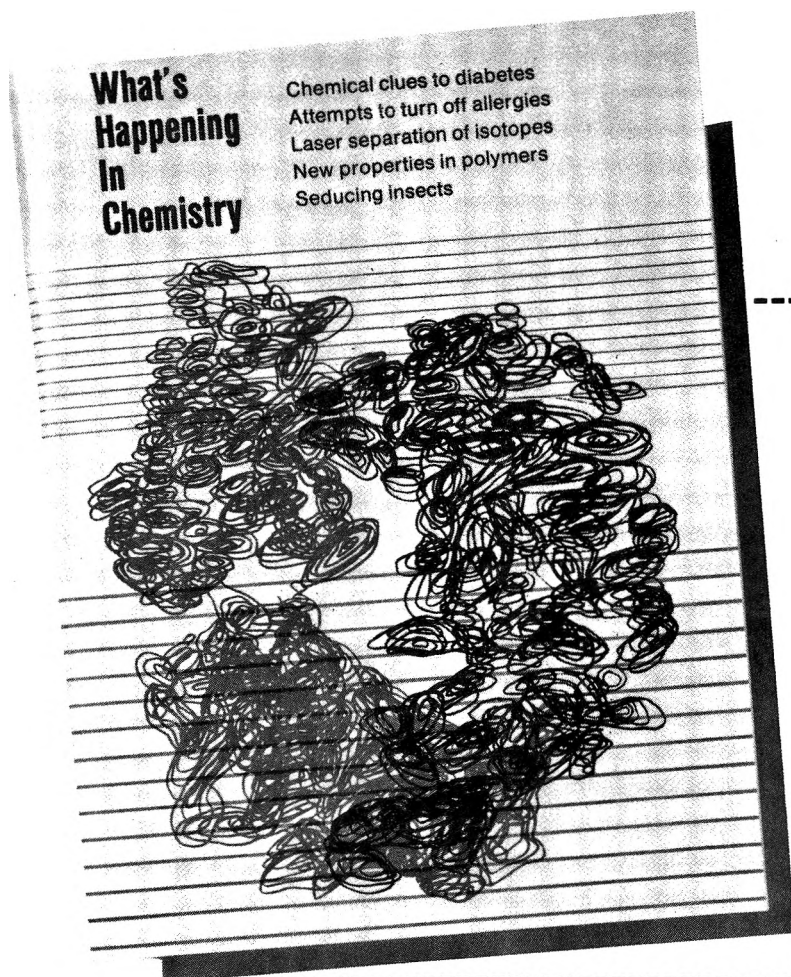
This latest compilation of recent events in chemical research makes absorbing and exciting reading. Every chemist, scientist, instructor, student, and interested layman will find it invaluable as a source of succinct information.

A glance at the contents listed below, will show you the scope of "WHAT'S HAPPENING IN CHEMISTRY?":

- NEW CHEMICAL CLUES TO DIABETES
- ADVANCES IN IMMUNOCHEMISTRY
- CHEMISTRY BY LASER LIGHT
- LEAD POISONING—MORE QUESTIONS AND ANSWERS
- NEW POLYMERS ON THE HORIZON
- A FRESH LOOK AT INSECT CONTROL
- NEW INSIGHTS TO THE DETECTION AND TREATMENT OF CANCER
- FUTURE FOODS
- OLD ENERGY SOURCES, NEW IDEAS
- OZONE—AEROSOL SPRAY . . . FACTS FALL INTO PLACE
- THE 1975 NOBEL PRIZE
- NATIONAL MEDAL OF SCIENCE

Because the book is printed in magazine format, the cost is only \$1.50 per copy. Order 15 copies or more and the cost drops to just \$.75 for each book.

Just fill out the order form below along with your payment and mail it back to us today. Your copy will be in the mail just as soon as we can process your order.



Special Issues Sales

American Chemical Society
1155—16th Street, N.W.
Washington, D.C. 20036

Please send me _____ copies of
"WHAT'S HAPPENING IN CHEMISTRY?"

Name

Address

City

State

Zip Code

WH 76

AUTHOR INDEX

- | | | | |
|------------------------|-----------------------------------|---------------------------|-----------------------------------|
| Abe, M., 1181 | Durig, J. R., 1129, 1188,
1199 | Kyogoku, Y., 1181 | Robinson, D. W., 1234 |
| Aldridge, J. P., 1203 | Emslie, A. G., 1224 | Laane, J., 1172 | Salares, V. R., 1137 |
| Aronson, J. R., 1224 | Falk, M., 1212 | Lafferty, W. J., 1199 | Shimanouchi, T., 1153 |
| Avirah, T. K., 1141 | Finch, C. B., 1226 | Lundt, S. L., 1123 | Snider, A. M., Jr., 1262 |
| Bates, J. B., 1226 | Finseth, D. H., 1248 | Malloy, T. B., Jr., 1141 | Sourisseau, C., 1248 |
| Bauman, L. E., 1172 | Forrest, G., 1127 | Mayo, D. W., 1217 | Stidham, H. D., 1226 |
| Bellamy, L. J., 1217 | Günthard, H. H., 1238 | McDowell, R. S., 1203 | Takamatsu, T., 1153 |
| Bernstein, H. J., 1137 | Hall, L. W., 1188 | Meinzer, A. L., 1178 | Tamiya, N., 1153 |
| Breslow, E., 1123 | Harada, I., 1153 | Mendelsohn, R., 1137 | Thomas, G. J., Jr.,
1157, 1164 |
| Bucy, W. E., 1129 | Hartman, K. A., 1157 | Miller, F. A., 1248, 1262 | Turano, T. A., 1157 |
| Buhay, H., 1208 | Holland, R. F., 1203 | Mills, I. M., 1187 | Villarreal, J. R., 1172 |
| Cannon, C. G., 1247 | Hunt, G. R., 1195 | Miyazawa, T., 1153 | Watanabe, E., 1181 |
| Carey, P. R., 1137 | Kalasinsky, V. F., 1188,
1199 | Odom, J. D., 1188 | Wurrey, C. J., 1129,
1188 |
| Carreira, L. A., 1149 | Kitagawa, T., 1181 | Ogoshi, H., 1181 | Yoshida, Z., 1181 |
| Carter, R. O., 1188 | Knop, O., 1212 | Oxton, I. A., 1212 | |
| Chao, S., 1141 | Krause, P. F., 1262 | Perry, C. H., 1208 | |
| Chou, C. H., 1164 | Kühne, H., 1238 | Prescott, B., 1164 | |
| Cole, A. R. H., 1221 | | Pringle, W. C., 1178 | |
| Cook, R. L., 1141 | | Ramsay, D. A., 1221 | |
| Cross, K. J., 1221 | | | |
| Downey, G. D., 1234 | | | |

THE JOURNAL OF PHYSICAL CHEMISTRY

Registered in U. S. Patent Office © Copyright, 1976, by the American Chemical Society

VOLUME 80, NUMBER 11 MAY 20, 1976

Electron Spin Resonance Studies of Neurophysin and Its Interaction with Spin-Labeled Peptides^{1a}

Susan Lord Lundt*^{1b} and Esther Breslow*

Department of Biochemistry, Cornell University Medical College, New York, N.Y. 10021 (Received December 30, 1975)

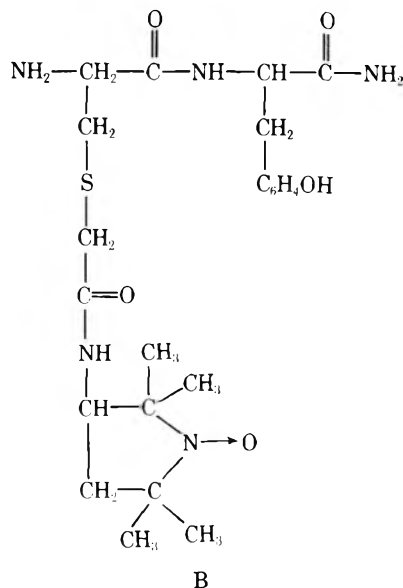
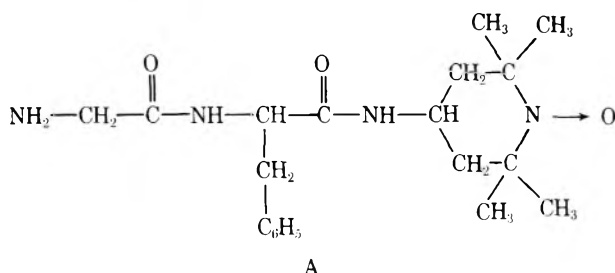
Publication costs assisted by the National Institutes of Health

The binding of two nitroxide spin-labeled peptides to the protein neurophysin was studied by electron spin resonance. The spin-labeled peptides were shown to bind to the hormone-binding site of neurophysin with affinities in general accord with those found for similar unlabeled peptides by other methods, but evidence for direct participation of at least one of the spin labels in binding was also obtained. Additionally, neurophysin was covalently spin labeled with a nitroxide. Comparison of the ESR spectrum of the covalently bound nitroxide with that of one of the spin-labeled peptide-protein complexes suggests that the peptide is held more rigidly on the protein than is the covalent label.

Introduction

The noncovalent interaction of the protein neurophysin (NP) with its physiological ligands oxytocin and vasopressin has been investigated by several methods.^{2a} With the aim of obtaining additional information about residues on the protein involved in binding, we have prepared nitroxide spin-labeled analogues of peptides known to bind noncovalently to the hormone-binding site of NP and have additionally prepared a covalently spin-labeled analogue of bovine NP-I.

NP-I was covalently labeled at its single histidine residue. The two nitroxide spin-labeled peptides that have been synthesized are glycyl-L-phenylalanyl-4-(2,2,6,6-tetramethylpiperidiny-1-oxy) (A) and S-4-(2,2,5,5-tetramethylpyrrolidinyl-1-oxy)-L-cysteinyl-L-tyrosine amide (B). Both A and B



retain the principal peptide features necessary for interaction, an α -amino in position 1 and an aromatic residue in position 2^{2a} but, based on previous studies of neurophysin-peptide

interaction, A can be expected to bind more weakly than B because of its shorter side chain at residue 1. These peptides have been synthesized most specifically for use in NMR studies, but we report here the results of ESR studies which indicate that they bind to the hormone-binding site of NP. Additionally, the ESR spectrum of the covalently bound spin label is compared with that of the spin-labeled peptide-protein complex.

Experimental Section

Peptide A was prepared by coupling^{2b,3} the 1-hydroxy-benzotriazole ester of glycyl-L-phenylalanine with 4-amino-2,2,6,6-tetramethylpiperidine (Aldrich) followed by oxidation to the nitroxide with H₂O₂.⁴ Peptide B was prepared by treating L-cysteinyl-L-tyrosine amide with 3-(2-iodoacetamido)-2,2,5,5-tetramethylpyrrolidinyl-1-oxy (Syva). Peptides were isolated from smaller reactants by chromatography on Sephadex G-10 with 0.1 M acetic acid followed by lyophilization. Purity of the preparation was assessed at greater than 90% by thin layer silica gel chromatography in butanol:acetic acid:water, 9:1:2.5, v/v/v. Neurophysin I was prepared according to the method of Breslow et al.⁵ Spin-labeled neurophysin I was prepared by treating the protein at pH 7 with a 60-fold molar excess of 4-(2-iodoacetamido)-2,2,6,6-tetramethylpiperidinyl-1-oxy (Syva) at room temperature in the dark for 8 days. The reacted protein was isolated from the reactants by chromatography on Sephadex G-25 with 0.1 M acetic acid and lyophilized.⁵ After acid hydrolysis of the labeled protein, amino acid analysis showed the loss of only the single histidine residue. Circular dichroism assays^{2a} indicated that the modified protein retained the ability to bind peptides.

Electron spin resonance measurements were performed on a Varian Model E-9 spectrometer in cylindrical quartz sample cells of inner diameter 1.2 mm and outer diameter 5 mm (Wilma Glass).⁶ Most spectra were recorded at a modulation amplitude of 0.2 G with a time constant of 0.3 s and a scan time of 8 min.

Electron spin resonance binding studies were performed at various concentrations of labeled peptide and a constant concentration of NP-I in 0.16 M KCl, 1 × 10⁻³ M EDTA, pH 6.2 at 23 °C. The fraction of spin-labeled peptide not bound was determined⁴ as the ratio of the height of the resonance signal when the solution was at pH 6.2 to the height of the signal when the solution was at 1.5 < pH < 2.7. In agreement with the known^{2a} pH dependence of peptide binding to NP-I, control studies indicate that binding is negligible at these acid pH values relative to that at pH 6.2; i.e., spin label signal amplitudes at pH 3 in the presence of protein are the same as at pH 6.2 in the absence of protein. Other experiments demonstrated that, during the binding study, the free-radical concentration was not reduced at the acid pH. As recommended by Weiner,⁴ experiments were conducted such that the height of the resonance signal at pH 6.2 in the presence of protein was ≥80% of that at acid pH; under these conditions, the decrease in signal height when protein is added can be treated as a linear function of the extent of binding.⁴ Additionally, we have calculated, from the spectra of the bound species, that assumptions used in the binding calculations which neglect the contribution of the bound species to the ESR spectra are valid.

Results and Discussion

Figure 1 shows the ESR spectrum of B at pH 6.2 in the absence and presence of NP-I. The large decrease in peak height when NP-I is added (note the difference in gain in the two

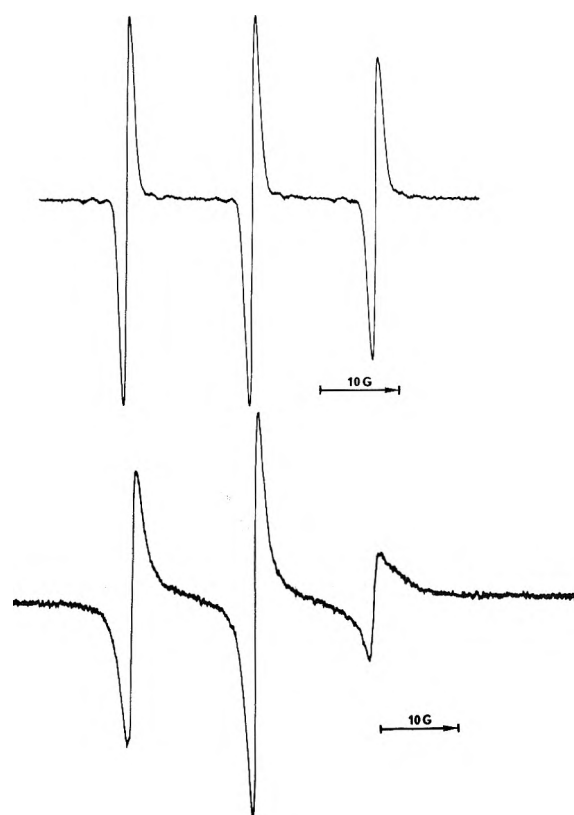


Figure 1. Electron spin resonance spectra of peptide B. The upper curve shows the spectrum of 0.5 mM peptide B in 0.16 M KCl, pH 6.2; the lower curve shows the spectrum of the same concentration of peptide B with 4.7 mM NP-I in 0.16 M KCl, 10⁻³ M EDTA, pH 6.2. The instrument gain for the upper curve was 2.5 × 10³, and 8 × 10³ for the lower curve.

spectra) permits the binding constant of B to be obtained using the method of Weiner.⁴ Accordingly, binding isotherms were constructed at a constant protein concentration and varying concentrations of B as described above. A double-reciprocal plot⁷ of the binding of B to NP-I is shown in Figure 2. Least-squares analysis of the data gives 0.91 binding sites per mole NP-I with a binding constant, $K_B^0 = 2.3 \times 10^3 \text{ M}^{-1}$. In the presence of a constant free concentration of the peptide L-phenylalanyl-L-tyrosine amide (Phe-Tyr NH₂) which is known^{2a} to bind to the hormone-binding site of NP-I, binding of B is reduced (Figure 2). Phe-Tyr NH₂ has been shown independently, using gel-filtration chromatography,⁸ to bind to a single site on NP-I at pH 6.2 with the binding constant $K_{\text{Phe-Tyr NH}_2}^0 = 7.2 \times 10^3 \text{ M}^{-1}$ at 25 °C. Using this value, the dashed line in Figure 2 represents the *expected* binding of B in the presence of Phe-Tyr NH₂, assuming strict competition between the two peptides, calculated from the equation:

$$K'_B = \frac{K_B^0}{1 + K_{\text{Phe-Tyr NH}_2}^0(\text{Phe-Tyr NH}_2)}$$

where K'_B is the apparent binding constant of B in the presence of the concentration of Phe-Tyr NH₂ used. Observed and calculated binding in the presence of Phe-Tyr NH₂ are in reasonable agreement. Alternatively, a value for $K_{\text{Phe-Tyr NH}_2}^0$ can be derived⁹ from the binding data in Figure 2, again assuming competition between the two peptides. The derived value for $K_{\text{Phe-Tyr NH}_2}^0$, 9.9×10^3 , is within experimental error (±20%) of the value obtained by gel filtration. These results indicate that B and Phe-Tyr NH₂ are competitors and can be interpreted with high probability as indicating that the two bind to the same site. We have also demonstrated indepen-

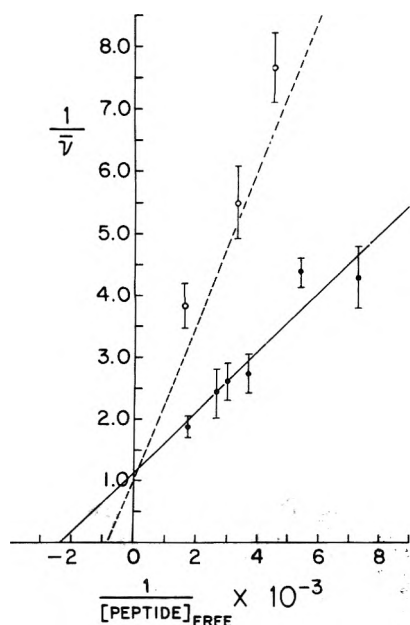


Figure 2. Double-reciprocal plot of the electron spin resonance binding data for peptide B. $\bar{\nu}$ = moles spin label bound per mole of protein, where 1 mol of NP-I = 9560 g. NP-I concentration was 0.12 mM. The total concentration of peptide B varied from 0.19 to 0.63 mM. Closed circles represent data obtained in the absence of the competitor, Phe-Tyr NH₂; the solid line is the least-squares analysis of these data. Open circles represent data obtained in the presence of 0.35 mM total Phe-Tyr NH₂. The dashed line is the theoretical binding of spin label calculated as indicated in the text and assuming that the free concentration of Phe-Tyr NH₂ is equal to the total concentration of Phe-Tyr NH₂; calculations indicate that less than 6% of the total Phe-Tyr NH₂ concentration is removed by binding to NP-I. Each data point is an average of results obtained from each of three nitroxide ESR lines at a single peptide concentration; the vertical line at each point represents the average of the deviations from the mean.

dently that B perturbs the circular dichroism spectrum of mononitrated NP-I in the manner characteristic^{2a} of peptides that bind to the hormone binding site.

Figure 3 shows the ESR spectrum of A alone and in the presence of NP-I; as above, the spectra indicate binding. The results of binding studies of A to NP-I are shown in Figure 4. A least-squares fit of the data gives 0.83 sites per mole with a binding constant $K^0_A = 2.7 \times 10^2 \text{ M}^{-1}$. In the presence of a constant total concentration of Phe-Tyr NH₂, A is displaced from NP-I, again strongly suggesting that A binds to the NP-I hormone-binding site. A value for $K^0_{\text{Phe-Tyr NH}_2}$ can be derived from the binding data, assuming that the two peptides are competitive, although in this instance corrections must be made for the fact that the free concentration of Phe-Tyr NH₂ was not constant over the course of the binding isotherm. The calculated value, 9.1×10^3 , is in very good agreement with that calculated from the competition data for peptide B and within experimental error of that obtained by gel filtration, supporting the concept that binding of A and of Phe-Tyr NH₂ are competitive. Additionally, as with B, we have independently determined that A perturbs mononitrated NP-I in a manner^{2a} indicative of binding to the active site.

It is of interest to compare the binding constant of A and B with the binding constants of closely related unlabeled peptides. The value of $2.7 \times 10^2 \text{ M}^{-1}$ for A can be compared with values of 5.3×10^1 and $2.5 \times 10^2 \text{ M}^{-1}$ for the binding of glycyl-L-tyrosine amide (Gly-Tyr NH₂) and glycyl-L-tyrosyl-L-phenylalanine amide (Gly-Tyr-Phe NH₂), respectively.¹⁰ The difference in binding between the latter two peptides

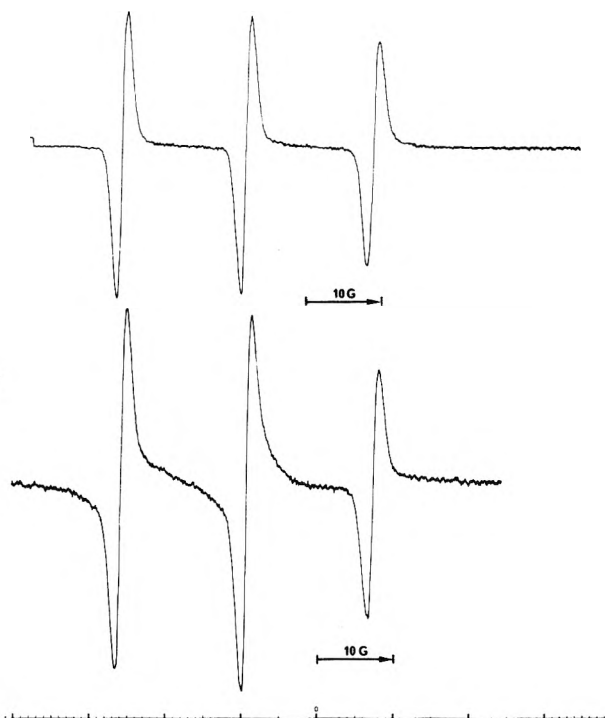


Figure 3. Electron spin resonance spectra of peptide A. The upper curve shows the spectrum of 0.35 mM peptide A in 0.16 M KCl, pH 6.2; the lower curve shows the spectrum of the same concentration of peptide A with 4.7 mM NP-I in 0.16 M KCl, 10^{-3} M EDTA, pH 6.2. The instrument gain for the upper curve was 2.5×10^3 , and 8×10^3 for the lower curve.

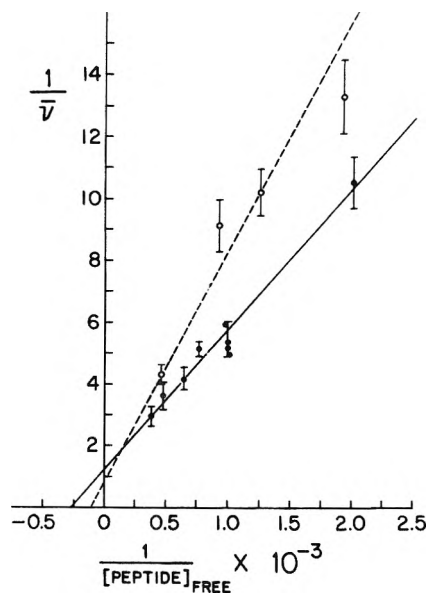


Figure 4. Double-reciprocal plot of the electron spin resonance binding data for peptide A. NP-I concentration was 0.93 mM; the total concentration of A varied from 0.59 to 3.0 mM. Closed circles represent data obtained in the absence of Phe-Tyr NH₂; the solid line is the least-squares analysis of the data. Open circles are data obtained in the presence of 0.5 mM Phe-Tyr NH₂; the dashed line delineates the data obtained in the presence of Phe-Tyr NH₂ but has no theoretical significance since the concentration of free Phe-Tyr NH₂ can be calculated to vary with the spin label concentration. For other details, see Figure 2.

is attributable to the apolar phenylalanine residue in position 3 of the Gly-Tyr-Phe NH₂. The similarity in binding between A and Gly-Tyr-Phe NH₂, when considered together with the fact that substitution of Phe for Tyr in position 2 is known to

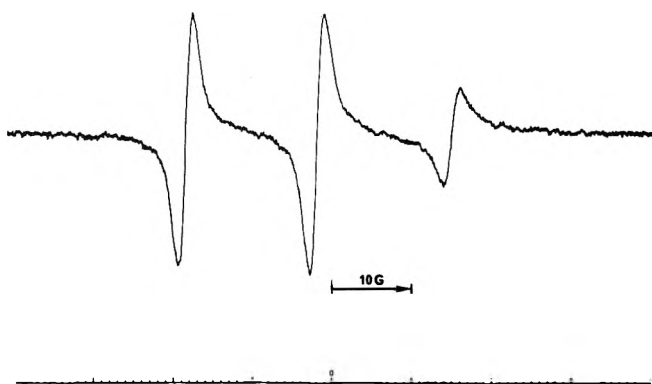


Figure 5. Electron spin resonance spectrum of 0.93 mM spin-labeled NP-I in 0.16 M KCl, 5×10^{-3} M EDTA, pH 6.2; the instrument gain was 8×10^3 .

have no effect on binding,^{2a} indicates that the tetramethylpiperidinyl-1-oxy group binds to a site on the protein normally occupied by residue 3 of the hormones and is in accord with the apparently low specificity of this site.^{2a} The binding constant $2.3 \times 10^3 \text{ M}^{-1}$ for B is best compared with a binding constant of $5.1 \times 10^3 \text{ M}^{-1}$ for *S*-methyl-L-cysteinyl-L-tyrosyl-L-phenylalanine amide corrected downward for the loss of position 3^{2a} to $1.3 \times 10^3 \text{ M}^{-1}$ or to the value of $1.7 \times 10^3 \text{ M}^{-1}$ for L-methionyl-L-tyrosine amide. The fact that B binds somewhat more strongly than these peptides suggests that the pyrrolidinoyl in position 1 may participate weakly in binding.

The ESR spectrum of bound B (Figure 1) also indicates relatively restricted motion of the pyrrolidinyl-1-oxy of B in the bound state both when compared with the spectrum of the unbound label and when compared with that of the covalently labeled protein. Figure 5 shows the spectrum of the covalently labeled protein. From the near equality in height of the center and low-field peaks and the relatively slight broadening of the high field peaks the correlation time for the spin label in Figure 5 can be approximated by known relationships¹¹ as $\sim 10^{-9}$ s. This value can be compared with rotational correlation times of $\sim 10^{-8}$ s found for other proteins the size of NP-I¹² and indicates that the histidine-bound spin label has mobility relative to the rest of the protein. The ESR spectrum of B in the presence of NP-I (Figure 1) represents 90% saturation with NP-I (as calculated from K^0_B). Measurable inequality exists between the center and low-field peaks and, relative to the other lines, that at high field is more broadened in Figure 1 than in Figure 5. Since the spectrum in Figure 1 in the presence of NP-I contains a 10% contribution from free spin label (the peak heights of which are a factor of 4–10 higher than those of the bound state), the broadening of the high-field line in the fully bound state is probably significantly greater than that seen in Figure 1. From relationships between nitroxide ESR spectra and correlation time,¹¹ assuming isotropic motion of the label, the results indicate that the ni-

troxide of B is more immobilized in the peptide-protein complex than is the nitroxide bound to the protein histidine.

We have observed no significant effect of binding peptides on the ESR spectrum of the spin-labeled NP-I. This observation, the relatively greater mobility of the histidine spin label, and the fact that the histidine is found in a region of the molecule that shows significant variability when different neurophysins are compared¹³ are in accord with the idea that the histidine is not involved in important functional interactions. On the other hand, immobilization of the spin label in B and its possible contribution to the binding constant have no necessary parallel in previous data. It is possible that the immobilization of the nitroxide of B results solely from its close attachment to the cysteinyl sulfur which is known to participate in binding.^{2a} Alternatively, some of the immobilization may arise from direct interactions between the pyrrolidinyl-1-oxy and the protein, perhaps at a site normally occupied by a hormone residue that is not represented in the smaller peptides described here. Molecular models interestingly suggest that the pyrrolidinyl-1-oxy on position 1 can orient itself spatially to mimic position 5 of the hormones.

Acknowledgments. This work was supported by Grant No. GM-17528 from the National Institutes of Health, and by a predoctoral fellowship to S.L.L. from a National Institutes of Health Public Health Service training grant. The authors wish to express their appreciation to Drs. P. Aisen and F. Landsberger for helpful discussions, and to the Department of Chemistry, Columbia University for use of their ESR spectrometer.

References and Notes

- (1) (a) Abstracted in part from the Ph.D. Thesis of S. L. Lundt, Cornell University Medical College, New York, N.Y. For previous papers in this series, see: (i) R. C. Lord, *J. Phys. Chem.*, **11**, 173 (1907); (ii) R. C. Lord, Jr., and D. H. Andrews, *ibid.*, **41**, 149 (1937). (b) Daughter of Professor Richard C. Lord; dedicated to my father on this very special occasion.
- (2) (a) E. Breslow, *Adv. Enzymol.*, **40**, 271 (1974); (b) W. König and R. Geiger, *Chem. Ber.*, **103**, 788 (1970).
- (3) S. L. Lundt, R. Stephani, and E. Breslow, to be submitted for publication.
- (4) H. Weiner, *Biochemistry*, **8**, 526 (1969).
- (5) E. Breslow, H. L. Aanning, L. Abrash, and M. Schmir, *J. Biol. Chem.*, **246**, 5179 (1971).
- (6) Specifications for sample cells were obtained from Dr. P. Aisen.
- (7) I. M. Klotz, "Protein Interactions", in "The Proteins", Vol. 1B, H. Neurath and K. Bailey, Ed., Academic Press, New York, N.Y., 1953, Chapter 8.
- (8) S. L. Lundt and E. Breslow, unpublished observations. NOTE ADDED IN PROOF: Recent gel-filtration studies give a binding constant for Phe-Tyr NH₂ closer to $1 \times 10^4 \text{ M}^{-1}$.
- (9) S. I. Rubinow, "Introduction to Mathematical Biology", Wiley, New York, N.Y., 1975, Chapter 2.
- (10) Binding constants for unlabeled peptides were determined by circular dichroism measurements^{2a} of binding of mononitrated bovine NP-II; comparative studies of binding of unlabeled peptides to native NP-I relative to nitrated NP-II indicate that both proteins have almost identical binding affinities.
- (11) T. J. Stone, T. Buckman, P. L. Nordio, and H. M. McConnell, *Proc. Natl. Acad. Sci. U.S.A.*, **54**, 1010, (1965).
- (12) R. W. Wien, J. D. Morrisett, and H. M. McConnell, *Biochemistry*, **11**, 3707 (1972).
- (13) W. G. North, R. Walter, D. H. Schlesinger, E. Breslow, and J. D. Capra, *Ann. N.Y. Acad. Sci.*, **248**, 408 (1975).

Deuterium Exchange in Pyridine Dinucleotide Coenzymes. Raman Spectroscopic Evidence for a Modified Amide Charge Distribution in β -Dihydronicotinamide Adenine Dinucleotide^{‡1}

G. Forrest¹⁵

Spectroscopy Laboratory and Department of Chemistry, Massachusetts Institute of Technology, Cambridge, Massachusetts 02139
(Received December 15, 1975)

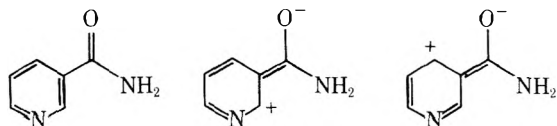
Publication costs assisted by the National Science Foundation

A new interpretation is proposed for the observed shifts of Raman amide vibrations in certain pyridine dinucleotide coenzymes. Differences in electron delocalization are proposed as the basic causes of the frequency shifts; comparison is made with previous interpretations in terms of solvent hydrogen-bonding effects. Consequences of the revised interpretation are explored briefly.

Analysis of Raman amide vibrations has played an important role in elucidation of protein conformations in solution. However, in cases where extended electron delocalization is possible, inferences from the normal coordinate analyses of formamide,² acetamide,³ and *N*-methylacetamide⁴ must be made with caution. A case in point is a recent report by Patrick, Wilson, and Leroi⁵ regarding the electronic structure of the amide residue in pyridine dinucleotide coenzymes. Considering 1-methyl-3-pyridinecarboxamide as a model for β -nicotinamide adenine dinucleotide (NAD), these investigators observed a significant solvent dependence of the Raman amide carbonyl frequency in D₂O (1667 cm⁻¹) and dimethyl sulfoxide (1696 cm⁻¹). The corresponding amide carbonyl frequency for NAD was 1667 cm⁻¹ in D₂O. Similar solvent effects were not observed for 3-pyridinecarboxaldehyde, 3-acetylpyridine, their 1-methyl derivatives, or β -dihydronicotinamide adenine dinucleotide (NADH).

The lower amide carbonyl frequencies for 1-methyl-3-pyridinecarboxamide and NAD in D₂O relative to dimethyl sulfoxide were attributed to solvent hydrogen bonding. However, Raman spectra of 1-methyl-3-pyridinecarboxamide and NAD in H₂O do not support this conclusion. Consideration of the normal vibrations comprising the amide carbonyl vibration and electron delocalization in NAD and NADH provides an explanation for the observed solvent effect and reaffirms that significant changes in the amide charge distribution occur on reduction of NAD to NADH.

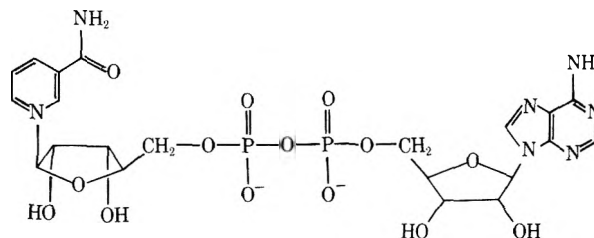
Inductive effects associated with β -substituted pyridine rings⁶ such as 3-pyridinecarboxamide are negated by qua-



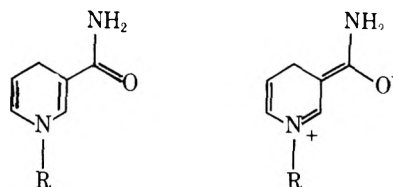
ternization of the pyridine nitrogen. For 1-methyl-3-pyridinecarboxamide the carbonyl frequency in dimethyl sulfoxide increases by 10 cm⁻¹ relative to 3-pyridinecarboxamide. The quaternization of the pyridine ring nitrogen that exists in

[‡] Editor's note: The authors of ref 5 suggest that this interpretation may be responsible for a portion of the observed carbonyl frequency shift, but that it does not satisfactorily account for all of the data. Both interpretations indicate that amide group resonance may be important in the interactions of these coenzymes.

NAD is responsible for the relatively high value of the carbonyl frequency in dimethyl sulfoxide (1697 cm⁻¹).



For NADH, however, resonance delocalization of electrons is possible.



Consistent with this electron delocalization, x-ray crystallographic studies of models for pyridine dinucleotide coenzymes suggest a significant shortening of the amide C-C bond on reduction of NAD to NADH.^{7,8}

As expected from the extended conjugation, the Raman carbonyl vibration for NADH (1688 cm⁻¹) is much more intense than that of either NAD (1698 cm⁻¹) or 3-pyridinecarboxamide in 0.25 M neutral aqueous solution. The frequencies in D₂O are confirmed to be 1689 cm⁻¹ for NADH and 1667 cm⁻¹ for NAD as reported.⁵ Since the amide carbonyl frequencies observed in dimethyl sulfoxide (1697 cm⁻¹ for NAD and 1696 cm⁻¹ for 1-methyl-3-pyridinecarboxamide) are similar to those observed in H₂O (1698 and 1697 cm⁻¹, respectively), it is unlikely the changes observed for NAD and 1-methyl-3-pyridinecarboxamide in D₂O result from hydrogen bonding.

Normal coordinate calculations for formamide² and acetamide³ indicate that the decrease in carbonyl frequency associated with amide deuteration is consistent with a decrease in coupling between the C=O stretching and ND₂ bending vibrations as compared to that between C=O stretching and NH₂ bending. The absence of a solvent isotope shift for NADH suggests either that exchange has not occurred or that

coupling is absent in NADH in both H₂O and D₂O. Raman spectra of NADH reveal a shift in a polarized 1085-cm⁻¹ vibration in H₂O to 911 cm⁻¹ in D₂O. A similar shift in the formamide frequency assigned to an NH₂ rocking vibration occurs from 1098 cm⁻¹ in H₂O to 911 cm⁻¹ in D₂O. No such changes are observed with adenosine 5'-diphosphate or adenosine 5'-diphosphoribose, which confirms that the shift arises from the nicotinamide moiety. In addition, proton magnetic resonance spectra of 1-methyldihydronicotinamide in D₂O support the conclusion that exchange of the amide protons of NADH occurs in D₂O.⁹

Because of the increased electron delocalization in NADH compared to NAD one might expect the carbonyl frequency of NADH in D₂O to be less than that of NAD in D₂O when the complications arising from NH₂ coupling are absent. In fact the opposite is observed, which suggests a decrease in the NADH amide resonance between the forms



One consequence is a decreased electron density at the amide oxygen and an increased electron density at the amide nitrogen for NADH relative to NAD. As a result decreased amide hydrogen bonding and electrostatic interactions may contribute to the decreased affinity of NADH for glyceraldehyde-3-phosphate dehydrogenase compared to NAD.¹⁰ X-ray crystallographic studies indicate NAD is bound to glyceraldehyde-3-phosphate dehydrogenase in an extended conformation and suggest carbonyl hydrogen bonding to an asparagine residue of the enzyme.¹¹

The absence of coupling in H₂O and the increased carbonyl frequency in D₂O for NADH are consequences of increased electron delocalization in the dihydropyridine ring. The similar carbonyl frequencies and solvent isotope shifts for 1-methyl-3-pyridinecarboxamide, β-nicotinamide mononucleotide, and NAD (Table I) indicate the amide properties of NAD are determined solely by the nicotinamide ring. Similarly, β-dihydronicotinamide mononucleotide and NADH have identical carbonyl frequencies which are insensitive to amide hydrogen exchange in D₂O. Since NAD and NADH may exist in solution with the adenine and nicotinamide rings stacked,¹²⁻¹⁴ it is significant that the carbonyl frequencies are independent of temperature.⁵ In solvents promoting unstacking (70% methanol, 30% H₂O or 70% methanol-*d*₁, 30% D₂O) the Raman carbonyl frequency of NADH is identical with the frequencies in dimethyl sulfoxide, H₂O, and D₂O. Insensitivity of the carbonyl frequencies to concentration over the range 0.05–0.5 M suggests minimal intermolecular stacking effects on the carbonyl frequency.

The conclusions reached by Patrick et al.⁵ regarding the

TABLE I: Raman Carbonyl Frequencies (cm⁻¹) of 0.25 M Solutions in Dimethyl Sulfoxide, H₂O, and D₂O^a

Compound	Me ₂ SO	H ₂ O	D ₂ O
3-Pyridinecarboxamide	(1686)	1679	(1637)
1-Methyl-3-pyridinecarboxamide	(1696)	1697	(1667)
NAD	1697	1698	(1667)
β-Nicotinamide mononucleotide	1699	1698	1670
NADH	(1689)	(1688)	(1689)
β-Dihydronicotinamide mononucleotide	1688	1689	(1689)
Formamide	1699	1692	1658

^a The results of Patrick et al.⁵ are indicated in parentheses.

significant contribution of amide resonance to the electronic structure of NAD are correct; however, the basis for the decreased amide conjugation in NADH is the increased electron delocalization in the dihydronicotinamide ring and not related to solvent hydrogen bonding as proposed by Patrick et al. This leads to the significant prediction that the amide should be sensitive to interactions of the dihydronicotinamide ring with the enzyme surface to which it is exposed. An analogous interaction between NAD and a cysteine thiol of glyceraldehyde-3-phosphate dehydrogenase has been proposed as the basis for the 360-nm Racker band absorption associated with NAD binding.¹¹

Acknowledgments. Provocative discussions with Professor Richard C. Lord regarding the interpretation of amide vibrations and the biological consequences of amide geometries are gratefully acknowledged. This research was sponsored by the National Science Foundation under Grant No. CHE 75-17040.

References and Notes

- (1) Dedicated to Professor Richard C. Lord on the occasion of his formal retirement from M.I.T.
- (2) I. Suzuki, *Bull. Chem. Soc. Jpn.*, **33**, 1359 (1960).
- (3) I. Suzuki, *Bull. Chem. Soc. Jpn.*, **35**, 1279 (1962).
- (4) T. Miyazawa, T. Shimanouchi, and S. Mizushima, *J. Chem. Phys.*, **29**, 611 (1958).
- (5) D. M. Patrick, J. E. Wilson, and G. E. Leroi, *Biochemistry*, **13**, 2813 (1974).
- (6) G. W. Wheland and L. Pauling, *J. Am. Chem. Soc.*, **57**, 2086 (1935).
- (7) I. L. Karle, *Acta Crystallogr.*, **14**, 497 (1961).
- (8) P. L. Johnson, C. A. Maier, and I. C. Paul, *J. Am. Chem. Soc.*, **95**, 5370 (1973).
- (9) R. F. Hutton and F. H. Westheimer, *Tetrahedron*, **3**, 73 (1958).
- (10) G. von Ellenreider, K. Kirschner, and I. Schuster, *Eur. J. Biochem.*, **26**, 220 (1974).
- (11) M. Buehner, G. C. Ford, D. Moras, K. W. Olsen, and M. G. Rossman, *J. Mol. Biol.*, **90**, 25 (1974).
- (12) G. Weber, *Nature (London)*, **180**, 1409 (1957).
- (13) D. W. Miles and D. W. Urry, *J. Biol. Chem.*, **243**, 4181 (1968).
- (14) M. Blumenstein and M. A. Raftery, *Biochemistry*, **11**, 1643 (1972).
- (15) Ph.D. degree with Richard C. Lord at M.I.T. expected 1976.

Vibrational Spectra and Normal Coordinate Analysis of Ethyl Cyanides

C. J. Wurrey,¹

Department of Chemistry, University of Missouri—Kansas City, Kansas City, Missouri 64110

W. E. Bucy,² and J. R. Durig¹

Department of Chemistry, University of South Carolina, Columbia, South Carolina 29208 (Received August 8, 1975)

Publication costs assisted by the University of South Carolina

The infrared spectra of $\text{CH}_3\text{CH}_2\text{CN}$, $\text{CD}_3\text{CH}_2\text{CN}$, $\text{CH}_3\text{CD}_2\text{CN}$, $\text{CD}_3\text{CD}_2\text{CN}$, and $\text{CH}_3\text{CH}_2^{13}\text{CN}$ have been observed in the vapor phase from 4000 to 200 cm^{-1} . Both the vapor and solid phase spectra of the $-d_0$ and $-d_5$ molecules were observed in the infrared region from 4000 to 150 cm^{-1} . The Raman spectra of all five isotopes were observed in the vapor, liquid, and solid phases from 4000 to 50 cm^{-1} , with the exception of the solid phase of the ^{13}CN isotope. An assignment of the 21 fundamental vibrations has been proposed, based on depolarization values, band contours, and group-frequency correlation. A normal coordinate calculation was also carried out in which 19 force constants were used to fit the observed frequencies to within 1.3%.

Introduction

Much research interest over the past several years has been centered on the vibrational spectra and, in particular, the normal coordinate analysis of the ethyl halides. Using the frequencies determined by Miller and Kiviat³ for ethyl chloride and its deuterated derivatives, Dempster and Zerbi⁴ performed a normal coordinate analysis and proposed re-assignments for several modes. Similarly, ethyl bromide and its deuterated derivatives were investigated and a normal coordinate analysis was also carried out.⁵ More recently, Crowder⁶ and Durig et al.⁷ have studied the spectra of several ethyl iodides. Crowder used a 28-parameter force field to fit four isotopic species while Durig et al. used 19 force constants to fit three isotopic ethyl iodides.

Since the cyanide functionality can be thought of as a pseudo halide it was thought to be of interest to investigate the spectra of ethyl cyanide and a number of its isotopically substituted derivatives in order to help confirm assignments in the other ethyl halides.

Duncan and Janz⁸ performed the first complete vibrational analysis of ethyl cyanide and performed a normal coordinate analysis for the skeletal modes only. Yamadera and Krimm⁹ used a 29-parameter force field to fit the 21 observed frequencies of ethyl cyanide. Klaboe and Grundnes¹⁰ also proposed an assignment for ethyl cyanide; however, like Yamadera and Krimm they assign the torsion to an accidentally depolarized Raman peak at 226 cm^{-1} , which is much too intense to be assigned to a methyl torsion. This also led to a misassignment of the a' in-plane CCN bending mode in both cases. Heretofore, no vibrational work has been done on any isotopically substituted ethyl cyanides. In order to help corroborate the assignments and make a normal coordinate analysis meaningful in the case of ethyl cyanide's low symmetry (C_s), isotopic data are virtually essential. Isotopic derivatives of ethyl cyanide have, however, been investigated by microwave spectroscopy^{11,12} where a Coriolis interaction between the torsion and the CCN bending mode was found to exist in $\text{CH}_3\text{CH}_2^{13}\text{CN}$ ¹³ but not in $\text{CD}_3\text{CD}_2\text{CN}$.¹⁴

Thus, in order to confirm the vibrational assignment of ethyl cyanide, especially in the low-frequency region where discrepancies exist, a vibrational study and normal coordinate

analysis of five isotopic species of ethyl cyanide was undertaken.

Experimental Section

Ethyl- d_0 cyanide was obtained from Columbia Organic Chemicals Co. and was purified by vapor phase chromatography. Merck Sharp and Dohme of Canada supplied the ethyl- d_5 cyanide which was used without further purification. Stohler Isotope Chemicals Co. supplied the ethyl-1,1- d_2 iodide, the ethyl-2,2,2- d_3 iodide, and the K^{13}CN used in the preparation of the isotopically substituted ethyl cyanide species. The ethyl- d_3 cyanide was prepared by refluxing a dimethyl sulfoxide solution of ethyl- d_3 iodide with KCN for 8 h. Ethyl cyanide- $^{13}\text{C}(N)$ was prepared analogously using ethyl- d_0 iodide and K^{13}CN . Fractions boiling at 82 and 94 °C were collected separately and purified by vapor-phase chromatography using a 15% Carbowax 20 M on 60/80 Chromosorb W column heated to 105 °C. The higher boiling fraction contained almost pure ethyl cyanide while the lower boiling fraction contained a significant amount of ethyl iodide. In preparing the ethyl- d_2 cyanide by this procedure, solvent exchange with the deuterated positions occurred, yielding an equal mixture of ethyl- d_0 , $-d_1$, and $-d_2$ cyanide. Therefore the preparation of ethyl- d_2 cyanide was done using $\text{Me}_2\text{SO}-d_6$, supplied by CEA of France, as the solvent. The purification of the $-d_2$ compound was also done by vapor phase chromatography. The isotopic purity was checked by observing the microwave spectrum using a Hewlett-Packard Model 8460A MRR spectrometer in the frequency region 26.5–40.0 GHz. The observed spectrum showed the sample to be at least 95% isotopically pure. The pure samples were stored over activated molecular sieves to remove any final traces of water.

The Raman spectra were recorded on a Cary Model 82 spectrophotometer equipped with a Coherent Radiation Model 53 G argon ion laser source using the 5145-Å line for excitation. The instrument was calibrated with emission lines from a neon lamp over the spectral range 0–4000 cm^{-1} . Generally 1.5–2.5 W of power were used for gases and about 1 W for solids and liquids. Raman spectra of the vapor were obtained using the Cary multipass accessory and a standard Cary multipass cell which was adapted with a PTFE greaseless stopcock and a side-arm reservoir. The windows of the cell and

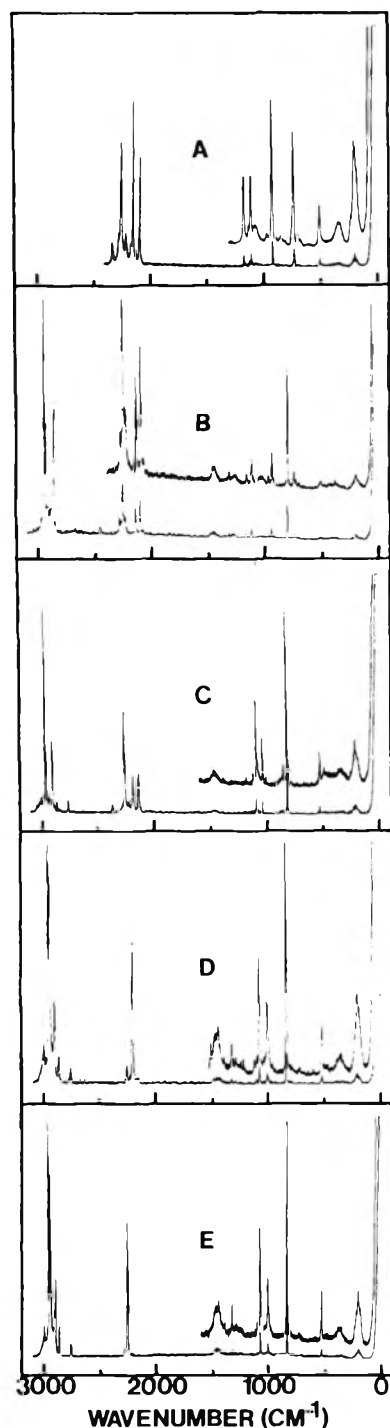


Figure 1. Raman spectra of gaseous ethyl cyanides. Spectra were recorded at 40–50 °C with 5-cm⁻¹ spectral band width: (A) CD₃CD₂CN, (B) CD₃CH₂CN, (C) CH₃CD₂CN, (D) CH₃CH₂¹³CN, and (E) CH₃CH₂CN.

signments are rather straightforward, only a summary of the more interesting or difficult points will be presented. Assignment of the normal modes for the ¹³C(N) molecule is almost identical with that of the -d₀ assignment.

C-H and C-D Stretching Regions. By combining both infrared and Raman data of the gas phase, it was possible to assign the five CH stretching vibrations in four isotopic species. The totally deuterated species added confidence to our assignment of the CH region by showing similar features in the CD region. Our assignment is consistent with the

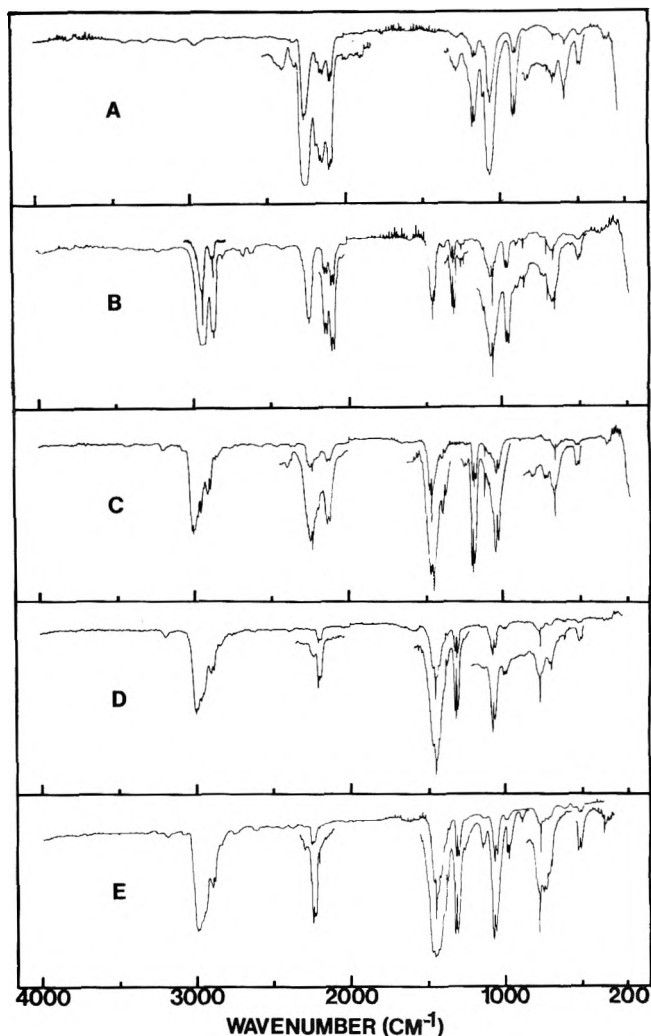


Figure 2. Infrared spectra of gaseous ethyl cyanides. Spectra were recorded at room temperature with cells of 20-cm and 1-m pathlengths: (A) CD₃CD₂CN, (B) CD₃CH₂CN, (C) CH₃CD₂CN, (D) CH₃CH₂¹³CN, and (E) CH₃CH₂CN.

argument presented by Durig et al. for several isotopic ethyl iodides⁷ and the assignment by Günthard et al. for several isotopic nitroethanes.¹⁸

In the -d₂ compound a strong A-type band centered at 3002 cm⁻¹ in the infrared spectrum with a weak Raman counterpart at 2999 cm⁻¹ with a high depolarization ratio, 0.7, is assigned as the doubly degenerate CH₃ antisymmetric stretch, ν_1 and ν_{14} , assuming local C_{3v} symmetry. The very strong Raman band at 2959 cm⁻¹ is assigned as the totally symmetric a' CH₃ stretch, ν_2 .

There is an additional strong polarized band at 2900 cm⁻¹ in the Raman spectrum with a B-type infrared counterpart centered at 2903 cm⁻¹. Fermi resonance between ν_2 and the first overtone of the CH₃ antisymmetric deformation, $2\nu_{16}$, always leads to a medium intensity band in both the infrared and Raman.¹⁹ This effect was observed in all of our spectra and we feel this assignment is correct.

A strong polarized Raman band at 2948 cm⁻¹ in the -d₃ compound is assigned as ν_3 , the CH₂ symmetric stretch. A broad region of strong intensity in the infrared spectrum is observed at about 2940 cm⁻¹ with the only noticeable feature being a C-type Q branch at 2936 cm⁻¹. Table III shows the assignment of this region as resulting from a binary combi-

nation. A rather weak shoulder at 2969 cm^{-1} in the infrared with a Raman counterpart, which is depolarized, at 2965 cm^{-1} is assigned as the CH_2 antisymmetric stretch, ν_{15} .

The CH stretching assignments of the ethyl- d_0 cyanide and ^{13}C N follow directly from the $-d_2$ and $-d_3$ assignments. The ν_{15} band is obscured by the R branch of ν_2 . However, in the solid phase a band of medium intensity is observed at 2973 and 2967 cm^{-1} in the infrared and Raman spectra, respectively.

The assignment of the CD region is complicated by presence of the CN stretch, ν_4 . However the frequency of this mode is rather insensitive to deuteration and is assigned between 2250 and 2259 cm^{-1} in all ^{12}C N species. A shift to 2207 cm^{-1} for the CN stretch is observed in the ^{13}C N molecule. The partially deuterated species provide the key to many of the assignments of the $-d_5$ compound. In the $-d_2$ compound two medium bands appear in both the infrared and Raman spectra in the 2100 – 2200-cm^{-1} region where ν_3 , the CD_2 symmetric stretch, should occur. Following the same arguments as presented by Durig et al.,⁷ the higher frequency band at 2184 cm^{-1} may be attributed to 2×1085 , in Fermi resonance with ν_3 which falls at 2133 cm^{-1} . A medium C-type Q branch is observed at 2237 cm^{-1} in the infrared spectrum, which is therefore assigned as ν_{15} , the CD_2 antisymmetric stretch.

In the $-d_3$ spectra two medium intensity bands are observed in both the infrared and Raman spectra at 2142 and 2099 cm^{-1} . Fermi resonance between $2\nu_{16}$ and ν_2 is postulated to explain their similar intensity and the abnormally large anharmonicity of ν_{16} . ν_2 is assigned as the strongly polarized Raman band at 2138 cm^{-1} whose infrared counterpart at 2142 cm^{-1} has an A-type band contour.

The assignment of ν_1 and ν_{14} in the totally deuterated and $-d_3$ species is complicated by the CN stretch. In the $-d_5$ compound a Q branch shoulder appears on the very strong and broad CN stretch. The intensity of this band in both the $-d_3$ and $-d_5$ compounds in comparison to the weak bands in both the $-d_0$ and $-d_2$ compounds leads us to the assignment of ν_1 and ν_{14} as almost degenerate with ν_4 in both the $-d_3$ and $-d_5$ molecules. Therefore the antisymmetric CD_3 stretches in the $-d_3$ and $-d_5$ molecules are assigned at 2254 cm^{-1} . A broad weak band about 2235 cm^{-1} in the Raman spectrum of gaseous ethyl- d_3 cyanide is assigned to the sum $1446 + 799\text{ cm}^{-1}$. There is no equivalent band in the $-d_0$ compound and there is no evidence of an infrared counterpart which was observed to be very strong in the $-d_0$ and $-d_2$ molecules. The assignment of the other CD modes in ethyl- d_5 cyanide follows directly from the $-d_3$ and $-d_2$ assignments.

CH_3 and CH_2 Deformation Region. The methyl deformations are well-established group frequencies,²⁰ which are demonstrated by our isotopic data. In the $-d_2$ molecule, a medium intensity A-type band occurred at 1470 cm^{-1} in the infrared spectrum, and is assigned as ν_6 , the CH_3 a' antisymmetric deformation. A sharp, strong C-type A branch at 1460 cm^{-1} is readily assigned to ν_{16} , the a'' antisymmetric CH_3 deformation whose Raman counterpart at 1459 cm^{-1} is depolarized. A weak B-type band centered at 1391 cm^{-1} in the infrared spectrum is assigned to ν_7 , the a' totally symmetric methyl deformation. In the $-d_3$ molecule a medium band in the Raman liquid spectrum at 1434 cm^{-1} and at 1448 cm^{-1} in the Raman spectrum of the gas phase is assigned to ν_5 , the CH_2 scissors. A B-type band centered at 1446 cm^{-1} was observed in the gas-phase infrared spectrum. This assignment is directly applicable to the $-d_0$ and ^{13}C N molecules. It should be noted that from the potential energy distribution among symmetry coordinates obtained from the normal coordinate analysis, ν_6 is calculated at 1456 cm^{-1} and ν_5 at 1475 cm^{-1} .

However, the calculations give very good agreement with the observed frequencies for ν_5 and ν_6 for the $-d_2$ and $-d_3$ molecules. Further discussion of this point will follow in the normal coordinate analysis.

CH_2 Motions. The assignment of the a' CH_2 wag, ν_8 , at 1313 and 1323 cm^{-1} in the $-d_3$ and $-d_0$, respectively, is unambiguous. A medium intensity A-type contour was observed in the infrared spectrum with weak Raman counterparts. The a'' CH_2 twist was observed at 1270 and 1258 cm^{-1} in the $-d_0$ and $-d_3$ compounds, respectively. Depolarized Raman bands and sharp C-type band contours made this assignment straightforward. C-type Q branches at 894 and 915 cm^{-1} in the $-d_2$ and $-d_5$, respectively, are assigned as ν_{17} , the CD_2 twist. The band at 915 cm^{-1} is almost degenerate with a B-type infrared band whose Raman counterpart is polarized. A band with a sharp Q branch in the infrared spectrum of the $-d_0$ molecule at 784 cm^{-1} , with a depolarized Raman counterpart in the liquid phase, is assigned as the a'' CH_2 rocking motion. This motion shifts to 665 and 594 cm^{-1} in the $-d_2$ and $-d_5$ molecules, respectively. A C-type Q branch at 861 cm^{-1} in the $-d_3$ molecule has been assigned as the CH_2 rock, apparently shifted from the $-d_0$ molecule. However, this is in good agreement with the calculated value of 896 cm^{-1} .

C–C Stretching and CH_3 Rocking Regions. The assignment of the spectral region from 800 to 1200 cm^{-1} is best described as a mixing region. Group frequencies in this region are generally not well defined for the ethyl fragment. The assignment of this region was done by comparing similar band types and consistent intensities between infrared and Raman data for all the isotopes.

In the $-d_2$ and $-d_5$ molecules medium A-type bands at 1183 and 1165 cm^{-1} , respectively, were calculated to be mainly ν_8 , the CD_2 wagging motions. Similar B-Type bands at 1113 and 1103 cm^{-1} in the infrared spectrum of the $-d_3$ and $-d_5$ species, respectively, were calculated to be mainly ν_9 , the ethyl C–C stretch. Polarized Raman bands were observed to support this assignment. A strongly polarized band at 1078 cm^{-1} in the $-d_0$ molecule with an B-type infrared counterpart was assigned to ν_9 . A similar band at 1085 cm^{-1} was observed in the $-d_2$ molecule. A polarized Raman band at 1121 cm^{-1} in the $-d_5$ molecule was calculated to be ν_7 , the CD_3 symmetric deformation. This is in good agreement with the 1113-cm^{-1} band of the $-d_3$ molecule, which is equally mixed between the CD_3 symmetric deformation and the carbon–carbon stretch of the ethyl group.

The a' antisymmetric CD_3 deformation, ν_6 , was observed as a very strong A-type band at 1061 cm^{-1} in the infrared spectrum of the $-d_5$ molecule and was calculated to be almost a pure mode. It is interesting that a strong C-type Q branch at 1058 and 1060 cm^{-1} in the $-d_5$ and $-d_3$ molecules, respectively, are almost degenerate with ν_6 . Local C_{3v} symmetry can be invoked to assign these bands as ν_{16} , the CD_3 a'' antisymmetric deformation. A Raman band at 1030 cm^{-1} in the $-d_3$ molecule had a depolarization ratio of about 0.73. This band was then assigned as ν_6 .

The a' CH_3 rocking mode and C–C(N) stretch are highly mixed modes and their assignment to a particular frequency is highly ambiguous. Strong, polarized Raman bands occurring near $820 \pm 20\text{ cm}^{-1}$ may be assigned as one of these fundamentals, most likely the C–C stretch. Infrared counterparts are very weak in the gas phase, but are of medium intensity in the solid phase. A weak A-type band in the infrared spectrum at 1008 cm^{-1} in the $-d_0$ molecule is assigned as the last a' fundamental expected in this region. Corresponding bands are observed in the other isotopes at $1000 \pm 40\text{ cm}^{-1}$ which

TABLE V: Product Rule Check of Assignments and Principal Moments of Inertia ($\text{amu } \text{Å}^2$)²

	Calcd	Obsd	Δ , %
CH ₃ CH ₂ ¹³ CN/CH ₃ CH ₂ CN	a' 0.9419	0.9404	-0.16
	a'' 0.9454	0.9813	3.80
CH ₃ CD ₂ CN/CH ₃ CH ₂ CN	a' 0.3736	0.3727	-0.26
	a'' 0.4094	0.4266	4.19
CD ₃ CH ₂ CN/CH ₃ CH ₂ CN	a' 0.1974	0.2092	6.00
	a'' 0.2994	0.3055	2.04
CD ₃ CD ₂ CN/CH ₃ CH ₂ CN	a' 0.0735	0.0736	0.19
	a'' 0.1206	0.1250	3.62
	<i>I</i> _a	<i>I</i> _b	<i>I</i> _c
CH ₃ CH ₂ CN	18.626	107.209	119.562
CH ₃ CH ₂ ¹³ CN	18.642	107.761	120.131
CH ₃ CD ₂ CN	23.451	109.838	123.911
CD ₃ CH ₂ CN	22.469	120.227	133.269
CD ₃ CD ₂ CN	27.632	122.468	137.568

^a Calculated from the structure presented in ref 11 which was also used in the normal coordinate analysis.

also have weak to medium intensity Raman bands. Further discussion of the remaining a' fundamentals will follow in the discussions about the Teller-Redlich product rule analysis and the normal coordinate analysis.

The CH₃ a'' rocking motion, ν_{18} , was observed as a medium intensity C-type Q branch at 1000 cm^{-1} in the infrared spectrum of the -*d*₀ molecule. Similar medium intensity bands were observed at 712 and 834 cm^{-1} in the infrared spectrum of the -*d*₃ and -*d*₅ molecules. A very weak shoulder at 1033 cm^{-1} in the infrared spectrum of the -*d*₂ gas was also assigned as ν_{18} .

Bending Vibrations and Torsions. The C-C-C bends, ν_{12} , were assigned to peaks at $520 \pm 20 \text{ cm}^{-1}$ in the various isotopes, in good agreement with group frequencies. Both ν_{13} and ν_{20} , the C-C-N bending modes, are weak to medium bands observed at 201 ± 10 and $355 \pm 17 \text{ cm}^{-1}$ in all isotopes. Both bands have high degrees of depolarization in the Raman effect, a fact characteristic of C-C \equiv N bending modes. However, consistent with the assignment of Durig et al.²¹ of isopropyl cyanide, the band at 371 cm^{-1} in the infrared spectrum of the -*d*₀ molecule has a C-type Q branch, characteristic of the a'' mode and the ν_{13} band at 211 cm^{-1} has a B-type contour.

The torsional mode ν_{21} was not observed directly. Microwave splitting results from the -*d*₀ and -*d*₅ molecules gave frequencies of ~ 220 and $\sim 162 \text{ cm}^{-1}$, respectively.^{13,14} A possible $2\nu_{21}$ band was observed for the -*d*₃ compound in the Raman effect at 313 cm^{-1} , which is consistent with the microwave results. The broad Raman line arising from the C-C-N out-of-plane bend obscures most of the $2\nu_{21}$ region of the other isotopes.

Teller-Redlich Product Rule Calculations. An attempt to check the consistency of the isotopic assignments was made through the Teller-Redlich product rule. Generally, an agreement of 3-5% between calculated and observed ratios is sufficient to suggest the validity of the assignment. Our results are shown in Table V.

The product rule was used as an aid in assigning the "missing" fundamentals in the a' block of the -*d*₂, -*d*₃, and -*d*₅ molecules. A weak Raman band at 855 cm^{-1} in the gas phase spectrum of the -*d*₂ molecule and a medium band in the solid phase at 856 cm^{-1} was consistent with the a' block Teller-Redlich product rule calculation. A weaker Raman band at

904 cm^{-1} was discounted because it placed the calculation over 5%. The assignment of fundamentals at 915 and 671 cm^{-1} in the -*d*₅ compound also gave a consistent product rule calculation. The 915- cm^{-1} B-type band was of medium intensity in the infrared spectrum and weak in the Raman effect. The large intensity of this band in the solid phase also made us feel it was a fundamental, not an overtone or combination band. The band at 671 cm^{-1} was chosen over the band at 725 cm^{-1} to be consistent with product rule calculations.

The -*d*₃ molecule presented the greatest difficulty in our assignment. The strong band in the Raman spectra of the gas at 799 cm^{-1} was considered a fundamental. This is in direct contrast to the prediction of the normal coordinate analysis which calculates this band at about 700 cm^{-1} . A band at 743 cm^{-1} in the Raman spectrum of this gas was discounted as this fundamental due to lack of intensity. It should be noted that the 799- cm^{-1} band was observed only in the Raman effect which was consistent with intensity of other C-C(N) stretching vibrations. However the lowest frequency mode should be mostly the CD₃ rock. However the assignment of both the 799- and 743- cm^{-1} bands as fundamentals made the product rule calculations inconsistent with the assignment of the other fundamentals which are believed to be correct. The "missing" fundamental was therefore assigned to the Raman peak at 938 cm^{-1} .

Normal Coordinate Analysis. As an aid in describing the molecular vibrations in a more quantitative manner, a normal coordinate analysis was undertaken. The calculations were carried out by the Wilson FG matrix method²² with computer programs written by Schachtschneider.²³ The observed frequencies were given a weight of $1/\lambda$ in the least-squares fitting procedure of the force constants, and no attempt was made to correct for frequency shifts due to energy level interactions, i.e., Fermi resonance. The internal coordinates for ethyl cyanide are defined in Figure 3. Symmetrization was accomplished using the symmetry coordinates listed in Table VI. The S₁₄ and S₁₅ symmetry coordinates have been defined as zero-coordinate four-branch redundancies. To have symmetry coordinates which would be to a degree consistent with the previous literature,^{5,7} we use the following procedure to define S₆ and S₁₂. The S₆' was written as $(1/\sqrt{2})(\Delta\delta - \Delta\pi)$ which is orthogonal to S₁₅. The S₁₂' was then written as

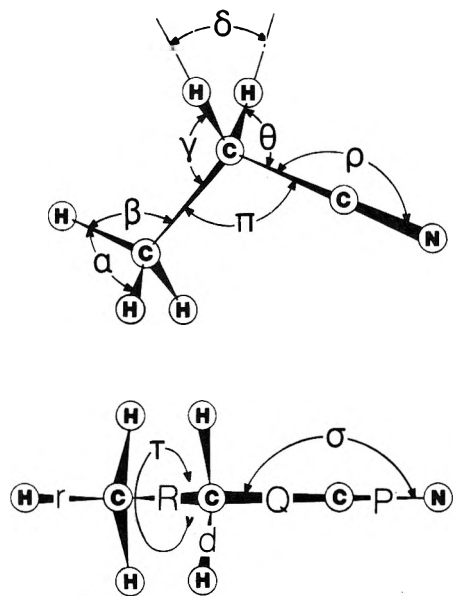


Figure 3. Internal coordinates for ethyl cyanide.

$(1/\sqrt{12})(2\Delta\delta + 2\Delta\pi - \Delta\theta_1 - \Delta\theta_2 - \Delta\gamma_1 - \Delta\gamma_2)$ where the coefficients were determined by the Schmidt orthogonalization method to complete the orthogonal set of A' symmetry coordinates. However, this new set does not separate the contributions of S_6' and S_{12}' in the potential energy distribution. Therefore we tried the new combinations

$$\begin{bmatrix} S_6 \\ S_{12} \end{bmatrix} = \begin{bmatrix} 1 & 1 \\ \sqrt{2} & \sqrt{2} \\ 1 & -1 \\ \sqrt{2} & \sqrt{2} \end{bmatrix} \begin{bmatrix} S_6' \\ S_{12}' \end{bmatrix}$$

which were found to be separated in the potential energy distribution. Table VI clearly shows S_6 to be mainly $\Delta\delta$, the CH_2 deformation, and S_{12} as $\Delta\pi$, the C-C-C bend.

The calculated vibrational frequencies are listed in Tables I-IV along with the associated symmetrized potential energy distribution among the diagonal elements of the F matrix. Using the relatively simple force field shown in Table VII, the average agreement between calculated and observed frequencies was found to be 1.27% or 11.4 cm^{-1} . In general, the results of the calculation support the commonly accepted "group frequency" descriptions associated with the methyl and methylene groups for the $-d_0$ and $^{13}\text{C}(\text{N})$ molecules.

However, the CH_3 deformation region should be explained in more detail. It was found that very small changes in the force field had an effect of reversing the assignment of ν_5 and ν_6 . In an attempt to best fit the 105 observed frequencies, the entire force field was allowed to vary. It was this procedure that reversed the assignment of ν_5 and ν_6 . However it must be emphasized that small changes in the force field will reverse the assignment, with a corresponding small increase in the percent error.

Since $3N - 6 = 21$ for ethyl cyanide, we tried to restrict the number of force constants to less than 21. It would have been possible with the amount of isotopic data we had to include all possible interaction constants, many of which would have been very small. However, we tried to find those force constants whose significance was such that fewer than 21 were required to reasonably reproduce the observed frequencies. Force constants $F_{\pi\rho}$, $F_{\alpha\beta}$, F_{RQ} , $F_{Q\gamma}$, $F_{Q\beta}$, $F_{R\pi}$, $F_{Q\pi}$, $F_{\gamma\theta}$, $F_{\alpha\alpha'}$, $F_{\beta\beta'}$, $F_{Q\theta}$, $F_{Q\delta}$, and $F_{\pi\beta}$ were tried and found to have very little

TABLE VI: Symmetry Coordinates for Ethyl Cyanides

A'	Species	
CH_3	Antisymmetric stretch	$S_1 = 6^{-1/2}(2\Delta r_1 - \Delta r_2 - \Delta r_3)$
CH_3	Symmetric stretch	$S_2 = 3^{-1/2}(\Delta r_1 + \Delta r_2 + \Delta r_3)$
CH_2	Symmetric stretch	$S_3 = 2^{-1/2}(\Delta d_1 + \Delta d_2)$
CH_3	Antisymmetric deformation	$S_4 = 6^{-1/2}(2\Delta\alpha_2 - \Delta\alpha_1 - \Delta\alpha_3)$
CH_3	Symmetric deformation	$S_5 = 6^{-1/2}(\Delta\alpha_1 + \Delta\alpha_2 + \Delta\alpha_3 - \Delta\beta_1 - \Delta\beta_2 - \Delta\beta_3)$
CH_2	Deformation	$S_6 = 24^{-1/2}[(\sqrt{6} + 2)\Delta\delta - (\sqrt{6} - 2)\Delta\pi - \Delta\gamma_1 - \Delta\gamma_2 - \Delta\theta_1 - \Delta\theta_2]$
CH_2	Wag	$S_7 = \frac{1}{2}(\Delta\gamma_1 + \Delta\gamma_2 - \Delta\theta_1 - \Delta\theta_2)$
CH_3	In-plane rock	$S_8 = 6^{-1/2}(2\Delta\beta_1 - \Delta\beta_2 - \Delta\beta_3)$
C-C	Stretch (ethyl)	$S_9 = \Delta R$
C-C(N)	Stretch	$S_{10} = \Delta Q$
C-N	Stretch	$S_{11} = \Delta P$
C-C-C	Bend	$S_{12} = 24^{-1/2}[(\sqrt{6} - 2)\Delta\delta - (\sqrt{6} + 2)\Delta\pi + \Delta\gamma_1 + \Delta\gamma_2 + \Delta\theta_1 + \Delta\theta_2]$
C-C-N	In-plane bend	$S_{13} = \Delta\rho$
Redundancy		$S_{14} = 6^{-1/2}(\Delta\alpha_1 + \Delta\alpha_2 + \Delta\alpha_3 + \Delta\beta_1 + \Delta\beta_2 + \Delta\beta_3) = 0$
Redundancy		$S_{15} = 6^{-1/2}(\Delta\gamma_1 + \Delta\gamma_2 + \Delta\theta_1 + \Delta\theta_2 + \Delta\delta + \Delta\pi) = 0$

A''	Species	
CH_3	Antisymmetric stretch	$S_{16} = 2^{-1/2}(\Delta r_2 - \Delta r_3)$
CH_2	Antisymmetric stretch	$S_{17} = 2^{-1/2}(\Delta d_1 - \Delta d_2)$
CH_3	Antisymmetric deformation	$S_{18} = 2^{-1/2}(\Delta\alpha_1 - \Delta\alpha_3)$
CH_2	Twist	$S_{19} = \frac{1}{2}(-\Delta\gamma_1 + \Delta\gamma_2 + \Delta\theta_1 - \Delta\theta_2)$
CH_2	Rock	$S_{20} = \frac{1}{2}(\Delta\gamma_1 - \Delta\gamma_2 + \Delta\theta_1 - \Delta\theta_2)$
CH_3	Out-of-plane rock	$S_{21} = 2^{-1/2}(\Delta\beta_2 - \Delta\beta_3)$
CH_3	Torsion	$S_{22} = \Delta\tau$
C-C-N	Out-of-plane bend	$S_{23} = \Delta\sigma$

effect on the force field. It has been shown that the relationship $F_{R\alpha} = -F_{R\beta}$ exists for tetrahedral angles.^{24,25} Our value for $F_{R\alpha}$ of -0.25 is in good agreement with the $F_{R\beta}$ values for ethyl iodide⁷ of 0.20 and for ethyl chloride⁴ of 0.17 mdyn/Å. Our value for $F_{R\gamma}$ of 0.56 is much higher than the value of 0.21 mdyn/Å in the ethyl chlorides and iodides.^{4,7} However, this value is more consistent with the 0.328 mdyn/Å value used by Yamedera and Krimm.⁹ The high value of this interaction constant with respect to other similar molecules (ethyl halides) might be attributed to a much different electronic structure. Experimental evidence is conclusive that the C-C (ethyl) bond in ethyl cyanide (1.54 Å) is longer than in the ethyl halides.^{11,12} A shortening of the C-C(N) bond to 1.46 Å in ethyl cyanide has been attributed to partial double bond character. Our force constants H_Q and H_R are consistent with approximately the 20% double bond character indicated.¹¹ The lower methyl barrier to internal rotation in ethyl cyanide with respect to the ethyl halides is more evidence that ethyl cyanide has a very different electron distribution about the C-C bond than is observed in the halogens.

Various attempts were made to raise the calculated frequency of the CD_3 rock at 691 cm^{-1} . However, none were

TABLE VII: Internal Force Constants for CH₃CH₂CN and Its Deuterated Derivatives^{a,b}

Force constant	Coordinates involved	Value
K_r	C-H, methyl	4.89 ± 0.02
K_d	C-H, methylene	4.77 ± 0.02
K_R	C-C, ethyl	3.97 ± 0.17
K_Q	C-C(N)	4.93 ± 0.26
K_P	C-N	17.52 ± 0.21
H_α	H-C-H, methyl	0.542 ± 0.006
H_β	C-C-H, methyl	0.619 ± 0.014
H_δ	H-C-H, methylene	0.611 ± 0.016
H_γ	C-C-H, methylene	0.520 ± 0.020
H_θ	(N)C-C-H, methylene	0.802 ± 0.018
H_π	C-C-C	1.970 ± 0.167
H_ρ	C-C-N in-plane	0.211 ± 0.021
H_σ	C-C-N out-of-plane	0.306 ± 0.019
H_τ^b	-CH ₃ ^c	0.010 ± 0.001
F_{rr}	C-H, C-H	0.075 ± 0.013
F_{dd}	C-H, C-H	0.043 ± 0.023
$F_{R\alpha}$	C-C, H-C-H	-0.253 ± 0.036
$F_{R\gamma}$	C-C, C-C-H	0.565 ± 0.052
$F_{\delta\theta}$	H-C-H, C-C-H	0.128 ± 0.016

^a Stretching force constants in mdyn Å⁻¹; bending constants in mdyn Å radian⁻²; stretch-bend interaction constants in mdyn radian⁻¹. ^b See Figure 3. ^c Torsional coordinate is defined as the sum of three trans torsions about the C-C bond.

successful. Concluding that the -d₃ molecule was behaving anomalously, we did not use the -d₃ data in one calculation. As was expected, the fit improved to 0.91% or 8.9 cm⁻¹. The overall force field, however, did not change significantly. Therefore, the reported force field is the result of the calculation from the data of all five isotopes.

In conclusion, we feel that our results provide a more complete understanding of the vibrational spectrum of ethyl cyanide and its -d₂, -d₃, -d₅, and ¹³C(N) derivatives. The relatively simple force field used in this paper accounts for most

of the fundamental vibrations, and also provides something more than a qualitative description of these motions.

Acknowledgment. The authors gratefully acknowledge the financial support by the National Aeronautics and Space Administration by Grant No. NGL-41-002-003.

Miniprint Material Available: Full-sized photocopies of Tables I-IV (12 pages). Ordering information is available on any current masthead page.

References and Notes

- (1) C. J. Wurrey received his Ph.D. from MIT under the direction of Professor Lord in 1973. Professor J. R. Durig received his Ph.D. from MIT under the direction of Professor Lord in 1962.
- (2) To be submitted in partial fulfillment of the Ph.D. requirements.
- (3) F. A. Miller and F. E. Kiviat, *Spectrochim. Acta, Part A*, **25**, 1363 (1969).
- (4) A. B. Dempster and G. Zerbi, *J. Mol. Spectrosc.*, **39**, 1 (1971).
- (5) R. Gaudres and M. Bejand-Bianchi, *Spectrochim. Acta, Part A*, **27**, 2249 (1971).
- (6) G. A. Crowder, *J. Mol. Spectrosc.*, **48**, 467 (1973).
- (7) J. R. Durig, J. W. Thompson, V. W. Thyagesan, and J. D. Witt, *J. Mol. Struct.*, **24**, 41 (1975).
- (8) N. E. Duncan and G. J. Janz, *J. Chem. Phys.*, **23**, 434 (1955).
- (9) R. Yamadera and S. Krimm, *Spectrochim. Acta, Part A*, **24**, 1677 (1968).
- (10) P. Klabeo and J. Grundnes, *Spectrochim. Acta, Part A*, **24**, 1905 (1968).
- (11) G. Lerner and B. P. Dailey, *J. Chem. Phys.*, **26**, 678 (1957).
- (12) H. M. Heise, H. Lutz, and H. Dreizler, *Z. Naturforsch. A*, **29**, 1345 (1974).
- (13) V. W. Laurie, *J. Chem. Phys.*, **31**, 1500 (1959).
- (14) Y. S. Li and J. R. Durig, *J. Mol. Spectrosc.*, **54**, 296 (1975).
- (15) R. N. Jones and A. Nadeau, *Spectrochim. Acta*, **20**, 1175 (1964).
- (16) R. T. Hall and J. M. Dowling, *J. Chem. Phys.*, **47**, 2459 (1967); **52**, 1161 (1970).
- (17) F. G. Baglin, S. F. Bush, and J. R. Durig, *J. Chem. Phys.*, **47**, 2104 (1967).
- (18) P. Groner, R. Meyer, and Hs. H. Günthard, *Chem. Phys.*, in press.
- (19) G. Herzberg, "Infrared and Raman Spectra of Polyatomic Molecules", Van Nostrand, New York, N.Y., 1945.
- (20) L. J. Bellamy, "The Infrared Spectra of Complex Molecules", Wiley, New York, N.Y., 1962.
- (21) J. R. Durig, C. M. Player, Jr., Y. S. Li, J. Bragin, and C. W. Hawley, *J. Chem. Phys.*, **57**, 4544 (1972).
- (22) E. B. Wilson, Jr., J. C. Decius, and P. C. Cross, "Molecular Vibrations", McGraw-Hill, New York, N.Y., 1955.
- (23) J. H. Schachtschneider, "Vibrational Analysis of Polyatomic Molecules", V and VI, Technical Reports No. 231-64 and 57-65, respectively, Shell Development Co., Emeryville, Calif.
- (24) H. Hollenstein and Hs. H. Günthard, *Chem. Phys.*, **4**, 368 (1974).
- (25) P. Groner and Hs. H. Günthard, *J. Mol. Spectrosc.*, in press.

Correlation between the Absorption Spectra and Resonance Raman Excitation Profiles of Astaxanthin^{1a}

V. R. Salares,* R. Mendelsohn,^{1b} P. R. Carey, and H. J. Bernstein

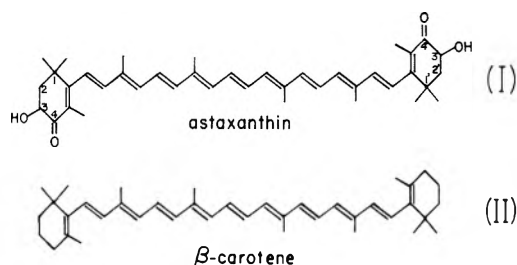
Division of Chemistry and Division of Biological Sciences, National Research Council of Canada, Ottawa, Canada K1A 0R6
(Received January 5, 1976)

Publication costs assisted by the National Research Council of Canada

Resonance Raman excitation profiles in the region 4579–5287 Å are reported for the carotenoid molecule astaxanthin at –162 and 23 °C. At these temperatures the visible absorption spectra are structured and unstructured, respectively. The experimental data, simulated using a simple model, demonstrate that there is a correlation between the development of vibrational structure in the absorption spectrum and in the excitation profile. For astaxanthin the excitation profiles at room temperature do not resolve the vibrational structure of the broad absorption band but do show that the 0–0 transition occurs near 18 850 cm⁻¹.

Introduction

Excitation profiles (variation of Raman intensity with exciting wavelength) have recently been suggested as a probe of vibrational structure in absorption spectra.^{2–5} This implies that vibrational structure which lies hidden in an absorption band may be resolved by measuring Raman excitation profiles. To date excitation profiles have been measured primarily for molecules with structured absorption spectra.^{2b–5} Thus, it is not clear if any correlation exists between the resolution obtainable in the Raman excitation profiles and in the absorption spectrum. To study this correlation, the carotenoid molecule astaxanthin (3,3'-dihydroxy-β,β-carotene-4,4'-dione) (I) was selected since its Raman excitation profiles could be



obtained under conditions of both structured (low temperature) and unstructured (room temperature) absorption spectra. A simple model, similar to that applied in previous Raman studies,^{2b–4} was used to analyze the intensity data and semiquantitatively evaluate the temperature dependence.

Experimental Section

Solvents and Reagents. Spectrochemical grade chemicals were used when available.

Astaxanthin. Astaxanthin was extracted from cleaned and ground lobster carapace with acetone at 5 °C. Purification and recrystallization from dichloromethane–petroleum ether (bp 30–60 °C) by the method of Buchwald and Jencks⁶ yielded red-violet platelets. The crystals or solutions in dichloromethane were stored at –23 °C.

The absorption spectra in different solvents were identical with those reported earlier.⁶ Thin-layer chromatography on silica gel 60F-254 (0.25 mm, Merck) developed with 20% ace-

tone–petroleum ether (bp 60–70 °C) gave a single band. The recrystallized material consists of only one isomer, and this is believed to be the all-trans form.⁷

Absorption Spectra. Absorption spectra were measured with a Cary 14 spectrophotometer. Low temperature spectra in EPA (diethyl ether–isopentane–ethanol, 5:5:2 by volume) were obtained using a dewar equipped with quartz windows. A 2-mm quartz cell which fitted inside the dewar cavity was cooled by flowing cold nitrogen gas. Temperatures were monitored with a chromel–alumel thermocouple.

Raman Spectra. Raman spectra were recorded using 90° scattering geometry on a Jarrell-Ash Model 25-102 double monochromator equipped with an RCA-C31034 photomultiplier tube and photon counting detection. A Spectra Physics 166 Ar⁺ laser provided nine excitation lines from 4579 to 5287 Å; output at 5287 Å was obtained by modifying the laser optics. Laser powers were kept between 4 and 9 mW. The vibrations of interest were scanned alternately with the reference lines at least three times.

For room temperature measurements, the rotating cell technique⁸ was used to minimize local heating. The solution of astaxanthin in chloroform ($A_{\text{max}} = 0.96$) was first deoxygenated and purged with nitrogen gas. Under these conditions, the absorbance and resonance Raman spectra were invariant indicating the absence of photochemical degradation or isomerization. The intensities of the 1524- and 1157-cm⁻¹ vibrations of astaxanthin (Figure 1) were measured relative to that of a chloroform line at 366 cm⁻¹.

For low temperature measurements, an astaxanthin solution in EPA ($A_{\text{max}} = 1.40$) was sealed in a glass capillary and mounted on an unsilvered, double-jacketed glass dewar.⁹ Cooling was achieved by flowing a stream of cold nitrogen gas. The intensities of the two fundamentals at 1524 and 1157 cm⁻¹ and of the overtone at 3045 cm⁻¹ were measured relative to the total area of solvent bands at 2808, 2874, 2938 and 2982 cm⁻¹. Each set of measurements with the nine exciting lines was obtained continuously. Intensity ratios with 5145-Å excitation at the beginning and at the end of the measurements were reproducible to ±5%.

Treatment of Experimental Data. Intensities were measured as band areas with a planimeter. An average value of three or more measurements on each line was taken and this was corrected for the wavelength dependence of the instrument response. The latter had previously been calibrated

* Address correspondence to this author at the Division of Chemistry, National Research Council of Canada.

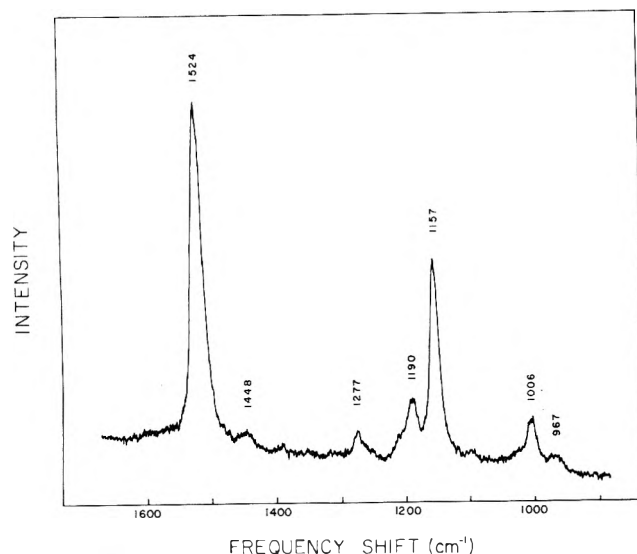


Figure 1. Resonance Raman spectrum of astaxanthin in CHCl_3 at $+23^\circ\text{C}$, 4658-Å excitation; 4 mW laser power, 6.5 cm^{-1} spectral slit width, scan speed $0.5\text{ cm}^{-1}/\text{s}$; full scale sensitivity 3000 counts/s.

using a standard lamp. Since the reference lines were not adjacent to the astaxanthin vibrations, a λ^4 correction³ was also applied. The solutions were sufficiently dilute ($8.5 \times 10^{-6}\text{ M}$ in chloroform, $1.25 \times 10^{-5}\text{ M}$ in EPA) that corrections due to self-absorption were considered to be negligible.³

Theoretical

The model used to calculate the excitation profile is based on the form of the scattering tensor derived by Albrecht¹⁰ and co-workers. The $\alpha_{\rho\sigma}$ component of the tensor is given by:

$$(\alpha_{\rho\sigma})_{g_i, g_j} = A + B$$

where

$$A = \sum_{e \neq g} \sum_{\nu} \left(\frac{(g^0 | R_{\sigma} | e^0)(e^0 | R_{\rho} | g^0)}{E_{e\nu, g_i} - E_0 + i\gamma} + \frac{(g^0 | R_{\rho} | e^0)(e^0 | R_{\sigma} | g^0)}{E_{e\nu, g_j} + E_0 + i\gamma} \right) \times \langle i | \nu \rangle \langle \nu | j \rangle \quad (1)$$

and

$$B = \sum_{e \neq g} \sum_{\nu} \sum_{s \neq e} \sum_a \left(\frac{(g^0 | R_{\sigma} | e^0)(e^0 | h_a | s^0)(s^0 | R_{\rho} | g^0)}{E_{e\nu, g_i} - E_0 + i\gamma} \right) \times \frac{\langle i | Q_a | \nu \rangle \langle \nu | j \rangle}{E_e^0 - E_s^0} \quad (2)$$

plus similar terms involving the interchange of i and j and s and e (see ref 10). In this notation, i and j are the vibrational levels of the ground electronic state g , ρ and σ are any of the Cartesian coordinates x , y , or z , R is the dipole moment operator, the ν 's are vibrational levels of the excited electronic state e with which resonance occurs, $E_{e\nu, g_i}$ is the vibronic energy, E_0 is the excitation energy, h_a is the (Herzberg-Teller) vibronic coupling operator, Q_a is the a th normal coordinate of the ground state, γ is the damping factor related to the half-width of the absorption band, s is an excited state not in resonance, and finally $|g^0\rangle$, $|e^0\rangle$, and $|s^0\rangle$ are wave functions for the indicated states.

The B term is utilized when resonance enhancement develops because of vibronic coupling between two excited electronic states, while the A term is applicable when only one state is involved in the scattering process. In the present case, the A term was found to give a satisfactory representation of

the excitation profiles. Simplification of the A term occurs because only one excited electronic state is assumed to be in resonance and because under resonance conditions the second term in eq 1 becomes negligible.

The depolarization ratios for the vibrations studied for astaxanthin were about 0.3, indicating that only one term in the scattering tensor (α_{zz}) was contributing to the observed intensity. In this instance eq 1 reduces to the following form:

$$(\alpha_{zz})^2 = \text{constant} \times f_a^2$$

where

$$f_a = \sum_{\nu} \frac{\langle i | \nu \rangle \langle \nu | j \rangle}{E_{e\nu, g_i} - E_0 + i\gamma} \quad (3)$$

where the terms involving the dipole moment matrix elements are included in the constants. Several approximations are introduced to evaluate f_a : (a) harmonic oscillator wave functions are assumed for the g and e states, (b) it is assumed that no change in force constant occurs in the upper state, and (c) it is assumed that the potential energy curves are displaced from each other horizontally by a parameter x such that

$$x = (\nu_{\text{vib}}\pi/h)^{1/2}Q \quad (4)$$

Computer programs were written to calculate and plot the excitation profiles. The sum over ν was taken up until $\nu = 6$. Inclusion of higher ν terms led to no change in the results. The parameters x and γ were varied to obtain a good fit to the experimental data.

The absorption spectra resulting from a sum of progressions in 2 vibrations was given by the following expression:

$$\epsilon(\nu) = \sum_{Q_1, Q_2} \sum_{\nu} \nu \langle 0 | \nu \rangle^2 g(\nu) \quad (5)$$

where $g(\nu)$ is a line shape function. The line shapes were assumed to be Gaussian with a half-width = γ . As the calculated absorption spectra led to poor quantitative agreement with experiment (see text), Lorentzian line shapes were introduced into eq 5. No improvement was observed in the fit.

Results and Discussion

The observed excitation profiles for ν_1 and ν_2 at 23 and -162°C and for $2\nu_1$ at -162°C are shown as triangles in Figures 2-4. The experimental points for ν_1 and ν_2 at room temperature suggest an intensity maximum near 5200 Å but no additional resolved structure. In the intensity profiles at -162°C , a resolved peak appears around 4600 Å for ν_1 and 4750 Å for ν_2 in addition to the main maximum near 5250 Å. For $2\nu_1$, the experimental excitation profile has a peak near 4880 Å and shows a second weaker maximum near 5200 Å.

The calculated excitation profiles are shown as solid lines in Figures 2-4. For the purposes of calculation, the 0-0 frequency of the electronic transition was set at $18\,850\text{ cm}^{-1}$. A reasonable fit to the excitation profiles was obtained at both 23 and -162°C without changing the 0-0 frequency.

The excitation profiles of ν_1 (Figures 2a and 2b) were simulated by assuming a value of $x = 0.9$ for both 23 and -162°C , with $\gamma = 950\text{ cm}^{-1}$ at 23°C and $\gamma = 500\text{ cm}^{-1}$ at -162°C . The calculated excitation profiles show a broad shoulder at room temperature while structure develops at low temperature. The short wavelength maximum in the excitation profile at -162°C arises from the 0-2 transition ($\nu = 2$ in the excited state) while the 0-1 transition appears only as a shoulder. When smaller γ values were used, a resolved peak did occur at the $\nu = 1$ level as was found for ν_1 of β -carotene.³ However, the overall fit was better with $\gamma = 500\text{ cm}^{-1}$.

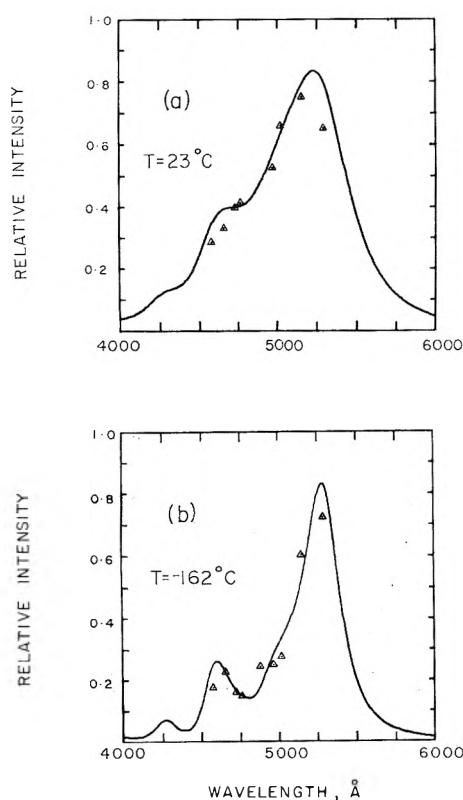


Figure 2. Observed (Δ) and calculated (—) profiles for ν_1 (1524 cm^{-1}) at (a) 23°C and (b) -162°C . The calculated curves were each scaled to equal the observed point at 4727 Å .

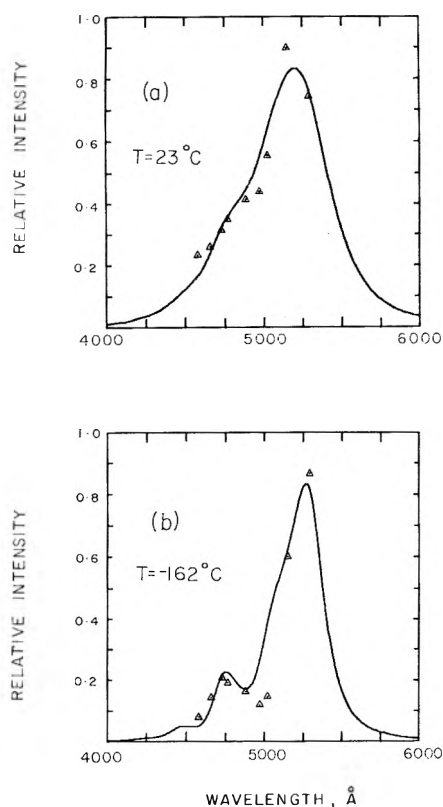


Figure 3. Observed (Δ) and calculated (—) excitation profiles for ν_2 (1157 cm^{-1}) at (a) 23°C and (b) -162°C . Scaled as for ν_1 .

The excitation profiles of ν_2 were calculated using the same γ values as those for ν_1 at the two temperatures, while the

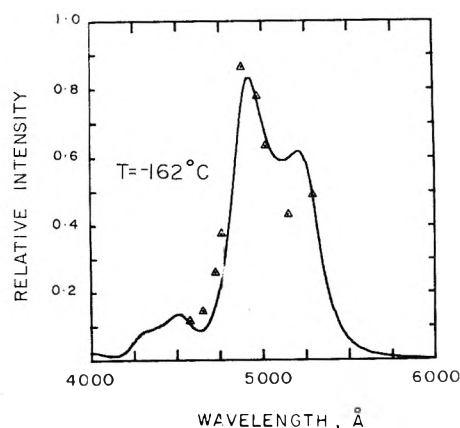


Figure 4. Observed (Δ) and calculated (—) excitation profiles for $2\nu_1$ at -162°C . The calculated curve was scaled to equal the observed datum at 4880 Å .

value of x was 0.8. Again, the calculated excitation profiles shows a shoulder at 23°C (Figure 3a) but a resolved structure at low temperature (Figure 3b). The second maximum for ν_2 at -162°C also occurs at the $\nu = 2$ position for this mode.

The excitation profile for $2\nu_1$ at -162°C was simulated using identical parameters as those for ν_1 at this temperature. The qualitative shape (Figure 4) corresponds well with the observation that the intensity maximum at the 0-1 transition is greater than that at the 0-0 transition. The fit is considered satisfactory in view of the experimental error in measuring low intensities of the overtone.

A summary of the parameters used in the calculation for astaxanthin at 23°C and -162°C , as well as those previously reported for β -carotene, is given in Table I. The values of x have been converted to changes in bond length upon excitation by a procedure similar to that described in ref 3. Slight differences are noted for β -carotene and astaxanthin. However, the approximations necessary for the calculation of x in this simple model, namely, that all C=C bonds have the same length and all C-C bonds have the same length and furthermore, that ν_1 and ν_2 are pure C=C and C-C stretching modes, respectively, suggest that these differences may not be significant.

The absorption spectrum of astaxanthin at room temperature, shown in Figure 5a, is devoid of fine structure. β -Carotene (II), on the other hand, has three resolved peaks in the visible region.⁷ The broad absorption band of astaxanthin is typical for carotenoid molecules which contain one or more conjugated carbonyl groups.¹¹ At low temperatures, however, fine structure develops (Figure 5b). Absorption in the visible region is known to arise from $\pi\text{-}\pi^*$ transitions of the polyene chain and the fine structure is due to transitions from the ground state to various vibrational energy levels in the first excited state.¹²

An attempt was made to simulate the observed absorption spectra by assuming that it is composed of a sum of progressions in ν_1 and ν_2 . The results are presented in Figures 6a and 6b. The parameters used for each mode were the same as those for the excitation profiles. Qualitatively, the development of structure observed in the absorption spectrum is reproduced by decreasing the half-width from 950 cm^{-1} at room temperature to 500 cm^{-1} at 162°C . However, the quantitative agreement is quite poor. There are several possible reasons for this discrepancy:

(1) Previous studies on β -carotene have shown that the ν_3 vibration contributes in significant fashion to the absorption

TABLE I: Parameters Used in the Calculation of Excitation Profiles of ν_1 , ν_2 , and $2\nu_1$ of Astaxanthin

$T, ^\circ\text{C}$	ν, cm^{-1}	γ, cm^{-1}	$x, \text{\AA}$
Astaxanthin			
23 (in CHCl_3)	1524	950	+0.023
-162 (in EPA)	1524	500	
-162 (in EPA)	3045	500	-0.025
23 (in CHCl_3)	1157	950	
-162 (in EPA)	1157	500	
β -Carotene ^a			
-150 (in isopentane)	1520	250	+0.020
-150 (in isopentane)	1157	250	-0.031

^a Reference 3.

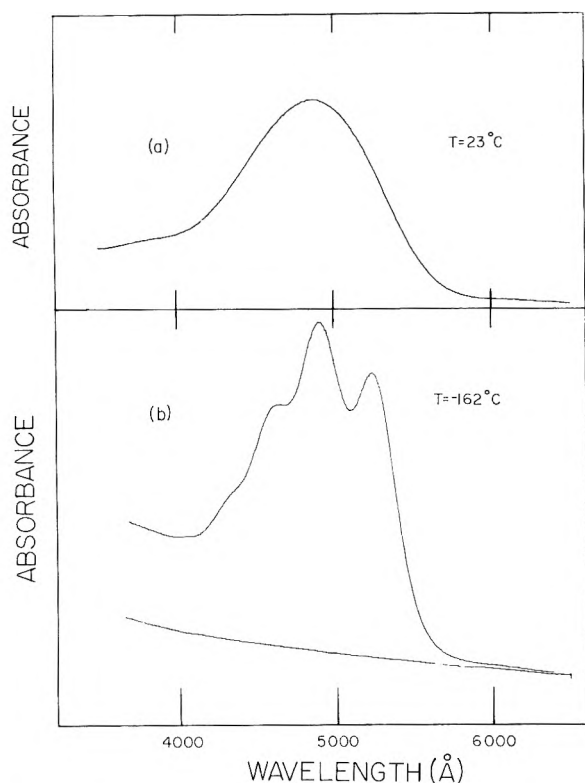


Figure 5. Absorption spectra of astaxanthin (a) in CHCl_3 solution at 23 $^\circ\text{C}$, λ_{max} 4880 \AA ; (b) in EPA solution at -162 $^\circ\text{C}$, λ_{max} 5240, 4900, and 4630 \AA .

spectrum.³ As the excitation profile for this mode was not measured, no value of x necessary for inclusion in the absorption spectrum calculation was available. A calculation was attempted in which the value of x for ν_3 was taken from the β -carotene work,³ and the calculated absorption spectrum resembled the observed much more closely.

(2) Other weak vibrations in the Raman spectrum (Figure 1) were not included in the calculations. The extent of their contributions to the absorption spectrum is unknown.

(3) The room temperature absorption spectrum is complicated by the presence of molecules which are not in their ground vibrational states prior to excitation.

(4) The $n-\pi^*$ transitions of the carbonyl groups may appear in the visible region whereas only the $\pi-\pi^*$ transition has been considered in the calculated absorption spectrum.

The value of γ used in the excitation profile calculation provides a measure of the width of the absorption band for the

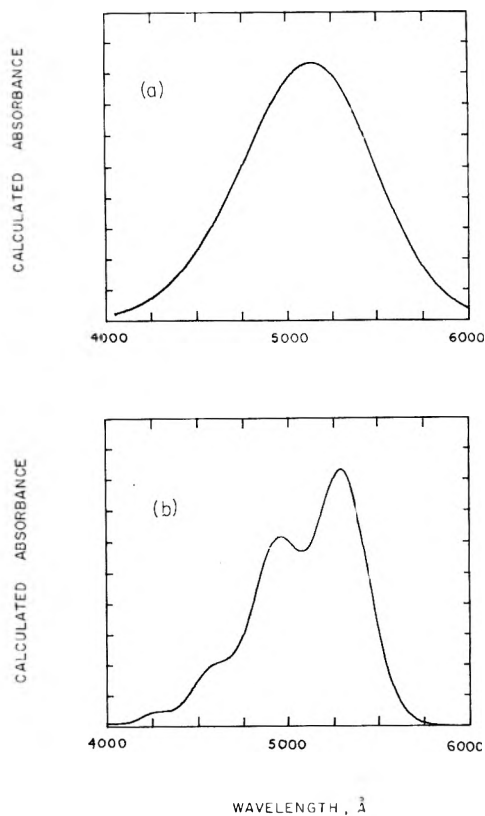


Figure 6. Calculated absorption spectra for astaxanthin. Gaussian line shapes were used: (a) $\gamma = 950 \text{ cm}^{-1}$; (b) $\gamma = 500 \text{ cm}^{-1}$.

0-0 level in these molecules. The larger value of γ for astaxanthin compared to β -carotene (500 cm^{-1} in EPA at -162 $^\circ\text{C}$ and 250 cm^{-1} in isopentane at -150 $^\circ\text{C}$,³ respectively) is undoubtedly due to the presence of carbonyl groups in astaxanthin. The hydroxyl groups cannot be responsible for the broadening since crustaxanthin (3,4,3',4'-tetrahydroxy- β -carotene) shows vibrational structure in its room temperature absorption spectrum. The carbonyl groups impart polarity to the molecule as shown by the reduced solubility of astaxanthin in nonpolar solvents. Greater interactions of solvent molecules with astaxanthin in the ground and excited states lead to increased broadening¹³ of the 0-0 level compared to β -carotene.

X-ray crystal studies have shown that the presence of carbonyl groups in the β -ionone rings enhances the noncoplanarity of the rings with the polyene chain.^{14,15} In solutions, the greater noncoplanarity of astaxanthin compared to β -carotene may cause a greater distribution of angular conformations about the bond joining the ring and the polyene chain for astaxanthin. This would lead to broadening of the 0-0 transition for the latter molecule.

The decrease in width of the 0-0 transition from 950 cm^{-1} at 23 $^\circ\text{C}$ to 500 cm^{-1} at -162 $^\circ\text{C}$ may be explained by a temperature effect on solvent organization around the solute molecules. In a more rigid environment such as in a glassy medium at low temperatures, slower solvent rearrangement leads to narrowing of the 0-0 transition.

Conclusion

It is clear that in circumstances where an unresolved absorption spectrum is composed of more than one vibrational progression and the 0-0 energy cannot be obtained, the res-

onance Raman excitation profiles may provide an estimate of this quantity. However, for astaxanthin the spacing between the 0-0, 0-1, 0-2, . . . , etc. transitions cannot be resolved from the excitation profiles at room temperature. A comparison of the experimental excitation profiles at 23 and -162 °C shows that the development of structure in the resonance Raman excitation profiles parallels its development in the absorption spectrum. It seems apparent for the molecule studied here that Raman excitation profiles depend in a fundamental way on absorption spectral line width and that excitation profiles will not be a general method for resolving vibrational structure of an unresolved absorption spectrum.

Acknowledgments. We wish to thank Mr. P. Bernath for writing some of the computer programs used in the current work and Dr. W. F. Murphy for the loan of his plotting sub-

outines, and for considerable advice about the programming.

References and Notes

- (1) (a) NRCC No. 15219. (b) Ph.D. with F. C. Lord, 1972.
- (2) (a) B. P. Gaber, V. Miskowski, and T. G. Spiro, *J. Am. Chem. Soc.*, **96**, 6868 (1974); (b) M. Mingardi, W. Siebrand, D. Van Labeke, and M. Jacon, *Chem. Phys. Lett.*, **31**, 208 (1975).
- (3) F. Inagaki, M. Tasumi, and T. Miyazawa, *J. Mol. Spectrosc.*, **50**, 286 (1974).
- (4) F. Galuzzi, M. Garozzo, and F. F. Ricci, *J. Raman Spectrosc.*, **2**, 351 (1974).
- (5) L. Rimai, R. G. Kilponen, and D. Gill, *J. Am. Chem. Soc.*, **92**, 3824 (1970).
- (6) M. Buchwald and W. P. Jencks, *Biochemistry*, **7**, 834 (1968).
- (7) L. Zechmeister, *Chem. Rev.*, **34**, 267 (1944).
- (8) W. Kiefer and H. J. Bernstein, *Appl. Spectrosc.*, **25**, 500 (1971).
- (9) F. A. Miller and B. M. Harney, *Appl. Spectrosc.*, **24**, 291 (1970).
- (10) A. C. Albrecht, *J. Chem. Phys.*, **34**, 476 (1961).
- (11) B. Ke, F. Imsgard, H. Kjosien, and S. Liaaen-Jensen, *Biochim. Biophys. Acta*, **210**, 139 (1970).
- (12) J. Dale, *Acta. Chem. Scand.*, **8**, 1235 (1954).
- (13) N. S. Bayliss and E. G. McRae, *J. Phys. Chem.*, **58**, 1002 (1954).
- (14) C. Sterling, *Acta Crystallogr.*, **17**, 1224 (1964).
- (15) J. C. J. Bart and C. H. MacGillivray, *Acta Crystallogr., Sect. B*, **24**, 1587 (1968).

Identification and Estimation of the Relative Abundance of Two Conformers of 1,2,3,6-Tetrahydropyridine from the Microwave Spectrum

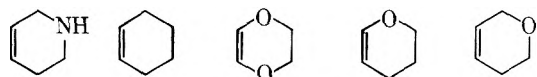
S. Chao, T. K. Avirah, Robert L. Cook, and Thomas B. Malloy, Jr.*¹

Department of Physics and Department of Chemistry, Mississippi State University, Mississippi State, Mississippi 39762
(Received December 22, 1975)

The microwave spectra of 1,2,3,6-tetrahydropyridine and its N-d analogue have been studied in the R-band (26.5-40 GHz) and X-band (7-12.4 GHz) regions with a Hewlett-Packard 8400C Stark-modulated microwave spectrometer. Transitions for two distinct conformers have been assigned and the change in the rotational constants on deuteration has allowed identification of the conformers as half-chair axial and half-chair equatorial. Half-chair refers to the conformation of the ring skeleton and axial-equatorial to the orientation of the N-H. For the *d*₀ compound the rotational constants are (in MHz) $A = 4897.47 \pm 0.01$, $B = 4709.16 \pm 0.01$, $C = 2641.48 \pm 0.01$ for the axial conformer and $A = 4950.50 \pm 0.01$, $B = 4743.05 \pm 0.01$, $C = 2647.82 \pm 0.01$ for the equatorial conformer. Measurement of the relative intensities of a number of lines yields an estimate of the rather small difference in stability of the two forms of $50 \pm 30 \text{ cm}^{-1}$ ($\sim 0.15 \text{ kcal/mol}$), the equatorial form being the more stable. Because of the distribution of the dipole moment among the principal axis components and the selection rules, the most prominent lines by far are due to the less abundant axial conformer. Under conditions of high resolution several of the lines exhibited resolvable splitting which can be attributed to quadrupole coupling from the nitrogen nucleus. Analysis of the observed hyperfine structure gave $\chi_{cc} = 1.32 \pm 0.02 \text{ MHz}$; $\eta\chi_{cc} = 0.72 \pm 0.02 \text{ MHz}$ for the axial conformer and $\chi_{cc} = -4.48 \pm 0.04 \text{ MHz}$; $\eta\chi_{cc} = 0.09 \pm 0.09 \text{ MHz}$ for the equatorial conformer. The drastic difference in the coupling constants for the two conformers is attributed to the difference in the relative orientations of the principal axes of the inertial and quadrupole coupling tensors, respectively.

Introduction

As part of a continuing effort in the study of the conformations and low-frequency vibrational modes of cyclic molecules, we undertook an investigation of the microwave spectrum of 1,2,3,6-tetrahydropyridine, C₅H₉N, which is an analogue of cyclohexene. Microwave, far-infrared, and/or Raman studies of cyclohexene, 1,4-dioxene, $\Delta^{2,3}$ -dihydropyran, and $\Delta^{3,4}$ -dihydropyran have been reported.²⁻⁸ These



studies indicate that the stable conformation is a twisted, or half-chair form. In addition, the barriers to planarity of the rings range from ~ 19 to 25 kcal/mol and the interconversion of the two equivalent stable twisted forms occurs via a bent (half-boat) form with barriers to interconversion ranging from ~ 6 to 10 kcal/mol . No direct evidence of the existence of a minimum corresponding to the less stable bent form has been found. It was expected that 1,2,3,6-tetrahydropyridine would also exist with a half-chair ring skeleton. The presence of the imino hydrogen, however, renders the two twisted forms nonequivalent, there being two distinct conformers, half-chair axial and half-chair equatorial, respectively. In addition, the

possibility existed of finding two bent forms depending on the orientation of the imino hydrogen (Figure 1).

In this work, the microwave spectra of 1,2,3,6-tetrahydropyridine and its *N-d* derivative are reported. Transitions arising from two conformers have been assigned for both the normal and the deuterated species. A study of the Stark effect has yielded the dipole moment components in the principal axis system for the two conformers and these data, along with the shift in the rotational constants on deuteration, have allowed identification of the conformers. A determination of the quadrupole coupling constants has been made from the observed splittings of some of the lines.

Experimental Section

The sample of 1,2,3,6-tetrahydropyridine was purchased from Aldrich Chemical Co., Inc. and used without further purification. The *N-d* derivative was prepared by successive exchange with NaOD in D₂O. The separation of these miscible solutions was effected by increasing the concentration of NaOD until two layers formed. The spectra were obtained in both the R-band (26.5–40.0 GHz.) and X-band (7–12.4 GHz.) frequency regions with a Hewlett-Packard Model 8400C Stark-modulated phase-stabilized microwave spectrometer. Measurements were made both at room temperature and with the Stark cell packed in dry ice. Methylacetylene ($\mu = 0.7837$ D) and carbonyl sulfide ($\mu = 0.7152$ D) were used to calibrate the Stark cell in R-band, and the $0 \rightarrow 1$ transition of OCS was used for calibration in X-band.⁹ The cell was saturated with D₂O before the introduction of the *N-d* derivative to prevent back-exchange with adsorbed H₂O in the cell. The observation of the relative intensities of D₂O and HOD lines in X band was quite helpful in monitoring the saturation process.

Assignment

A survey scan of the spectrum of 1,2,3,6-tetrahydropyridine in the R-band region is shown in Figure 2. The spectrum is characterized by three groups of rather prominent perpendicular Q-branch transitions of a near oblate symmetric top. The beginning of these series is marked "a", indicating that the complete analysis led to the identification of these transitions as arising from the half-chair axial conformer. Not immediately obvious are three much weaker groups of Q-branch transition marked "e", which correspond to the half-chair equatorial conformer. This spectrum may be compared to that of $\Delta^{3,4}$ -dihydropyran which was reported earlier from this laboratory.⁵ The prominent transitions are the same and the asymmetry parameter, κ , is $\sim +0.8$ in both cases, but the present spectrum is considerably denser due to the presence of the second conformer. It is also noteworthy that the most prominent lines (marked "a") are due to the less abundant conformer, their prominence being due to the selection rules and the relative magnitudes of the *a* components of the dipole moments.

Shown in Figure 3 is a survey scan of the spectrum of the *N-d* derivative. Again there are three prominent groups of lines assigned as perpendicular Q-branch transitions of an oblate near symmetric top molecule. These series are one K_1 higher than the corresponding transitions in the lighter compound reflecting the smaller values of the rotational constants on deuteration. Similarly, the corresponding series for the equatorial conformer are indicated on the figure with an "e".

After Q-branch assignments were made, it was quite simple to locate the $(J+1)_{0,J+1} \leftarrow J_{0,J}$ and $(J+1)_{1,J+1} \leftarrow J_{1,J}$ a type transitions which were coincident in frequency, where $J = 4,$

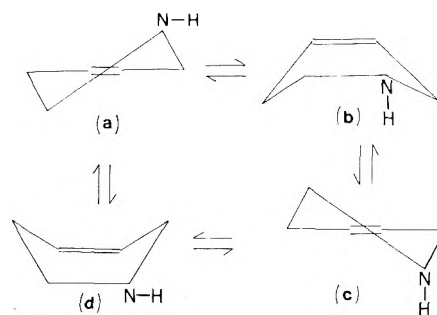


Figure 1. Nonplanar conformations for 1,2,3,6-tetrahydropyridine: (a) half-chair equatorial; (b) half-boat axial; (c) half-chair axial; (d) half-boat equatorial. The arrows indicate possible interconversions by analogy with other cyclohexene analogues.²⁻⁸

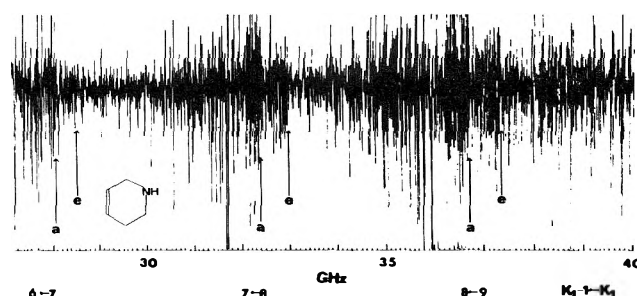


Figure 2. Survey scan of the R-band spectrum of 1,2,3,6-tetrahydropyridine at a Stark field of ~ 300 V/cm. "a" indicates the beginning of perpendicular Q-branch transitions for the axial conformer. "e" indicates the same series for the equatorial conformer.

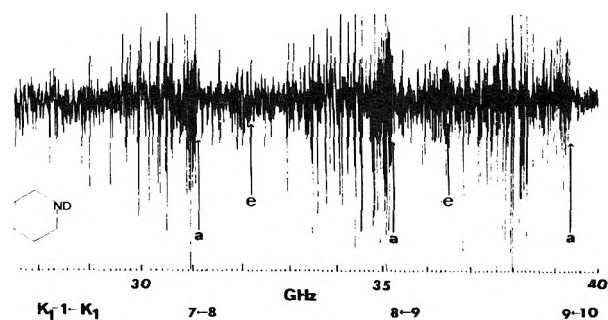


Figure 3. Survey scan of the R-band spectrum of 1,2,3,6-tetrahydropyridine-*N-d* at a Stark field of ~ 300 V/cm. "a" and "e" denote series due to axial and equatorial conformers as in Figure 2.

5, or 6, and the corresponding b type transitions, $(J+1)_{1,J+1} \leftarrow J_{0,J}$; $(J+1)_{0,J+1} \leftarrow J_{1,J}$ also having the same frequency. This assignment, however, left rather large uncertainties in the rotational constants. Due to the density of the spectrum, it was rather difficult to extend the assignment to lower K_1 lines. This difficulty was finally overcome by extending the measurements to X-band and locating the $1 \leftarrow 0$ transitions. The other lines were then predicted rather well from the rotational constants. Measurements were made on a number of the lines in R-band and X-band up to $J = 7$. Higher J lines exhibited noticeable effects of centrifugal distortion.

Tables I–IV indicate the transitions measured, assignments, and the rigid rotor fits for both the axial and equatorial conformers for the normal and for the *N-d* compound. The values of the rotational constants determined from fitting these transitions are summarized in Table V. Some additional high J lines were measured. These transitions exhibit distortion effects and were hence not included in the analysis for the

TABLE I: Transitions Used in the Determination of the Rotational Constants for 1,2,3,6-Tetrahydropyridine (Equatorial Conformer)^a

Transitions	Obsd, MHz	Obsd - calcd, MHz	Transition	Obsd, MHz	Obsd - calcd, MHz
a Type			b Type		
$5_{0,5} \leftarrow 4_{0,4}$	28 674.77	-0.01	$5_{4,2} \leftarrow 5_{3,3}$	11 118.84	-0.14
$5_{1,5} \leftarrow 4_{1,4}$		0.01	$5_{5,1} \leftarrow 5_{4,2}$	8 202.69	-0.13
$5_{3,3} \leftarrow 4_{3,2}$	37 381.27	-0.06	$6_{0,6} \leftarrow 5_{1,5}$	33 970.34	-0.02
$5_{3,2} \leftarrow 5_{3,3}$	10 630.64	-0.11	$6_{1,6} \leftarrow 5_{0,5}$		-0.02
$6_{0,6} \leftarrow 5_{0,5}$	33 970.34	-0.02	$6_{1,5} \leftarrow 5_{2,4}$	38 364.06	-0.07
$6_{1,6} \leftarrow 5_{1,5}$		-0.02	$6_{4,2} \leftarrow 6_{3,3}$	10 366.42	-0.10
$6_{2,5} \leftarrow 5_{2,4}$	38 364.04	-0.10	$6_{5,2} \leftarrow 6_{4,3}$	11 248.10	-0.22
$6_{4,2} \leftarrow 6_{4,3}$	10 312.85	-0.13	$6_{6,1} \leftarrow 6_{5,2}$	8 859.51	-0.31
$7_{0,7} \leftarrow 6_{0,6}$	39 265.89	-0.08	$7_{0,7} \leftarrow 6_{1,6}$	39 625.89	-0.08
$7_{1,7} \leftarrow 6_{1,6}$		-0.08	$7_{1,7} \leftarrow 6_{0,6}$		-0.08
$7_{5,2} \leftarrow 7_{5,3}$	9 858.76	-0.19			
b Type			c Type		
$1_{1,1} \leftarrow 0_{0,0}$	7 598.27	-0.05	$1_{1,0} \leftarrow 0_{0,0}$	9 693.61	0.06
$3_{3,1} \leftarrow 3_{2,2}$	7 228.25	0.14	$3_{1,2} \leftarrow 2_{0,2}$	29 022.64	0.12
$4_{2,2} \leftarrow 3_{3,1}$	31 342.35	-0.05	$3_{2,2} \leftarrow 2_{1,2}$	29 080.74	0.09
$4_{3,2} \leftarrow 3_{2,1}$	32 801.82	0.22	$3_{2,1} \leftarrow 2_{1,1}$	28 779.06	0.08
$4_{4,1} \leftarrow 3_{3,0}$	37 576.20	0.15	$3_{3,0} \leftarrow 2_{2,0}$	29 138.97	0.18
$4_{3,2} \leftarrow 4_{2,3}$	11 042.57	0.04	$3_{3,1} \leftarrow 2_{2,1}$	29 400.94	0.25
$4_{4,1} \leftarrow 4_{3,2}$	7 658.98	-0.09	$4_{2,2} \leftarrow 3_{1,2}$	38 643.39	0.09
$5_{0,5} \leftarrow 4_{1,4}$	28 674.77	0.01	$4_{3,1} \leftarrow 3_{2,1}$	38 390.75	0.12
$5_{1,5} \leftarrow 4_{0,4}$		-0.01	$4_{3,2} \leftarrow 3_{2,2}$	38 785.63	0.01
$5_{3,2} \leftarrow 5_{2,3}$	10 648.67	-0.10	$4_{4,0} \leftarrow 3_{3,0}$	38 916.46	-0.08
			$6_{6,0} \leftarrow 6_{5,2}$	9 622.55	-0.02

^aStandard deviation of the least-squares fit is 0.12 mHz. Observed frequencies have been corrected for the effects of quadrupole coupling.

TABLE II: Transitions Used in the Determination of the Rotational Constants (in MHz) for 1,2,3,6-Tetrahydropyridine-N-d (Equatorial Conformer)^a

Transition	Obsd, MHz	Obsd - calcd, MHz	Transition	Obsd, MHz	Obsd - calcd, MHz
a Type			b Type		
$4_{1,3} \leftarrow 3_{1,2}$	27 139.63	-0.10	$6_{6,1} \leftarrow 6_{5,2}$	9 846.08	0.09
$4_{2,3} \leftarrow 3_{2,2}$	26 993.37	-0.07	$6_{0,6} \leftarrow 5_{1,5}$	33 073.27	0.09
$5_{0,5} \leftarrow 4_{0,4}$	27 918.96	0.13	$6_{1,6} \leftarrow 5_{0,5}$		0.08
$5_{1,5} \leftarrow 4_{1,4}$		0.25	$7_{1,7} \leftarrow 6_{0,6}$	38 227.46	-0.20
$5_{2,3} \leftarrow 4_{2,2}$	36 742.53	-0.06	$7_{0,7} \leftarrow 6_{1,6}$		-0.20
$5_{3,3} \leftarrow 4_{3,2}$	36 333.74	-0.08	$7_{5,2} \leftarrow 7_{4,3}$	9 015.26	-0.21
$6_{0,6} \leftarrow 5_{0,5}$	33 073.27	0.08			
$6_{1,6} \leftarrow 5_{1,5}$		0.09	c Type		
$6_{4,2} \leftarrow 6_{4,3}$	9 386.52	0.19	$1_{1,0} \leftarrow 0_{0,0}$	9 457.50	0.05
$7_{0,7} \leftarrow 6_{0,6}$	38 227.46	-0.20	$3_{3,0} \leftarrow 2_{2,0}$	28 501.21	0.03
$7_{1,7} \leftarrow 6_{1,6}$		-0.20	$3_{2,1} \leftarrow 2_{1,1}$	27 933.18	0.13
$7_{6,2} \leftarrow 7_{4,3}$	12 129.71	-0.16	$3_{3,1} \leftarrow 2_{2,2}$	28 853.06	0.14
b Type			$3_{1,2} \leftarrow 2_{0,2}$	28 243.67	0.12
$4_{2,3} \leftarrow 3_{1,2}$	27 154.89	-0.17	$3_{2,2} \leftarrow 2_{1,2}$	28 372.44	0.08
$4_{4,1} \leftarrow 3_{3,0}$	37 132.75	0.21	$4_{4,0} \leftarrow 3_{3,0}$	38 137.54	-0.06
$4_{4,1} \leftarrow 4_{3,2}$	8 044.43	-0.21	$4_{4,1} \leftarrow 3_{3,1}$	38 504.05	0.00
$5_{0,5} \leftarrow 4_{1,4}$	27 918.96	0.26	$4_{3,1} \leftarrow 3_{2,1}$	37 287.70	-0.04
$5_{1,5} \leftarrow 4_{0,4}$		0.13	$4_{2,2} \leftarrow 3_{1,2}$	37 547.71	-0.04
$6_{4,2} \leftarrow 6_{3,3}$	9 563.62	-0.14	$4_{3,2} \leftarrow 3_{2,2}$	37 855.36	-0.05
			$4_{2,3} \leftarrow 3_{1,3}$	37 770.33	0.02

^aStandard deviation of the least-squares fit is 0.14 MHz. Observed frequencies have been corrected for the effects of quadrupole coupling.

rotational constants; however, some were used in the analysis of the nuclear quadrupole coupling effects.

Stark Effect and the Dipole Moment

With the possibility of three nonzero components of the dipole moment for each of the two conformers, it was necessary to measure the Stark displacements for a number of lines. Due to interference in the X-band region from rather strong HOD and D₂O lines, as well as the presence of impurity lines of the normal compound, the measurement of the Stark effect

for the N-d compound was abandoned and only the Stark effect of the parent molecule was measured.

The calculation of the necessary Stark coefficients was accomplished by the method of Golden and Wilson.¹⁰ Several levels involved in the transitions were near other interacting levels and it was necessary to treat these using degenerate perturbation theory. The transitions used, $|M\rangle$ components, and, where applicable, second-order Stark coefficients determined for the two conformers are given in Table VI. The calculated values of the Stark coefficients represent those

TABLE III: Transitions Used in the Determination of the Rotational Constants of 1,2,3,6-Tetrahydropyridine (Axial Conformer)^a

Transition	Obsd, MHz	Obsd - calcd, MHz	Transition	Obsd, MHz	Obsd - calcd, MHz
a Type			b Type		
1 _{0,1} ← 0 _{0,0}	7 350.76	0.11	4 _{3,2} ← 4 _{2,3}	10 849.38	0.06
3 _{1,2} ← 3 _{1,3}	10 755.55	0.01	4 _{4,1} ← 4 _{3,2}	7 448.19	0.11
4 _{2,2} ← 4 _{2,3}	10 668.52	0.09	5 _{3,2} ← 5 _{2,3}	10 515.66	-0.02
4 _{3,2} ← 4 _{1,3}	10 852.91	0.09	5 _{4,2} ← 5 _{3,3}	10 913.76	-0.04
4 _{1,3} ← 3 _{1,2}	27 644.37	0.00	5 _{5,1} ← 5 _{4,2}	7 940.36	0.06
4 _{2,2} ← 3 _{2,1}	32 326.82	0.11	5 _{0,5} ← 4 _{1,4}	28 574.64	-0.05
4 _{4,1} ← 4 _{2,2}	7 629.08	0.12	5 _{1,5} ← 4 _{0,4}		-0.07
4 _{3,1} ← 3 _{3,0}	35 296.18	0.03	5 _{1,4} ← 4 _{2,3}	32 894.14	0.24
5 _{3,2} ← 5 _{3,3}	10 501.66	-0.06	5 _{2,4} ← 4 _{1,3}	32 897.45	-0.11
5 _{4,2} ← 5 _{2,3}	10 927.75	-0.02	5 _{2,3} ← 4 _{3,2}	37 132.77	0.06
5 _{0,5} ← 4 _{0,4}	28 574.64	-0.07	5 _{3,3} ← 4 _{2,2}	37 327.63	0.07
5 _{1,5} ← 4 _{1,4}		-0.05	6 _{4,2} ← 6 _{3,3}	10 271.16	-0.01
5 _{1,4} ← 4 _{1,3}	32 897.45	0.04	6 _{5,2} ← 6 _{4,3}	11 023.36	0.09
5 _{2,4} ← 4 _{2,3}	32 894.14	0.08	6 _{6,1} ← 6 _{5,2}	8 535.21	-0.03
5 _{2,3} ← 4 _{2,2}	37 313.59	-0.00	6 _{0,6} ← 5 _{1,5}	33 857.65	0.02
5 _{3,3} ← 4 _{3,2}	37 146.63	-0.04	6 _{1,6} ← 5 _{0,5}		0.02
6 _{4,2} ← 6 _{4,3}	10 229.54	-0.08	6 _{1,5} ← 5 _{2,4}	38 177.84	-0.00
6 _{5,2} ← 6 _{3,3}	11 064.71	-0.11	6 _{2,5} ← 5 _{1,4}		-0.16
6 _{6,1} ← 6 _{4,2}	9 328.91	0.02	7 _{5,2} ← 7 _{4,3}	9 938.35	-0.01
6 _{0,6} ← 5 _{0,5}	33 857.65	0.02	7 _{1,6} ← 7 _{0,7}	28 071.38	-0.03
6 _{1,6} ← 5 _{1,5}		0.02	7 _{2,6} ← 7 _{1,7}		-0.03
6 _{1,5} ← 5 _{1,4}	38 177.84	-0.16	7 _{6,2} ← 7 _{5,3}	11 191.00	-0.23
6 _{2,5} ← 5 _{2,4}		-0.01	7 _{7,1} ← 7 _{6,2}	9 231.70	-0.12
7 _{2,6} ← 7 _{0,7}	28 071.38	-0.03	7 _{1,7} ← 6 _{0,6}	39 140.55	-0.03
7 _{1,6} ← 7 _{1,7}		-0.03	7 _{0,7} ← 6 _{1,6}		-0.03
7 _{5,3} ← 7 _{5,2}	9 835.70	-0.18	c Type		
7 _{0,7} ← 6 _{0,6}	39 140.55	-0.03	1 _{1,0} ← 0 _{0,0}	9 606.78	0.14
7 _{1,7} ← 6 _{1,6}		-0.03	3 _{3,0} ← 2 _{2,0}	28 868.60	-0.11
7 _{6,2} ← 7 _{4,3}	11 293.47	-0.24	3 _{3,1} ← 2 _{2,1}	29 109.90	0.08
b Type			4 _{4,0} ← 3 _{3,0}	38 546.50	0.13
1 _{1,1} ← 0 _{0,0}	7 539.11	0.15	4 _{4,1} ← 3 _{3,1}	38 826.40	0.09
3 _{1,2} ← 3 _{0,3}	10 756.23	0.19			
4 _{2,2} ← 4 _{1,3}	10 672.01	0.07			
4 _{2,2} ← 3 _{3,1}	31 197.41	0.07			

^aStandard deviation of the least-squares fit is 0.10 MHz. Observed frequencies have been corrected for the effects of quadrupole coupling.

TABLE IV: Transitions Used in the Determination of the Rotational Constants (in MHz) for 1,2,3,6-Tetrahydropyridine-*N-d* (Axial Conformer)^a

Transition	Obsd, MHz	Obsd - calcd, MHz	Transition	Obsd, MHz	Obsd - calcd, MHz
a Type			b Type		
4 _{2,2} ← 4 _{2,3}	10 220.41	0.05	4 _{2,3} ← 3 _{1,2}	27 182.71	-0.19
4 _{3,2} ← 4 _{1,3}	10 417.32	0.10	4 _{3,2} ← 4 _{2,3}	10 413.11	-0.16
4 _{1,3} ← 3 _{1,2}	27 179.03	0.08	5 _{4,2} ← 5 _{3,3}	10 481.85	-0.05
4 _{2,2} ← 3 _{2,1}	31 679.52	0.20	5 _{0,5} ← 4 _{1,4}	28 232.03	0.08
5 _{3,2} ← 5 _{3,3}	10 043.48	-0.02	5 _{1,5} ← 4 _{0,4}		0.06
5 _{4,2} ← 5 _{2,3}	10 497.55	-0.09	5 _{2,4} ← 4 _{1,3}	32 379.32	-0.08
5 _{0,5} ← 4 _{0,4}	28 232.03	0.06	6 _{4,2} ← 6 _{3,3}	9 803.71	0.14
5 _{1,5} ← 4 _{1,4}		0.08	6 _{5,2} ← 5 _{4,3}	10 598.24	0.10
5 _{1,4} ← 4 _{1,3}	32 379.32	0.11	6 _{0,6} ← 5 _{1,5}	33 463.95	0.04
5 _{2,4} ← 4 _{2,3}	32 375.62	0.18	6 _{1,6} ← 5 _{0,5}		0.04
5 _{2,3} ← 4 _{2,2}	36 625.44	0.11	6 _{1,5} ← 5 _{2,4}	37 608.32	-0.07
5 _{3,3} ← 4 _{3,2}	36 448.28	0.12	6 _{2,5} ← 5 _{1,4}		-0.26
6 _{5,2} ← 6 _{3,3}	10 644.80	-0.12	7 _{5,2} ← 7 _{4,3}	9 460.57	-0.04
6 _{4,2} ← 6 _{4,3}	9 756.74	-0.05	7 _{6,2} ← 7 _{5,3}	10 775.79	-0.23
6 _{0,6} ← 5 _{0,5}	33 463.95	0.04	7 _{7,1} ← 7 _{6,2}	9 007.05	0.08
6 _{1,6} ← 5 _{1,5}		0.04	7 _{0,7} ← 6 _{1,6}	38 695.83	-0.06
6 _{1,5} ← 5 _{1,4}	37 608.32	-0.25	7 _{1,7} ← 6 _{0,6}		
6 _{2,5} ← 5 _{2,4}		-0.08	c Type		
7 _{5,2} ← 7 _{5,3}	9 345.40	0.01	1 _{1,0} ← 0 _{0,0}	9 379.98	-0.20
7 _{6,2} ← 7 _{4,3}	10 891.08	-0.15	3 _{3,0} ← 2 _{2,0}	28 192.41	-0.23
7 _{0,7} ← 6 _{0,6}	38 695.83	-0.06	3 _{3,1} ← 2 _{2,1}	28 434.77	0.25
7 _{1,7} ← 6 _{1,6}		-0.06	4 _{4,0} ← 3 _{3,0}	37 648.59	0.18
			4 _{4,1} ← 3 _{3,1}	37 926.94	0.20
			4 _{2,3} ← 3 _{1,3}	37 495.93	-0.15

^aStandard deviation of the least-squares fit is 0.14 MHz.

TABLE V: Rotational Constants for 1,2,3,6-Tetrahydropyridine^a

	Equatorial (N-H)	Axial (N-H)	Equatorial (N-D)	Axial (N-D)
<i>A</i>	4950.50 ± 0.01	4897.47 ± 0.01	4882.41 ± 0.01	4785.44 ± 0.01
<i>B</i>	4743.05 ± 0.01	4709.16 ± 0.01	4575.05 ± 0.01	4594.74 ± 0.01
<i>C</i>	2647.82 ± 0.01	2641.48 ± 0.01	2577.26 ± 0.02	2616.00 ± 0.01
<i>κ</i>	0.819 814	0.833 056	0.733 329	0.824 201
<i>I_a</i>	102.0856	103.1910	103.5095	105.6070
<i>I_b</i>	106.5508	107.3177	110.4635	109.9901
<i>I_c</i>	190.8649	191.3230	196.0904	193.1865

^a Rotational constants in MHz and moments of inertia in u Å². Conversion factor 505 376 MHz μ Å² from ref 9.

TABLE VI: Stark Coefficients (in MHz cm²/V²) for 1,2,3,6-Tetrahydropyridine

Transition	Axial <i>M</i>	Δ <i>v</i> /E ² × 10 ⁶		Transition	Equatorial <i>M</i>	Δ <i>v</i> /E ² × 10 ⁶	
		Obsd	Calcd ^a			Obsd	Calcd ^a
1 ₁₁ ← 0 ₀₀	0	10.2	10.2	1 ₁₁ ← 0 ₀₀	0	+8.43	+8.20
1 ₀₁ ← 0 ₀₀	0	13.5	13.5	3 ₂₁ ← 2 ₁₁	2	+31.8	+32.1
6 ₀₆ ← 5 _{05b}	5			3 ₃₀ ← 2 ₂₀	1	+7.94	+7.99
	4				2	-3.97	-3.98
	3				1	-1.25	-1.26
	2				0	-0.364	-0.356
	1						
7 ₅₂ ← 7 ₅₃	7	-53.2	-55.8	6 ₆₁ ← 6 ₅₂	6	-28.4	-28.3
	6	-39.5	-41.0		5	-20.1	-19.6
	5	-28.4	-28.5		4	-11.2	-12.5
	4	-18.0	-18.2		3	-6.36	-7.04
	3	-10.5	-10.2				
8 ₆₂ ← 8 ₆₃	8	-18.9	-19.1				
	7	-14.8	-14.6				
	6	-11.0	-10.7				
	5	-7.92	-7.45				
	4	-5.16	-4.76				

^a Calculated using the appropriate Stark coefficients and the dipole components obtained from a least-squares analysis of all the data. See Table VII. ^b 6₀₆ interacts with 6₁₆ and 5₀₅ interacts with 5₁₅, both interactions with a μ_c connection.

calculated employing dipole components obtained from a least-squares fit to all of the measured displacements, including those for transitions which did not exhibit second-order Stark effects. In the case of the axial conformer, 132 measured displacements were fit with a root mean square deviation of 0.38 MHz. The fit to 45 displacements for the equatorial form gave a root mean square deviation of 0.24 MHz. The dipole moment components for each of the conformers are given in Table VII along with the total dipole moments. It is interesting to note the rather dramatic change of the components for the two conformers, while with 99% confidence intervals (approximately three standard deviations) the total dipole moments essentially overlap for the two conformers.

Nuclear Quadrupole Coupling

Several of the lines of the equatorial conformer under conditions of high resolution showed resolvable splitting which can be attributed to nuclear quadrupole coupling from the nitrogen nucleus. Some of the low *J* lines showed resolvable quadrupole fine structure along with some of the higher *J* Q-branch transitions. The quadrupole hyperfine structure can be conveniently treated for an oblate asymmetric rotor in terms of the two coupling constants χ_{cc}, and ηχ_{cc} = χ_{bb} - χ_{aa}. Except for a few low *J* transitions, which were observed as triplets, the remaining lines were observed as doublets. The best values of the quadrupole coupling constants obtained from a least-squares analysis of the observed splittings are

$$\chi_{cc} = -4.48 \pm 0.04 \text{ MHz}, \eta\chi_{cc} = 0.09 \pm 0.09 \text{ MHz}$$

TABLE VII: Dipole Moment Components (in Debye) for the Two Conformers of 1,2,3,6-Tetrahydropyridine^a

	Axial	Equatorial
<i>μ_a</i>	0.757 ± 0.008	0.293 ± 0.003
<i>μ_b</i>	0.530 ± 0.015	0.428 ± 0.005
<i>μ_c</i>	0.401 ± 0.002	0.843 ± 0.005
<i>μ_{total}</i>	1.007 ± 0.006	0.990 ± 0.005

^a Errors listed are twice the standard deviations obtained from a least-squares analysis.

The uncertainties quoted for the coupling constants represent one standard deviation. The observed fine structure was primarily dependent on χ_{cc} and the coupling constant ηχ_{cc} is not well determined. Similar hyperfine structure was observed for the weaker spectrum of N-d derivative of the equatorial form. Most transitions were observed as closely spaced doublets which could be accounted for with a value of χ_{cc} close to that found for the hydrogen compound

$$\chi_{cc} = -4.51 \pm 0.06 \text{ MHz}$$

On the other hand, the hyperfine structure for the axial conformer was quite different from the equatorial form. The high *J* Q-branch lines, which were particularly sensitive to χ_{cc}, did not show any hyperfine structure under similar conditions of resolution. This is illustrated in Figure 4. The lack of ob-

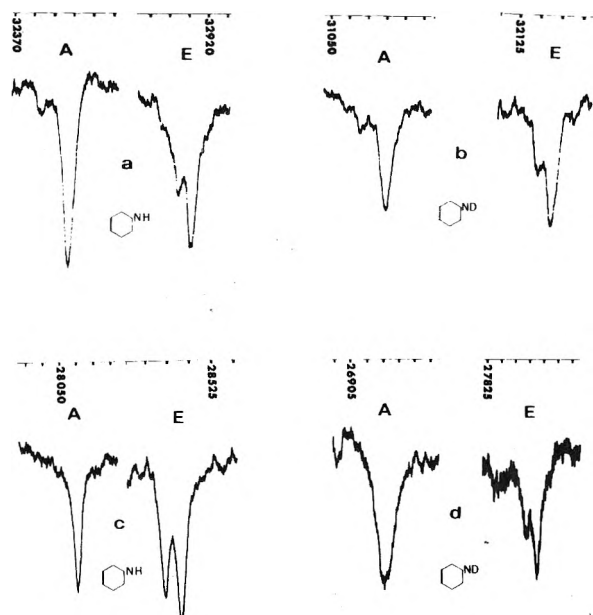


Figure 4. The symbols A and E refer to axial and equatorial. Each line is comprised of four transitions which are coincident in frequency. The separation between the frequency markers is 1 MHz. Transitions in the equatorial form under these conditions of resolution show a splitting while there is no observed splitting for the same transition in the axial form. The quadrupole splitting is primarily dependent on χ_{cc} . (a) The $10_{2,8} \rightarrow 10_{3,7}$ transition. The equatorial line is split by 0.69 MHz. (b) The $10_{2,8} \rightarrow 10_{3,7}$ transition showing the same quadrupole pattern as in (a) for the light compound. (c) The quadrupole pattern of the $9_{3,7} \rightarrow 9_{4,6}$ transition. The equatorial line is split by 0.73 MHz. (d) The $9_{3,7} \rightarrow 9_{4,6}$ transitions showing the same quadrupole pattern as in (c) for the light compound.

served splitting indicates for this conformer a value of $|\chi_{cc}|$ with a magnitude less than 3 MHz. Furthermore, during the course of the analysis of the spectrum it became apparent that the line width for the equatorial and axial forms were different and consistent with smaller quadrupole coupling in the axial form. A more careful look at the Q-branch transitions under conditions of maximum resolution revealed they were doublets split by approximately 0.2 MHz. Measurements of a number of other transitions all with relatively small splittings gave the following coupling parameters for the axial form

$$\chi_{cc} = 1.32 \pm 0.02, \eta\chi_{cc} = 0.72 \pm 0.02$$

These coupling constants are quite different from those obtained for the equatorial conformer. The origin of this result is in the rather different orientations of the principal quadrupole coupling axes with respect to the principal inertial axes in the two conformers. This point is discussed further in the last section.

Intensity Measurements

Knowing the dipole moment components, it was possible to estimate the relative abundance of the two conformers by measuring the relative intensities of a number of lines. This was complicated by the effect of quadrupole splitting or broadening of the lines and the fact that, with a few exceptions, the line widths for the same transition were quite different for the axial and equatorial forms. The identification of the lines corresponding to the different conformers is discussed in the next section. Also, due to the density of the spectrum, it was rather difficult to find lines free from interference by nearby lines.

The intensities of some nine different pairs of lines for the

two conformers were measured. The pressure was adjusted to ensure that we were in the pressure broadened region and the crystal current was matched for the pairs of lines. Also low microwave power was employed to prevent saturation effects. Since the line widths were usually different for a given pair of lines, the ratio of the area under the absorption line was used rather than the line heights. The line area or integrated absorption coefficient is proportional to the product of the line height and the half-width of the line. Despite this there was still a fair spread in values of the energy difference determined, the final result being that the equatorial form is more stable by $50 \pm 30 \text{ cm}^{-1}$ ($\sim 0.14 \text{ kcal/mol}$). The quoted uncertainty is twice the standard deviation. The temperature dependence of a few pairs of lines was also studied and the results were consistent with the equatorial form being the lower energy conformer in that lines attributable to the equatorial conformer invariably increased relative to the lines of the axial conformer when the temperature was lowered to that of dry ice.

This result was somewhat surprising based on the survey spectra (Figures 2 and 3) in which the lines due to the less abundant axial form are by far the most prominent. Examination of the dipole components in Table VII, however, yields an explanation. The most prominent transitions are perpendicular Q-branch transitions of a near oblate top $K_1 - 1 \leftarrow K_1$. For low J , each line is actually four overlapped lines, two a type and two b type. As J increases, these split into doublets, each being an overlapped a,b pair. Further increase in J splits the lines into a quartet. From Table VII, it is noted that the b components of the dipole moments of the two conformers are comparable, while the a component of the axial form is considerably larger than that of the equatorial form. This accounts for the greater intensity of the prominent Q-branch transitions of the axial form.

Results and Discussion

From the analysis of the microwave spectrum, lines attributable to two distinct conformers of 1,2,3,6-tetrahydropyridine have been assigned. It is possible to put the identification of the conformers on a firmer basis by demonstrating that the experimental data can be reproduced using structural parameters that are quite reasonable based on the values reported for related molecules. In particular, we used as starting values for the calculations, the structural parameters reported for propylene¹¹ and dimethylamine.¹² In addition to the six rotational constants for each conformer, three for each of the isotopic species, the dipole moment components gave us additional information (Table VII). As was noted earlier, the dipole moment for $\Delta^{3,4}$ -dihydropyran (1.28 D)⁵ is virtually identical with that in dimethyl ether (1.30 D)¹³ and the components are quite consistent with the molecular dipole moment almost parallel to the C–O–C bisector, which is, of course, the direction of the dipole moment in dimethyl ether. As seen from Table VII, the dipole moments of the two conformers of tetrahydropyridine are extremely close to that of dimethylamine (1.01 D).¹² By assuming that the dipole moment was oriented halfway between the N–H bond and the CNC bisector, i.e., essentially along the lone pair on the nitrogen, we were able to calculate the principal axis components of the dipole moment, as well as the rotational constants for the various assumed structures. The direction chosen for the dipole moment vector is within 2.5° of the direction of the dipole vector in dimethylamine.¹²

We were not attempting a rigorous structure determination with the limited data and in this spirit assumed equality be-

TABLE VIII: Structural Parameters Used for 1,2,3,6-Tetrahydropyridine^a

Parameter	Uncertainty	Axial conformer ^b	Equatorial conformer ^b
C=C 1.34 Å	±0.01 Å	1.337 Å	1.336 Å
=C-C 1.51 Å	±0.02 Å	1.512 Å	1.505 Å
C-N 1.47 Å	±0.03 Å	1.467 Å	1.471 Å
-C-C 1.53 Å	±0.02 Å	1.532 Å	1.534 Å
∠C-C=C 122°	±3°	122.3°	122.7°
∠C-C-N 113°	±3°	114.1°	109.7°
τ 30° ^c	±5°	28.1°	33.2°

^a The hydrogen parameters are not varied in the fit but fixed so that =C-H = 1.09 Å and lies on the ∠C-C=C bisector; -C-H = 1.10 Å, ∠HCH = 109° 28' and shares a common bisector with the interior ring angle. N-H = N-D = 1.02 Å and makes an angle of 125° with the bisector of ∠C-N-C in a plane perpendicular to the C-N-C plane.

^b These do not represent the true structural parameters but represent a set which reproduce the experimental data with a minimum distortion of the original set based on the estimated uncertainties. ^c τ is the angle between the plane containing the nitrogen atom, carbon 2, and the midpoint of the C₃-C₆ line, and the C₃-C₄=C₅-C₆ plane.

tween certain structural parameters that are not symmetrically equivalent. For example, the two nonequivalent C-N distances were assumed to be equal. This considerably reduced the number of adjustable parameters. In addition, since the hydrogen parameters have only a minor effect, we fixed their values at the assumed values. With all of these assumptions, we were fitting nine experimental data for each conformer, three rotational constants for each of the two isotopic species and three dipole moment components for the light compound, with seven adjustable parameters. In principle the parameters are over determined and may be adjusted by least-squares fitting the data. In fact, the matrix of coefficients of the normal equations was very nearly singular indicating that the data are not sensitive to some of the parameters. There are other causes of difficulty arising from the fact that the assumption of equality between symmetrically nonequivalent parameters and the fixing of the values of other parameters might have required artificially large adjustments in the other parameters to compensate and reproduce the experimental data. A procedure which avoids these pitfalls has been described by Curl.¹⁴ In this procedure, the parameters are weighted by the inverse of their estimated uncertainties, the matrix of coefficients of the normal equations diagonalized, and the eigenvalues compared to an estimated standard deviation for the experimental data. Only the eigenvectors for those eigenvalues greater than the squared standard deviation are used to compute the shift in the parameters. In the calculations on tetrahydropyridine only four of the seven eigenvectors were used for each of the conformers. This is equivalent to fitting the experimental data *not* with seven parameters, but with four linear combinations of the seven parameters which are sensitive to the experimental data. The assumed parameters and their estimated uncertainties are given in Table VIII. Also indicated in the table are the values of the parameters adjusted by the procedure described above to reproduce the experimental data for the axial conformer and for the equatorial conformer. Only minor adjustments in the parameters have been made to fit the data. Table IX indicates the observed and calculated values of the rotational constants and dipole moment components. It is seen that all of the data are quite adequately reproduced with the possible exception of μ_b , and, to a lesser extent, μ_c for the

TABLE IX: Observed and Calculated Rotational Constants and Dipole Moment Components for 1,2,3,6-Tetrahydropyridine

	Axial		Equatorial	
	Obsd	Calcd	Obsd	Calcd
	N-H		N-H	
A	4897.47	4894.99	4950.50	4954.37
B	4709.16	4712.58	4743.05	4741.53
C	2641.48	2642.55	2647.82	2651.74
μ_a	0.757	0.706	0.293	0.278
μ_b	0.530	0.561	0.428	0.169
μ_c	0.401	0.431	0.843	0.946
	N-D		N-D	
A	4785.44	4787.99	4882.41	4882.29
B	4594.74	4590.36	4575.05	4576.23
C	2616.00	2617.09	2577.26	2580.37

^a Rotational constants in MHz; dipole components in Debye units.

equatorial conformer. This can be remedied by a more flexible model, i.e., one in which the two nonequivalent C-N-H angles are adjusted independently while the dipole vector follows the direction of the lone pair. However, considering the nature of the approximation involved in transferring the dipole moment from dimethylamine in the first place, it was felt that the discrepancy was not serious and that little was to be gained. The major features for the two conformers, i.e., the dramatic change in μ_a and μ_c between the two is quite well represented.

Much more difficult to describe is the fact that the data cannot be adequately reproduced by bent (half-boat) conformations. Much of the discussion for $\Delta^{3,4}$ -dihydropyran⁵ applies in this case and will not be repeated here. Suffice it to say that it is not possible to reproduce the rotational constants, much less the dipole moment components, by transferring structural parameters from dimethylamine and propylene with half-boat forms and restricting the range over which the parameters are allowed to vary. Aside from attempting to reproduce the experimental data, a few calculations quickly show that it is impossible to fix the C=C-C angles near 120°, maintain normal bond distances, and have the other interior ring angles anywhere near their expected values. This is particularly true of the C-N-C angle and the N-C₂-C₃ angle.

Several other interesting points arose in considering the data for 1,2,3,6-tetrahydropyridine. Table VIII indicates the similarity of the structural parameters which reproduce the experimental data for each conformer, with the exception of ∠C-C-N and the twist angle τ (~28° as opposed to ~33°). These differences in the ring structure lead to some interesting comparisons of the data for the two conformers and these are summarized in Table X. Figure 5 indicates the approximate orientation of the c principal axis in the molecule. The principal z axis of the quadrupole tensor is also indicated. The orientation of the latter is assumed to be the same as in dimethylamine and lies essentially along the nitrogen lone pair.

One thing that was found was that the change in the C rotational constant between the conformers for the light compound was not a reliable criterion for distinguishing between the conformers. Examination of Figure 5 indicated that the imino hydrogen is much closer to the c axis in the axial form and that, if the ring structure is invariant, the C rotational constant for the axial conformer should be larger. The first entry in Table X indicates the range of values for the difference in C rotational constants calculated for a series of ring structures. The observed shift in C is in the opposite direction,

TABLE X: Comparison of Data for the Two Conformers of 1,2,3,6-Tetrahydropyridine

$(C_{ax} - C_{eq})^a$, MHz	Calcd +45 to +60		Obsd -6.33	
	Axial		Equatorial	
	Calcd	Obsd	Calcd	Obsd
$(C_H - C_D)^a$, MHz	+27.5 to +19.2	+25.48	+68.5 to +73.0	+70.56
c^b , Å	1.30	1.29	0.21	0.24
χ_{cc}^b , MHz	+1.03	+1.32	-4.53	-4.48
$\eta\chi_{cc}^b$, MHz	+1.47	+0.72	+0.25	+0.09

^a Calculated values are for dimethylamine and propylene structural parameters for a range of twist angles, $\tau = 25-35^\circ$ in 2.5° increments. ^b Calculated values for the parameters in Table VIII.

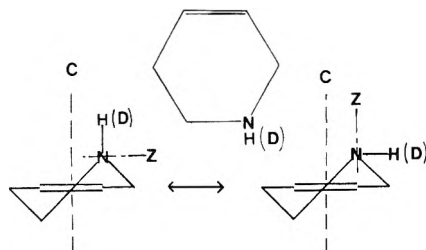


Figure 5. Approximate orientation of the c principal axis for the axial and equatorial conformers. The approximate orientation of the principal z axis of the quadrupole coupling tensor is also included.

indicative of the change in ring structures between the conformers (Table VIII).

On the other hand, the change in the C rotational constant on deuteration or the c substitution coordinates derived for the imino hydrogen by applying the Kraitchman equations¹⁵ clearly allow identification of the conformers (Table X). The agreement is quite reasonable, particularly considering that the N-H parameters were fixed in the adjustment procedure.

Consideration of the relative orientations of the c principal inertial axis and the z principal quadrupole axis shown in Figure 5 clearly shows that one expects quite different values of χ_{cc} for the two forms. A detailed calculation has been made assuming the principal axis coupling constants ($\chi_{xx} = 3.04$ MHz, $\chi_{yy} = 2.01$ MHz, $\chi_{zz} = -5.05$ MHz) and principal quadrupole axis orientation of $(\text{CH}_3)_2\text{NH}$.¹² Transforming the coupling tensor to the principal inertial axis system for the two conformers yields the calculated values in Table X. Considering the nature of the approximations involved in transferring the principal axis coupling constants from dimethylamine and the uncertainties in these constants,¹² it is gratifying that quite reasonable agreement in sign and magnitude is obtained using structural parameters adjusted on the basis of data independent of the quadrupole coupling (Table IX). This agreement is consistent with the electronic environment or bonding to the nitrogen atom being basically the same in both conformers and very similar to that in dimethylamine.

Another qualitative consideration leads to the same conclusion as to the identity of the conformers. Referring again to Figure 5 and considering the dipole moment components in Table VII, it is seen that the relative magnitudes of the c components of the dipole moments for the two conformers are consistent with the identification of the conformers. One would expect the c component of the dipole moment of the equatorial conformer to be quite large considering the position of the electronegative nitrogen relative to the other atoms. Alternatively, in the axial form, the imino hydrogen is on one side of the nitrogen while the rest of the ring is on the other side and, due to partial cancellation, a small c component is

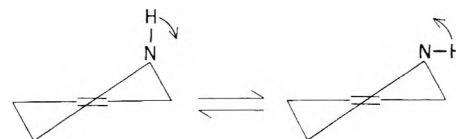


Figure 6. Alternate pathway for interconversion of the stable conformers of 1,2,3,6-tetrahydropyridine via the N-H rocking motion. Compare this with the path indicated in Figure 1.

expected. These observations are quite consistent with the components listed in Table VII and with the identification of the conformers.

In summary, two conformers of 1,2,3,6-tetrahydropyridine have been found, both with half-chair ring skeletons: one with the imino hydrogen axial, the other equatorial. The rotational constant data indicate the ring structures are slightly different. On the other hand, the total dipole moments are virtually identical, and the same as in dimethylamine, although the distribution among the principal axis components is markedly different. This is consistent with the orientation of the principal axes and the electronegativities of the atoms. In addition, the principal axis quadrupole coupling constants for dimethylamine¹² account reasonable well for the coupling constants determined for the two conformers, taking into account the relative orientations of the principal axes of the inertial and quadrupole coupling tensors, respectively.

Consideration of alternate pathways for interconversion of the two conformers leads to several interesting points. One way this may be accomplished is through a path similar to that found for cyclohexene and some of its oxygen analogues and is illustrated in Figure 1. In this path, interconversion proceeds via intermediate half-boat forms. Interconversion via the planar form for the ring skeleton for the cyclohexene analogues involve barriers of 19–25 kcal/mol, while interconversion via the half-boat conformers involve barriers of 6–10 kcal/mol. On the other hand, the interconversion may occur via the rocking motion of the N-H, illustrated in Figure 6. Barriers for this in other N-H compounds range from 4 to 10 kcal/mol.^{12,16} It is not clear which of these paths is the lowest energy path for tetrahydropyridine. If the N-H rocking is the lowest energy path, this is certainly accompanied by some mixing of the other motion since the experimental data definitely indicate some relaxation of the ring between the axial and equatorial conformers.

By analogy with the other molecules studied, we are probably safe in putting a lower limit of 3000 cal/mol on the interconversion process. The energy difference between the two conformers is only 140 cal/mol. Thus we have two conformers differing only slightly in energy separated by a high (but unknown) barrier. If the barrier to interconversion is ~ 5 kcal/mol or higher it should be possible to determine it by line shape

analysis of the temperature dependence of the ^{13}C magnetic resonance spectrum. We are planning to carry out these experiments.

Acknowledgments. This paper is dedicated to Professor Richard C. Lord on his retirement as Director of the Spectroscopy Laboratory at M.I.T. Acknowledgment is made to the Donors to the Petroleum Research Fund administered by the American Chemical Society for the partial support of this research. Acknowledgment is made to the Research Corporation for a Cottrell Grant.

References and Notes

- (1) Research Associate with R. C. Lord, Spectroscopy Laboratory, M.I.T., March 1970–September 1971; June–September 1972; June–September 1975.
- (2) (a) L. H. Scharpen, J. E. Wollrab, and D. P. Ames, *J. Chem. Phys.*, **49**, 2368 (1968); (b) T. Ogata and K. Kozima, *Bull. Chem. Soc. Jpn.*, **42**, 1263 (1969).
- (3) J. Sheridan, private communication.
- (4) J. A. Wells and T. B. Malloy, Jr., *J. Chem. Phys.*, **60**, 2132 (1974).
- (5) J. A. Wells and T. B. Malloy, Jr., *J. Chem. Phys.*, **60**, 3987 (1974).
- (6) R. C. Lord, T. C. Rounds, and T. Ueda, *J. Chem. Phys.*, **57**, 2572 (1972).
- (7) J. R. Durig, R. O. Carter, and L. A. Carreira, *J. Chem. Phys.*, **60**, 3098 (1974).
- (8) T. B. Malloy, Jr., Thirtieth Annual Symposium on Molecular Structure and Spectroscopy, The Ohio State University, Columbus, Ohio, June 16–20, 1975, Paper WE 12.
- (9) W. Gordy and R. L. Cook, "Microwave Molecular Spectra", Wiley-Interscience, New York, N.Y., 1970, p 357, Table 10.10.
- (10) S. Golden and E. B. Wilson, Jr., *J. Chem. Phys.*, **16**, 669 (1948).
- (11) D. R. Lide, Jr., and D. E. Mann, *J. Chem. Phys.*, **27**, 868 (1957).
- (12) J. E. Wollrab and V. W. Laurie, *J. Chem. Phys.*, **48**, 5058 (1968).
- (13) U. Blukis, P. H. Kasai, and R. J. Meyers, *J. Chem. Phys.*, **38**, 2753 (1963).
- (14) R. F. Curl, *J. Comp. Phys.*, **6**, 367 (1970).
- (15) J. Kraitchman, *Am. J. Phys.*, **21**, 17 (1953).
- (16) M. K. Kemp and W. H. Flygare, *J. Am. Chem. Soc.*, **90**, 6267 (1968).

Raman Spectrum and Torsional Potential Function of Acrolein

L. A. Carreira[†]

Department of Chemistry, University of Georgia, Athens, Georgia 30601 (Received October 28, 1975)

A series of six lines in the Raman spectrum of acrolein has been observed and assigned as torsional overtones. The data have been analyzed using a potential function of the form $V(\phi) = \sum_i (V_i/2)(1 - \cos i\phi)$. The less stable species is found to be in the cis configuration with a cis–trans energy difference of $584 \pm 180 \text{ cm}^{-1}$. The barrier for trans \rightarrow cis interconversion was found to be $2236 \pm 135 \text{ cm}^{-1}$. An analysis as to the origin of the potential terms is attempted.

Introduction

Acrolein has been the subject of a great many conformational studies. Both microwave¹ and electron diffraction² studies have shown the trans conformer to be the most stable. The ultraviolet investigations of acrolein by Alves³ et al. and Bair⁴ et al. have shown the existence of a second conformer $660 \pm 40 \text{ cm}^{-1}$ less stable than the trans conformer but these studies could not determine whether the less stable species was in the cis or gauche conformation. De Groot and Lamb⁵ studied the trans–cis (gauche) isomerism in the liquid state and found the less stable species to lie 720 cm^{-1} above the ground state with a barrier for trans–cis (gauche) interconversion of 2460 cm^{-1} .

In principle, if one could accurately determine the potential function governing the torsion about the C–C single bond, the twist angle of the second conformer, its height above the ground state, and the barrier separating it from the ground state could be determined. The potential function hindering internal rotation about the C–C single bond is of the form

$$V(\phi) = \sum_i \frac{V_i}{2} (1 - \cos i\phi)$$

where $\phi = 0$ corresponds to the stable trans configuration. Fateley⁶ et al. and Harris⁷ have attempted to obtain the constants, V_i , by observing the torsional transitions in the far-infrared spectrum of acrolein but, under their experimental conditions, were only able to observe the fundamental at 157

cm^{-1} . This allowed them to calculate the quantity $V^* = \sum_i i^2 V_i = 21.2 \text{ kcal/mol}$. More recently Cole and Green⁸ have investigated the infrared active torsion of acrolein under higher resolution and observed the fundamental and several excited state transitions associated with the trans well. They were unable to see any torsional transitions in the less stable well and were only able to calculate the quantities $V^* = \sum_i i^2 V_i = 21.7 \text{ kcal/mol}$ and $V_d = \sum_i i^4 V_i = 31.3 \text{ kcal/mol}$. The V_i parameters cannot be calculated separately since the second differences (after perturbation correction⁸) were all about the same.

In light of the success of gas phase Raman spectroscopy in the determination of the torsional potential function in 1,3-butadiene⁹ an investigation of the low frequency gas phase Raman spectrum of acrolein has been undertaken.

Experimental Section

The freshly distilled sample of acrolein was obtained from Chemical Samples Co. The sample was contained at its vapor pressure in a standard gas cell with Brewster angle windows. The Raman spectra were recorded with a Spex Ramlog spectrophotometer equipped with a Spectra Physics 164-03 argon ion laser which produced 1 W of power in the $4880\text{-}\text{\AA}$ line at the sample. At room temperature the sample was stable for long periods. Decomposition was a problem at elevated temperatures but produced no new lines in the spectral range of interest, causing only a decrease in Raman signal.

TABLE I: Observed and Calculated Raman Overtone Transitions for the Torsional Mode of Acrolein

Transition ^a	Inferred ^b from ir	Obsd Raman, cm ⁻¹ (ir)	Obsd - calcd ^c	Calcd rel Intensity
0T-2T	314.8	315.8	0.7	1.0
1T-3T	312.4	311.8	-1.2	1.4
2T-4T	311.2	311.8	+1.2	1.3
3T-5T	308.5	308.0	0.4	0.9
4T-6T		303.4	0.2	0.7
0C-2C		273.0	0.1	0.2
1C-3C		264.0	-0.1	0.2
0T-1T		(158.6)	0.0	
1T-2T		(156.2)	-0.3	
2T-3T		(156.2)	-0.3	
3T-4T		(155.0)	0.2	
4T-5T		(153.5)	0.7	

^a 0T designated the lowest energy level whose wave function is confined to the trans well, 0C the lowest in the cis well. ^b Obtained from sums of single jump frequencies (peak maxima) found in ref 8. ^c Calculated using the potential function $V = (306.1/2)(1 - \cos \phi) + (1918.5/2)(1 - \cos 2\phi) + (338.0/2)(1 - \cos 3\phi) - (96.2/2)(1 - \cos 4\phi) - (57.6/2)(1 - \cos 5\phi)$ and a perturbation correction of 1.2 cm^{-1} see text and Figure 2.

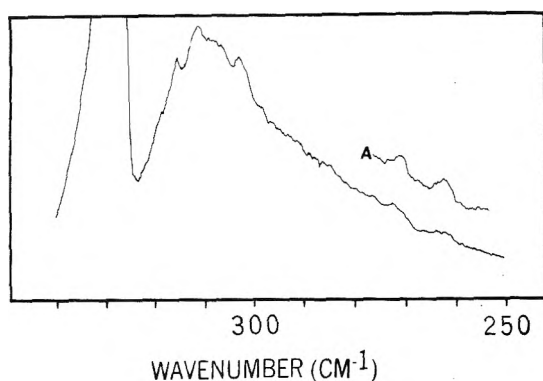


Figure 1. Low-frequency Raman spectrum of acrolein recorded with a special slit width of 2.0 cm^{-1} at its vapor pressure at room temperature. The intensity is in arbitrary units. Spectrum A taken at 30°C .

Results

The low frequency Raman spectrum of the torsional overtones in acrolein is shown in Figure 1. The spectrum is very similar to that obtained for 1,3-butadiene. There are two "clumps" of lines. A stronger series beginning at 315.8 cm^{-1} and a weaker series beginning at 277.4 cm^{-1} . At elevated temperatures the higher vapor pressure of acrolein allowed an enhancement of signal in the region below 280 cm^{-1} , but rapid decomposition did not allow a reliable temperature study to be made. The first few $\Delta V = 2$ torsional transitions observed in the Raman spectrum compare favorably with sums of the $\Delta V = 1$ transitions observed by Cole and Green.⁸ The V_{13} bend appears at 327 cm^{-1} . All frequencies reported here are the Q branch maxima and may be displaced somewhat from the true band center.^{8,9}

Discussion

The preliminary analysis of the observed spectrum is straightforward in light of the analysis of the 1,3-butadiene spectrum.⁹ The first few Raman lines in the strong series compare favorably with the appropriate sums of the $\Delta V = 1$ torsional transitions observed by Cole and Green⁸ and are

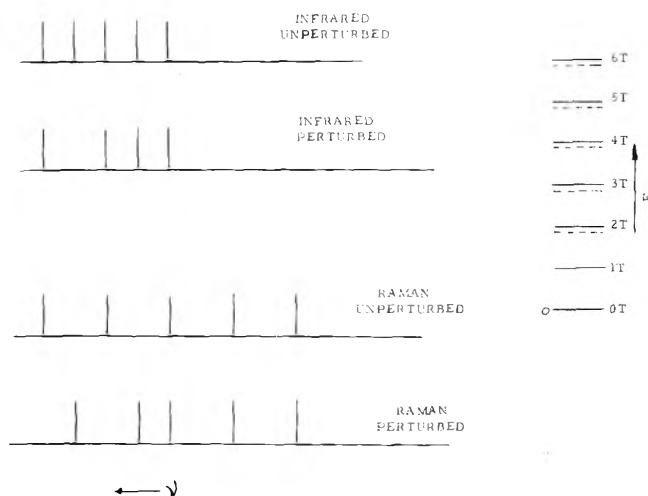


Figure 2. Pictorial representation of perturbation effects on the infrared and Raman spectrum of the torsional mode in acrolein.

assigned as $\Delta V = 2$ torsional transitions associated with the stable trans species. The weaker series has been assigned as $\Delta V = 2$ overtone transitions associated with the less stable species.

The Fermi resonance effects observed by Cole and Green⁸ have been confirmed in the Raman spectrum of acrolein. Brand¹⁰ first suggested a possible Fermi resonance between $V_{18} = 2 \{0,2\}$ and $V_{13} = 1 \{1,0\}$ and was later invoked by Cherniak and Costain¹ to explain anomalies in the rotational constants of torsionally excited molecules. Torsional levels $V_{18} = 2$ and above will be slightly perturbed by interactions of the sort $\{1,0\} \leftrightarrow \{0,2\}$, $\{1,1\} \leftrightarrow \{0,3\}$, $\{1,2\} \leftrightarrow \{0,4\}$, etc. Cherniak and Costain found all torsional satellite lines except the first were displaced equally implying Fermi resonance affects all torsional levels above $\{0,1\}$ equally. This was shown to be the case in the infrared spectrum and is confirmed here. The levels above $\{0,1\}$ appear to all be shifted to lower frequency by $1.2\text{--}1.6 \text{ cm}^{-1}$. In the far-infrared spectrum this shows up as an apparent "missing line" since the second differences are about 1.4 cm^{-1} (see Figure 2). In the Raman spectrum the second differences are twice as large and the effect is to make one line appear as an unresolved closely spaced doublet (see Figure 2). The spacing of this doublet can be roughly predicted from the results of Cole and Green⁸ to be about 1.2 cm^{-1} . Before fitting the observed Raman lines to a potential of the form $V(\phi) = \sum_i (V_i/2)(1 - \cos i\phi)$ the $\nu_{0 \rightarrow 2}$ and $\nu_{1 \rightarrow 3}$ transitions in the trans well were corrected for perturbation effects by adding 1.2 cm^{-1} to the observed frequencies.

As in 1,3-butadiene, resonance stabilization is expected to play a major role in determining the torsional potential function of acrolein. This would lead to stabilization of the planar trans and cis conformations and introduce a large V_2 term into the torsional potential function. One would also expect nonbonded interactions in the cis configuration to be larger than in the trans configuration. This type of interaction will introduce a V_1 term into the torsional potential function. If one uses the Pauling¹¹ model of a double bond as two bent single bonds, then the symmetry about the single bond in acrolein would be essentially trigonal introducing a sizable V_3 term into the torsional potential function to represent the bond-bond interactions. Therefore, it is expected that the first three terms will be the largest and as a first approximation the torsional potential function was chosen as $V(\phi) = \sum_{i=1}^3 (V_i/2)(1 - \cos i\phi)$. The Hamiltonian would then be of the form

TABLE II: Cartesian Coordinates Used for the Calculations of the F Number for the Cis Configuration of Acrolein

Atom	X	Y	Z
O	0.0	0.505 939	1.376 529
C	0.0	-0.513 442	0.719 814
C	0.0	-0.600 367	-0.756 873
C	0.0	0.529 089	-1.492 349
H	0.0	-1.497 393	1.239 378
H	0.0	-1.567 709	-1.270 153
H	0.0	0.484 450	-2.584 422
H	0.0	1.513 193	-1.020 917

$$H = -\frac{d}{d\phi} F(\phi) \frac{d}{d\phi} + \sum_{i=1}^3 \frac{V_i}{2} (1 - \cos i\phi)$$

where $F = h/8\pi^2 c I_\gamma$, and I_γ is the reduced moment of inertia as defined by Pitzer.¹² The F value changes dramatically as the torsional angle (ϕ) is increased. In order to better represent the potential function^{9,13} F was not taken as a constant but represented as a cosine series of the form $F(\phi) = F_0 + \sum_i F_i \cos i\phi$. The series converges rapidly yielding (in cm^{-1}) $F_0 = 3.586$, $F_1 = -0.7674$, $F_2 = 0.3882$, $F_3 = -0.1192$, and $F_4 = 0.0584$. The structures used in calculating the F numbers at several values of the torsional angle were obtained from the molecular mechanics program of Allinger.¹⁴ This program reproduced the trans structure well and opened the C=C-C and O=C-C angles 1.5 and 1.4°, respectively, as the torsional angle increased to 180°. The C-C bond was slightly longer at a torsional angle of $M\pi/2$. The structure used in determining the F number at 180° is given in Table II.

A computer program modeled after that of Lewis¹³ et al. was written to calculate the energy levels and wave functions associated with the above Hamiltonian. The Hamiltonian matrix was set up in a plane rotor ($\exp(i\ell\phi)$) basis and rotated to the symmetry adapted sin-cos basis. Seventy basis functions were used in the calculation. The program was written to handle potential terms up to V_6 and kinetic terms up to F_6 . The potential constants were iterated in a least-squares manner in order to fit both the observed $\Delta V = 2$ torsional transitions and the $\Delta V = 1$ transitions observed by Cole and Green.⁸ After this preliminary determination of the potential function higher order terms up to V_6 were added to see if they would improve the fit. The addition of small V_4 and V_5 terms very slightly improved the fit and were allowed to remain. The potential constants thus determined are $V_1 = 306 \pm 100 \text{ cm}^{-1}$, $V_2 = 1919 \pm 70 \text{ cm}^{-1}$, $V_3 = 338 \pm 13 \text{ cm}^{-1}$, $V_4 = -96 \pm 5 \text{ cm}^{-1}$, and $V_5 = -57 \pm 9 \text{ cm}^{-1}$ where the error limits were estimated from the variance covariance matrix generated in the least-squares procedure and the uncertainties in the F numbers. The calculated and observed frequencies are listed in Table I. This potential leads to minima at 0 (trans) and 180° (cis). Therefore the less stable species of acrolein is calculated to be in the cis rather than the gauche configuration. The large uncertainty in V_1 is due to the fact that this term has little effect on the first or second differences observed. A more lengthy explanation using the results of first-order perturbation theory is given in ref 9.

Recently Durig¹⁵ et al. have reinterpreted the torsional overtone progression observed⁹ in the gas phase Raman spectrum of 1,3-butadiene. In attempting to reproduce the F number given for the cis configuration of 1,3-butadiene Durig et al. opened only the C=C-C angles while leaving all other internal parameters fixed at the same values as in the trans configuration. This led them to believe that the opening of the

C=C-C angles used in ref 9 were "exaggerated". Actually the C=C-C angles used in ref 9 were only opened 3.5°. This is in good agreement with the theoretical calculation of Radom and Pople¹⁶ and is similar to the behavior found experimentally for glyoxal by Ramsay and Zauli.¹⁷ In calculating the F numbers for 1,3-butadiene and acrolein all internal parameters were varied for each angle, ϕ , and these relaxed geometries were used in calculating $F(\phi)$. It is felt that the geometries used in ref 9 were more realistic than those generated by Durig et al.

By using only a frequency fit to the observed transitions, Durig et al. were able to find two other potential functions which reproduced the spectroscopic frequency data. Unfortunately when one uses the wave functions calculated for these two other potential functions to calculate relative intensities, the calculated values deviate greatly from the observed values. For their potential function where the second stable form is the cis conformer, the calculated intensity ratio of $\nu_{0 \rightarrow 2}^{\text{trans}}/\nu_{0 \rightarrow 2}^{\text{cis}}$ is off by a factor of 3. For their potential function where the second stable form is the gauche conformer, the calculated intensities for the $\nu_{3 \rightarrow 4}^{\text{gauche}}$ and $\nu_{3 \rightarrow 5}^{\text{gauche}}$ are nearly the same but no $\nu_{3 \rightarrow 5}$ transition was observed although the $\nu_{2 \rightarrow 4}$ transition was easily seen. Therefore when dealing with asymmetric potential functions relative intensity data are often useful in alleviating this type of uniqueness problem.

Most of the uncertainty in the conformational energy difference comes from the uncertainty in the V_1 term. In order to alleviate any uniqueness problems due to the insensitivity of the V_1 term, the relative intensities at room temperature were used as additional data in fitting the potential constants. The relative intensities of the $\nu_{0 \rightarrow 2}^{\text{trans}}$ and $\nu_{0 \rightarrow 2}^{\text{cis}}$ transitions are very sensitive to the magnitude of the V_1 term and were used in the fitting procedure. The fact that the cis configuration is found to be more stable than the gauche configuration is related to the result that the quantity $\sum_i (-1)^i i^2 V_i$ is positive. This quantity remains quite positive at all extremes of the error limits.

Since the peak maxima for the Raman $\Delta V = 2$ transitions compare favorably with sums of the appropriate peak maxima for the $\Delta V = 1$ transitions the band centers for the $\Delta V = 2$ transitions are expected to be about 1 cm^{-1} displaced from their peak maxima. This correction could have been made for the trans lines but the correction (both magnitude and sign) is not known for the cis lines. In the above analysis peak maxima were always used and the uncertainty in frequencies was taken as 2.0 cm^{-1} and the uncertainty in second differences as 0.5 cm^{-1} .

As in the case of 1,3-butadiene, the relative intensities cannot be explained by a simple Boltzmann factor argument since the $\nu_{0 \rightarrow 2}$ transition in the cis well is considerably weaker than the $\nu_{3 \rightarrow 5}$ transition in the trans well although they both occur from roughly the same energy (see Figure 3). As in the case of 1,3-butadiene the relative intensities of these transitions can be calculated using the equation

$$I \propto e^{-(\Delta E/kT)} \langle \psi_V | \alpha_{\text{op}} | \psi_V \rangle$$

where the polarizability operator (α_{op}) used⁹ transforms like $\cos \phi$. The calculated relative intensities are given in Table I. Unfortunately, a temperature study of the relative intensities was impossible since at higher temperatures the acrolein polymerized rapidly.

A comparison of the potential constants of acrolein with those of 1,3-butadiene is given in Table III. For 1,3-butadiene⁹ and acrolein the V_2 terms are quite large (2068 and 1919 cm^{-1} , respectively) and of nearly the same magnitude. The second

TABLE III: Comparison of Potential Constants Obtained for Acrolein and 1,3-Butadiene

	V_1	V_2	V_3	V_4	V_5	V_6	Barrier trans-cis	$E_{cis} - E_{trans}$
1,3-Butadiene	600	2068	273	-49			2504	873
Acrolein	306	1919	338	-96	-57		2236	584

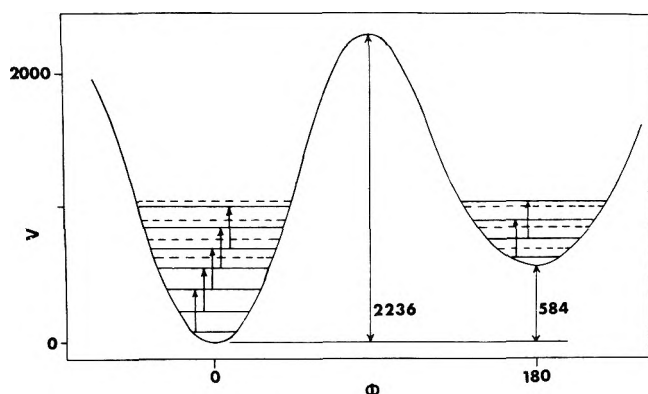


Figure 3. Potential function, energy levels, and observed transitions for the torsional vibration in acrolein. (0° corresponds to the trans configuration.)

term in the even expansion representing the resonance contribution is V_4 . The V_4 terms for 1,3-butadiene and acrolein are -49 and -96 cm^{-1} , respectively. These are down by more than an order of magnitude from the leading V_2 term, showing a fast convergence for the even series. The nearly identical V_2 terms indicate that the resonance stabilization in these two molecules is large and nearly identical.

For 1,3-butadiene the first two terms in the odd expansion are $V_1 = 600$ cm^{-1} and $V_3 = 273$ cm^{-1} . The large value of the second term (V_3) relative to the V_1 term suggests that the magnitude of this term may have significant contribution from bond-bond interactions whose leading term would be V_3 using the Pauling model.

In going to acrolein one would expect less steric interactions since the 1,4 hydrogens in 1,3-butadiene are very close in the cis configuration whereas in acrolein there are no close hydrogen-hydrogen interactions but only a more distant hydrogen-oxygen interaction. Since the steric terms should be smaller for acrolein one might expect all terms in the odd expansion for acrolein to be smaller than the corresponding terms for 1,3-butadiene if there is little contribution to the odd series (to V_3 in particular) from the bond-bond interactions.

One finds that the V_1 term in acrolein is 306 cm^{-1} which is considerably lower than the 600 - cm^{-1} value found for 1,3-butadiene. But the magnitudes of the V_3 terms in the torsional potential functions of acrolein and 1,3-butadiene are comparable and suggest that the leading term in the bond-bond interactions is V_3 and that this term may be a transferable potential constant for torsions in conjugated dienes.

Conclusions

The observation of several torsional overtones in both the cis and trans wells of acrolein has allowed an analysis of the torsional potential function to be carried out. The less stable conformer of acrolein is found to have the cis configuration and lies 584 cm^{-1} above the stable trans conformer. The barrier to interconversion (trans \rightarrow cis) is found to be 2236 cm^{-1} . The magnitudes of the V_3 terms in the torsional potential functions of acrolein and 1,3-butadiene are comparable and suggest some trigonal symmetry about the C-C single bond, and a possible transferability of the potential constant V_3 , representing bond-bond interactions in the torsions of conjugated dienes.

References and Notes

- † Ph.D with Professor Richard C. Lord, 1969.
- (1) A. Cherniak and C. C. Costain, *J. Chem. Phys.*, **45**, 104 (1966).
- (2) K. Kuchitsu, T. Kukuyama, and Y. Morino, *J. Mol. Struct.*, **1**, 463 (1968).
- (3) A. C. P. Alves, J. Christoffersen, and J. M. Hollas, *Mol. Phys.*, **20**, 625 (1971).
- (4) E. J. Bair, W. Goetz, and D. A. Ramsay, *Can. J. Phys.*, **49**, 2710 (1971).
- (5) M. S. De Groot and J. Lamb, *Proc. R. Soc. London, Ser. A*, **242**, 36 (1967).
- (6) W. G. Fateley, R. K. Harris, F. A. Miller, and R. E. Withowski, *Spectrochim. Acta*, **21**, 231 (1965).
- (7) R. K. Harris, *Spectrochim. Acta*, **20**, 1129 (1964).
- (8) A. R. H. Cole and A. A. Green, *J. Mol. Spectrosc.*, **48**, 232 (1973).
- (9) L. A. Carreira, *J. Chem. Phys.*, **62**, 3851 (1975).
- (10) J. C. D. Brand and D. G. Williamson, *Discuss. Faraday Soc.*, **35**, 184 (1963).
- (11) L. Pauling, "The Nature of the Chemical Bond", 3rd ed, Cornell University Press, Ithaca, N.Y., 1960, pp 130-142, 292.
- (12) K. S. Pitzer, *J. Chem. Phys.*, **14**, 239 (1946).
- (13) J. D. Lewis, T. B. Malloy, Jr., T. Chao, and J. Laane, *J. Mol. Struct.*, **12**, 427 (1972).
- (14) N. L. Allinger, J. T. Sprague, and T. Liljefors, *J. Am. Chem. Soc.*, **96**, 5100 (1974).
- (15) J. R. Durig, W. E. Bucy, and A. R. H. Cole, *Can. J. Chem.*, submitted for publication.
- (16) L. Radom and J. A. Pople, *J. Am. Chem. Soc.*, **92**, 4786 (1970).
- (17) D. A. Ramsay and C. Zauli, *Acta Phys. Acad. Sci. Hung.*, **35**, 79 (1974).

Raman Spectra of Some Neurotoxins and Denatured Neurotoxins in Relation to Structures and Toxicities

Issei Harada,*¹ Tadahisa Takamatsu, Takehiko Shimanouchi,

Department of Chemistry, Faculty of Science, The University of Tokyo, Bunkyo-ku, Tokyo, Japan

Tatsuo Miyazawa,

Department of Biophysics and Biochemistry, Faculty of Science, The University of Tokyo, Bunkyo-ku, Tokyo, Japan

and Nobuo Tamiya

Department of Chemistry, Tohoku University, Sendai, Japan (Received December 23, 1975)

Publication costs assisted by The University of Tokyo

Raman spectra are reported of aqueous solutions of neurotoxins, erabutoxins a and b and *Laticauda semifasciata* III, and denatured neurotoxins, reduced and *S*-carboxymethylated erabutoxin b and tryptophan-modified erabutoxin b. The molecular structures as revealed by the analyses of Raman spectra are discussed in relation with toxicities.

Introduction

About 40 neurotoxic and cardiotoxic proteins have been isolated from the venoms of Hydrophiidae and Elapidae snakes and sequenced.^{2a} Neurotoxins are classified into two groups, namely, the short-chain toxins, containing 60–62 amino acid residues with four disulfide bridges, and long-chain toxins, containing 71–74 amino acid residues with five disulfide bridges.^{2b} The secondary structures of the neurotoxins are considered to be quite similar to each other and fifteen amino acids including the eight half cystines that are found in common at the same positions for these neurotoxins may be particularly responsible for their lethal activity.^{2a,3} Cardiotoxins that are less lethal to animals than are neurotoxins also consist of 60–62 amino acid residues with four disulfide bridges.⁴ Four of the fifteen amino acid residues found in common for neurotoxins are replaced by other amino acids in cardiotoxins and this may be related to the lack of neurotoxicity.^{2a,3} It has been known that the reduction of disulfide bridges or the chemical modification of the tryptophan residue causes almost complete loss of toxicity.^{5,6}

Erabutoxins a, b, and c (Ea, Eb, and Ec) are the neurotoxic proteins from the venom of a sea snake, *Laticauda semifasciata*, and their amino acid sequences are known.^{7–10} They belong to the short-chain toxins and each Ea and Ec differs from Eb only at one position, i.e., Ea contains asparagine instead of histidine 26 of Eb and Ec contains asparagine instead of lysine 51 of Eb, respectively. The same venom contains also a weakly neurotoxic component, *Laticauda semifasciata* III (component Ls III), consisting of 66 amino acid residues with five disulfide bridges. Component Ls III has some neurotoxicity (about one-eighth that of erabutoxins) but no cardiotoxicity.^{2a} Component Ls III is considered as a fossil component preserved in the venom.^{2a}

The Raman spectra of snake toxins have been investigated including cobramine B and toxins isolated from venoms of sea snakes *Lapemis hardwickii* and *Enhydrina schistosa*.^{11,12} In the present study, Raman spectra are observed of aqueous solutions of erabutoxins a and b, *Laticauda semifasciata* III, reduced and *S*-carboxymethylated erabutoxin b (RCM Eb), and tryptophan-modified erabutoxin b (Trp-modified Eb)

and the relationships between the structures and toxicities are discussed.

Experimental Section

Ea, Eb, and component Ls III were isolated from the venom of *Laticauda semifasciata* as previously described.^{2a,7–9} RCM Eb was prepared as described by Sato and Tamiya.⁹ Trp-modified Eb was obtained through the treatment of erabutoxin b with 2-hydroxy-5-nitrobenzyl bromide.⁶

The Raman spectra were obtained on a Spex 1401 spectrophotometer with the 647.1-nm line of a Spectra Physics Model 166-01 krypton ion laser as the exciting line.¹³ A quartz tube cell 2 mm in diameter with a quartz plate on one end and about 15 μ l of the solution were used for each measurement. Ea, Eb, and Trp-modified Eb dissolved in water easily. RCM Eb was dissolved in aqueous 0.5 M pyridine solution. Component Ls III was dissolved in aqueous 0.1 M pyridine solution. The protein solutions were prepared at concentrations of 100–200 mg/ml. All spectra were recorded with a laser power at the sample of about 400 mW and a spectral slit width of 7 cm^{-1} in about 2.5 h.

Original charts of Raman spectra of the proteins are shown in Figures 1–5.

Results and Discussion

1. *Erabutoxin b*. The amide I line is strong and sharp at 1674 cm^{-1} (Figure 1), which indicates a large fraction of β -pleated-sheet conformation.^{14,15} The amide III mode is observed as a broad and strong band in the region 1252–1235 cm^{-1} ; scattering peaks are found at 1252 and 1236 cm^{-1} indicating the predominant coexistence of random-coil and β -pleated-sheet structures.^{14,15} The weak shoulder at 1266 cm^{-1} may be assigned to the minor α -helical form.^{14,15}

According to the study on the correlation of SS stretching frequency with the disulfide conformation, the gauche-gauche (G-G), gauche-trans (G-T), and trans-trans (T-T) structures of the CC-SS-CC linkage exhibit Raman frequencies at about 510, 525, and 540 cm^{-1} , respectively.^{16,17} The SS-stretching Raman lines of Eb molecule are observed at 511 (strong) and 524 cm^{-1} (shoulder) with an approximate intensity ratio of

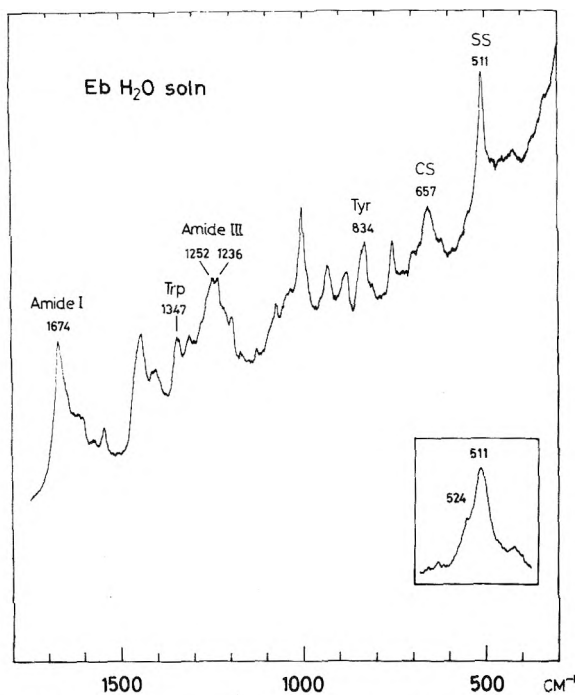


Figure 1. Raman spectrum of erabutoxin b in water.

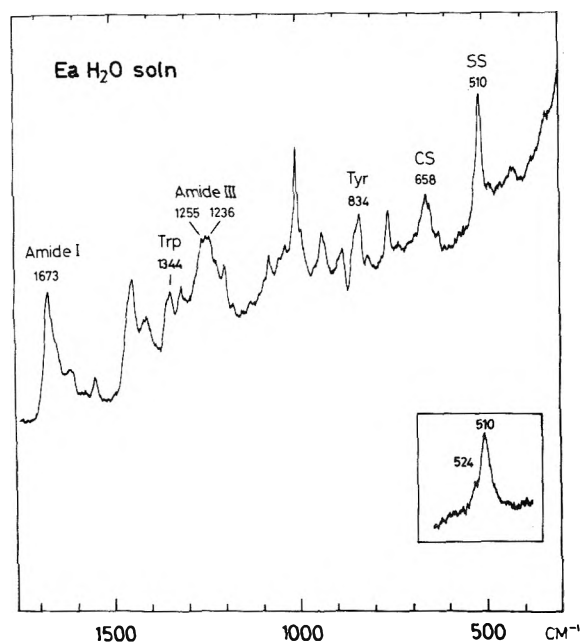


Figure 2. Raman spectrum of erabutoxin a in water.

3 to 1. This shows that three out of four cystine bridges of Eb take the G-G structure and the remaining one takes the G-T structure with respect to the $C_{\alpha}C_{\beta}$ -SS- $C_{\beta}C_{\alpha}$ linkage. The CS stretching vibration is observed as a broad band at 657 cm^{-1} indicating the existence of trans form about HC_{α} - $C_{\beta}S$ bond.^{16,18}

According to the recent study on the doublet at 850 and 830 cm^{-1} due to the tyrosyl residue, the intensity ratio of the two peaks is found to be sensitive to the nature of the hydrogen bonding of the phenolic hydroxyl group or its ionization, but much less so to the environment of the phenyl ring and the conformation of the amino acid backbone.¹⁹ The peaks due to the single tyrosyl residue of Eb molecule are strong at 835

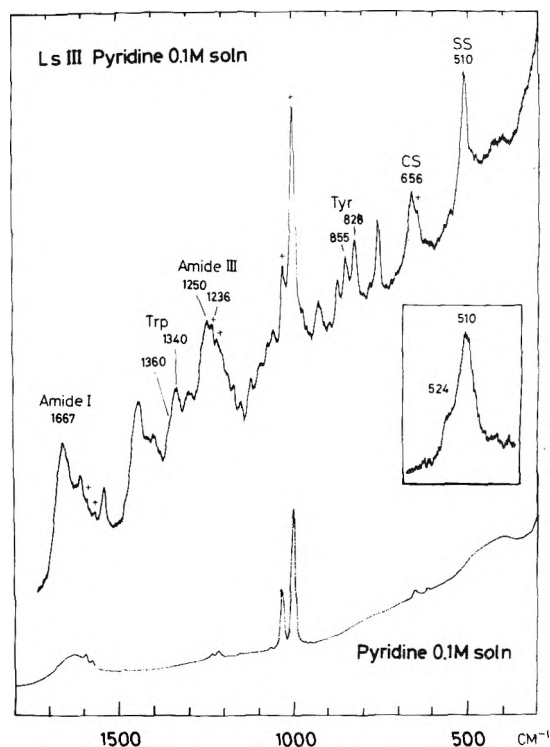


Figure 3. Raman spectra of *Laticauda semifasciata* III in aqueous 0.1 M pyridine solution (upper) and aqueous 0.1 M pyridine solution (lower). Each + indicates the possible overlap with the band due to pyridine.

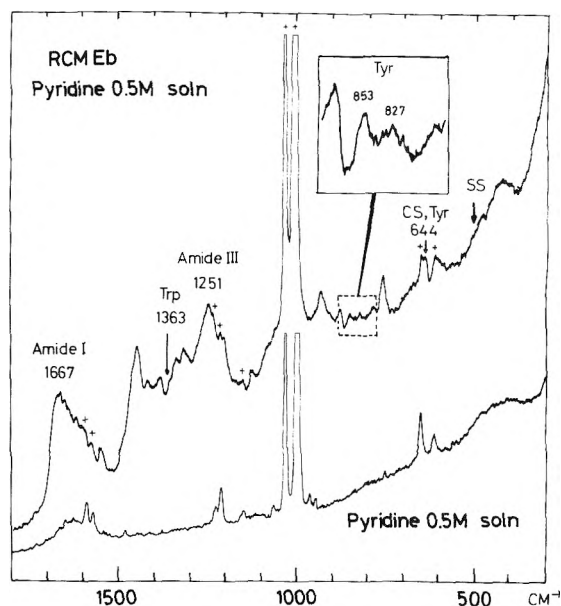


Figure 4. Raman spectra of reduced and *S*-carboxymethylated erabutoxin b in aqueous 0.5 M pyridine solution (upper) and aqueous 0.5 M pyridine solution (lower). Each + indicates the possible overlap with the band due to pyridine.

cm^{-1} and weak (shoulder) at 847 cm^{-1} . This is interpreted to indicate that the single tyrosine at 25th position (Figure 6) is buried in the interior of the molecule and is forming a hydrogen bond with a strong proton-acceptor such as CO_2^- or NH_2 .¹⁹

The lack of a distinct peak at 1361 cm^{-1} due to tryptophan residue indicates that the single tryptophan residue at the 29th position is exposed to the solvent.^{20,21}

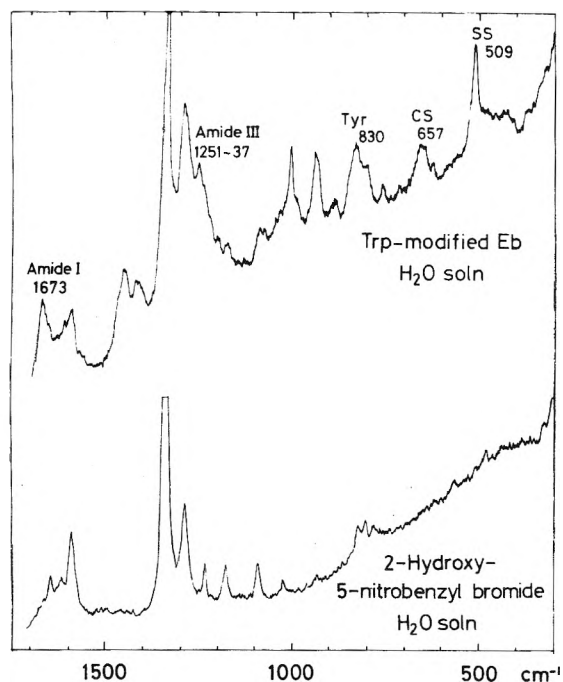
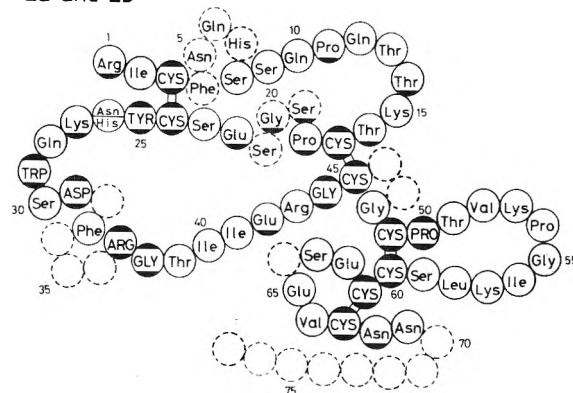


Figure 5. Raman spectra of Trp-modified erabutoxin b in water (upper) and 2-hydroxy-5-nitrobenzyl bromide in water (lower).

2. *Erabutoxin a*. The Raman spectrum of erabutoxin a is essentially the same as that of erabutoxin b (Figure 2). The main features of the typical peaks are as follows: amide I, 1673 cm^{-1} ; amide III, 1255–1236 cm^{-1} with a shoulder at 1265 cm^{-1} ; ν_{SS} , 510 and 524 cm^{-1} with an intensity ratio similar to Eb; ν_{CS} , 658 cm^{-1} ; Tyr, 834 cm^{-1} (strong) and 850 cm^{-1} (weak shoulder); and Trp, 1344 cm^{-1} . The replacement of a single amino acid residue at the 26th position (see Figure 6) does not seem to cause appreciable changes to the Raman spectrum.

3. *Component Ls III*. The amide I peak at 1667 cm^{-1} is broad (Figure 3) as compared with those of erabutoxins a and b. The amide III band has its maximum at 1250 cm^{-1} with shoulders at 1260 cm^{-1} (weak) and 1236 cm^{-1} (medium, overlapped by a band of pyridine). These facts indicate that the random-coil structure is dominant in the molecule and that the β -pleated-sheet and α -helix exist to some extent.^{14,15} The strong peak at 510 cm^{-1} and the weak shoulder at 524 cm^{-1} are assigned to the SS stretching vibrations of the G–G and G–T structures, respectively.^{16,17} The intensity ratio of the two bands is about 4 to 1, indicating that four out of the five disulfide linkages of the molecule take the G–G structure and the remaining one takes the G–T structure. If we assume that the local structures of the four disulfide parts that are common to Ea, Eb, and component Ls III are analogous, the structure of the Cys 30–Cys 34 part must be taking the G–G structure (Figure 6). The strong peak at 656 cm^{-1} is assigned to the CS stretching vibration of the trans form with respect to the $\text{HC}_\alpha\text{--C}_\beta\text{S}$ linkage.^{16,18} Component Ls III contains three tyrosyl residues, Tyr 4, Tyr 25, and Tyr 70 (Figure 6). Tyr 25 is at the same position as the tyrosyl residues in Ea and Eb, i.e., next to the disulfide linkage. The tyrosine peaks are at 855 and 828 cm^{-1} with equal intensities. This is interpreted to indicate that one out of the three tyrosyl residues is forming a strong hydrogen bond as a proton-donor and the other two are in the state of moderate hydrogen bonding at most.¹⁹ From a simple analogy to the cases of Ea and Eb, it is possible that Tyr 25 corresponds to the former. This point will be discussed again in the final section. Two tryptophan residues, Trp 29 and Trp

Ea and Eb



Ls III

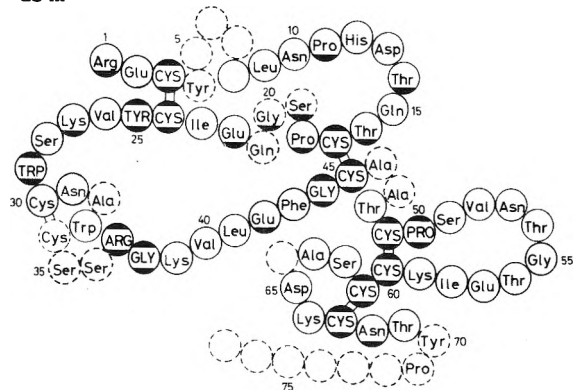


Figure 6. Primary structures of erabutoxins a and b (upper) and *Laticauda semifasciata* III (lower). The amino acids in the 26th position of Ea and Eb are asparagine and histidine, respectively: (●) invariant in neurotoxins; (◐) common to Ea, Eb, and component Ls III; (⋯) lacking in some neurotoxins.

33, are both exposed to the solvent as indicated by the weak intensity of the shoulder at 1360 cm^{-1} .^{20,21}

4. *Reduced and S-Carboxymethylated Erabutoxin b*. The SS stretching band is not observed in the 500- cm^{-1} region indicating that the breakage of the disulfide bonds has proceeded as intended (Figure 4). The relative intensity of the amide III peak at 1251 cm^{-1} to the peak at 1236 cm^{-1} has increased compared with the case of erabutoxin b. The amide I band has shifted from 1674 to 1667 cm^{-1} and has broadened considerably. These facts indicate that the β -pleated-sheet region of erabutoxin b has changed, at least in part, to the random-coil structure.

The effect of chemical denaturation is also seen for the peaks due to the aromatic side chains. The tyrosine bands have changed significantly in intensities and the weak peaks appear at 853 and 827 cm^{-1} . This is interpreted to indicate that the breakage of the disulfide bond of Cys 3–Cys 24 has caused a great change in the environment of Tyr 25, simultaneously breaking the strong hydrogen bond.¹⁹ The tryptophan peak at 1363 cm^{-1} has emerged as a shoulder indicating the small change in the environment of Trp 29.

5. *Tryptophan-modified Erabutoxin b*. Most of the peaks due to the tryptophan residue are missing entirely (the peak at 1550 cm^{-1}) or observed with much reduced intensities (the peaks at 882 and 758 cm^{-1}) indicating that the chemical modification of tryptophan by 2-hydroxy-5-nitrobenzyl bromide has proceeded (Figure 5). On the other hand, no significant change seems to have occurred in the main-chain structure and in the environment of the tyrosyl residue. The

amide I peak is at 1673 cm^{-1} . The amide III band is observed in the $1251\text{--}1237\text{ cm}^{-1}$ region though it is obscured by the partial overlap with the bands of the modifying group. The SS and CS stretching vibrations are at 509 and 657 cm^{-1} with band shapes similar to those of erabutoxin b. The tyrosine peaks are strong at 830 cm^{-1} and weak (shoulder) at 849 cm^{-1} , being overlapped on the lower-frequency side by the bands of the modifying group. Except for the peaks due to the tryptophan residue the spectral features remain essentially unchanged by the modification of tryptophan. This suggests that the tryptophan residue is exposed to the solvent, since otherwise the modification should have caused the structural changes observable in the Raman spectrum. This is consistent with the results of the dependence of the relative intensity of the fluorescence on the concentration of ethylene glycol in the solvent⁶ and of the Raman spectra of Ea and Eb described above.

6. *Relationships between Toxicities and Structures as Revealed by Raman Spectra.* The complete loss of toxicity of Ea by the modification of the single tryptophan residue at the 29th position has been known and the tryptophan residue is considered to be essential to the toxicity on the post-synaptic membrane.⁶ It is of interest to see whether the modification is localized in tryptophan moiety or if it causes additional structural changes that might also be responsible for the loss of toxicity. As is described above, the present analysis of the Raman spectra of Eb and Trp-modified Eb indicates that the conformations of the main-chain and four disulfide bridges and the environment of Tyr 25 of the Eb molecule are not affected by the modification. Therefore, it is evident that the loss of toxicity by the modification of the tryptophan residue is primarily due to the local change, and that the tryptophan plays the role of the key to the key-hole of acetylcholine receptor in the lethal activity of erabutoxins.

The loss of toxicity by the reduction and carboxymethylation of the disulfide bridges is correlated to the drastic deformation of the overall structure as well as the change of the local environment. This is seen in the Raman spectrum, where the conversion of the β -pleated-sheet to the random-coil structure and the breakage of the strong hydrogen bond of Tyr 25 are evident. The proper locations for Trp 29 and certain basic amino acid residues to block the acetylcholine receptor sites on the post-synaptic membrane⁶ would have been destroyed through the above-mentioned process of denaturation.

The neurotoxicity of component Ls III is about one-eighth that of erabutoxins.^{2a} This may be related to the fact that Asp 31, which is one of the 15 common amino acid residues in neurotoxins, is replaced by asparagine in component Ls III. This point will be discussed further in the next section. The Raman spectrum of component Ls III shows that the random-coil structure is more dominant over the β -pleated-sheet structure as compared to the cases of erabutoxins while the local structures of the disulfide bridges are similar to those of erabutoxins. It is probable that the random-coil-rich structure precludes the tryptophan residue from the optimum positioning.

7. *Search for the Proton Acceptor of the Hydrogen Bond of Tyr 25.* Tyr 25 is found in common for the neurotoxins sequenced so far and is known to be buried in the interior of the molecule from the result that it is not iodinated under the same condition as His 26 of Eb.²² From the above facts, Tyr 25 is considered to play an important role in the construction of the tertiary structures of neurotoxins.³

Present study shows that the hydroxyl group of Tyr 25 in each of the erabutoxins is forming a hydrogen bond with a

strong proton-acceptor like CO_2^- or NH_2 .¹⁹ The Raman spectrum of the toxin of *Enhydrina schistosa* (a neurotoxin of known sequence) gives quite similar patterns to those of erabutoxins.¹² The only tyrosyl residue, Tyr 25, of this toxin is also considered to be buried and strongly hydrogen-bonded. If we assume that the position of the proton-acceptor site is common to erabutoxins and the toxin of *Enhydrina schistosa*, one of the candidates as the strong proton-acceptor in erabutoxins, Glu 22, is eliminated because the 22d position of the toxin of *Enhydrina schistosa* is serine instead of glutamic acid of erabutoxins.

It is probable that this strong hydrogen bonding found in erabutoxins and the toxin of *Enhydrina schistosa* is an essential factor for the construction of the tertiary structures of neurotoxins in general and that all the neurotoxins with different sequences have Tyr 25's in a condition common to those in erabutoxins. A closer inspection of the primary structures of neurotoxins suggests several positions as the candidates of the strong proton-acceptor site. All of the 28 neurotoxins (excluding component Ls III) so far sequenced³ possess NH_2 groups at the 37th and 53d positions and an NH_2 or CO_2^- group at the 68th position in common. Furthermore, they possess a CO_2^- group at the 42d position in common with one exception (Asn in *Ophiophagus hannah* B²³). From the point of view of the invariant residues-toxicities relationships, however, the proton acceptor for the hydroxyl group of Tyr 25 is probably Asp 31 since this is the only candidate available as a strong proton acceptor among the 14 common amino acid residues (excluding Tyr 25) in neurotoxins. Possibly Tyr 25 of component Ls III is forming rather weaker hydrogen bonding than the Tyr 25's of erabutoxins because the 31st position of component Ls III is asparagine instead of aspartic acid. This, in turn, might result in lack of the definite tertiary structure that is optimum for strong neurotoxicity.

Investigations of the Raman spectra of other neurotoxins and cardiotoxins are necessary for more detailed clarification of the problem.

Acknowledgment. We are indebted to the Japan Academy for a grant in aid of this research.

References and Notes

- (1) Postdoctoral Research Associate with Richard C. Lord, 1967–1969.
- (2) (a) N. Maeda and N. Tamiya, *Biochem. J.*, **141**, 389 (1974); (b) D. J. Strydom, *Comp. Biochem. Physiol.*, **44B**, 269 (1973).
- (3) N. Tamiya, "The Biology of Sea Snakes", W. A. Dunson, Ed., University Park Press, Baltimore, Md., 1975, Chapter 18.
- (4) C. Y. Lee, *Annu. Rev. Pharmacol.*, **12**, 265 (1972).
- (5) C. C. Yang, *Biochem. Biophys. Acta*, **133**, 346 (1967).
- (6) A. Seto, S. Sato, and N. Tamiya, *Biochim. Biophys. Acta*, **214**, 483 (1970).
- (7) N. Tamiya and H. Arai, *Biochem. J.*, **99**, 624 (1966).
- (8) Y. Endo, S. Sato, S. Ishii, and N. Tamiya, *Biochem. J.*, **122**, 463 (1971).
- (9) S. Sato and N. Tamiya, *Biochem. J.*, **122**, 453 (1971).
- (10) N. Tamiya and H. Abe, *Biochem. J.*, **130**, 547 (1972).
- (11) N. T. Yu, B. H. Jo, and D. C. O'Shea, *Arch. Biochem. Biophys.*, **156**, 71 (1973).
- (12) N. T. Yu, T. S. Lin, and A. T. Tu, *J. Biol. Chem.*, **250**, 1782 (1975).
- (13) H. Hamaguchi, I. Harada, and T. Shimanouchi, *J. Raman Spectrosc.*, **2**, 517 (1974).
- (14) (a) M. C. Chen and R. C. Lord, *J. Am. Chem. Soc.*, **96**, 4750 (1974); (b) T. J. Yu, J. L. Lippert, and W. L. Peticolas, *Biopolymers*, **12**, 2161 (1973).
- (15) N. T. Yu and C. S. Lin, *J. Am. Chem. Soc.*, **94**, 5127 (1972).
- (16) H. Sugeta, A. Go, and T. Miyazawa, *Chem. Lett.*, 83 (1972); *Bull. Chem. Soc. Jpn.*, **46**, 2752 (1973).
- (17) R. B. Martin, *J. Phys. Chem.*, **78**, 855 (1974).
- (18) E. J. Bastian, Jr., and R. B. Martin, *J. Phys. Chem.*, **77**, 1129 (1973).
- (19) M. M. Siamwiza, R. C. Lord, M. C. Chen, T. Takamatsu, I. Harada, H. Matsuura, and T. Shimanouchi, *Biochemistry*, **14**, 4870 (1975).
- (20) M. C. Chen, R. C. Lord, and R. Mendelsohn, *Biochim. Biophys. Acta*, **328**, 252 (1973).
- (21) N. T. Yu, *J. Am. Chem. Soc.*, **96**, 4664 (1974).
- (22) S. Sato and N. Tamiya, *J. Biochem.*, **68**, 867 (1970).
- (23) F. Joubert, *Biochim. Biophys. Acta*, **317**, 85 (1973).

Studies of Virus Structure by Laser-Raman Spectroscopy. 3. Turnip Yellow Mosaic Virus

T. A. Turano, K. A. Hartman,*¹

Department of Biochemistry and Biophysics, University of Rhode Island, Kingston, Rhode Island 02881

and G. J. Thomas, Jr.²

Department of Chemistry, Southeastern Massachusetts University, North Dartmouth, Massachusetts 02747

(Received December 29, 1975)

Laser-excited Raman spectra of a plant virus, the turnip yellow mosaic virus (TYMV), reveal vibrational frequencies characteristic of both the nucleic acid (RNA) and coat-protein components. The prominent Raman lines of the virus were assigned to specific subgroups of the constituent macromolecules and were examined as a function of temperature for both H₂O and D₂O solutions. The Raman data indicate the following structural features of aqueous TYMV. Amide I and III frequencies of the coat-protein molecules exclude the presence of appreciable amounts of both α -helical and antiparallel- β -sheet structures and suggest that the polypeptide chain is mostly in an irregular conformation. All of the four cysteine residues of the coat-protein molecule have SH groups and no S-S linkages exist in TYMV. All SH groups are accessible to the solvent, as evidenced by their deuterium exchange. A tentative finding is that many or all of the carboxyl groups of aspartic and glutamic acid residues in the coat protein are ionized at pH 7. Tryptophan residues are exposed to solvent H₂O molecules, whereas tyrosine residues are apparently not in contact with the solvent and form strong hydrogen bonds between the tyrosyl -OH donor and negative acceptor groups within the virion. These structural properties of TYMV are unchanged over the temperature range 0–54 °C, above which the virus structure collapses. The encapsulated RNA molecule of TYMV contains an unusually low amount of ordered secondary structure (~60%), in comparison with those other single-stranded RNA species which have been studied (~85%). The secondary structure of encapsulated RNA is also largely resistant to changes in temperature up to 54 °C. The cytosine residues of TYMV RNA are not protonated at pH 7, either for protein-free RNA or for RNA encapsulated within the virus. It is therefore unlikely that specific hydrogen bonding interaction between cytosine residues of RNA and carboxyl groups of coat proteins are a major source of stabilization of the native TYMV virion, at pH 7.

Introduction

Considerable progress has been made recently in the application of laser-Raman spectroscopy to the elucidation of the structures of biological molecules.^{3,4} Raman spectra of the constituents of nucleic acids were first observed in the laboratory of Professor R. C. Lord in the early 1960's (for a discussion of this work see ref 3–5). More detailed investigations of polynucleotides and naturally occurring nucleic acids soon followed^{6–9} as more powerful laser sources became generally available.

Lord and Yu¹⁰ next began the modern era of laser-Raman spectroscopy of proteins, by assigning spectral lines of the amino acids and successfully utilizing their results in an analysis of the enzyme, lysozyme. In addition to the study of other proteins, Chen and Lord¹¹ in 1974 produced a correlation between the chain conformations of model polypeptides and their corresponding Raman lines. This work suggested the use of conformationally sensitive Raman frequencies of the peptide group, the so-called amide frequencies, as a means of estimating protein conformation without necessitating a detailed and laborious crystallographic analysis.

In 1973 enough data had been accumulated to allow Hartman, Clayton, and Thomas¹² to initiate the use of laser-Raman spectroscopy in nucleoprotein research by obtaining spectra of the bacterial virus, R17, and assigning its individual Raman lines to vibrations of specific subgroups of viral RNA and coat protein. In 1975, Thomas and Murphy¹³ and Thomas, Prescott, Ordzie, and Hartman¹⁴ studied the DNA viruses, Pfl and fd, and the RNA virus, MS2, respectively.

Several structural properties of the nucleic acid and protein components of these viruses were revealed by the Raman data.

The advantages of laser-Raman spectroscopy in investigations of viruses and other nucleoproteins are that small amounts of sample are required, that a wealth of information is available from the many vibrational scattering lines assignable to subgroups of both nucleic acid and protein components, and that the entire vibrational spectrum is open to analysis for aqueous (H₂O and D₂O) solutions of viruses. Structural information of the kind obtained from Raman spectra of viruses is difficult or impossible to obtain by other means. It is for these reasons that we have undertaken structural studies of viruses, including the turnip yellow mosaic virus (TYMV), using laser-Raman spectroscopy.

A single TYMV particle (virion) contains about one-third by weight nucleic acid (one molecule of RNA of molecular weight, mol wt = 1.91×10^6) and about two-thirds by weight protein (180 molecules of "ccat" protein, each of mol wt = 20 133, which together form the capsid).¹⁵

TYMV has been extensively studied by x-ray crystallography, electron microscopy, and various chemical and hydrodynamic methods.¹⁵ These analyses reveal the gross morphological properties of the capsid, but indicate virtually nothing about the locus or conformation of the encapsulated RNA. The finer details of the capsid structure are also unknown. For example, the x-ray diffraction data are accounted for by an icosahedral capsid assembled from 20 hexamers and 12 pentamers of the coat-protein monomer. However, the conformations of the coat-protein molecules and the nature

of the interactions between them in the assembled capsid are questions still unanswered.

Evidence suggests that the RNA of the virion laces in and out between the coat-protein molecules. In a model proposed by Kaper¹⁵ the RNA is considered to be bound to the capsid protein by hydrogen-bonding interaction between protonated cytosine residues of the RNA and protonated carboxyl groups (of aspartic and/or glutamic acid residues) of the protein (pH <6). However, direct evidence of the existence of such ionized groups and interaction between them within native TYMV has yet to be obtained.

It is anticipated that Raman spectra of TYMV may help to shed further light on these questions by addressing the following: Are the potentially interacting cytosine residues and carboxyl groups of TYMV ionized or not ionized? Does bonding occur between specific subgroups of RNA and protein? Does coat protein contain chain segments with α -helical, β -sheet, or other types of structure? What is the extent of ordered secondary structure in the viral RNA molecule? Are base-stacked and base-paired configurations of RNA stabilized by the coat protein? Are the SH groups of the coat-protein molecules sufficiently exposed to exchange with deuterium atoms of D₂O solvent? Are other amino-acid residues (protein side groups) exposed to the solvent or buried in hydrophobic regions? How do the structural features of TYMV change as a function of biologically relevant parameters, such as temperature?

Methods and Materials

Raman spectra were recorded on a Spex Ramalog instrument equipped with a Coherent Radiation, Model CR-2, argon-ion laser. In the present experiments the laser was operated at 488.0 nm with radiant power at the sample usually in the range 200–400 mW. Raman cells were thermostated to ± 0.5 °C using a device described previously.¹⁶ Further details of instrumentation and accessories for Raman spectroscopy, as well as sample-handling procedures, are as discussed elsewhere.¹⁴ Raman frequencies reported here are accurate to ± 2 cm⁻¹ for intense or sharp lines and to ± 4 cm⁻¹ for weak or broad lines as well as for poorly resolved shoulders. Raman intensities were reproducible to $\pm 10\%$, among spectra recorded independently on the same or similar sample preparations.

The virus used in this study was generously provided by Dr. J. M. Kaper of the United States Department of Agriculture, Agricultural Research Service, Beltsville, Md. It was of sufficient purity to yield fluorescence-free Raman spectra of high signal-to-noise ratio.

Solutions of the virus in H₂O were prepared for Raman spectroscopy as follows. The aqueous solution received from Dr. Kaper (containing 14 mg in 1 ml of H₂O) was centrifuged for 1 h at 153 000g in a Beckman L5-50 ultracentrifuge with a Model 65 rotor. The pellet formed was then dissolved in 100 μ l of 0.75 M KCl in H₂O to produce a solution containing 90 μ g of TYMV/ μ l. Aliquots of this solution were loaded into capillary tubes (Kimax no. 34507) from which spectra were recorded. Solutions containing TYMV in D₂O were prepared by pelleting the virus as above and then dissolving the pellet in the required D₂O-salt solution. D₂O solutions prepared in this manner generally contained appreciable amounts of HDO as the spectra below indicate. Aliquots of the D₂O solution were introduced into capillary tubes and spectra recorded. For both H₂O and D₂O solutions of TYMV, spectra were measured at temperatures ranging from 0 °C to the temperature

at which the sample degraded, i.e., precipitated from solution (about 60 °C).

RNA was extracted from TYMV by treatment with phenol. The RNA was precipitated from the separated aqueous phase by adding cold ethanol. The pellet formed by centrifuging this precipitate (10 000g for 10 min in a Sorval RC-2B centrifuge with an SS-34 rotor) was then dissolved in 0.2 M KAc and reprecipitated with ethanol. After several reprecipitations to remove phenol, the pellet was dissolved in 100 μ l of 0.375 M KAc in H₂O, yielding a solution containing 30 μ g of TYMV RNA/ μ l. Capillary tubes were filled and spectra obtained.

Sucrose-gradient sedimentation of virus was performed using 5 to 20% (w/v) sucrose solution made in 0.75 M KCl. Samples (0.2 ml) were layered on 4.8 ml gradients which were centrifuged at 49 000 rpm in an SW 50.1 rotor in the Beckman L5-50 centrifuge (4 °C). Tubes were then fractionated and absorbance values of the diluted fractions were determined with a Beckman DBG spectrophotometer.

Electrophoresis was performed using 3% polyacrylamide gels as previously described.¹⁷

Results and Conclusions

(a) *Integrity of the Virus and Its Components.* The interpretation of the Raman spectra of viruses in terms of the secondary structures of and interaction between component molecules requires that samples of the virus and its isolated components should have as little degradation as possible. The extent of any degradation or inhomogeneity in the sample should be measured and considered when interpreting the spectra.

Such degradation exists and appears to be to some extent unavoidable, in the case of TYMV. Even fresh samples of this virus contain some virions with partially hydrolyzed RNA. In older samples, each virion is likely to contain several fragments of the single molecule of RNA which was originally present in the native particle (J. M. Kaper, private communication). We therefore extracted the RNA from TYMV and estimated the polydispersity by obtaining the sedimentation profile (by sucrose gradient centrifugation) and the electrophoretic profile (using polyacrylamide gels) for this RNA. As expected, we found the RNA to be polydisperse with an average molecular weight of about 10 000. Nevertheless, despite the existence of numerous chain scissions in the encapsulated RNA, the resultant fragments are expected to retain some of the secondary structure which exists in the native virus.

The integrity of the virus was also estimated by obtaining sedimentation and electrophoresis profiles. Both profiles gave a sharp peak at the positions expected for intact virions which suggests that the virions had not unfolded to larger particles and had not released a significant portion of RNA or protein. The latter conclusions were also supported by the ultraviolet spectrum which was as expected for an RNA-protein particle of the composition of TYMV. Therefore, even when the viral RNA is partially degraded, the fragments remain encapsulated and the overall hydrodynamic properties of the capsid are unaffected.

(b) *Raman Spectrum of TYMV.* Raman spectra of TYMV in H₂O and D₂O solutions, each containing also 0.75 M KCl, are shown in Figures 1a and 1b, respectively. KCl is required for stabilization of the capsid structure¹⁵ and does not contribute to the Raman scattering spectrum. The assignment of Raman lines to amino-acid residues of the coat protein and nucleotide residues of the viral RNA (Table I) is facilitated by use of the spectrum of protein-free RNA shown in Figure 1c, as well as by reference to our previously published as-

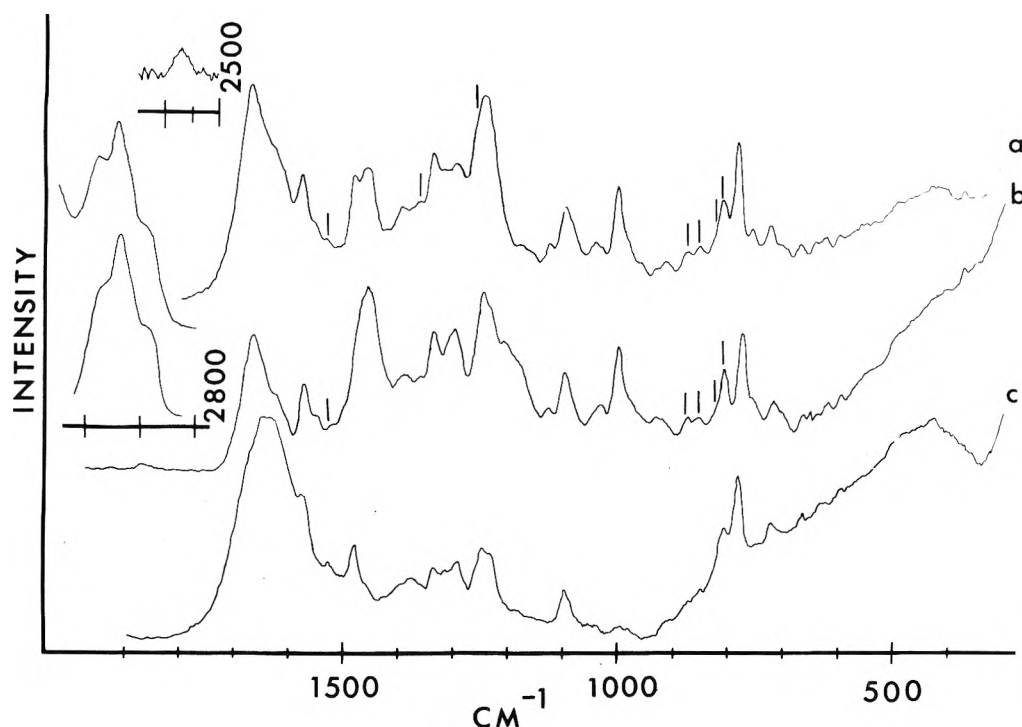


Figure 1. Raman spectra of TYMV and protein-free TYMV RNA. (a) TYMV in H₂O (containing 0.75 M KCl) at 32 °C: pH 7, slit width 10 cm⁻¹, scan speed 50 cm⁻¹/min, rise time 3 s, relative amplification (A) = 1 (300–1800 cm⁻¹), A = 3 (2500–2600 cm⁻¹), A = 1/3 (above 2800 cm⁻¹). The reference marks above the spectrum indicate respectively 1535, 1362, 1255, 879, 856, 825, and 812 cm⁻¹. (b) TYMV in D₂O (0.75 M KCl, pH 7) at 32 °C: same as in part a, except the 2500–2600-cm⁻¹ region is not shown. The reference marks above the spectrum indicate respectively 1535, 878, 860, 825, and 812 cm⁻¹. (c) RNA in H₂O (0.75 M KCl, pH 7) at 32 °C: same as in part a, except spectrum not shown above 1800 cm⁻¹.

signments for compositionally similar RNA and capsids.^{6,8,12,14} Since sufficient quantities of virus were not available to permit repeated isolation of RNA for obtaining spectra of its D₂O solution and for obtaining reproducibly accurate spectra of RNA-free capsids, we have not included in Figure 1 the scant data obtained for them. In the subsequent discussion we therefore give emphasis to the data collected from H₂O solutions of TYMV and TYMV RNA, with occasional reference to the data of deuterated samples and capsids, as appropriate.

The structural implications of the Raman spectra of Figure 1 are as follows. In the conformationally sensitive amide I and amide III regions of the Raman spectrum (usual intervals 1625–1675 and 1225–1300 cm⁻¹, respectively), TYMV exhibits intense lines centered at 1669 and 1248 cm⁻¹ (Figure 1a). Comparison with Figure 1c shows that these features are due predominantly to the coat protein rather than to the encapsulated RNA, although the solvent (H₂O) is primarily responsible for the broad shoulder to the amide I line near 1645 cm⁻¹. This is confirmed by the Raman spectrum of the RNA-free capsid which also shows one line with a maximum near 1243 cm⁻¹ and no "shoulders" or small lines nearby (unpublished data). Lord and co-workers¹¹ have shown that α -helical polypeptides give amide I and III lines near 1650 and 1275 cm⁻¹, the latter weak, whereas β -sheet structures give lines near 1660 and 1230 cm⁻¹, both intense. Polypeptides in extended or "random-chain" structures, such as (low pH) poly-L-lysine and denatured proteins, generally exhibit amide I and III lines near 1670 and 1248 cm⁻¹, again both intense.¹¹ Accordingly, the present results indicate that the coat-protein molecules of TYMV contain neither α -helical nor β -sheet structures to any appreciable extent. The implications of these results will be dealt with in the Discussion section.

The absence of Raman scattering near 500 cm⁻¹ for TYMV

(Figures 1a and 1b) and the appearance of a broad Raman line centered near 2569 cm⁻¹ (Figure 1a, insert) assignable to SH stretching vibrations indicate that S–S bridges are absent from the virion and further that the four cysteine residues per coat-protein molecule (Table II) are indeed present in the reduced form. Therefore the Raman spectra confirm previous conclusions drawn from chemical studies.¹⁵ In Figure 1a, the Raman scattering in the region 2500–2600 cm⁻¹ was recorded with a threefold higher amplification than was employed for either the lower frequency range (below 1700 cm⁻¹) of the same spectrum or the spectrum of Figure 1b. Accordingly the Raman line near 1868 cm⁻¹ in Figure 1b, due to SD stretching of deuterated cysteine residues, appears with about a sixfold lower intensity, as expected if all SH groups are exchanged by deuterium. (Theoretical considerations suggest that I_{S-D} is about one-half I_{S-H} .) We found the exchange was complete at the time the spectrum was first recorded after the virus had been placed in D₂O (elapsed time of several days). A more complete determination of the kinetics of deuterium exchange of the S–H groups is planned.

Many lines in the spectrum of TYMV can be assigned to aromatic amino acids which are sparingly present or to non-aromatic amino acids which are abundantly present in the TYMV coat protein (Tables I and II). Here we draw attention to several of these which are useful in predicting structural features.

The environment of the hydrophobic side group of tryptophan has been correlated with its Raman line at 1362 cm⁻¹, due to a vibration of the indole ring.¹⁸ If tryptophan residues are, on the average, buried in hydrophobic regions within the protein, the indole vibration near 1362 cm⁻¹ is characteristically intense and sharp in the Raman effect. This can be clearly seen in the Raman spectrum of lysozyme (first part of ref 11) in which the sharp line at 1362 cm⁻¹ is nearly as intense

TABLE I: Raman Frequencies, Relative Intensities, and Assignments for TYMV in H₂O and D₂O Solutions (0.75 M KCl) at 32 °C

Assignments ^a	TYMV H ₂ O	TYMV D ₂ O	TYMV- RNA H ₂ O
	598 (0.11)	602 (—)	
phe, U, C	626 (0.10)	625 (0.14)	625 (0.26)
Tyr	644 (0.17)	645 (—)	
G	671 (0.17)	668 (0.16)	668 (—)
C-S	703 (0.13)	*	
C-S, A	726 (0.35)	723 (0.32)	725 (—)
Trp, C	759 (0.27)	762 (0.31)	*
C, U, Thr	785 (1.48)	778 (—)	786 (1.65)
P	812 (0.71)	812 (0.69)	812 (0.98)
Tyr	825 (0.29)	825 (0.20)	
Tyr	856 (0.17)	860 (0.15)	
Trp, C-C str	879 (0.20)	878 (0.19)	
r	919 (0.16)	*	918 (0.14)
C-C str	*	938 (0.15)	
	962 (0.13)		
AIII'	*	994 (—)	
phe, A, U, C	1005 (1.0)	1005 (1.0)	1000 (—)
r, Phe	1045 (0.18)	1041 (—)	1050 (0.07)
C-N, P	1100 (0.72)	1102 (0.66)	1100 (0.72)
C-N, C, U	1127 (0.24)	1132 (0.23)	*
C-N	1159 (0.09)	*	
Tyr, phe	1178 (0.09)	*	
Tyr, phe	*	1214 (0.64)	
AIII, C, U	1248 (1.57)	1252 (1.15)	1249 (0.96) ^b
C, A, U	1296 (0.29)	1305 (0.64)	1302 (0.49)
G, (CHdef)	1319 (0.33)	*	1321 (—)
Trp, A, (CHdef)	1339 (0.61)	1341 (0.62)	1338 (0.50)
Trp, (CHdef)	1362 (0.05)	1361 (—)	
U, A, G, (CO ₂ ⁻ sym str)	1395 (0.19)	1390 (—)	1384 (0.34)
(CHdef)	1458 (0.99)	1460 (1.51)	1468 (—)
A, G	1481 (0.95)	*	1484 (0.88)
C, A, G	*	1521 (—)	*
C	1535 (—)		*
Trp	1553 (0.11)	1559 (—)	
Trp, A, G, phe, tyr	1577 (0.59)	1577 (0.64)	1578 (0.5)
Tyr, phe, trp	1625 (—)	1634 (—)	
AI, AI'	1669 (—)	1669 (1.49)	
S-D Cys		1868 (—)	
S-H Cys	2569 (—)		
Aliphatic C-H str	2900 (—)	2900 (—)	
Aliphatic C-H str	2941 (—)	2937 (—)	
		2965 (—)	
Aliphatic C-H str	2975 (—)		
Aromatic C-H str		3062 (—)	

^a Standard three-letter symbols for amino acids and one-letter symbols for RNA bases. Also r = ribose, P = phosphate, C-S, C-N, C-C denote atoms bonded together as usual. AI and AIII mean amide I and III. Primes mean those modes for deuterated amide groups. Sym = symmetric, str = stretch, def = deformation. Numbers in parentheses are relative intensities with a value of 1.00 assigned to the 1005-cm⁻¹ line of phenylalanine. A dash in a parentheses shows that the intensity value was not reproducible to $\pm 10\%$. An asterisk means lines too weak for accurate measurement. ^b An unresolved doublet.

as the line at 760 cm⁻¹ (also due to tryptophan). At least four of the six tryptophan residues in lysozyme appear to be in hydrophobic regions of the molecule. If these residues are, on the other hand, exposed to solvent, the intensity of the 1362-cm⁻¹ line is diminished and the line is broadened as a consequence of hydrogen bonding interactions. The com-

TABLE II: Amino-Acid Composition of the Coat-Protein Molecule of TYMV^a

Amino acid	No.	Amino acid	No.
Glutamic acid	7	Cysteine	4
Aspartic acid	7	Methionine	4
Glutamine	7	Glycine	—
Asparagine	4	Valine	14
Lysine	7	Alanine	15
Arginine	3	Isoleucine	16
Tryptophane	2	Leucine	17
Tyrosine	3	Serine	17
Histidine	3	Proline	20
Phenylalanine	5	Threonine	26
		Total	189

^a Reference 15.

panion Raman lines of the indole ring, near 760 and 879 cm⁻¹, are insensitive to this effect, and are clearly visible for indole in either environment.^{11,18} The spectrum of TYMV, which shows distinct lines at 760 and 879 cm⁻¹, but little intensity at 1362 cm⁻¹, indicates that most of the side groups of tryptophan in the coat protein are exposed to the solvent (compare with spectra of ref 11 and 18 which show limiting cases). This conclusion does not agree with inferences drawn from the lack of reactivity of tryptophan residues with *N*-bromosuccinimide.¹⁵

A correlation has also been found between the relative intensities of the pair of lines near 856 and 825 cm⁻¹, due to tyrosine residues, and the nature of hydrogen bonding of the tyrosyl OH group in proteins.^{18,19} The intensity ratio of the doublet (I_{856}/I_{825}) should be between 1.25 and 1.4 when the tyrosyl OH group is exposed and hydrogen bonded to solvent H₂O molecules. However, when tyrosyl OH groups are inaccessible to solvent water molecules and are instead involved in much stronger hydrogen bonding interaction with the OH group as donor to more highly negative acceptor groups (e.g., -COO⁻), the ratio I_{856}/I_{825} is expected to approach the value 0.30. In the case of TYMV (Figure 1a), we observe the components of the tyrosine doublet at 856 and 825 cm⁻¹ (to ± 2 cm⁻¹), and with intensity ratio of 0.55 ± 0.10 , reasonably approximating the extreme case of very strong hydrogen bonding to negative acceptor groups. In the spectrum of Figure 1, note that the 825-cm⁻¹ component appears as a shoulder on the much stronger line at 815 cm⁻¹. This ratio is as small as has yet been reported in any protein,¹⁹ and its possible significance will be reviewed in the Discussion section. This conclusion is in agreement with interpretation of spectroscopic titration curves (see p 269 of ref 15).

Of special significance in TYMV is the state of ionization of its many carboxyl groups. Each coat protein contains a minimum of 7 glutamic and 7 aspartic acid residues (Table II) as well as a terminal carboxyl group on the polypeptide chain. With 180 coat-protein molecules per capsid, the resultant 2700 carboxyl groups may be expected to play an important role in stabilizing the assembled virion. Interest in the ionization states of these groups is further heightened by the possibility that, if protonated, they may interact specifically with protonated cytosine residues of capsulated RNA¹⁵ (see Discussion). The number of cytosine residues in TYMV RNA is close to 2100. We have carefully examined the Raman spectra of TYMV and TYMV RNA to explore these questions.

For carboxyl ions in proteins, the symmetric stretching vibration of the -CO₂⁻ group is expected near 1415 cm⁻¹,¹⁰ although the frequency may be lowered somewhat (ca. 1400

cm^{-1}) by strong hydrogen bonding to an acidic donor group. Nonionized carboxyl groups of proteins ($-\text{COOH}$) are recognized by their carbonyl stretching vibration normally appearing at 1715 cm^{-1} .¹⁰ By examining the Raman spectra of dilute solutions of sodium acetate and acetic acid we have established that the 1415- and 1715-cm^{-1} lines should be just barely detectable over the background of scattering by other molecular subgroups and solvent, for the case of aqueous TYMV. This may seem surprising in view of the large number of carboxyl groups present in TYMV, but it happens that the Raman intensities of these group vibrations are much weaker than the characteristic group frequencies of aromatic rings, such as the ring modes of the tyrosine and tryptophane residues mentioned earlier. Moreover, the frequency intervals under consideration are precisely those in which strong Raman scattering also is expected from either amide I vibrations (ca. 1670 cm^{-1}) or CH deformations (ca. 1450 cm^{-1}), and the molar percentages of these groups exceed that of the carboxyl group. Finally, in the case of the whole TYMV virus, some scattering in these intervals is expected from the RNA.^{5,6} Taking all these factors into consideration, we have concluded the following: If all carboxyl groups of TYMV are protonated (i.e., exist in the $-\text{COOH}$ form) a very weak Raman line should appear near 1715 cm^{-1} in the spectrum of TYMV in D_2O solution. This line should be a clearly recognizable shoulder on the high-frequency side of the strong amide I line. (The latter is centered near 1660 cm^{-1} where D_2O replaces H_2O as the solvent and more properly is called the amide I' line; see Table I.) However such a shoulder would be impossible to detect in a spectrum of TYMV in H_2O solution because of the greater interference from amide I in that case. If all carboxyl groups of TYMV are ionized (i.e., in the COO^- form), a weak Raman line should appear near $1400\text{-}1415\text{ cm}^{-1}$, over and above the Raman background generated by other protein and RNA groups in this region. Such a feature should be discernible in spectra of TYMV in either H_2O or D_2O solution. If comparable amounts of ionized and protonated carboxyl groups exist simultaneously in TYMV, it would be virtually impossible to detect either the 1415- or 1715-cm^{-1} components in relation to their respective strong backgrounds.

Thus the data shown in Figure 1 indicate that for TYMV at pH 7, *not all of the carboxyl groups of TYMV are protonated*. Spectra recorded at higher resolution and with greatly increased amplification (not shown in Figure 1) consistently lack evidence of a 1715-cm^{-1} shoulder assignable to $-\text{COOH}$ groups. Beyond this point the situation is less clear-cut. The Raman spectra of TYMV do not contain a recognizable feature between 1400 and 1415 cm^{-1} that would confirm conclusively a predominance of ionized carboxyl groups. However, spectra of TYMV always reveal a very weak line near $1395\text{-}1398\text{ cm}^{-1}$ (Table I and Figures 1a and 1b). This line is not due to RNA, but to the protein fraction of TYMV, as verified by its absence from the spectrum of protein-free RNA (Figure 1c) and its presence in the spectrum of RNA-free capsids (not shown in Figure 1). We are, however, yet unable to decide whether the $1395\text{-}1398\text{-cm}^{-1}$ line is to be assigned exclusively to carboxyl groups, or exclusively to other functional groups (CH deformations and ring modes of aromatic residues¹⁰), or partly to both. We are therefore unable to state whether the vast majority of carboxyl groups of TYMV are ionized or whether comparable amounts of both ionized and protonated residues coexist simultaneously. It is clear, however, that not all carboxyl groups are protonated ($-\text{COOH}$) and therefore those which are ionized ($-\text{COO}^-$) can be considered as potential sites for interaction with other molecular subgroups

of the coat protein or of RNA. In this regard, it is worth noting that the position of the Raman line in question ($1395 \pm 4\text{ cm}^{-1}$) is below 1415 cm^{-1} (the frequency of acetate in D_2O solution), so that if it is due in whole or in part to COO^- groups, then the hydrogen bonding interactions involved must be stronger than those between D_2O and $-\text{COO}^-$ in aqueous solutions of acetate.

Our next concern was to evaluate the possibility that the cytosine residues in TYMV RNA are protonated.¹⁵ Fortunately, nonprotonated cytosine residues have a very different spectrum in the $1250\text{-}1600\text{-cm}^{-1}$ region than do protonated cytosine residues. The pK_a value of the ring nitrogen in cytidine (the model compound in this case) is near 4.5 so in neutral solutions the cytosine residue will be nonprotonated. Neutral solutions of cytidine exhibit strong lines at 1245 and 1295 cm^{-1} and a moderately intense line at 1530 cm^{-1} .⁵ Protonated cytidine (in solutions with $\text{pH} < 3$) exhibits an extremely strong line at 1255 cm^{-1} and a weak line at 1546 cm^{-1} (all values for H_2O solutions⁵). No other constituents of TYMV give significant lines between 1525 and 1550 cm^{-1} .^{5,10} Also, no comparably intense Raman scattering from ribonucleosides or protein residues occurs near 1255 or 1295 cm^{-1} and the amide III line (centered near 1248 cm^{-1} for TYMV and at 1243 cm^{-1} in the RNA-free capsid) would not prevent the detection of a line at 1255 cm^{-1} if protonated cytidine residues predominated in TYMV. This is reinforced by the fact that the 1255-cm^{-1} line of protonated cytidine is the most intense Raman line ever observed for any nucleotide base.⁵ Moreover, the present analysis is advanced by the fact that TYMV is particularly rich in cytidine residues as compared with other nucleosides (the nucleoside composition in mol % is A, 22.4; G, 17.2; C, 38.3; and U, 22.1: ref 15). Therefore the presence of a strong line at 1295 cm^{-1} , a weak line at 1530 cm^{-1} , and no line or shoulder at 1255 cm^{-1} in the spectra of TYMV and of TYMV RNA (Figures 1a and 1c) show that a large majority of the cytosine residues are not protonated in solutions at pH 7. We plan to reevaluate this question for solutions below pH 6 in the future. It should be noted that the cytidine line at 1530 cm^{-1} is much weaker in the spectrum of TYMV (Figure 1a) or TYMV RNA (Figure 1c) than anticipated from its counterpart in the spectra of nucleoside and nucleotide monomers.⁵ This is a Raman hypochromic effect resulting from the ordered secondary structure of the RNA molecule, evident for both encapsulated and protein-free states. Large hypochromicity in the 1530-cm^{-1} line is found whenever cytosine residues are in base-stacked configurations, as occur in neutral GpC,²⁰ in polyribonucleotide complexes,⁷ and in ribosomal and transfer RNAs.⁸ The "lost" intensity is recovered when the RNA secondary structure is eliminated by heating to 90°C .²⁰ A further indication of the absence of protonated cytosine in TYMV RNA can be seen by comparison of the present results with spectra of a dinucleoside monophosphate containing protonated cytosine, namely GpC⁺.²⁰ The above conclusion is also confirmed by a similar analysis of the available D_2O solution spectra of TYMV (not shown) and model compounds.

Many other Raman lines in the spectrum of TYMV are assigned to one or more subgroups of the encapsulated RNA. Of particular interest are the lines of 815 and 1100 cm^{-1} , which are due to symmetrical stretching vibrations of the phosphodiester ($-\text{O}-\text{P}-\text{O}-$) and dioxy (PO_2^-) groups, respectively.⁹ The former may be coupled to a small extent with adjacent C-O and C-C bond stretching motions of the ribose residues. The intensity ratio $I_{815}:I_{1100}$ has been correlated with the fraction of RNA nucleotides that are in ordered configura-

tions, with a value of 1.64 assigned to completely ordered structures such as double-helical polyribonucleotide complexes.⁹ In the case of TYMV the measured ratio $I_{815}:I_{1100}$ is only 60% of the maximum value of 1.64, indicating an upper limit of 60% of the phosphodiester groups in the ordered configuration. The significance of this result is as follows. Each nucleotide which is base-stacked between nearest neighbors, as in single-stranded poly (rA), or stacked and paired, as in double-helical polyribonucleotides, is found to contribute equally to the intensity at 815 cm^{-1} .³ Our results show that no more than 60% of the nucleotide residues of TYMV RNA may exist in such regions. The actual percentage may in fact be somewhat less ($\sim 55\%$) because the correlation was established for lower ionic strength solutions in which the 1100-cm^{-1} line (which constitutes the normalization basis) is slightly more intense than at present.⁹

The amount of secondary structure of TYMV RNA is considerably lower than the values near 85% observed for molecules of tRNA, 16S rRNA, R17 RNA, and MS2 RNA.^{3,12,14} This low result could be due in part to chain scissions of the native TYMV molecule, mentioned earlier. However, it is possible that the ordered regions of native TYMV RNA, which are known to be immune to hydrolysis by RNase,¹⁵ are unaffected by the chain scissions detected in present samples. Therefore the present results are considered a reasonable first approximation to the amount of secondary structure in RNA of native TYMV. We plan to reevaluate this question using TYMV which contains more nearly intact RNA.

(c) *Dependence of Raman Spectra on Temperature.* The Raman spectra of TYMV in H_2O and D_2O solutions were recorded as a function of the solution temperature between 0 and 54°C . The results obtained for H_2O solutions are shown in Figure 2. The same results are obtained for D_2O solutions (unpublished). Above 54°C , spectra of reproducible quality could not be recorded. This was attributed to aggregation and precipitation of the coat protein attendant with a breakdown of the capsids above 54°C .

These spectra demonstrate the thermal stability of TYMV up to 54°C (Figure 2). There are no major changes and only one minor change in the Raman scattering frequencies and intensities throughout the spectral interval shown. We observe a small decrease in the Raman intensity at 815 cm^{-1} (amounting to a 9% reduction in the ratio $I_{815}:I_{1100}$) between 41 and 54°C . This reflects a small decrease in the amount of ordered secondary structure of the viral RNA. An accompanying intensity increase at 785 cm^{-1} is more likely due to the shift of the Raman intensity originally present at 815 cm^{-1} to the neighborhood of 790 cm^{-1} rather than to a real change in the intensity of the 785-cm^{-1} pyrimidine line.²⁰ In all other respects the TYMV spectrum is unchanged by increasing temperature.

Discussion

We now offer some observations concerning the results and conclusions presented above.

A conclusion of primary importance concerns the lack of regions of α -helix and β -sheet structure in the coat-protein molecules of TYMV. This result is in contrast to the known structures of many globular proteins in which regions of α -helix and β -sheet are common.²¹ To test this conclusion, we predicted the secondary structure of the TYMV coat-protein molecule from its amino-acid sequence¹⁵ by the method of Chou and Fasman.²² The results of this calculation are given in Table III. An earlier prediction using a different method

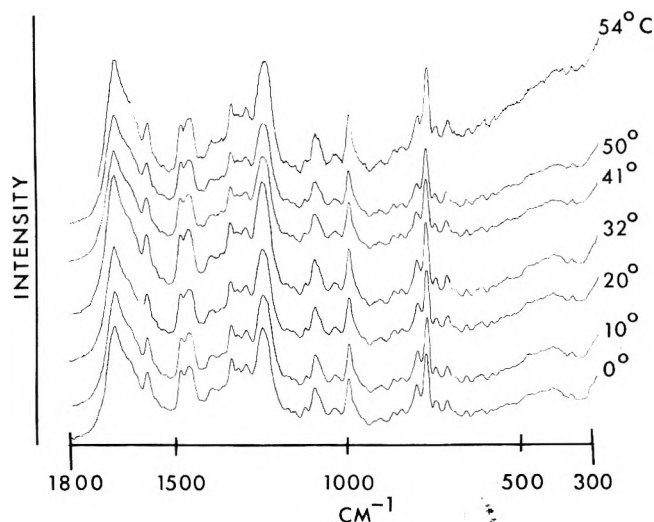


Figure 2. Raman spectra of TYMV in H_2O (0.75 M KCl, pH 7) at 0, 10, 20, 32, 41, 50, and 54°C . Conditions are the same as Figure 1a.

TABLE III: Secondary Structure Calculated for the TYMV Coat-Protein Molecule^a

Residues	Conformation	Residues	Conformation
1-8	α -Helix	97-101	Irregular
9-12	Irregular ^b	102-116	β -Sheet
13-23	β -Sheet	117-127	Irregular
24-34	Irregular	128-132	β -Sheet
35-42	α -Helix	133-144	Irregular
43-46	Irregular	145-149	β -Sheet
47-54	α -Helix	150-153	Irregular
55-60	Irregular	154-160	β -Sheet
61-67	β -Sheet	161-167	Irregular
68-73	α -Helix	168-177	β -Sheet
74-78	β -Sheet	178-182	Irregular
79-88	Irregular	183-187	β -Sheet
89-96	β -Sheet	188-189	Irregular

^a Reference 22. ^b The term irregular includes the terms "random" and " β turn" as used in ref 22.

suggested only two regions of α -helix (residues 35-42 and 71-79 or a total of 16 residues) in TYMV coat protein.¹⁵ Our results agree with one of these regions, but suggest that residues 74 to 78 are in the β structure. From Table III we find that 16% of the amino acid residues are in regions of α -helix, 41% are in regions of β -sheet, and 43% are in regions of irregular structure. Although our predictions from the Raman spectrum could well have missed this relatively small amount of α -helix, the discrepancy concerning the β -sheet structure is less easily explained since the Raman line due to β structure (1229 to 1235 cm^{-1}) is below the region expected to contain the line due to irregular structures (1243 to 1253 cm^{-1}) so that 41% β structure should produce at least a "shoulder" in this region.

We also found that RNA in TYMV contained a comparatively low amount of ordered secondary structure. At least 40% of the nucleotide residues exist in regions with no base pairing or base stacking. All other single-stranded RNA molecules so far examined have only about 15% of the nucleotides in disordered regions.³ The large number of nonpaired bases in TYMV RNA could allow the chain to assume configurations otherwise not possible and could facilitate the interlacing of

the RNA through the protein molecules of the capsid. Also the C=O and N-H groups of these unpaired bases would be available to form H bonds to subgroups of the coat protein.

The Raman effect appears to provide a rapid and reliable means of detecting S-H groups due to the cysteine residues in the proteins of viruses.¹⁴ The presence or absence of S-S linkages may also be easily confirmed. The high resolution and lack of interference from the solvent provide advantages over such methods as Fourier-transform infrared spectroscopy.²³

We also wish to mention that the Raman line from SH groups in TYMV is at a lower frequency and is much broader than the same line in the spectrum of the bacteriophage MS2.¹⁴ This suggests that the SH groups in TYMV may be hydrogen bonded to a greater extent than those in MS2, or that TYMV contains two or more overlapping, but poorly resolved, Raman lines due to SH groups. We have consistently obtained evidence for the latter hypothesis in scans of the SH stretching region with narrower spectral slit widths. Although the appearance of the Raman scattering in this region is similar to that of a doublet (with principal peak at 2569 cm⁻¹ and weak shoulder at 2540 cm⁻¹), two definite peaks cannot be resolved, probably because of intrinsically large half-widths of the lines involved.

We also found that all four SH groups of the TYMV coat-protein molecules will readily exchange to become SD groups when TYMV is dissolved in D₂O. No heating or special treatment was required to produce this exchange. This shows that all SH groups are "in contact" with the solvent and no difference is observed for the four SH groups per molecule. This is different from the kinetics of the reaction of SH groups with *p*-mercuribenzoate in which one SH group reacts more rapidly than the remaining three, which suggests that one SH group is exposed, but that the others are shielded and that changes in capsid structure may be necessary before the second, third, and fourth SH may react (for an authoritative discussion of this point, see ref 15, chapter 8). The advantage of using H → D exchange to study the location of SH groups in proteins is that no changes should be induced in the protein conformation by this method whereas mercurials have been found to degrade TYMV.¹⁵

The aromatic amino-acid residues of the coat protein appear to be distributed between hydrophobic and hydrophilic regions of the TYMV particle in the following manner. The two tryptophan residues per coat-protein molecule are exposed to and interact with solvent H₂O molecules, whereas the three tyrosine residues per coat-protein molecule exist in environments (on the average) where water molecules are largely or totally excluded from hydrogen bonding with them. The Raman data indicate that the tyrosyl OH group is the donor in hydrogen bonding to a negative acceptor group other than H₂O. The present results can be explained by assuming that all tyrosine residues are involved in such hydrogen bonds with acceptors somewhat more negative than the oxygen atom of solvent H₂O, or that two out of three tyrosine residues are involved in such hydrogen bonds with acceptors very much more negative than H₂O oxygen. Either case would seem to allow ionized carboxyl groups as likely candidates. Since such groups outnumber tyrosine (Table II), carboxyl-tyrosyl interactions are clearly a possible source of stabilization of

TYMV. However, the RNA phosphate groups are also available candidates for interaction with tyrosine and further resolution of this question must await more detailed studies of TYMV capsids (free of RNA). Although the coat-protein molecule of TYMV contains three histidine residues, the Raman spectra do not yet permit any conclusions regarding the possible roles of these residues in capsid stabilization.

We have shown that the cytosine residues of the RNA of TYMV in solutions of pH 7 are not protonated to any appreciable extent. Therefore the existence of a significant number of interactions between protonated cytosine residues and protonated carboxyl groups is excluded.¹⁵ The existence of cytosine-cytosine hemiprotonated base pairs also is unlikely.¹⁵ Either of these types of interaction could however occur at pH 6.

The Raman spectra show clearly that TYMV RNA is unusually abundant in cytosine and deficient in guanine residues (cf. Figures 1 and 2 with data of ref 3, 5, 12, and 14); and further that none of the purine or pyrimidine bases are ionized (protonated or deprotonated).

Acknowledgments. The support of the U.S. Public Health Service (Grants AI-11855 and AI-11856) is gratefully acknowledged. We thank Dr. J. M. Kaper for generously providing the bulk preparations of TYMV which were used in this work. We also thank Miss B. Prescott and Mrs. P. E. McDonald-Ordzie for technical assistance and discussions.

References and Notes

- (1) K. A. Hartman received his Ph.D. Degree with Professor R. C. Lord in 1962 and was a Postdoctoral Research Associate with Professor Lord, 1962-1963.
- (2) G. J. Thomas, Jr. received his Ph.D. Degree with Professor R. C. Lord in January 1967 and was thereafter a Postdoctoral Research Associate with Professor Lord to April 1967.
- (3) K. A. Hartman, R. C. Lord, and G. J. Thomas, Jr., in "Physico-Chemical Properties of Nucleic Acids", Vol. 2, J. Duchesne, Ed., Academic Press, New York, N.Y., 1974, p 1.
- (4) R. C. Lord, *Proc. Int. Congr. Pure Appl. Chem., Suppl.*, 23rd, 7, 179 (1971).
- (5) R. C. Lord and G. J. Thomas, Jr., *Spectrochim. Acta, Part A*, 23, 2551 (1967); *Dev. Appl. Spectrosc.*, 6, 179 (1968).
- (6) G. J. Thomas, Jr., *Biochim. Biophys. Acta*, 213, 417 (1970).
- (7) L. Laffeur, J. Rice, and G. J. Thomas, Jr., *Biopolymers*, 11, 2423 (1972).
- (8) G. J. Thomas, Jr., G. C. Medeiros, and K. A. Hartman, *Biochim. Biophys. Acta*, 277, 71 (1972); *Biochem. Biophys. Res. Commun.*, 44, 587 (1971).
- (9) G. J. Thomas, Jr., and K. A. Hartman, *Biochim. Biophys. Acta*, 312, 311 (1973).
- (10) R. C. Lord and N-T. Yu, *J. Mol. Biol.*, 50, 509 (1970); 51, 203 (1970).
- (11) M. C. Chen and R. C. Lord, *J. Am. Chem. Soc.*, 96, 3038, 4750 (1974).
- (12) K. A. Hartman, N. Clayton, and G. J. Thomas, Jr., *Biochem. Biophys. Res. Commun.*, 50, 942 (1973).
- (13) G. J. Thomas, Jr., and P. Murphy, *Science*, 188, 1205 (1975).
- (14) G. J. Thomas, Jr., B. Prescott, P. E. McDonald-Ordzie, and K. A. Hartman, *J. Mol. Biol.*, in press.
- (15) J. M. Kaper, "The Chemical Basis of Virus Structure Dissociation and Reassembly", North Holland/American Elsevier, New York, N.Y., 1975.
- (16) G. J. Thomas, Jr., and J. R. Barylski, *Appl. Spectrosc.*, 24, 463 (1970).
- (17) K. A. Hartman, J. Amaya, and E. Schachter, *Science*, 170, 171 (1970).
- (18) N-T. Yu, T-S. Lin, and A. T. Tu, *J. Biol. Chem.*, 250, 1782 (1975).
- (19) M. N. Siamwiza, R. C. Lord, M. C. Chen, T. Takamatsu, I. Harada, H. Matsura, and T. Shimanouchi, *Biochemistry*, 14, 4870 (1975).
- (20) B. Prescott, R. Gamache, J. Livramento, and G. J. Thomas, Jr., *Biopolymers*, 13, 1821 (1974).
- (21) R. E. Dickerson and I. Geis, "The Structure and Action of Proteins", Harper & Row, New York, N.Y., 1969.
- (22) P. Y. Chou and G. D. Fasman, *Biochemistry*, 13, 211, 222 (1974).
- (23) J. O. Alben, G. H. Bare, and P. A. Bromberg, *Nature (London)*, 252, 736 (1974).

A Raman Spectroscopic Study of Complexes of Polylysine with Deoxyribonucleic Acid and Polyriboadenylic Acid^{1a}

B. Prescott, C. H. Chou, and G. J. Thomas, Jr.*^{1b}

*Department of Chemistry, Southeastern Massachusetts University, North Dartmouth, Massachusetts 02747
(Received December 31, 1975)*

Laser-excited Raman spectra of complexes of polylysine with DNA reveal the frequencies and intensities of Raman scattering from both the polypeptide and nucleic acid components. Most sensitive to complex formation are characteristic vibrational frequencies of the DNA bases. The results show that the DNA-polylysine complex is formed with conservation of the backbone structure normally occurring in aqueous DNA, the so-called B-DNA structure. However, interactions between bases in the DNA double helix are significantly altered by polylysine binding. The same results are obtained for DNA-polylysine complexes formed in either high or low ionic-strength solutions and by either direct mixing or annealing of the constituent biopolymers. The results are consistent with a model in which the extended polylysine chain is bound by electrostatic interactions between positively charged lysyl side chains and negatively charged DNA phosphate groups. Laser-Raman spectra of the complex of polyriboadenylic acid and polylysine show, on the other hand, that both the geometry of the backbone and the mode of interaction between stacked bases of polyriboadenylic acid are altered by complex formation. In this complex, the extended polylysine chain may also be bound to polyriboadenylic acid by electrostatic interaction between lysyl and phosphate groups. However, the gauche⁺-gauche⁺ configuration normally occurring in the phosphodiester linkages of aqueous polyriboadenylic acid is distorted as a consequence of polylysine binding.

Introduction

Interactions between proteins and nucleic acids play a central role in the biology of the living cell by controlling, either directly or indirectly, the processes of cellular metabolism, replication, and development. Such interactions are also of importance in determining the proper assembly and function of certain extracellular agents such as viruses. In many cases the interacting proteins are bound only to highly specific nucleotide sequences or sites of the nucleic acid substrate.² The molecular basis for such remarkably specific and accurate recognition remains, however, a major unsolved problem of molecular biology.

In an effort to learn more about nucleic acid-protein interactions, selected model systems have been examined by a variety of physicochemical methods,³⁻⁹ including infrared (but not Raman) spectroscopy.³ A model system typically consists of a natural or synthetic polynucleotide and a synthetic polypeptide, each of well-defined composition and conformational structure, such as the interacting pair: DNA and polylysine. Here, the nucleotide composition and secondary structure of DNA can be carefully controlled, and the repeat unit (L-lysine) and configurational properties of polylysine are relatively simple when compared with native proteins. Polylysine also has the advantage of serving as a realistic model for lysine-rich proteins (e.g., histones and protamines) which have an affinity for binding to chromosomal DNA.^{2a}

Precipitates formed by the complexing of DNA with polylysine have been studied in considerable detail. Leng and Felsenfeld⁴ established conditions (viz., in 1.0 M NaCl) at which complex formation is reversible and demonstrated the dependence of interaction upon the degree of polymerization (DP) of polylysine and the molecular weight, adenine-thymine (AT) content, and secondary structure of DNA. Tsuboi et al.⁵ have proposed that at lower salt concentrations (0.1-0.4 M NaCl) the complex is formed in an essentially irreversible manner and with a 1:1 ratio of lysine amino ($-\text{NH}_3^+$) to DNA

phosphate ($>\text{PO}_2^-$) groups. This stoichiometry is consistent with a structure in which the extended polypeptide chain is wound helically around a groove of the DNA double helix.⁶ Olins et al.^{7,8} confirmed the specificity of polylysine for AT-rich regions of DNA, noting that lysine-bound sites are far more stable than unbound sites with respect to thermal denaturation of substrate DNA, and established further that a minimum of eight lysyl residues is needed to effect cooperative binding at moderate salt concentrations.

The more recent literature on this subject reveals further details of the DNA-polylysine interaction, as well as some unresolved conflicts. For example, hydrogen-tritium exchange studies⁹ indicate that a substantial fraction (about one-fourth) of DNA base protons, involved in interchain hydrogen bonding, are promoted to an instantaneously changing (i.e., solvent exposed) class as a consequence of polylysine binding. The peptidyl hydrogens of bound polylysine exchange as a single class, though more slowly than in the case of unbound polylysine. These results suggest that the secondary structure of DNA is altered by complex formation and that the peptidyl backbone of polylysine is partially shielded from the aqueous environment by the DNA substrate. It was conjectured^{2a,9} that the DNA bases, which are perpendicular to the helix axis in unbound DNA (the so-called "B" geometry of DNA¹⁰), may be tilted by several degrees from the plane normal to the helix axis (as in the "A" geometry of DNA or RNA¹⁰) when polylysine binding occurs. This simple hypothesis, despite its attractiveness, appears to be in conflict with the published work of Higuchi and Tsuboi¹¹ which demonstrates both qualitative and quantitative differences between the binding of polylysine to nucleic acids of the B (DNA) and A (RNA) types. Moreover, steric conflicts are encountered when attempting to accommodate a polylysine strand into the groove of nucleic acid double helices of the A type.¹¹ Also, while DNA and polylysine easily complex in the presence of 1.0 M NaCl,^{4,12} RNA and polylysine apparently form a complex quantitatively only at lower (0.1-0.4 M NaCl) salt concentrations.^{11,13-15}

In a detailed study of DNA–polylysine complexes, Shapiro et al.¹² demonstrated the reversibility of interaction, over a wide range of salt concentrations. These authors emphasized that despite the insolubility of the complex (ranging from a flocculent precipitate to suspended spherical particles of mean radius 1700 Å, depending upon solute and solvent conditions), the separated phase should be regarded as a “complex coacervate” in equilibrium with the solution phase, readily exchanging its DNA with excess DNA in the solution. More importantly, the preference of polylysine for AT-rich regions of DNA with a binding ratio of one lysine residue per nucleotide was unambiguously established, thus further supporting the notion that DNA–polylysine complexes may be structurally quite different from complexes of polylysine with polyribonucleotides that lack both A and T bases.^{5,11,13} In DNA–polylysine, the data¹² reveal a well-ordered complex formed cooperatively and stabilized by electrostatic interaction between the positively charged ϵ -amino group of each lysyl residue and the negatively charged phosphodiester group of each nucleotide in the bound regions of DNA. In this structure the optical rotatory dispersion (ORD) and circular dichroism (CD) spectra of complexed DNA differ strikingly from ORD and CD spectra of free DNA,^{12,16} suggesting a conformational change of the nucleic acid though not necessarily one involving either base-tilting or a B \rightarrow A transition. While many workers^{17–22} have contended that the B-DNA structure is altered appreciably by the binding of either polylysine or lysine-rich histones, x-ray diffraction,^{23,24} electron microscopy,^{25–27} and infrared dichroism^{3,28,29} measurements of the complexes do not in general support this contention. The best available x-ray diffraction patterns of DNA–polylysine²³ exclude the likelihood of any major degree of distortion of the B-DNA double helix, but provide instead evidence of supercoiling and formation of liquid-crystalline or micellar structures. The formation of such ordered liquid-crystalline phases could also explain the observed CD, ORD, and infrared spectra of DNA–polylysine.

Nevertheless, there remains considerable controversy in this matter. Some most recently published CD studies of DNA–polylysine^{20,30} advance the view that the B-DNA structure is perturbed in the direction of a C-DNA structure (also base-tilted¹⁰) as a consequence of polylysine binding, while identical data obtained independently³¹ have been given a different interpretation. Finally, it has been proposed that structural details of the complex at the molecular level,^{32,33} as well as thermodynamic properties,³⁴ depend upon whether the complex is prepared by direct mixing of the constituent biopolymers or by annealing (reconstitution) in a salt gradient dialysis.

We have thus undertaken a study of DNA–polylysine and other polynucleotide–polypeptide complexes using laser Raman spectroscopy in order to determine whether structural changes accompany complex formation and which molecular subgroups may participate. The Raman spectrum of a nucleic acid generally reveals both qualitative and quantitative information relating to its secondary structure, including the backbone conformation of the macromolecule.^{35–37} Raman spectra of proteins and polypeptides also provide information on the macromolecular conformation,^{38,39} though at present the data are more reliably employed for qualitative rather than quantitative purposes.

In this paper we discuss the Raman spectra of the DNA–polylysine and polyriboadenylic acid–polylysine complexes. The results obtained are helpful in confirming or rejecting some of the proposals, discussed above, concerning the nature

of DNA–polylysine interaction. The data are additionally useful in providing a better understanding of the Raman spectra and intermolecular interactions of native nucleoproteins, such as viruses, that have been under investigation in our laboratory for the past several years.^{40–42}

The subject of this paper would seem an appropriate one for this volume, in view of the fact that present-day developments in laser-Raman spectroscopy of both nucleic acids and proteins can be traced to the initial studies carried out on such biomolecules during the late 1960's at the MIT Spectroscopy Laboratory under the direction of Professor Lord.^{43,44} The application of Raman spectroscopy to investigate nucleic acid–protein interactions is a logical outgrowth of these earlier studies.

Experimental Methods

Highly polymerized calf-thymus DNA (molecular weight $\approx 10^6$ – 10^7) and poly-L-lysine (average degree of polymerization (\overline{DP}) ~ 300) were obtained from Sigma Chemical Co. Polyriboadenylic acid poly(rA) of high molecular weight ($\geq 100\,000$) was obtained from Miles Laboratories, Inc. All other reagents were of the highest grades commercially available.

The so-called “directly mixed” complex of DNA and polylysine was prepared using a method similar to that of Felsenfeld and co-workers.^{4,12} Equal volumes of aqueous polylysine (0.1 M in peptide monomer) and aqueous DNA (0.1 M on nucleotide monomers) were mixed directly, vortex agitated, and allowed to stand for several hours at room temperature after the complex, recognizable as a separate phase, had formed. The polymer stock solutions were originally at pH 7.5 and contained either 0.025 M NaCl (low salt) or 1.0 M NaCl (high salt) concentration. The relatively high concentrations of DNA and polylysine employed here are required for Raman spectroscopy, so that a relatively dense precipitate is obtained in a small volume of supernatant. Identical results were obtained when either cacodylate buffer (pH 6.5), Tris buffer (pH 8), or EDTA (pH 8) was present in the stock solutions.

The directly mixed poly(rA)–polylysine complex was prepared in the same way, except that 0.01 M sodium phosphate buffer (pH 7.5) was present in the stock solutions.

The “reconstituted” DNA–polylysine complex was prepared by the salt gradient dialysis method, also described previously.^{4,12,31} Cellulose dialysis tubing was boiled for 1 h in 5% NaHCO₃ + 0.1 M EDTA, followed by boiling twice in distilled water, the last time immediately before use. Equal volumes of DNA (0.025 M) and polylysine (0.025 M) in 4 M NaCl solution (pH 7) were mixed and dialyzed against successively more dilute salt solutions, leading eventually to a final salt concentration of 0.025 M NaCl. The complex formed in this manner was also insoluble at the concentrations of DNA and polylysine employed.

Each of the above complexes that was prepared in a low ionic strength medium (viz., DNA–polylysine in 0.025 M NaCl, either directly mixed or reconstituted, and poly(rA)–polylysine in 0.01 M sodium phosphate buffer) appeared as a white, fibrous precipitate. However, the high ionic strength complex of DNA and polylysine (in 1.0 M NaCl) invariably appeared as a gel, either opaque or transparent. In all cases the nucleotide:lysine ratios were the same, namely, 1:1, and Raman spectra were reproducible to within $\pm 5\%$ in scattering frequencies and intensities for independently prepared complexes of a given type. The fact that all of the solution DNA was precipitated by the added polylysine was confirmed

by obtaining spectra of the supernatants which were indistinguishable from H_2O .

For Raman spectroscopy, the complexes were transferred from the mixing vessel to a sample cell (1.0-mm glass capillary tube). Raman spectra of high signal-to-noise quality could be obtained provided the separated phase was suspended in its corresponding supernatant (mother liquor). For a given complex, the Raman spectrum displayed the same frequencies and intensities, regardless of the physical state of the sample. However, optimum scattering was achieved with the aqueous suspensions described above, or with gels of low opacity.

Aqueous solutions ($\sim 3\%$ weight/volume) of DNA, poly(rA), and polylysine were also contained in glass capillary tubes, filled to approximately $10 \mu\text{l}$, for obtaining Raman spectra.

All spectra were excited with 200–400 mW of 514.5-nm radiation from an Ar^+ laser (Coherent Radiation, Model CR2), and were recorded on a Spex Ramalog spectrometer. Further details of Raman instrumentation are described elsewhere.⁴⁵

Results and Discussion

1. DNA–Polylysine Complexes. Raman spectra of DNA, polylysine, and the directly mixed DNA–polylysine complex, each in 1.0 M NaCl, are compared in Figure 1. Spectra of DNA, polylysine, the directly mixed DNA–polylysine complex, and the reconstituted DNA–polylysine complex, each in 0.025 M NaCl, are compared in Figure 2. In order to interpret these results it is useful to consider briefly the previously published Raman data on DNA^{46–48} and polylysine.^{39,49}

The A, B, and C structures of DNA are distinguished from one another by the frequency and intensity of Raman scattering near 800 cm^{-1} , due largely to the OPO symmetric stretching vibration of the phosphodiester backbone.^{35,46} In A structures a strong sharp line occurs at 807 cm^{-1} and in B structures there is a weak broad line at $830 \pm 5 \text{ cm}^{-1}$.^{46–48} In C structures the corresponding vibrational frequency presumably occurs outside the range $790\text{--}850 \text{ cm}^{-1}$, where it is masked by other Raman scattering from vibrations of the DNA bases.⁴⁶ The sensitivity of the phosphodiester group frequency to changes in backbone conformation is well established both for nucleic acids and model compounds.³⁵ Another feature distinguishing Raman spectra of A, B, and C structures is the relative intensity of the pair of lines at 670 and 680 cm^{-1} . The former is more intense for A-DNA, the latter more intense for B-DNA, and the two of equal intensity for C-DNA.^{46–48} The 670- and 680-cm^{-1} lines are due to in-plane ring vibrations of thymine and guanine, respectively,⁴³ and the intensity reversal accompanying the $A \rightarrow B$ transition probably reflects the different base stacking geometries in the two types of helix. Furthermore, there is a strong thymine line at 750 cm^{-1} in B-DNA appearing with greatly diminished intensity in A- or C-DNA.⁴⁶ C-DNA is also distinguished from both A- and B-DNA by a strikingly different pattern of Raman frequencies in the $1250\text{--}1400\text{-cm}^{-1}$ interval,⁴⁶ again attributable to its altered base stacking geometry. Finally the PO_2^- dioxy symmetric stretching vibration, which occurs near $1092\text{--}1095 \text{ cm}^{-1}$ in B-DNA, is elevated to 1100 cm^{-1} in A-DNA and to 1104 cm^{-1} in C-DNA.⁴⁶ However, this elevation represents the effect of dehydration of the phosphate groups, rather than an intramolecular conformational change.⁴⁷ In any case the overall shift ($\sim 10 \text{ cm}^{-1}$) is small and not as useful for diagnostic purposes as the shifts described above.

In the case of polylysine, the extended or random-chain structure gives characteristic Raman lines at approximately 1245 cm^{-1} (amide III) and 958 cm^{-1} (C–C stretching) which

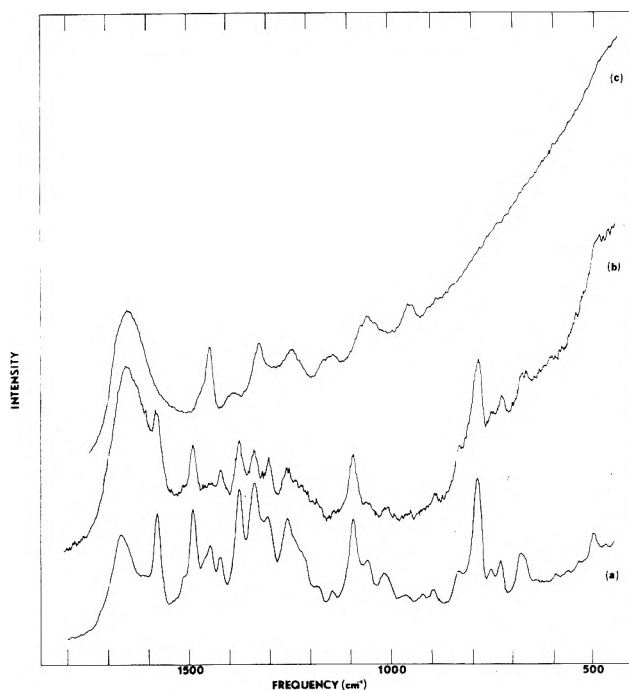


Figure 1. Raman spectra at $32 \text{ }^\circ\text{C}$ of the following in 1.0 M NaCl solution (pH 7): (a) DNA–polylysine complex, directly mixed; (b) DNA; (c) polylysine. Excitation wavelength 514.5 nm; radiant power $\sim 300 \text{ mW}$; spectral slit width 10 cm^{-1} ; scan speed $25 \text{ cm}^{-1}/\text{min}$; rise time 10 s.

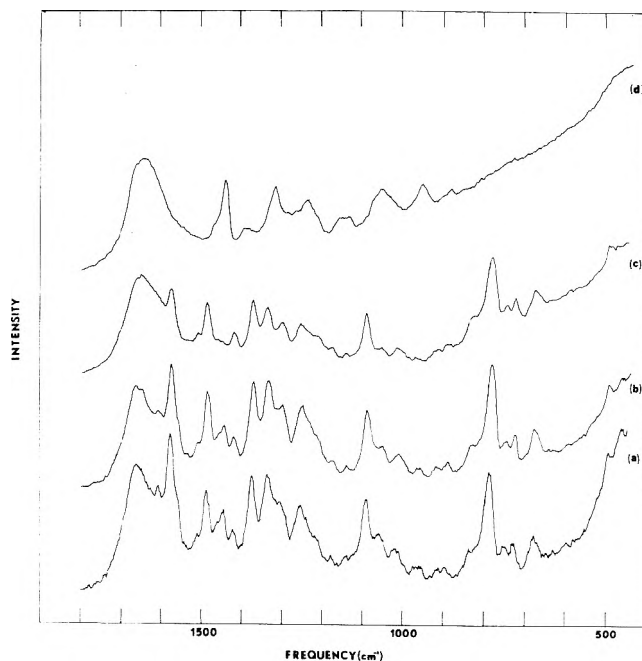


Figure 2. Raman spectra at $32 \text{ }^\circ\text{C}$ of the following in 0.025 M NaCl solution (pH 7): (a) DNA–polylysine complex, directly mixed; (b) DNA–polylysine complex, reconstituted; (c) DNA; (d) polylysine. Conditions as in Figure 1.

differ both in frequency and intensity from the corresponding lines obtained when α -helical or β -sheet structures prevail.^{39,49} The amide III and skeletal C–C stretching modes are considered to be the most responsive to conformational changes in the polylysine backbone, though other differences have also been noted.⁴⁹

Thus the spectra of DNA (noncomplexed) in Figures 1b and 2c correspond to the B conformation and spectra of polylysine

(noncomplexed) in Figures 1c and 2d correspond to the extended or random-chain conformation. The fact that spectra of DNA are identical, whether the NaCl concentration is 1.0 M (Figure 1b) or 0.025 M (Figure 2c), indicates that the B conformation is unchanged over this range of salt concentration. The identity of Figures 1c and 2d has a similar significance for polylysine.

When the DNA-polylysine complex is formed, the PO_2^- group frequency remains at 1093 cm^{-1} and is unaffected in either intensity or half-width. This result may seem at first surprising, since interaction between lysyl ($-\text{NH}_3^+$) and nucleotide ($>\text{PO}_2^-$) groups is considered to be the basis for complex formation.^{6,12} However, as discussed below, the PO_2^- group frequency is virtually insensitive to a variety of intra- and intermolecular interactions of nucleic acids. The unaltered condition of the 1093-cm^{-1} line of DNA is evident for the directly mixed complex in 1.0 M NaCl (Figure 1a), the directly mixed complex in 0.025 M NaCl (Figure 2a), and the reconstituted complex in 0.025 M NaCl (Figure 2b). (See also Figure 3.)

Nevertheless, in other respects the Raman spectrum of each complex differs from spectra of its constituents. In order to demonstrate more clearly the spectral differences between DNA-polylysine complexes and noncomplexed DNA plus polylysine, the Raman spectrum of each complex is redrawn in Figure 3 together with a tracing of the sum of spectra of the constituent (noncomplexed) polymers at the same experimental conditions.

The tracings of Figure 3 were made from the best available data as follows. The spectrum of a given complex was reproduced from the originally recorded spectrum by plotting the Raman scattering intensity over a flat baseline tangent to intensity maxima near 600 , 900 , 1400 , and 1800 cm^{-1} . Thus, Figure 1a yields the broken line curve of Figure 3a. The synthesized spectrum was obtained by adding together the separately recorded Raman spectra of DNA and polylysine, each at the same experimental conditions with the same baseline as employed for the corresponding complex. Before adding the constituent spectra it was necessary to normalize them in such a way as to preserve the 1:1 molar ratio of lysine to nucleotide that is assumed for the complex. Accordingly, the contributions of DNA and polylysine were normalized so that their respective Raman lines at 1093 cm^{-1} (PO_2^- dioxy symmetric stretching) and 1444 cm^{-1} (C-H deformation) were of the same intensity as observed in the complex. Thus, the spectra of Figures 1b and 1c, so added, give the solid line curve of Figure 3a.

The rationale for this normalization procedure rests upon the fact that for a given nucleic acid (in the present case, DNA), the PO_2^- group frequency is independent of the kind and extent of interaction between the nucleic acid bases. Indeed, the dioxy symmetric stretching vibration generates the Raman line which is the most insensitive to conformational changes of aqueous RNA,³⁵ aqueous DNA,⁴⁸ and synthetic polynucleotides.^{36,37,50} Its position and half-width appear to be affected only by gross changes in the degree of hydration of nucleic acid fibers⁴⁷ (as noted above), and then only to a rather small extent. A very slight broadening of the 1100-cm^{-1} Raman line of aqueous tRNA has also been observed when large excesses of divalent cations (e.g., Mg^{2+}) are present in solution.⁵¹ Therefore the 1093-cm^{-1} line is considered to provide the best available basis for normalization of other Raman intensities of DNA. Likewise, the 1444-cm^{-1} line of polylysine is unaffected by conformational changes in the peptidyl backbone, by side chain ionizations, and so forth.^{39,49}

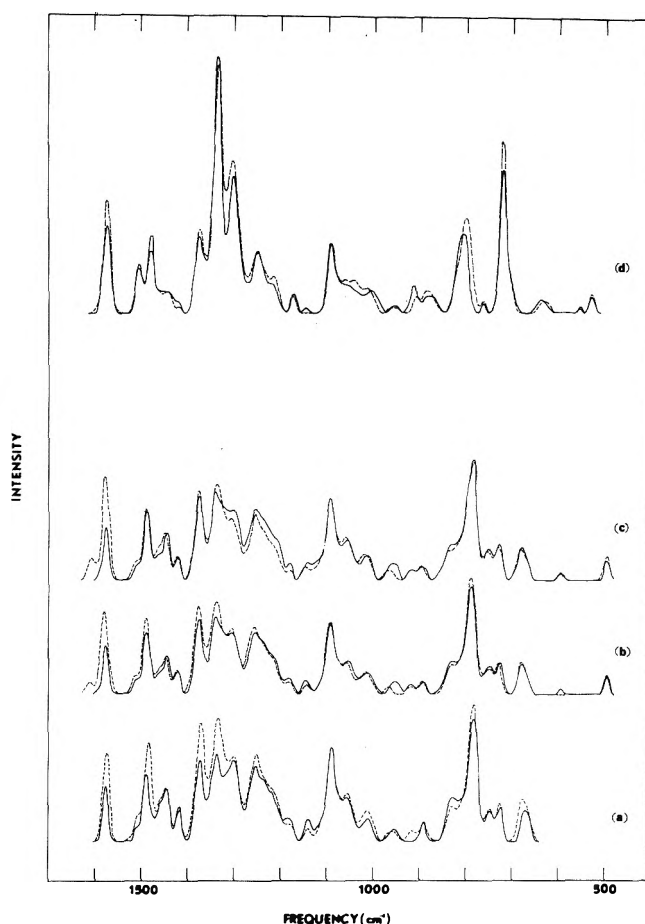


Figure 3. Comparison of the observed Raman spectra of a complex (---) with the sum of the spectra of the constituent polymers (—), for each of the following: (a) DNA-polylysine, directly mixed in 1.0 M NaCl (pH 7); (b) DNA-polylysine, reconstituted in 0.025 M NaCl (pH 7); (c) DNA-polylysine, directly mixed in 0.025 M NaCl (pH 7); (d) poly(rA)-polylysine, directly mixed in 0.01 M sodium phosphate (pH 7.5).

This is not surprising in view of the origin of the 1444-cm^{-1} line in C-H deformations of the lysyl methylene groups.⁴⁹ It is fortunate that polylysine gives no Raman scattering at 1092 cm^{-1} and DNA very little at 1444 cm^{-1} .

On the other hand it is not possible to demonstrate independently the validity of the above normalization procedure, since an internal standard cannot be incorporated quantitatively into the aggregated complexes. It is also recognized that the normalization procedure used here does not compensate for Raman scattering by the aqueous solvent (or supernatant). Nevertheless, the contribution from H_2O is about the same for each spectrum of Figure 2, and only about a factor of 2 smaller for the complex of Figure 1. Therefore errors introduced in this regard are probably negligible, except for the regions below 950 and above 1600 cm^{-1} in Figure 3a, where considerably different solvent backgrounds prevailed in the original spectra.

Despite these limitations, it is still possible to observe the following features in Raman spectra of DNA-polylysine complexes of Figure 3. First, the B conformation of DNA is conserved in each complex. This is evident by the appearance in each case of a Raman line near $828\text{--}835\text{ cm}^{-1}$ with little or no change from the Raman line of free DNA at this frequency. Also, the pair of lines at 671 and 680 cm^{-1} , observed here as an unresolved doublet, is always centered at approximately

TABLE I: Raman Spectral Changes of DNA and Polylysine Accompanying Complex Formation^a

Complex	Frequency	Rel intensity	Assignment	Effect of complex formation
DM (1.0 M NaCl)	954	w	C-C str (PLL)	Shift to 965 cm ⁻¹ and intensity decrease
	1254	s	C,A	Small intensity increase
	1301	s	A	Small intensity increase
	1338	s	A	Large intensity increase
	1374	s	T,A,G	Large intensity increase
	1489	s	G,A	Large intensity increase
	1577	s	G,A	Large intensity increase
R (0.025 M NaCl)	954	w	C-C str (PLL)	Shift to 966 and intensity decrease
	1254	s	C,A	Small intensity increase
	1302	s	A	Small intensity increase
	1339	s	A	Moderate intensity increase
	1374	s	T,A,G	Moderate intensity increase
	1488	s	G,A	Moderate intensity increase
	1577	s	G,A	Large intensity increase
DM (0.025 M NaCl)	954	w	C-C str (PLL)	Shift to 964 and intensity decrease
	1241	m	amide III, A,T,C	Small intensity decrease (?)
	1254	s	C,A	Small intensity decrease (?)
	1302	s	A	Small intensity decrease (?)
	1339	s	A	Small intensity increase
	1577	s	G,A	Large intensity increase

^a Abbreviations: Complex: DM = directly mixed, R = reconstituted; Rel intensity: s = strong, m = medium, w = weak; Assignment: A = adenine, T = thymine, G = guanine, C = cytosine, PLL = polylysine, str = stretching, other letter abbreviations refer to functional groups.

678 cm⁻¹, indicative of the fact that the guanine component is the more intense as expected for B-DNA. This is confirmed by scans of the 650–700-cm⁻¹ region (not shown) at 5-cm⁻¹ resolution, which clearly resolve the doublet and the stronger intensity of the 680-cm⁻¹ component. Likewise the line at 750 cm⁻¹ and other ring vibrational frequencies of the DNA bases reveal the B structure, but neither the A nor C structure. Second, the extended conformation of polylysine is conserved in each complex. Small changes in the Raman scattering intensity of complexed polylysine, vis-a-vis free polylysine, are evident in each case near 1250 cm⁻¹ and small shifts to higher frequency are also observed for the 954-cm⁻¹ line. However, these changes are not sufficient to indicate an appreciable conversion to structures other than of the extended chain type.^{39,49} Third, the major differences between Raman spectra of a complex and its constituents occur in the region 1250–1500 cm⁻¹ and are due to enhanced Raman scattering by DNA base vibrations. Fourth, except for the 954-cm⁻¹ line of polylysine mentioned above, spectral differences between a complex and its constituents in the region below 1200 cm⁻¹ are small, restricted to weaker Raman lines, and estimated to be within experimental error. (In the case of Figure 3a, a substantial uncertainty in the spectral baseline could account for the larger spectral differences noted there, as discussed earlier.) A summary of the significant spectral differences between each complex and its constituents is given in Table I. It is apparent from Table I that the *major* elements of change are qualitatively similar for each complex, but quantitatively largest for the high-ionic strength complex. By far the most dramatic effect of complex formation is the enormous increase in the Raman intensity of the 1577-cm⁻¹ line of DNA (due to G and A ring vibrations⁴³), apparent even in the original data shown in Figures 1 and 2. The magnitude of this intensity increase is comparable for each type of complex.

On the other hand, the 1489-cm⁻¹ line, which has a similar origin (G and A bases⁴³), shows a large intensity increase only for the directly mixed complex in 1.0 M NaCl.

In summary, the DNA–polylysine complex, directly mixed at high ionic strength, reveals the most drastically altered Raman spectrum as the result of complex formation, followed in order by the reconstituted low-ionic-strength complex and the directly mixed low-ionic-strength complex. It is of interest to note that with one exception (954-cm⁻¹ line of polylysine) all of the Raman lines in each complex which differ significantly in frequency and/or intensity from Raman scattering by the constituent polymers originate from vibrations of the DNA bases and, more specifically, are due in whole or in part to adenine.

2. *Poly(rA)–Polylysine Complex.* In view of the above, and the work of other investigators concerning the formation of a stable complex between poly(rA) and polylysine^{31,52–54} we have obtained Raman spectra of this complex and its constituent polymers as shown in Figure 4. For comparison with the results obtained on DNA–polylysine complexes, we include in Figure 3d the spectrum observed for poly(rA)–polylysine (broken line) and that synthesized from adding together the appropriately normalized (see above) spectra of poly(rA) and polylysine, assuming a 1:1 molar ratio of adenylic acid to lysine residues (solid line). It is worth noting that because the solution of poly(rA) is much less viscous than that of DNA, and therefore more easily rid of suspended matter, its Raman spectrum displays a higher signal-to-noise ratio than does that of DNA. Accordingly, higher concentrations of poly(rA) can be employed and attendant with them is a lower background of scattering from H₂O, as shown in Figure 4. Consequently, there is much less uncertainty in the positions and relative intensities of Raman lines traced in Figure 3d, than was encountered for the DNA–polylysine spectra (Figures 3a–c). We

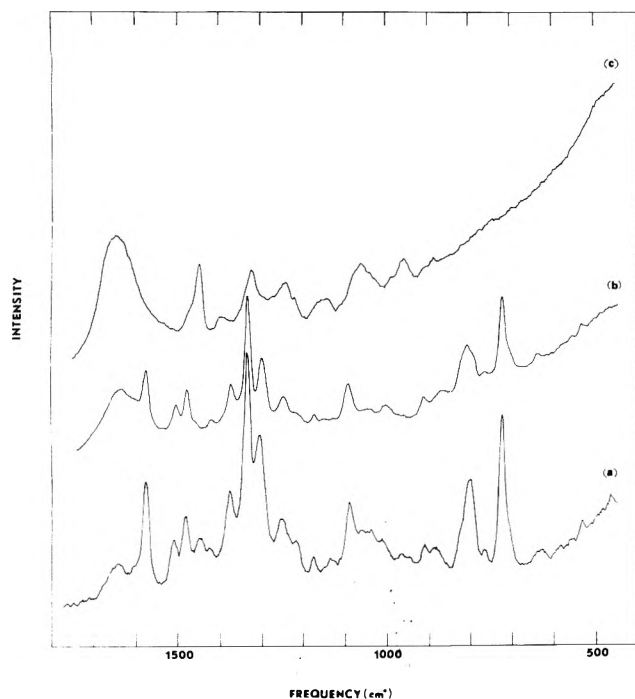


Figure 4. Raman spectra at 32 °C of the following in 0.01 M sodium phosphate (pH 7.5): (a) poly(rA)-polylysine complex, directly mixed; (b) poly(rA); (c) polylysine. Conditions as in Figure 1.

are confident that all of the discrepancies between observed and synthesized spectra of Figure 3d (accurately reproducible) are significant and due to intermolecular interaction between polynucleotide and polypeptide. The same results are also obtained when a stoichiometric excess of phosphate buffer, pH 7.5, is present to ensure that poly(rA) is maintained in the single-stranded, nonprotonated form. It is of course clear from the spectra shown (cf. Figure 4 with data of ref 43) that, even in the absence of excess buffer, there is no appreciable conversion of poly(rA) to the protonated double-helical structure, poly(rA⁺)-poly(rA⁺). The latter exhibits a completely different Raman spectrum,^{55,56} by virtue of the protonation of the adenine bases and the formation of a double-stranded helix.

Raman spectra of single-stranded poly(rA) and of its interaction products with other polynucleotides have been discussed in considerable detail previously.^{35-37,50,56-58} For the present discussion we take note of the following correlations between Raman spectra and structural properties of this polynucleotide. (i) Single-stranded poly(rA) at low temperatures (0-40 °C) assumes a predominantly ordered structure in which most of the bases are stacked one above another.⁵⁹ Such base stacking causes several Raman lines due to in-plane vibrations of the bases to suffer intensity loss (Raman hypochromism).⁵⁰ Most hypochromic are the lines at 726, 1306, 1377, 1508, and 1576 cm⁻¹,^{50,60} all of which recover their lost intensity when the base stacking is eliminated by heating poly(rA) to high temperatures (~100 °C). (ii) Raman spectra indicate that the single-stranded, base-stacked structure of poly(rA) contains a backbone geometry very similar to that of double-helical polyribonucleotides and RNA,^{35,36} which are in turn structurally similar to A-DNA.^{10,46,47} In such polyribonucleotide structures the phosphodiester symmetric stretching vibration (which may be coupled with adjacent C-O stretching vibrations) generates an intense Raman line at approximately 812 cm⁻¹.³⁵ Recent calculations⁶¹ support our

original assignment^{35,62} and indicate further that the C-O-P-O-C network is most likely in the gauche⁺-gauche⁺ (g⁺-g⁺) configuration. When poly(rA) is disordered by heating, the phosphodiester group frequency shifts to 795-797 cm⁻¹ with little change in overall intensity.³⁶ The Raman scattering in this frequency range is in fact somewhat dependent upon ionic strength. The relative Raman intensities at 812 and 795 cm⁻¹ nevertheless provide a rough measure of the relative numbers of adenylic acid residues of poly(rA) in ordered and disordered states, respectively.^{35,36} A more detailed understanding of the relationship between Raman scattering intensity near 800 cm⁻¹ and polynucleotide backbone conformation must await additional studies of model compounds and reliable normal coordinate calculations. However, a reasonable explanation is that coupling of P-O and C-O (and possibly C-C) bond stretching motions may elevate this frequency to 812 cm⁻¹ in ordered ribopolymer structures (as compared with 760-780 cm⁻¹ in alkyl phosphate esters⁶³) and such coupling may be reduced or eliminated when the A geometry of the backbone is thermally denatured. This would require a conversion of C-O-P-O-C dihedral angles from the g⁺-g⁺ configuration to another (or several) different configuration(s) which are sterically and energetically accessible.⁶¹ (iii) Finally, there are a number of less dramatic changes in the Raman spectrum of poly(rA) accompanying thermal denaturation.^{36,50,60} One of the more interesting of these is the apparent disappearance of a weak Raman line near 710 cm⁻¹, usually observed as a shoulder to the intense 726-cm⁻¹ line in low temperature spectra. We have speculated³⁶ that this line is due to a vibration of the ribose ring, since it also appears in Raman spectra of other ordered (low temperature) ribonucleotides, including monomers, oligomers, and polymers. Its presence only in low-temperature spectra clearly suggests conformational dependence and a reasonable hypothesis is that C₃-endo ring puckering¹⁰ of the ribofuranosyl moiety is responsible.

Examination of Figure 4b shows that at 32 °C poly(rA) contains a predominantly ordered structure, by virtue of the peak at 811 cm⁻¹ with only a weak shoulder near 797 cm⁻¹. This spectrum is similar to that published previously³⁶ and we have estimated from curve fitting⁶⁰ that ~65% of the nucleotide residues are in the ordered configuration.

Attendant with complex formation the Raman lines of poly(rA) in the complex undergo the changes generally characteristic of thermal denaturation, as discussed above, with the following exceptions. The Raman line at 1483 cm⁻¹ loses intensity upon complex formation, whereas it is virtually unchanged in intensity upon thermal denaturation of poly(rA); the line at 1508 cm⁻¹ is unaffected by complex formation, whereas it gains intensity upon thermal denaturation; the weak shoulder at 708 cm⁻¹ is unaffected by complex formation whereas it is eliminated by denaturation. Table II summarizes the effects of complex formation upon Raman spectra of poly(rA) and polylysine.

Thus in poly(rA)-polylysine, as in DNA-polylysine, the Raman spectrum reveals substantial structural change only in the polynucleotide component. Moreover, in both cases the Raman intensities associated with ring vibrational frequencies of the nucleotide bases are affected. However, in poly(rA)-polylysine the binding of polylysine perturbs the configuration of the polynucleotide backbone, whereas in DNA-polylysine the backbone configuration of B-DNA is conserved.

Conclusions

The present results allow us to draw the following conclu-

TABLE II: Raman Spectral Changes of Poly(rA) and Polylysine Accompanying Complex Formation^a

Frequency	Rel Intensity	Assignment	Effect of complex formation
726	s	A ring	Intensity increase
811	s	O-P-O sym str	Shift to 804 cm ⁻¹ and intensity increase
887	w	C-O, C-C str (RP)	Intensity increase
917	w	A ring	Shift to 912 cm ⁻¹ and intensity decrease
1007	m	C-O, C-C str (RP)	Shift to 1014 cm ⁻¹
1025-1075	m	C-O, C-C, C-N str (PLL, RP)	Intensity increase
1221	w	A ring	Intensity increase
1306	s	A ring	Intensity increase
1379	m	A ring	Intensity increase
1483	m	A ring	Intensity decrease
1578	s	A ring	Intensity increase

^a Abbreviations: RP = ribose phosphate; other abbreviations as in Table I.

sions concerning the model nucleic acid-protein complexes under investigation.

(1) Binding of extended-chain polylysine to B-DNA alters appreciably the secondary structure of the nucleic acid but not that of the polypeptide.

(2) The extent of alteration of the DNA secondary structure depends upon the concentration of NaCl in solution and the method of preparation of the complex. The largest effects were noted for directly mixed complexes which yielded a gel at high NaCl concentration (1.0 M).

(3) The kind of structural change induced in DNA by polylysine binding does not depend upon either the concentration of NaCl or the method of preparation of the complex. In particular, directly mixed and reconstituted complexes differ in the amount but not in the kind of structural perturbation of DNA.

(4) The backbone configuration of B-DNA is not significantly altered by polylysine binding. The secondary structure of bound DNA appears to differ from that of unbound DNA only in the interactions between bases (i.e., in intensities of Raman lines due to base vibrations). In particular, DNA-polylysine complexes give no evidence of containing either A-DNA or C-DNA structures.

(5) Raman lines of the purine bases, particularly adenine, are the most sensitive to polylysine binding. They undergo intensity increases similar but not identical with those observed upon thermal denaturation of DNA.^{48,64}

(6) The binding of extended chain polylysine to single-stranded poly(rA) alters appreciably the secondary structure of the polynucleotide but not that of the polypeptide.

(7) In poly(rA)-polylysine *both* the backbone geometry of the polynucleotide *and* the mode of base stacking are altered by polylysine binding. Specifically, the g^+-g^+ phosphodiester configuration and the appreciable base stacking which are assumed to occur in single-stranded poly(rA) are displaced in favor of the type of structure prevailing for thermally denatured poly(rA) as a consequence of polylysine binding.

The complexes studied here are considered to be similar to the DNA-polylysine complexes described by Tsuboi and co-workers^{5,11,13,65} and Felsenfeld and co-workers^{4,12} and to the poly(rA)-polylysine complexes described by Davidson and Fasman.⁵² In each case the stoichiometry of lysine to nucleotide is 1:1. Unfortunately it is not possible to demonstrate the stoichiometry of interaction using Raman spectra, since suitable data are obtained only from thick precipitates or gels which result from mixtures initially containing stoichiometric equivalents of lysine and nucleotide. Likewise it is important

to recognize that at the solute concentrations required for Raman spectroscopy a direct comparison with data of previous workers may be of doubtful significance. For ultraviolet absorption spectroscopy^{5,65} and CD spectroscopy,^{4,12,52} for example, the complexes are prepared from solutions containing nucleotide and lysine concentrations as much as 10⁴-fold lower than those employed here. Nevertheless the precipitates we have examined are true complexes and are probably similar to the aggregates or "separated phases" studied previously.

In any case, the presently examined DNA-polylysine complexes do not reveal structural features at the molecular level which depend in kind upon the method of complex formation, viz. direct mixing vs. annealing in a salt gradient dialysis. Furthermore, in no case have we found a complex containing DNA in the A or C geometry. These results are therefore consistent with the point of view, advanced earlier,^{23,31} that anomalous CD and ORD spectra of annealed complexes are due to aggregative phenomena and not to structural peculiarities at the molecular level which depend upon the method of complex formation.

We view the present results as consistent with the DNA-polylysine model proposed by Tsuboi⁶⁵ and Wilkins.⁶ Since binding is essentially quantitative to all nucleotides, the larger response of Raman lines of adenine to complex formation reflects the greater sensitivity of those lines to altered base interactions rather than a specificity of interaction of adenine bases or AT base pairs. Apparently the neutralization of negatively charged phosphate groups of DNA by lysyl groups is sufficient to alter the balance of forces ordinarily stabilizing DNA so that the mutual base interactions in the complex are substantially different from those in unbound DNA. This disruption obviously takes place without a significant change in the backbone geometry characteristic of B-DNA.

In the poly(rA)-polylysine complex, a detailed molecular model has not been proposed. However, the present results indicate that a satisfactory model should account for both the altered base stacking and deviation of the phosphodiester torsion angles from the g^+-g^+ configuration which accompany complex formation. The fact that several Raman lines due to vibrations of the ribose moiety are altered by polylysine binding (Table II) suggests further that conformational changes in the poly(rA) backbone extend beyond the immediate sites of the phosphodiester groups. Apparently, the structural feature responsible for the 708-cm⁻¹ line (C_3 -endo?) is not affected, however, by polylysine binding.

In all cases of polylysine binding, we find that the Raman frequencies and intensities of the polypeptide are little af-

fect. This result can be explained by assuming that a nearly fully extended polypeptide chain is required for filling the groove of B-DNA as in proposed models of the DNA-polylysine complex.^{6,65} Apparently a similar situation prevails for binding of polylysine to single-stranded poly(rA). We may also conclude from these results that even when rather strong electrostatic interaction occurs between proteins and their substrates, it may not be possible to detect evidence of the interaction in terms of altered Raman scattering by the protein subgroups.

The similarities between Raman spectra of complexed DNA (Figure 3) and denatured DNA^{48,64} may be of more than casual interest. Many proteins are thought to bind to DNA either by seizing upon a local "opening-up" of the double helix or by causing the DNA structure to open subsequent to binding.^{2a} Clearly Raman spectroscopy cannot distinguish between these two possibilities. However, the Raman data do provide evidence that the base interactions are altered in lysine-bound DNA and the alterations appear to be in the direction of a more open DNA structure. On the other hand, it is well established that DNA-polylysine complexes are thermally more stable than noncomplexed DNA,^{5,7,8} so one must not interpret such a structure, despite its altered base interactions, as being less resistant to thermal denaturation. It is unfortunate that the requirements for Raman scattering have precluded the possibility of obtaining spectra as a function of temperature on the complexes prepared here. This limitation of Raman spectroscopy vis-a-vis CD and ORD methods is offset to some extent by the fact that Raman spectra of condensed phases are much less sensitive to artifacts of the type encountered in CD and ORD spectra.

Finally, we note that Raman spectroscopy should prove useful in the study of other nucleic acid-protein complexes including nucleohistones and nucleoprotamines, by revealing whether such complexes, like the model systems examined here, contain nucleic acid backbones of the B type.

NOTE ADDED IN PROOF: After submitting this manuscript we were informed of a recently published study of DNA-polylysine complexes using infrared linear dichroism spectroscopy [J. Liquier, M. Pinot-Lafaix, E. Taillandier, and J. Brahm, *Biochemistry*, **14**, 4191-4197 (1975)]. The ir investigations were made on oriented fibers at experimental conditions differing from those employed here. Nevertheless, Liquier et al. report that binding of polylysine to B-DNA does not convert the DNA backbone to either A or C structures and does not appreciably affect the structural transitions which B-DNA fibers normally undergo as a function of relative humidity. The ir data show that bound polylysine has only a small effect on the orientation of DNA phosphate groups relative to the helix axis (termed a B*-DNA structure) and therefore indicate consistency with the Raman results reported here.

Acknowledgment. This work was supported by Grant No. AI-11855 from the U.S. Public Health Service.

References and Notes

- (1) (a) Paper XV in the series, Raman Spectral Studies of Nucleic Acids. Paper XIV is ref 56. (b) Ph.D. Degree with Professor Richard C. Lord, Department of Chemistry, MIT, Jan, 1967.
- (2) (a) P. H. von Hippel and J. D. McGhee, *Annu. Rev. Biochem.*, **41**, 231 (1972); (b) S. Casjens and J. King, *ibid.*, **44**, 555 (1975).
- (3) E. M. Bradbury, C. Crane-Robinson, H. W. E. Rattle, and R. M. Stephens, in "Conformation of Biopolymers", Vol. 2, G. N. Ramachandran, Ed., Academic Press, New York, N.Y., 1967, p 583.
- (4) M. Leng and G. Felsenfeld, *Proc. Natl. Acad. Sci. U.S.A.*, **56**, 1325 (1966).
- (5) M. Tsuboi, K. Matsuo, and P. O. P. Ts'o, *J. Mol. Biol.*, **15**, 256 (1966).
- (6) M. H. F. Wilkens, *Cold Spring Harbor Symp. Quant. Biol.*, **21**, 75 (1956).
- (7) D. E. Olins, A. L. Olins, and P. H. von Hippel, *J. Mol. Biol.*, **24**, 157 (1967).
- (8) D. E. Olins, A. L. Olins, and P. H. von Hippel, *J. Mol. Biol.*, **33**, 265 (1968).
- (9) C. W. Lees and P. H. von Hippel, *Biochemistry*, **7**, 2480 (1968).
- (10) S. Arnott, *Prog. Biophys. Mol. Biol.*, **21**, 256 (1970).
- (11) S. Higuchi and M. Tsuboi, *Biopolymers*, **4**, 837 (1966).
- (12) J. T. Shapiro, M. Leng, and G. F. Felsenfeld, *Biochemistry*, **8**, 3219 (1969).
- (13) K. Matsuo and M. Tsuboi, *Biopolymers*, **8**, 153 (1969).
- (14) H. A. Sober, S. Schlossman, A. Yaron, S. A. Latt, and G. W. Rushizky, *Biochemistry*, **5**, 3608 (1966).
- (15) S. A. Latt and H. A. Sober, *Biochemistry*, **6**, 3293, 3307 (1967).
- (16) P. Cohen and C. Kidson, *J. Mol. Biol.*, **35**, 241 (1968).
- (17) G. D. Fasman, B. Schaffhausen, L. Goldsmith, and A. Adler, *Biochemistry*, **9**, 2814 (1970).
- (18) T. Y. Shih and G. D. Fasman, *Biochemistry*, **10**, 1675 (1971).
- (19) T. Y. Shih and G. D. Fasman, *J. Mol. Biol.*, **52**, 125 (1970).
- (20) M. F. Pinkston and H. J. Li, *Biochemistry*, **13**, 5227 (1974).
- (21) R. S. Johnson, A. Chan, and S. Hanlon, *Biochemistry*, **11**, 4348 (1972).
- (22) H. J. Li, C. Chang, and M. Weiskopf, *Biochemistry*, **12**, 1763 (1973).
- (23) M. Haynes, R. A. Garrett, and W. B. Gratzel, *Biochemistry*, **9**, 4410 (1970).
- (24) G. Zubay and M. H. F. Wilkins, *J. Mol. Biol.*, **4**, 444 (1962); **9**, 246 (1964).
- (25) J. Sonnenbichler, *Nature (London)*, **223**, 205 (1969).
- (26) R. A. Garrett, *J. Mol. Biol.*, **38**, 249 (1968).
- (27) D. E. Olins and A. L. Olins, *J. Mol. Biol.*, **57**, 437 (1971).
- (28) E. M. Bradbury, W. C. Price, and G. R. Wilkinson, *J. Mol. Biol.*, **4**, 39 (1962).
- (29) E. M. Bradbury, W. C. Price, G. R. Wilkinson, and G. Zubay, *J. Mol. Biol.*, **4**, 50 (1962).
- (30) C. Chang, M. Weiskopf, and H. J. Li, *Biochemistry*, **12**, 3328 (1973).
- (31) D. Carroll, *Biochemistry*, **11**, 421, 426 (1972).
- (32) H. J. Li, B. Brand, A. Rotter, C. Chang, and M. Weiskopf, *Biopolymers*, **13**, 1681 (1974).
- (33) H. J. Li, C. Chang, M. Weiskopf, B. Brand, and A. Rotter, *Biopolymers*, **13**, 649 (1974).
- (34) V. Giancotti, A. Cesàro, and V. Crescenzi, *Biopolymers*, **14**, 675 (1975).
- (35) G. J. Thomas, Jr., and K. A. Hartman, *Biochim. Biophys. Acta*, **312**, 311 (1973).
- (36) B. Prescott, R. Gamache, J. Livramento, and G. J. Thomas, Jr., *Biopolymers*, **13**, 1821 (1974).
- (37) G. J. Thomas, Jr., in "Vibrational Spectra and Structure", Vol. 3, J. R. Durig, Ed., Marcel Dekker, New York, N.Y., 1975, p 239.
- (38) R. C. Lord, *Proc. Int. Congr. Pure Appl. Chem., Suppl.*, **23rd**, **7**, 179 (1971).
- (39) M. C. Chen and R. C. Lord, *J. Am. Chem. Soc.*, **96**, 4750 (1974).
- (40) K. A. Hartman, N. Clayton, and G. J. Thomas, Jr., *Biochem. Biophys. Res. Commun.*, **50**, 942 (1973).
- (41) G. J. Thomas, Jr., and P. Murphy, *Science*, **188**, 1205 (1975).
- (42) G. J. Thomas, Jr., B. Prescott, P. E. McDonald-Ordzie, and K. A. Hartman, *J. Mol. Biol.*, in press.
- (43) R. C. Lord and G. J. Thomas, Jr., *Spectrochim. Acta, Part A*, **23**, 2551 (1967); *Biochim. Biophys. Acta*, **142**, 1 (1967); *Dev. Appl. Spectrosc.*, **6**, 179 (1968).
- (44) R. C. Lord and N.-T. Yu, *J. Mol. Biol.*, **50**, 509 (1970); **51**, 203 (1970).
- (45) G. J. Thomas, Jr., in "Physical Techniques in Biological Research", Vol. 1A, "Optical Techniques", G. Oster, Ed., Academic Press, New York, N.Y., 1971, p 277.
- (46) S. C. Erfurth, E. J. Kiser, and W. L. Peticolas, *Proc. Natl. Acad. Sci. U.S.A.*, **69**, 938 (1972).
- (47) S. C. Erfurth, P. J. Bond, and W. L. Peticolas, *Biopolymers*, **14**, 1245 (1975).
- (48) L. Rimai, V. M. Maher, D. Gill, I. Salmeen, and J. J. McCormick, *Biochim. Biophys. Acta*, **361**, 155 (1974).
- (49) T. J. Yu, J. L. Lippert, and W. L. Peticolas, *Biopolymers*, **12**, 2161 (1973).
- (50) E. W. Small and W. L. Peticolas, *Biopolymers*, **10**, 69 (1971).
- (51) G. J. Thomas, Jr., M. C. Chen, and K. A. Hartman, *Biochim. Biophys. Acta*, **324**, 37 (1973).
- (52) B. Davidson and G. D. Fasman, *Biochemistry*, **8**, 4116 (1969).
- (53) F. Brun, J. J. Toulmè, and C. Hélène, *Biochemistry*, **14**, 558 (1975).
- (54) M. Durand, J. C. Maurizot, H. N. Borazan, and C. Hélène, *Biochemistry*, **14**, 563 (1975).
- (55) N.-T. Yu, Ph.D. Thesis, Department of Chemistry, MIT, Cambridge, Mass., 1969.
- (56) G. J. Thomas, Jr., and J. Livramento, *Biochemistry*, **14**, 5210 (1975).
- (57) L. Lafleur, J. Rice, and G. J. Thomas, Jr., *Biopolymers*, **11**, 2423 (1972).
- (58) K. Morikawa, M. Tsuboi, S. Takahashi, Y. Kyogoku, Y. Mitsui, Y. Itaka, and G. J. Thomas, Jr., *Biopolymers*, **12**, 799 (1973).
- (59) B. S. Stannard and G. Felsenfeld, *Biopolymers*, **14**, 299 (1975).
- (60) G. J. Thomas, Jr., and J. Livramento, unpublished results.
- (61) W. K. Olson, *Biopolymers*, **14**, 1797 (1975).
- (62) G. J. Thomas, Jr., *Biochim. Biophys. Acta*, **213**, 417 (1970).
- (63) T. Shimanouchi, M. Tsuboi, and Y. Kyogoku, *Adv. Chem. Phys.*, **7**, 435 (1964).
- (64) S. C. Erfurth and W. L. Peticolas, *Biopolymers*, **14**, 247 (1975).
- (65) M. Tsuboi in ref 3, p 689.

Ring-Puckering Vibrational Spectra of Cyclopentene-1- d_1 and Cyclopentene-1,2,3,3- d_4

J. R. Villarreal, L. E. Bauman, and J. Laane*¹

Department of Chemistry, Texas A&M University, College Station, Texas 77843 (Received January 13, 1976)

The far-infrared and low-frequency Raman spectra of cyclopentene-1- d_1 and -1,2,3,3- d_4 have been recorded. For each molecule approximately a dozen infrared bands in the 60–200- cm^{-1} region and a like number of Raman bands in the 90–250- cm^{-1} region were assigned to ring-puckering transitions. A series of ring-twisting infrared Q branches was also obtained for each molecule, near 370 cm^{-1} for the d_1 and near 338 cm^{-1} for the d_4 . The d_4 molecule showed a series of side bands resulting from the ring-twisting excited state. The seventh excited state ($\nu = 7$) of the ring puckering was found to be split by an unusual Fermi resonance with the $\nu = 2$ puckering state in the twisting excited state. Extensive potential energy calculations were carried out using various models (with and without CH_2 rocking) for the puckering vibration for the d_0 , d_1 , d_4 , and d_8 molecules. Inclusion of rocking gave slight improvement for the frequency fit, but rocking parameters could not be well determined. The barriers to inversion of the four molecules were found to be 233, 231, 224, and 215 cm^{-1} in order of increasing deuteration. The dihedral angle of each isotopic form was determined to be 26°.

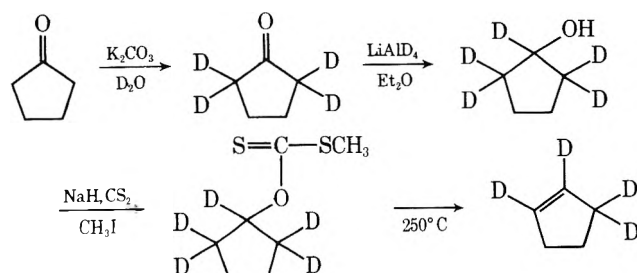
Introduction

The barrier to inversion of cyclopentene was first determined by Laane and Lord² to be 0.66 kcal/mol (232 cm^{-1}). Their analysis of the far-infrared spectrum established the ring-puckering potential energy function for this molecule and showed conclusively that the cyclopentene ring is bent with a dihedral angle exceeding 20°. Low-frequency Raman studies later confirmed these far-infrared results.^{3,4}

Very recently the far-infrared and Raman spectra of cyclopentene- d_8 were reported and analyzed by Villarreal and co-workers.⁵ The results for the d_8 derivative were very similar to those of the d_0 compound except that the inversion barrier had apparently decreased to 215 cm^{-1} and the one-dimensional potential energy function had changed slightly. These differences were attributed to the mixing of other motions, including CH_2 (or CD_2) rocking, into the ring-puckering normal coordinate. In order to better understand the ring-puckering motion and to examine the effect of isotopic substitution on the potential function and barrier height, we have prepared cyclopentene-1- d_1 and cyclopentene-1,2,3,3- d_4 and recorded their far-infrared and low-frequency Raman spectra. The data were then analyzed using various one-dimensional models for the ring-puckering motion.

Experimental Section

Cyclopentene-1,2,3,3- d_4 was prepared according to the following reaction scheme. Cyclopentene-1- d_1 was prepared similarly except that the undeuterated cyclopentanone was used instead of the d_4 derivative.



Cyclopentanone-2,2,5,5- d_4 . Cyclopentanone (Aldrich,

99.5%), anhydrous K_2CO_3 (Mallinckrodt Analytical reagent), and D_2O (Stohler, 99.8%) were mixed according to the procedure of Ellis and Maciel.⁶ Three successive exchanges were required for complete deuteration.

1-Cyclopentanol-1,2,2,5,5- d_5 . Cyclopentanone-2,2,5,5- d_4 , 14.9 g (0.17 mol) in 110 ml of anhydrous ether, was added dropwise to 2.9 g (0.062 mol) of LiAlD_4 (Stohler, 99.8%) suspended in 225 ml of anhydrous ether. The procedure used was that of Lipnick.⁷ Excess LiAlD_4 was destroyed with saturated ammonium chloride solution. Filtration, concentration, and vacuum distillation gave 10.8 g (0.119 mol, 70%) of the deuterated alcohol.

O-1,2,2,5,5-Cyclopentyl S-Methyl Xanthate. 1-Cyclopentanol-1,2,2,5,5- d_5 (10.8 g) was added to a suspension of NaH in mineral oil (5.63 g, K & K) following the procedure of Roberts and Sauer.⁸ After addition of CS_2 (10.9 g, Fischer Scientific Reagent Grade) and CH_3I (21.6 g, Fischer Scientific, Certified) the mixture was stirred overnight. The xanthate was concentrated using a 1-ft beaded glass column and used without further purification.

Cyclopentene-1,2,3,3- d_4 . Crude O-1,2,2,5,5-cyclopentyl S-methyl xanthate was dropped into boiling biphenyl (Matheson Coleman and Bell) under a fast N_2 purge.⁸ The products were collected in two successive dry ice/acetone traps. Distillation of the trapped products resulted in 4.1 g of cyclopentene-1,2,3,3- d_4 (48% from cyclopentanol- d_5). The purity and authenticity of the product was verified by its NMR, ir, and mass spectra.

Cyclopentene-1- d_1 . Cyclopentanone (Aldrich 99%+) was reduced with LiAlD_4 (as above) to 1-cyclopentanol-1- d_1 . Formation of the xanthate of this alcohol and its subsequent pyrolysis were accomplished in the same manner (and with comparable yields) as in the cyclopentene-1,2,3,3- d_4 synthetic scheme.

The far-infrared spectra were recorded on a Digilab FTS-20 vacuum spectrophotometer using a Wilks multiple-reflection long-path cell. Raman spectra were recorded on a Cary 82 spectrophotometer using a Coherent Radiation 53 argon ion laser as the exciting source. Experimental conditions for both kinds of spectra were similar to those previously described.⁵ Infrared frequencies are accurate to $\pm 0.2 \text{ cm}^{-1}$ whereas the broader Raman lines are ± 0.5 to $\pm 1.0 \text{ cm}^{-1}$. Infrared resolu-

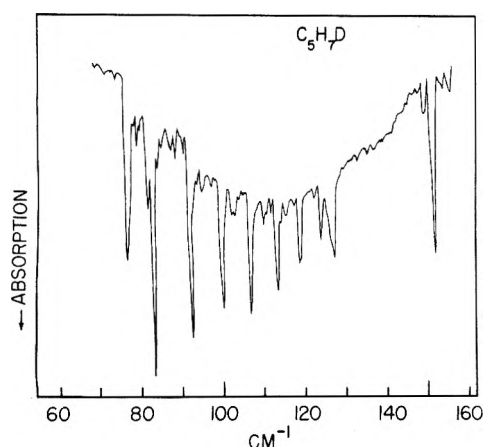


Figure 1. Far-infrared ring-puckering spectrum of cyclopentene-1- d_1 : path length, 5.3 m; vapor pressure, 80 Torr; resolution, 1.0 cm^{-1} . The ordinate scale is 0 to 100% transmittance.

tions ranged from 0.25 to 1.0 cm^{-1} and Raman band widths were 2 to 4 cm^{-1} .

Results

Ring-Puckering Spectra. Figures 1–4 show the far-infrared and Raman spectra of cyclopentene-1- d_1 and cyclopentene-1,2,3,3- d_4 vapors in the ring-puckering region. Tables I and II list the recorded band maxima and assignments along with the calculated frequencies which will be discussed later. As in the previous studies on cyclopentene- d_0 and - d_8 , the far-infrared frequencies correspond to single quantum transitions (except for several triple jumps originating from levels below the barrier) and the Raman bands correspond to changes of two in the ring-puckering quantum number ν . The complementary nature of the two types of spectra and the excellent correlation between the data make the interpretation clear cut for each molecule. The cyclopentene-1- d_1 spectrum is very similar to that of the undeuterated species with most frequencies being shifted by about 1 cm^{-1} or less. The d_4 spectra show evidence for an extra ring-puckering level at $\nu = 7$ and this will be discussed later in the section on Fermi resonance. The d_4 infrared spectrum also shows a side band series (see Table III) resulting from the excited state of the ring-twisting mode (see Figure 7), similar to the series reported for the undeuterated molecule.² Three or four such bands can also be seen for the d_1 molecule but a series sufficient for determining a potential function was not obtained.

Ring-Twisting Spectra. Due to the reduction of symmetry, the cyclopentene- d_1 and - d_4 molecules give rise to ring-twisting Q branches in the infrared and these spectra can be seen in Figures 5 and 6. The fundamental twisting frequencies are at 369.3 and 337.6 cm^{-1} for the d_1 and d_4 , respectively. The other Q branches in the spectra arise from transitions between various twisting states, and some of these may also be associated with excited puckering levels. No definite assignment is presented at this time, but these will be analyzed in greater detail at a later time using a two-dimensional potential function involving both ring-puckering and ring-twisting coordinates.

In the Raman spectra of the d_0 , d_1 , d_4 , and d_8 compounds the broad twisting bands (with no Q branches) have center gaps at 392, 369, 338, and 325 cm^{-1} , respectively.

Fermi Resonance. The far-infrared and Raman spectra of cyclopentene- d_4 show a remarkable case of Fermi resonance involving one of the puckering levels. If we designate the twisting and puckering quantum numbers as ν_T and ν_P , re-

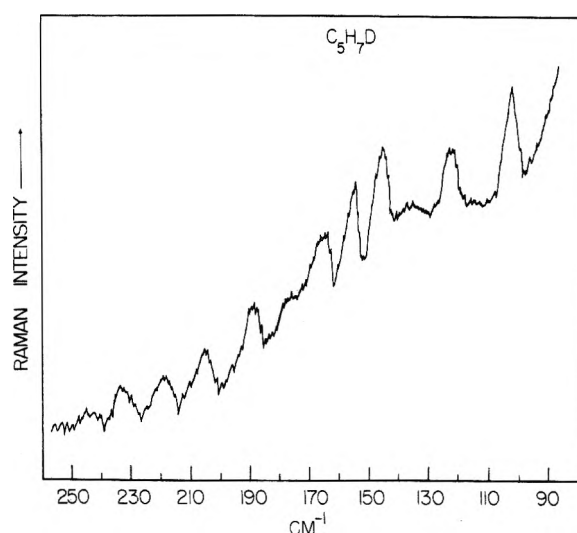


Figure 2. Raman spectrum of cyclopentene-1- d_1 : vapor pressure, 300 Torr; resolution, 3 cm^{-1} .

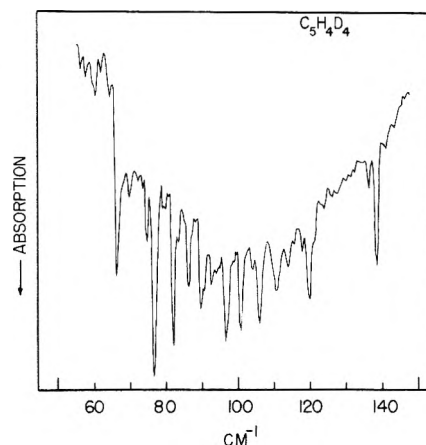


Figure 3. Far-infrared spectrum of cyclopentene-1,2,3,3- d_4 : path length, 6.3 m; vapor pressure, 84 Torr; resolution, 1.0 cm^{-1} . The ordinate scale is 0 to 60% transmittance.

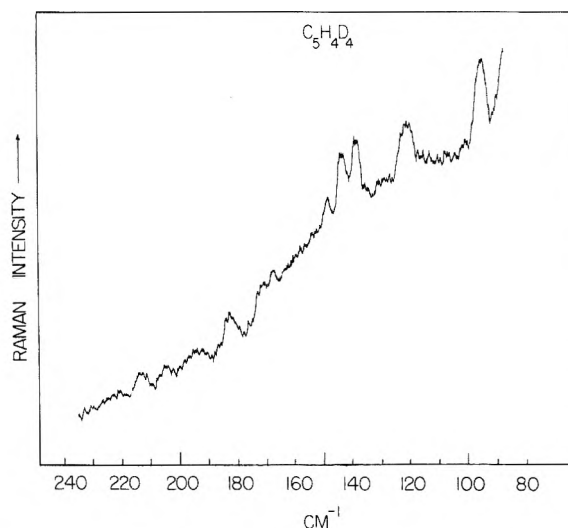


Figure 4. Raman spectrum of cyclopentene-1,2,3,3- d_4 : vapor pressure, 300 Torr; resolution, 3 cm^{-1} .

TABLE I: Observed and Calculated Ring-Puckering Transitions of Cyclopentene-1-*d*₁ from Far-Infrared and Raman Spectra

Transition	Frequency, cm ⁻¹			Rel. intensity	
	Obsd	Calcd I ^a	Calcd II ^b	Obsd	Calcd
Far-Infrared Spectrum					
0-1		0.85	0.87		
1-2	126.0	125.9	125.8	0.4	1.0
2-3		24.0	24.0		
3-4	82.8	81.8	81.9	1.4	1.1
4-5	76.1	75.7	75.8	0.7	0.9
5-6	91.5	90.9	91.0	(1.0)	(1.0)
6-7	99.5	98.9	98.9	0.7	0.9
7-8	106.2	106.5	106.5	0.7	0.7
8-9	112.6	113.1	113.0	0.5	0.5
9-10	118.1	119.1	119.0	0.3	0.3
10-11	123.5	124.5	124.3	0.2	0.2
0-3	151.3	150.6	150.8	1.1	1.1
2-5	182.9	181.3	181.8	0.2	0.4
Raman Spectrum					
0-2	127.2	126.7	126.7	0.7	0.7
1-3	150.0	149.8	149.9	(1.0)	(1.0)
2-4	107.9	105.6	105.9	1.0	0.5
3-5	159.0	157.5	157.8	0.9	0.8
4-6	168.3	166.6	166.8	0.7	0.7
5-7	190.1	189.8	189.9	0.6	0.7
6-8	205.2	205.4	205.4	0.5	0.6
7-9	218.8	219.6	219.5	0.4	0.5
8-10	231.0	232.2	232.0	0.3	0.3
9-11	~242	243.7	243.3	0.1	0.2

^a $V = 25.05 (Z^4 - 6.07Z^2) \text{ cm}^{-1}$; no rocking model. ^b $V = 25.22 (Z^4 - 6.05Z^2) \text{ cm}^{-1}$; rocking included ($\gamma = -0.10$; $\delta = +0.10$).

spectively, and label our levels as (ν_T, ν_P), the resonance occurs between levels (0,7) and (1,2). Evidence for the Fermi interaction comes from the fact that extra bands are present in both the infrared and Raman puckering spectra. These extra bands are readily explained if the (0,7) level is considered to be a doublet split by 3.4 cm^{-1} . Two infrared bands (86.2 and 89.6 cm^{-1}) can then be assigned to the (0,6) \rightarrow (0,7) doublet transition and two (92.9 and 96.3 cm^{-1}) to the (0,7) doublet \rightarrow (0,8) transition. Two Raman bands at 167.6 and 171.5 cm^{-1} correspond to the (0,5) \rightarrow (0,7) doublet jump and the very broad band (~ 194 and $\sim 196 \text{ cm}^{-1}$) corresponds to the (0,7) doublet \rightarrow (0,9) transition. By summing five infrared transition frequencies up to the $\nu_P = 7$ state, the pair of (0,7) levels are calculated to be 449.2 and 452.6 cm^{-1} above the ground state. The pair of (1,2) levels are calculated to be at 452.7 and 456.3 cm^{-1} by summing the (0,0) \rightarrow (1,0) transition frequency (337.6 cm^{-1}) and the (1,1) \rightarrow (1,2) frequencies (114.6 and 118.2 cm^{-1}) and adding the calculated (1,0) \rightarrow (1,1) separation of 0.5 cm^{-1} . Although the two calculations are not in exact agreement, it is highly probable that the (1,2) and (0,7) levels are in resonance. Both levels have A' symmetry for the C_s point group. [The (0,8) and (1,4) levels are also calculated to be similar in energy but have A' and A'' symmetry representations, respectively, and therefore no resonance is possible.] It should be remembered that band maxima do not normally correspond exactly to band origins (for trimethylene sulfide, differences of about 0.5 cm^{-1} for each puckering band were calculated⁹), consequently the difference in the two frequency summations of less than 4 cm^{-1} resulting from combining eight frequencies is not entirely unexpected. Another possibility is that the (0,0) \rightarrow (1,0) transition actually corresponds to one of the bands in Figure 6 at a frequency below 337 cm^{-1} .

TABLE II: Observed and Calculated Ring-Puckering Transitions of Cyclopentene-1,2,3,3-*d*₄ from Far-Infrared and Raman Spectra

Transition	Frequency, cm ⁻¹			Rel. intensity	
	Obsd	Calcd I ^a	Calcd II ^b	Obsd	Calcd
Far-Infrared Spectrum					
0-1		0.53	0.56		
1-2	120.0	119.5	119.6	0.3	0.9
2-3		17.8	18.0		0.01
3-4	76.5	75.4	75.8	1.1	1.0
4-5	66.0	65.5	65.7	0.6	0.7
5-6	81.7	81.1	81.2	(1.0)	(1.0)
6-7	}	86.2	88.2	88.2	0.3
		89.6			0.4
7-8	}	92.9	95.4	101.2	0.2
		96.3			0.4
8-9	100.5	101.5	101.2	0.4	0.5
9-10	106.0	107.1	106.7	0.3	0.4
10-11	110.4	112.2	111.6	0.2	0.3
11-12	114.6	116.9	116.2	0.1	0.2
0-3	138.8	137.9	138.3	0.6	1.0
2-5	161.2	158.7	159.5	0.2	0.4
Raman Spectrum					
0-2	120.5	120.1	120.2	1.0	0.7
1-3	138.0	137.3	137.7	(1.0)	(1.0)
2-4	95.0	93.2	93.8	1.0	0.4
3-5	143.1	140.9	141.5	0.9	0.9
4-6	148.5	146.6	146.9	0.3	0.7
5-7	}	167.6	169.3	169.4	0.3
		171.5			0.3
6-8	182.8	183.6	183.5	0.5	0.7
7-9	}	~194	196.9	196.5	0.3
		~196			0.3
8-10	206.3	208.6	207.9	0.3	0.5
9-11	215.0	219.3	218.3	0.3	0.3

^a $V = 22.40 (Z^4 - 6.32Z^2) \text{ cm}^{-1}$; no rocking model. ^b $V = 22.77 (Z^4 - 6.27Z^2) \text{ cm}^{-1}$; rocking included ($\gamma_H = -0.10$; $\gamma_D = -0.25$; $\delta = +0.10$).

TABLE III: Observed and Calculated Far-Infrared Frequencies for the Cyclopentene-1,2,3,3-*d*₄ Side Band Series^a

Transition	Frequency, cm ⁻¹		
	Obsd	Calcd	Δ
0-1		0.73	
1-2	118.2	115.6	0.8
	114.6		
2-3		21.3	
3-4	74.6	74.6	0.0
4-5	69.6	68.9	0.7
5-6	83.4	83.0	0.4
0-3	136.5	137.7	-1.2

^a $V = 22.63 (Z^4 - 6.13Z^2) \text{ cm}^{-1}$; no rocking model. Barrier = 213 cm^{-1} .

At any rate, five pairs of transition frequencies with a consistent separation of about 3.4 cm^{-1} support the existence of a doublet at about 450 cm^{-1} above the ground state. Only the ring-puckering and ring-twisting modes can combine to give levels in this region. All other vibrations have frequencies above 500 cm^{-1} .¹⁰ Figure 7 summarizes the scheme of levels and transitions observed in the vicinity of the Fermi doublet. On the left of the diagram are shown pure ring-puckering (infrared and Raman) transitions; on the right are those involving the ring-twisting excited state, including the "side-band" series.

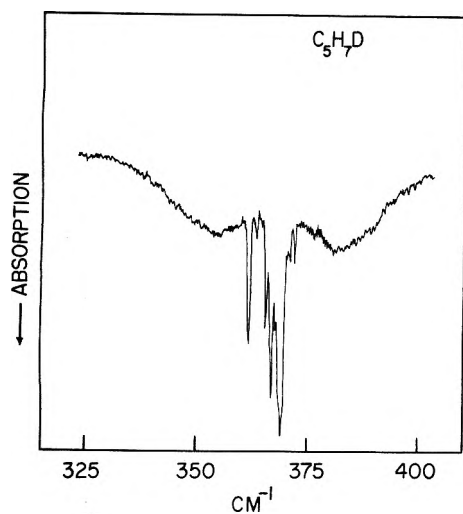


Figure 5. Infrared ring-twisting spectrum of cyclopentene-1- d_1 : path length, 75 cm; vapor pressure, 84 Torr; resolution, 0.5 cm^{-1} . The ordinate scale is 5 to 100% transmittance.

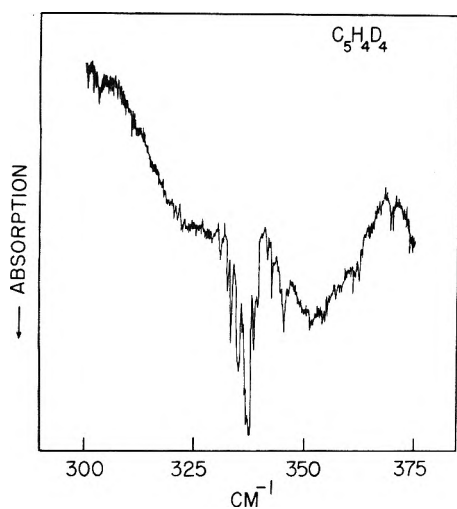


Figure 6. Infrared ring-twisting spectrum of cyclopentene-1,2,3,3- d_4 : path length, 7 m; vapor pressure, 84 Torr; resolution, 0.25 cm^{-1} . The ordinate scale is 0 to 100% transmittance.

Calculations

The use of the quartic-quadratic one-dimensional potential energy function, $V = ax^4 \pm bx^2$, for analyzing ring-puckering vibrations is well established.¹¹⁻¹³ This kind of double-minimum potential has been applied^{2,5} to cyclopentene- d_0 and - d_8 , and it is also used in this study. In addition to the potential function, which for mathematical purposes is used in reduced (undimensioned) form, the calculated transition frequencies depend to a lesser extent on the model assumed for the puckering motion. This model determines the reduced mass expansion used in the kinetic energy part of the matrix calculation.

We have selected three different types of reduced mass functions to be used in the calculations. First, a fixed reduced mass, independent of puckering coordinate x , is utilized. Even though this is not realistic, many ring-puckering calculations have been carried out in this fashion, and we include this calculation for comparison purposes. In the second type of calculation, a reduced mass function depending on the puckering coordinate is made use of. This function is calcu-

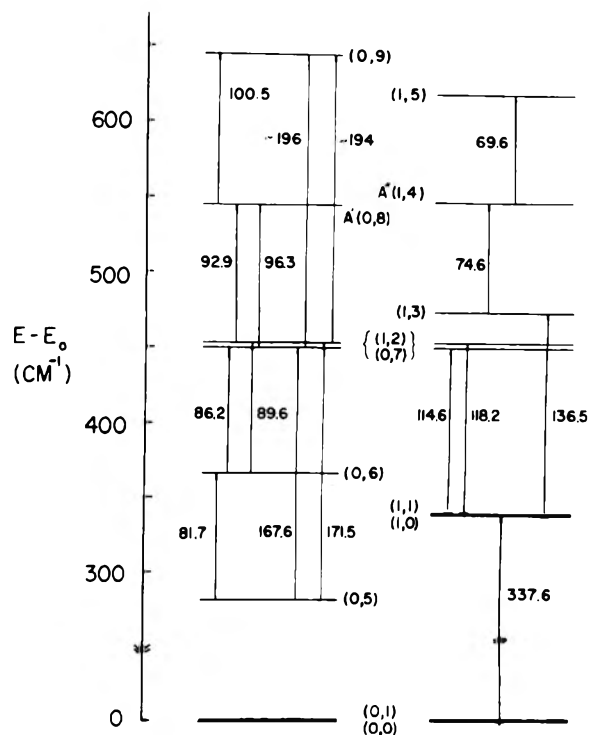


Figure 7. Ring-puckering (left) and ring-twisting (right) energy levels showing Fermi resonance between the (0,7) and (1,2) levels.

lated by a computer program which we have written and which assumes the basic bisector model described by Malloy.¹³ The motion of the ring atoms is assumed to be curvilinear and the HCH angle bisectors are constrained to be colinear with the CCC angle bisectors. That is, no CH_2 rocking is allowed. In the third type of calculation rocking of the both the α and β CH_2 groups is allowed. For consistency, the rocking motion and parameters are identical in definition to that of Malloy.¹³ A positive δ represents a motion of the β - CH_2 group rocking in the same direction as the β -carbon atom moves during the puckering; a positive γ measures equal rocking motions of each of the α - CH_2 groups in the direction of the puckering of the α -carbon atoms. For cyclopentene- d_4 , γ_{H} and γ_{D} are used to distinguish between the independent α - CH_2 and α - CD_2 rocking motions. The rocking angle is assumed to vary linearly with the dihedral angle of the ring and no rocking ($\delta = \gamma = 0$) is assumed for the planar cyclopentene structure. Although this rocking model may not be the most realistic, it is virtually the only one which can be accommodated into a one-dimensional analysis of the potential function.

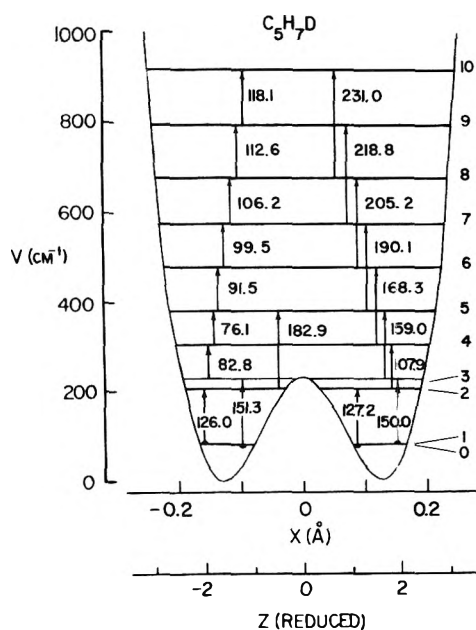
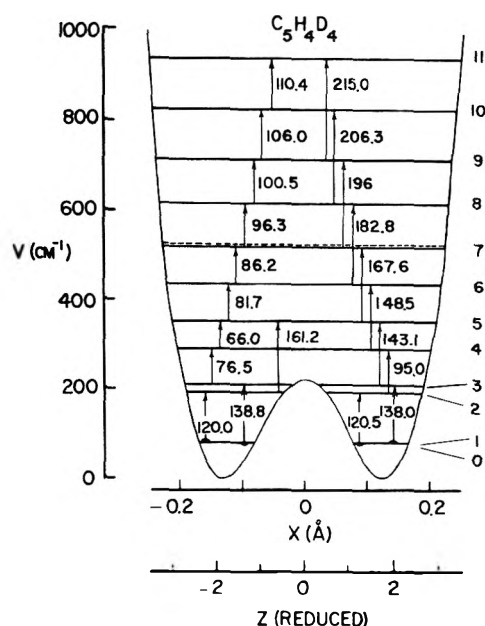
Malloy has analyzed the cyclopentene- d_0 data and has shown that use of $\gamma = -0.10$ and $\delta = +0.10$ improves the frequency agreement. We have used these rocking parameters to generate a set of kinetic energy expressions for cyclopentene- d_1 , - d_4 , and - d_8 , realizing that the contribution of rocking to the puckering motion will change upon deuteration. We have also generated more than 30 other reduced mass expansions for the d_4 and d_8 species in order to investigate which sets of rocking parameters lead to the best frequency fit. Our basic conclusion is that a wide variety of rocking parameters will improve the calculation somewhat, but the degree of improvement is relatively insensitive to the rocking model. Consequently, not much physical significance can be ascribed to the δ and γ values which yield the optimum calculated frequencies.

Table IV summarizes a few selected calculations which were

TABLE IV: Ring-Puckering Potential Energy Functions for Cyclopentene and Its Deuterated Derivatives

C ₂ H ₈ species	Reduced mass, au ^a	Rocking parameters		Potential functions							
		γ	δ	Reduced: V = A(Z ⁴ - BZ ²)		Dimensioned: V = ax ⁴ - bx ⁻³		Barrier, cm ⁻¹	Dihedral angle ^b	Av ^c Δ ²	
				A, cm ⁻¹	B	a, cm ⁻¹ /Å ⁴	b, cm ⁻¹ /Å ²				
d ₀	117.88	0	0	24.36	6.17	7.06 × 10 ⁵	25.6 × 10 ³	232.1	26.5	1.64	
	117.88 + μ ₀ (x)	0	0	25.31	6.06	7.93 × 10 ⁵	27.2 × 10 ³	232.7	25.8	0.50	
	115.00 + μ ₀ ^R (x)	-0.1	+0.1	25.50	6.04	7.72 × 10 ⁵	26.8 × 10 ³	232.8	26.0	0.25	
d ₁	119.78	0	0	24.12	6.20	7.08 × 10 ⁵	25.5 × 10 ³	231.8	26.5	3.40	
	119.78 + μ ₁ (x)	0	0	25.05	6.07	7.93 × 10 ⁵	27.0 × 10 ³	230.6	25.8	0.48	
	117.01 + μ ₁ ^R (x)	-0.1	+0.1	25.22	6.05	7.72 × 10 ⁵	26.7 × 10 ³	230.4	25.9	0.34	
d ₄	138.95	0	0	21.86	6.40	7.11 × 10 ⁵	25.3 × 10 ³	224.0	26.4	2.31	
	138.95 + μ ₄ (x)	0	0	22.40	6.32	7.63 × 10 ⁵	26.1 × 10 ³	223.9	25.9	0.93	
	132.72 + μ ₄ ^R (x)	-0.1	+0.1	22.58	6.30	7.13 × 10 ⁵	25.3 × 10 ³	223.9	26.3	0.62	
	122.88 + μ ₄ ^T (x)	{-0.10(H)} {-0.25(D)}	+0.1	22.77	6.27	6.27 × 10 ⁵	23.7 × 10 ³	224.0	27.2	0.44	
d ₈	184.51	0	0	17.92	6.95	6.89 × 10 ⁵	24.4 × 10 ³	216.4	26.5	0.74	
	184.51 + μ ₈ (x)	0	0	18.27	6.87	7.30 × 10 ⁵	25.1 × 10 ³	215.3	26.0	0.32	
	178.43 + μ ₈ ^R (x)	-0.1	+0.1	18.41	6.84	6.99 × 10 ⁵	24.5 × 10 ³	215.1	26.3	0.23	
	142.79 + μ ₈ ^T (x)	-0.2	-0.1	18.63	6.79	4.63 × 10 ⁵	19.9 × 10 ³	214.5	29.2	0.09	

^a μ₀(x) = 319.1x² + 2792x⁴ + 19 492x⁶; μ₁^R(x) = 400.3x² + 2901x⁴ + 21 535x⁶; μ₁(x) = 199.7x² + 3702x⁴ + 17 954x⁶; μ₁^R(x) = 277.6x² + 3544x⁴ + 19 616x⁶; μ₄(x) = 219.5x² + 3701x⁴ + 18 448x⁶; μ₄^R(x) = 298.6x² + 3544x⁴ + 20 160x⁶; μ₄^T(x) = 343.0x² + 3361x⁴ + 20 803x⁶; μ₈(x) = 222.4x² + 5066x⁴ + 23 148x⁶; μ₈^R(x) = 345.8x² + 4882x⁴ + 26 048x⁶; μ₈^T(x) = 299.6x² + 4281x⁴ + 22 369x⁶. ^b Calculated by averaging extremes of the potential function for the ground state. ^c Taken for the ten most prominent far-infrared frequencies.

Figure 8. Ring-puckering potential energy function for cyclopentene-1-d₁.Figure 9. Ring-puckering potential energy function for cyclopentene-1,2,3,3-d₄.

carried out. For completeness, all four isotopic forms are included. Results for all the various rocking models could not be included, and only those leading to the smallest average Δ² (Δ is the difference between observed and calculated frequencies) are shown. It should be reemphasized that we do not consider this a meaningful determinant of the rocking parameters, but rather an indication of how important a role rocking plays in the overall motion. The rocking parameters are not well determined and other sets of parameters may lead to average Δ² nearly as small as those in Table IV. Furthermore, it should be noted that Malloy's values, γ = -0.10 and δ = +0.10, for cyclopentene-d₀ are not consistent with our d₈

values of γ = -0.20 and δ = -0.10 in that one of the rocking motions has changed directions.

Tables I and II compare the calculated frequencies for cyclopentene-d₁ and -d₄ to those observed, and Figures 8 and 9 show the potential energy functions determined for these compounds. For each molecule calculation I lists the frequencies for the reduced mass expansion with no rocking; calculation II utilizes addition of rocking into the puckering motion. In both cases calculation II gives slightly better agreement than calculation I. However, two additional parameters were required for this model. In addition, use of rocking parameters has a pronounced effect on the calculated

reduced masses and thus, on the dihedral angle. Since the calculated dihedral angle should be reasonably consistent from one isotopic form to another, the last calculations for the d_4 and d_8 molecules in Table IV are in poor agreement with the other calculations indicating that these selections of rocking parameters are not good ones, even though they lead to improved frequency determinations. It is interesting that when no rocking is used, the observed isotope shift is quite well matched by the calculation. We feel, therefore, that the most meaningful potential functions determined are those with no rocking. Undoubtedly, rocking is present, but the slight improvement in the calculations does not warrant the addition of two more parameters, which are themselves ill-determined.

The dihedral angles listed in Table IV were calculated by averaging the extremes of the potential for the ground state. The minima of the potential functions occur approximately a degree higher. Each of the calculations with kinetic energy expansion and no rock gives an angle (within 0.1°) of 25.9° . On the other hand, the barrier to inversion drops from 233 to 231 to 224 to 215 cm^{-1} in going from the d_0 to d_1 to d_4 to d_8 . It is interesting to note that the energy between the top of the barrier and the ground state appears to remain constant at $151 \pm 1 \text{ cm}^{-1}$ for each isotopic form.

Discussion

The spectra of four different isotopically substituted cyclopentene molecules were analyzed in order to examine the variation in barrier height and the effect of the rocking motion on the ring-puckering coordinate. We have found that a regular decrease in barrier height occurs in going from the d_0 compound (233- cm^{-1} barrier) to the d_1 (231 cm^{-1}) to the d_4 (224 cm^{-1}) and to the d_8 compound (215 cm^{-1}). These barrier values are very insensitive to the one-dimensional model and the inclusion of various rocking motions leaves them virtually unchanged ($\pm 1 \text{ cm}^{-1}$). It is apparent, then, that mixing of the rocking motion can not account for the change in barrier, even though some rocking is no doubt present in the puckering normal coordinate, and use of rocking parameters does slightly improve the frequency calculation. A similar conclusion was reached by Malloy and Lafferty¹⁴ for cyclobutane and cyclobutane- d_8 where a barrier difference of 14 cm^{-1} was found for the two molecules.¹⁵ Bauder and co-workers¹⁶ also concluded that the exact form of the kinetic energy operator has only a very small effect on the barrier determination for nitroethylene.

The calculated variation in barrier height may be the result of inherent deficiencies in the one-dimensional model of the puckering. The ring-twisting vibration, which is also a low-frequency motion, may be sufficiently coupled to the puckering motion to cause the apparent decrease in barrier with deuteration. For this reason, we have begun a two-dimensional analysis, with ring-puckering and ring-twisting coordinates, on the cyclopentene molecules. A two-dimensional potential function has been calculated for the ring-puckering and twisting of 2,5-dihydrofuran,¹⁶ but no series of twisting frequencies was available for the analysis. However, the spectra of the d_1 and d_4 derivatives make cyclopentene more suitable since the ring-twisting mode for these is infrared active and gives rise to a number of Q branches. Cyclopentene- d_0 and - d_8 have C_s symmetry but their spectra conform closely to the C_{2v} selection rules expected for a planar molecule. The d_1 and d_4 derivatives have C_1 symmetry but their

spectra behave close to C_s selection rules. The ring-twisting is A_2 (infrared forbidden) in C_{2v} for the d_0 and d_8 molecules but becomes A'' (infrared active) in C_s for the d_1 and d_4 derivatives.

As noted in our discussion⁵ of cyclopentene- d_8 the reduced mass calculations quite accurately determine the expected isotope shift for that molecule. The same is true for the d_1 and d_4 shifts, and it can be seen that for the same type of puckering model the dimensioned potential function parameters are relatively constant. If we constrain the dimensioned potential function to be identical for all four molecules, fairly good frequency agreement is obtained for all spectra. For example, the best function for all the molecules together would be very close to that of the d_4 molecule (using the kinetic energy expansion but no rocking): $V = 7.62 \pm 0.32 \times 10^5 x^4 - 26.1 \pm 1.1 \times 10^3 x^2$. This calculates all the observed energy level spacings to within approximately 2 cm^{-1} for all four molecules. While we feel that different amounts of mixing of other vibrations in the various isotopic forms should result in somewhat different one-dimensional potential functions, it appears that we have achieved about as good a picture of the kinetic and potential energy functions as can be hoped for within the limitations of the one-dimensional approximation.

The dihedral angle for each of the isotopic forms is consistently calculated near 26° for the models with no rocking or with the rocking parameters as previously estimated. Large changes in the rocking parameters can have a marked effect on the calculated angles. Nevertheless, we feel the rocking contribution is sufficiently small so that the value of 26° is a good one. This may be compared to the value of $22.3 \pm 2^\circ$ reported from microwave studies.^{18,19}

Acknowledgments. The authors wish to dedicate this paper to Professor R. C. Lord on his 65th birthday and retirement. His contributions to spectroscopy and chemistry are unsurpassed. This work was supported by the Robert A. Welch Foundation. The FTS-20 spectrophotometer was purchased with the aid of NSF Grant No. GP-37029. One of us (L.E.B.) wishes to thank the John and Fannie Hertz Foundation for a predoctoral fellowship.

References and Notes

- (1) J. Laane received his Ph.D. under the direction of Professor R. C. Lord in 1967.
- (2) J. Laane and R. C. Lord, *J. Chem. Phys.*, **47**, 4941 (1967).
- (3) T. H. Chao and J. Laane, *Chem. Phys. Lett.*, **14**, 595 (1972).
- (4) J. R. Durig and L. A. Carreira, *J. Chem. Phys.*, **56**, 4966 (1972).
- (5) J. R. Villarreal, L. E. Bauman, J. Laane, W. C. Harris, and S. F. Bush, *J. Chem. Phys.*, **63**, 3727 (1975).
- (6) P. D. Ellis and G. E. Maciel, *J. Am. Chem. Soc.*, **92**, 5829 (1970).
- (7) R. L. Lipnick, *J. Mol. Struct.*, **21**, 411 (1974).
- (8) J. D. Roberts and C. W. Sauer, *J. Am. Chem. Soc.*, **71**, 3928 (1949).
- (9) T. R. Borgers and H. L. Strauss, *J. Chem. Phys.*, **45**, 947 (1966).
- (10) J. R. Villarreal, J. Laane, W. C. Harris, and S. F. Bush, to be submitted for publication.
- (11) J. Laane, *Appl. Spectrosc.*, **24**, 73 (1970).
- (12) C. S. Blackwell and R. C. Lord, "Vibrational Spectra and Structure", Vol. 1, J. R. Durig, Ed., Marcel Dekker, New York, N.Y., 1972, pp 1-25.
- (13) T. B. Malloy, Jr., *J. Mol. Spectrosc.*, **44**, 504 (1972).
- (14) T. B. Malloy, Jr., and W. J. Lafferty, *J. Mol. Spectrosc.*, **54**, 20 (1975).
- (15) The situation for C_4H_8 and C_4D_8 is rather different, however, in that without rocking the correlation between calculated potential functions for the two species is very poor.
- (16) A. Bauder, E. Mathier, R. Meyer, M. Ribeaud, and Hs. H. Günthard, *Mol. Phys.*, **15**, 597 (1968).
- (17) L. A. Carreira, I. M. Mills, and W. B. Person, *J. Chem. Phys.*, **56**, 1444 (1972).
- (18) G. W. Rathjens, *J. Chem. Phys.*, **36**, 2401 (1962).
- (19) S. S. Butcher and C. C. Costain, *J. Mol. Spectrosc.*, **15**, 40 (1965).

Effect of Carbonyl Substitution on the Barrier to Planarity in Cyclobutanes

A. L. Meinzer¹ and W. C. Pringle*²

Department of Chemistry, Wesleyan University, Middletown, Connecticut 06457 (Received January 20, 1976)

The effect of carbonyl substitution on the ring planarity and ring-puckering vibration has been analyzed in terms of a one-dimensional potential model in the series of molecules, cyclobutane, oxetane, and thietane. The model incorporates a "torsional strain" parameter in addition to the contributions of ring angle deformations and unstrained torsions about the ring bonds. The potential constants determined by comparison of the experimental potential functions from the literature and this model analysis indicate that the increased planarity of the carbonyl substituted molecules is due mainly to reduction in torsional repulsion. Also torsional forces are very significantly perturbed in these strained four-membered ring molecules compared to torsional forces in open chain analogue molecules.


Introduction

The study of far-infrared and microwave spectra associated with the ring puckering vibration in a large number of four-membered ring molecules has yielded considerable experimental information concerning the planarity or nonplanarity of the ring and the nature of the vibrational potential function for this out-of-plane degree of freedom.³ In general the vibration is quite anharmonic and often a barrier to ring planarity exists which results in a nonplanar ring conformation. Chemical substitution endo and exo to the ring often causes large changes in the forces, barriers to planarity, and structures of these highly strained ring molecules.⁴

The barrier to ring planarity can be described in terms of the forces resulting from the competition between torsional forces about ring bonds, which ordinarily favor a nonplanar ring in order to relieve repulsion in the eclipsed planar conformation, and ring strain forces, which favor a planar ring in which the compressed, strained ring angles are a maximum. Chemical and structural changes which increase torsional repulsion also increase the barrier to planarity while changes which increase ring strain have the opposite effect of decreasing the barrier. For example, the lower barrier in cyclobutanone (7 cm^{-1}) compared to cyclobutane (500 cm^{-1}) has been qualitatively attributed to the combination of the lower torsional barrier of acetone than propane and the increased ring strain associated with the sp^2 carbonyl vs. the less strained sp^3 methylene in cyclobutane.^{5c}

In order to gain a more quantitative measure of the change in forces with chemical substitution, we use a model developed by Harris and co-workers⁶ to analyze the experimentally determined potential functions in terms of valence forces associated with deformation and torsion. In a previous study of the changes associated with fluorine substitution on cyclobutane and oxetane (trimethylene oxide), we found it necessary to modify this model slightly by the addition of a force, torsional strain, which describes the change in the torsional energy of an open chain molecule arising from the formation of the ring molecule.⁴ A four-membered ring molecule in the planar conformation is in an eclipsed state in which the cross ring bonds are much closer than they would be in an open chain analogue such as propane. With previous models, which assumed that torsional barriers in unstrained open chain analogues were equal to those in ring molecules, we could not reasonably account for the large reduction in the barrier to planarity for difluoro substitution in both cyclobutane and

TABLE I: Unstrained Angles and Torsional Barriers for Nonring Analogue Molecules

Ref molecule	Angle	Value θ_θ , deg	Torsional barrier, cm^{-1}
Propane	C-C-C	112.4 ^a	$V_P = 1162^f$
2,2-Difluoropropane	C-C-C	112.4 ^b	1325 ^g upper limit 1049 ^h lower limit
Acetone	 C-C-C	116.23 ^c	$V_{ACE} = 272^c$
Dimethyl ether	C-O-C	112	$V_{DME} = 950^d$
Dimethyl sulfide	C-S-C	98.9 ^e	$V_{DMS} = 746^e$

^aD. R. Lide, *J. Chem. Phys.*, **33**, 1514 (1960). ^bAssumed to be the same as propane. ^cJ. D. Swalen and C. C. Costain, *J. Chem. Phys.*, **31**, 1562 (1959). ^dU. Blukis, P. H. Kasai, and R. J. Myers, *ibid.*, **38**, 2753 (1963). ^eL. Pierce and M. Hayashi, *ibid.*, **35**, 479 (1961). ^fE. Hirota, C. Matsumura, and Y. Morino, *Bull. Chem. Soc. Jpn.*, **40**, 1124 (1967). ^gReference 7a. ^hReference 7b.

oxetane since the torsional barriers of unstrained propane and 2,2-difluoropropane⁷ are nearly equal. The magnitude of the change in the torsional strain and deformation force constants are quantitatively similar in both molecules and also the substitution caused a similar shift in the dynamics of the relative bending about the two ring diagonals away from the axis of fluorine substitution. Thus torsional strain and the deformation parameters and the changes in these with chemical substitution might be parameters transferable among ring molecules.

In this work the effect of carbonyl substitution on the ring planarity and on the ring puckering potential function is investigated in the molecules, cyclobutane, oxetane, and thietane. The experimental potential functions used to determine the parameters of the model are derived from the infrared and microwave studies of the ring puckering spectra of the molecules cyclobutane,⁸ cyclobutanone,^{5,9} oxetane,¹⁰ 3-oxetanone,¹¹ thietane,^{9,12} and 3-thietanone.¹³

Results

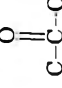

The valence forces which determine the planarity of the four-membered ring molecules and the barriers to planarity are evaluated for this series of molecules. Then the changes in these forces can be compared for carbonyl substitution in the series. The model potential analysis is carried out as described in detail in ref 4 using the literature values of unstrained torsional barriers, structures, and experimental po-

TABLE II: Experimental Potential Functions (cm^{-1}) as a Function of Ring-Puckering Coordinate (\AA), Ring Bending Dynamics, and Structural References

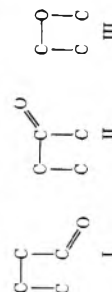
Molecule	Potential function, cm^{-1}	Ref	Dynamics ω	Structural ref
Cyclobutane	$V(Z) = -37.4 \times 10^3 Z^2 + 6.95 \times 10^5 Z^4$	8a	0.0	a
Cyclobutanone	$V(Z) = -2.88 \times 10^3 Z^2 + 4.32 \times 10^5 Z^4$	9b	-0.5	5c
Oxetane	$V(Z) = -6.63 \times 10^3 Z^2 + 7.70 \times 10^5 Z^4$	10a	+0.2	b
3-Oxetanone	$V(Z) = +37.0 \times 10^3 Z^2 + 2.07 \times 10^5 Z^4$	11, c	-0.6 to -1	11
Thietane	$V(Z) = -23.5 \times 10^3 Z^2 + 5.06 \times 10^5 Z^4$	9b	+0.3	12, d
3-Thietanone	$V(Z) = +6.7 \times 10^3 Z^2 + 1.12 \times 10^5 Z^4$	13, e	-0.68	13

^aJ. D. Dunitz and V. Shoemaker, *J. Chem. Phys.*, **20**, 1703 (1952). ^bS. I. Chan, J. Zinn, J. Fernandez, and W. D. Gwinn, *ibid.*, **33**, 1643 (1960). ^cThe potential function reported in terms of dihedral angle in ref 11 was converted to $V(Z)$ by expanding the dihedral angle in an odd power series in Z . ^dNo structural data available; the structure is consistent with the ground state rotational constants reported. ^eThe potential function is given in a reduced coordinate in ref 13 which is converted to Z by calculating the reduced mass of 184.3 based on structural parameters given in ref 13.

TABLE III: Model Potential Functions and Calculated Torsional Strain and Deformation Constants

Molecule	Model potential function $V(Z)$, ^a cm^{-1}	$\Delta\theta$, radian	Calcd potential constant	
			Torsional strain V' , cm^{-1}	Deformation k , $\text{mdyn \AA radian}^{-2}$
Cyclobutane	$(2.56k_{\text{CCC}} - 59.1(V_p + V_p'))Z^2 + (5.40k_{\text{CCC}} + 354(V_p + V_p'))Z^4$	C-C-C 0.39	$V_p' = +450$	$k_{\text{CCC}} = 0.449$
Cyclobutanone	$(2.51k_{\text{CCC}} + 0.35k_{\text{CC(O)C}} - 29.8(V_p + V_{\text{CR}}) - 30.9(V_{\text{ACE}} + V_{\text{CP}}))Z^2$ + $(6.83k_{\text{CCC}} + 0.36k_{\text{CC(O)C}} + 178(V_p + V_{\text{CR}}) + 191(V_{\text{ACE}} + V_{\text{CP}}))Z^4$	 C-C-C 0.40	$V_{\text{CR}}' + V_{\text{CP}}' = +160$	
Oxetane	$(0.98k_{\text{CCC}} + 0.87k_{\text{CCO}} + 0.80k_{\text{COC}} - 35.4(V_{\text{DME}} + V_{\text{OP}}) - 30.3(V_p + V_{\text{OR}}))Z^2 + (2.11k_{\text{CCC}} + 2.11k_{\text{CCO}} + 2.71k_{\text{COC}} + 256(V_{\text{DME}} + V_{\text{OP}}) + 184(V_p + V_{\text{OR}}))Z^4$	C-C-C 0.43 C-C-C 0.38 C-C-C 0.49 C-C-O 0.34 C-O-C 0.30	$V_{\text{OR}}' + V_{\text{OP}}' = +370$	$k_{\text{CCO}} + k_{\text{COC}} = 1.226$
3-Oxetanone	$(0.38k_{\text{CC(O)C}} + 2.40k_{\text{CCO}} + 0.23k_{\text{COC}} - 34.9(V_{\text{DME}} + V_{\text{OP,CR}}) - 31.0(V_{\text{ACE}} + V_{\text{OR,CP}}))Z^2 + (0.23k_{\text{CC(O)C}} + 8.66k_{\text{CCO}} + 0.29k_{\text{COC}} + 241(V_{\text{DME}} + V_{\text{OP,CR}}) + 198(V_{\text{ACE}} + V_{\text{OR,CP}}))Z^4$	 C-C-C 0.55 C-C-O 0.41 C-O-C 0.30	$V_{\text{OPCR}}' + V_{\text{ORCP}}' = -1200$	
Thietane	$(0.55k_{\text{CCC}} + 0.75k_{\text{CCS}} + 0.52k_{\text{CSC}} - 22.4(V_p + V_{\text{SR}}) - 30.6(V_{\text{DMS}} + V_{\text{SP}}))Z^2 + (2.31k_{\text{CCC}} + 1.05k_{\text{CCS}} + 1.34k_{\text{CSC}} + 98.8(V_p + V_{\text{SR}}) + 195(V_{\text{DMS}} + V_{\text{SP}}))Z^4$	C-C-C 0.25 C-C-S 0.37 C-S-C 0.33	$V_{\text{SP}}' + V_{\text{SR}}' = +600$	$k_{\text{CCS}} + k_{\text{CSC}} = 1.12$
3-Thietanone	$(0.15k_{\text{CC(O)C}} + 1.93k_{\text{CCS}} + 0.13k_{\text{CSC}} - 22.3(V_{\text{DMS}} + V_{\text{SP,CR}}) - 31.9(V_{\text{ACE}} + V_{\text{SR,CP}}))Z^2 + (0.15k_{\text{CC(O)C}} + 6.34k_{\text{CCS}} + 0.08k_{\text{CSC}} + 107(V_{\text{DMS}} + V_{\text{SP,CR}}) + 194(V_{\text{ACE}} + V_{\text{SR,CP}}))Z^4$	C-C-C 0.28 C-C-S 0.39 C-S-C 0.33	$V_{\text{SPCR}}' + V_{\text{SRCP}}' = -940$	

^aSubscripts CR, CP, OR, OP, SP, and SR refer to carbonyl on the rotor nucleus, I, carbonyl on the pivot nucleus, II, oxygen as a rotor nucleus, oxygen as a pivot nucleus, III, etc.



tential functions given in Tables I and II. The combinations of torsional strain and ring angle deformation force constants, determined by comparison of the model potential in Table III with experimental potential functions, are given in Table III.

This simplified analysis of a very complex problem leads to several conclusions although the valence force constants derived from the approximate vibrational model should be interpreted with caution. The combinations of ring angle deformation force constants given in Table III are quite similar to force constants for angle bending in nonring molecules. On the other hand, ring formation causes very large changes in torsional interactions of open chain molecules. The combinations of torsional strain potential constants in Table III represent the changes in the unstrained torsional barriers accompanying formation of the rings. Note that the changes in torsional barriers for ring formation are as large as the actual barriers in the open chain molecules in Table I. Carbonyl substitution causes such a large reduction in the torsional strain repulsion that the resultant torsional interaction (unstrained plus strained) is a minimum at the planar conformation of oxetanone and thietanone and has only a small planar barrier for cyclobutanone. This resultant torsional minimum at the planar conformation has been discussed for oxetanone by Gibson and Harris.⁶ Finally the changes in the torsional strain barriers for carbonyl substitution in the series of molecules cyclobutane, oxetane, and thietane are in the same direction (lower) and qualitatively but not quantitatively

the same, ranging from 4 kcal/mol in cyclobutane to approximately 9 kcal/mol in oxetane and thietane. The origin of the forces which result in these large reductions in torsional repulsion upon substitution of electronegative groups fluorine or carbonyl on four-membered ring molecules has not been determined.

References and Notes

- (1) Part of a thesis submitted in partial fulfillment for the degree of Doctor of Philosophy, Wesleyan University, 1974.
- (2) Ph.D. Degree with Richard C. Lord, Jr., 1966.
- (3) Review articles: (a) R. C. Lord and S. Blackwell, *Vib. Spectra Struct.*, **1**, 1 (1972); (b) V. Laurie, *Acc. Chem. Res.* **3**, 331 (1970).
- (4) W. C. Pringle and A. L. Meinzer, *J. Chem. Phys.*, **61**, 2071 (1974).
- (5) (a) J. R. Durig and R. C. Lord, *J. Chem. Phys.*, **45**, 61 (1966); (b) T. R. Borgers and H. L. Strauss, *ibid.*, **45**, 947 (1966); (c) L. H. Sharpen and V. W. Laurie, *ibid.*, **49**, 221 (1968).
- (6) J. S. Gibson and D. O. Harris, *J. Chem. Phys.*, **52**, 5234 (1970).
- (7) (a) K. D. Moller, A. R. deMeo, D. R. Smith, and L. H. London, *J. Chem. Phys.*, **47**, 2609 (1967); (b) R. A. Beaudet, personal communication.
- (8) (a) J. R. Stone and I. A. Mills, *Mol. Phys.*, **18**, 631 (1970); (b) T. Ueda and T. Shimanouchi, *J. Chem. Phys.*, **49**, 470 (1968).
- (9) (a) L. H. Sharpen and V. W. Laurie, *J. Chem. Phys.*, **49**, 221 (1968); (b) T. R. Borgers and H. L. Strauss, *ibid.*, **45**, 947 (1966).
- (10) (a) S. I. Chan, J. Zinn, and W. D. Gwinn, *J. Chem. Phys.*, **34**, 1319 (1961); (b) A. Dante, W. J. Lafferty, and R. C. Lord, *ibid.*, **33**, 294 (1960); (c) S. I. Chan, T. R. Borgers, J. W. Russell, H. L. Strauss, and W. D. Gwinn, *ibid.*, **44**, 1103 (1966).
- (11) J. S. Gibson and D. O. Harris, *J. Chem. Phys.*, **57**, 2318 (1972).
- (12) D. O. Harris, H. W. Harrington, A. C. Luntz, and W. D. Gwinn, *J. Chem. Phys.*, **44**, 3467 (1966).
- (13) T. K. Avirah, R. L. Cook, and T. B. Malloy, Ohio State Symposium on Molecular Structure and Spectroscopy, Ohio State University, Columbus, Ohio, June 1974.

Resonance Raman Spectra of Metalloctaethylporphyrins. Low Frequency Vibrations of Porphyrin and Iron–Axial Ligand Stretching Modes

T. Kitagawa,* M. Abe, Y. Kyogoku,¹

Institute for Protein Research, Osaka University, Suita, Osaka, Japan, 565

H. Ogoshi, E. Watanabe, and Z. Yoshida

Department of Synthetic Chemistry, Faculty of Engineering, Kyoto University, Yoshida, Sakyo-ku, Kyoto, Japan, 606
(Received January 5, 1976)

Resonance Raman spectra of THF solutions of various metalloctaethylporphyrin complexes [M(OEP): M = Pd²⁺, Ni²⁺, Co²⁺, and Cu²⁺], their meso-deuterated derivatives [M(OEP)-d₄: M = Ni²⁺ and Pd²⁺], [Fe³⁺(OEP)X: X = F, Cl, Br, and I], Fe³⁺(OEP)Cl-d₄, and Fe³⁺(OEP)(Im)₂ClO₄ are measured in the frequency region below 850 cm⁻¹. Vibrational modes corresponding to individual Raman lines are shown in terms of Cartesian displacement vectors which have been obtained from normal coordinate analysis of the observed Raman and infrared data of Ni(OEP) and Ni(OEP)-d₄. On the basis of the normal coordinate calculations, only one vibrational mode (B_{1g} in D_{4h}) of M(OEP) is deduced to show a large isotopic frequency shift. Further, depolarized Raman lines are found at 751 and 684 cm⁻¹ for Ni(OEP) and Ni(OEP)-d₄, respectively, and at 758 and 687 cm⁻¹ for Pd(OEP) and Pd(OEP)-d₄, respectively. The Raman lines due to Fe-axial ligand stretching modes are assigned for some Fe complexes. In high-spin derivatives [Fe³⁺(OEP)X], the Fe-X stretching modes are assigned at 606, 364, and 279 cm⁻¹ when X = F, Cl, and Br, respectively, while for low-spin derivatives [Fe³⁺(OEP)L₂], the L-Fe-L symmetric stretching mode gives rise to the Raman line at 290 cm⁻¹ when L = imidazole. A rather intense and polarized Raman line is observed at around 670 cm⁻¹ in spectra of M(OEP) derivatives excited with 488.0-nm radiation and its intensity depends apparently upon the geometrical structures of the complexes.

Introduction

Resonance Raman spectra of metalloporphyrin complexes have been extensively studied to reveal the molecular symmetry and the excitation profile of Raman scattered intensity.²⁻⁹ In previous work from this laboratory, Raman lines associated primarily with the methine-bridge stretching vibrations were assigned empirically¹⁰ and the assignments were confirmed by normal coordinate calculations.¹¹⁻¹³ The dependence of porphyrin vibrational frequencies upon the nature of the substituted metal ion has also been discussed in terms of a model which proposes either π -electron interaction between metal and porphyrin¹⁴ or distortion of the porphyrin ring.¹⁵ These Raman studies, and previous infrared studies¹⁶⁻¹⁸ as well, have been concerned mainly with the higher frequency modes (above 850 cm⁻¹) of the porphyrin ring system.

However, it is reasonable to expect that lower frequency modes should be particularly sensitive to the structural changes of interest. For example, ring deformation vibrations below 850 cm⁻¹ can be expected to differ according to whether the porphyrin ring is planar [as in low spin Fe(OEP)(Im)₂ClO₄¹⁹] or domed [as in high spin Fe(PP)Cl²⁰ where PP = protoporphyrin]. The stretching vibration of the coordination bond between Fe and its axial ligand (L) may also appear in this frequency region. Indeed a Raman line due to the Fe-O₂ stretching mode was found recently at 567 cm⁻¹ in oxyhemoglobin.²¹ Since the frequency of this mode is closely related to the nature of the Fe-L bond, its position in the resonance Raman spectrum might be useful for characterizing native hemoproteins. Thus further study of Fe-L stretching frequencies in hemoprotein model compounds seems appropriate.

In this paper, we report and assign the Raman frequencies

due to Fe-L (high spin) and L-Fe-L (low spin) stretching vibrations of Fe(OEP) derivatives and also point out that the intensities of some Raman lines in the low-frequency region are apparently structure sensitive.

Experimental Section

Syntheses and methods of preparation of nondeuterated [M(OEP)] and meso-deuterated complexes [M(OEP)-d₄] have been described previously.^{17,22} The iron-protoporphyrin-bis(imidazole) complex [Fe(PP)(Im)₂] was obtained by adding imidazole [Im] to aqueous bovine hemin (Sigma type I) at pH 11. The Raman spectra were obtained with excitation by an Ar⁺ ion laser (Spectra Physics Model 164) and recorded on a JEOL-02AS Raman spectrometer equipped with a cooled RCA-C31034 photomultiplier (Figures 1 and 3A) or a JEOL-400D Raman spectrometer equipped with an HTV-R649 photomultiplier (Figures 2 and 3B). Procedures for the measurement of Raman spectra were as described previously,¹⁴ except that, in the present study, a spinning (1800 rpm) cell of 2 cm diameter was used in order to avoid overheating of sample. Calibration of the spectrometer was performed with the use of D₂ gas.²³ The estimated errors of frequencies and depolarization ratios are within the limits of 2 cm⁻¹ and 0.1, respectively.

Normal Coordinate Treatment

Normal coordinate calculations were carried out for in-plane vibrations of nickel octamethylporphyrin [Ni(OMP)] and its meso-deuterated derivative [Ni(OMP)-d₄]. The peripheral methyl groups were regarded as point masses in the calculations and the proposed D_{4h} symmetry of the porphyrin frame²⁴ was assumed. Details of the calculation procedure, as well as results obtained in applying this procedure to

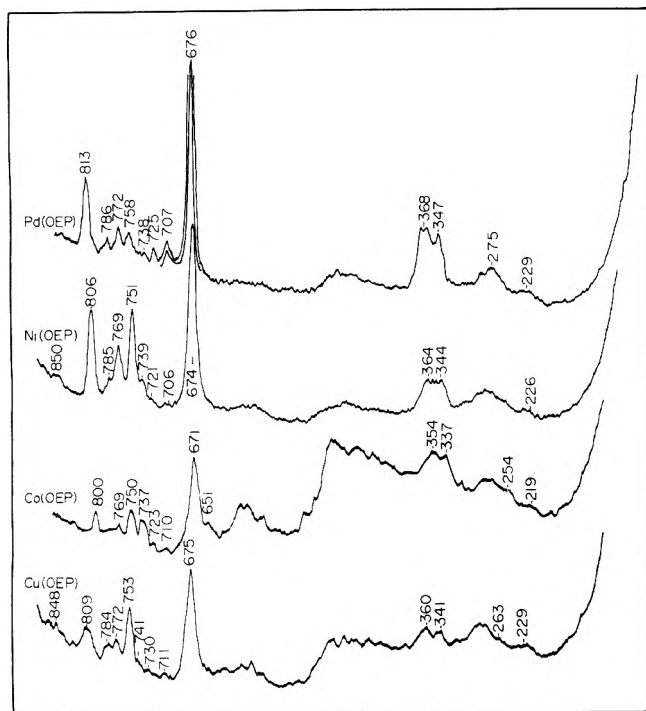


Figure 1. Raman spectra of square-planar metalloctaethylporphyrin complexes in THF, excited by the 488.0-nm line. Raman frequencies are in cm^{-1} units. Weak Raman lines at 285, 600 and 665 cm^{-1} are due to THF.

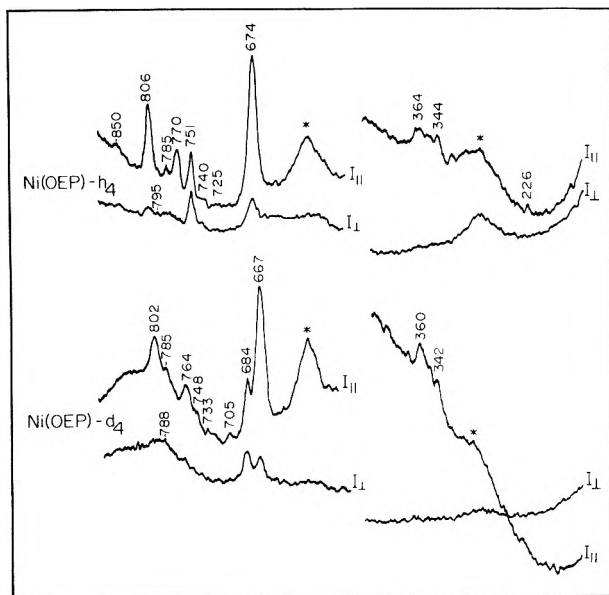


Figure 2. Polarized Raman spectra of Ni(OEP) and Ni(OEP)- d_4 in THF, excited by the 488.0-nm line. $I_{||}$ and I_{\perp} indicate the electric vector of the scattered radiation to be parallel and perpendicular, respectively, to that of the incident laser light. Raman lines marked by an asterisk are due to THF.

frequencies of Ni(OEP) in the region above 850 cm^{-1} , were given recently.¹² Here attention is focused on vibrations below 850 cm^{-1} .

The in-plane vibrations are classified into 18 infrared-active degenerate modes ($18E_u$) and 35 Raman active modes ($9A_{1g} + 9B_{1g} + 8A_{2g} + 9B_{2g}$). The potential function employed consisted of a Urey-Bradley force field with additional terms

for stretching-stretching interaction between adjacent bonds. This modified function thus incorporated the effect of resonance of conjugated double bonds in the porphyrin ring. Repulsion force constants were transferred from similar molecules and were used without adjustment. Other force constants were adjusted by trial and error until the calculated frequencies fit those of Raman and infrared bands observed for Ni(OEP) and Ni(OEP)- d_4 . The calculated frequencies and potential energy distribution [PED] for lower frequency modes are given in Table I together with the corresponding observed frequencies. Further details are given elsewhere.¹²

Results

Raman spectra of four M(OEP) complexes with square-planar structure are shown in Figure 1. Each compound has an intense and polarized Raman line at $\sim 674 \text{ cm}^{-1}$, as well as other common spectral features below 800 cm^{-1} . In Figure 1, the poorly resolved doublet of Ni(OEP) (ca. 364 and 344 cm^{-1}) was clearly separated into two lines at 364 and 350 cm^{-1} by cooling the sample from room temperature to 193 K in THF solution. On the other hand, the fairly broad Raman line ca. 229 cm^{-1} (Figure 1) did not become sharp even at low temperature.

Figure 2 illustrates the polarization properties of the Raman lines of Ni(OEP) and Ni(OEP)- d_4 , where $I_{||}$ and I_{\perp} denote the parallel and perpendicular components of the scattered radiation, respectively. We thus find no prominent anomalously polarized Raman lines in this lower frequency region, although several Raman lines with inverse polarization have been clearly identified in the higher frequency region.¹⁴ It is noteworthy that the Raman lines at 751 cm^{-1} for Ni(OEP) and 684 cm^{-1} for Ni(OEP)- d_4 are definitely depolarized. Therefore, the 751 cm^{-1} line of Ni(OEP) appears to shift to 684 cm^{-1} upon deuterium substitution of methine hydrogen atoms. The corresponding Raman line of Pd(OEP) is observed at 758 cm^{-1} and is shifted to 687 cm^{-1} in Pd(OEP)- d_4 . Since four totally symmetric ring modes are expected in this frequency region for the proposed D_{4h} symmetry,²⁴ we assign the four polarized Raman lines at 806 , 674 , 364 , and 226 cm^{-1} [Ni(OEP), Figure 2] to these modes (see also Table I).

Raman spectra of Fe(OEP)X (X = F, Cl, Br, and I) and Fe(OEP)(Im) $_2$ ClO $_4$ are shown in Figure 3. Inspection of Figure 3 reveals that while these derivatives exhibit closely similar spectra in the higher frequency region (Figure 3A, CH $_2$ Cl $_2$ solution), their spectra are considerably different from one another in the lower frequency region (Figure 3B, THF solution). Comparison of the Raman spectrum of Fe(OEP)F with those of other Fe(OEP)X suggests further that there is a Raman line at 606 cm^{-1} when X = F, although this line is partially overlapped by a broad line of the solvent.

The Raman lines at 364 cm^{-1} for Fe(OEP)Cl and 279 cm^{-1} for Fe(OEP)Br are seen only for X = Cl and X = Br, respectively. The corresponding Raman line for Fe(OEP)Cl- d_4 is identified at 360 cm^{-1} . Therefore the vibrational mode responsible cannot be associated with appreciable displacement of methine bridges. Frequencies of these Raman lines agree closely with those of the infrared bands of the Fe-X stretching vibrations, observed in the solid state at 605.5 cm^{-1} for Fe(OEP)F, at 357 cm^{-1} for Fe(OEP)Cl, and at 270 cm^{-1} for Fe(OEP)Br.²² Accordingly, the Raman lines at 606 , 364 , and 279 cm^{-1} are assigned to Fe-F, Fe-Cl, and Fe-Br stretching vibrations, respectively.

None of the Raman lines of Fe(OEP)X (high spin) in the interval 660 – 680 cm^{-1} are nearly as intense as the line at 674 cm^{-1} in either Ni(OEP) or Fe(OEP)(Im) $_2$ ClO $_4$ (low spin).

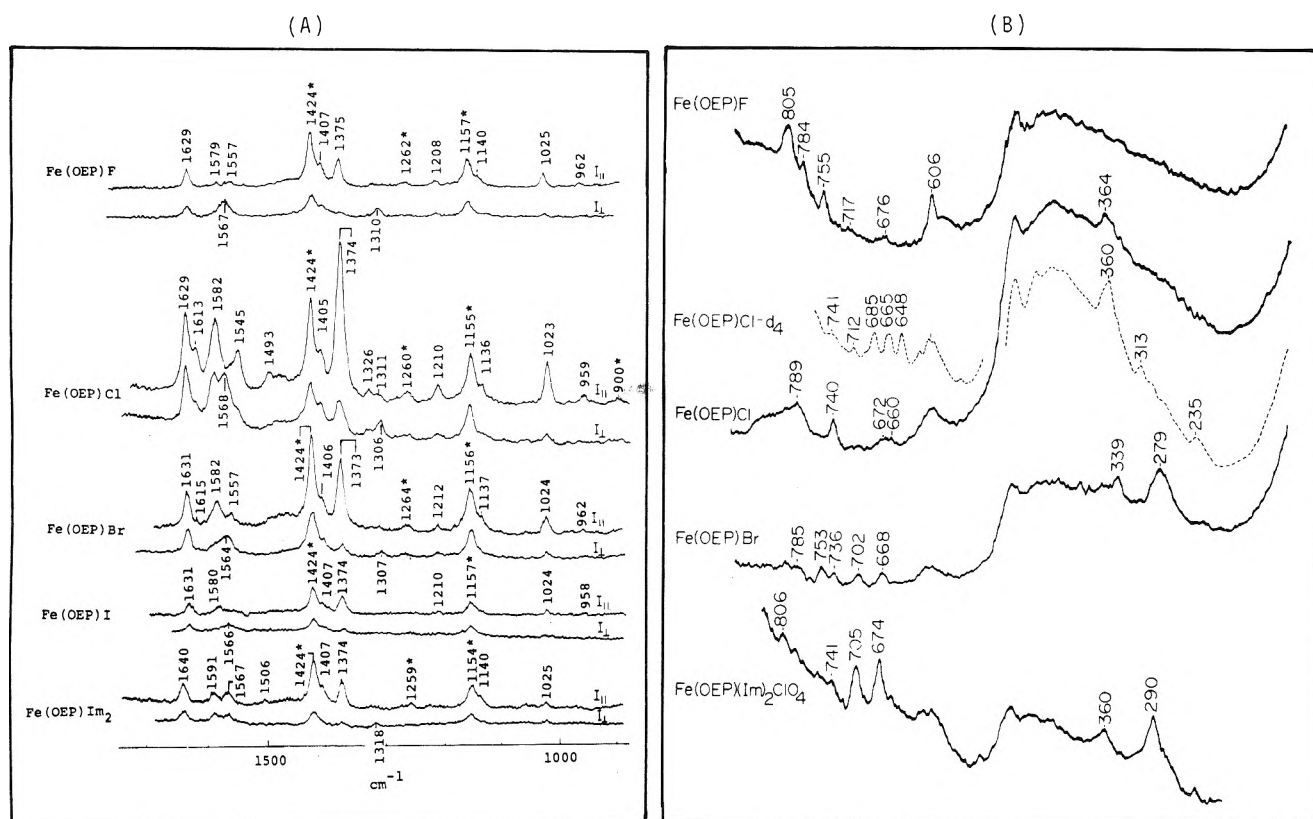


Figure 3. Raman spectra of iron-octaethylporphyrin derivatives, excited by the 488.0-nm line. (A) Parallel ($I_{||}$) and perpendicular (I_{\perp}) components of the Raman spectra in the higher frequency region (CH_2Cl_2 solutions). Raman lines marked by an asterisk are due to CH_2Cl_2 . (B) Raman spectra in the lower frequency region (THF solutions). Unmarked lines are due to either THF or the cell. The broken curve, with change of base line near 500 cm^{-1} , is the spectrum of the meso-deuterated derivative of Fe(OEP)Cl.

TABLE I: Observed and Calculated Frequencies of the Raman Active Vibrations of Ni(OEP) and Ni(OEP)- d_4 (cm^{-1})^a

	Ni(OEP)		Ni(OEP)- d_4		Isotopic shift		PED
	Obsd	Calcd	Obsd	Calcd	Obsd	Calcd	
A_{1g}	806	805	802	791	4	14	$\nu(\text{C}_\alpha\text{N})36$, $\delta(\text{C}_\alpha\text{C}_m\text{C}_\alpha)20$
	674	658	667	649	7	9	$\nu(\text{C}_\alpha\text{C}_\beta)20$, $\delta(\text{C}_\beta\text{C}_\alpha\text{N})19$
	364	362	360	362	4	0	$\delta(\text{C}_\beta\text{Me})70$, $\nu(\text{C}_\beta\text{C}_\beta)10$
	226	238		238		0	$\nu(\text{C}_\alpha\text{C}_m)23$, $\nu(\text{MN})20$
B_{1g}	784	748	(785)	748	(0)	0	$\nu(\text{C}_\beta\text{Me})34$, $\nu(\text{C}_\alpha\text{C}_\beta)23$
	751	660	684	605	67	55	$\delta(\text{C}_\beta\text{C}_\alpha\text{N})31$, $\delta(\text{C}_\alpha\text{NC}_\alpha)21$
	~344	350	~342	350	2	0	$\delta(\text{C}_\beta\text{Me})78$
	226	221		221		0	$\nu(\text{MN})40$, $\delta(\text{C}_\beta\text{C}_\alpha\text{C}_m)28$
B_{2g}	(850)	859	(845)	858	(5)	1	$\delta(\text{C}_\beta\text{Me})50$, $\nu(\text{C}_\alpha\text{C}_m)25$
		529		527		2	$\delta(\text{C}_\alpha\text{C}_\beta\text{C}_\beta)37$, $\nu(\text{C}_\beta\text{Me})14$
		218		217		1	$\delta(\text{NMN})20$, $\nu(\text{C}_\alpha\text{C}_m)15$
		167		167		0	$\delta(\text{NMN})21$, $\delta(\text{C}_\beta\text{C}_\alpha\text{C}_m)21$
A_{2g}	795	783	(788)	782	(7)	1	$\delta(\text{C}_\beta\text{Me})34$, $\delta(\text{C}_\beta\text{C}_\alpha\text{C}_m)31$
		528		522		6	$\delta(\text{C}_\alpha\text{C}_\beta\text{C}_\beta)45$, $\nu(\text{C}_\beta\text{Me})19$
		309		306		3	$\delta(\text{C}_\beta\text{C}_\alpha\text{C}_m)45$, $\delta(\text{C}_\beta\text{Me})29$

^a Observed frequencies are accurate to $\pm 2\text{ cm}^{-1}$ except for values in parentheses which are accurate to $\pm 5\text{ cm}^{-1}$. Polarization properties of the Raman lines in parentheses are uncertain because of weakness. Abbreviations: ν , stretching coordinate; δ , angle deformation coordinate; Me, peripheral methyl group treated as a single dynamical unit; M, metal; PED, potential energy distribution, cited as a percentage of the total for each bond stretching or angle deformation given in parentheses. Notation for individual atoms is given in Figure 5.

(Note also that the intensity ratio $I_{751}/I_{674} < 0.5$ in both Ni(OEP) and Fe(OEP)(Im)₂ClO₄, but in Fe(OEP)X the ratio I_{751}/I_{674} is much greater than 0.5 for all lines in the region 660–680 cm^{-1} .) Since Fe(PP)Cl (PP = protoporphyrin) is

known to have a domed structure²⁰ and both Ni(OEP) and Fe(OEP)(Im)₂ClO₄ planar structures,^{19,24} we may conclude that the absence of an intense polarized line near 674 cm^{-1} is characteristic of the domed structure while the presence of

an intense line near 674 cm^{-1} (such that $I_{750}/I_{674} < 0.5$) is characteristic of the planar structure. Accordingly, from the data of Figures 1 and 3B, we propose that $\text{Fe}(\text{OEP})\text{X}$ ($\text{X} = \text{F}$, Cl , and Br) are domed while $\text{M}(\text{OEP})$ ($\text{M} = \text{Pd}^{2+}$, Co^{2+} , and Cu^{2+}) are planar.

An alternative explanation is that the observed intensity ratios are dependent in whole or in part upon the absorption (profile) of the chromophore. However, we have examined the resonance Raman spectra of $\text{Fe}^{2+}(\text{PP})(\text{Im})_2$ and $\text{Fe}^{3+}(\text{PP})(\text{Im})_2$ and found that the ratio I_{748}/I_{676} is nearly identical for both of these complexes (0.4), in spite of their different absorption spectra in the visible region. Therefore we view the former explanation as a more reasonable one and suggest that the intensity ratio I_{750}/I_{674} may be useful as an indicator of planar and domed porphyrin frames for a given type of heme.

We also note that the 674-cm^{-1} line is more intense for planar structures and for shorter wavelengths of excitation. On the other hand, the 751-cm^{-1} line is more intense when electron-withdrawing groups, such as $-\text{CH}=\text{O}$, are present as peripheral substituents of the porphyrin frame.

In Figure 4 we show the infrared spectra obtained from CsI disks of $\text{Ni}(\text{OEP})$ and $\text{Ni}(\text{OEP})\text{-}d_4$ since the latter has not been reported previously. It is seen that the strong band at 355 cm^{-1} for $\text{Ni}(\text{OEP})$ shows a fairly large frequency shift (to 334 cm^{-1}) upon meso deuteration, implying that this frequency cannot be due to an in-plane vibration as previously proposed.^{13,17} On the other hand, the two Raman lines at 364 and 344 cm^{-1} for $\text{Ni}(\text{OEP})$ show only small isotopic frequency shifts (see Figure 2). It is therefore evident that the infrared band and Raman lines are due to different modes although their frequencies are fortuitously close.

Another important point to be noted is that the infrared band of $\text{Ni}(\text{OEP})$ at 1673 cm^{-1} is missing in $\text{Ni}(\text{OEP})\text{-}d_4$. The highest frequency infrared fundamental of $\text{Ni}(\text{OEP})\text{-}d_4$ is located at 1543 cm^{-1} (Figure 4). However, a fundamental vibration corresponding to a porphyrin-ring bond-stretching mode should not exhibit an isotopic frequency shift as large as 130 cm^{-1} solely as the result of meso deuteration. Accordingly, we conclude that the 1673-cm^{-1} band of $\text{Ni}(\text{OEP})$ cannot be due to a fundamental stretching mode of the porphyrin ring as assigned previously.¹³ This new fact has been incorporated into the normal coordinate calculations and the refinement results in a large change of the stretching force constants reported previously.^{12,13}

Discussion

Fe-L Stretching Vibrations. There is a Raman line at 290 cm^{-1} for $\text{Fe}(\text{OEP})(\text{Im})_2\text{ClO}_4$ which is not recognizable either in spectra of other $\text{Fe}(\text{OEP})\text{X}$ type derivatives or in spectra of square-planar $\text{M}(\text{OEP})$. However, a corresponding Raman line is identified at 299 cm^{-1} for $\text{Fe}^{2+}(\text{PP})(\text{Im})_2$ and at 276 cm^{-1} for $\text{Fe}^{3+}(\text{PP})(\text{Im})_2$.³ Accordingly, the Raman line at 290 cm^{-1} for $\text{Fe}(\text{OEP})(\text{Im})_2\text{ClO}_4$ is presumably associated with the $(\text{Im})\text{N}-\text{Fe}-\text{N}(\text{Im})$ symmetric stretching mode. The Raman line at 301 cm^{-1} for ferrous cytochrome c^{25} may also be due to a similar vibrational mode, although here the two axial ligands are N (histidine) and S (methionine). Thus we propose that this particular out-of-plane vibrational mode appears with recognizable intensity in resonance Raman spectra of both the bis(imidazole) model compounds and cytochrome c .

If we assume that the Soret and Q bands in the visible absorption spectra of metalloporphyrins are due to $A_{1g} \rightarrow E_u$ transitions (D_{4h} symmetry), then resonance enhancement of Raman scattering intensity is expected only for vibrations of

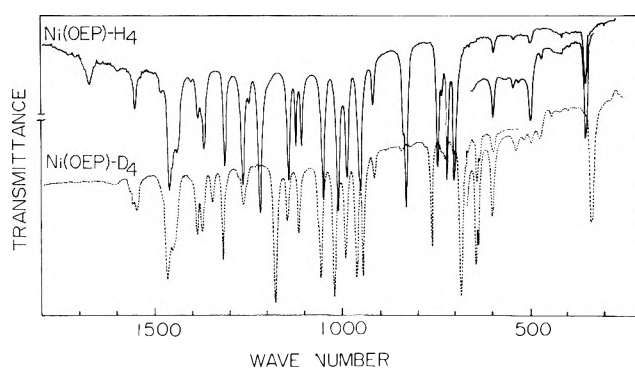


Figure 4. Infrared absorption spectra of CsI disks of $\text{Ni}(\text{OEP})$ and $\text{Ni}(\text{OEP})\text{-}d_4$. A higher substrate to matrix ratio was employed to obtain spectra of disks below 700 cm^{-1} .

A_{1g} , A_{2g} , B_{1g} , and B_{2g} species. The $L-\text{Fe}-L$ symmetric stretching vibration of $\text{Fe}(\text{OEP})\text{L}_2$, despite the fact that it is an out-of-plane vibration, belongs to the A_{1g} species and therefore its appearance in the resonance Raman spectrum is not prohibited on grounds of symmetry. Furthermore, it may borrow additional Raman intensity through vibrational coupling with other A_{1g} modes. These considerations would explain the appearance of an out-of-plane mode in the spectra.

The antisymmetric $L-\text{Fe}-L$ stretching mode belongs to the A_{2u} species. Assignment²² of the ir band at 376.5 cm^{-1} in $\text{Fe}(\text{OEP})(\text{Im})_2\text{ClO}_4$ to this mode seems reasonable. The corresponding Raman line is, however, missing. This suggests that $\text{N}-\text{Fe}-\text{N}$ in solution assumes a linear configuration, as in the case of the crystal.¹⁹

When $\text{M}(\text{OEP})$ molecules have the domed (C_{4v}) structure as in chlorohemin,²⁰ the vibrational modes in the A_{1g} and A_{2u} species of the D_{4h} group are mixed and combined into the A_1 species which is simultaneously infrared and Raman active. It seems likely that the $\text{Fe}-\text{X}$ stretching mode in $\text{Fe}(\text{OEP})\text{X}$ (A_1 species) gains Raman intensity through mixing with other resonance-enhanced modes corresponding to the in-plane (A_{1g}) vibrations of planar $\text{M}(\text{OEP})$. Evidence for such vibrational coupling comes from the fact that the Raman frequencies below 850 cm^{-1} of $\text{Fe}(\text{OEP})\text{X}$ depend upon the identity of the axial ligands (see Figure 3B).

Previously the Raman lines at 299 cm^{-1} for $\text{Mn}(\text{TPP})\text{Cl}$ (TPP = tetraphenylporphyrin) and 278 cm^{-1} for $\text{Mn}(\text{TPP})\text{Br}$ were assigned to $\text{Mn}^{3+}-\text{Cl}$ and $\text{Mn}^{3+}-\text{Br}$ stretching modes, respectively.²⁶ The frequency of the $\text{Mn}^{3+}-\text{Br}$ stretching mode is close to that of $\text{Fe}^{3+}-\text{Br}$ (279 cm^{-1}). However, the frequency of the $\text{Mn}^{3+}-\text{Cl}$ stretching mode differs considerably from that of $\text{Fe}^{3+}-\text{Cl}$ (364 cm^{-1}). If the stretching force constants are assumed to be almost identical (i.e., $K_{\text{Fe}-\text{Cl}} \approx K_{\text{Fe}-\text{Br}}$), and if no vibrational coupling occurs, then the $\text{Fe}-\text{Cl}$ stretching frequency $\nu_{\text{Fe}-\text{Cl}}$ may be approximated by

$$\nu_{\text{Fe}-\text{Cl}} = (\mu_{\text{Fe}-\text{Br}}/\mu_{\text{Fe}-\text{Cl}})^{1/2}\nu_{\text{Fe}-\text{Br}}$$

where $\mu_{\text{Fe}-\text{Br}}$ and $\mu_{\text{Fe}-\text{Cl}}$ are the reduced masses for the assumed $\text{Fe}-\text{Br}$ and $\text{Fe}-\text{Cl}$ oscillators. With 279 cm^{-1} for $\nu_{\text{Fe}-\text{Br}}$, we calculate 343 cm^{-1} for $\nu_{\text{Fe}-\text{Cl}}$ from the above equation. However, the stretching force constants differ in the order $K_{\text{Fe}-\text{F}} > K_{\text{Fe}-\text{Cl}} > K_{\text{Fe}-\text{Br}}$ and therefore $\nu_{\text{Fe}-\text{Cl}}$ is expected to be appreciably higher than 343 cm^{-1} . Accordingly, the assignment of the 364-cm^{-1} line to the $\text{Fe}-\text{Cl}$ stretching mode seems quite reasonable.

Recently Kincaid and Nakamoto²⁷ assigned the Raman line of $\text{Fe}(\text{OEP})\text{F}$ at 606 cm^{-1} to the $\text{Fe}-\text{F}$ stretching mode. We also confirm their assignment in the present study.

Assignment of Low Frequency Raman Lines of Ni(OEP). Raman frequencies of Ni(OEP) in the region below 850 cm^{-1} are assignable to specific vibrational modes with the help of normal coordinate calculations. Just as most of the depolarized Raman lines in the region above 850 cm^{-1} of Ni(OEP)¹⁴ and hemoproteins²⁸ have been assigned to vibrations of B_{1g} species, the depolarized lines below 850 cm^{-1} of Ni(OEP) are also assignable to the B_{1g} vibrations. In the lower frequency region there is only one mode for which a fairly large isotopic frequency shift is expected on the basis of normal coordinate calculations. We observe such a line for Ni(OEP) at 751 cm^{-1} , shifted to 684 cm^{-1} for Ni(OEP)- d_4 . The involvement of C_m -D deformations is very likely responsible for the large isotopic frequency shift (see Table I). However, agreement between the calculated and observed frequencies for this mode is not yet satisfactory. This may be due partly to the treatment of peripheral CH_3 groups as single dynamic units.

Degenerate in-plane modes (E_u) are infrared active. Three bands are expected to appear in the infrared between 250 and 500 cm^{-1} for Ni(OEP), corresponding to the calculated E_u modes at 372, 312, and 299 cm^{-1} . Since these vibrations do not involve displacements of the CH groups at the methine bridges, only small isotopic frequency shifts are expected in the infrared upon deuterium substitution, irrespective of the set of force constants employed. Accordingly, the strong infrared band of Ni(OEP) at 355 cm^{-1} , with isotopic frequency shift ($\Delta\nu$) of 21 cm^{-1} (Figure 4), must be due to an out-of-plane deformation vibration of porphyrin. The previous assignment to coupled Ni-N stretching and in-plane deformation is less likely.¹⁷

Figure 5 illustrates the vibrational displacements (L_X)¹² of four A_{1g} modes and one B_{1g} mode. The latter mode shows the large isotopic frequency shift discussed above. The atomic displacement vectors indicate that the Raman line at 806 cm^{-1} is due to a deformation vibration of the 16-membered inner ring (macrocycle). The vibrational mode for the Raman line at 674 cm^{-1} has the appearance of a breathing vibration of the macrocycle, with only slight displacement of the C_β atoms. The 806- and 674-cm^{-1} frequencies also involve contributions from porphyrin-ring bond-stretching motions, although such contribution is rather small (<10% PED) for the 751-cm^{-1} mode. Pyrrole ring deformations contribute about equally in magnitude but opposite in phase to the 674- and 751-cm^{-1} frequencies. For the 674-cm^{-1} line, adjacent pyrrole rings buckle in phase, whereas they deform out-of-phase for the 751-cm^{-1} line.

With the understanding that only limited conclusions can be drawn from comparing resonance Raman intensities derived from a single wavelength (in this case, 488.0 nm), we suggest the following interpretation of the data of Figure 3. The counterparts of the 674- and 751-cm^{-1} lines exhibit wide variations of intensity among Fe(OEP)X derivatives. This situation is similar to that reported for myoglobin derivatives, also with 488.0-nm excitation.²⁹ We propose that the observed intensities for a given type of heme differ according to the geometrical structure of the porphyrin rings, i.e., whether the ring is planar or domed. It is evident from Figure 3 that the complexes which are likely to be planar [Fe(OEP)(Im)₂ClO₄ and M(OEP); M = Pd, Cu, Co and Ni] have an intense Raman line near 674 cm^{-1} , while those likely to be domed [Fe(OEP)X; X = F, Cl, and Br] have very much weaker lines near 674 cm^{-1} .

Thus, in nonresonance Raman spectra we expect that the ring-breathinglike mode (674 cm^{-1}) would give rise to an intense Raman line when the porphyrin ring is planar, and further that the intensity of this line would gradually diminish

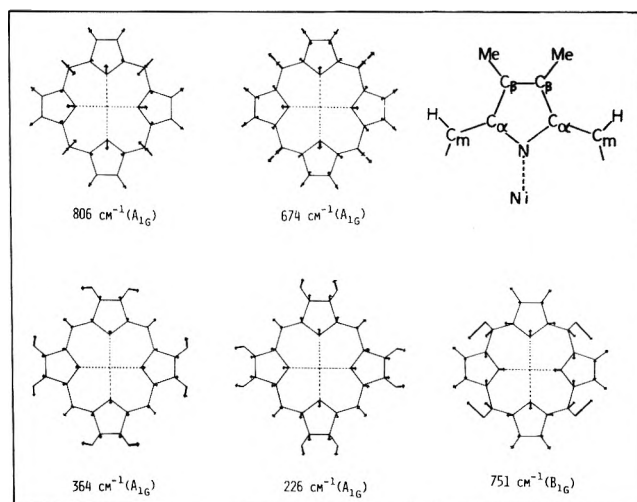


Figure 5. Vibrational modes corresponding to the one depolarized and four polarized Raman lines of Ni(OEP). Frequencies in cm^{-1} are those observed for Ni(OEP) in THF. The inset (upper right) shows the notation of porphyrin ring atoms used in the text and in Table I.

as the ring is domed and the vibration loses its "breathing" character. However, it should be kept in mind that other factors may also affect the observed intensities. For example, in resonance Raman scattering, the Franck-Condon overlap integral is also an important determinant of the intensity of polarized lines (674 cm^{-1}). On the other hand, vibronic coupling would play a significant role in determining the intensity of a depolarized line (751 cm^{-1}).³⁰ The influence of these two factors is thought to be significant for bond-stretching motions¹⁴ (viz. conjugated bonds of the porphyrin ring) but may be less significant in the present case of deformation modes.

The above proposal also seems reasonable in view of the following: (i) Ring stretching modes of the A_{2g} species give rise to intense and inversely polarized Raman lines upon excitation by 514.5-nm radiation,¹⁴ but no inversely polarized Raman line appears in the lower frequency region for Ni(OEP), even when the 514.5-nm line is used for excitation. (ii) Normal coordinate calculations implied that the contribution of ring stretching motions to the lower frequency modes of A_{2g} species is insignificant. (iii) When the wavelength of excitation is increased, the 751-cm^{-1} line should gain intensity, as do the *depolarized* lines above 1000 cm^{-1} , while the 674-cm^{-1} line should lose intensity, as do the *polarized* lines above 1000 cm^{-1} . This is qualitatively what is observed for ferrous C-type cytochromes.^{25,31,32}

Further study of the excitation-wavelength dependence of the resonance Raman intensities of Fe(OEP)X complexes will allow us to either confirm or reject the above hypothesis. Calculations are now in progress to determine the normal modes of domed metalloporphyrins and to evaluate the role of the Franck-Condon overlap integral in the excitation profile of Raman scattering intensity.

The Raman line at 226 cm^{-1} for Ni(OEP) is associated with a mode in which the four pyrrole rings move outward in-phase (Figure 5). The corresponding frequencies for Fe(OEP)Cl- d_4 , Fe²⁺(PP)(Im)₂, Fe³⁺(PP)(Im)₂, and ferrous cytochrome c_3 occur at 235, 236, 232, and 229 cm^{-1} , respectively (Figure 3B and ref 25). The broadness of the Raman line in each case is not due to vibrational anharmonicity otherwise sharpening would occur at low temperature. Choice of an excitation wavelength within the region of charge transfer bands might cause this line to be strongly enhanced.

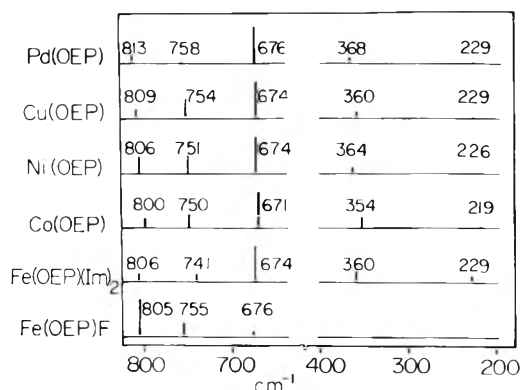


Figure 6. Dependence of the one B_{1g} and four A_{1g} Raman lines of metalloctaethylporphyrin upon the substituted metal ion. The most intense Raman line in the frequency region below 850 cm^{-1} is normalized to unity. Numbers indicate the observed Raman frequencies in cm^{-1} units.

The important low frequency modes ($4A_{1g} + B_{1g}$) observed in Raman spectra of planar $M(\text{OEP})$ complexes are summarized in the correlation diagram of Figure 6. Recognizing that there should be virtually no motion of the metal ion for each of these vibrational modes (g species of D_{4h} symmetry), any frequency differences among the complexes cannot be due to the different masses of the metal ions, at least to a first approximation. (This approximation does not apply to infrared-active low-frequency fundamentals, where displacements of the metal ion could be significant and therefore mass effects could not be ignored.) Hence, the frequency difference in Figure 6 are attributed to differences in the stretching force constants change of the $M\cdots N$ bonds.

It is evident from Figure 6 that the force constants change rather little among the square-planar complexes, indicating that the degree of covalent character in the $M\cdots N$ bonds decreases only slightly in the order $\text{Pd} > \text{Cu} > \text{Ni} > \text{Co}$. This order is partly reversed in the higher frequency modes treated previously, which is consistent with the assumption that both π and σ electron interactions influence the $M\cdots N$ stretching force constants but that only π electron interactions influence the higher frequency modes.¹⁴

In conclusion, the Raman spectra in the lower frequency region (below 850 cm^{-1}) contain useful information on the structure of metalloporphyrin complexes, even though the Raman intensities are generally weaker in this region than in the higher frequency region. The frequency of the symmetric stretching vibration of the bonds between metal ion and two

axial ligands was located ca. 290 cm^{-1} in resonance Raman spectra of several bis(imidazole)-iron-porphyrin complexes and some cytochromes. These results suggest that the Fe -axial ligand bond-stretching frequencies may be detectable and of structural significance in hemoproteins.

Acknowledgment. The authors wish to express their gratitude to Professor G. J. Thomas, Jr., of Southeastern Massachusetts University for stimulating discussion and for correcting the manuscript.

References and Notes

- (1) Y. Kyogoku, Postdoctoral Research Associate with Richard C. Lord, 1965-1967.
- (2) A. L. Verma, R. Mendelsohn, and H. J. Bernstein, *J. Chem. Phys.*, **61**, 383 (1974).
- (3) (a) A. L. Verma and H. J. Bernstein, *J. Chem. Phys.*, **61**, 2560 (1974); (b) *J. Raman Spectrosc.*, **2**, 163 (1974).
- (4) R. Plus and M. Lutz, *Spectrosc. Lett.*, **7**, 73, 133 (1974).
- (5) R. H. Felton, N. T. Yu, D. C. O'Shea, and J. A. Shelnutz, *J. Am. Chem. Soc.*, **96**, 3675 (1974).
- (6) S. Sunder, R. Mendelsohn, and H. J. Bernstein, *Biochem. Biophys. Res. Commun.*, **62**, 12 (1975).
- (7) R. Mendelsohn, S. Sunder, and H. J. Bernstein, *J. Raman Spectrosc.*, **3**, 303 (1975).
- (8) S. Sunder, R. Mendelsohn, and H. J. Bernstein, *J. Chem. Phys.*, **63**, 573 (1975).
- (9) R. Mendelsohn, S. Sunder, A. L. Verma, and H. J. Bernstein, *J. Chem. Phys.*, **62**, 37 (1975).
- (10) T. Kitagawa, H. Ogoshi, E. Watanabe, and Z. Yoshida, *Chem. Phys. Lett.*, **30**, 451 (1975).
- (11) P. Stein, J. M. Burke, and T. G. Spiro, *J. Am. Chem. Soc.*, **97**, 2304 (1975).
- (12) M. Abe, T. Kitagawa, and Y. Kyogoku, *Chem. Lett.*, 249 (1976).
- (13) H. Ogoshi, Y. Saito, and K. Nakamoto, *J. Chem. Phys.*, **57**, 4194 (1972).
- (14) T. Kitagawa, H. Ogoshi, E. Watanabe, and Z. Yoshida, *J. Phys. Chem.*, **79**, 2629 (1975).
- (15) L. D. Spaulding, C. C. Chang, N. T. Yu, and R. H. Felton, *J. Am. Chem. Soc.*, **97**, 2517 (1975).
- (16) L. J. Boucher and J. J. Katz, *J. Am. Chem. Soc.*, **89**, 1340 (1967).
- (17) H. Ogoshi, N. Masai, Z. Yoshida, J. Takemoto, and K. Nakamoto, *Bull. Chem. Soc. Jpn.*, **44**, 49 (1971).
- (18) H. Ogoshi and Z. Yoshida, *Bull. Chem. Soc. Jpn.*, **44**, 1722 (1971).
- (19) A. Takenaka, Y. Sasada, E. Watanabe, H. Ogoshi, and Z. Yoshida, *Chem. Lett.*, 1235 (1972).
- (20) J. L. Hoard, M. J. Hamor, T. A. Hamor, and W. S. Caughey, *J. Am. Chem. Soc.*, **87**, 2312 (1965).
- (21) H. Brunner, *Naturwissenschaften*, **61**, 129 (1974).
- (22) H. Ogoshi, E. Watanabe, Z. Yoshida, J. Kincaid, and K. Nakamoto, *J. Am. Chem. Soc.*, **95**, 2845 (1973).
- (23) B. P. Stoicheff, *Can. J. Phys.*, **35**, 730 (1957).
- (24) D. A. Cullen and E. F. Meyer, Jr., *J. Am. Chem. Soc.*, **96**, 2095 (1974).
- (25) T. Kitagawa, Y. Kyogoku, T. Iizuka, M. I. Saito, and T. Yamanaka, *J. Biochem.*, **78**, 719 (1975).
- (26) R. R. Gaughan, D. F. Shriver, and L. J. Boucher, *Proc. Natl. Acad. Sci. U.S.A.*, **72**, 433 (1975).
- (27) J. Kincaid and K. Nakamoto, *Spectrosc. Lett.*, in press.
- (28) T. G. Spiro and T. C. Streckas, *Proc. Natl. Acad. Sci. U.S.A.*, **69**, 2622 (1972).
- (29) Y. Ozaki, T. Kitagawa, and Y. Kyogoku, *FEBS Lett.*, **62**, 369 (1976).
- (30) A. C. Albrecht, *J. Chem. Phys.*, **34**, 1476 (1961).
- (31) L. A. Nafie, M. Pezolet, and W. L. Peticolas, *Chem. Phys. Lett.*, **20**, 563 (1973).
- (32) T. G. Spiro and T. C. Streckas, *Proc. Natl. Acad. Sci. U.S.A.*, **69**, 2622 (1972).

Vibrationally Averaged Interatomic Distances

I. M. Mills¹

Department of Chemistry, University of Reading, Reading RG6 2AD, England (Received January 5, 1976)

Equations are presented for the average internuclear distances r_g and r_α in terms of elements of the L matrix and the L tensor. These are an alternative to the equations presented by Kuchitsu and Morino.

In the analysis of gas electron diffraction data and rotational spectra to determine molecular structures, various vibrational averages of the internuclear distances are involved. Of particular interest are the average internuclear distance r_g , and the distance between the average nuclear positions r_α , which are related to the equilibrium internuclear distance r_e by equations which are usually written in the form

$$r_g = r_e + \langle \Delta z \rangle + \frac{\langle \Delta x^2 \rangle + \langle \Delta y^2 \rangle}{2r_e} \quad (1)$$

$$r_\alpha = r_e + \langle \Delta z \rangle \quad (2)$$

These equations were originally derived by Morino and co-workers^{2,3} and the underlying theory has recently been well reviewed by Kuchitsu⁴ who gives references to the original papers.

In eq 1 and 2, Δx , Δy , and Δz denote differences between the Cartesian displacements of the two atoms involved, in molecule-fixed (Eckart) axes oriented so that the z axis is aligned with the internuclear direction. The averages may represent thermal averages over a Boltzmann vibrational distribution, or averages in the ground (or any other) vibrational state. In the ground state the distance r_α is denoted r_z and defines the "zero-point average" structure of the molecule.⁵ Gas electron diffraction data give the r_g distances, while molecular rotation spectra give the rotational constants B_0 which may be corrected if the harmonic force field is known to give the rotational constants B_z of the zero-point average structure.⁵

It is the object of this note to show that the relations between these average distances may be conveniently formulated in terms of the L tensor introduced by Hoy, Mills, and Strey.⁶

The L tensor defines the nonlinear transformation from internal to normal coordinates. If r_i denotes an interatomic distance, which may be between either a bonded or a non-bonded atom pair, then

$$r_i = r_{ie} + \Delta r_i \quad (3)$$

where Δr_i is the displacement from the equilibrium distance r_{ie} , and

$$\Delta r_i = \sum_r L_i^r Q_r + \frac{1}{2} \sum_{r,s} L_i^{rs} Q_r Q_s + (1/3!) \sum_{r,s,t} L_i^{rst} Q_r Q_s Q_t + \dots \quad (4)$$

Here L_i^r is an element of the familiar L matrix, $L_i^{rs} = \partial^2 r_i / \partial Q_r \partial Q_s$ is a second derivative L tensor element, and so on. The subscript/superscript notation for the indices is convenient for the higher derivative elements. Equation 4 is exact, but in practice of course the series must be truncated; in general it converges well, each term being smaller than the

preceding term by a factor of about 10 for typical vibrational amplitudes.

Hoy et al. give formulae for L tensor elements up to the third derivative; for interatomic distance coordinates they are particularly simple (eq 22, 23, and 24 in ref 6). Although they describe their formulae as applying to "bond stretching coordinates", they apply equally to either bonded or non-bonded interatomic distances. Of course the complete set of interatomic distances in a polyatomic molecule will generally form a set of *redundant* nonlinear internal coordinates, so that the L matrix for example will be deeper than it is wide; however, the L matrix and the L tensor are still uniquely defined and may be calculated from the same equations.

Consider the average internuclear distance r_g for the i th interatomic pair, which we now denote r_{ig} :

$$r_{ig} = \langle r_i \rangle = r_{ie} + \langle \Delta r_i \rangle$$

Using eq 4 for Δr_i , and noting that $\langle Q_r Q_s \rangle = 0$ if $\omega_r \neq \omega_s$ ⁷

$$r_{ig} = r_{ie} + \sum_r L_i^r \langle Q_r \rangle + \frac{1}{2} \sum_s L_i^{ss} \langle Q_s^2 \rangle + \dots \quad (5)$$

The linear average $\langle Q_r \rangle$ in the second term on the right-hand side of (5) arises from cubic anharmonicity; by perturbation theory we find

$$\begin{aligned} \langle Q_r \rangle &= \sum_s \gamma_r^{-1/2} (-\phi_{rss}/2\omega_r) \langle Q_s^2 \rangle \\ &= \sum_s -(\phi_{rss}/2\gamma_r^{1/2}\omega_r) \left(\nu_s + \frac{1}{2} \right) \end{aligned} \quad (6)$$

in any particular vibrational state, where $\gamma_r = 2\pi c \omega_r / \hbar$, and ϕ_{rss} is a cubic anharmonic force constant in wavenumber units.⁶ The quadratic average $\langle Q_s^2 \rangle$ in the third term of (5) may be evaluated using harmonic wave functions

$$\langle Q_s^2 \rangle = \gamma_s^{-1} \langle q_s^2 \rangle = \gamma_s^{-1} \left(\nu_s + \frac{1}{2} \right) \quad (7)$$

The averages in (6) and (7) apply to a specified vibrational state, but they are easily changed to a Boltzmann thermal average in the usual way, and thus the leading terms in $r_{ig} - r_{ie}$ are readily calculated from the L tensor. In the presence of a strong anharmonic resonance (e.g., Fermi resonance) eq 6 and 7 may be inadequate, and it may be necessary to calculate the averages using wave functions obtained by matrix diagonalization as discussed by Kuchitsu;³ however, eq 5 remains valid.

The order of magnitude of the second and third terms on the right-hand side of (5) is similar. If we write κ for the ratio of a typical vibrational displacement to a typical bond length $\Delta r/r$, and if we also assume $\phi_{rss}/\omega_r \simeq \kappa$ as in Oka's scheme of orders of magnitude for the terms in the rovibrational Hamiltonian,^{8,9} then both the second and third terms in (5) are of

magnitude $\kappa^2 r_e$. This is because $L_i^r/\gamma_r^{1/2}$ is of magnitude κr_e , whereas L_i^{ss}/γ_s is of magnitude $\kappa^2 r_e$, but $\langle q_r \rangle$ is of magnitude κ , whereas $\langle q_s^2 \rangle$ is of magnitude 1. In practice both terms are typically around 0.005 Å. Continuing this reasoning the next two terms in (5) would be of magnitude $\kappa^4 r_e$, perhaps 100 times smaller still, and negligible compared to the precision of present measurements.

Finally we show that the second and third terms in eq 5 correspond exactly to the second and third terms in eq 1. From eq 22 and 23 of Hoy et al.,⁶ and the definition of P_i^r in their eq 20 and 21

$$\sum_r L_i^r Q_r = \sum_r (\partial z_i / \partial Q_r) Q_r = \Delta z_i \quad (8)$$

$$\begin{aligned} \sum_s L_i^{ss} Q_s^2 &= \sum_s [P_i^s \cdot P_i^s - (L_i^s)^2] Q_s^2 \\ &= \sum_s [(\partial x_i / \partial Q_s)^2 + (\partial y_i / \partial Q_s)^2] Q_s^2 \\ &= \Delta x_i^2 + \Delta y_i^2 \end{aligned} \quad (9)$$

where Δx_i , Δy_i , and Δz_i are the local Cartesian difference coordinates defined earlier, linearly related to the normal coordinates. Averaging (8) and (9) over a vibrational state proves the term by term equivalence of (1) and (5).

Similarly it is clear that eq 2 can be written in the form

$$r_{i\alpha} = r_{ie} + \sum_r L_i^r \langle Q_r \rangle \quad (10)$$

giving the correction from r_{ie} to $r_{i\alpha}$ (or to r_{iz} in the ground vibrational state).

The possible advantage of the formulation in eq 5 and 10 over that in eq 1 and 2 is partly in the physical significance of the terms, and partly in convenience of calculation. Equation 5 brings out the fact that the $L_i^r \langle Q_r \rangle$ term arises from the average displacement in the totally symmetric coordinates due to cubic anharmonicity, whereas the $L_i^{ss} \langle Q_s^2 \rangle$ term arises from the nonlinear nature of the transformation from interatomic distances to normal coordinates. It also appears to be a more direct relation between the quantities of interest than eq 1. Finally the calculation of the necessary L tensor elements is simple to program, and provides a convenient method of calculating vibrational averaging effects.

References and Notes

- (1) Research associate with Professor R. C. Lord, 1963–1964.
- (2) Y. Morino, J. Nakamura, and P. W. Moore, *J. Chem. Phys.*, **36**, 1050 (1962).
- (3) K. Kuchitsu, *Bull. Chem. Soc. Jpn.*, **40**, 505 (1967).
- (4) K. Kuchitsu in "Molecular Structures and Vibrations", S. J. Cyvin, Ed., Elsevier, Amsterdam, 1972, Chapter 12.
- (5) Y. Morino, K. Kuchitsu, and T. Oka, *J. Chem. Phys.*, **36**, 1108 (1962).
- (6) A. R. Hoy, I. M. Mills, and G. Strey, *Mol. Phys.*, **24**, 1265 (1972).
- (7) If the index s refers to a degenerate normal coordinate, the sum over s in eq 5 should be carried over each component of the degenerate mode.
- (8) T. Oka, *J. Chem. Phys.*, **47**, 5410 (1967).
- (9) $\kappa = (m/M)^{1/4}$ is the Born–Oppenheimer expansion parameter; in terms of κ , $E_{rot}/E_{vib} \approx E_{vib}/E_{electr} \approx \kappa^2$, and $\Delta r/r \approx \kappa$.

Microwave, Infrared, and Raman Studies of Several Isotopic Species of Vinylidifluoroborane

J. R. Durig,^{*1a} L. W. Hall,^{1b} R. O. Carter, C. J. Wurrey,^{1c} V. F. Kalasinsky,^{1d} and J. D. Odom

Department of Chemistry, University of South Carolina, Columbia, South Carolina 29208 (Received December 15, 1975)

Publication costs assisted by the University of South Carolina

The microwave spectra of $F_2^{11}B^{13}CHCH_2$, $F_2^{11}BCDCH_2$, $F_2^{10}BCDCH_2$, $F_2^{11}B^{13}CDCD_2$, $F_2^{11}BCDCH_2$, $F_2^{11}BCHCHD(2)$, $F_2^{10}BCHCHD(2)$, $F_2^{11}BCDCHD(2)$, and $F_2^{10}BCDCHD(2)$ have been obtained and assigned in the range from 18 to 40 GHz. The 26 independent rotational constants along with the four previously determined ones were used to obtain a least-squares fit of the 13 structural parameters as follows: $r_{C-C} = 1.339 \pm 0.005$, $r_{B-C} = 1.532 \pm 0.003$, $r_{B-F} = 1.331 \pm 0.002$, $r_{B-F} = 1.331 \pm 0.002$, $r_{C_{\alpha}-H} = 1.086 \pm 0.007$, $r_{C_{\beta}-H} = 1.087 \pm 0.006$, $r_{C_{\beta}-H} = 1.087 \pm 0.006$, $\angle HC_{\beta}C_{\alpha} = 122.31 \pm 0.56$, $\angle H'C_{\beta}C_{\alpha} = 119.50 \pm 0.36$, $\angle F'BC = 121.72 \pm 0.48$, $\angle FBF' = 116.04 \pm 0.41$, $\angle CCB = 121.96 \pm 0.25$, and $\angle H_{\alpha}C_{\alpha}C_{\beta} = 117.84 \pm 0.69$. Several of these structural parameters were obtained also by the r_s method and they were found to be within the error limits of those obtained by the least-squares method. The most important parameter is the B–C distance which appears to be normal. The infrared (200–4000 cm^{-1}) of gaseous and solid and Roman spectra (0–4000 cm^{-1}) of gaseous, liquid, and solid F_2BCDCH_2 have been obtained and the spectra interpreted in detail. A normal coordinate calculation has been carried out using 17 diagonal force constants and four interaction constants to fit 36 fundamental frequencies. Slight coupling was found between the B–C and B–F stretching motions.

Introduction

The microwave, infrared, and Raman spectra of $F_2B(C_2H_3)$ have been reported in a previous study carried out in our laboratories.² From this work a partial structure, dipole mo-

ment, and barrier to internal rotation of $F_2B(C_2H_3)$ were obtained. This earlier work was undertaken primarily because of our interest in the question of boron–carbon π bonding in the vinylboranes. The determination of the structure of $F_2B(C_2H_3)$ is of particular interest since our ^{13}C NMR study³

of the vinylboranes found B–C π conjugation to occur to the greatest extent in the monovinylhaloboranes. A more detailed structural determination should provide a means of assessing if there are any dramatic effects due to potential fluorine–boron p_π – p_π back-bonding. To provide such structural information a microwave and vibrational study of various isotopic species of vinyl difluoroborane was completed. The results of this study are presented herein.

Experimental Section

The synthesis of $F_2B(C_2H_3)$ has been previously presented in detail.^{2,4} Three separate syntheses were carried out in order to obtain the deuterated species of vinyl difluoroborane used in this investigation.^{1b}

In each of the three syntheses, the series of reaction steps was the same. Vinyl bromide was prepared by the gas-phase reaction of acetylene and hydrogen bromide. The hydrogen bromide species were purified by passage through a -112°C trap. Vapor pressures of 30 Torr at -112°C were used as a check of purity (lit.⁵ 28 Torr). Reactions of 1:1 mixtures were carried out in 2- or 3-l. gas bulbs with reactants in amounts that would keep the total pressure less than 1 atm. The reactions required uv radiation to proceed at ambient temperatures. The primary product, vinyl bromide, was separated from the dibromoethane species by fractionation through -78 , -112 , and -196°C traps. Vinyl bromide was collected in the -112°C trap and exhibited a vapor pressure of 420 Torr at 0°C (lit.⁵ 424 Torr).

Vinyl bromide was used in the preparation of a Grignard reagent by adding it to a solution of dry THF and powdered magnesium in an inert N_2 atmosphere. Stannic chloride was then added to the reaction flask. After the completion of the reaction, the volatile products were pumped through a -50°C trap. The material that remained in this trap was purified on a low-temperature sublimation column.⁶ The pure tetra-vinyltin was characterized by infrared and mass spectra.

The tetra-vinyltin was then condensed into a reaction flask along with an appropriate amount of BF_3 which had been purified by passage through a -112°C trap. The flask was sealed off and heated to 60°C for 16 h. At the end of this period, the volatile products were pumped off and purified by fractionation on a low-temperature column. Vinyl difluoroborane exhibited a vapor pressure of 562 Torr at -45°C and was characterized by infrared and mass spectra.

In the first synthesis, deuterated acetylene was prepared by the reaction of D_2O and CaC_2 under Ar flow. The mass spectrum of the product indicated that its composition was $\sim 88\%$ C_2D_2 and $\sim 12\%$ C_2DH . After subsequent reactions, the vinyl difluoroborane obtained was found to be $\sim 44\%$ each of the *cis*- and *trans*-vinyl difluoroborane- d_2 species, $\sim 6\%$ of the α - d_1 species, and $\sim 3\%$ of each of the β - d_1 species.

The second synthesis was designed to yield large amounts of the β - d_1 -vinyl difluoroborane. This was accomplished by allowing DBr to react with C_2H_2 to produce β - d_1 vinyl bromide.

Finally, pure $F_2BCD_2CD_2$ was prepared using a sample of C_2D_2 whose isotopic purity was raised from ~ 88 to $\sim 97\%$ by exchange in a $NaOD$ – D_2O solution. The purity of $F_2BCD_2CD_2$ produced from such a sample of C_2D_2 was determined from infrared, Raman, mass, and microwave spectra to be better than 97%.

The microwave spectra were recorded with a Hewlett-Packard 8460A MRR microwave spectrometer, using a Stark modulation frequency of 33.33 kHz. Frequency measurements were made with the Stark cell at room temperature or cooled

with dry ice. Scans to both high and low frequency were made to achieve frequency accuracy to ± 0.02 MHz.

Infrared spectra were recorded from 200 to 4000 cm^{-1} by using a Perkin-Elmer Model 621 spectrophotometer or from 450 to 4000 cm^{-1} by using a Digilab FTS-15B interferometer.⁷ Atmospheric water vapor was removed from the spectrophotometer housings by flushing with dry nitrogen. In the high-frequency region, the instruments were calibrated in the usual manner,^{8,9} whereas the lower frequency region was calibrated with atmospheric water vapor and the assignments of Hall and Dowling.¹⁰ The infrared frequencies are believed to be accurate to $\pm 2\text{ cm}^{-1}$. Cesium iodide plates were used as windows for the gas and cold cell as well as the substrate for the low-temperature experiment with the Perkin-Elmer Model 621 while potassium bromide windows were used in the interferometer.

Raman spectra were recorded on a Cary 82 Raman spectrophotometer equipped with a Coherent Radiation Model 53A argon ion laser. The Raman frequencies are known to $\pm 2\text{ cm}^{-1}$. The spectrum of the gas was recorded using a standard Cary multipass gas cell. The Raman spectra of solid $F_2B(C_2D_3)$ were obtained by using a Harney–Miller¹¹ type cell, cooled with the vapors of boiling liquid nitrogen. Raman spectra of liquid $F_2B(C_2D_3)$ were obtained using sealed glass capillaries. The 5145-Å laser line was used with the power at the sample varied between 0.5 and 2 W depending upon the physical state being examined. Spectra of the gas are shown in Figure 1 with Raman spectra of the liquid and crystalline solid states of $F_2BCD_2CD_2$ shown in Figure 2.

Microwave Spectrum and Assignment

The spectra of the various isotopic species reported were assigned as A-type rotors with R-branch transitions dominating the spectra. B-type Q-branch transitions were found to be very weak and, therefore, undetectable for many of the species of lesser abundance. The moments of inertia reported in our initial report² were adjusted as necessitated by recent improvements in the values of physical constants to give 52.465, 131.745, and 184.243 u \AA^2 in $F_2^{11}BCHCH_2$ and 52.464, 131.593, and 184.094 u \AA^2 in $F_2^{10}BCHCH_2$ or I_A , I_B , and I_C , respectively.

The microwave data for the additional 12 isotopic species are listed in Tables I–III (miniprint material; see paragraph at end of text regarding miniprint material). In addition, the three most intense satellite lines for the $F_2^{11}B^{12}CD^{12}CD_2$ species were also assigned, and these data are given in Table IV (miniprint material). The relative intensities and inertial defects, Δ , were found to be analogous to the corresponding excited state lines of the protonated species. The arguments applied to the assignments of these lines to the respective vibrations is based on the observed inertial defects as given in the earlier work² and will be discussed in a subsequent section.

The observed transitions were, in each case, fit to the rigid rotor model using an iterative least-squares computer program. The moments of inertia were obtained from the rotational constants using the conversion factor $505\,379\text{ MHz amu \AA}^2$. All of the ^{10}B and ^{13}C data were measured from species in natural abundance. Since these weaker species are often obscured by vibrational satellites, measurements were taken on only those lines which were not overlapped by excited state satellites.

Structure

The preparation of mono-, di-, and trideuteriovinyl difluoroborane and the natural abundances of ^{10}B and ^{13}C isotopic

Table I. Transition Frequencies (MHz), Rotational Constants (MHz), Kappa Values (κ), Moments of Inertia (u - Å^2),^a and Inertial Defects [$\Delta = I_C - (I_A + I_B)$] for some Vinylidifluoroborane Species.

Transition	$F_2^{11}B^{13}CH_2C_2$		$F_2^{11}BCD_2$		$F_2^{10}BCD_2$		$F_2^{11}B^{13}CD_2$	
	Obsd	Obsd - calcd	Obsd	Obsd - calcd	Obsd	Obsd - calcd	Obsd	Obsd - calcd
5 ₄₁ - 4 ₄₀	32,971.41	-0.11	—	—	—	—	—	—
5 ₁₅ - 4 ₁₄	—	—	26,829.24	-0.12	—	—	—	—
5 ₂₄ - 4 ₂₃	—	—	29,420.77	0.13	29,458.85	0.10	—	—
5 ₃₃ - 4 ₃₂	33,028.10	0.01	—	—	—	—	—	—
5 ₄₂ - 4 ₄₁	—	—	—	—	—	—	30,022.09	-0.18
5 ₁₄ - 4 ₁₃	—	—	31,485.61	0.15	31,527.73	0.11	31,304.55	0.50
5 ₂₃ - 4 ₂₂	24,634.31	0.09	31,294.95	0.18	—	—	31,222.05	-0.27
5 ₃₂ - 4 ₃₁	—	—	27,705.99	0.08	—	—	—	—
5 ₀₅ - 4 ₀₄	—	—	31,986.87	0.00	32,022.92	0.10	31,787.22	0.02
6 ₁₆ - 5 ₁₅	35,075.47	0.00	32,615.71	-0.06	—	—	—	—
6 ₂₅ - 5 ₂₄	35,722.30	0.05	32,615.71	-0.06	—	—	—	—
6 ₀₆ - 5 ₀₅	38,559.97	-0.02	35,091.71	-0.07	35,136.17	-0.07	34,883.68	0.30
6 ₁₅ - 5 ₁₄	—	—	37,319.16	-0.04	37,336.56	-0.03	37,099.64	-0.46
6 ₂₄ - 5 ₂₃	—	—	38,076.77	-0.02	38,134.72	0.13	37,867.57	0.30
6 ₃₄ - 5 ₃₃	—	—	38,050.38	-0.31	36,100.05	-0.28	35,842.99	-0.19
A	9,541.92 ± 0.07		8,853.74 ± 0.5		8,853.59 ± 0.6		8,791.52 ± 2.8	
B	3,808.86 ± 0.02		3,452.87 ± 0.01		3,458.16 ± 0.02		3,434.21 ± 0.04	
C	2,721.89 ± 0.02		2,484.08 ± 0.01		2,468.74 ± 0.02		2,468.17 ± 0.04	
κ	-0.681240		-0.695811		-0.694783		-0.694453	
I _A	52.964 ± 0.004		57.081 ± 0.003		57.082 ± 0.004		57.485 ± 0.019	
I _B	132.685 ± 0.002		146.365 ± 0.001		146.141 ± 0.001		147.160 ± 0.003	
I _C	185.672 ± 0.002		203.447 ± 0.001		203.230 ± 0.001		204.759 ± 0.003	
Δ	0.023		0.001		0.007		0.114	

^a Moments of inertia were obtained with the conversion factor 505379 MHz $\mu\text{Å}^2$. The errors in the moments of inertia are those implied by the errors in the corresponding rotational constants.

Table III. Transition Frequencies (MHz), Rotational Constants (MHz), Kappa Values (κ), Moments of Inertia (u - Å^2),^a and Inertial Defects [$\Delta = I_C - (I_A + I_B)$] for some Vinylidifluoroborane- d_2 Species.

Transition	$trans-F_2^{11}BCDCH_2^b$		$cis-F_2^{11}BCDCH_2^b$		$trans-F_2^{10}BCDCH_2^b$		$cis-F_2^{10}BCDCH_2^b$	
	Obsd	Obsd - calcd	Obsd	Obsd - calcd	Obsd	Obsd - calcd	Obsd	Obsd - calcd
3 ₁₂ - 2 ₁₁	—	—	—	—	20,425.00	0.19	—	—
4 ₁₄ - 3 ₁₃	—	—	—	—	22,762.85	0.24	—	—
4 ₀₄ - 3 ₀₃	—	—	—	—	23,825.33	-0.15	—	—
4 ₂₃ - 3 ₂₂	—	—	—	—	25,082.00	0.20	—	—
4 ₂₂ - 3 ₂₁	—	—	—	—	26,457.07	0.38	—	—
4 ₁₃ - 3 ₁₂	26,987.53	0.02	—	—	—	—	—	—
5 ₀₅ - 4 ₀₄	26,966.85	-0.19	—	—	—	—	—	—
5 ₁₅ - 4 ₁₄	28,218.88	0.39	27,945.61	0.09	—	—	—	—
5 ₀₄ - 4 ₀₄	29,044.98	0.18	28,802.70	0.12	—	—	—	—
5 ₂₄ - 4 ₂₃	31,126.65	0.06	30,213.22	-0.01	—	—	—	—
5 ₃₃ - 4 ₃₂	31,860.47	-0.10	—	—	31,899.90	-0.09	30,857.23	0.11
5 ₄₂ - 4 ₄₁	32,132.88	-0.06	—	—	32,174.69	0.08	—	—
5 ₁₄ - 4 ₁₃	33,356.46	-0.11	32,736.01	0.03	—	—	32,375.50	0.15
5 ₂₃ - 4 ₂₂	33,938.12	0.13	32,252.10	-0.07	—	—	32,297.40	0.26
5 ₃₂ - 4 ₃₁	—	—	32,829.95	0.07	—	—	—	—
6 ₁₆ - 5 ₁₅	—	—	33,461.61	0.00	—	—	33,513.40	0.10
6 ₂₅ - 5 ₂₄	34,854.33	-0.23	—	—	—	—	37,072.62	-0.23
6 ₃₄ - 5 ₃₃	—	—	—	—	37,123.00	-0.13	—	—
6 ₂₅ - 5 ₂₄	—	—	—	—	39,010.45	-0.37	37,575.58	-0.15
6 ₃₃ - 5 ₃₂	—	—	—	—	—	—	38,367.40	-0.13
7 ₁₅ - 6 ₁₄	33,565.72	0.01	33,336.09	0.01	—	—	—	—
7 ₀₆ - 6 ₀₅	—	—	37,536.06	0.06	—	—	—	—
7 ₀₇ - 6 ₀₆	—	—	38,461.28	-0.05	—	—	—	—
7 ₁₇ - 6 ₀₆	—	—	39,015.56	-0.11	—	—	—	—

Table III. Continued

Transition	$trans-F_2^{11}BCDCH_2^b$		$cis-F_2^{11}BCDCH_2^b$		$trans-F_2^{10}BCDCH_2^b$		$cis-F_2^{10}BCDCH_2^b$	
	Obsd	Obsd - calcd	Obsd	Obsd - calcd	Obsd	Obsd - calcd	Obsd	Obsd - calcd
A	8,880.84 ± 0.09		9,074.90 ± 0.03		8,881.43 ± 1.4		9,074.86 ± 0.07	
B	3,487.47 ± 0.01		3,947.19 ± 0.01		3,492.55 ± 0.06		3,552.14 ± 0.03	
C	2,605.36 ± 0.01		2,501.10 ± 0.01		2,507.79 ± 0.05		2,552.57 ± 0.03	
κ	-0.655132		-0.694369		-0.654185		-0.694990	
I _A	56,907 ± 0.001		55,690 ± 0.001		56,903 ± 0.009		55,690 ± 0.001	
I _B	137,053 ± 0.001		142,473 ± 0.001		136,864 ± 0.003		142,275 ± 0.002	
I _C	193,977 ± 0.001		198,180 ± 0.001		193,796 ± 0.005		197,988 ± 0.003	
Δ	+0.017		+0.017		+0.028		+0.023	

^a See Table I.
^b cis and trans refer to the relative positions of the two ²H atoms with respect to the double bond.

molecules has made it possible to determine substitution coordinates for some of the atoms. The r_s parameters and their errors were calculated by the single-substitution method as outlined by Kraitchman¹² and Costain¹³ and, in certain cases, by the double-substitution method of Krisher and Pierce.¹⁴ The following values have been obtained: $r_{B-C} = 1.533 \pm 0.008$, $r_{C-H} = 1.083 \pm 0.009$, and $\angle HCB = 123.1 \pm 1.5^\circ$. The coordinates of the β protons were also determined, but the data for the β carbon-13 species were questionable and not included in the calculations or tables.

The structural parameters given in Table V have been determined from a least-squares fitting of the experimentally determined moments of inertia. Initially, the r_s coordinates were used as constraints in the calculations. Bonded and nonbonded distances determined from substitution coordinates were held fixed while the least-squares routine varied the remaining parameters in fitting the moments of inertia of the 15 isotopic species. After the structure seemed to have been optimized within these constraints, all the parameters were allowed to vary. The program allows for the moments of

Table II. Transition Frequencies (MHz), Rotational Constants (MHz), Kappa Values (κ), Moments of Inertia (u - Å^2),^a and Inertial Defects [$\Delta = I_C - (I_A + I_B)$] for some Vinylidifluoroborane- d_1 Species.

Transition	$F_2^{11}BCDCH_2$		$cis-F_2^{11}BCDCH_2^b$		$trans-F_2^{11}BCDCH_2^b$		$cis-F_2^{10}BCDCH_2^b$		$trans-F_2^{10}BCDCH_2^b$	
	Obsd	Obsd - calcd	Obsd	Obsd - calcd	Obsd	Obsd - calcd	Obsd	Obsd - calcd	Obsd	Obsd - calcd
4 ₁₄ - 3 ₁₃	23,402.92	0.19	—	—	—	—	—	—	—	—
4 ₁₃ - 3 ₁₂	—	—	27,325.57	0.17	—	—	—	—	—	—
4 ₁₅ - 3 ₁₄	—	—	28,795.61	0.15	28,081.84	0.15	28,423.75	0.21	28,110.23	0.21
5 ₁₅ - 4 ₁₄	29,038.38	0.07	29,876.74	0.08	29,720.84	0.09	29,061.30	0.01	29,447.82	0.02
5 ₂₄ - 4 ₂₃	32,052.87	-0.03	31,608.78	-0.04	—	—	—	—	31,643.69	0.12
5 ₁₄ - 4 ₁₃	34,353.45	0.11	33,836.80	0.02	—	—	—	—	33,875.31	0.18
5 ₂₃ - 4 ₂₂	34,575.67	0.02	33,784.60	0.00	—	—	—	—	—	—
6 ₁₆ - 5 ₁₅	34,585.96	-0.05	34,326.06	0.03	33,500.83	0.05	34,358.91	0.06	33,534.06	0.11
6 ₀₆ - 5 ₀₅	35,139.41	-0.06	34,981.53	-0.07	—	—	—	—	35,125.52	-0.20
6 ₂₅ - 5 ₂₄	38,179.18	-0.18	37,694.18	-0.21	36,608.96	-0.04	37,734.86	-0.06	36,649.66	-0.06
6 ₃₄ - 5 ₃₃	—	—	—	—	37,497.09	-0.29	38,798.74	-0.23	37,542.06	-0.28
6 ₃₃ - 5 ₃₂	—	—	—	—	37,897.15	-0.18	—	—	—	—
6 ₁₅ - 5 ₁₄	—	—	—	—	38,925.69	0.04	—	—	—	—
6 ₂₄ - 5 ₂₃	—	—	—	—	39,445.54	0.32	—	—	—	—
A	9,090.27 ± 0.4		9,425.91 ± 0.5		9,604.38 ± 0.8		9,425.91 ± 0.9		9,603.91 ± 1.1	
B	3,801.38 ± 0.02		3,715.63 ± 0.01		3,576.35 ± 0.02		3,720.44 ± 0.03		3,581.12 ± 0.03	
C	2,680.22 ± 0.01		2,664.78 ± 0.01		2,605.51 ± 0.02		2,667.21 ± 0.02		2,607.96 ± 0.02	
κ	-0.650185		-0.699151		-0.725272		-0.698332		-0.721795	
I _A	55,596 ± 0.003		53,616 ± 0.003		52,620 ± 0.005		53,616 ± 0.005		52,622 ± 0.007	
I _B	132,946 ± 0.001		136,014 ± 0.001		141,311 ± 0.002		135,838 ± 0.002		141,123 ± 0.002	
I _C	188,558 ± 0.001		189,651 ± 0.001		193,955 ± 0.002		189,479 ± 0.002		193,783 ± 0.002	
Δ	+0.016		+0.021		+0.034		+0.025		+0.038	

^a See Table I.
^b cis and trans refer to the relative positions of the ²H and BF₂ group with respect to the double bond.

Table VI. Observed Infrared and Raman Frequencies (cm⁻¹), Calculated Fundamentals (cm⁻¹), and Potential Energy Distribution of Vinylidifluoroborane.^a

Infrared, gas	Infrared, solid	Raman, ^b			Calculated	Assignment and potential energy distribution ^c		
		gas	liquid	solid				
3098 R	—	—	—	—	—	—		
3091 Q	A/B w	2090 w	3089 s	p	3089 m	3107	ν_1 CH ₂ antisym str (100%)	
3083 P	—	—	—	—	—	—	—	
3033 R	—	—	—	—	—	—	—	
3018 P	B w	—	3024 vs	p	3021 vs	3023 vs	3018	ν_2 CH ₂ sym str (93%), C-H str (7%)
3014	—	—	—	—	—	—	—	—
2998 R	A/B w	2991 w	2991 vs	p	2990 s	2992 m	2991	ν_3 C-H str (93%), CH ₂ sym str (7%)
2991 Q	—	—	—	—	—	—	—	—
2984 P	—	—	—	—	—	—	—	—
1632 R	—	—	—	—	—	—	—	—
1624 Q	A s	1618 s	1625 vs	p	1620 vs	1620	1628	ν_4 C=C str (44%), C-B str (31%), C-H in-plane bend (15%)
1615 P	—	—	—	—	—	—	—	—
1457	—	—	—	—	—	—	—	—
1450	—	—	—	—	—	—	—	—
1443	—	—	—	—	—	—	—	—
1431	—	—	-1440 b, sh	dp	1440 sh	p	1445 m	—
1425 Q	vs	1422 vs	1425 m	p	1426 m	1425 m	1429	ν_5 CH ₂ def (89%), C=C str (11%)
1418	—	—	1380 vs	—	—	—	1432	ν_6 10BF ₂ antisym str (48%), CH ₂ def (36%), BF ₂ rock (9%), C=C str (8%)
1382 R	B w	1344 vs	1375	—	—	—	1382	ν_7 11BF ₂ antisym str (53%), C-B str (14%), BF ₂ rock (11%), 11BF ₂ sym str (8%), BF ₂ def (5%), CCB bend (5%), C=C str (4%)
1348 R	A/B s, sh	—	1340 m	p	1332 m	1330 m	1351	10BF ₂ sym str (12%), C=C str (48%), 10BF ₂ str (11%), C-B str (10%), C-B str (13%), BF ₂ def (9%)
1328 Q	—	—	—	—	—	—	—	—
1327 P, R	—	—	—	—	—	—	—	—
1318 Q	A vs	1316 vs	1318 s	p	1317 s	1306 s	1329	11BF ₂ sym str (10%), C=C str (38%), 11BF ₂ antisym str (27%), C-H in-plane bend (13%)
1310 P	—	—						

Table IV. Transition Frequencies (MHz), Rotational Constants (MHz), Kappa Values (κ), Moments of Inertia ($\text{amu}\cdot\text{Å}^2$), and Inertial Defects [$\Delta = I_C - (I_A + I_B)$] for Three Excited Vibrational States of F_2BCDCl_2 .

Transition	$\nu_{18} (\nu = 1)$		$\nu_{17} (\nu = 1)$		$\nu_{13} (\nu = 1)$	
	Obsd	Obsd - calcd	Obsd	Obsd - calcd	Obsd	Obsd - calcd
$\nu_{18} + \nu_{18}$	27,747.36	-0.07	27,733.75	0.12	27,693.59	0.08
$\nu_{24} + \nu_{23}$	—	—	29,425.74	0.04	29,412.74	0.06
$\nu_{23} + \nu_{22}$	31,358.74	-0.20	31,373.65	0.11	31,292.07	0.06
$\nu_{16} + \nu_{15}$	32,053.71	0.20	32,031.45	-0.01	31,970.34	-0.05
$\nu_{16} + \nu_{16}$	32,476.22	-0.29	32,656.05	-0.06	32,599.68	0.03
$\nu_{25} + \nu_{24}$	35,103.69	0.27	35,100.80	-0.05	35,081.54	-0.08
$\nu_{15} + \nu_{14}$	37,296.03	0.09	—	—	37,312.76	-0.02
$\nu_{24} + \nu_{23}$	—	—	38,047.45	-0.08	38,074.02	-0.01
A	$8,778.9 \pm 1.1$	—	$8,803.2 \pm 0.7$	—	$8,859.9 \pm 0.2$	—
B	$3,444.29 \pm 0.03$	—	$3,447.48 \pm 0.02$	—	$3,453.14 \pm 0.01$	—
C	$2,492.62 \pm 0.03$	—	$2,489.74 \pm 0.02$	—	$2,482.38 \pm 0.01$	—
κ	-0.697223	—	-0.698604	—	-0.695568	—
I_A	57.567 ± 0.009	—	57.405 ± 0.004	—	57.0427 ± 0.002	—
I_B	146.730 ± 0.002	—	146.594 ± 0.001	—	146.353 ± 0.001	—
I_C	202.750 ± 0.003	—	202.985 ± 0.002	—	203.586 ± 0.001	—
Δ	-1.55	—	-1.02	—	+0.19	—

^a See Table I.

Table IX. Symmetry Coordinates for Vinylidifluoroborane.

$S_1 = R + P$	Symmetric CH_2 stretch
$S_2 = R - P$	Antisymmetric CH_2 stretch
$S_3 = Q$	C-H stretch
$S_4 = S$	C-H stretch
$S_5 = r$	C-B stretch
$S_6 = p + q$	Symmetric BF_2 stretch
$S_7 = p - q$	Antisymmetric BF_2 stretch
$S_8 = a + b + \gamma = 0$	Redundancy
$S_9 = 2a - b - \gamma$	CH_2 deformation
$S_{10} = b - \gamma$	CH_2 in-plane rock
$S_{11} = \delta + \epsilon + \zeta = 0$	Redundancy
$S_{12} = 2\epsilon - \delta - \zeta$	CDB bend
$S_{13} = \delta - \epsilon$	CH in-plane bend
$S_{14} = \epsilon + \rho + \sigma = 0$	Redundancy
$S_{15} = 2\sigma - \rho - \sigma$	BF_2 deformation
$S_{16} = \epsilon - \rho$	CF_2 in-plane bend (BF_2 rock)
$S_{17} = x$	CH_2 wag
$S_{18} = y$	CF_2 out-of-plane bend (BF_2 wag)
$S_{19} = w$	CH out-of-plane bend
$S_{20} = \tau_1$	CH_2 twist
$S_{21} = \tau_2$	BF_2 torsion

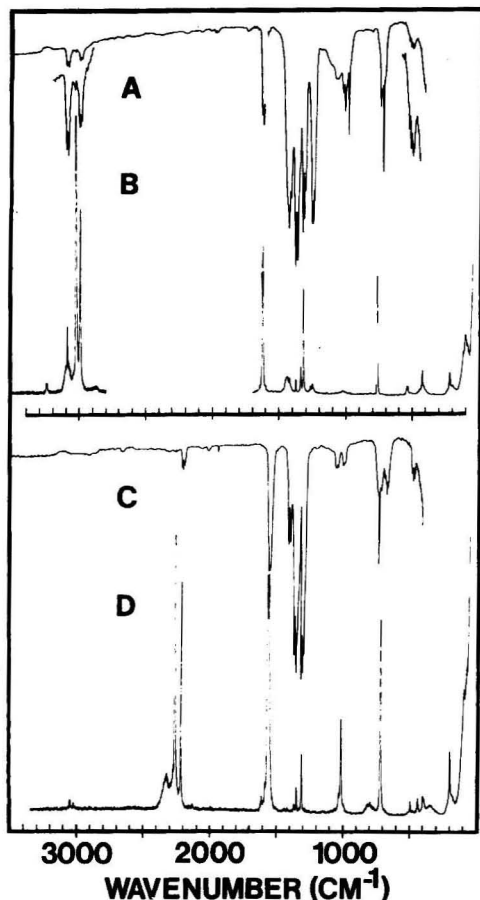


Figure 1. (A) Infrared and (B) Raman spectra of gaseous vinylidifluoroborane and (C) infrared and (D) Raman spectra of gaseous vinylidifluoroborane- d_3 .

Table VII. Observed Infrared and Raman Frequencies (cm^{-1}), Calculated Fundamentals (cm^{-1}), and Potential Energy Distribution of Vinylidifluoroborane- d_3 .

Infrared, gas	Infrared, solid	Raman, gas	Raman, liquid	Raman, solid	Calculated	Assignment and potential energy distribution ^b	
—	—	2323 m p	2322 m dp	2326 s	2324	ν_1 CD_2 antisym str (100%)	
2225 R	—	2261 vs p	2260 vvs p	2261 vs	2240	ν_2 CD_2 sym str (54%), C-D str (39%), C-C str (7%)	
2217 Q A	2220 m	2217 s p	2216 vs p	2219 s	2199	ν_3 C-D str (58%), CD_2 sym str (42%)	
2209 P	—	—	—	—	—	—	
1868 s	—	—	—	1662 w	—	—	
1562 s	1554 s	1566 s p	1560 vs p	1552 vs	1585	ν_4 C-C str (44%), C-B str (37%), C-D in-plane bend (9%), BF_2 def (5%), BF_2 sym str (5%)	
1558 sh s	—	—	—	—	—	—	
—	—	1440 vw p	—	—	—	$2 \times \nu_{10} = 1440$	
1425 R B	1377 s	—	—	—	1422	ν_6 $^{10}\text{BF}_2$ antisym str (79%), BF_2 rock (13%), C-B str (8%)	
1411 P	—	—	—	—	—	—	
1376 R B	vs	1324 vs	1370 sh	—	1323 w	1372	ν_8 $^{11}\text{BF}_2$ antisym str (78%), BF_2 rock (13%), C-B str (9%)
1361 P B	vs	—	—	—	—	—	
1325 Q A/B s,sh	1343 s	1351 w p	1350 w p	1343 w	1317	ν_7 $^{10}\text{BF}_2$ sym str (29%), C-C str (44%), C-B str (15%), BF_2 def (13%), $^{10}\text{BF}_2$ antisym str (10%)	
1323 R	—	—	—	—	—	—	
1315 Q A/B vs	1301 vs	1313 m p	1305 m p	1302 m	1289	ν_7 $^{11}\text{BF}_2$ sym str (21%), C-C str (38%), C-B str (17%), BF_2 def (15%), $^{11}\text{BF}_2$ antisym str (11%)	
1075 w	—	—	—	—	—	—	
1069 Q w	—	—	—	—	—	—	
1064 Q w	1062 s	—	—	1062 w	1073	ν_5 CD_2 def (62%), CD in-plane bend (18%), BF_2 sym str (9%), CD_2 rock (6%), BF_2 def (5%)	
1061 w	—	—	—	—	—	—	
1027 R	1027 sh	—	—	—	—	—	
1015 Q A/B w	1023	1014 m p	1014 s p	1014 s	988	C-D in-plane bend (47%), CD_2 def (27%), CD_2 rock (14%), BF_2 sym str (8%), CCB bend (4%)	
1009 P	1020 sh	—	—	—	—	—	
—	—	—	—	969 vw	—	—	
—	—	813 vw	802 w dp	807 m dp	815 vs	818	ν_{14} CD_2 wag (73%), C-D out-of-plane bend (27%)
—	—	784 w	—	786 w	786	ν_9 CD_2 rock (50%), C-D in-plane bend (50%)	

Table VII. Continued

Infrared, gas	Infrared, solid	Raman, gas	Raman, liquid	Raman, solid	Calculated	Assignment and potential energy distribution ^b	
758 m	—	—	—	—	—	—	
752 sh	—	—	—	—	—	—	
748 Q C s	743 s	—	—	747 w	745	ν_{15} CD_2 twist (87%), CD_2 wag (13%)	
735 m	—	—	—	—	—	—	
—	—	716 w	720 s p	720 vs p	717 s	703	ν_{10} C-B str (19%), BF_2 sym str (51%), CD_2 rock (26%), C-D in-plane bend (4%)
711 Q w	—	—	—	—	—	—	
699 w	—	—	—	—	—	—	
691 Q m	697 s	—	—	~700 vw	—	$\nu_{11} + \nu_{13} = 693$	
684 w	—	—	—	—	—	Impurity	
—	—	566 w	—	—	—	568	C-D out-of-plane (62%), CD_2 twist (29%), CD_2 wag (9%)
503 R	—	—	—	—	—	—	
495 A w	497 s	497 w p	496 w p	493 w	505	ν_{11} BF_2 def (59%), BF_2 sym str (16%), C-B str (15%)	
467 P	—	—	—	—	—	—	
—	—	440 w p	439 vw p	—	—	Impurity	
406 R B	vw	414 m	397 w p	404 w p	412 m	397	ν_{12} BF_2 rock (54%), CCB bend (18%), BF_2 antisym str (11%)
393 P	—	—	—	—	—	—	
—	—	346 w dp	342 w dp	347 m	—	Impurity	
—	—	(Impurity)	—	—	—	—	
—	—	198 m p	199 m p	200 m	198	ν_{13} CCB bend (69%), BF_2 rock (31%)	
—	—	185 vw dp	190 vw dp	—	183	ν_{17} BF_2 wag (100%)	
—	—	—	—	143 w	—	Lattice mode	
—	—	94	—	122 m	94	ν_{18} BF_2 torsion (95%), C-D out-of-plane bend (5%)	
—	—	~8	—	97 w	—	Lattice modes	

^a For abbreviations used, see Table VII.

^b Contributions of less than 4% are not included.

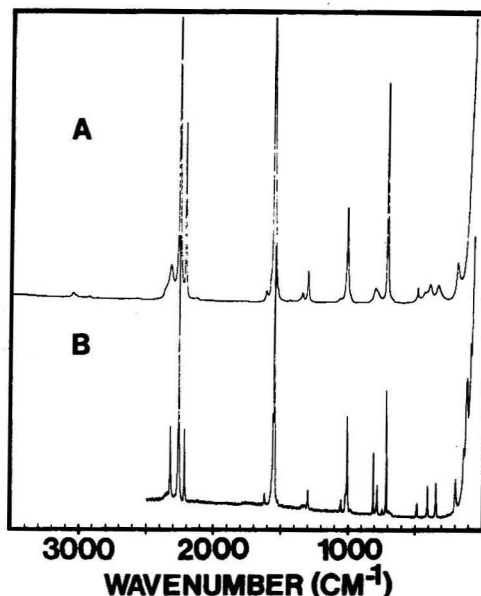


Figure 2. Raman spectra of (A) liquid and (B) solid vinylidifluoroborane- d_3 .

$\text{HC}\equiv\text{CBF}$ (1.513 Å).¹⁷ The CC distance is typical for ethylenic molecules.¹⁸⁻²¹

The B-F distances were allowed to vary independently at first, as were the $\text{C}_\beta\text{-H}$ distances. We found that the least-squares routine would "trade off" the B-F', $\text{C}_\alpha\text{-H}_\alpha$, and $\text{C}_\beta\text{-H}'$

TABLE V: Structural Parameters for Vinylidifluoroborane

r_0 Parameters	
$r_{B-C} = 1.532 \pm 0.003$	$\angle CCB = 121.96 \pm 0.25$
$r_{C=C} = 1.339 \pm 0.005$	$\angle H_\alpha CB^b = 120.20 \pm 0.73$
$r_{C_\alpha-H_\alpha} = 1.086 \pm 0.007$	$\angle H_\alpha C_\alpha C_\beta = 117.84 \pm 0.69$
$r_{C_\beta-H^a} = 1.087 \pm 0.006$	$\angle H^a C_\beta C_\alpha = 119.50 \pm 0.36$
$r_{C_\beta-H} = 1.087 \pm 0.006$	$\angle H^b C_\beta H^b = 118.19 \pm 0.67$
$r_{B-F^a} = 1.331 \pm 0.002$	$\angle HC_\beta C_\alpha = 122.31 \pm 0.56$
$r_{B-F} = 1.331 \pm 0.002$	$\angle F^b BC = 121.72 \pm 0.48$
	$\angle F^a BF = 116.04 \pm 0.41$
	$\angle FBC^b = 122.24 \pm 0.63$
r_s Parameters	
$r_{B-C} = 1.533 \pm 0.008$	$\angle H_\alpha CB = 123.1 \pm 1.9$
$r_{C_\alpha-H_\alpha} = 1.083 \pm 0.009$	

^a H' refers to the proton that is cis to the -BF₂ group. F' refers to the fluorine atom closest to H'. ^b These angles are implied by the values of the two adjacent angles.

distances simply to reach a mathematical minimum. So separate additional calculations were carried out in which (1) the B-F distances were set equal and allowed to vary together and (2) both the B-F distances and C_β-H distances were set equal. The results of this latter calculation comprise Table VI. The former calculation gave results well within the errors of those in Table VI with $r(C_\beta-H') = 1.093 \pm 0.008$ Å and $r(C_\beta-H) = 1.082 \pm 0.008$ Å. It is not possible to tell if the C_β-H distances are actually different. In propylene,¹⁹ the corresponding distances were 1.090 ± 0.003 and 1.081 ± 0.003 Å, respectively, as determined from substitution coordinates. We cannot tell if we are seeing a similar effect because both sets are within experimental error of one another. The B-F distances of 1.331 Å are consistent with those found in HC≡CBF₂ (1.323 Å).¹⁷

Vibrational Assignment

The 18 normal vibrations of vinylidifluoroborane span the representation 13A' + 5A'' of C_s symmetry. The totally symmetric vibrations (A') are all motions within the molecular plane and will give rise to polarized Raman lines and A, B, or A/B hybrid infrared, gas-phase band contours. Depolarized Raman lines and characteristic C-type band contours will result from the nontotally symmetric, out-of-plane A'' vibrations. Assignment of the spectra was made using the Raman depolarization data, infrared gas-phase band contours, and group frequency correlations. Observed frequencies for F₂BCHCH₂ and F₂BCD₂ are listed in Tables VI and VII (miniprint material), respectively. Typical spectra are shown in Figure 1. Spectra of F₂BCHCH₂ have been previously reported² and those frequencies along with the frequencies for F₂BCD₂ have been used in the normal coordinate analysis.

Table VIII summarizes the assignments of the fundamental frequencies of vinylidifluoroborane-*d*₀ and -*d*₃. The three C-D stretching modes can be clearly identified from the Raman spectra. In the gas phase the CD₂ antisymmetric and symmetric stretching frequencies are at 2323 and 2261 cm⁻¹. Even though both are A' motions, the line at higher frequency appears depolarized. The CD stretch is assigned at 2217 cm⁻¹, which is the frequency of the Q branch of an A-type infrared band and a polarized Raman line. The C=C stretching vibration gives rise to a complex infrared band with local maxima at 1568 and 1562 cm⁻¹ while the Raman frequency is 1563 cm⁻¹.

The B-F stretching motions in F₂¹¹BCD₂ are found to be only slightly shifted from their corresponding frequencies

TABLE VIII: Fundamental Vibrational Frequencies (cm⁻¹) of Vinylidifluoroborane and Vinylidifluoroborane-*d*₃

	Approximate description	F ₂ BCH CH ₂	F ₂ BCD CD ₂
A'			
ν_1	CH ₂ (CD ₂) antisymmetric stretch	3091	2323
ν_2	CH ₂ (CD ₂) symmetric stretch	3021	2261
ν_3	CH(CD) stretch	2991	2217
ν_4	C=C stretch	1624	1565
ν_5	CH ₂ (CD ₂) scissors	1425	1068
ν_6	¹⁰ BF ₂ antisymmetric stretch	1425	1418
ν_6	¹¹ BF ₂ antisymmetric stretch	1375	1369
ν_7	¹⁰ BF ₂ symmetric stretch	1338	1352
ν_7	¹¹ BF ₂ symmetric stretch	1318	1315
ν_8	CH(CD) in-plane bend	1250	1015
ν_9	CH ₂ rock	1021	786
ν_{10}	B-C stretch	765	720
ν_{11}	BF ₂ scissors	538	495
ν_{12}	CBF ₂ bend (BF ₂ rock)	427	397
ν_{13}	BCC in-plane bend	215	198
A''			
ν_{14}	CH ₂ (CD ₂) twist	1015	748
ν_{15}	CH ₂ (CD ₂) wag	989	802
ν_{16}	CH(CD) out-of-plane bend	729	566
ν_{17}	CBF ₂ bend (BF ₂ wag)	198	185
ν_{18}	BF ₂ torsion	103	95

in the "light" molecule. The infrared spectra of the gas show very strong absorptions between 1300 and 1430 cm⁻¹. The B-type band whose central minimum occurs at 1369 cm⁻¹ is assigned to the antisymmetric ¹¹BF₂ stretch. The A/B hybrid infrared band having a Q branch at 1315 cm⁻¹ corresponds to a medium intensity Raman line at 1313 cm⁻¹ and is attributed to a symmetric ¹¹BF₂ stretching motion. The ¹⁰B counterparts of these modes are also identifiable. Their respective band types are identical and the antisymmetric and symmetric vibrations occur at 1418 and 1352 cm⁻¹, respectively. Using these data, it is possible to verify the assignment of these modes in F₂BCHCH₂. The antisymmetric and symmetric ¹¹BF₂ stretches have been assigned at 1375 and 1318 cm⁻¹.² The ¹⁰BF₂ symmetric motion has been identified in the Raman and infrared at 1338 cm⁻¹.² The antisymmetric motion for the ¹⁰B isotope must fall in the region of the CH₂ scissors. The scissoring motion is assigned to the medium intensity polarized line at 1425 cm⁻¹ in the Raman spectra. The infrared shows maxima at 1418, 1431, and 1443 cm⁻¹ around the 1425-cm⁻¹ Q branch of the CH₂ scissors. The ¹⁰BF₂ stretch is expected to be a B-type band and could show maxima at 1418 and 1431 or at 1431 and 1443 cm⁻¹. We prefer the former assignment on the basis of the intensities.

The CD₂ scissors in F₂BCD₂ is assigned to a complex A/B hybrid centered at 1068 cm⁻¹. The CD in-plane bend gives rise to the A/B hybrid band in the infrared whose Q branch appears at 1015 cm⁻¹. There is also a corresponding Raman line at 1014 cm⁻¹.

The remaining CH(D) bending mode of A' symmetry is the CH₂(D₂) rock. In the previous study² the CH₂ rock was assigned to a Q branch at 1015 cm⁻¹ that seemed to be part of an A-type band with the R branch at 1027 cm⁻¹. For some time it has been felt that the CH₂ rock in vinyl fluoride (FCHCH₂) was very close in frequency to an out-of-plane motion.^{22,23} Only recently it has been determined, using matrix-isolation techniques, that these two modes are within 8 cm⁻¹ of each other.²⁴ In F₂BCHCH₂, the 1015-cm⁻¹ Q branch

could be a C-type band arising from an out-of-plane mode while the 1027-cm^{-1} band is the R branch of a B-type band whose P branch would be expected around 1013 cm^{-1} . This assignment is supported by the appearance of a polarized line at 1021 cm^{-1} in the Raman spectrum of the gas. In the $-d_3$ compound the only assignment for the CD_2 rock is at 786 cm^{-1} . This appears as a shoulder on the side of the 807-cm^{-1} line in the Raman spectrum of the room-temperature liquid, but, as the liquid is cooled, the line becomes more distinct, and is clearly a separate fundamental in the spectra of the crystalline solid. The alternative assignment for this motion is the A-type band centered at 691 cm^{-1} . This would give a shift factor of 1.48 so we prefer the former assignment.

Skeletal motions comprise the remaining four A' fundamentals for the F_2BCDCD_2 molecule. The B-C stretch is assigned to the strong polarized Raman line at 720 cm^{-1} . The BF_2 scissoring motion gives rise to an A-type infrared band centered at 495 cm^{-1} with a Raman coincidence at 497 cm^{-1} . The CBF_2 in-plane bend (BF_2 rock) and BCC in-plane bend are assigned to polarized Raman lines at 397 and 198 cm^{-1} , respectively.

The A'' vibrations produce dipole changes perpendicular to the molecular plane and give rise to C-type Q branches in the infrared spectra of the gas. In the infrared region investigated there are four apparent C-type bands for F_2BCHCH_2 . These occur at 1015 , 989 , 751 , and 729 cm^{-1} . In F_2BCDCD_2 the only certain C types are at 748 and 711 cm^{-1} . The three motions that must be assigned in this region are the $\text{CH}_2(\text{CD}_2)$ twist, the $\text{CH}_2(\text{CD}_2)$ wag, and the $\text{CH}(\text{CD})$ out-of-plane bend. Potts and Nyquist²⁵ have tabulated group frequencies for CH out-of-plane bending modes. They find that the twisting motion for vinyl compounds occurs in the region $920\text{--}1020\text{ cm}^{-1}$ while the CH_2 wag is between 830 and 970 cm^{-1} . They also find that the wagging motion is stronger in the infrared. The CH out-of-plane bend falls at lower frequencies and depends heavily on the substituent. The designation of the twisting and CH out-of-plane motions as such is for convenience since these motions are heavily mixed.^{23,25,26} For these reasons we assigned the CH_2 twist to the band at 1015 cm^{-1} and the wagging motion to the strong bands at 989 cm^{-1} in the $-d_0$ species. We would like to assign the twisting vibration in F_2BCDCD_2 to the weak depolarized Raman line at 802 cm^{-1} in the gas phase and the CD_2 wag to the strong C-type Q branch in the infrared at 748 cm^{-1} . On the basis of the normal coordinate analysis, however, we will reverse this assignment, although there is substantial mixing of the modes. The $\text{CH}(\text{CD})$ out-of-plane modes fall at 729 and 566 cm^{-1} in the infrared spectra, respectively, and show the expected shift.

The remaining vibrations are the CBF_2 out-of-plane bend (BF_2 wag) and the BF_2 torsion. These are assigned in F_2BCDCD_2 by analogy to the "light" compound and occur at 185 and 94 cm^{-1} , respectively. The intensities of microwave satellites aid in these assignments as well as with the assignment of the ν_{13} fundamental. The inertial defects associated with these three excited states (Table IV) indicate that they arise from two out-of-plane motions and an in-plane motion. The intensities predict vibrational frequencies of 85 ± 20 , 196 ± 20 , and $193 \pm 20\text{ cm}^{-1}$ for ν_{18} , ν_{17} , and ν_{13} , respectively.

The barrier to internal rotation about the C-B bond was calculated as has been previously described.^{27,28} We find a value for the twofold barrier to internal rotation of $1546.5 \pm 81.6\text{ cm}^{-1}$ (4.42 kcal/mol) using F values represented by $F(\alpha) = F_0 + \sum_{n=1}^6 F_n \cos n\alpha$, where $F_0 = 1.7273$, $F_1 = -0.01119$, and $F_2 = 0.1388$ for the $-d_0$ species and $F_0 = 1.3160$, $F_1 = -0.00781$, and $F_2 = 0.07077$ for the $-d_3$ species.

The assignments outlined above are supported by the results of Teller-Redlich product rule calculations. The theoretical τ values for the A' and A'' blocks are 7.305 and 2.520, respectively, while the observed ratios are 7.213 and 2.501. The results are good and the errors are within the limits set by the experimental accuracy of the frequencies.

Normal Coordinate Analysis

The normal coordinate calculations were carried out using the programs of Schachtschneider²⁹ which employ the standard Wilson FG matrix method.³⁰ The 21 internal coordinates consisting of the bond lengths, bond angles, out-of-plane wags, and torsions shown in Figure 3 were used as a basis for the vibrational analysis. For the purposes of minimizing the number of force constants and simplifying the force field, local C_{2v} symmetry was assumed about both the $=\text{CH}_2$ and $-\text{BF}_2$ groups. The symmetry coordinates used are listed in Table IX (miniprint material). A preliminary normal coordinate calculation using the 21 diagonal force constants implied by the internal coordinates showed mixing of modes to be quite strong in both symmetry blocks; thus, a simpler force field was sought to accommodate the possibility of using more interaction force constants and fewer diagonal force constants. It can be seen that the number of force constants used in the force field exceeds $3N - 6$, but in view of the isotopic data we obtained, not only for deuterium but also boron substitution, we feel justified in using this number of force constants.

The frequencies calculated by using the force constants given in Table X agree with the experimental ones to an average of 8.4 cm^{-1} (1.0%). For the out-of-plane vinyl vibrations, the force constants are very similar to those for $\text{C}_2\text{H}_3\text{Br}$.²⁶ Additionally K_Q has a value characteristic for carbon-carbon double bonds. The potential energy distributions given in Tables VI and VII show considerable mixing. The C=C stretch is mixed with the C-H bending modes, as well as the C-B stretch, in the A' block. Additionally, we find that the C-B and B-F stretching motions are mixed to the extent that it is difficult to identify them as separate modes. The out-of-plane motions show the expected mixing of the CH_2 twist, wag, and the CH out-of-plane bend.^{23,26}

In view of the low molecular symmetry, we feel that the force constants obtained are reasonable and the PED is valid for describing the molecular vibrations in a quantitative fashion.

Discussion

The interest in assessing the π character of B-C (ethylenic) bonds has prompted our more thorough investigation of vinyl difluoroborane. The recent ^{13}C NMR study³ of the C_β shifts indicated more delocalization of the double bonds in the monovinylhaloboranes than in the divinylhaloboranes. Variations in bond lengths might be expected to parallel the trends in the chemical shifts. Our microwave data indicate that the C=C bond length of $1.339 \pm 0.005\text{ \AA}$ in vinyl difluoroborane is within experimental error of the corresponding distance in vinyl fluoride ($1.329 \pm 0.006\text{ \AA}$),¹⁸ propylene ($1.336 \pm 0.004\text{ \AA}$),¹⁹ vinyl chloride ($1.332 \pm 0.002\text{ \AA}$),²⁰ and acrylonitrile ($1.338 \pm 0.009\text{ \AA}$).²¹ This consistency of bond lengths may extend to vinylsilane and vinylgermane, as well, in which these values are 1.347 ± 0.003 ³¹ and $1.347 \pm 0.015\text{ \AA}$,³² respectively. We may conclude that the C=C distances in vinyl compounds are insensitive to substituents. Thus, it is not surprising that evidence for delocalization cannot be found in this structural parameter. In acrylonitrile ($\text{H}_2\text{C}=\text{CH}-\text{CN}$), for instance, the C-C bond ($1.425 \pm 0.006\text{ \AA}$) is shorter than

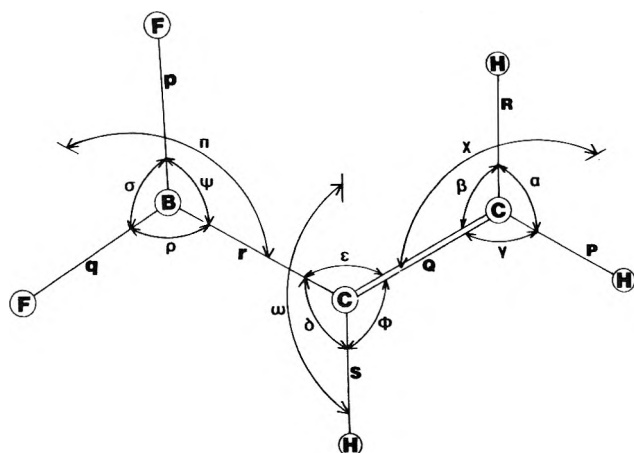


Figure 3. Internal coordinate definitions for vinyldifluoroborane. The CH_2 twist, τ_1 , and BF_2 torsion, τ_2 , are not shown.

TABLE X: Internal Force Constants for Vinyldifluoroborane

Force constant	Group	Value, $\text{mdyn}/\text{\AA}^a$
K_R	CH_2 stretch	5.10 ± 0.01
K_Q	$\text{C}=\text{C}$ stretch	8.25 ± 0.04
K_S	CH stretch	4.86 ± 0.01
K_T	CB stretch	5.59 ± 0.05
K_{PQ}	BF_2 stretch	5.20 ± 0.02
H_α	$\angle\text{HCH}$ bend	0.426 ± 0.003
$K_{\beta\gamma}$	$\angle\text{HCC}$ bend of CH_2	0.555 ± 0.003
H_δ	$\angle\text{HCB}$ bend	0.311 ± 0.007
H_ϵ	$\angle\text{CCB}$ bend	0.484 ± 0.018
H_ϕ	$\angle\text{HCC}$ bend of CH	0.658 ± 0.006
$H_{\psi\rho}$	$\angle\text{FBC}$ bend	0.753 ± 0.012
H_σ	$\angle\text{FBF}$ bend	1.64 ± 0.03
H_x	CH_2 out-of-plane bend	0.287 ± 0.003
H_π	BF_2 out-of-plane bend	0.055 ± 0.002
H_ω	CH out-of-plane bend	0.302 ± 0.004
H_{τ_1}	CH_2 twist	0.211 ± 0.002
H_{τ_2}	BF_2 torsion	0.016 ± 0.002
F_{TP}	CB stretch/ BF stretch	0.861 ± 0.024
$F_{Q\alpha}$	$\text{C}=\text{C}$ stretch/ HCH bend	-0.595 ± 0.014
$F_{S\delta}$	$\text{C}=\text{C}$ stretch/ CH bend	0.344 ± 0.020
$F_{\omega\tau_1}$	CH out-of-plane/ CH_2 twist	-0.131 ± 0.003

^a All bending coordinates weighted by 1 \AA .

a "normal" single bond (1.526 \AA), while the multiple bonds are unaffected.

It is equally difficult to evaluate the implications of the $\text{C}-\text{B}$ distance. The length of the $\text{C}-\text{B}$ bond in vinyldifluoroborane is bracketed by the corresponding distances in CH_3BF_2 ^{15,16} and HCCBF_2 .¹⁷ As pointed out by Lafferty and Ritter¹⁷ this may be a consequence of the hybridization around the carbon atom. The amount of s character of the $\text{C}-\text{B}$ bond increases as one follows the series CH_3BF_2 , F_2BCHCH_2 , and HCCBF_2 , with sp^3 , sp^2 , and sp hybridization, respectively, of the carbon. Multiple-bond character would be expected to compliment this effect and is difficult to assess for this reason.

The lengths of the $\text{B}-\text{F}$ bonds may be an indication of some delocalization of the ethylenic double bond. In vinyldifluo-

borane, this distance ($1.331 \pm 0.002 \text{\AA}$) is the longest yet reported for a tricoordinated boron atom. In HBF_2 , HCCBF_2 , and BF_2OH these distances are 1.311 ± 0.005 ,³³ 1.323 ± 0.005 ,¹⁷ and $1.32 \pm 0.02 \text{\AA}$,³⁴ respectively. Back donation of π -electron density from fluorine to boron presumably gives rise to the short bond in HBF_2 . In F_2BCHCH_2 a π donation from the vinyl group can be thought of as competition for the effects of fluorine donation. If this were the case, the $\text{B}-\text{F}$ distances would be expected to lengthen slightly. For tetrahedrally coordinated boron atoms, $\text{B}-\text{F}$ distances are longer (H_3PBF_3 , $r_{\text{B-F}} = 1.372 \text{\AA}$).³⁵

In our structural calculation we constrained the $\text{B}-\text{F}$ bonds by requiring them to be equal. It still seems clear that the differences between these lengths in the above series are real. The immense amount of data required to determine $\text{B}-\text{F}$ distances may limit its usefulness as an indicator of the amount of delocalization of the vinylic π electrons.

The vinyl force constants derived for vinyldifluoroborane (Table X) are not strikingly different from those in other substituted ethylenes. The $\text{C}=\text{C}$ stretching force constants is smaller than the currently accepted value in ethylene ($9.147 \text{mdyn}/\text{\AA}$),³⁶ while the CH_2 stretching constants are essentially the same. The force constants for the CH out-of-plane motions are in the same ranges as those in vinyl fluoride,²³ vinyl bromide,²⁶ and ethylene.²⁶ However, the twisting force constant in vinyldifluoroborane is somewhat smaller than in these other compounds. There also seems to be more mixing among the three vinyl out-of-plane modes in this case than in the other molecules, and we find that the amplitudes of vibration are also larger. Again, it is difficult to say whether these features are indicative of delocalization of the $\text{C}=\text{C}$ bond.

As pointed out in the earlier work,² the barrier to internal rotation about the $\text{C}-\text{B}$ bond is typical for twofold barriers and provides little information about the π character of this bond. The revised value of 4.42 kcal/mol for this barrier is slightly higher, but within experimental error of the previous value of 4.17 kcal/mol.² The difference between the barriers calculated from the data for F_2BCHCH_2 and F_2BCDCl_2 must arise from the mixing of the torsion with other normal modes. Excellent consistency is generally found for barriers in "light" and "heavy" molecules when the torsional modes are "pure". The errors in measuring the torsional frequencies in vinyldifluoroborane may be as large as 3cm^{-1} because the upper level "hot-band" transitions are separated by less than 1cm^{-1} . Since a number of excited vibrational states are expected to be populated at room temperature for a vibration of such low frequency, these "hot bands" can cause the maximum to be displaced from the fundamental frequency.

The spectra of the crystalline solid show some interesting features. The number of lattice modes in F_2BCHCH_2 indicates that there are at least two molecules per unit cell. It is not reasonable to assign these lattice modes specifically to librations and translations since the differences between the isotopic shift factors are less than those implied by the $\pm 2\text{-cm}^{-1}$ error of the frequencies. It is interesting to note the seemingly anomalous shifts upon condensation of the BF_2 torsional and antisymmetric stretching modes. The torsion shifts more than 30% in each case to higher frequency. Ordinarily shifts of 10% are noted for methyl rotors,³⁷ but we can expect a more pronounced effect for a planar molecule because of crystal packing considerations. The antisymmetric BF_2 stretches shift by $\sim 45 \text{cm}^{-1}$ while the symmetric modes only shift $\sim 12 \text{cm}^{-1}$. Again, this must be a consequence of the crystal packing and the nature of the motion involved.

We can conclude by summarizing our results. It is not

possible to state unequivocally whether there is delocalization of the π electrons of the C=C bond. There are subtle indications that this might indeed be the case, but the "classical" indicators do not imply this. The C=C bond is of "normal" length, but the B-F distance may be somewhat longer than expected. There are no values with which to compare r_{C-B} to assess that bond's π character. The normal coordinate calculations may indicate some delocalization, but the complex mixing of the normal vibrations makes this difficult to assess as well. This study neither contradicts nor confirms the conclusions drawn from the NMR data.³ It is possible that NMR is a more sensitive technique for drawing these conclusions. It may be necessary to revise the classical theories concerning delocalization and structure.

Acknowledgment. The authors gratefully acknowledge the financial support of this work by the National Science Foundation by Grant No. MPS74-12241-A0.

Miniprint Material Available: Full-sized photocopies of Tables I-IV, VI, VII, and IX (10 pages). Ordering information is available on any current masthead page.

References and Notes

- (1) (a) J. R. Durig received his Ph.D. from M.I.T. under the direction of Professor Lord in 1962. (b) Taken in part from the thesis of L. W. Hall which was submitted to the Department of Chemistry in partial fulfillment of the Ph.D. degree, May, 1975. (c) C. J. Wurrey received his Ph.D. from M.I.T. under the direction of Professor Lord in 1973. (d) V. F. Kalasinsky received his S.B. degree from M.I.T. under the direction of Professor Lord in 1972.
- (2) J. R. Durig, R. O. Carter, and J. D. Odom, *Inorg. Chem.*, **13**, 701 (1974).
- (3) L. W. Hall, J. D. Odom, and P. D. Ellis, *J. Am. Chem. Soc.*, **97**, 4527 (1975).
- (4) F. E. Brinckman and F. G. A. Stone, *J. Am. Chem. Soc.*, **82**, 6218 (1960).
- (5) D. F. Shriver, "The Manipulation of Air-Sensitive Compounds", McGraw-Hill, New York, N.Y., 1969.
- (6) J. Dobson and R. Schaefer, *Inorg. Chem.*, **9**, 2183 (1970).
- (7) This instrument was purchased with funds from a National Science Foundation Grant No. MPS-75-06296.
- (8) IUPAC, "Tables of Wavenumbers for the Calibration of Infrared Spectrometers", Butterworths, Washington, D.C., 1961.
- (9) R. N. Jones and A. Nadeau, *Spectrochim. Acta*, **20**, 1175 (1964).
- (10) R. T. Hall and J. M. Dowling, *J. Chem. Phys.*, **47**, 2454 (1967); **52**, 1161 (1970).
- (11) F. A. Miller and B. M. Harney, *Appl. Spectrosc.*, **24**, 291 (1970).
- (12) J. Kraitchman, *Am. J. Phys.*, **21**, 17 (1953).
- (13) C. C. Costain, *J. Chem. Phys.*, **29**, 864 (1958).
- (14) L. C. Krisher and L. Pierce, *J. Chem. Phys.*, **32**, 1619 (1960).
- (15) R. E. Naylor, Jr., and E. B. Wilson, Jr., *J. Chem. Phys.*, **26**, 1057 (1957).
- (16) S. H. Bauer and J. M. Hastings, *J. Am. Chem. Soc.*, **64**, 2686 (1942).
- (17) W. J. Lafferty and J. J. Ritter, *J. Mol. Spectrosc.*, **38**, 181 (1971).
- (18) B. Bak, D. Christensen, L. Hansen-Nygaard, and J. Rastrup-Anderson, *Spectrochim. Acta*, **13**, 120 (1958); D. R. Lide, Jr., and D. Christensen, *Spectrochim. Acta*, **17**, 665 (1961).
- (19) D. R. Lide, Jr., and D. E. Mann, *J. Chem. Phys.*, **27**, 868 (1957); D. R. Lide, Jr., and D. Christensen, *J. Chem. Phys.*, **35**, 1374 (1961).
- (20) D. Kivelson, D. B. Wilson, Jr., and D. R. Lide, Jr., *J. Chem. Phys.*, **32**, 205 (1960).
- (21) C. C. Costain and B. P. Stoicheff, *J. Chem. Phys.*, **30**, 777 (1959).
- (22) B. Bak and D. Christensen, *Spectrochim. Acta*, **12**, 355 (1958).
- (23) J. R. Scherer and W. J. Potts, *J. Chem. Phys.*, **31**, 1691 (1959).
- (24) G. R. Smith and W. A. Guillory, *J. Chem. Phys.*, **63**, 1311 (1975).
- (25) W. J. Potts and R. A. Nyquist, *Spectrochim. Acta*, **15**, 679 (1959).
- (26) J. R. Scherer and W. J. Potts, *J. Chem. Phys.*, **30**, 1527 (1959).
- (27) J. R. Durig, W. E. Bucy, C. J. Wurrey, and L. A. Carreira, *J. Phys. Chem.*, **79**, 988 (1975).
- (28) L. A. Carreira, *J. Chem. Phys.*, **62**, 3851 (1975).
- (29) J. H. Schachtschneider, Technical Report No. 231-64 and 57-65, Shell Development Company, Emeryville, Calif.
- (30) E. B. Wilson, J. C. Decius, and P. C. Cross, "Molecular Vibrations", McGraw-Hill, New York, N.Y., 1955.
- (31) J. M. O'Reilly and L. Pierce, *J. Chem. Phys.*, **34**, 1176 (1961).
- (32) J. R. Durig, K. L. Kizer, and Y. S. Li, *J. Am. Chem. Soc.*, **96**, 7400 (1974).
- (33) T. Kasuya, W. J. Lafferty, and D. R. Lide, Jr., *J. Chem. Phys.*, **48**, 1 (1968).
- (34) H. Takeo and R. F. Curl, *J. Chem. Phys.*, **56**, 4314 (1972).
- (35) J. D. Odom, V. F. Kalasinsky, and J. R. Durig, *Inorg. Chem.*, **14**, 2837 (1975).
- (36) D. C. McKean and J. L. Duncan, *Spectrochim. Acta, Sect. A*, **27**, 1879 (1971).
- (37) J. R. Durig, S. M. Craven, and W. C. Harris in "Vibrational Spectra and Structure", Vol. 1, J. R. Durig, Ed., Marcel Dekker, New York, N.Y., 1972.

Infrared Spectral Behavior of Fine Particulate Solids

Graham R. Hunt¹

U.S. Geological Survey, Denver, Colorado 80225 (Received January 12, 1976)

Publication costs assisted by the U.S. Geological Survey

Transmission and emission spectra of clouds and layers of fine particulate samples of quartz, magnesium oxide, and aluminum oxide in the 6.5–35- μ m wavelength range are presented. They demonstrate that the behavior of layers of particles constitutes a good analogue for a cloud of particles; that individual micrometer-sized particles emit most where they absorb most; that as the size of the particle is increased, the emission features reverse polarity and the spectrum approaches that of one obtained from a polished plate; and that as the particle layer-thickness increases, radiative interaction becomes increasingly important so that the emission maximum shifts from the strongest to weaker features, or produces a maximum at the Christiansen wavelength.

Introduction

The appearance of the spectrum of a cloud, or layers of micrometer-sized particles, cannot be simply related to the optical constants of the bulk material in the same way as can that of a polished plate of the substance. In addition to the

absorption and refractive indices, other parameters, such as particle size and shape, size distribution, particle density, cloud or layer thickness, and the thermal distribution throughout the sample all have an effect on the appearance of the spectrum.

Much of the laboratory work performed to explain the emission properties of finely particulate solids has been directed at evaluating the usefulness of infrared emission spectroscopy for compositional remote sensing of surface layers, particularly of the moon and planets,²⁻⁸ and several attempts have been made to explain theoretically the observed behavior.⁷⁻¹⁶

In an earlier paper, Hunt and Logan¹⁴ experimentally investigated the emission properties of individual micrometer-sized silicate particles, and explained the results in terms of Mie absorption efficiency factors, an explanation based largely on Conel's theoretical treatment of quartz particles.¹³ Detailed treatments of the Mie theory are available in a number of works.^{17,18}

In the Hunt and Logan paper,¹⁴ laboratory results obtained using a balloon-flight instrument were described. The instrument contained a circular variable wedge filter which restricted the wavelength coverage to the 6-11.8- μm range, and because all the materials investigated were silicates, only the extremely intense features due to the silicon-oxygen stretching fundamentals were investigated.

The purpose of this report is to extend the wavelength range investigated to 35 μm , and include materials other than silicates to demonstrate the general nature of the spectral behavior of particulate solids. The analogical behavior between a cloud and layers of particles is demonstrated in transmission. The need to understand this behavior is particularly relevant to studies of the spectral properties of clouds of fine particles, such as those present in the terrestrial (e.g., aerosol layer, solid pollutants, dust, and ice clouds) and planetary (e.g., the dust clouds on Mars) atmospheres, and of interstellar dust.

Experimental Section

Spectra were recorded using a Digilab Model FTS-14 interferometer spectrometer fitted with a coated germanium beam splitter designed to cover the range from 5 to 35 μm . Both transmission and emission spectra were recorded.

(a) *Transmission.* Spectra were recorded from samples prepared in several ways:

(1) A fine cloud of particles entrained in the nitrogen gas flow from a fluid energy mill¹⁹ was directed into a flow-through cell, equipped with KRS-5 windows 3 in. (8 cm) apart, located in the sample beam, and interferograms were recorded every second. These were coadded until a satisfactory signal-to-noise ratio was achieved, a period of less than 20 s.

(2) A layer of particles was deposited on the surface of a KRS-5 plate which was then placed in the normal transmission sample position. The particles were deposited either directly from the fluid energy mill or from an elutriation column that the particles had traversed, or, in the case of magnesium oxide, by collecting the smoke from burning magnesium wire.

(3) A layer of particles was deposited on a plane mirror (as described for the KRS-5 plate above), and then substituted for one of the plane mirrors in the optical path of the FTS-14, or it was placed in the conventional sample position of a microreflectance attachment.

(b) *Emission.* Spectra were recorded from samples deposited from an elutriation column or a fluid energy mill onto polished brass plates. These plates have a nearly flat spectral response and a reflectivity only a few percent less than that of gold coated glass mirrors through the 5- to 35- μm range, but, they have much better thermal conductivity. The brass plates were heated to approximately 100 °C using a stainless steel Hotwatt can heater, and the temperature of the plate was measured with a thermocouple embedded in the plate. Re-

flected energy from the ambient temperature surroundings was measured for each sample before the heating process commenced and was found to be sufficiently small to be ignored. The emission curves shown here represent the difference in emission between the recorded energy from the brass plate and sample, and from the brass plate alone, and have not been corrected for transmission of the plate emission through the sample. Because the plates are better than 95% reflecting, this is a minor effect.

Results and Discussion

The infrared emission from a cloud or layers of micrometer-sized particles is a complex function of emission, absorption, and scattering. The most important parameter for describing the emission from such systems is the spectral distribution of the energy emitted by the individual particles, because this is the "source function" that entirely defines how radiant energy is initially injected into the system. Also, the absorption and scattering properties determine how the "source function" energy is modified before it leaves the system.

In Figures 1, 3, and 4, transmission spectra are displayed at the top and emission spectra at the bottom to facilitate comparisons.

(a) *Transmission.* The curve at the top of Figure 1 is the transmission spectrum of a laboratory generated, very low density cloud of less than 5- μm diameter quartz particles dispersed in dry nitrogen. Immediately below is the transmission spectrum of a very thin layer (which contains approximately the same number of particles per unit beam area as the cloud) of particles deposited on a KRS-5 plate. It is evident that these two spectra are essentially identical, the only obvious discrepancy is a sharp feature near 15 μm which is due to atmospheric CO₂. The imbalance between the sample and reference beams is opposite for these two experimental procedures, and thus the direction of the peak is reversed in one spectrum relative to the other.

The same correspondence between particle cloud and deposited particle sample occurs for magnesium oxide and aluminum oxide, therefore only the spectrum of the sample deposited on the KRS-5 plate is included for magnesium oxide in Figure 3 and aluminum oxide in Figure 4.

The effect on the transmission spectrum of progressively increasing the thickness of a sample on the KRS-5 plate is illustrated in Figure 2. The spectra are numbered 1 through 10 in increasing order of thickness of layers of micrometer-sized magnesium oxide particles. The most intense features occur near 17.4 and 25 μm , with the 17.4- μm band displaying a strong shoulder near 15 μm . Features more than an order of magnitude weaker become apparent near 11.8 and 10.2 μm as the layer thickness is increased, and even weaker bands appear near 8.3 and 7.1 μm . The origin of these infrared active features has been discussed by several authors.^{20,21}

The steady decrease in intensity at wavelengths shorter than 9 μm , which becomes apparent with increasing layer thickness, is due to increased scattering out of the beam, and this, together with the genuine absorption at longer wavelengths produces a transmission maximum, the so-called Christiansen peak, at 9 μm .

(b) *Emission.* The emission spectrum of an approximate monolayer of micrometer-sized quartz particles is shown at the bottom of Figure 1. It is obvious that this emission spectrum is essentially the intensity inverse of the transmission spectra, and it is also apparent that micrometer-sized particles

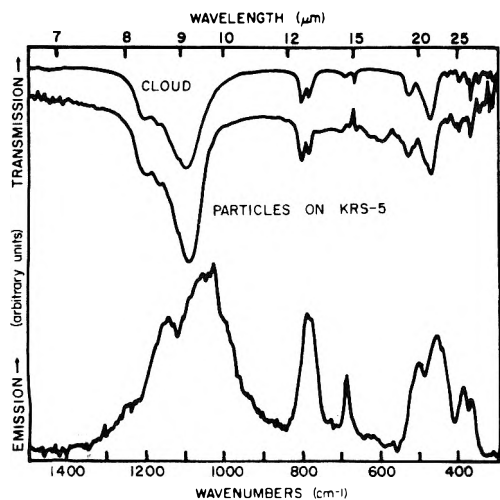


Figure 1. Transmission spectra of a low density cloud (upper curve), a monolayer on a KRS-5 plate (middle curve), and the emission spectrum on a brass plate (lower curve) of micrometer-sized particles of quartz.

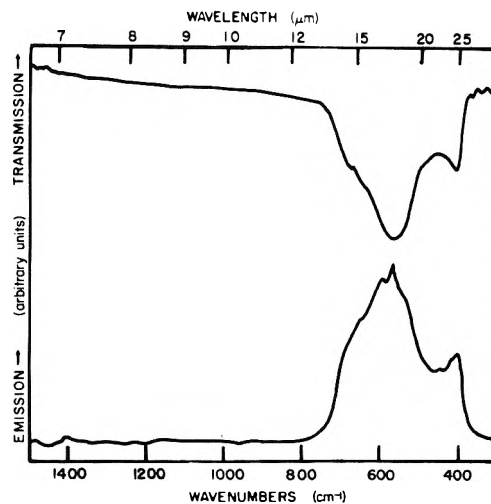


Figure 3. Transmission (upper curve) and emission (lower curve) spectra of micrometer-sized magnesium oxide particles.

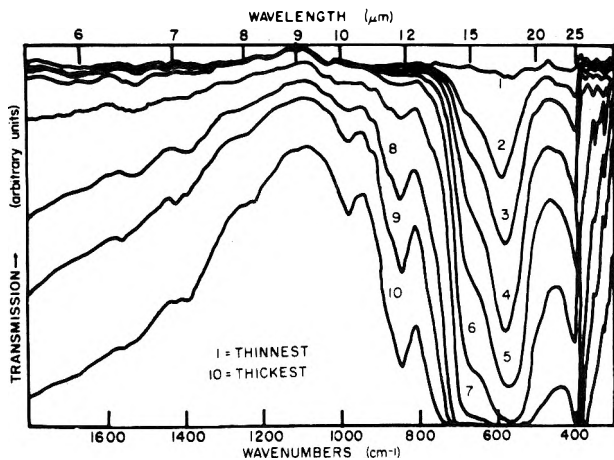


Figure 2. The effect of sample thickness on the transmission spectrum of micrometer-sized magnesium oxide particles.

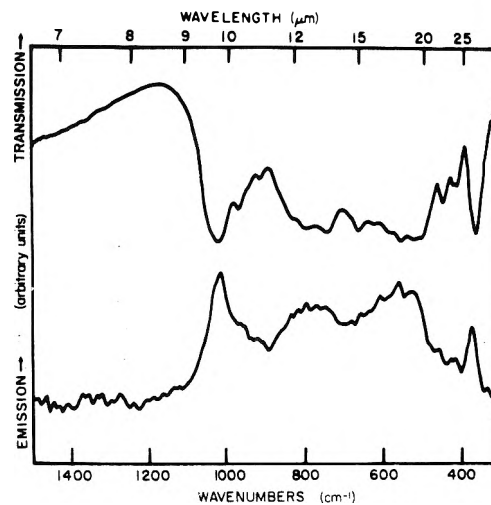


Figure 4. Transmission (upper curve) and emission (lower curve) spectra of micrometer-sized aluminum oxide particles.

emit most where they absorb most, and that this is true throughout the entire wavelength range shown.

The relative intensities of the features in the transmission spectra are retained by the bands in the emission spectrum at wavelengths greater than 10 μm. The major feature near 9 μm appears relatively less intense, but this is because the sample used for emission is located on a mirror surface, and therefore the layer acts as if it is twice as thick as it actually is; consequently there has been some obvious reabsorption of the intense 9-μm feature, which causes the emission spectrum to appear to be slightly displaced to longer wavelengths.

Emission spectra of magnesium oxide and aluminum oxide are shown at the bottom of Figures 3 and 4, and the same inversion relationship between the transmission and emission spectra as was evident for quartz is apparent here.

The spectral emission effects of gross variations in particle-size range²² is illustrated in Figure 5 for quartz particles. These spectra, displaced vertically for clarity, are arranged in order of increasing size from the bottom up, and the particle-size range is indicated on the curves. These spectra were recorded from a monolayer of particles deposited on a heated brass plate.

The smallest particle-size sample (less than 5 μm) displays an emission spectrum which is the inverse of the transmission spectra, as shown in Figure 1. The spectrum of the largest particle-size sample (250–1200 μm) is similar in form to that obtained from an optically thick polished plate of the sample material, where the emission, E_λ , may be simply expressed as $E_\lambda = E_{BB,\lambda}(1 - R_\lambda)$, where $E_{BB,\lambda}$ is the emission from a black body at the same temperature as the sample, and R_λ is the sample reflectivity.

The spectrum of the 74–250-μm particle-size sample is very similar to that of the larger particle size, indicating that these particles are large enough to be optically thick over this wavelength range. The spectrum of the less than 53-μm particle-size sample is a combination of the spectra of the smallest and largest particle spectra. Alone, it would not be recognizable as a quartz spectrum, because all the features normally associated with a quartz spectrum are not obvious. The limiting particle size at which a single particle emission spectrum becomes the inverse of the transmission spectrum has not been determined with the size-sorting techniques available, because the task requires the capability of isolating narrow-size ranges between 1 and 10 μm.

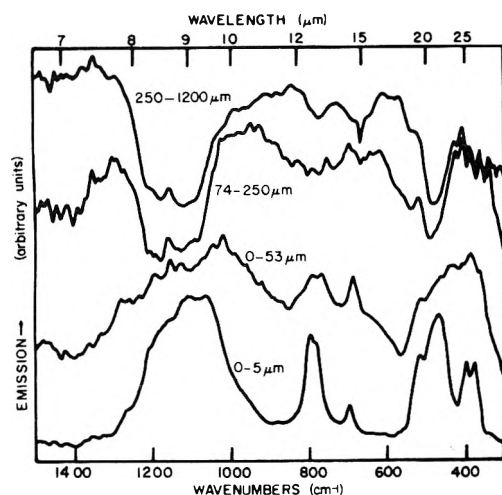


Figure 5. The effect of particle size on the emission spectrum of quartz. The particle size range of the samples used is indicated on the curves.

The effect of sample thickness was investigated using micrometer-sized magnesium oxide particles, and the spectra of increasingly thick samples are shown in Figure 6. The thinnest sample (curve 1) is thicker than that from which the emission spectrum shown in Figure 3 was recorded as is indicated by the fact that the two peaks near 18.2 and 15.4 μm are of the same relative intensity and the feature near 25 μm is relatively much weaker. This suggests that strong reabsorption has already occurred for the thinnest sample.

Increasing the thickness of the sample drastically alters the shape of the curve and shifts the position of maximum emission, in the case of magnesium oxide, to shorter wavelengths. The reabsorption in the 18.2- μm feature occurs to such an extent that the feature no longer appears as the maximum. The maximum in the spectrum occurs at 15.4- μm . Further increasing of the sample thickness allows the peak near 11 μm to develop more rapidly than the 15.4- μm band as reabsorption becomes increasingly significant, until it becomes the most intense feature in the thickest sample shown. This effect of shifting the maximum to shorter wavelengths in magnesium oxide will continue as long as there are absorption features at shorter wavelengths. Consequently, it is difficult to specify the region of maximum emission for a cloud or layer of particles without also specifying its thickness or density.

Conclusion

These results demonstrate the following:

(a) Individual micrometer-sized particles emit most energy in the wavelength they absorb most energy, so that their emission spectra are the intensity inverse of their transmission spectra. This behavior was reported previously¹⁴ for silicates in the 6–11.8- μm range, and an explanation based on Mie absorption efficiency factors was provided. The present study illustrates the general nature of this behavior by extending the wavelength range to 35 μm , and by considering materials other than silicates.

(b) As the particle size increases from approximately micrometer to tens of micrometers, the polarity of the bands reverse so that the emission maxima for micrometer-sized particles becomes the emission minimum for the larger particles.

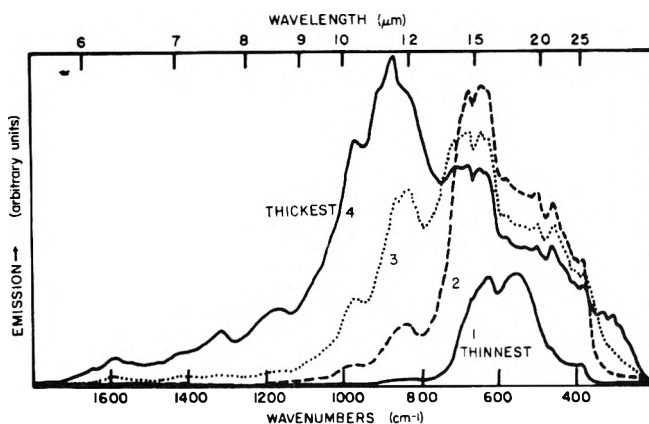


Figure 6. The effect of sample thickness on the emission spectrum of micrometer-sized magnesium oxide particles.

(c) As the cloud particle density or the thickness of the layer increases, and radiative interaction increases, the wavelength of the emission maximum shifts to progressively weaker bands, or appears as a Christiansen peak due to the combined effects of scattering at shorter wavelengths and absorption at longer wavelengths.

(d) The similarity between both the transmission and emission behavior of thin layers of particles deposited on a substrate and that of a cloud containing the same number of particles in the beam cross section suggests that particles deposited on a substrate provide a reasonably good analog for the study of thin clouds of particles.

References and Notes

- (1) Postdoctoral Research Associate with Professor Richard C. Lord, 1962–1963. Dedicated to Professor Lord on his 65th birthday and retirement.
- (2) (a) R. J. P. Lyon, NASA Report No. CR-100 (1964); (b) R. A. Van Tassel and I. Simon in "The Lunar Surface Layer", J. W. Salisbury and P. E. Glazer, Ed., Academic Press, New York, N.Y., 1964.
- (3) J. E. Conel, Jet Propulsion Laboratory Technical Memo 33243 (1965).
- (4) W. A. Hovis, Jr., and W. R. Callahan, *J. Opt. Soc. Am.*, **56**, 639 (1966).
- (5) A. F. H. Goetz, Ph.D. Thesis, California Institute of Technology, 1967.
- (6) G. R. Hunt and R. K. Vincent, *J. Geophys. Res.*, **73**, 6039 (1968).
- (7) L. M. Logan and G. R. Hunt, *Science*, **169**, 865 (1970).
- (8) L. M. Logan and G. R. Hunt, *J. Geophys. Res.*, **75**, 6539 (1970).
- (9) A. G. Emslie in "Progress in Astronautics and Aeronautics", Vol. 18, G. B. Heller, Ed., Academic Press, New York, N.Y., 1966.
- (10) J. R. Aronson, A. G. Emslie, R. V. Allen, and H. G. McLinden, *J. Geophys. Res.*, **72**, 687 (1967).
- (11) R. K. Vincent and G. R. Hunt, *Appl. Opt.*, **7**, 53 (1968).
- (12) J. R. Aronson and A. G. Emslie in "Infrared and Raman Spectroscopy of Lunar and Terrestrial Minerals", C. Karr, Jr., Ed., Academic Press, New York, N.Y., 1975, p. 143.
- (13) J. E. Conel, *J. Geophys. Res.*, **74**, 1614 (1969).
- (14) G. R. Hunt and L. M. Logan, *Appl. Opt.*, **11**, 142 (1972).
- (15) A. G. Emslie and J. R. Aronson, *Appl. Opt.*, **12**, 2563 (1973).
- (16) J. R. Aronson and A. G. Emslie, *Appl. Opt.*, **12**, 2573 (1973).
- (17) H. C. Van de Hulst, "Light Scattering by Small Particles," Wiley, New York, N.Y., 1957.
- (18) R. E. Samuelson, Ph.D. Dissertation, Georgetown University, Washington, D.C., 1967.
- (19) A device for reducing particle size through causing them to collide vigorously by entraining them in opposed jets of gas.
- (20) S. P. Srivastava, *Chem. Phys. Lett.*, **10**, 387 (1971).
- (21) J. I. Gourley and W. A. Runciman, *J. Phys. Chem. Solid State Phys.*, **6**, 583 (1973).
- (22) The three larger particle size ranges were prepared by crushing and grinding the samples in agate mortars, and then sizing the sample by sieving. The precise particle size distribution in each range was not determined, but it should be similar to that given by the grinding law. The less than 5- μm samples were prepared using a fluid energy mill.

Spectra and Structure of Small-Ring Molecules.

33.¹ Microwave Spectrum of SilacyclopentaneJ. R. Durig,^{*2,3}

Swiss Federal Institute of Technology, Laboratory for Physical Chemistry, Zürich, Switzerland

W. J. Lafferty,²

National Bureau of Standards, Washington, D.C.

and V. F. Kalasinsky

Department of Chemistry, University of South Carolina, Columbia, South Carolina 29208 (Received December 18, 1975)

Publication costs assisted by the University of South Carolina

The microwave spectrum of silacyclopentane, 1-silacyclopentane-1,1-*d*₂, and silacyclopentane-²⁹Si has been investigated in the spectral range of 8–40 GHz. The rotational lines of five vibrational excited states of the ring-puckering mode have also been assigned and are consistent with a high barrier to pseudorotation. Both the dipole moment measurements and the isotopic data indicate that the skeletal ring of this molecule is in the “twisted” C₂ conformation for the ground state. The *a* component of the dipole moment is 0.726 ± 0.005 D and the *c* component has been determined to be less than 0.01 D with a |μ_d| = 0.726 ± 0.006 D. The isotopic data are sufficient to determine the following parameters: ∠HSiH = 108.76 ± 0.26, *r*(Si–H) = 1.478 ± 0.004. Other important structural features have been estimated.

Introduction

The phenomenon of pseudorotation has been studied spectroscopically for a number of years and has recently been reviewed by Laane.⁴ The general theory for free and hindered pseudorotation has been developed by Harris et al.⁵ and successfully employed to interpret experimental data.⁶ More recently, Ikeda et al.⁷ have investigated the implications of a barrier to pseudorotation using a strict two-dimensional model.

The barriers to pseudorotation for a number of monosubstituted cyclopentanes have been determined from transitions in their far-infrared^{8–17} and Raman^{18,19} spectra; however, it is usually not possible to determine the structure of the most stable ring conformation from the vibrational data alone. Silacyclopentane is one of the molecules which has been studied previously and the value of the barrier to pseudorotation was found to be 3.9 kcal/mol.^{16,17} However, there was some uncertainty as to the most stable configuration, C₂ or C_s, although the evidence was strongly in favor of the twisted or C₂ conformation. Rotational spectra have been shown to be useful in answering these questions.^{20,21} In order to provide additional evidence for the relatively high barrier and to determine the symmetry of the heavy-atom skeleton in the ground vibrational state, the microwave spectra of silacyclopentane and silacyclopentane-1,1-*d*₂ have been recorded and analyzed in detail. The geometry of the ring has been estimated from a rigid model of the molecule in the ground state consistent with the observed rotational constants and the dipole moment has been determined from two different transitions.

Experimental Section

The samples of silacyclopentane and silacyclopentane-*d*₂ were prepared and kindly provided by Dr. J. N. Willis, Jr.^{16,22} No further purification was necessary and each sample was quite stable in the bronze waveguide. The microwave spectra

were recorded with the samples held at dry ice temperatures on a conventional spectrometer with 80-kHz square wave modulation. Frequency measurements were reproducible within 0.05 MHz with an absolute accuracy estimated to be 0.1 MHz for the ground state lines and for higher vibrational states and isotopic species to ±0.5 MHz. The dipole moment measurements were made with a Stark field applied from a precision high-voltage dc power supply with sufficient square wave superimposed to modulate the transition. The waveguide spacing was calibrated relative to the dipole moment of OCS.²³

Spectrum and Assignment

The spectrum in general was weak, but lines were sharp. The pattern of R-branch lines was typical of an a-type rotor with a |*K*| value close to zero in that lines associated with a given *J*-level transition were separated by as much as a few GHz.

Initial line assignments were made on the basis of a spectrum predicted from a structure in which the Si–H and Si–C distances were assumed to be the same as in dimethylsilane,²⁴ and the C–H and C–C bond lengths the same as in propane.²⁵ These assignments were verified by observing the Stark effect in various lines. The R-branch assignments were helpful in assigning some of the a-type Q branches in the spectrum.

A search for signals attributable to molecules with isotopic substitution in natural abundance was carried out. The ²⁹Si isotopic species was identified, with intensities consistent with its 4.7% abundance. Other weaker lines that might be due to ³⁰Si, or α- or β-¹³C were observed but the data were somewhat questionable and are not included.

Observed transition frequencies for the -*d*₀, -1,1-*d*₂, and ²⁹Si species are listed in Table I. The rotational constants shown have been calculated using an iterative least-squares program. All the transitions shown were used in the program, except in the case of the -*d*₀ compound where only the lower *J* levels were used. We feel that these eight R branches and one Q branch give rotational constants unaffected by centrifugal

TABLE I: Microwave Transition Frequencies (MHz), Rotational Constants (MHz), κ Values, Moments of Inertia ($\text{u } \text{Å}^2$),^a and Inertial Defects [$\Delta = I_c - (I_a + I_b)$] for Some Isotopic Species of Silacyclopentane

Transition	²⁸ Si		<i>1,1-d</i> ₂		²⁹ Si	
	Obsd	Obsd - calcd ^b	Obsd	Obsd - calcd	Obsd	Obsd - calcd
2 ₁₂ ← 1 ₁₁	12 121.76	-0.02	11 401.50	0.07		
2 ₀₂ ← 1 ₀₁	12 873.09	0.09	12 133.06	0.06		
2 ₁₁ ← 1 ₁₀	15 072.57	-0.01	13 864.87	0.02		
2 ₂₀ ← 1 ₀₁	22 617.57	-0.01				
3 ₁₃ ← 2 ₁₂	17 801.01	-0.02	16 833.37	0.03		
3 ₀₃ ← 2 ₀₂	18 206.58	-0.01	17 327.53	0.04		
3 ₂₂ ← 2 ₂₁	20 395.60	-0.09	18 949.81	0.09		
3 ₁₂ ← 2 ₁₁	21 971.40	0.11	20 388.35	-0.03		
3 ₂₁ ← 2 ₂₀	22 584.77	-0.02	20 571.90	-0.04		
4 ₁₄ ← 3 ₁₃	23 270.54	-0.32	22 089.92	-0.08	23 078.60	0.04
4 ₀₄ ← 3 ₀₃	23 404.97	-0.16	22 300.96	-0.02	23 227.29	0.16
4 ₂₃ ← 3 ₂₂	26 596.19	-0.16	24 860.99	-0.04	26 336.35	-0.01
4 ₁₃ ← 3 ₁₂	27 939.48	0.05			27 718.86	-0.02
4 ₃₂ ← 3 ₃₁	28 166.74	0.01	25 979.22	0.06	27 833.03	0.05
4 ₃₁ ← 3 ₃₀	29 400.00	0.01	26 710.50	0.01		
4 ₂₂ ← 3 ₂₁	30 311.15	0.04	27 794.15	-0.02		
5 ₁₅ ← 4 ₁₄	28 639.64	-0.24			28 408.92	0.19
5 ₀₅ ← 4 ₀₄	28 674.62	-0.17			28 449.28	0.11
5 ₂₄ ← 4 ₂₃	32 418.33	-0.34			32 131.73	-0.06
5 ₁₄ ← 4 ₁₃						
5 ₃₃ ← 4 ₃₂	34 902.20	-0.32				
5 ₂₃ ← 4 ₂₂	37 222.30	-0.09				
5 ₃₂ ← 4 ₃₁	37 760.10	-0.54				
6 ₁₆ ← 5 ₁₅	33 973.91	-0.47			33 701.79	-0.08
6 ₀₆ ← 5 ₀₅	33 981.96	-0.45			33 711.61	0.01
6 ₂₅ ← 5 ₂₄	37 962.48	-0.48				
7 ₁₇ ← 6 ₁₆	39 299.01	-0.62			38 984.47	-0.06
7 ₀₇ ← 6 ₀₆	39 300.72	-0.63			38 986.57	-0.11
7 ₂₅ ← 7 ₄₄	18 932.62	-0.28				
9 ₃₆ ← 9 ₅₅	22 538.30	-0.69				
A	5 473.39 ± 0.04		5 308.25 ± 0.16		5 473.42 ± 0.20	
B	4 137.01 ± 0.02		3 774.14 ± 0.03		4 085.26 ± 0.04	
C	2 661.55 ± 0.02		2 542.43 ± 0.03		2 639.99 ± 0.02	
κ	0.049		-0.109		0.020	
<i>I</i> _A	92.334 ± 0.002		95.206 ± 0.005		92.333 ± 0.004	
<i>I</i> _B	122.160 ± 0.001		133.906 ± 0.002		123.708 ± 0.002	
<i>I</i> _C	189.882 ± 0.001		198.778 ± 0.002		191.432 ± 0.002	
Δ	-24.612		-30.334		-24.609	

^a Moments of inertia were calculated using the conversion factor 505 379 u Å² MHz. Errors are those implied from the errors in the rotational constants. ^b Only the $J = 2 \leftarrow 1$ and $3 \leftarrow 2$ transitions were used in the least-squares determination of the rotational constants.

distortion. In the other cases, since no Q branches were identified, we have used all the data available.

In addition, a number of relatively strong excited state lines were apparent on the high-frequency side of the ground state lines. We have identified these in the $-d_0$ compound as excited states of the ring-puckering motion and were able to measure five higher levels of this mode. These data are found in Table II along with the derived rotational constants and moments of inertia.

Dipole Moment

Stark coefficients were calculated by the method of Golden and Wilson²⁶ from a computer program written by Beaudet²⁷ and modified by W. Kirchoff. Comparison of these rigid-rotor Stark coefficients to those obtained from a least-squares fit of the observed Stark transitions at various field values yield the dipole moment components. The two transitions chosen for these measurements were those which have very large type-c dependence but the c component was found to be less

than 0.01 D. The a component of the dipole moment was constant within the experimental error in the vibrational states, $\nu = 0, 1, 2, \text{ and } 3$; $|\langle \nu | \mu_a | \nu \rangle| = 0.726 \pm 0.005$ D. The total dipole moment was determined to be $|\mu_d| = 0.726 \pm 0.006$ D. The dipole moment, transition moments, and the transitions used to determine them are given in Table III. This is comparable to the value of 0.75 D found in dimethylsilane.²⁴

Molecular Conformation

Qualitatively it is possible to make use of the data to determine the molecular conformation of silacyclopentane. The least likely conformation is the planar, C_{2v} , form. More probable are the C_s (envelope) or C_2 (twisted) configurations.

Of the three possibilities only the C_s form is expected to have dipole-moment components in more than one direction, and in particular these would be a and c components. We have found that within the experimental error, μ_c is zero for silacyclopentane.

Additionally, the isotopic substitution of the silicon atom

TABLE II: Microwave Transition Frequencies (MHz), Rotational Constants (MHz), κ Values, Moments of Inertia ($\text{u}\text{\AA}^2$),^a and Inertial Defects [$\Delta = I_c - (I_a + I_b)$] for the ν_{39} Vibrational States of Silacyclopentane-²⁸Si

Transition	$\nu = 1$		$\nu = 2$		$\nu = 3$		$\nu = 4$		$\nu = 5$	
	Obsd	Obsd - calcd	Obsd	Obsd - calcd	Obsd	Obsd - calcd	Obsd	Obsd - calcd	Obsd	Obsd - calcd
$3_{03} \leftarrow 2_{02}$	18 220.64	0.23								
$3_{22} \leftarrow 2_{21}$	20 416.30	0.15								
$3_{12} \leftarrow 2_{11}$	21 988.76	-0.08	22 003.57	0.26	22 015.48	0.21	22 025.34	0.41	22 033.29	0.11
$3_{21} \leftarrow 2_{20}$	22 611.86	-0.03	22 634.55	0.15	22 653.36	0.23	22 668.38	0.01		
$4_{14} \leftarrow 3_{13}$	23 292.35	-0.76	23 313.86	0.12	23 331.99	0.11	23 348.15	-0.02	23 362.63	-0.02
$4_{04} \leftarrow 3_{03}$	23 425.69	0.34	23 444.32	0.12	23 460.95	0.18	23 475.88	0.13	23 489.38	0.14
$4_{23} \leftarrow 3_{22}$	26 620.59	0.11	26 641.48	0.01	26 659.34	0.02	26 674.58	0.06	26 687.62	-0.02
$4_{13} \leftarrow 3_{12}$	27 955.31	-0.20	27 969.05	0.03	27 980.41	0.16	27 989.33	-0.18	27 998.14	0.00
$4_{32} \leftarrow 3_{31}$	28 197.37	0.08	28 223.26	0.04	28 245.16	0.10	28 263.17	-0.05		
$4_{31} \leftarrow 3_{30}$	29 440.27	0.04	29 474.07	0.00						
$4_{22} \leftarrow 3_{21}$	30 341.02	-0.14	30 365.84	0.04	30 386.08	-0.07	30 402.50	0.03		
$5_{24} \leftarrow 4_{23}$	32 445.90	0.30	32 469.13	-0.20	32 489.33	-0.33	32 507.20	-0.02	32 522.57	-0.13
$5_{33} \leftarrow 4_{32}$	34 936.69	0.00	34 965.46	-0.28	34 989.91	-0.28	35 010.41	-0.16	35 027.63	0.01
A	5 467.92 \pm 0.48		5 462.45 \pm 0.27		5 457.43 \pm 0.42		5 452.68 \pm 0.34		5 449.23 \pm 0.24	
B	4 140.86 \pm 0.07		4 143.89 \pm 0.04		4 146.34 \pm 0.06		4 148.22 \pm 0.05		4 149.69 \pm 0.04	
C	2 664.52 \pm 0.08		2 667.36 \pm 0.05		2 669.89 \pm 0.06		2 672.21 \pm 0.05		2 674.26 \pm 0.03	
κ	0.053		0.056		0.059		0.062		0.063	
I_A	92.426 \pm 0.008		92.519 \pm 0.005		92.604 \pm 0.007		92.685 \pm 0.006		92.743 \pm 0.005	
I_B	122.047 \pm 0.002		121.958 \pm 0.002		121.886 \pm 0.002		121.830 \pm 0.002		121.787 \pm 0.002	
I_C	189.670 \pm 0.006		189.468 \pm 0.004		189.288 \pm 0.005		189.124 \pm 0.004		188.979 \pm 0.002	
Δ	-24.803		-25.009		-25.202		-25.391		-25.551	

^a See Table I.**TABLE III: Stark Coefficients [(MHz/cm²)/V²] and Dipole Moment of Silacyclopentane**

Transitions	M	Obsd $\times 10^6$	Calcd $\times 10^6$
$4_{04} \leftarrow 3_{03}$	3	0.8131	0.8135
	2	0.2817	0.2823
$4_{14} \leftarrow 3_{13}$	3	1.246	1.243
	2	0.4927	0.4931
	$\mu_a = 0.726 = 0.005$ D		
	$\mu_c = 0.00 \pm 0.01$		
	$\mu_t = 0.726 \pm 0.006$ D		

gives no change (within experimental error) in the moment of inertia about the a axis (see Table I). This implies that the silacyclopentane molecule has an axis of symmetry and that it passes through the silicon atom.

Finally, we rule out the planar, C_{2v} , form on the basis of the values of the inertial defect, Δ , shown in Table I. These values are too large for any reasonable out-of-plane hydrogen coordinates. We must conclude, ther., that silacyclopentane exists in a permanently twisted, C_2 , configuration in the ground state.

Structure

With the isotopic data available, certain features of the molecular structural can be determined, while others may be inferred. By taking advantage of the symmetry of silacyclopentane in the formulation of Kraitchman's equations²⁸ it is possible to calculate substitution coordinates for the silicon atom and its protons. We find $r(\text{Si-H}) = 1.478 \pm 0.004$ \AA and $\angle(\text{H-Si-H}) = 108.76 \pm 0.26^\circ$. These are similar to the corresponding quantities in dimethylsilane.²⁴

While it is not possible to determine the exact structure of silacyclopentane we may estimate some of the other salient features. By assuming the remaining bond lengths and exte-

TABLE IV: Assumed and Calculated Structural Parameters for Silacyclopentane

Substitution parameters	$r(\text{Si-H}) = 1.478 \pm 0.004$ \AA
Assumed parameters	$\angle\text{HSiH} = 108.76 \pm 0.26^\circ$
	$r(\text{Si-C}) = 1.87$ \AA
	$r(\text{C-C}) = 1.54$ \AA
	$r(\text{C-H}) = 1.09$ \AA
	$\angle(\text{HC}_\alpha\text{Si}) = 109.5^\circ$
	$\angle(\text{HC}_\beta\text{C}_\beta) = 109.5^\circ$
Estimated parameters	$\angle(\text{CSiC}) = 96.7^\circ$
	$\angle(\text{SiCC}) = 105.1^\circ$
	$\angle(\text{CCC}) = 113.7^\circ$
	$\tau = 21^\circ$

rior bond angles, we can concentrate on the more important internal ring angles and, of course, τ , the twist angle. The twist angle can be thought of as the dihedral angle between the plane defined by $\text{C}_{\alpha 1}\text{-Si-C}_{\alpha 2}$ and one that contains the Si and C_β atoms. The assumed and subsequently derived parameters are given in Table IV.

We found that the a moment of inertia was sensitive only to variations in the C-Si-C angle. This is to be expected for a molecule with silacyclopentane's symmetry. The other two valence angles and τ were determined in each case from all three moments of inertia after $\angle\text{C-Si-C}$ was fixed at a value consistent with I_a .

The structure given in Table IV reproduces the ground state rotational constants of the three isotopic species to within 1.0%. Error limits on the structural features have not been included since they would be very large and difficult to determine. We feel that this structure is a reasonable one, even though a number of assumptions were made.

Vibrational Excited States

We have measured five excited states of the ring-puckering motion in the normal isotopic species and the results are found

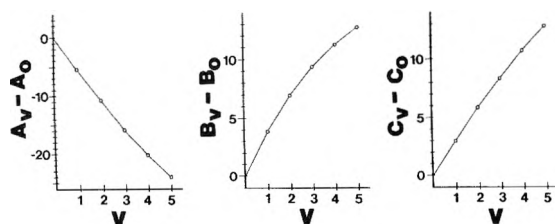


Figure 1. Plot of the change in rotational constants (MHz) with increasing vibrational quantum number of the ring-puckering motion.

in Table II. The increase in the values of the inertial defect, Δ , with increasing vibrational state are consistent with a motion of this sort. The value of the barrier to interconversion of the two equivalent twisted forms is expected, from the observed satellite pattern, to be fairly large.

The variation in the rotational constants with increasing vibrational state is plotted in Figure 1. The linearity in the graphs is typical of molecules with appreciable barriers to interconversion.^{29,30} Also indicative of a high barrier in silacyclopentane is the lack of observed splitting in the first five excited states. This implies that the fifth vibrational level, which is about 500 cm^{-1} above the ground state, is still well below the top of the potential well. This is consistent with the value of the barrier (3.9 kcal/mol) determined from far-infrared data.^{16,17}

Discussion

The conformation of silacyclopentane has been established on the basis of dipole-moment components, isotopic substitution, and inertial defects to be the twisted, C_2 , form. In the vibrational studies,^{16,17} it had not been possible to distinguish between the C_2 and C_s forms. The C_2 configuration had been assumed, as this is in qualitative agreement with the treatment of Pitzer and Donath.³¹ The twisted form has also been found to be the stable one in germacyclopentane,²⁰ cyclopentanone,³⁰ and methylenecyclopentane.²⁹ These molecules show barriers to pseudorotation of 4.14 ,^{15,19} 2.15 ,^{32,33} and 1.8 ^{29,34} kcal/mol, respectively.

It has been implied^{16,17} that the large difference between the observed barrier to pseudorotation and that predicted using the formulation of Pitzer and Donath is due to the nontransferability of torsional barriers from simple molecules to ring compounds. The structural features of ring compounds are probably an important factor causing this to be true. The difference between the C-Si-C angles in dimethylsilane (110.98°)²⁴ and silacyclopentane (96.7°) is certainly significant in this respect. In addition, this smaller angle introduces ring strain that is absent in unsubstituted cyclopentane. The twist angle, τ , must be important since the nonbonded interactions between adjacent CH_2 groups are affected by this parameter. It is not surprising that quantitative agreement with theory³¹ is generally poor.

The recent treatments of pseudorotation as a two-dimensional problem^{19,33} involving the puckering and radial modes have been interesting insofar as the barriers obtained have been lower than the previous simpler treatments. Additional vibrational data necessary for these studies were obtained from the far-infrared spectra of a number of isotopic species³³ or the Raman spectra of gaseous samples.¹⁹ The Raman spectra of silacyclopentane should prove to be very useful in determining a more complete potential surface governing the low-frequency ring vibrations.

Acknowledgment. The authors gratefully acknowledge the financial support of this study by the donors of the Petroleum Research Fund administered by the American Chemical Society.

References and Notes

- (1) For part XXXII, see *J. Chem. Phys.*, **63**, 2015 (1975).
- (2) W. J. Lafferty received his Ph.D. under the direction of Professor Lord in 1961. J. R. Durig received his Ph.D. under the direction of Professor Lord in 1962.
- (3) Work done at the National Bureau of Standards and the Swiss Federal Institute of Technology while on sabbatical leave from the University of South Carolina.
- (4) J. Laane in "Vibrational Spectra and Structure", Vol. I, J. R. Durig, Ed., Marcel Dekker, New York, N.Y., 1972, Chapter 2.
- (5) D. O. Harris, G. G. Engerholm, C. A. Tolman, A. C. Luntz, R. A. Keller, H. Kim, and W. D. Gwinn, *J. Chem. Phys.*, **50**, 2438 (1969).
- (6) G. G. Engerholm, A. C. Luntz, W. D. Gwinn, and D. O. Harris, *J. Chem. Phys.*, **50**, 2446 (1969).
- (7) T. Ikeda, R. C. Lord, T. B. Malloy, Jr., and T. Ueda, *J. Chem. Phys.*, **56**, 1434 (1972).
- (8) W. J. Lafferty, D. W. Robinson, R. V. St. Louis, J. W. Russel, and H. L. Strauss, *J. Chem. Phys.*, **42**, 2915 (1965).
- (9) J. R. Durig, G. L. Coulter, and D. W. Wertz, *J. Mol. Spectrosc.*, **27**, 285 (1968).
- (10) J. R. Durig and D. W. Wertz, *J. Chem. Phys.*, **49**, 675 (1968).
- (11) J. A. Greenhouse and H. L. Strauss, *J. Chem. Phys.*, **50**, 124 (1969).
- (12) D. W. Wertz, *J. Chem. Phys.*, **51**, 2133 (1969).
- (13) W. H. Green, A. B. Harvey, and J. A. Greenhouse, *J. Chem. Phys.*, **54**, 850 (1971).
- (14) J. R. Durig, J. M. Karriker, and D. W. Wertz, *J. Mol. Spectrosc.*, **31**, 237 (1969).
- (15) J. R. Durig and J. N. Willis, Jr., *J. Chem. Phys.*, **52**, 6108 (1970).
- (16) J. R. Durig and J. N. Willis, Jr., *J. Mol. Spectrosc.*, **32**, 320 (1969).
- (17) J. Laane, *J. Chem. Phys.*, **50**, 1946 (1969).
- (18) L. A. Carreira, G. J. Jiang, W. B. Person, and J. N. Willis, Jr., *J. Chem. Phys.*, **56**, 1440 (1972).
- (19) J. R. Durig, Y. S. Li, and L. A. Carreira, *J. Chem. Phys.*, **58**, 2393 (1973).
- (20) E. C. Thomas and V. W. Laurie, *J. Chem. Phys.*, **51**, 4327 (1969).
- (21) J. A. Wells and T. B. Malloy, Jr., *J. Chem. Phys.*, **60**, 2132 (1974).
- (22) J. N. Willis, Jr., Ph.D. Thesis, University of South Carolina, 1970.
- (23) J. S. Muentzer, *J. Chem. Phys.*, **48**, 4544 (1969).
- (24) L. Pierce, *J. Chem. Phys.*, **34**, 498 (1961).
- (25) D. R. Lide, Jr., *J. Chem. Phys.*, **33**, 1519 (1960).
- (26) S. Golden and E. B. Wilson, *J. Chem. Phys.*, **7**, 669 (1948).
- (27) R. A. Beaudet, Ph.D. Thesis, Harvard University, 1961.
- (28) J. Kraitichman, *Am. J. Phys.*, **21**, 17 (1953).
- (29) J. R. Durig, Y. S. Li, and L. A. Carreira, *J. Chem. Phys.*, **57**, 1896 (1972).
- (30) H. Kim and W. D. Gwinn, *J. Chem. Phys.*, **51**, 1815 (1969).
- (31) K. S. Pitzer and W. E. Donath, *J. Am. Chem. Soc.*, **81**, 3213 (1959).
- (32) L. A. Carreira and R. C. Lord, *J. Chem. Phys.*, **51**, 3225 (1969).
- (33) T. Ikeda and R. C. Lord, *J. Chem. Phys.*, **56**, 4450 (1972).
- (34) T. B. Malloy, Jr., F. Fisher, J. Laane, and R. M. Hedges, *J. Mol. Spectrosc.*, **40**, 239 (1971).

Vibrational Constants and Force Field of Sulfur Hexafluoride^{1,2}

Robin S. McDowell,^{*3} Jack P. Aldridge, and Redus F. Holland

Los Alamos Scientific Laboratory, University of California, Los Alamos, New Mexico 87545 (Received January 19, 1976)

Publication costs assisted by the U. S. Energy Research and Development Administration

The infrared-active combination bands of SF₆ gas were remeasured and the band origins estimated. These data were combined with the Raman frequencies of Bosworth et al., and with the spectrum of SF₆ in cryogenic liquid oxygen solutions reported by Bertsev et al., to obtain estimates for the 21 anharmonicity constants X_{ij} . The resulting harmonic vibrational frequencies were used in a calculation of the general quadratic harmonic force field of SF₆. The most useful constraint in the F_{1u} symmetry block was the Coriolis constant $\zeta_3 = 0.693 \pm 0.004$ obtained from an analysis of ν_3 resolved with tunable diode lasers; but ζ_4 estimated from a similar analysis of ν_4 , and the ³²S-³⁴S isotope frequency shifts reported by Brunet and Perez for these fundamentals, are all in general agreement. The more important valence force constants are $f_r = 5.45 \pm 0.03$, f_{rr} (cis interaction) = 0.36 ± 0.01 , $f_{rr'}$ (trans interaction) = -0.02 ± 0.03 , and $f_\alpha \approx 0.83$, all in m dyn/Å. From the absolute band intensities of Schatz and Hornig and the present force field, the S-F bond moment and its derivative are estimated to be $\mu_0 = 2.44 \pm 0.12$ D and $\partial\mu/\partial r = 4.2 \pm 0.3$ D/Å.

Introduction

In the last decade several general quadratic force fields have been reported for SF₆.⁴⁻⁸ To avoid approximation methods, which are always of doubtful validity, one needs at least one additional constraint besides the two fundamental frequencies in the infrared-active F_{1u} symmetry block. In the papers cited, this has been supplied by the Coriolis constants ζ_3 and ζ_4 as estimated from the contours of unresolved bands,⁴ by the Coriolis constant ζ_4 obtained from an analysis of the partially resolved rotational structure of ν_4 ,⁹ and by the ³²S-³⁴S isotope shifts in ν_3 and ν_4 .^{7,9} The general features of the force field of this molecule are thus understood, but the indifferent agreement between the various force constant estimates indicates that the values are not known with much precision.

Recently extensive rotational fine structure in the ν_3 fundamental of SF₆ has been resolved using tunable diode laser spectroscopy, and rotational and octahedral splitting quantum numbers have been assigned.¹⁰ These assignments were then extended to portions of the band that had been heterodyne-calibrated against the P(14), P(18), and P(20) CO₂ laser lines, and the spectroscopic constants of ν_3 were determined.¹¹ We have also made a preliminary analysis of laser spectra of the bending fundamental ν_4 . These data provide the most precise constraints available on the F_{1u} block, and we present here a new determination of the force constants of SF₆. This paper is the fourth in a series on the vibrational force fields of hexafluoride molecules; previous work has covered MoF₆,¹² WF₆,¹³ and UF₆.¹⁴

Experimental Section

Conventional infrared spectra were obtained with a Perkin-Elmer Model 180 double-beam grating spectrometer, and calibrated using the IUPAC tables.^{15,16} All bands were recorded with a spectral slit width of 0.5 cm⁻¹ at 300 K; the fundamentals were examined also at 190 K. The measurements are summarized in Table I.

The diode laser spectra of ν_3 at 10.5 μm have been described previously.^{10,11} Similar scans were made of ν_4 at 16 μm using a different Pb_{1-x}Sn_xSe diode. The sample temperatures and pressures were ~130 K and 0.2 Torr for the Q-branch region;

and ~150 K and 1 Torr for the P and R branches, with a few runs at 300 K and 1 Torr. The spectra were calibrated using a germanium etalon with a free spectral range of 0.048 56 cm⁻¹, and absorption lines of ¹²CO₂, ¹³CO₂, NH₃, and N₂O.

Vibrational Data

1. *Observed and Harmonic Frequencies.* The six observed fundamental frequencies (ν_i) are listed in Table II. The value for ν_3 is that of the band origin (ν_0) determined from an analysis of the diode laser spectrum at 10.5 μm;¹¹ the origin of ν_4 was similarly obtained from an unpublished preliminary analysis of laser spectra of the 16-μm region. The frequencies of the Raman-active fundamentals ν_1 , ν_2 , and ν_5 are those reported by Bosworth et al.¹⁷ These should not differ much from the band origins, since each of these transitions has a narrow, symmetrical Q branch. For the inactive mode ν_6 we have accepted the value of Bosworth et al.,¹⁷ which is simply one-half the measured frequency of the overtone $2\nu_6$.¹⁸

To obtain accurate anharmonicity constants, it is desirable to know the band origins of the combinations and overtones. For cases where this was possible, we have given in Table I estimated ν_0 's obtained by subtracting one spectral slit width from the position of the high-frequency edge of the Q branch.¹² This procedure is valid for bands whose Q branches degrade to low frequencies (i.e., those for which most of the applicable anharmonicity constants are negative),¹² and it can be quite accurate: note the close agreement between the ν_0 's estimated for ν_3 and ν_4 in Table I, and the values obtained from band analyses in Table II.

These ν_0 's were used in conjunction with the Raman data¹⁷ to determine the anharmonicity constants X_{13} , X_{14} , X_{22} , X_{23} , and X_{24} .¹⁹

$$X_{ij} = (\nu_i + \nu_j) - \nu_i - \nu_j \quad (i \neq j)$$

$$X_{22} = \frac{1}{2}[(2\nu_2 + \nu_3) + \nu_3 - 2(\nu_2 + \nu_3)]$$

The anharmonicity constants involving the low-frequency fundamental ν_6 are given by the spacing of the hot-band Q branches from the main Q branches (these spacings were determined with an estimated precision of ± 0.1 cm⁻¹):

TABLE I: Infrared Grating Spectra of $^{32}\text{SF}_6$

Assignment	Structure	Position of absorption maximum, cm^{-1}	Estimated ν_0 , cm^{-1}	$\Delta\nu(\text{P-R})$ at 300 K, cm^{-1}
$2\nu_2 + \nu_3$	PQR	2226.5	2227.5 ± 0.3	~ 6
$\nu_1 + \nu_3$	PQR	1719.2	1719.5 ± 0.3	(5) ^a
$\nu_1 + \nu_3 + \nu_6 - \nu_6$	Q	1717.7		
$\nu_2 + \nu_3$	PQR	1587.9	1588.1 ± 0.3	(11.5) ^a
$\nu_3 + \nu_5$	None ^b	1456		
$\nu_1 + \nu_4$	PQR ^b	1388.1	1388.8 ± 0.3	21.4 ± 0.5 (18.6) ^a
$\nu_1 + \nu_4 + \nu_6 - \nu_6$	Q ^b	1386.9		
$\nu_2 + \nu_4$	PQR	1257.0	1257.3 ± 0.3	(12) ^a
$\nu_2 + \nu_4 + \nu_6 - \nu_6$	Q	1255.0		
$\nu_4 + \nu_5$? ^c	1140.4		
$\nu_2 + \nu_6$	PQR ^d	991.2		
$\nu_2 + 2\nu_6 - \nu_6$	Q	989.7		
ν_3	PQR	947.7	948.1 ± 0.1	(3.6) ^a [5.3 ^e]
$\nu_3 + \nu_6 - \nu_6$	Q	946.7		
$\nu_5 + \nu_6$	PQR	869.9	870.6 ± 0.3	25.5 ± 1 (26.8) ^a
ν_4	PQR	614.7	615.0 ± 0.1	21.4 ± 0.5 (21.6) ^a
$\nu_4 + \nu_6 - \nu_6$	Q	613.7		

^a The values in parentheses are $2(\nu_R - \nu_{Q_{\text{max}}})$. ^b These bands are illustrated in ref 14. ^c The combination $\nu_4 + \nu_5$ consists of a strong narrow peak (Q branch?) with an adjoining "P branch" about 6 cm^{-1} distant, similar in shape to $\nu_2 + \nu_4$ of UF_6 .¹⁴ ^d The Q branch of $\nu_2 + \nu_6$ is not centered, but lies near the R-branch maximum. ^e Value calculated for $\zeta_3 = 0.693$. ^f $\Delta\nu(\text{P-R}) = 17.1 \pm 0.5 \text{ cm}^{-1}$ at 190 K.

TABLE II: Vibrational Parameters of $^{32}\text{SF}_6$ ^a

	$i = 1$	$i = 2$	$i = 3$	$i = 4$	$i = 5$	$i = 6$
Γ_i	A_{1g}	E_g	F_{1u}	F_{1u}	F_{2g}	F_{2u}
ν_i	773.6 ± 0.5^b	642.1 ± 0.5^b	947.968 ± 0.001	615.03 ± 0.02	522.9 ± 0.5^b	346 ± 1^b
ω_i	782 ± 3	649 ± 2	966 ± 3	620 ± 5	528 ± 5	352 ± 2
X_{i1}	-0.9 ± 0.6^c					
X_{i2}	-2.3 ± 1.0^c	-0.4 ± 0.3^d				
X_{i3}	-2.1 ± 0.6^d	-2.0 ± 0.6^d	-3.1 ± 0.3^c			
X_{i4}	$+0.2 \pm 0.6^a$	$+0.2 \pm 0.6^d$	$(-0.5 \pm 1.0)^e$	$(-0.5 \pm 1.0)^e$		
X_{i5}	$(-0.5 \pm 1.0)^e$	$(-0.5 \pm 1.0)^e$	$(-0.5 \pm 1.0)^e$	$(-0.5 \pm 1.0)^e$	$(-0.5 \pm 1.0)^e$	
X_{i6}	-0.3 ± 0.2^f	-1.0 ± 0.1^f	-1.0 ± 0.1^f	-1.0 ± 0.1^f	$(-0.5 \pm 1.0)^e$	-0.3 ± 0.1^f
ζ_i	(0)	(0)	0.693 ± 0.004	-0.213 ± 0.019	$(-1/2)$	$(-1/2)$
Isotope shifts, $^{32}\text{SF}_6$ - $^{34}\text{SF}_6$:						
$\Delta\nu_i$			17.4 ± 0.3^g	3.3 ± 0.4^g		
$\Delta\omega_i$	(0)	(0)	17.97 ± 0.3	3.35 ± 0.4	(0)	(0)

^a Units are cm^{-1} , except for the ζ_i , which are dimensionless. ^b From Raman data of Bosworth et al.¹⁷ ^c Obtained from bands of SF_6 in cryogenic solutions as measured by Bertsev et al.²⁰ ^d From the estimated ν_0 's of infrared bands (Table I) and Raman frequencies of Bosworth et al.¹⁷ ^e Estimated value. ^f Obtained from spacing of hot-band Q branches (Table I). ^g Measured by Brunet and Perez;⁹ probable error of $\Delta\nu_2$ is estimated; that of $\Delta\nu_4$ was given by Thakur,⁸ citing a personal communication from H. Brunet.

$$X_{i6} = [(\nu_i + \nu_j + \nu_6 - \nu_6) - (\nu_i + \nu_j)] - [(\nu_j + \nu_6 - \nu_6) - \nu_j] \quad (i = 1, 2; j = 3, 4)$$

$$X_{i6} = (\nu_i + \nu_6 - \nu_6) - \nu_i \quad (i = 3, 4)$$

$$2X_{66} = [(\nu_2 + 2\nu_6 - \nu_6) - (\nu_2 + \nu_6)] + [(\nu_4 + \nu_6 - \nu_6) - \nu_4] - [(\nu_2 + \nu_4 + \nu_6 - \nu_6) - (\nu_2 + \nu_4)]$$

Finally, Bertsev et al.²⁰ have studied SF_6 in cryogenic liquid oxygen solutions. The narrow absorption bands were measured with errors not exceeding $\pm 0.5 \text{ cm}^{-1}$, and allow three more X_{ij} 's to be evaluated:

$$2X_{11} = (2\nu_1 + \nu_3) + \nu_3 - 2(\nu_1 + \nu_3)$$

$$X_{12} = (\nu_1 + \nu_2 + \nu_4) + \nu_4 - (\nu_1 + \nu_4) - (\nu_2 + \nu_4)$$

$$6X_{33} = (3\nu_3) - 3(\nu_3)$$

We have thus determined 13 of the 21 anharmonicity constants (Table II). Those involving a bending fundamental (ν_4 , ν_5 , or ν_6) fall in the range $+0.2$ to -1.0 cm^{-1} , with a mean near -0.5 cm^{-1} , so for each of the eight undetermined X_{ij} 's we have adopted an estimated value of $-0.5 \pm 1.0 \text{ cm}^{-1}$.

Recently Nowak and Lyman,²¹ in analyzing absorption measurements on SF_6 that had been shock-heated to 400–1500 K, treated the anharmonicity constants involving ν_3 by an approximation method. They assumed that the anharmonic shift for a given hot band is proportional to the amount of vibrational energy in the lower state:

$$X_{3i} = A\nu_i / (1 + \delta_{3i}) \quad (1)$$

where $\delta_{3i} = 1$ when $i = 3$ and $\delta_{3i} = 0$ otherwise, and A is an adjustable parameter. By matching calculated with observed band contours, they estimated $A = -(2.6 \pm 0.3) \times 10^{-3}$. This

gives $X_{13} = -2.0$, $X_{23} = -1.7$, and $X_{36} = -0.9 \text{ cm}^{-1}$, all in excellent agreement with the values of Table II; $X_{33} = -1.2 \text{ cm}^{-1}$ is somewhat lower than ours. Their $X_{34} = -1.6$ and $X_{35} = -1.4 \text{ cm}^{-1}$ are higher than the values we have estimated, but fall within our probable error limits. It appears that eq 1 is suitable as an approximation to the anharmonicity corrections when one is unable to obtain the X_{ij} 's individually, as in high-temperature band analyses.

The harmonic frequencies (ω_i) for the six fundamentals derived from our set of anharmonicity constants are given in Table II.

2. *Coriolis Constants.* The analysis of ν_3 yielded¹¹

$$B_3 + B_0 - 2(B\zeta)_3 = 0.055\,688 \pm 0.000\,016 \text{ cm}^{-1} \quad (2)$$

$$B_3 - B_0 = (-1.518 \pm 0.012) \times 10^{-4} \text{ cm}^{-1}$$

In an electron diffraction study²² of SF₆ gas the S-F bond length was found to be $1.564 \pm 0.010 \text{ \AA}$, so the effective rotational constant is $B = 0.0907 \pm 0.0012 \text{ cm}^{-1}$, and the difference between $B_3 + B_0$ and $2B$ is of the order of 0.1%. Thus to well within the accuracy of the electron diffraction determination of B , we can replace $B_3 + B_0 - 2(B\zeta)_3$ in eq 2 with $2B(1 - \zeta_3)$, which gives $\zeta_3 = 0.693 \pm 0.004$.

The full analysis of ν_4 is not yet complete, but we have measured sufficient vibration-rotation lines to be able to estimate ζ_4 reliably. The lines R(2) through about R(20) show no indication of octahedral splitting (unlike their counterparts in ν_3),¹⁰ and the spacing in this region is $0.220 \pm 0.002 \text{ cm}^{-1} \approx 2B(1 - \zeta_4)$. This spacing agrees closely with that determined by Brunet and Perez⁹ using a grille spectrometer ($0.22 \pm 0.005 \text{ cm}^{-1}$), and yields $\zeta_4 = -0.213 \pm 0.019$.

The precision of these Coriolis constants is determined mainly by the uncertainty in the S-F bond length r : the mean error in r is 0.64%; and that in $B = h/32\pi^2cr^2m_F$ is 1.3%, which is the approximate error in the values of $1 - \zeta_i$. Under these conditions, the more accurately determined of the two ζ 's will be the one nearer to the limiting value of +1: in this case, ζ_3 . We note that $\zeta_3 + \zeta_4 = 0.480 \pm 0.019$, in agreement with the value $1/2$ required by the sum rule.²³

The SF₆ fundamentals provide an opportunity to check the accuracy for octahedral molecules of the Edgell-Moynihan method of determining the Coriolis constants of unresolved bands.^{23,24} From the P-R branch spacing in ν_4 (Table I), we have

$$\zeta_4 = 1 - [\Delta\nu(\text{P-R})(hc/16kTB)^{1/2}] = -0.23 \pm 0.03$$

at both 300 and 190 K, in satisfactory agreement with the high-resolution results. For ν_3 the hot-band structure obscures the P-branch maximum, and attempts have been made to estimate the P-R spacing by doubling the distance between the Q- and R-branch maxima.⁴ It can be seen from Table I that this is satisfactory for ν_4 , but for ν_3 the value of $\Delta\nu(\text{P-R})$ thus obtained yields $\zeta = 0.79$ instead of the true value of 0.69. This approximation of course neglects the R-branch convergence caused by the change in the rotational constants between the ground and excited states (the $B_3 - B_0$ term), which will decrease the Q-R distance, but the discrepancy seems greater than can be accounted for by this effect alone. An additional complication is that at 300 K the branch maxima correspond to rotational levels of $J \approx 50$, and in this region of ν_3 the Coriolis splitting is much larger than the distance between adjoining J manifolds, and thus dominates the band structure.¹¹

3. ³²S-³⁴S Isotope Shifts. Brunet and Perez⁹ have measured isotope shifts in natural SF₆ (4.2% ³⁴S) of 17.4 cm^{-1} in ν_3 and 3.3 cm^{-1} in ν_4 . These shifts are consistent with those reported

by other authors with somewhat less precision.^{7,20} With anharmonicity corrections¹⁴ they become 17.97 and 3.35 cm^{-1} . The harmonic product ratio $\omega_3\omega_4(^{34}\text{SF}_6)/\omega_3\omega_4(^{32}\text{SF}_6)$ is then 0.9761 ± 0.0006 , compared with a theoretical value of 0.9768. This agreement is only marginally satisfactory; there is a possibility that one of the shifts measured by Brunet and Perez⁹ is slightly too large.

The pertinent vibrational data are summarized in Table II.

Force Field

Results of the force constant calculations using the harmonic frequencies are presented in Table III.²⁵ The errors quoted there reflect the uncertainties in the ω_i 's, and, for F_{33} and F_{44} , the error limits on F_{34} . So that the force constants of SF₆ can be compared with those of other molecules for which the anharmonicity corrections are not available, we have included in Table III the results of calculations using the observed frequencies.

As for all two-dimensional secular equations, there are two sets of force constants that reproduce the F_{1u} frequencies, the ζ 's, and the isotopic frequency shifts equally well; these are both given in Table III. For most molecules, one of these two can be selected on the basis of vibrational amplitudes, but for SF₆ the choice is not obvious (Table IV). Only the S-F amplitude is sensitive to the force field, and there is not much difference between the two calculated values. Ewing and Sutton²² directly determined only the short F...F amplitude, so their data are inconclusive. (Insofar as their assumed value of $u(\text{S-F})$ is near that of set I and gives good agreement between the observed and calculated values of the F...F amplitudes, it may be said to provide some support for that set.) On the basis of the valence force constants f_r and $f_{rr'}$, set I is physically the more reasonable of the two, but the choice is not as compelling as it usually is in these cases. Most (but not all⁷) other authors have chosen constants corresponding to our set I, though apparently some were unaware that an alternate solution lies nearby.

It is evident from Table III that although all the constraints are in general agreement, ζ_3 is by far the most effective in defining the force field. Because of the rather low observed product ratio mentioned above, the values of F_{34} determined by the isotope shifts in ω_3 and ω_4 differ by $0.059 \pm 0.061 \text{ mdyne/\AA}$; normally one would expect better agreement. Ruoff⁶ elected to use only $\Delta\nu_3$ in his calculations, noting that the ν_4 Q branch of ³⁴SF₆ is difficult to measure in natural samples because of interference by the hot bands of ³²SF₆. On the other hand, Thakur⁸ preferred $\Delta\nu_4$ because its anharmonicity corrections are smaller. The shifts should probably be re-measured to resolve these uncertainties, but meanwhile the force field is now adequately fixed by the Coriolis constant ζ_3 . The isotope shifts would be as effective as ζ_3 if they could be measured to about $\pm 0.05 \text{ cm}^{-1}$; this would probably require the resolution and analysis of the ³⁴SF₆ fundamentals.

Discussion

We will defer a full discussion of the force field of SF₆ until similar harmonic data are available for SeF₆ and TeF₆. However, we may note that the valence force constants of Table III (set I) are reasonable for a covalently bound molecule for which nonbonded F...F repulsions are significant. The arguments for the importance of such repulsions are the following: (1) the cis interaction constant $f_{rr} = 0.36 \text{ mdyne/\AA}$ is positive, which implies that stretching one bond favors contraction of the four adjacent bonds, and it is fairly large (cf. the values 0.23 and 0.27 mdyne/\AA in MoF₆ and WF₆);^{12,13} while

TABLE III: Force Constants of SF₆ (mdyn/Å)

	Using harmonic frequencies, ω_i		Using observed frequencies, ν_i	
	I ^a	II ^b	I ^a	II ^b
A. Determination of F_{34} from the various constraints				
ζ_3	0.909 ± 0.005	1.456 ± 0.008	0.902	1.421
ζ_4	0.883 ± 0.025	1.416 ± 0.038	0.877	1.382
³² S- ³⁴ S shift in ω_3	0.883 ± 0.026	1.416 ± 0.039	0.896	1.412
³² S- ³⁴ S shift in ω_4	0.942 ± 0.055	1.503 ± 0.079	0.929	1.461
Final value of F_{34}	0.907 ± 0.005 ^c	1.453 ± 0.008 ^c	0.90	1.42
B. Symmetry force constants				
$F_{11} = f_r + 4f_{rr} + f_{rr}'$	6.845 ± 0.053	6.845 ± 0.053	6.70	6.70
$F_{22} = f_r - 2f_{rr} + f_{rr}'$	4.715 ± 0.029	4.715 ± 0.029	4.61	4.61
$F_{33} = f_r - f_{rr}'$	5.465 ± 0.046	3.282 ± 0.042	5.30	3.23
$F_{44} = f_\alpha + 2f_{\alpha\alpha} - 2f_{\alpha\alpha}'' - f_{\alpha\alpha}'''$	1.051 ± 0.021	2.143 ± 0.011	1.034	2.07
$F_{34} = 2(f_{r\alpha} - f_{r\alpha}'')$	0.907 ± 0.005	1.453 ± 0.008	0.90	1.42
$F_{55} = f_\alpha - 2f_{\alpha\alpha}' + f_{\alpha\alpha}'''$	0.780 ± 0.015	0.780 ± 0.015	0.765	0.765
$F_{66} = f_\alpha - 2f_{\alpha\alpha} + 2f_{\alpha\alpha}'' - f_{\alpha\alpha}'''$	0.693 ± 0.008	0.693 ± 0.008	0.670	0.670
C. Valence force constants				
f_r	5.445 ± 0.026	4.354 ± 0.025	5.30	4.27
f_{rr} (adjacent bonds)	0.355 ± 0.010	0.355 ± 0.010	0.348	0.348
f_{rr}' (opposite bonds)	-0.020 ± 0.026	1.071 ± 0.025	0.003	1.04
$f_\alpha - f_{\alpha\alpha}'$ ($\approx f_\alpha$)	0.826 ± 0.009	1.099 ± 0.008	0.809	1.07
$f_{r\alpha} - f_{r\alpha}''$	0.454 ± 0.002	0.727 ± 0.004	0.45	0.71

^a Preferred solution. ^b Alternate solution. ^c Average weighted according to the inverse squares of the estimated errors.

TABLE IV: Root-Mean-Square Vibrational Amplitudes and Shrinkage Effects in SF₆ (Å)

	$T = 0$ K		$T = 300$ K		Obsd ^c
	Calcd (I) ^a	Calcd (II) ^b	Calcd (I) ^a	Calcd (II) ^b	
$u(\text{S-F})$	0.0407	0.0455	0.0416	0.0475	(0.0410) ^d
$u(\text{F}\cdots\text{F}, \text{short})$	0.0554	0.0554	0.0603	0.0603	0.060 ± 0.002
$u(\text{F}\cdots\text{F}, \text{long})$	0.0508	0.0508	0.0528	0.0528	(0.0507) ^d
$\delta(\text{F}\cdots\text{F}, \text{short})$	0.0006	0.0004	0.0006	0.0003	
$\delta(\text{F}\cdots\text{F}, \text{long})$	0.0021	0.0018	0.0025	0.0022	

^a Preferred solution. ^b Alternate solution. ^c Values reported in the electron-diffraction study of Ewing and Sutton.²² ^d Assumed value, calculated using an approximate valence force field.²²

the trans interaction constant f_{rr}' , which is not influenced by such repulsion, is near zero. (2) The primary bending force constant $f_\alpha \approx 0.83$ mdyn/Å is by far the largest of any known hexafluoride molecule.²⁶ (3) The stretch-bend interaction constant $f_{r\alpha} - f_{r\alpha}'' = 0.45$ mdyn/Å is positive (i.e., stretching a bond causes the four adjacent bonds to bend toward it), and also is much larger than for any other hexafluoride.²⁶ Furthermore, all three of these force constants decrease sharply in the series SF₆, SeF₆, TeF₆, as the size of the central atom, and hence the F...F distance, increases.^{26,27} (4) While the S-F and long F...F vibrational amplitudes of 0.042 and 0.053 Å (at 300 K), respectively, are close to those of most other hexafluorides,²⁸ the short F...F amplitude (0.060 Å) is much less than the 0.09–0.12 Å observed in metal hexafluorides,²⁸ suggesting that this motion is constrained.

We conclude with a brief discussion of the bond moment in SF₆. Schatz and Hornig²⁹ have measured the absolute intensities of the infrared-active SF₆ fundamentals in the vapor, with uncertainties of ±10%. (Bertsev et al.²⁰ recently reported intensities in liquid oxygen solutions that agree with the earlier gas-phase results to within ±5%.) The Schatz-Hornig intensities yield the following values for the derivatives of the vector dipole moments with respect to the normal coordinates:

$$\partial\mu/\partial Q_3 = \pm(226 \pm 11) \text{ esu}$$

$$\partial\mu/\partial Q_4 = \pm(54.6 \pm 2.7) \text{ esu}$$

From the force constants of Table III (set I) we calculate the following elements of the eigenvector matrix in units of amu^{-1/2}:

$$L_{33} = 0.3371 \quad L_{34} = 0.0395$$

$$L_{43} = -0.4206 \quad L_{44} = 0.4226$$

The sign ambiguity in the dipole moment derivatives results in two sets of solutions for the effective S-F bond moment and its derivative:

$$\mu_0 = 2.44 \pm 0.12 \text{ D} \quad \partial\mu/\partial r = 4.16 \pm 0.31 \text{ D/\AA}$$

or

$$\mu_0 = 0.85 \pm 0.12 \text{ D} \quad \partial\mu/\partial r = -6.79 \pm 0.31 \text{ D/\AA}$$

Only the first of these two sets is reasonable on the basis of electronegativity arguments.²⁹ The error limits quoted here include both the uncertainties in the measurement of the intensities, and those introduced into the elements of the L and L⁻¹ matrices by the estimated errors in the frequencies and

force constants. Our value of μ_0 is about 8% lower, and of $\partial\mu/\partial r$ about 8% higher, than the original results of Schatz and Hornig;²⁹ this is remarkable agreement considering that the latter had only an approximate force field with which to reduce their data. Several bond moment calculations published more recently^{8,30} have differed greatly from Schatz and Hornig's, and apparently are erroneous.

NOTE ADDED IN PROOF: In an infrared-infrared double resonance experiment, I. Burak, A. V. Nowak, J. I. Steinfeld, and D. G. Sutton, *J. Chem. Phys.*, **51**, 2275 (1969), have measured the absorption curve of the $2\nu_3 \leftarrow \nu_3$ transition in SF₆. It has an anharmonicity shift of "approximately 7 cm⁻¹"; i.e., $X_{33} \approx -3.5$ cm⁻¹, in agreement with the value of -3.1 ± 0.3 cm⁻¹ in our Table II. We thank Professor M. F. Becker of the University of Texas for calling our attention to this reference.

While Bertsev et al.²⁰ reported the ³²SF₆-³⁴SF₆ isotope shift in ν_3 , and various combination bands involving ν_3 , to be 17 ± 1 cm⁻¹, it is worth noting that their measurements on ν_3 itself are actually reported to the nearest 0.1 cm⁻¹: $\Delta\nu_3 = 17.0$ cm⁻¹, which with anharmonicity corrections becomes $\Delta\omega_3 = 17.5_6$ cm⁻¹, or $F_{34} = 0.918$ mdyne/Å. They also measured a ³²SF₆-³³SF₆ shift of 8.8 cm⁻¹, giving $\Delta\omega_3(^{32}\text{S}-^{33}\text{S}) = 9.0_9$ cm⁻¹ and $F_{34} = 0.912$ mdyne/Å. These values of F_{34} are in closer agreement with that obtained using ζ_3 as the constraint (Table II) than is F_{34} obtained from the isotope shift measured by Brunet and Perez.⁹

Acknowledgment. We thank Ruth J. Sherman for assistance with the grating spectrometer measurements.

References and Notes

- (1) Dedicated to Professor Richard C. Lord on his 65th birthday and retirement.
- (2) This work was supported by the U.S. Energy Research and Development Administration.
- (3) Ph.D. degree with Richard C. Lord, 1961.
- (4) S. Abramowitz and I. W. Levin, *J. Chem. Phys.*, **44**, 3353 (1966).
- (5) H. Kim, P. A. Souder, and H. H. Claassen, *J. Mol. Spectrosc.*, **26**, 46 (1968).
- (6) A. Ruoff, *J. Mol. Struct.*, **4**, 332 (1969).
- (7) V. D. Klimov and E. A. Lobikov, *Opt. Spectrosc.*, **30**, 25 (1971).
- (8) S. N. Thakur, *J. Mol. Struct.*, **7**, 315 (1971).
- (9) H. Brunet and M. Perez, *J. Mol. Spectrosc.*, **29**, 472 (1969).
- (10) J. P. Aldridge, H. Filip, H. Flicker, R. F. Holland, R. S. McDowell, N. G. Nereson, and K. Fox, *J. Mol. Spectrosc.*, **58**, 165 (1975).
- (11) R. S. McDowell, H. W. Galbraith, B. J. Krohn, C. D. Cantrell, and E. D. Hinkley, *Opt. Commun.*, submitted for publication.
- (12) R. S. McDowell, R. J. Sherman, L. E. Asprey, and R. C. Kennedy, *J. Chem. Phys.*, **62**, 3974 (1975).
- (13) R. S. McDowell and L. E. Asprey, *J. Mol. Spectrosc.*, **48**, 254 (1973).
- (14) R. S. McDowell, L. E. Asprey, and R. T. Paine, *J. Chem. Phys.*, **61**, 3571 (1974).
- (15) IUPAC Commission on Molecular Structure and Spectroscopy, "Tables of Wavenumbers for the Calibration of Infrared Spectrometers", Butterworths, London, 1961.
- (16) A. R. H. Cole, R. N. Jones, and R. C. Lord, *Pure Appl. Chem.*, **33**, 605 (1973).
- (17) Y. M. Bosworth, R. J. H. Clark, and D. M. Rippon, *J. Mol. Spectrosc.*, **46**, 240 (1973).
- (18) W. Holzer and R. Ouilion, *Chem. Phys. Lett.*, **24**, 589 (1974), have observed ν_6 directly by collision-induced Raman scattering in SF₆ gas at high pressures, at 336 cm⁻¹; in liquid SF₆ it appears at 350 cm⁻¹. This vapor frequency seems inconsistent with the position of the allowed transition $2\nu_6$, which Holzer and Ouilion; Bosworth et al.;¹⁷ and H. H. Claassen, G. L. Goodman, J. H. Holloway, and H. Selig, *J. Chem. Phys.*, **53**, 341 (1970), all found at 692-694 cm⁻¹ in the gas; it has been observed also in the solid at 694 \pm 2 cm⁻¹ by H. F. Shurvell and H. J. Bernstein, *J. Mol. Spectrosc.*, **30**, 153 (1969); and in the liquid at the same frequency by Holzer and Ouilion. Perhaps the molecular interaction that enables ν_6 to be active in scattering also affects its frequency; in any case, we have preferred to place this fundamental near 346 cm⁻¹.
- (19) The vibrational energy level expression may be found, for example, in ref 13 and 14.
- (20) V. V. Bertsev, T. D. Kolomitseva, and N. M. Tsyganenko, *Opt. Spectrosc.*, **37**, 263 (1974).
- (21) A. V. Nowak and J. L. Lyman, *J. Quant. Spectrosc. Radiat. Transfer*, **15**, 945 (1975). The estimated error limit for A was quoted in a personal communication from J. L. Lyman (1976).
- (22) V. C. Ewing and L. E. Sutton, *Trans. Faraday Soc.*, **59**, 1241 (1963).
- (23) R. S. McDowell, *J. Chem. Phys.*, **43**, 319 (1965).
- (24) W. F. Edgell and R. E. Moynihan, *J. Chem. Phys.*, **27**, 155 (1957).
- (25) References to FG-matrix treatments of the force constants may be found in ref 4, 5, 8, and 13. (In ref 4 and 8, the symmetry coordinates are chosen so that F_{34} has the opposite sign from the convention adopted here.) The 1973 values of the physical constants were used, with $m_F = 18.998$ amu and $m_S = 31.972$ or 33.967 86 amu. All force constants are given in units of mdyne/Å (1 mdyne/Å = 10² N/m). The vibrational amplitudes were calculated for ³²SF₆.
- (26) L. H. Jones, "Inorganic Vibrational Spectroscopy", Marcel Dekker, New York, N.Y., 1971, pp 94-100.
- (27) J. W. Linnett and C. J. S. M. Simpson, *Trans. Faraday Soc.*, **55**, 857 (1959).
- (28) S. J. Cyvin, J. Brunvoll, and A. Müller, *Acta Chem. Scand.*, **22**, 2739 (1968).
- (29) P. N. Schatz and D. F. Hornig, *J. Chem. Phys.*, **21**, 1516 (1953).
- (30) L. M. Sverdlov, *Opt. Spectrosc.*, **8**, 96 (1960).

Resonant Raman Scattering in the Ferroelectric Semiconductor SbSI

H. Buhay

Department of Physics, Northeastern University, Boston, Massachusetts 02115

and Clive H. Perry*¹

Hochfeld-Magnetlabor des Max-Planck-Instituts für Festkörperforschung, 38042 Grenoble, France (Received January 19, 1976)

Publication costs assisted by the Department of Physics, Northeastern University

Resonant Raman scattering studies have been performed on SbSI near the fundamental absorption edge. Measurements were made as a function of temperature (above and below the ferroelectric phase transition) and of incident laser excitation. The results indicate that all the phonon modes investigated show similar resonant behavior and their intensity variations compare favorably with the simple Loudon theory for a direct-energy-gap semiconductor. The nature of the energy gap appears to be the same in both phases.

Introduction

SbSI undergoes a paraelectric to ferroelectric phase transition at ~ 288 K with an associated structural change from $D_{2h}^{16}(Pnam) \rightarrow C_{2v}^9(Pna2_1)$. Detailed infrared and Raman data^{2,3} have been reported previously. SbSI is also a semiconductor with a band gap of 1.84–1.88 eV for E parallel to c and 1.96–1.97 eV for E perpendicular to c at room temperature^{4–9} (where 1 eV = 8065.8 cm^{-1}). These values were determined from measurements of the absorption edge and its definition is somewhat arbitrary. In our use of the band gap we have been guided by the work of Harbeke⁵ and we have taken the value of the band-gap energy, E_g , to be the wavelength where the absorption coefficient $\alpha = 100 \text{ cm}^{-1}$. Kern⁴ found that $E_g(T) \approx E_g(298) - \beta T$, where $\beta \sim 1.5 \times 10^{-3} \text{ eV/K}$ between 77 and 300 K. Harbeke reported that both edges shift with temperature without altering their shape, but the temperature dependence of the edge (and hence the band gap) cannot be adequately described by Kern's simple expression (i.e., β represents only an average value).

However the exact nature of the absorption edge has undergone some debate. In ref 6 and 7 it is concluded that the edges are due to phonon assisted indirect optical transitions whereas the work reported in ref 5, 8, and 9 describe the edge as exponential, corresponding to a direct gap.

Our earlier Raman results^{2a} favored the latter picture as no bands corresponding to two-phonon processes could be observed and all the one-phonon modes in our spectra showed intensity enhancement.

In this work we have performed polarized resonant Raman scattering (RRS) studies on SbSI in the vicinity of the absorption edge using two methods: one was to use several different laser sources to vary the incident radiation (at a fixed band gap); the other was to vary E_g for both E parallel to c and E perpendicular to c by changing the sample temperature at a fixed incident energy. Both methods are virtually equivalent for investigating the resonance behavior and for comparing the scattering intensities with different theoretical models providing all appropriate corrections to the observed Raman intensities can be made. Unfortunately in our most recent measurements unexpected changes had taken place in our samples after a long period of time and the results obtained by the first method could not be satisfactorily analyzed.

* Address correspondence to this author at the Department of Physics, Northeastern University, Boston, Mass. 02114.

However the temperature dependent measurements of the phonon modes in SbSI using He–Ne 6328 Å and later measurements using Kr 6471- and 6764-Å excitation on new samples show that the RRS intensity is in accord with the simple Loudon theory¹⁰ for a two-band parabolic model with a direct gap.

Experimental Section

The single crystals used in the Raman investigations were thin needles (about 1-mm² cross section), with the c axis along the needle axis. The crystals were grown from the vapor phase and the growth faces were perpendicular to the [100] and [010] directions. No attempt was made to positively identify the crystal a and b axes as only relatively minor intensity changes were observed by interchanging the designated x and y directions.

The Raman spectra were recorded using an Spectra-Physics Model 125 He–Ne laser, a Spectra-Physics Model 164 krypton laser and an argon pumped Coherent Radiation Model 490 Jet Stream dye laser. The measurements were taken with a Spex 1401 double/triple monochromator and a cooled ITT FW130 or RCA C31034 photomultiplier operating in a photon-counting mode. Low laser powers were used (~ 15 mW) to avoid excessive heating of the samples and were measured to within 5% at the position of the sample. An oblique incidence corresponding to an approximately back-scattering configuration was used, except with the Kr laser where right-angle scattering was employed. The spectral resolution $\Delta\nu$ was $\sim 2 \text{ cm}^{-1}$. The temperature control both above and below room temperature was achieved with either an Air Products helium cryotip equipped with a heater or a continuous nitrogen-gas-transfer cryostat. The temperatures were monitored by thermocouples mounted on the crystal holder in close proximity to the sample. Temperature stability of less than ± 1 K could be achieved.

Results and Discussion

In order to study the resonance Raman effect in SbSI two methods were utilized. In the first method we kept the energy gap constant and varied the energy of the incident radiation by simple tuning the dye laser or by choosing selected laser lines so that E_g could be approached from below. An alternative and slightly more convenient method was to change the position of the gap by some external means (e.g., temperature,

pressure, electric field, etc.) while maintaining a constant frequency of the incident light.

In our initial studies only a He-Ne laser was available for performing these measurements and we were forced to utilize the second method. Consequently we undertook Raman measurements of SbSI as a function of temperature from room temperature to liquid helium temperatures. We observed a marked increase in intensity on cooling from T_c to ~ 240 K. Further cooling to 15 K resulted in a decrease in intensity by about a factor of 3. The temperature dependence of the relative intensities of the 110- and 140- cm^{-1} bands were measured using a $y(zz)y$ configuration and the results are shown in Figure 1. With a laser excitation energy of 1.96 eV, a rather broad maximum of the Raman scattering intensity is observed at ~ 240 K for each phonon mode.

Using the two-band parabolic model due to Loudon,¹⁰ the frequency dependence of the resonant term in the Raman tensor for direct energy gap semiconductors is found to be

$$R(E_i, E_2, E_0) \propto \int_0^{K_{\max}} d\mathbf{K} \left[(E_g + E_0 - E_i + \frac{K^2}{2\mu})(E_g - E_i + \frac{K^2}{2\mu}) \right]^{-1} \quad (1)$$

and the Raman scattering intensity is proportional to

$$[(E_g(T) + E_0 - E_i)^{1/2} - (E_g(T) - E_i)^{1/2}]^2 \quad (2)$$

where E_i , E_2 , and E_0 are the incident, Stokes, and lattice-vibrational frequencies, respectively. The direct energy gap is $E_g(T)$, the reduced mass is μ and the electronic wave vector is \mathbf{K} . Thus there is an enhancement but no singularity as $E_i \rightarrow E_g$.

In the exciton picture¹¹ the electron and hole in an intermediate state are caused to interact and for simple parabolic bands the spectrum is now the discrete plus continuum states of a single exciton series. Calculation¹² shows that as $E_i \rightarrow E_g - R'$ (where R' is the exciton Rydberg in eV), the Raman amplitude becomes $A(E_i, E_g(T))$

$$\propto [(E_g - R' - E_i)(E_g - R' + E_0 - E_i)]^{-1} \quad (3)$$

The addition of a phenomenological damping term, Γ_g , to round off the divergence leads to a RRS intensity

$$\propto [((E_g - R' - E_i)^2 + \Gamma_g^2)((E_g - R' + E_0 - E_i)^2 + \Gamma_g^2)]^{-1} \quad (4)$$

The theoretical intensity curves for the 140- cm^{-1} phonons for the Loudon picture for noninteracting states (eq 2) and for the exciton picture (eq 4 with $\Gamma_g = 0$) are also shown in Figure 1.

The Raman intensities given in our earlier work¹ were not corrected for absorption but nevertheless the data indicated that the two band direct gap model is the more appropriate. From Figure 1 it can be seen that the intensities below the band-gap diverge as $(E_g - E_i)^{-1/2}$ rather than $(E_g - E_i)^{-1}$ which would be expected from the exciton picture. Using Harbeke's absorption data at room temperature and the variation of the band gap with temperature⁵ a series of absorption curves as a function of incident radiation and temperature was constructed and the necessary corrections for the absorption were applied. The Raman scattering intensities using a dye laser (tunable range 1.91–2.15 eV) were measured on the same SbSI samples previously investigated 4 years earlier with 6328-Å radiation. In these studies both methods were employed and the variation of the intensities as a function of temperature (i.e., varying E_g) and as a function of the

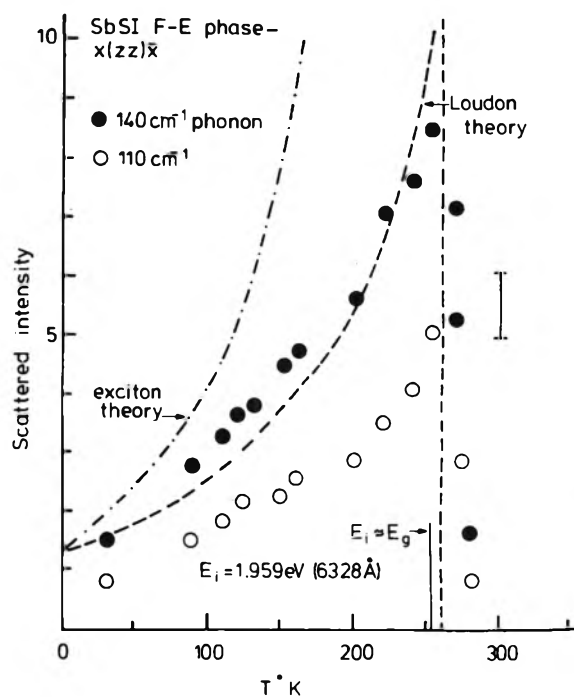


Figure 1. Raman scattering intensities for the 110- and 140 cm^{-1} bands plotted as a function of temperature. Theoretical intensity curves are shown for the Loudon theory and the exciton theory for the 140- cm^{-1} phonon.

incident light, E_i , were obtained.¹³ The RRS above and below the ferroelectric phase transition was investigated by studying the phonon modes (E_0) at ~ 110 and ~ 320 cm^{-1} for $y(xx)y$ and the ~ 110 , ~ 140 cm^{-1} , and the temperature dependent soft mode for $y(zz)y$.

A few examples of the results (not corrected for absorption) are shown in Figures 2 and 3. The sharp decrease in the scattering at higher frequencies (or at higher temperatures) is due to the rapid increase in absorption in the vicinity of the band edge. The increase in intensity at low frequencies is probably due to impurity induced absorption,¹⁴ due to the change in stoichiometry of our samples over a long period. The "absorption" tail in the samples was found to be approximately a factor of 10 larger than that reported by Harbeke.⁵ As no reliable estimate could be made of the "effective" thickness of the domains, it was meaningless to make any attempt to correct for the absorption. When observed under a microscope the samples showed wide variations in the transmittance from one domain to another, and it was concluded that they were no longer of uniform composition. The back-scattered light collected from our samples is dominated primarily by the transmitted light, rather than changes in the scattering coefficient and this has probably provided the anomalous results shown in Figures 2 and 3 at low energies and at low temperatures, respectively. In a previous report¹³ we assumed that the increase in absorption was possibly due to free carriers and using the theoretical treatment of RS from metallic surfaces by Mills et al.¹⁵ we were able to qualitatively reproduce the measurements by assuming the integrated RS intensity varied as δ^5 (where δ is the classical skin depth) and that such a term modulated eq 2. However, from our optical absorption data we now believe that the increase in the scattering at frequencies below the band gap was mainly due to impurities and imperfections created by a change in sample composition with time.

Temperature dependent measurements of the Raman ac-

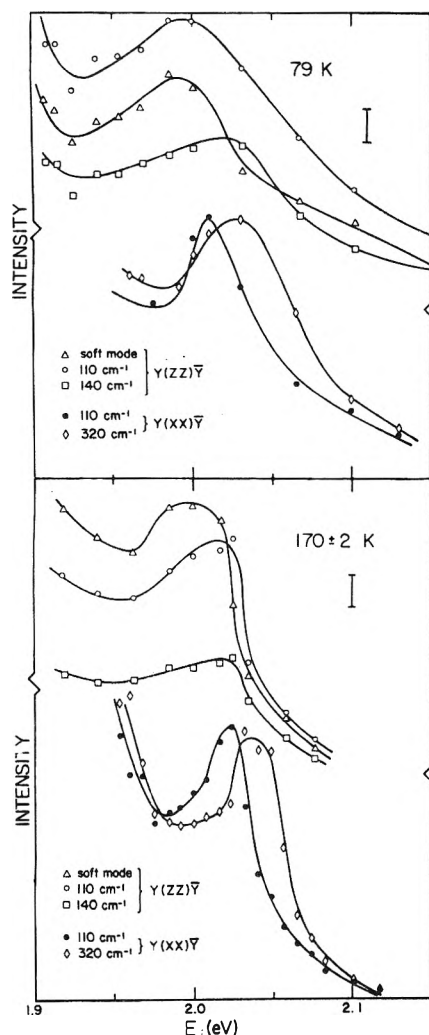


Figure 2. Raman scattering intensities for the ferroelectric soft mode and the 110- and 140- cm^{-1} phonons with $\gamma(zz)\bar{\gamma}$ and 110- and 320- cm^{-1} phonons for $\gamma(xx)\bar{\gamma}$ at ~ 80 and $\sim 170\text{ K}$ as a function of incident energy, E_i .

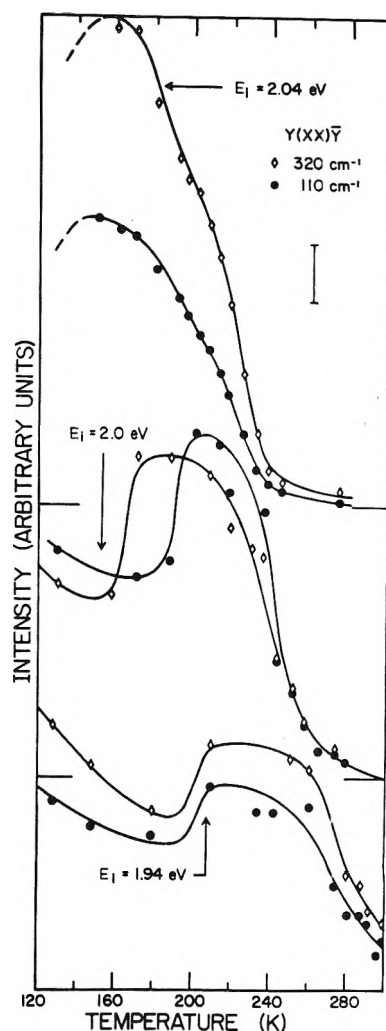


Figure 3. Raman scattering intensities for the 110- and 320- cm^{-1} phonons with $\gamma(xx)\bar{\gamma}$ at $E_i = 1.97, 2.0,$ and 2.04 eV as a function of temperature (i.e., E_g).

tive phonons with a Kr laser using $6471\text{-}\text{\AA}$ radiation and $x(zz)y$ geometry on a "fresh" sample in the ferroelectric phase compared favorably with the earlier results obtained with a He-Ne laser and the results are shown in Figure 4 for the 140-cm^{-1} phonon.

Measurements taken with $6764\text{-}\text{\AA}$ Kr in the paraelectric phase (Figure 5) were in good agreement with those reported by Spilbauer¹⁶ and both Figures 4 and 5 confirm the applicability of the simple Loudon theory in a semiconductor with a direct gap.¹⁰ These are in accord with the Raman results of Spilbauer¹⁶ and those reported recently by Yu et al.¹⁷ They are also consistent with the results of Harbeke,⁵ Zeinally et al.,⁸ and Kamimura et al.⁹ where the optical absorption edge is found to be exponential, such that in the range of $\alpha = 40\text{--}1000\text{ cm}^{-1}$ the absorption coefficient obeys the empirical Urbach rule. Possibly the most appropriate theory that can be applied to explain the exponential nature of the optical absorption edge for SbSI, is that developed by Mahan¹⁸ for polar crystals, where he showed that LO phonons predominate in the formation of the absorption edge but other phonons may participate in the process away from the edge. Kamimura et al.⁹ and Zeinally et al.⁸ conclude from their analysis of the absorption edge data that the excitons are strongly coupled to phonons in the range $210\text{--}220\text{ cm}^{-1}$. In our ir measurements

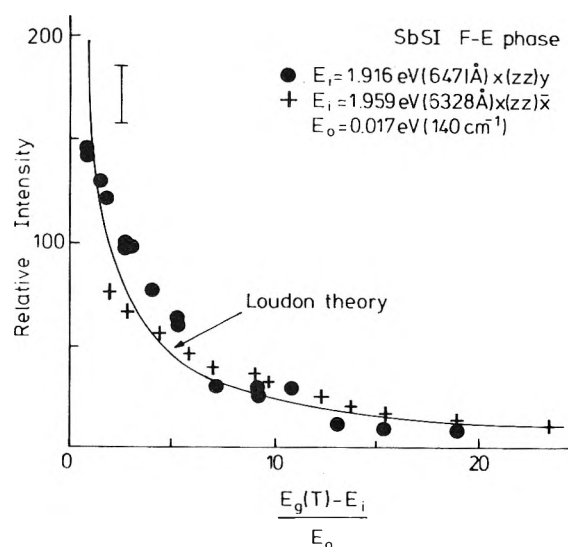


Figure 4. Scattering intensity of the 140-cm^{-1} phonon in the ferroelectric phase for $E_i = 1.916$ and 1.959 eV as a function of $E_i - E_{i0}$. E_{i0} was varied by changing the temperature. The solid line is the theoretical curve for a two-band parabolic model.

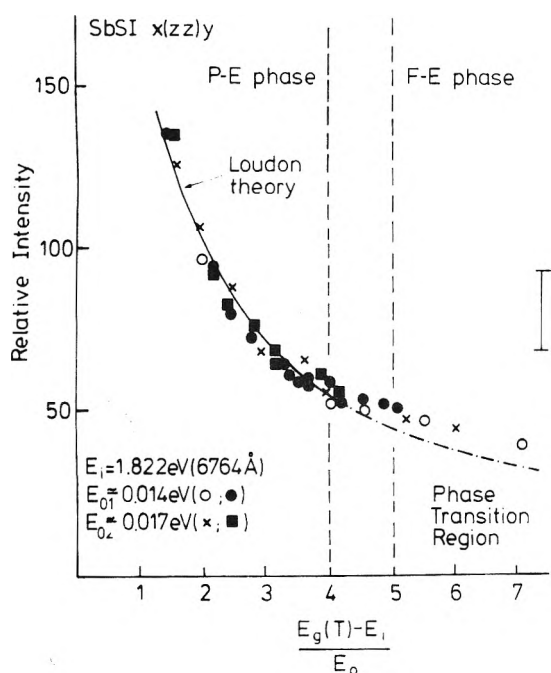


Figure 5. Scattering intensity for $x(zz)y$ geometry in the paraelectric phase for the 110- and 140- cm^{-1} phonons with $E_i = 1.822$ eV as a function of $(E_g(T) - E_i)/E_0$. E_g was varied by changing the temperature. ($E_0 \approx 0.014$ and 0.017 eV, respectively.) The solid curve is the intensity variation according to the Loudon theory and the solid circles and squares are taken from unpublished data in ref 16.

we report^{2a} a strong LO phonon at $\sim 217 \pm 10$ cm^{-1} associated with atomic displacements along the c axis. It has been shown by Balkanski et al.^{2b} that vibrations in the 150–320- cm^{-1} range, which includes these phonons, represent rotation and internal vibrations of $\text{Sb}^+ - \text{S}$ diatomic groups and are in fact valence vibrations of the $\text{Sb}^+ - \text{S}$ bonds. These vibrations are observed in both phases and show similar resonant behavior (when plotted as a function of $(E_g - E_i)/E_0$) and comparison of the intensity data above and below the phase transition suggests that the nature of the fundamental gap remain essentially unchanged at the phase transition. According to Yu

et al.¹⁷ this result is consistent with band structure calculations which show the top valence band and the bottom conduction band mainly derive from the p band of I and the S band of Sb, respectively. At the phase transition the S and Sb atoms are displaced along the c axis with respect to the I atoms by 0.2 and 0.05 Å, respectively,¹⁹ and the band ordering remains approximately the same.

Acknowledgments. The authors gratefully acknowledge the contributions of Mr. F. Llevada, Dr. N. E. Tornborg, and Mrs. G. Tang to this work. We also wish to thank Professor M. Balkanski, Laboratoire de Physique des Solides de l'Université Pierre et Marie Curie, Paris, for helpful discussions and making available to us the thesis of Marie-Noëlle Spilbauer. This work was supported in part by NSF Grant No. DMR72-03282A02 and the Research Corporation.

References and Notes

- (1) M.I.T. Sloan Post-doctoral Fellow and Research Associate with Richard C. Lord, 1960–1962. Alexander-von-Humboldt Foundation Senior U.S. Scientist Awardee, 1975–1976.
- (2) (a) D. K. Agrawal and C. H. Perry, *Solid State Commun.*, **8**, 225 (1970); *Phys. Rev. B* **4**, 1893 (1971); (b) M. Balkanski, M. K. Teng, S. M. Shapiro, and M. K. Ziolkiewicz, *Phys. Status Solidi*, **44**, 355 (1971).
- (3) E. F. Steigmeier, G. Harbeke, and R. K. Wehner, "Light Scattering in Solids", M. Balkanski, Ed., Flammarion Science, Paris, 1971, p 396.
- (4) R. Kern, *J. Phys. Chem. Solids*, **23**, 249 (1962).
- (5) G. Harbeke, *J. Phys. Chem. Solids*, **24**, 957 (1963); private communication.
- (6) E. I. Gerzanich, *Sov. Phys. Solid State*, **9**, 2358 (1968).
- (7) V. M. Fridkin, E. I. Gerzanich, II. Groshik, and V. A. Lyakhovitskaya, *JETP Lett.*, **4**, 139 (1966).
- (8) A. Kh. Zeinaly, A. M. Mamedov, and Sh. M. Efendiev, *Sov. Phys. -Semicond.*, (*Engl. Transl.*), **7**, 271 (1973); *Ferroelectrics*, **6**, 119 (1973).
- (9) H. Kamimura, S. M. Shapiro, and M. Balkanski, *Phys. Lett. A*, **33**, 277 (1970).
- (10) R. Loudon, *Proc. R. Soc. London, Ser. A*, **275**, 218 (1963); *J. Phys. Radium*, **26**, 677 (1965).
- (11) A. K. Ganguly and J. L. Birman, *Phys. Rev.*, **162**, 806 (1967).
- (12) B. Bendow, J. L. Birman, A. K. Ganguly, T. C. Damen, R. C. C. Leite, and J. F. Scott, *Opt. Commun.*, **1**, 267 (1970).
- (13) H. Buhay and C. H. Perry, 11th European Congress on Molecular Spectroscopy, July 1–4, 1975, Strasbourg, France. M. Grossman, Ed., Elsevier Scientific, Amsterdam, 1975, p 271.
- (14) T. Tamiki and T. Miyata, *J. Phys. Soc. Jpn.*, **27**, 658 (1969).
- (15) D. L. Mills, A. A. Maradudin, and E. Burstein, *Ann. Phys.*, **56**, 504 (1970).
- (16) M-N. Spilbauer, 3ème Cycle Thèse, Université de Paris VI, 1974, unpublished.
- (17) P. Y. Yu, N. M. Amer, Y. Petroff, and Y. R. Shen, "International Conference on Light Scattering Spectra of Solids," 1975, M. Balkanski, Ed., Flammarion, Paris, in press.
- (18) G. D. Mahan, *Phys. Rev.*, **145**, 602 (1966).
- (19) A. Kikuchi, Y. Oka, and E. Sawaguchi, *J. Phys. Soc. Jpn.*, **20**, 337 (1967).

Determination of the Symmetry of the Ammonium Ion in Crystals from the Infrared Spectra of the Isotopically Dilute NH_3D^+ Species¹

Ian A. Oxton, Osvald Knop,*

Department of Chemistry, Dalhousie University, Halifax, Nova Scotia, Canada B3H 4J3

and Michael Falk²

Atlantic Regional Laboratory, National Research Council of Canada, Halifax, Nova Scotia, Canada B3H 3Z1

(Received December 11, 1975)

A method is described whereby the symmetry of the ammonium ion in crystals may be determined from the number and relative intensities of the N–D stretching and bending fundamentals of isotopically dilute NH_3D^+ ions. These modes give rise, at liquid-nitrogen temperature, to sharp bands in the infrared spectrum. The method has been applied to the study of the ammonium ion in a variety of crystalline environments, as exemplified by $(\text{NH}_4)_2\text{SnCl}_6$, $(\text{NH}_4)_2\text{TiF}_6$, NH_4IO_4 , $(\text{NH}_4)_2\text{PdCl}_4$, $\text{NH}_4\text{NO}_3(\text{V})$, and $(\text{NH}_4)_2(\text{COO})_2\cdot\text{H}_2\text{O}$.

The symmetry of a site occupied in a crystal by an ammonium ion can be, in principle, any one of the 32 crystallographic point-group symmetries, and more than half of these have in fact been reported as site symmetries of the ion. The site symmetry is almost always deduced from the result of a crystal-structure determination. However, such a determination is often not available, and even when it is, the indication of the site symmetry occasionally is ambiguous or incorrect. An alternative approach to the problem is thus of value. In this paper we propose to investigate what can be learned about the site symmetry of an ammonium ion from the infrared spectrum.

The spectroscopic characteristics of an NH_4^+ ion at a site of symmetry S depend on the effective symmetry of the ion at that site. The effective symmetry E is determined by the maximum subgroup common to T_d and S , i.e., by the intersection $T_d \cap S = E$. Inasmuch as the intersections of T_d with the 32 crystallographic point groups are the subgroups of T_d , E can at most indicate the site symmetry within the homomorphisms $S \rightarrow E$ of Table I. The determination of site symmetry is further limited by the spectroscopic distinguishability of the subgroups of T_d for NH_4^+ . From the number of infrared-active fundamentals only those sets of S can be identified that correspond to one of the following sets of subgroups of T_d : (T_d, T) ; (C_{3v}, C_3) ; D_{2d}, C_{2v} ; $(S_4, D_2, C_s, C_2, C_1)$. However, establishing the number of fundamentals in the infrared spectrum of the ion in undeuterated (or those of ND_4^+ in fully deuterated) ammonium compounds is generally not feasible. Perhaps the most serious difficulty is due to extensive Fermi resonance which exists in the N–H (or N–D) stretching region and involves principally the vibrational modes $\nu_3, \nu_2 + \nu_4$, and $2\nu_4$.³ This resonance is expected to become more serious as the symmetry of the ion decreases, owing to the increasing number of components able to resonate with the fundamentals ν_1 and ν_3 . The intensity redistribution arising from this effect is often sufficient to render the assignment of fundamentals uncertain. However, even when Fermi resonance does not interfere severely, misinterpretation of any observed bands may occur as a result of ambiguities introduced by the possible presence of nonequivalent ammonium ions, factor-group splitting, and site-group splitting. This difficulty may be illustrated by the infrared studies of the complex fluorides $(\text{NH}_4)_2\text{NiF}_4$ and $(\text{NH}_4)_2\text{CuF}_4$. Crockett and Haendler⁴ attributed a splitting of the absorption due to ν_4 to the presence of two nonequiva-

lent sets of ammonium ions in the crystals of these salts. The x-ray diffraction work by Rüdorff et al.,⁵ however, revealed the presence of only one type of ammonium ion in each compound.

A method which avoids the complications that are encountered with NH_4^+ (or ND_4^+) is offered by the use of the isotopically dilute NH_3D^+ ion. It has been shown⁶ that, in the infrared spectra of NH_3D^+ ions at sites of symmetry T_d , the modes of principal interest, $\nu_1(a_1)$ and $\nu_{4bc}(e)$, are not subject to Fermi resonance and occur in frequency regions which are usually clear of other absorptions. These modes correspond essentially to N–D stretching and bending, respectively. At liquid-nitrogen temperature they give rise to sharp bands which reflect more clearly the symmetry of the ammonium ion. A low-level deuteration, such as results on recrystallizing the ammonium compound from an $\text{H}_2\text{O}-\text{D}_2\text{O}$ mixture of low D content, ensures that the NH_3D^+ ions are dispersed in the crystal at random and widely separated ("isotopically isolated"), so that the NH_3D^+ ion acts as a true probe of the symmetry and orientation of the ammonium ion in the structure. While in principle NHD_3^+ in an ND_4^+ matrix would serve equally well, in practice the requirement of an almost complete deuteration is less easily satisfied. The NHD_3^+ ion may turn out to be less suitable for yet another reason: in $(\text{NH}_4)_2\text{PtCl}_6$ the N–H stretching mode of NHD_3^+ , ν_{3a} , was found⁶ to give rise to a band almost as broad as that due to $\nu_3(\text{NH}_4^+)$.

The replacement by D of one of the H atoms in an NH_4^+ ion bound to a crystal site will give rise to four equally probable permutations (or orientations) whose equivalence will depend on the effective symmetry E of the NH_4^+ ion. The effective symmetry (or symmetries) E' of the NH_3D^+ ion(s) resulting from this substitution will be the intersection $C_{3v} \cap E$ of the maximum point group of the NH_3D^+ ion with E or a subgroup of that intersection, i.e., C_{3v}, C_3, C_s , or C_1 . Under these symmetries the N–D stretching and bending modes of the isolated NH_3D^+ ion will take the form

$$\begin{array}{lll}
 E': C_{3v} & \nu_1: a_1 & \nu_{4bc}: e \\
 C_3 & a & e \\
 C_s & a' & a' + a'' \\
 C_1 & a & a + a
 \end{array}$$

The number, and relative intensities, of bands expected from ν_1 and ν_{4bc} are then determined from the appropriate entry,

TABLE I: Effective Symmetries of the NH_4^+ (E) and NH_3D^+ (E') Ions at Crystal Sites of Symmetries S

S ^a	E	E' ^b
$O_h, {}^c T_d$	T_d	$C_{3v}(4)$
O, T_h, T	T	$C_3(4)$
$D_{6h}(2), D_{3h}, C_{6v}(2),$ D_{3d}, C_{3v}	C_{3v}	$C_{3v}, C_s(3)$
$D_6, C_{6h}, C_{3h}, C_6, D_3,$ S_6, C_3	C_3	$C_3, C_1(3)$
$D_{4h}(2), D_{2d}$	D_{2d}	$C_s(4)$
C_{4h}, S_4	S_4	$C_1(4)$
$C_{4v}(2), D_{2h}(3), {}^d C_{2v}$	C_{2v}	$C_s(2), C_s(2)$
$D_4(2), D_{2h}, {}^d D_2$	D_2	$C_1(4)$
$C_{2h}, {}^d C_s$	C_s	$C_s, C_s, C_1(2)$
$C_4, C_{2h}, {}^d C_2$	C_2	$C_1(2), C_1(2)$
C_i, C_1	C_1	C_1, C_1, C_1, C_1

^a The number of nonequivalent choices of symmetry operations of E from the symmetry operations of S is indicated in parentheses, e.g., $D_{6h}(2)$. ^b The number in parentheses indicates the number of equivalent orientations of the NH_3D^+ ion of given symmetry E' relative to the parent NH_4^+ ion of symmetry E. ^c Supergroup of T_d , $T_d \subset S_4$. ^d This S symmetry yields two different E symmetries, depending upon the choice of the symmetry operation from this point group.

for a particular S, in the column E' of Table I. These entries correspond to the symmetries of the four possible orientations of the NH_3D^+ ion; the numbers in parentheses refer to the number of equivalent orientations. In predicting the expected ratios it is assumed that, within each compound, each component of a vibrational mode contributes unit intensity.

The presence of sets of nonequivalent ammonium ions in a crystal may or may not be immediately detected by this method, depending upon the symmetries of the different sites and their relative abundance. For example, two nonequivalent sets of C_{2v} symmetry and equal abundance could not be distinguished from one set of equivalent C_1 sites.

Results and Discussion

To demonstrate the practical usefulness of this isotopic dilution method, an effort has been made to provide examples of most of the effective NH_4^+ symmetries E of Table I. Infrared spectra of authenticated polycrystalline samples in Nujol mulls at 80 K were obtained with a Perkin-Elmer Model 180 spectrophotometer. When necessary, additional cooling was achieved using an Air Products and Chemicals Inc. Cryo-Tip capable of maintaining a temperature of 22 K. Typical D content of a sample was 1%.

Site Symmetry T_d . Ammonium hexachlorostannate(IV), $(\text{NH}_4)_2\text{SnCl}_6$. In this compound, which is isostructural with $(\text{NH}_4)_2\text{PtCl}_6$,⁷ all ammonium ions are equivalent (cf. Figure 1 of ref 6). From Table I it would be expected that the isotopically isolated NH_3D^+ ion retains its C_{3v} symmetry and that all four N-D orientations are equivalent. The fundamentals $\nu_1(a_1)$ and $\nu_{4bc}(e)$ should thus each give rise to a single absorption band.

The N-D stretching and bending regions of $(\text{NH}_4)_2\text{SnCl}_6$ (1% D) (Figure 1) are seen to contain the expected features. The absorption arising from $\nu_1(a_1)$ consists of a very sharp, single band of about 5 cm^{-1} half-width, while that due to $\nu_{4bc}(e)$ appears as a considerably more intense absorption. Since the N-D stretching fundamental $\nu_1(a_1)$ at 2374.5 cm^{-1} is separated by about 120 cm^{-1} from the $2\nu_{4bc}(e)$ level at $2 \times$

$1246.4 = 2492.8\text{ cm}^{-1}$, no serious Fermi resonance is expected. The weak band observed at 2480 cm^{-1} and assigned to $2\nu_{4bc}$ confirms this expectation.

Site Symmetry C_{3v} . Ammonium hexafluorotitanate, $(\text{NH}_4)_2\text{TiF}_6$, is trigonal (space group $P\bar{3}m1$, No. 164)⁷ and isostructural with $\beta\text{-}(\text{NH}_4)_2\text{SiF}_6$ (cf. Figure 1 of ref 9). It contains only one type of ammonium ion. According to Table I two effective symmetries are possible for the NH_3D^+ ion at a C_{3v} site. These correspond to the N-D bond directed axially (C_{3v}) or nonaxially (C_s), and have a probability ratio of 1:3. The predicted absorptions for an isolated NH_3D^+ ion are then $\nu_1(a_1)$ for the axial and $\nu_1(a')$ for the nonaxial orientation, corresponding to $\nu_1(a_1)$ of T_d , and $\nu_{4bc}(e)$ for the axial and $\nu_{4b}(a') + \nu_{4c}(a'')$ for the nonaxial orientation, corresponding to $\nu_{4bc}(e)$ of T_d . We expect two bands in the N-D stretching region, in an intensity ratio of 1:3, and three bands in the N-D bending region. For the latter, the expected approximate intensity ratio is 2:3:3.⁸

The N-D stretching and bending regions of the infrared spectrum of $(\text{NH}_4)_2\text{TiF}_6$ (1% D) are shown in Figure 2. The two sharp bands attributed to $\nu_1(a_1)$ and $\nu_1(a')$ have an intensity ratio close to 1:3, as expected. The band due to ν_{4bc} appears as a shoulder on one of the more intense absorptions by the nonaxial NH_3D^+ ion.

Other examples have been reported earlier⁹: $\beta\text{-}(\text{NH}_4)_2\text{SiF}_6$, $(\text{NH}_4)_2\text{GeF}_6$, and $(\text{NH}_4)_2\text{Pb}(\text{SO}_4)_2$.

Site Symmetry S_4 . Ammonium periodate, NH_4IO_4 , has the tetragonal scheelite-type structure,⁷ with an environment of the ammonium ion as illustrated in Figure 1 of ref 10 for the isostructural NH_4ReO_4 . The ammonium ion in the periodate occupies a site of symmetry S_4 and is surrounded by eight oxygen atoms, four at a distance of about $2.9(3)\text{ \AA}$ and four at ca. $3.0(3)\text{ \AA}$.¹¹

For site symmetry S_4 we predict $E' = C_1(4)$. The N-D stretching and bending regions of isotopically isolated NH_3D^+ ions will thus be expected to contain one and two bands, respectively. The observed spectrum of NH_4IO_4 (1% D) (Figure 3) is in good agreement with the prediction. As was found to be the case in NH_4ReO_4 ,¹⁰ in NH_4IO_4 at liquid-nitrogen temperature all ammonium ions have the same orientation in the crystal. That this need not be so has been demonstrated in a previous study¹⁰ using this technique: in $(\text{NH}_4)_2\text{CuCl}_4 \cdot 2\text{H}_2\text{O}$ equivalent ammonium ions at sites of symmetry S_4 are divided between the two possible orientations.

Site Symmetry D_{2h} . Ammonium tetrachloropalladite(II), $(\text{NH}_4)_2\text{PdCl}_4$, is tetragonal, with all ammonium ions equivalent.⁷ The site point group D_{2h} is not a subgroup of T_d but of O_h . Ross¹² supposes that the ammonium ion in such circumstances undergoes free rotation to maintain the symmetry of the site. This may be the case at ambient or higher temperatures, but at low temperatures it seems more likely that the ions assume different orientations in the crystal. With isotopically isolated NH_3D^+ these different orientations are equivalent in that they yield identical spectral features. Figure 4 shows the immediate environment of an ammonium ion in this compound. The eight chlorine atoms are equidistant from the N atom, at about 3.33 \AA .¹³

Site symmetry D_{2h} can yield either C_{2v} or D_2 as the effective symmetry E of the ammonium ion, depending on the choice of symmetry operations from D_{2h} (Table I). The possible effective symmetries E' for NH_3D^+ are thus $C_s(2) + C_s(2)$ and $C_1(4)$, respectively. The single band due to $\nu_1(\text{NH}_3\text{D}^+)$ and the doublet due to $\nu_{4bc}(\text{NH}_3\text{D}^+)$ in the spectrum of $(\text{NH}_4)_2\text{PdCl}_4$ (1% D) (Figure 5) are only consistent with the latter.

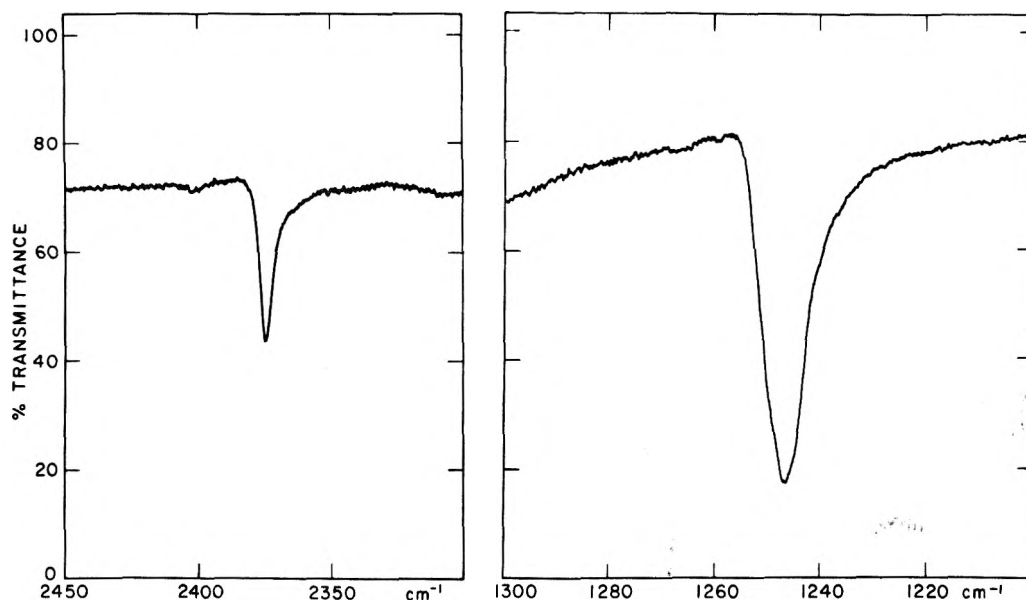


Figure 1. The N-D stretching and bending regions of the infrared spectrum of $(\text{NH}_4)_2\text{SnCl}_6$ (1% D) at 80 K.

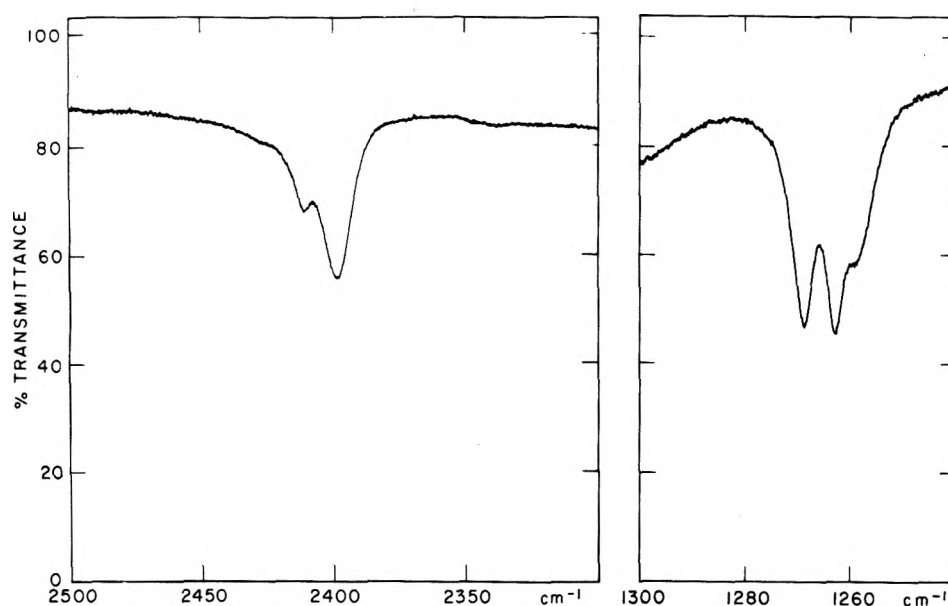


Figure 2. The N-D stretching and bending regions of the infrared spectrum of $(\text{NH}_4)_2\text{TiF}_6$ (1% D) at 80 K.

The splitting of $\nu_{4bc}(\text{NH}_3\text{D}^+)$ is not compatible with the free rotation of the ammonium ion suggested by Ross, hence we conclude that two orientations of NH_4^+ relative to the crystallographic axes occur in the crystal, both completely equivalent for an isotopically isolated NH_3D^+ ion. In a crystal of the undeuterated compound the two orientations of the NH_4^+ ion could be distributed at random or arranged in an ordered manner. A random distribution can be realized in the space group $P4/mmm$ (No. 123), which is the space group of the isostructural K_2PtCl_6 , if the equipoint 16(u) is half-occupied by H atoms, four about each nitrogen. The ordered arrangement is realizable in a subgroup of $P4/mmm$, $P422$ (No. 89), if the H atoms are placed in the 8(p) equipoint; the site symmetry at the N atom is then D_2 . Both distributions are compatible with the observed x-ray diffraction symmetry.

Site Symmetry C_2 . Phase V of ammonium nitrate, stable

at temperatures below -18°C , has been reported¹⁴ to be tetragonal and to contain ammonium ions at sites of symmetry C_2 . In the crystal structure refinement the four nonequivalent ammonium ions in the unit cell appear to have been constrained to be *metrically* equivalent. A schematic view of the surroundings of an ammonium ion in $\text{NH}_4\text{NO}_3(\text{V})$ is shown in Figure 6. The nearest neighbours of the ion are eight oxygen atoms, each deriving from a different NO_3^- group; four are at an N...O distance of 3.01 Å, two at 2.89 Å, and two at 3.10 Å.

The E' expected for an NH_3D^+ ion at a site of symmetry C_2 is $C_1(2) + C_1(2)$. This effective symmetry would manifest itself as two stretching modes arising from ν_1 , with an intensity ratio of 1:1, and four bending modes arising from ν_{4bc} . The N-D stretching region of $\text{NH}_4\text{NO}_3(\text{V})$ (1% D) at liquid-nitrogen temperature is shown in Figure 7. Instead of the expected two

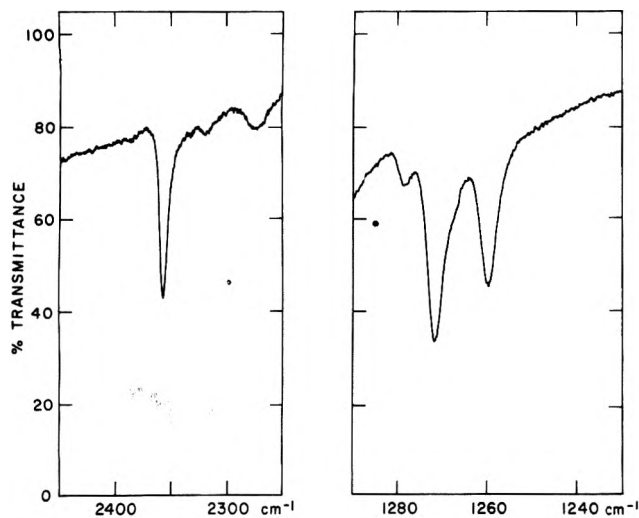


Figure 3. The N-D stretching and bending regions of the infrared spectrum of NH_4IO_4 (1% D) at 80 K.

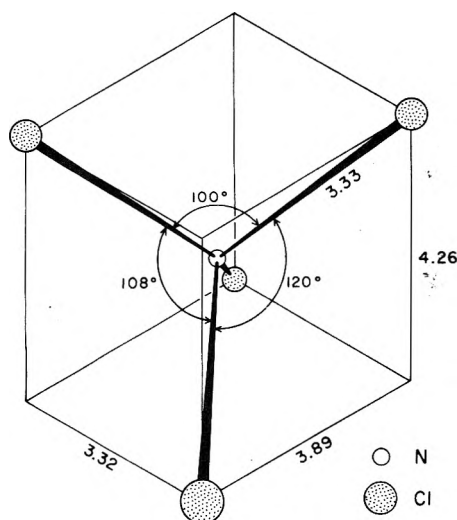


Figure 4. The immediate environment of an NH_4^+ ion in $(\text{NH}_4)_2\text{PdCl}_4$, after ref 7. The coordination about the ion consists of eight equidistant Cl atoms, arranged in two equivalent, approximately tetrahedral sets. Only one such set is shown in the figure. The distances are in Å.

bands we observe four bands of approximately equal intensities. Unfortunately, the N-D bending region of NH_4NO_3 is overlaid by intense anion absorptions.

The reported crystal structure can be reconciled with the existence of four components of ν_1 if each of the four nonequivalent sets of ammonium sites is populated by NH_4^+ ions in two different, structurally nonequivalent orientations of equal abundance at liquid-nitrogen temperature. Such a situation is geometrically conceivable. However, unless the energies of the two orientations are *closely* similar, or equal, one would expect the lower-energy orientation to become more abundant on further decrease of temperature, and this would be evident in the relative intensities of the four bands. To test this possibility, the NH_4NO_3 mull was cooled to 22 K, but the spectrum remained essentially unchanged. Annealing and maintaining the sample at 22 K for several hours produced no difference. The observed spectrum is consistent with the proposed crystal structure on this additional assumption of the NH_4^+ ions occurring in the crystal in two different orientations of very similar energies or of high potential barrier for reorientation.

Other possible interpretations may be considered:

(1) The assumed metric equivalence of unrelated ammonium ions at the four nonequivalent sites holds for *two pairs* of ion types instead for all four types, and only one orientation exists. This would be consistent with the observed occurrence of two pairs of closely spaced N-D stretching doublets.

(2) The proposed crystal structure is incorrect. In that case the possibility of $E = C_1$ would have to be considered.

(3) The observed spectrum is not that of $\text{NH}_4\text{NO}_3(\text{V})$ but of another phase. This is not very likely, for the four bands were present in spectra taken over a wide range of low temperatures; this range included the temperatures of the x-ray diffraction experiments of ref 14.

Attention is drawn to the narrowness of the observed four bands. Their half-widths are about 6 cm^{-1} at 80 K and less at 22 K. Bands as narrow as these would be consistent with the close metric similarity ("equivalence") of the NH_4^+ ions at the nonequivalent sites.

The result for $\text{NH}_4\text{NO}_3(\text{V})$ is inconclusive, but the NH_3D^+ spectrum has provided structural information *additional* to that deduced from the available x-ray diffraction study. At -18°C the bands are too broad to observe any changes in the

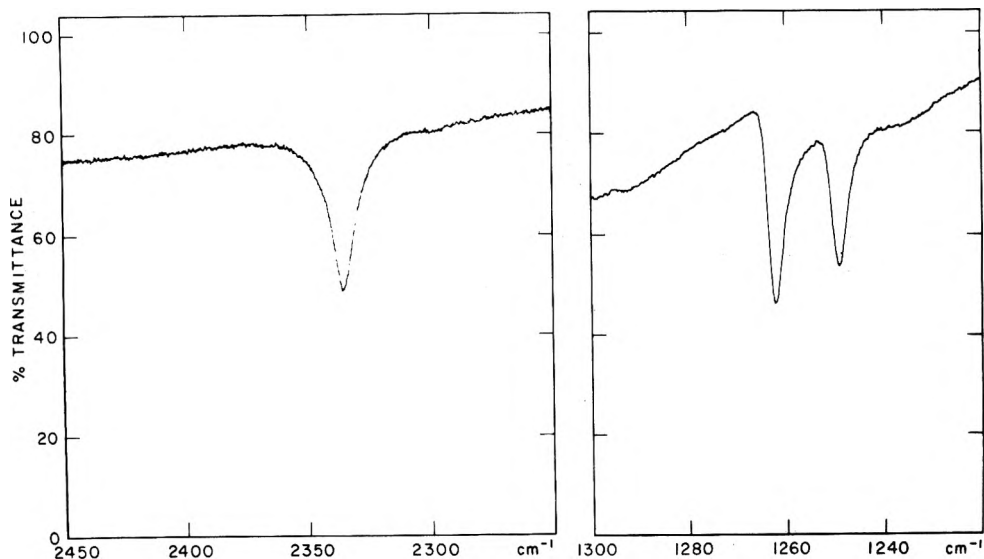


Figure 5. The N-D stretching and bending regions of the infrared spectrum of $(\text{NH}_4)_2\text{PdCl}_4$ (1% D) at 80 K.

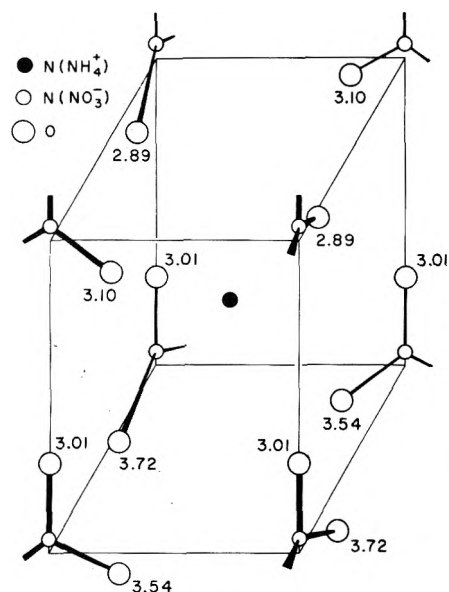


Figure 6. Surroundings of an ammonium ion in $\text{NH}_4\text{NO}_3(\text{V})$, after ref 14. Only one-eighth of the unit cell is shown. For clarity, some of the oxygen atoms have been omitted. The numbers indicate the distances (in Å) from the ammonium nitrogen.

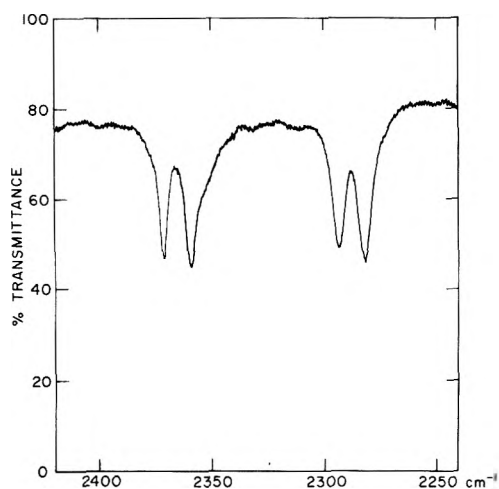


Figure 7. The N-D stretching region of the infrared spectrum of $\text{NH}_4\text{NO}_3(\text{V})$ (1% D) at 80 K.

spectral features that may be due to the IV \leftrightarrow V phase transition.

Site Symmetry C_1 . Determination of the crystal structure of ammonium oxalate monohydrate $(\text{NH}_4)_2(\text{COO})_2\cdot\text{H}_2\text{O}$, by x-ray¹⁵ and neutron¹⁶ diffraction has shown that all ammonium ions are equivalent and located at sites of symmetry C_1 . The immediate environment of an ammonium ion is shown in Figure 8.¹⁷ For this symmetry Table I leads us to expect four N-D stretching bands of equal intensity.

The N-D stretching region of $(\text{NH}_4)_2(\text{COO})_2\cdot\text{H}_2\text{O}$ (1% D) is shown in Figure 9. The band occurring at just under 2400 cm^{-1} is assigned to the O-D stretching mode of isotopically dilute HDO; the three bands in the 2280–2220- cm^{-1} region are attributed to components of $\nu_1(\text{NH}_3\text{D}^+)$. Of the latter group of bands the two at higher frequency are very sharp, $\nu_{1/2} = 6 \text{ cm}^{-1}$, while the half-width of the lowest-frequency band is about 12 cm^{-1} . The D...O distance is greatest for the N-D...O(w) bond and the corresponding N-D vibration is ex-

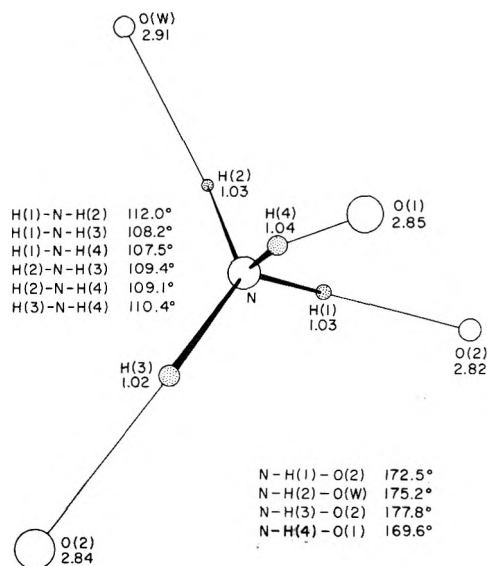


Figure 8. The immediate environment of an ammonium ion in $(\text{NH}_4)_2(\text{COO})_2\cdot\text{H}_2\text{O}$. The interatomic distances (in Å) and bond angles shown refer to the refinement from three-dimensional neutron-diffraction¹⁶ data; they do not differ substantially from those from three-dimensional x-ray intensities collected¹⁵ at 30 K.

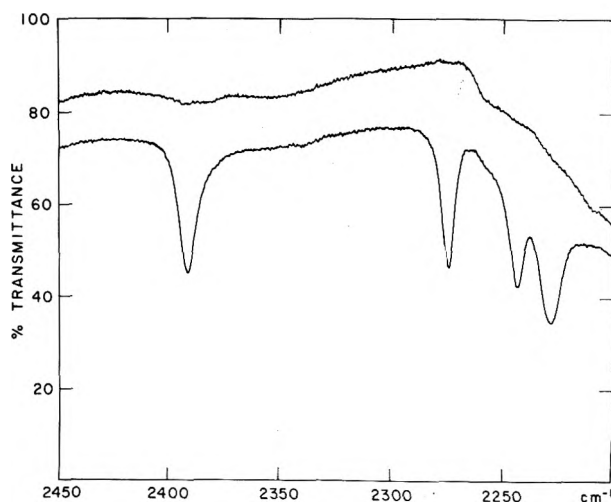


Figure 9. The N-D stretching region of the infrared spectrum of $(\text{NH}_4)_2(\text{COO})_2\cdot\text{H}_2\text{O}$ (1% D) at 80 K. The corresponding region of the spectrum of the undeuterated compound is shown for comparison.

pected to be of higher frequency than the others; the band at 2275 cm^{-1} is therefore assigned to this vibration. The band at lowest frequency has approximately twice the integrated intensity of either of the other two bands. From this we conclude that it represents the band envelope of two components of $\nu_1(\text{NH}_3\text{D}^+)$ whose band centers differ by 4 cm^{-1} or less. Attempts to resolve the components by cooling to 22 K were unsuccessful.

It is of interest to note that the O-D absorption is well clear of the NH_3D^+ absorptions, which permits ammonium salt hydrates to be investigated by this method.

Conclusions

The isotopic dilution technique appears to offer the best approach yet to the infrared spectroscopic study of ammonium ions in crystals. Introduction into the crystal of an ammonium compound of the NH_3D^+ ion at low concentration

makes it possible to obtain a spectrum which reflects the effective symmetry E' of this ion at its lattice site. The site symmetry S of the NH_4^+ in the undeuterated crystal may be deduced from E' , within the restrictions imposed by theory (Table I).

This method and the analysis presented in this paper are capable of natural extension to the PH_4^+ and BH_4^- ions and in principle to any tetrahedral species XY_4 in crystalline compounds.

Acknowledgment. This investigation was supported by a grant in aid of research from the National Research Council of Canada to one of us (O.K.).

References and Notes

- (1) NRCC No. 15064.
- (2) Postdoctoral Research Associate with Richard C. Lord, 1960–1962.
- (3) Our designation of vibrational modes follows that of G. Herzberg, "Infrared and Raman Spectra of Polyatomic Molecules", Van Nostrand, New York, N.Y., 1945.
- (4) D. S. Crockett and H. M. Haendler, *J. Am. Chem. Soc.*, **82**, 4158 (1960).
- (5) W. Rüdorff, J. Kändler, G. Lincke, and D. Babel, *Angew. Chem.*, **71**, 672 (1959); W. Rüdorff, J. Kändler, and D. Babel, *Z. Anorg. Allg. Chem.*, **317**, 261 (1962).
- (6) I. A. Oxtan, O. Knop, and M. Falk, *Can. J. Chem.*, **53**, 2675 (1975).
- (7) R. W. G. Wyckoff, "Crystal Structures", 2nd ed, Vol. 3. Interscience, New York, N.Y., 1965.
- (8) The doubly degenerate mode ν_{4bc} of an axial NH_3D^+ ion is expected to have approximately twice the intensity of either ν_{4b} or ν_{4c} of a nonaxial NH_3D^+ ion.
- (9) I. A. Oxtan, O. Knop, and M. Falk, *Can. J. Chem.*, **53**, 3394 (1975).
- (10) I. A. Oxtan, O. Knop, and M. Falk, *Can. J. Chem.*, **54**, 892 (1976).
- (11) These distances have been estimated assuming that the positional parameters of the oxygen atom in NH_4IO_4 are similar to those in $KReO_4$.⁷ An accurate determination of the crystal structure of NH_4IO_4 is not available.
- (12) S. D. Ross, "Inorganic Infrared and Raman Spectra", McGraw-Hill, London, 1972.
- (13) This distance and the angles shown in Figure 4 have been calculated on the assumption that the positional parameter of the Cl atom in $(NH_4)_2PdCl_4$ is 0.23.⁷ An accurate determination of the crystal structure of $(NH_4)_2PdCl_4$ is not available.
- (14) J. L. Amorós, F. Arrese, and M. Canut, *Z. Kristallogr.*, **117**, 92 (1962).
- (15) J. H. Robertson, *Acta Crystallogr.*, **18**, 410 (1965).
- (16) J. C. Taylor and T. M. Sabine, *Acta Crystallogr., Sect. B*, **28**, 3340 (1972).
- (17) The N...O(w) distance in ref 16 is stated incorrectly. It should be 2.910 Å for the neutron-diffraction refinement.

Infrared Frequency Effects of Lone Pair Interactions with Antibonding Orbitals on Adjacent Atoms

L. J. Bellamy*¹ and D. W. Mayo^{2,3}

Procurement Executive, Ministry of Defence, Explosives Research and Development Establishment, Powdermill Lane, Waltham Abbey, Essex, EN9 1BP England (Received February 9, 1976)

Publication costs assisted by a Du Pont Educational Grant to Bowdoin College

A study of infrared frequencies suggests that the lone pair effect, which is responsible for weakening of the CH bonds of OCH_3 and NH_3 groups and which results in a nonequivalence of methyl hydrogen atoms, appears to influence several other structural arrangements. It is suggested that similar interactions occur with $=CH_2$, $=CH$, NH_2 , NH , $=NH$, OH , and SiH bonds when these groups have a hydrogen atom positioned approximately trans to a lone pair orbital on an adjacent atom. The low CH stretching frequencies characteristic of aldehydes and of some $CH_2=N$ systems also may be interpreted in this way. The possibility that C–C, C–O, and other bonds are responsive to these effects is briefly considered.

1. Introduction

The exceptionally low symmetric CH stretching frequencies of CH_3 groups attached to oxygen or nitrogen atoms with a lone pair of electrons was first reported as long ago as 1957–1958,^{4–6} and subsequently it was shown that the involved frequencies rose to more normal values if the lone pair electrons were delocalized via resonance structures. Since that time the characteristic absorption near 2800 cm^{-1} has been widely used for the identification of OCH_3 and NCH_3 groups and much supporting data have accumulated.⁷ Correspondingly low frequencies have been found for CH_2 and CH groups when one of the hydrogen atoms is in a trans position to the lone pair.^{8,9} The suggestion that this effect originates in a donation of electrons from the lone pair into an antibonding orbital of a trans CH group was first put forward by Hamlow et al.¹⁰ This has been elaborated by others^{11,12} and has undergone general acceptance.

The impact of this effect, however, did not begin to become fully apparent until McKean et al.^{13–15} carried out elegant infrared studies on partial deuteration products of a wide variety of compounds such as dimethyl ether, trimethylamine, etc. The observation that two bands were apparently generated from a single CHD_2 group in the CH stretching region demonstrated unequivocally the nonequivalence of the methyl group hydrogen atoms, and the observed frequency separations (100 cm^{-1} for dimethyl ether, 153 cm^{-1} for trimethylamine) indicate that the inequalities are surprisingly large. If such separations are considered in light of McKean's¹⁵ empirical relationship between ν_{CH} and the bond dissociation energies, it seems clear that the differences between the individual CH bonds are of the order of 9–13 kcal and the differences in their activation energies could, of course, be even greater.

It has been rather firmly established that these low CH

stretching frequencies do not arise from artifacts of coupling or from Fermi resonance, but from a form of bond interaction which could be of considerable importance in the molecular properties of compounds found in many fields of chemistry, as, for example, in stereospecific biochemical reactions. As the interaction mechanism proposed involves donation into an antibonding orbital of the adjacent group there would seem to be no reason in principle why the effect should not operate very much more widely, being limited only by the efficiency of donation. We have, therefore, reviewed the existing data to see whether similar effects occur: with unsaturated CH₂ or CH groups; whether the lone pair can be donated from an unsaturated oxygen or nitrogen atom; and whether other XH bonds are affected. We have also looked briefly at the possibilities of lone pair interaction with bonds other than those of adjacent atoms to hydrogen atoms.

2. Data and Interpretation

A. Lone Pair Effects on XH Bonds other than CH. (1) *NH₂, NH Groups.* In view of the interaction observed with C-H bonds it would seem likely that a nitrogen atom might donate its lone pair into an antibonding orbital of an adjacent NH₂ or NH bond and this seems to be the case and to be well substantiated by the partial deuteration studies of Hadzi et al.¹⁶ on substituted hydrazines. These studies are particularly interesting in that they demonstrate the potentially large impact of such donation effects. Thus, it is observed in *uns*-dimethylhydrazine that two NH stretching bands occur at 3371 and 3190 cm⁻¹, while in the NHD isotopic derivative two bands are found at 3362 and 3197 cm⁻¹. From these observations it is clear that the individual NH bonds differ in frequency by 165 cm⁻¹ and that the effect of coupling these N-H frequencies is relatively small, as it increases the separation by only 16 cm⁻¹. Similar results are observed in a number of other hydrazine derivatives. *It would, therefore, be more appropriate to describe the two NH stretching bands of these NH₂ compounds as separate stretching modes of two slightly different NH bonds, which are only weakly affected by coupling, rather than by the conventional designations of antisymmetric and symmetric vibrations.*

These authors do not discuss the CH₃ symmetric stretching frequencies of *uns*-dimethylhydrazine, but values are assigned for these vibrational modes by Durig et al.¹⁷ as 2816 and 2777 cm⁻¹. Similar low values have been identified in *s*-dimethylhydrazine¹⁸ and in methylhydrazine.¹⁹ These observations indicate that the donation of the lone pair of a central nitrogen atom into an antibonding orbital of a trans NH bond, does not totally monopolize the interaction and that a simultaneous donation into an alternate CH bond trans to the lone pair may occur.

In addition, Hadzi et al.¹⁶ have shown that there are two different NH stretching bands in *s*-diphenylhydrazine indicating that the NH group, as well as NH₂ groups, respond to lone pair interactions. It was also observed that two NH stretching bands occur in the partially deuterated series C₆H₅CH=NNHD, indicating that lone pair donation may occur from an unsaturated sp² nitrogen atom into the adjacent N-H orbital.

It might have been expected that the oxygen atom of hydroxylamine would also be capable of donating electrons into a suitably oriented NH bond, but studies on hydroxylamine and on its methyl derivatives²⁰ suggest that the preferred conformations are such that the oxygen lone pairs are not predominantly trans to an NH bond, and indeed, a rise toward

normal symmetric NH₂ stretching frequencies and normal coupling separations are observed in this series.

It also appears that =NH bonds will interact if suitably positioned. For example, in the *cis* form of the unstable species, diimide (NH=NH), the NH stretching frequency appears at the low value of 3070 cm⁻¹.²¹ It is unfortunate that in the *trans* form of diimide, in which an interaction with the nitrogen lone pairs would not be expected to occur, symmetry dictates that the NH band is too weak to be identified. The value for the *cis* form, however, is clearly very much less than for normal imines or for methyleneimine (3280 cm⁻¹).^{22,23}

(2) *OH Groups.* The assessment of lone pair effects on OH bonds obviously cannot be demonstrated by partial deuteration studies, and therefore, these interactions can only be established, if at all, by inference. For example, hydrogen peroxide is known to have a skew conformation in which no interactions with *trans* OH groups are possible. This system absorbs at 3610 cm⁻¹. The sharp drop from this value to 3530 cm⁻¹ for hydroperoxides is large in relation to the expected influence of the inductive effect of the R group at the β position and might well arise from a *trans* lone pair effect. The very low OH stretching frequency of 3414 cm⁻¹ observed for the monomeric radical -OOH²⁴ is also a potential case of *trans* lone pair donation. The most clear cut case in which lone pair interactions would appear to operate, however, is that of nitrous acid. This molecule has been demonstrated to exist in the vapor in both *cis* and *trans* forms. The OH stretching frequencies of these two forms are *cis* 3426 cm⁻¹ and *trans* 3590 cm⁻¹.²⁵ If we take the OH stretching frequency (3610 cm⁻¹) of H₂O₂ to be representative of a noninteractive lone pair -OH bond system, the rather low value observed for the *cis* form of nitrous acid suggests that the drop in frequency is the result of a weakening of the OH bond through a lone pair donation. The large frequency differences between the OH, N=O, and other vibrations of these two forms are very difficult to account for on the basis of a simple change in the geometry of otherwise identical bonds. A contribution to the known differences in the polarity of *cis* and *trans* N=O bonds in simple alkyl nitrites may also arise via a similar route.²⁶

The OH stretching frequencies of oximes are also observed to occur in the 3640-cm⁻¹ region, and therefore, are presumably not influenced by any interaction with the nitrogen lone pair electrons. Such an interaction could only occur in oximes if the OH group was oriented *cis* to the N=C bond and it seems likely that oximes take the *trans* configuration which they must adopt when associated to form cyclic dimers and trimers.

(3) *SiH₃ Groups.* There is usually no effective separation of the antisymmetric and symmetric stretching frequencies of SiH₃ and SiH₂ groups. This is probably due to the relatively large mass of the silicon atom and its correspondingly small amplitude. In such silanes as have been studied at high resolution the band separation is usually only 2-3 cm⁻¹. It is, therefore, interesting to observe that in OSiH₃ and NSiH₃ groups (and apparently only in such groups), there is a substantial separation of ν_{as} and ν_s. For example, in H₃SiOCH₃ the splitting amounts to about 60 cm⁻¹ and in SiH₃(NCH₃)₂ the separation is about 50 cm⁻¹.^{27,28} This apparent coupling vanishes in resonant systems such as CH₃COOSiH₃.²⁹ It does, therefore, seem reasonable to assume that the SiH bonds are affected in a similar way as the CH₃ bonds of OCH₃ and NCH₃ compounds and that the majority of the splitting effect we are observing is the result of a lone pair interaction rather than simple mechanical coupling.

B. Interactions at an Unsaturated CH Group. The CH₂=C

TABLE I: Observed X-H Values

Ref	Compd	cm ⁻¹	Ref	Compd	cm ⁻¹	Ref	Compd	cm ⁻¹
a	H ₂ CO	2813	30	CD ₂ =CH ₂	3095, 3019	47	CH ₂ =N=N	3188, 3077
a	CH ₃ CHO	2770	30	CH ₂ =C=CD ₂	3084, 3013	38, b	XC ₆ H ₅ CH=N-C ₆ H ₅	2907-2886
a	NH ₂ CHO	2852	30	CH ₂ =CHCH ₃	3090, 3013	48	(CH ₃) ₂ N-N=CH ₂	3081, 2947
a	HC≡CCHO	2858	30	CH ₂ =CHCl	3124, 3038	49	CH ₂ =N-N=CH ₂	3072, 2940
a	HCOOCH ₃	2943				50	CH ₂ =NOH	3098, 2976
a	HCOOH	2947	24	-OOH	3414	c	C ₃ H ₇ CH=NOH	2870 (Raman value)
			21	<i>cis</i> -NH=NH	3070			
46	HCOSH	2850				22, d	CH ₂ =NH	3032, 2936
46	HCOS ⁻ Na ⁺	2810				40	CH(NH ₂)=NOH	2824
						51	CH ₂ =NCH ₃	3005, 2894

^a From Table II ref 15. ^b 27 examples: Band vanishes at these wavenumbers on coordination at N atom. ^c Spectrum 55 of ref 41. ^d H's nonequivalent by deuteration.

group has antisymmetric and symmetric CH stretching frequencies near 3095 and 3019 cm⁻¹ (values for CH₂=CD₂),³⁰ with a separation close to 76 cm⁻¹. Duncan³⁰ has shown that this separation is a function of the HCH bond angle and is independent of the frequencies themselves provided the angle remains close to 120°. It has been observed that in ketene, for example, the frequencies rise to 3166 and 3070 cm⁻¹, but that the band separation remains roughly the same as in CH₂=CD₂. Some of Duncan's data is included in Table I. A single sp² CH= group usually absorbs near 3030 cm⁻¹.

If donation can occur from an oxygen atom lone pair through a double bond into an antibonding orbital of a "trans" link, one would expect to find a large effect in formaldehyde where the system is presumably oriented for interaction and involves shorter distances and more effective overlap than in the OCH₃ type system. The low CH stretching frequencies of CH₂O, and other aldehydes (2770 cm⁻¹) are, of course, well known and have been the subject of several recent studies.^{31,32} If this frequency drop is partly the result of a lone pair effect one might expect to find somewhat higher CH stretching frequencies in compounds in which a resonance system competes for the availability of a carbonyl oxygen lone pair, just as in the case where OCH₃ and NCH₃ systems are incorporated into delocalized structures. In Table I data on a number of such compounds are given and it will be seen that there is, indeed, a substantial frequency rise on passing from acetaldehyde to methyl formate and to formic acid (2947 cm⁻¹). One might also expect that the inductive influence of the aldehyde substituent would produce predictable shifts within this series and this appears to be the case.³²

There would, therefore, seem to be reasonable grounds (see also later discussion of cyclopropanone) for proposing that the lone pair effect is operative through the C=O double bond and that it is at least partially responsible for the low CH stretching frequencies generally observed in aldehydes.³³

Substituent influence appears to be reflected in the relatively high CH stretching frequencies observed for CF₃CHO and CCl₃CHO (2851 cm⁻¹), examples in which there are no obvious possibilities for normal resonance competition. Although inductive effects might be expected to play a major role in raising these frequencies it is interesting to observe that in this case the orientation is such that "reverse trans donation" via the halogen bond would be in competition with oxygen lone pair donation into the aldehyde C-H bond. This effect would be similar to that observed in *p*-trifluoromethylaniline.³⁴ Further potential examples of this effect have been reported in completely saturated systems in which the donation of a lone pair is observed to be significantly reduced

by the presence of trans oriented halogen atoms positioned on a β carbon atom. A good case in point of this latter situation is that of secondary propanols. In particular it has been reported that the two CD stretching bands of CH₃CDOHCH₃, corresponding to the two conformers, are separated by 73 cm⁻¹,⁹ but this frequency separation falls to less than half this value in CF₃CDOHCF₃³⁵ and CH₃CDOHCF₃.³⁶

If aldehydes possess low CH stretching frequencies due to "trans" lone pair interactions via the double bond, it might be anticipated that similar perturbed CH stretching frequencies would occur in systems containing the CH₂=N group. In Table I are listed the CH₂= and CH= stretching frequencies of a number of representative compounds of this kind. It will be seen that CH₂=N=N which has no lone pair available for donation from the central atom possesses the typically high frequencies of an sp² CH₂ group, but that the remainder of the series all show the CH₂ symmetric stretch at markedly lower values than diazomethane. In methylenimine itself, the CH₂ frequencies are at 3032 and 2936 cm⁻¹ and the CH bonds have been demonstrated to be nonequivalent.²² The substantial frequency shifts of ν_s as compared with the relatively small shifts of ν_{as}, and the consequent widening of their separation has been shown by Bellamy³⁷ to be an invariable result of inequalities in XH₂ bonds. It seems highly likely then that lone pair interactions are also involved in the origin of the low CH₂ symmetric stretching frequencies observed in this series of compounds. Indeed, if this were not the case it would be necessary to assume from the Duncan relationship that the HCH bond angles have opened out to values in excess of 130° which seems rather improbable.

Data on similar interactions with CH=N groups are limited because of the masking effects of alkyl groups. The extensive series of benzilidene anilines studied by Margerum and Sousa,³⁸ however, appear to demonstrate the effect. Such compounds would not be expected to possess CH stretching bands below 3030 cm⁻¹, but all examples studied thus far have a well marked band close to 2895 cm⁻¹ which could arise from the perturbed CH= stretching frequency. Moreover, related compounds in which the nitrogen lone pair is chelated to a metal atom, and, therefore, is not available for interaction, appear to have no absorption in this region.³⁹ In the case of formamidoxime,⁴⁰ in which the CH bond is subject to the influence of two trans lone pairs, the CH= stretching frequency is identified by a well-defined band at 2824 cm⁻¹. Comparison studies of the syn and anti forms of aldoximes would be of particular interest in this regard as only one form should be capable of undergoing the interaction. In the infrared, the 2900-cm⁻¹ region is overlaid by broad H-bonded OH bands,

even at high dilutions. It is interesting to note, however, that in the Raman spectrum of butyraldehyde oxime, where this masking interference is eliminated because of the weak scattering by the OH group, there is observed a strong band at 2870 cm^{-1} . This band is absent from the corresponding spectrum of 2-butanone oxime.⁴¹

Preliminary evidence would, therefore, seem to indicate that lone pair effects are also operating in $\text{N}=\text{CH}$ systems by similar mechanisms as identified in aldehydes. It appears, however, that the shifts produced are rather less than those found in aldehydes. This drop in the efficiency of electron donation observed in the nitrogen series may well be related to the shift in lone pair orbital hybridization to sp^2 from p in the oxygen series which should tend to depress the "trans" mechanism of donation.

C. Evidence Other than Infrared Data for the Lone Pair Effect. Trans effects of the magnitude observed above would be expected to be reflected in chemical reactivities, and there is a good deal of evidence that this is so. For example, a C-H group will not normally react with ozone as does an aldehyde CH, but it will do so if it is attached to two oxygen or nitrogen atoms provided their conformation is such that the hydrogen atom is trans to two separate lone pairs.⁴² β -Glucopyranoses which have this form react whereas α -glucopyranoses do not.

Reactions have also been reported which suggest the possibility that trans lone pair effects also may operate on C-C, C-O, and C-N bonds as well as on XH bonds. In *N*-disubstituted imidates,⁴³ the course of the reaction with alkali, and the nature of the hydrolysis products, depends wholly on the initial orientation of the alkoxyl group. This orientation determines whether it is the C-O or C-N bond of the tetrahedral intermediate which is trans to two separate lone pairs, and therefore, becomes the point of fission. One isomer, thus, yields an amine and an ester, while the other isomer gives an amide and an alcohol. A similar treatment of the tetrahedral intermediates for the reaction of other carbonyl groups with alkali provides a clear rationalization for the cleavage mechanisms of such reactions as the Cannizzaro, haloform, benzilic rearrangement, and for that matter many others.⁴²

There is also some physical evidence that bonds other than X-H may be subject to trans lone pair effects. For example, the NMR quadrupole coupling of chlorine in C-Cl bonds of α -chloroethers varies with the orientation of the oxygen lone pair.⁴⁴ In addition, Jorgensen and Salem¹² have remarked on the lengthening of the $\text{C}_1\text{-C}_2$ bonds of cyclopropanone (1.58 \AA) as compared with cyclopropane (1.51 \AA). The parallel of this case with the lengthening of the CH bonds of formaldehyde is a clear one.

3. Conclusion

It seems very probable, therefore, that the *trans lone pair effect* is a widespread chemical phenomenon affecting many different types of bonds. It appears on the basis of the current limited data that the interaction is most effective in the donation from lone pair orbitals into X-H bonds. One piece of infrared evidence which tends to support this latter view is the work of Kreuger et al.⁹ This group has suggested that in alcohols there is a small rise in ν_{OH} when the oxygen lone pair is trans to a CH bond, and thus in a donating orientation but none when it is trans to a C-C bond. The evidence supporting this conclusion is the broadening of the OH bands of primary and secondary alcohols and the gradual frequency

rise from tertiary alcohols to methanol. This study does not appear to be entirely conclusive as Van der Maes and Lutz⁴⁵ have not found the OH band of methanol to be significantly sharper than those of a number of primary alcohols and they have also demonstrated multiple OH peaks in tertiary alcohols. They prefer, therefore, to ascribe the frequency shifts to normal substituent effects.

References and Notes

- (1) Collaborator in eighteen infrared summer programs with Richard C. Lord.
- (2) B.S. degree (1952) and Postdoctoral Research Associate (1959-1960) with Richard C. Lord.
- (3) On leave during Spring 1975 from the Department of Chemistry, Bowdoin College, Brunswick, Maine 04011.
- (4) H. B. Henbest, G. D. Meakins, B. Nicholls, and A. A. Wagland, *J. Chem. Soc.*, 1462 (1957).
- (5) J. T. Braunholtz, E. A. V. Ebsworth, F. G. Mann, and N. Sheppard, *J. Chem. Soc.*, 2780 (1958).
- (6) R. D. Hill and G. D. Meakins, *J. Chem. Soc.*, 760 (1958).
- (7) L. J. Bellamy, "The Infrared Spectra of Complex Molecules", 3rd ed, Wiley, New York, N.Y., 1975.
- (8) F. Bohmann, *Chem. Ber.*, 91, 2157 (1958).
- (9) P. J. Kreuger, J. Jan, and H. Weiser, *J. Mol. Struct.*, 5, 375 (1970).
- (10) H. P. Hamlow, S. Okuda, and N. Nakagawa, *Tetrahedron Lett.*, 2553 (1964).
- (11) J. A. Pople, *Tetrahedron*, 30, 1605 (1974).
- (12) W. J. Jorgensen and H. Salem, "The Organic Chemists Book of Orbitals", Academic Press, New York, N.Y., 1973, p 38.
- (13) A. Allan, D. C. McKean, J. P. Perchard, and M. L. Josien, *Spectrochim. Acta, Part A*, 27, 1409 (1971).
- (14) D. C. McKean, *Chem. Commun.*, 1373 (1961).
- (15) D. C. McKean, J. L. Duncan, and L. Batt, *Spectrochim. Acta, Part A*, 29, 1037 (1973).
- (16) D. Hadzi, J. Jan, and A. Ocvirk, *Spectrochim. Acta, Part A*, 25, 97 (1969).
- (17) J. R. Durig and W. C. Harris, *J. Chem. Phys.*, 51, 4457 (1969).
- (18) J. R. Durig and W. C. Harris, *J. Chem. Phys.*, 55, 1735 (1971).
- (19) P. Kreuger and J. Jan, *Can. J. Chem.*, 48, 3227 (1970).
- (20) M. Davies and N. D. Spiers, *J. Chem. Soc.*, 3971 (1959).
- (21) K. Rosengren and G. C. Pimentel, *J. Chem. Phys.*, 43, 507 (1965).
- (22) C. B. Moore, G. C. Pimentel, and T. D. Goldfarb, *J. Chem. Phys.*, 43, 63 (1965).
- (23) D. E. Milligan, *J. Chem. Phys.*, 35, 1490 (1961).
- (24) D. E. Milligan and M. E. Jacob, *J. Chem. Phys.*, 38, 2627 (1963).
- (25) L. H. Jones, R. M. Badger, and G. E. Moore, *J. Chem. Phys.*, 19, 1599 (1951).
- (26) L. J. Bellamy, C. P. Conduit, R. J. Pace, and R. L. Williams, *Trans. Faraday Soc.*, 55, 1677 (1959).
- (27) G. S. Weiss and G. R. Nixon, *Spectrochim. Acta*, 21, 203 (1965).
- (28) M. J. Butler and D. C. McKean, *Spectrochim. Acta*, 21, 485 (1965).
- (29) A. G. Robiette and J. C. Thompson, *Spectrochim. Acta*, 21, 2023 (1965).
- (30) J. L. Duncan, *Spectrochim. Acta, Part A*, 26, 429 (1970).
- (31) G. Lucczeau and C. Sandorfy, *Can. J. Chem.*, 48, 3694 (1970).
- (32) S. L. Rock and R. M. Hammaker, *Spectrochim. Acta, Part A*, 23, 1899 (1971).
- (33) Professor N. Sheppard, University of East Anglia, has independently arrived at a similar interpretation of this effect, private communication.
- (34) J. D. Roberts, R. L. Webb, and E. A. McElhill, *J. Am. Chem. Soc.*, 72, 408 (1950).
- (35) J. Murto, A. Kivinen, R. Viitala, and J. Hyomaki, *Spectrochim. Acta, Part A*, 29, 1121 (1973).
- (36) J. Murto, A. Kivinen, K. Edelmann, and E. Hassinen, *Spectrochim. Acta, Part A*, 31, 479 (1975).
- (37) L. J. Bellamy and R. J. Pace, *Spectrochim. Acta, Part A*, 28, 1869 (1972).
- (38) J. D. Margerum and J. A. Sousa, *Appl. Spectrosc.*, 19, 91 (1965).
- (39) A. Bigotto and G. DeAlti, *Spectrochim. Acta, Part A*, 30, 27 (1974).
- (40) W. J. Orville Thomas and A. E. Parsons, *Trans. Faraday Soc.*, 54, 460 (1958).
- (41) F. R. Dollish, W. G. Fateley, and F. F. Bentley, "Characteristic Raman Frequencies of Organic Compounds", Wiley, New York, N.Y., 1974, Spectra 55 and 56.
- (42) P. Deslongchamps, P. Atlani, D. Fréhel, A. Malaval, and C. Moreau, *Can. J. Chem.*, 52, 3651 (1974).
- (43) P. Deslongchamps, C. Lebreux, and R. Taillefer, *Can. J. Chem.*, 51, 1665 (1973).
- (44) E. A. C. Lucken, *J. Chem. Soc.*, 2954 (1959).
- (45) J. H. Van Der Maes and E. T. C. Lutz, *Spectrochim. Acta, Part A*, 30, 2005 (1974).
- (46) R. Engler and G. Gattow, *Z. Anorg. Allg. Chem.*, 78, 388 (1972).
- (47) C. B. Moore and G. C. Pimentel, *J. Chem. Phys.*, 40, 342 (1964).
- (48) W. G. Harris, F. L. Glenn, and L. B. Knight, *Spectrochim. Acta, Part A*, 31, 11 (1975).
- (49) J. F. Ogilvie and H. C. Cole, *Spectrochim. Acta, Part A*, 27, 877 (1971).
- (50) S. Califano and W. Luttkie, *Z. Phys. Chem.*, 6, 83 (1956).
- (51) J. Henze and R. F. Curl, *J. Am. Chem. Soc.*, 86, 5068 (1964).

Rotational Structure of the (0-0) Visible Band of Glyoxal- d_1 . A Reanalysis¹

A. R. H. Cole,^{*2} K. J. Cross,

School of Chemistry, University of Western Australia, Nedlands, Western Australia 6009

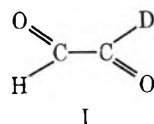
and D. A. Ramsay

National Research Council, Ottawa, Canada (Received January 26, 1976)

The (0-0) band in the gas-phase visible absorption spectrum of monodeuterioglyoxal has been remeasured at high resolution and reanalyzed. Many subbands have been assigned to higher J values than previously and, by use of a line-fitting program, statistically significant values of the centrifugal distortion constants have been determined. Values of the major rotational constants previously measured by Paldus and Ramsay have been confirmed.

I. Introduction

The $\pi^* \rightarrow n$ visible absorption bands of *trans*-glyoxal and its isotopically substituted analogues near 4550 Å have been the subject of a comprehensive investigation under high resolution by Paldus and Ramsay,³ Birss et al.⁴ and Agar et al.⁵ The initial analysis of the (0-0) band of glyoxal- d_1 (I) by



Paldus and Ramsay³ was somewhat incomplete because it was based on the method of combination differences. In many of the subbands the range of J for which suitable lines could be assigned in more than one branch was quite restricted, and it was not possible to obtain statistically significant values of the centrifugal distortion constants. Subsequent analyses of other bands of these systems^{4,5} have been carried out by using a line-fitting program,⁶ and this method has been used in the present work.

Glyoxal- d_1 is an asymmetric top ($\kappa = -0.977$ in the ground state) and its rotational levels are controlled by quantum numbers J , K_a , and K_c . Since the molecule is almost a prolate symmetric top, K_a is expected to behave like the symmetric top K . The nature of the visible absorption band of glyoxal has been described in the earlier papers,³⁻⁵ and only the salient points will be summarized here. The transition gives rise to a type C band, which, for high values (>3) of K_a , resembles a perpendicular band of a symmetric top. For low values of K_a , however, the energy levels, and hence the subbands, are split by K -type doubling (Figure 1). Unlike glyoxal and dideuterioglyoxal, there is no intensity alternation in the J lines of the split subbands, because the monodeuterio compound has no center of symmetry.

The change in rotational constants on excitation is relatively large ($A' > A''$, $B' < B''$, $C' < C''$) so that the subbands corresponding to $\Delta K_a = +1$ consist predominantly of R branches, which converge markedly to form band heads, and Q branches, which diverge fairly rapidly to low wave numbers (Figure 2), while those for $\Delta K_a = -1$ are characterized by similar Q branches plus P branches which diverge more rapidly in the direction of low frequencies (Figure 3).

II. Experimental Section

Monodeuterioglyoxal was prepared by oxidation of 1,1-dideuterioethylene with a mixture of selenium dioxide and phosphorus pentoxide at about 200 °C. The spectrum was photographed on Kodak III-0 plates in the thirteenth order of a 7.3-m Ebert spectrograph (resolving power $\sim 600\,000$) with the samples in a 2-m cell at a temperature of 213 K and a pressure of 60 Pa (0.5 Torr). This resolving power corresponds to an isolated line width of about 0.035 cm^{-1} at $22\,000\text{ cm}^{-1}$. Emission lines from an iron hollow cathode lamp were photographed adjacent to the glyoxal absorption spectrum for calibration. The iron lines were recorded in all orders of the spectrum (by removing the order-sorting prism) in order to give a sufficient density of calibration lines. The plates were measured using a comparator fitted with a photoelectric scanning device and standard wavelengths were taken from the tables of Crosswhite;⁷ vacuum corrections according to Edlén⁸ were applied. Independent measurements from different plates agreed to $\pm 0.003\text{ cm}^{-1}$.

III. Analysis and Results

As in the earlier work³⁻⁵ the analysis was commenced in the $\Delta K_a = +1$ region where strong R and Q branches of many subbands could be readily assigned. Extensive use of the asymmetric rotor computer program ASYROT⁶ was made in predicting line positions and progressively refining the rotational constants as the analysis was extended across the band center into the $\Delta K_a = -1$ region. In the early stages the "one state fit" option was employed whereby the excited state constants were constrained at values determined from the analysis of other bands involving the same upper level,^{3,9,10} but as the analysis neared completion "two state fits" were used to determine all 13 constants independently of other work.

In all, 1807 lines were assigned and, of these, 1779 were accepted by the computer and used to calculate the constants tabulated in Table I. Lines deviating from their predicted positions by more than 0.034 cm^{-1} were rejected; this is of the order of the isolated line width and represents only a minor discrepancy between theory and experiment. In general, rejected lines are blends, and since blending usually results in some change in peak position this accounts for the occasional

TABLE I: Rotational Constants from the (0-0) Band of Glyoxal-*d*₁

	This work ^a	Paldus and Ramsay ^b	($\nu_0-\nu_5''$) ^c	($\nu_0-2\nu_7''$) ^{a,d}
Ground State				
A''/cm^{-1}	$1.483\ 6 \pm 0.000\ 17$	$1.483\ 4 \pm 0.000\ 2$		
B''/cm^{-1}	$0.159\ 70 \pm 0.000\ 07$	$0.159\ 76 \pm 0.000\ 08$		
C''/cm^{-1}	$0.144\ 24 \pm 0.000\ 07$	$0.144\ 30 \pm 0.000\ 08$		
D_K''/cm^{-1}	$(1.00 \pm 0.06) \times 10^{-5}$	$(8.8 \pm 0.5) \times 10^{-6}$		
D_{JK}''/cm^{-1}	$(-2.9 \pm 1.5) \times 10^{-7}$			
D_J''/cm^{-1}	$(7.5 \pm 2.7) \times 10^{-8}$			
κ	$-0.976\ 9 \pm 0.000\ 15$	$-0.976\ 9$		
$\Delta^e/\text{g cm}^{-2}$	$(-0.08 \pm 0.12) \times 10^{-40}$	$(-0.10 \pm 0.14) \times 10^{-40}$		
Excited State				
A'/cm^{-1}	$1.569\ 4 \pm 0.000\ 16$	$1.569\ 5 \pm 0.000\ 2$	$1.569\ 8$	$1.569\ 9 \pm 0.000\ 9$
B'/cm^{-1}	$0.154\ 72 \pm 0.000\ 07$	$0.154\ 72 \pm 0.000\ 08$	$0.154\ 70$	$0.154\ 70 \pm 0.000\ 09$
C'/cm^{-1}	$0.140\ 79 \pm 0.000\ 07$	$0.140\ 81 \pm 0.000\ 08$	$0.140\ 82$	$0.140\ 81 \pm 0.000\ 09$
D_K'/cm^{-1}	$(1.64 \pm 0.05) \times 10^{-5}$	$(1.6 \pm 0.1) \times 10^{-5}$	1.4×10^{-5}	$(1.4 \pm 0.1) \times 10^{-5}$
D_{JK}'/cm^{-1}	$(-5.7 \pm 1.5) \times 10^{-7}$		-0.94×10^{-7}	$(-0.74 \pm 2.4) \times 10^{-7}$
D_J'/cm^{-1}	$(7.5 \pm 2.7) \times 10^{-8}$		3.7×10^{-8}	$(3.3 \pm 3.9) \times 10^{-8}$
κ	$-0.980\ 5 \pm 0.000\ 15$	$-0.980\ 5$	$-0.980\ 6$	
$\Delta/\text{g cm}^{-2}$	$(+0.06 \pm 0.12) \times 10^{-40}$	$(+0.09 \pm 0.15) \times 10^{-40}$	$+0.09 \times 10^{-40}$	
ν_0/cm^{-1}	$21\ 993.342 \pm 0.003$	$21\ 993.334$		

^a Errors quoted are 3 standard deviations. ^b Errors quoted are 5 standard deviations. ^c Reference 9. ^d Reference 10. ^e $\Delta = I_c - I_a - I_b$, I_x (g cm^{-2}) = $27.9908 \times 10^{-40}/X$ (cm^{-1}), where $X = A, B$, or C .

TABLE II: Sample of Results with Lines in Order of Wave Number

Upper State			Lower State			Rel intensity	Obsd	Calcd	Obsd - Calcd
<i>J</i>	<i>KA</i>	<i>KC</i>	<i>J</i>	<i>KA</i>	<i>KC</i>				
18	11	8	17	10	8	4.68	22 036.099	22 036.107	-0.008
36	13	24	36	12	24	2.34	22 036.026	22 036.025	0.001
17	11	6	16	10	6	4.74	22 035.953	22 035.953	0.000
16	11	6	15	10	6	4.78	22 035.786	22 035.792	-0.006
15	12	4	15	11	4	1.32	22 035.733	22 035.747	-0.014
37	13	25	37	12	25	2.29	22 035.733	22 035.714	0.019
15	11	4	14	10	4	4.83	22 035.620	22 035.622	-0.002
16	12	5	16	11	5	1.57	22 035.620	22 035.613	0.007
17	12	6	17	11	6	1.79	22 035.444	22 035.471	-0.027
14	11	4	13	10	4	4.87	22 035.444	22 035.444	0.000
38	13	26	38	12	26	2.24	22 035.404	22 035.394	0.010
18	12	7	18	11	7	1.99	22 035.324	22 035.320	0.004
13	11	2	12	10	2	4.92	22 035.248	22 035.257	-0.009
19	12	8	19	11	8	2.17	22 035.150	22 035.161	-0.011
39	13	27	39	12	27	2.18	22 035.055	22 035.067	-0.012
12	11	2	11	10	2	4.97	22 035.055	22 035.062	-0.007
20	12	9	20	11	9	2.32	22 035.018	22 034.994	0.024
11	11	0	10	10	0	5.03	22 034.853	22 034.859	-0.006
21	12	10	21	11	10	2.46	22 034.811	22 034.818	-0.007
40	13	28	40	12	28	2.12	22 034.742	22 034.731	0.011
22	12	11	22	11	11	2.55	22 034.645	22 034.633	0.012
23	12	12	23	11	12	2.68	22 034.419	22 034.440	-0.021
41	13	29	41	12	29	2.06	22 034.374	22 034.385	-0.011
24	12	13	24	11	13	2.77	22 034.219	22 034.240	-0.021
42	13	30	42	12	30	1.99	22 034.028	22 034.031	-0.003
25	12	14	25	11	14	2.84	22 034.028	22 034.030	-0.002
26	12	15	26	11	15	2.89	22 033.825	22 033.811	0.014
43	13	31	43	12	31	1.92	22 033.651	22 033.668	-0.017
27	12	16	27	11	16	2.93	22 033.590	22 033.585	0.005

slight difference between observed and calculated line positions. The 1779 accepted lines were fitted with a standard deviation of $0.013\ \text{cm}^{-1}$ by the constants listed. Table II shows a sample of the assignment details, and full details of the wave numbers and quantum numbers are contained in Table III.¹¹

The values obtained for the major rotational constants *A*,

B, and *C* for each level agree closely with those of Paldus and Ramsay³ and, in addition, good values are obtained for the centrifugal distortion constants D_K , D_{JK} , and D_J for each level.¹² Only D_{JK}' merits special comment since the values obtained from other bands^{9,10} differ from the present result (Table I). We are confident, however, that the present value

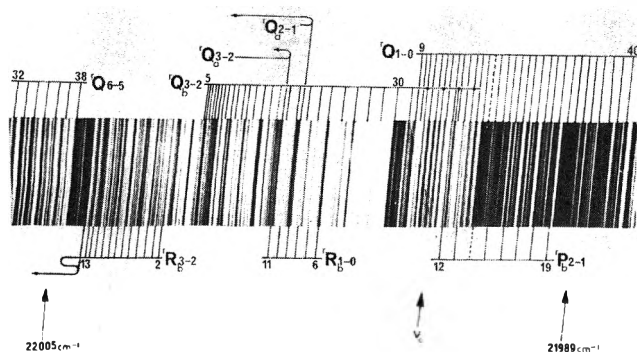


Figure 1. The region near the band center showing the effects of asymmetry on the subbands of low K_a .

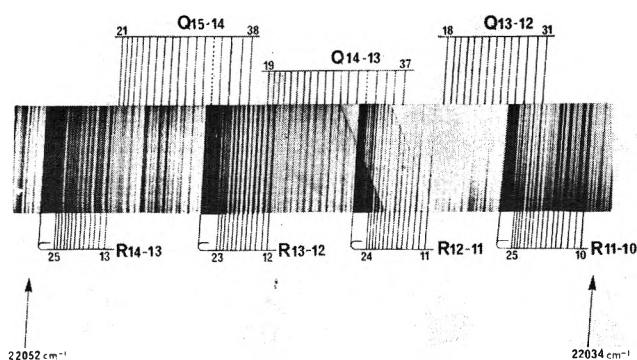


Figure 2. Section showing 'R and 'Q branches of subbands of high K_a .

is correct, since those found for $C_2H_2O_2^3$ and $C_2D_2O_2^5$ are -8.4×10^{-7} and $-2.4 \times 10^{-7} \text{ cm}^{-1}$, respectively. It might fairly be assumed that C_2HDO_2 would have a value of $D_{JK'}$ near the average of these two (-5.4×10^{-7}) and we obtain $-5.7 \times 10^{-7} \text{ cm}^{-1}$. Such an approximate average value also holds for the ground state $D_{JK''}$ where the values are: $C_2H_2O_2$, -0.39×10^{-6} ; C_2HDO_2 , -0.29×10^{-6} ; $C_2D_2O_2$, $-0.03 \times 10^{-6} \text{ cm}^{-1}$. The discrepancy between the present value of $D_{JK'}$ and those from $\nu_0-\nu_5''$ and $\nu_0-2\nu_7''$ almost certainly arises from the fact that overlap with neighboring bands prevented the assignments in those two bands from being followed to sufficiently high values of J and K_a .

IV. Concluding Remarks

The ultimate aim of this type of work is not the analysis of a single band of a molecule since the information available from a single band is limited in scope. Rather, an analysis of

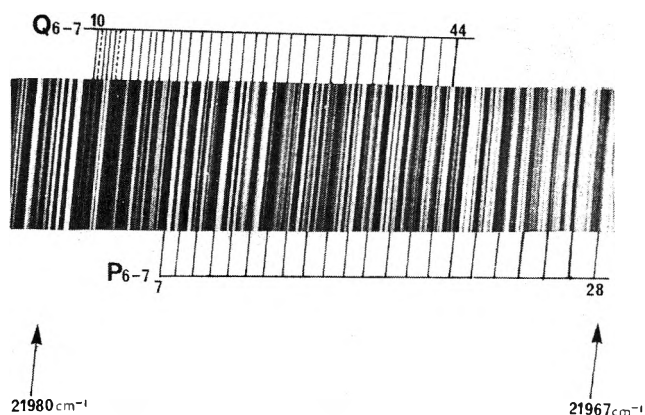


Figure 3. Section showing 'PQ and 'PP branches of subbands of high K_a .

as many bands as possible for as many isotopically substituted species as possible is desired. The information then to be derived falls into two classes which are related to each other: accurate molecular geometry and accurate molecular force fields. Such an analysis awaits the completion of the study of a number of other bands of monodeuteriogyoxal.

Acknowledgments. We wish to thank Mr. W. Goetz for photographing the bands and Dr. R. E. Pulfrey and Mr. M. Barnett for assistance with the computing.

References and Notes

- (1) Dedicated to Professor R. C. Lord on his retirement, and in acknowledgment of the high standard he has always set in spectroscopy.
- (2) Research Associate with R. C. Lord, Massachusetts Institute of Technology, 1959.
- (3) J. Paldus and D. A. Ramsay, *Can. J. Phys.*, **45**, 1389 (1967).
- (4) F. W. Birss, J. M. Brown, A. R. H. Cole, A. Lofthus, S. L. N. G. Krishnamachari, G. A. Osborne, J. Paldus, D. A. Ramsay, and L. Watmann, *Can. J. Phys.*, **48**, 1230 (1970).
- (5) D. M. Agar, E. J. Bair, F. W. Birss, P. Borrell, P. C. Chen, G. N. Currie, A. J. McHugh, B. J. Orr, D. A. Ramsay, and J.-Y. Roncin, *Can. J. Phys.*, **49**, 323 (1971).
- (6) F. W. Birss and D. A. Ramsay, unpublished.
- (7) H. M. Crosswhite, Johns Hopkins Spectroscopic Report, No. 13 (1958).
- (8) B. Edlén, *J. Opt. Soc. Am.*, **43**, 339 (1953).
- (9) G. A. Osborne and D. A. Ramsay, unpublished results on $\nu_0-\nu_5''$.
- (10) A. R. H. Cole, F. R. Honey, and D. A. Ramsay, unpublished results on $\nu_0-2\nu_7''$.
- (11) Table III comprises approximately 100 pages of computer print-out and is available, at a nominal charge, from the Depository of Unpublished Data, CISTI, National Research Council of Canada, Ottawa, Canada K1A052. Copies may be obtained on application to the Librarian.
- (12) Throughout the glyoxal project it has been found satisfactory to use the symmetric top centrifugal distortion constants. The program will handle τ 's but the analysis is not thereby improved.

Continuum and Discrete-Medium Theories of Radiative Transfer in Powders^{1a}

A. G. Emslie^{1b} and J. R. Aronson^{1c}

Arthur D. Little, Inc., 15 Acorn Park, Cambridge, Massachusetts 02140 (Received February 4, 1974)

Publication costs assisted by Arthur D. Little, Inc.

Continuum and discrete-medium theories of radiative transfer in powders are compared for the case of a two-beam model. It is found that the continuum theory gives a smaller value for the reflectance of a semiinfinite powder medium than does the preferred discrete-medium theory. However, the continuum theory can be made to agree with the discrete-medium theory if "effective" values of the absorption and scattering coefficients are used. These effective values are the K and S of the Kubelka-Munk theory, as found by experiment rather than by theory alone.

I. Introduction

In previous papers dealing with the spectral reflectance of mineral powders,^{2,3} we have pointed out that a continuum theory of radiative transfer such as that of Chandrasekhar⁴ is, in general, not appropriate for a scattering and absorbing medium composed of closely packed particles, but must be replaced by a noncontinuum theory. In this note, we compare the two types of theory quantitatively for the simple case of a two-beam radiative transfer model. The problem has also been discussed from a different point of view by Lathrop.⁵

II. Theories

In the continuum theory, the absorption and scattering properties of the individual particles are averaged over many particles and expressed as absorption and scattering coefficients which are continuous functions of position in the medium. This is valid for widely spaced particles, as occur in dust clouds,⁶ but not for closely packed particles in powders where the radiation intensity may change by a large fraction in a distance of the order of the particle size. To treat the dense particle case, one must replace the differential equations of the continuum theory by difference equations in which the spatial step or discontinuity is of the order of the particle size.

For simplicity, we consider only the case of a two-beam radiative transfer model with no emission of radiation by the particles. The continuum theory then takes the form of the well-known equations of Schuster⁷ or Kubelka-Munk⁸:

$$dI/dx = -(K + S)I + SJ \quad (1)$$

$$-dJ/dx = -(K + S)J + SI \quad (2)$$

where x is a spatial coordinate aligned with the two beams of intensities I , J in the forward and backward directions, respectively, and K , S are absorption and back-scattering coefficients related to the particle absorption and back-scattering cross sections σ_a and σ_s , and N , the number of particles per unit volume, by the relations:

$$K = N\sigma_a \quad (3)$$

$$S = N\sigma_s \quad (4)$$

One can calculate the cross sections σ_a and σ_s by Mie⁹ theory in the special case of spherical particles or by a more general method² for particles of arbitrary shape. The solutions of (1) and (2) are of the form

$$I = Ae^{-\gamma x} + Be^{\gamma x} \quad (5)$$

$$J = RAe^{-\gamma x} + \frac{1}{R}Be^{\gamma x} \quad (6)$$

where A and B are arbitrary constants, γ is the propagation constant, given by

$$\gamma = (K^2 + 2KS)^{1/2} \quad (7)$$

and R is the diffuse reflectance of a semiinfinite layer of the powder, given by

$$R = 1 + \frac{K}{S} - \left[\left(1 + \frac{K}{S} \right)^2 - 1 \right]^{1/2} \quad (8)$$

In the discrete medium theory, we consider that the particles are arranged in monolayers of thickness d and that each monolayer has an average reflectance ρ , transmittance τ , and absorptance α related by the energy conservation condition

$$\rho + \tau + \alpha = 1 \quad (9)$$

The differential equations (eq 1 and 2) are then replaced by the difference equations

$$I_{n+1} = \tau I_n + \rho J_{n+1} \quad (10)$$

$$J_n = \tau J_{n+1} + \rho I_n \quad (11)$$

where

$$n = x/d \quad (12)$$

denotes the n th monolayer measured from the surface of the powder, I_n is the intensity of the forward-directed beam incident on the n th monolayer, and J_n is the backward-directed beam leaving the n th monolayer.

The solution of (10) and (11) is

$$I_n = Cr^n + D \frac{1}{r^n} \quad (13)$$

$$J_n = \left(\frac{r - \tau}{\rho} \right) Cr^n + \left(\frac{1 - \tau}{\rho} \right) D \frac{1}{r^n} \quad (14)$$

where C and D are arbitrary constants and r is the intensity decay ratio of either the forward or the backward beam across one monolayer. The decay ratio is given by

$$r = \frac{1 + \tau^2 - \rho^2}{2\tau} - \left[\left(\frac{1 + \tau^2 - \rho^2}{2\tau} \right)^2 - 1 \right]^{1/2} \quad (15)$$

One can calculate³ the monolayer parameters α and ρ , and therefore τ from (9), from the particle cross sections σ_a and σ_s .

We obtain the discrete-medium reflectance R_d for a semi-infinite powder by putting $D = 0$ in (13) and (14) and solving for the ratio J_n/I_n .

$$R_d = \frac{\tau - \tau}{\rho} = \frac{1 + \rho^2 - \tau^2}{2\rho} - \left[\left(\frac{1 + \rho^2 - \tau^2}{2\rho} \right)^2 - 1 \right]^{1/2} \quad (16)$$

III. Results

We now compare the predictions of the two theories for the case of a medium composed of discrete layers with absorbance α and reflectance ρ . In order to apply the continuum theory to this noncontinuum situation, we suppose that α and ρ are simply averaged spatially to give continuum absorption and back-scattering coefficients $K = \alpha/d$ and $S = \rho/d$. Then

$$K/S = \alpha/\rho \quad (17)$$

Therefore, from (8) and (9), the continuum reflectance R_c is given by

$$R_c = \frac{1 - \tau}{\rho} - \left[\left(\frac{1 - \tau}{\rho} \right)^2 - 1 \right]^{1/2} \quad (18)$$

Figure 1 shows the error in R_c relative to R_d due to the averaging process, for various values of ρ and τ . It is seen that the discrete-medium theory always gives the larger reflectance and that the difference in the reflectances is quite large when a monolayer of particles interacts strongly enough with the radiation to produce significant values of ρ or α . Figure 1 shows that in the limiting case of small ρ and α (i.e., small ρ and large τ), the discrete-medium theory gives the same reflectance as the continuum theory, as one would expect. The curves for $\tau = 0$ also represent a limiting case, but one that would be unlikely to occur in practice.

IV. Discussion

It is worth noting that the solutions (5), (6) for the continuum theory and (13), (14) for the discrete-medium theory are both of exponential form. This suggests that the two theories will give identical results for both reflection and transmission through a powder layer of any thickness if "effective" values of K and S are used in the continuum theory.

Two conditions have to be met. First, the forward intensities I_n and I must change by the same factor over the distance $x = d$, corresponding to $\Delta n = 1$, for the case of a semiinfinite medium, for which $B = D = 0$. This condition gives

$$e^{-\gamma d} = \tau \quad (19)$$

Second, the ratio J/I must be the same as the ratio J_n/I_n for the semiinfinite medium. In other words, the reflectances must be the same. Thus, from (8) and (16)

$$1 + \frac{K_{\text{eff}}}{S_{\text{eff}}} = \frac{1 + \rho^2 - \tau^2}{2\rho} \quad (20)$$

From (19), (20), (7), and (15) one obtains for the effective continuum absorption and scattering coefficients.

$$S_{\text{eff}} = \frac{\ln [b + (b^2 - 1)^{1/2}]}{d(a^2 - 1)^{1/2}} \quad (21)$$

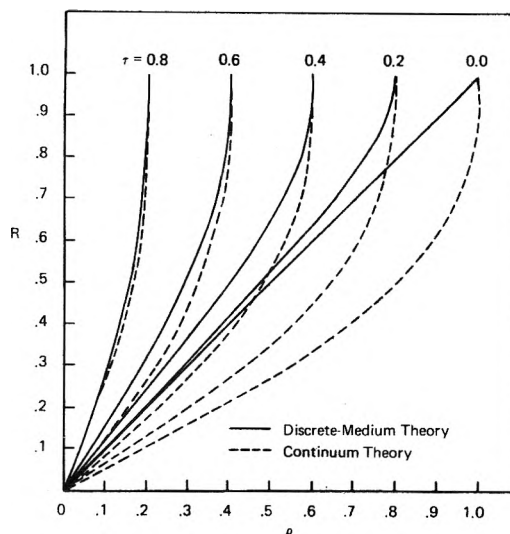


Figure 1. Comparison of reflectances for discrete-medium and continuum theories.

$$K_{\text{eff}} = (a - 1)S_{\text{eff}} \quad (22)$$

where

$$a = \frac{1 + \rho^2 - \tau^2}{2\rho} \quad (23)$$

$$b = \frac{1 + \tau^2 - \rho^2}{2\tau} \quad (24)$$

The foregoing considerations apply when one attempts to make radiative transfer calculations based on the optical properties, particle shape, and geometrical configuration of the particles in a powder. On the other hand, the great success of the Kubelka-Munk theory in the practical areas of paints and other pigmented coatings stems from the fact that this theory is only rarely based on first principles, but instead, depends on measured values of K and S for some standard coating to allow prediction of the optical performance of a similar coating of different thicknesses applied to a different substrate. It is to be noted that the measured values of K and S are really K_{eff} and S_{eff} defined by (21) and (22). In practice, therefore, the Kubelka-Munk theory bypasses the distinction between continuum and discrete-medium concepts.

References and Notes

- (1) (a) This paper is dedicated to Professor Lord on his 65th birthday and retirement. (b) Guest Lecturer in "The Physics of Infrared Radiation" course organized by Professor Richard C. Lord, 1958. (c) Postdoctoral Research Associate with Professor Richard C. Lord, 1958-1959.
- (2) A. G. Emslie and J. R. Aronson, *Appl. Opt.*, **12**, 2563 (1973).
- (3) J. R. Aronson and A. G. Emslie, "Applications of Infrared Spectroscopy and Radiative Transfer to Earth Sciences", in "Infrared and Raman Spectroscopy of Lunar and Terrestrial Minerals", C. Karr, Jr., Ed., Academic Press, New York, N.Y., 1975.
- (4) S. Chandrasekhar, "Radiative Transfer", Clarendon Press, Oxford, 1950 (reprinted by Dover, New York, N.Y., 1960).
- (5) A. L. Lathrop, *J. Opt. Soc. Am.*, **56**, 926 (1966).
- (6) J. R. Aronson and A. G. Emslie, *J. Geophys. Res.*, **80**, 4925 (1975).
- (7) A. Schuster, *Astrophys. J.*, **21**, 1 (1905).
- (8) P. Kubelka and F. Munk, *Z. Tech. Phys.*, **12**, 593 (1931).
- (9) G. Mie, *Ann. Phys.*, **25**, 377 (1908).

Vibrational Spectra of Synthetic Single Crystal Tephroite, Mn_2SiO_4 ^{1a}

H. D. Stidham,^{1b} J. B. Bates,* and C. B. Finch

Solid State Division and Metals and Ceramics Division, Oak Ridge National Laboratory, Oak Ridge, Tennessee 37830
(Received November 17, 1975)

Publication costs assisted by Oak Ridge National Laboratory

The Raman, infrared, and visible absorption spectra of synthetic tephroite, Mn_2SiO_4 , have been measured. The bands observed in the vibrational spectra are assigned to the $k \approx 0$ transverse optical modes of Mn_2SiO_4 , and several longitudinal optical mode frequencies of ν_3 were estimated from features observed in transverse magnetic reflection spectra. The Raman active components of the internal modes of SiO_4^{4-} do not appear to interact with the motions of Mn^{2+} ions, but the infrared components of ν_2 and ν_4 appear to be highly mixed with the external modes of the manganese sublattice.

Introduction

Numerous investigations of the vibrational spectra of minerals and microcrystalline preparations of silicates of the olivine structure have been reported. The early literature has been reviewed by Hohler and Funck.^{2a} Pure synthetic single crystals of the olivine forsterite, Mg_2SiO_4 , have been prepared, and the vibrational spectrum has been studied.^{2,3} No other study of the vibrational spectrum of a pure synthetic single-crystal silicate olivine appears to have been reported. The olivine structure readily substitutes a variety of metal ions without essential modification of the underlying silicate framework,⁴ and naturally occurring olivines are mixed crystals. More than half of the low-frequency lattice vibrations predicted for tephroite, Mn_2SiO_4 , were not observed in the spectrum reported for the mineral.^{2a}

The simplicity of the internal mode approximation makes it attractive for use in qualitative descriptions of the vibrations of the olivines, but some vibrations of the crystal are more complicated than is implied by its use. Some of the internal modes of the SiO_4^{4-} ions mix with the external modes as shown by Paques-Ledent and Tarte.⁵ The authors prepared ²⁶Mg substituted, powdered forsterite and found that most of the infrared bands below 475 cm^{-1} are sensitive to metal ion isotopic substitution, indicating participation of metal-ion sublattice motion in the ν_2 and ν_4 bending vibrations. The mixing of internal and external modes implied by this result should be somewhat relieved if an ion heavier than Mg^{2+} were used in synthesizing a pure synthetic silicate olivine, and its spectrum should provide some insight into the factors governing the extent of applicability of the internal mode approximation. The manganese ion was selected for use in this work because of the visible color it imparts to the crystal. Juxtaposition of the Mn^{2+} absorption bands in the crystal with the principal lines of the He-Ne and argon ion lasers used for excitation of the Raman spectra allows a search for a possible resonance Raman effect. Such an effect would be of interest if found, for the electronic transitions of an isolated Mn^{2+} ion are both spin and parity forbidden, while most resonance Raman spectra reported have involved electric dipole allowed electronic transitions.

In this paper the preparation of high-purity single-crystal synthetic tephroite is described. The visible, Raman, and infrared spectra of tephroite are reported, and a search for a

resonance Raman effect is discussed. An assignment of the vibrational spectrum is made using the internal mode approximation. The results are compared with those previously reported for forsterite and natural tephroite, permitting some tentative statements to be made about the nature of some of the low-frequency lattice vibrations, and the circumstances in which the internal mode approximation is qualitatively useful.

Experimental Section

The Mn_2SiO_4 tephroite single crystals were grown from the melt at $1315 \pm 5^\circ\text{C}$ and 1 atm total pressure by the Czochralski (pulling) method. To assure the divalent form of manganese, an oxygen partial pressure of 10^{-10} Torr was applied over the melt in the form of an argon-4% hydrogen gas current through the growth system. The melt was contained in a heavy walled (2-mm thick) platinum crucible which was inductively heated by a 410-kHz generator. The starting materials consisted of pelletized and intimately mixed powders of MnO (prepared by reduction of >99.999% pure MnO_2 with H_2 gas at 600°C) and of >99.999% pure SiO_2 . The apparatus and other crystal growth details are described elsewhere.⁷ Optically transparent, cylindrical crystals up to 1 cm in diameter \times 3 cm in length were grown from melts of a 2:1 molar MnO: SiO_2 composition. Growth rates of 3–10 mm/h with seed rotation at 10–25 rpm gave good growth results, although progressively slower rates were required as the melt deviated from an integral 2:1 MnO: SiO_2 stoichiometry due to MnO uptake by the platinum crucible. The rose-colored crystals were identified as Mn_2SiO_4 by x-ray diffraction. The following parameters were found for the orthorhombic unit cell: $a_0 = 4.875 \pm 0.002\text{ \AA}$; $b_0 = 10.521 \pm 0.003\text{ \AA}$; $c_0 = 6.238 \pm 0.003\text{ \AA}$. The measured density (Jolly balance) of $4.12 \pm 0.01\text{ g/cm}^3$ approximated that theoretically calculated from the unit cell parameters, viz. 4.191 g/cm^3 . The predominant cleavage plane is [010], and the Mohs hardness is approximately 6.5.

Samples were prepared for spectroscopic measurements from boules which had been oriented by x-ray diffraction. Axis orientation with respect to polished faces was checked with a polarizing microscope. The samples varied in size from $7 \times 7 \times 3\text{ mm}$ to $10 \times 3 \times 0.5\text{ mm}$, depending on the measurements to be made.

Polarized Raman spectra of Mn_2SiO_4 were measured with a modified Jarrell-Ash 25-300 spectrometer which has been

* Address correspondence to this author at the Solid State Division.

described elsewhere.⁸ The 488.0-nm line of a Coherent Radiation 52 argon ion laser operated at about 1 W was the usual source of excitation. A search for possible resonance Raman phenomena was conducted using the 514.5- (750 mw), 476.5- (250 mw), and 457.9-nm (150 mw) lines of the ion laser, and the 632.8-nm (50 mw) line of Spectra Physics 125 He-Ne laser. The emission lines of the ion laser plasma were used as frequency calibration standards. Spectra were recorded at 300 and at ~ 14 K from samples mounted in an Air Products CSA-202 closed-cycle helium refrigerator.

Polarized infrared reflectance spectra were obtained between 1200 and 200 cm^{-1} at room temperature with a Perkin-Elmer 621 spectrometer and between 400 and 50 cm^{-1} with a Digilab Model FTS-20 Fourier transform spectrometer. The spectrometers were equipped with a gold grid polarizer cast on AgBr (1200–400 cm^{-1}) and on polyethylene (400–50 cm^{-1}). Reflectance data were measured as a function of incidence angle in both transverse electric (TE) and transverse magnetic (TM) polarization using a modified Wilks attenuated total reflectance stage. The prism assembly was removed and replaced by a stainless steel sample mount attached to a slide that allowed the incidence angle to be varied continuously between limits of about 6° and nearly grazing. Infrared spectra of a Nujol mull of Mn_2SiO_4 were measured at 77 K using the FTS instrument. The mull was supported on CsI for the mid-ir region (1200–300 cm^{-1}) and on a silicon window for the far-ir region (300–50 cm^{-1}).

Visible and ultraviolet absorption spectra were obtained with the samples cooled to 14 K in the helium refrigerator using a Cary 15 spectrophotometer. Polarizations were determined by mounting a piece of optical grade Polaroid sheet in front of the sample and orienting it to pass the electric vector in either the vertical or horizontal direction. Sample polarizations were checked by rotating the crystals by 90° and remeasuring the spectra at 14 K.

Results and Discussion

A. Electronic Spectrum. The visible regions of the polarized electronic absorption spectra of Mn_2SiO_4 are displayed in Figure 1. A complete assignment of the electronic transitions of Mn^{2+} in tephroite is beyond the scope of this work, but the bands shown in Figure 1 are of interest in the attempts made at observing resonance Raman effects in this crystal. The bands in the 425–675-nm region correspond to single components observed at 425.3 and 514.2 nm in the spectrum of MnF_2 that were assigned to the ${}^6A_{1g} \rightarrow {}^4T_{2g}$ and ${}^6A_{1g} \rightarrow {}^4T_{1g}$ transitions, respectively, of octahedrally coordinated Mn^{2+} .⁹ Because the Mn^{2+} ions occupy C_s and C_i sites in Mn_2SiO_4 , the multiplicity of bands observed in the visible region may be caused by site splitting of the triply degenerate excited states. Furthermore, transition energies at the two types of non-equivalent sites may be different, which can also give rise to apparent multiplet splitting. The parity restriction on electric dipole transitions could be lifted for Mn^{2+} ions on the C_s sites. In any case, the ${}^6A_1 \rightarrow {}^4T_1$ and ${}^6A_1 \rightarrow {}^4T_2$ transitions are spin forbidden and therefore spin-orbit interaction is partly responsible for the appearance of the bands in Figure 1.¹⁰

The search for a resonance Raman effect was conducted using the laser lines indicated by dotted lines on Figure 1. Spectra recorded with different exciting lines were examined for changes in relative band intensities and for appearance of new features, especially in the low-frequency region. When the 632.8-nm line of the He-Ne laser was used, the sample emitted a broad, intense luminescence centered at ~ 707 nm at 14 K, and no Raman spectrum could be observed. Raman

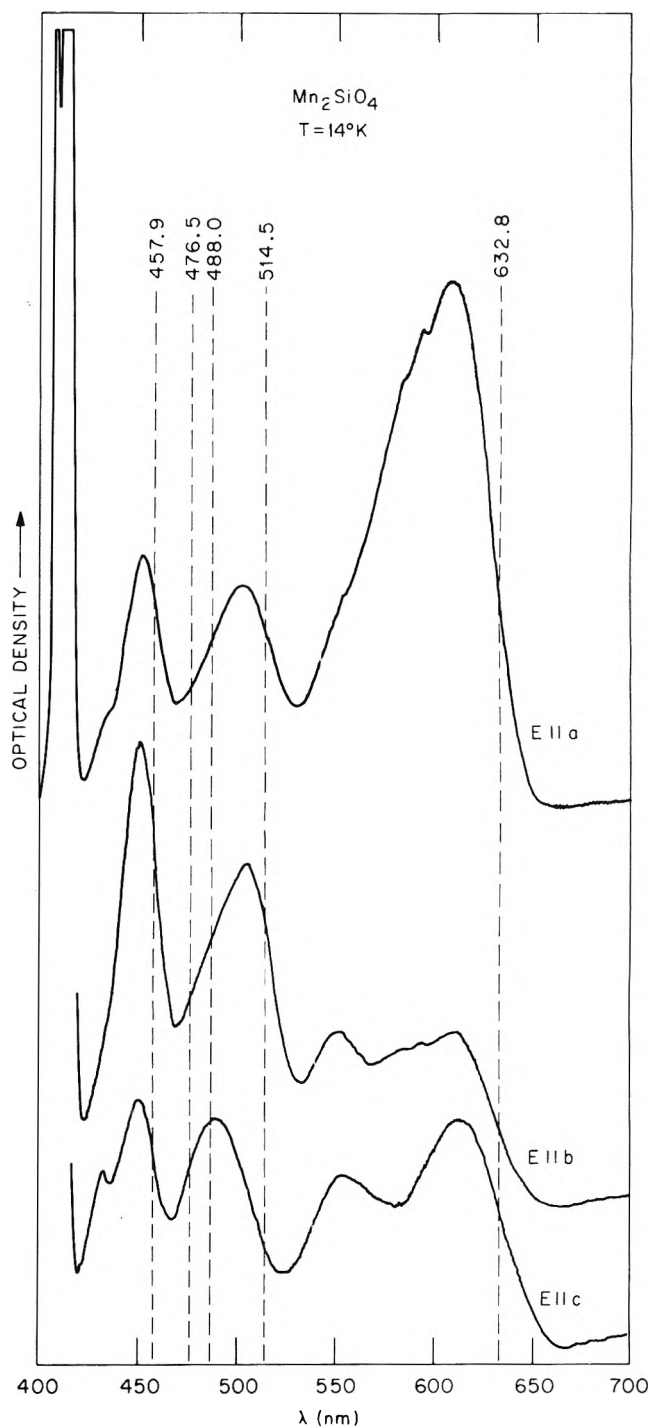


Figure 1. Visible absorption spectrum of tephroite at 14 K. The dotted lines represent the principal laser lines used to excite the Raman spectrum.

spectra of good quality were obtained from each of the other available laser lines. On changing the exciting line, none of the polarized spectra showed any changes in relative band intensities that could not be attributed to reabsorption effects, and no new features appeared in any region of the spectra. Our results, therefore, contain no evidence of any resonance Raman effects with the visible transitions of Mn^{2+} in tephroite. Similar negative results have been obtained on exciting into the optical band of a spin allowed but parity forbidden transition of Ni^{2+} in $\text{Rb}_2\text{NiCl}_4 \cdot 2\text{H}_2\text{O}$.¹¹

B. Vibrational Spectrum. 1. Internal and External

TABLE I: Symmetry Species for the Internal and External Modes of $\text{Mn}_2\text{SiO}_4^a$

A. Internal Modes

$$\nu_1(A_1) \rightarrow A_g + B_{1g} + B_{2u} + B_{3u}$$

$$\nu_2(E) \rightarrow A_g + B_{1g} + B_{2g} + B_{3g} + A_u + B_{1u} + B_{2u} + B_{3u}$$

$$\left. \begin{array}{l} \nu_3(F_2) \\ \text{or} \\ \nu_4(F_2) \end{array} \right\} \rightarrow 2A_g + 2B_{1g} + B_{2g} + B_{3g} + A_u + B_{1u} + 2B_{2u} + 2B_{3u}$$

$$\Gamma^{\text{int}}(\text{SiO}_4^{4-}) = 6A_g + 6B_{1g} + 3B_{2g} + 3B_{3g} + 3A_u + 3B_{1u} + 5B_{2u} + 5B_{3u}$$

B. External Modes

$$\Gamma^{\text{ext}}(\text{SiO}_4^{4-}) = R(\text{SiO}_4^{4-}) + T(\text{SiO}_4^{4-})$$

$$\Gamma^R(\text{SiO}_4^{4-}) = A_g + B_{1g} + 2B_{2g} + 2B_{3g} + 2A_u + 2B_{1u} + B_{2u} + B_{3u}$$

$$\Gamma^T(\text{SiO}_4^{4-}) = 2A_g + 2B_{1g} + B_{2g} + B_{3g} + A_u + B_{1u} + 2B_{2u} + 2B_{3u}$$

$$\Gamma^i(\text{Mn}^{2+}) = 3A_u + 3B_{1u} + 3B_{2u} + 3B_{3u}$$

$$\Gamma^s(\text{Mn}^{2+}) = 2A_g + 2B_{1g} + B_{2g} + B_{3g} + A_u + B_{1u} + 2B_{2u} + 2B_{3u}$$

^a int = internal, ext = external, R = rotations, T = translations, i = C_i , s = C_s .

Transverse Optical Modes. The olivines belong to the orthorhombic space group, D_{2h}^{16} .^{4,12} Orthorhombic systems admit six different crystallographic settings for the same unit cell, and this fact has occasioned confusion in the literature as pointed out by Devarajan and Funck.³ In this work, the setting $Pbnm$ is chosen, in agreement with the common choice of mineralogists.⁴ The permutation of the standard abc orientation for the setting $Pnma$ as described in the International Tables for X-Ray Crystallography¹³ makes the c axis in setting $Pbnm$ perpendicular to the mirror planes, which are then parallel to the a and b axes. The four SiO_4^{4-} tetrahedra and four of the Mn^{2+} ions are situated on mirror planes (C_s sites). The remaining four Mn^{2+} ions are on C_i sites. The irreducible representations for the $k = 0$ internal and external optical and acoustic modes were obtained from correlation diagrams and are presented in Table I. The $k = 0$ optical modes of the crystal are classified as $11A_g$ (aa , bb , cc) + $11B_{1g}$ (ab) + $7B_{2g}$ (ac) + $7B_{3g}$ (bc) + $10A_u$ + $9B_{1u}$ (c) + $13B_{2u}$ (b) + $13B_{3u}$ (a) where the polarizations of the spectroscopic activities in the setting selected in this work are indicated in parentheses following each species symbol.

The results presented in Table I show that there are many opportunities for mixing of internal modes which have the same symmetry. Because the extent of mixing depends on the proximity of the two combining states, it is expected to be most pronounced for the neighboring components of ν_1 and ν_3 and for those of ν_2 and ν_4 . The polarized Raman and infrared spectra provide the frequencies and symmetries of the optically active $k = 0$ phonons, but the extent of mixing of ν_1 and ν_3 or ν_2 and ν_4 cannot be determined from these data. Therefore, the assignments proposed below were made without regard to possible mixing of the internal modes. There is evidence, however, for mixing of ν_2 with the external modes of Mn_2SiO_4 , and this type of coupling will be discussed in connection with the internal mode approximation.

In many respects, the Raman spectrum of tephroite, shown in Figure 2, is very similar to that reported for forsterite. A number of bands active in one polarization appear in others, as found for the olivines reported in earlier work.² This spillover or leakage of intensities of a component in a forbidden polarization can occur because of crystal misorientation and because of the large solid angle at which the scattered light is collected. In tephroite, there appear to be several cases in which, for a particular polarization, the frequency of a forbidden (leakage) component is coincident (within experimental error) with that of another component that is allowed. There are two different types of this leakage of intensity from one polarization into another. The first type arises because

the intensity of any given totally symmetric mode is different in the aa , bb , and cc polarizations. The consequence is that two totally symmetric modes may appear with quite different spillover intensities in different nontotally symmetric polarizations. For this reason, the assignment of the band at 288 cm^{-1} to B_{1g} as given in Table II is uncertain due to the presence of the A_g fundamental at 291 cm^{-1} . In the second type of leakage, a mode that is active in a nontotally symmetric species has only one contributor to any leakage of intensity into any of the other polarizations. The nontotally symmetric modes of the same species then appear with the same relative intensities in polarizations other than the one to which they belong. This is the basis for the assignment of the band at 274 cm^{-1} in ac polarization to a B_{2g} fundamental, for it is far too intense to be accounted for solely by leakage from the evident B_{3g} fundamental at 276 cm^{-1} . A similar argument applies to the B_{3g} and B_{1g} assignments proposed for the bands at 304 and 307 cm^{-1} , respectively. The assignment of the band at 575 cm^{-1} in the ac polarization to the B_{2g} component of ν_4 is uncertain due to the appearance of a band at 575 cm^{-1} in the diagonal polarizations, even though the ac intensity is of the same order of magnitude as the bb or cc components.

The Raman spectrum of tephroite is further complicated by self-absorption, which may have precluded observation of the low-intensity components of ν_3 . Accidental degeneracy of an allowed, weak nontotally symmetric component with the relatively much more intense leakage from one of the very intense, totally symmetric components may also be a factor. There are several nontotally symmetric SiO stretching fundamentals that occur with low intensity in the Raman spectrum of forsterite, which has no visible absorption bands.^{2b} In general, the frequencies of the strong Raman bands in tephroite lie 15–25 cm^{-1} lower than the corresponding bands in forsterite. This suggests searching for the weak Raman bands in tephroite at frequencies 15–25 cm^{-1} lower than those at which these appear in forsterite. These regions in the off-diagonal polarizations showed no evident Raman scattering in the spectrum of tephroite, even though repeated efforts were made to discern weak or unresolved bands.

The infrared absorption spectrum of powdered tephroite in a hydrocarbon suspension at 77 K (Figure 3) provides most of the frequencies of the transverse components of the infrared active vibrations. Transverse electric infrared reflectance spectra of the oriented principal faces obtained at near normal incidence also shown in Figure 3 provide polarization data, information concerning relative intensities, and band widths which give a measure of the longitudinal optical (LO) and transverse optical (TO) mode frequency splitting. Transverse

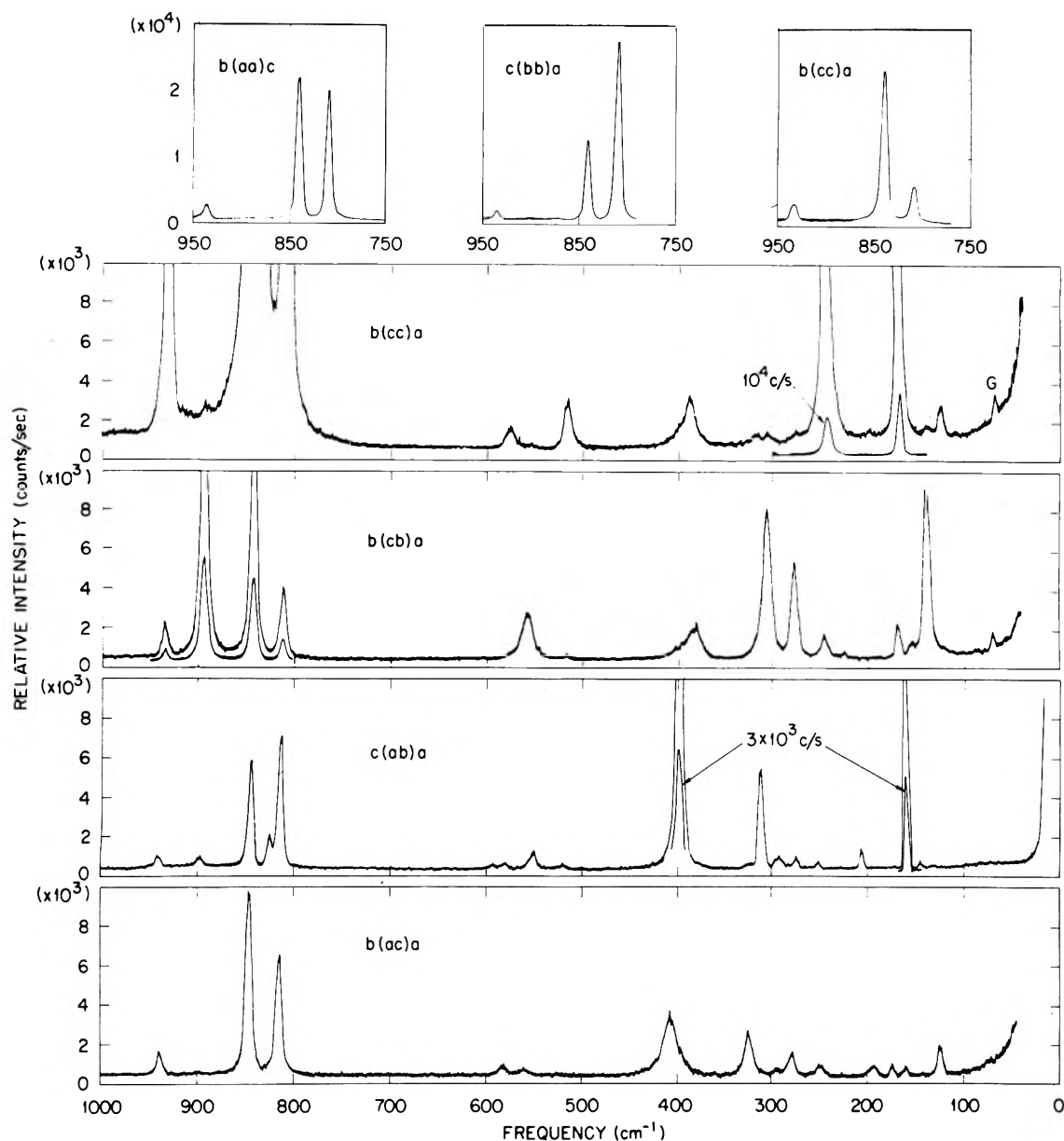


Figure 2. Raman spectrum of tephroite at 14 K. G is a grating ghost.

magnetic infrared reflectance spectra obtained at high angles of incidence from principal faces (oriented to bring the incidence and principal crystal planes into coincidence) contain evidence of coupling of some of the out-of-face polarized LO modes with the electric vector of the incident light. These spectra are shown in Figure 4.

Two infrared components of ν_1 are expected in the 800- cm^{-1} region, and the band at 818 cm^{-1} in both the absorption and b polarized reflectance spectra is assigned to one of these. Five components of ν_4 are expected in the 500- cm^{-1} region. Four of these are assigned to bands at 565, 508, 482, and 459 cm^{-1} in the absorption spectrum on the basis of the polarization results shown in Figure 4. The weak band at 433 cm^{-1} occurs with c polarization, rather than with the a polarization required for the missing ν_4 component, or for any mixed-mode of ν_4 with a B_{3u} component of ν_2 or with an external phonon. Therefore, the band at 433 cm^{-1} must be assigned either to an external B_{1u} mode of unusually high frequency or to a B_{1u} two-phonon mode. There is some evidence of two broad bands

of very low intensity in the a polarized reflectance spectrum near 800 and 490 cm^{-1} . The low-frequency contour of the 818- cm^{-1} absorption band appears asymmetric, and the high-frequency contour of the 482- cm^{-1} band is in a region of very intense absorption and is thus obscured. Exact frequencies cannot be given for the missing components of ν_1 and ν_4 . These are somewhat arbitrarily taken near 815 and 490 cm^{-1} in this assignment, though these frequencies may be as much as 15 cm^{-1} away from the actual values. These selections, taken together with the assignments for the components of ν_3 , are listed in Table III and exhaust the frequencies available for assignment above 450 cm^{-1} .

One infrared component of ν_2 is expected in each of the three polarizations at frequencies lower than those assigned to ν_4 . Apart from the isolated 433- cm^{-1} band discussed above, the only candidates for assignment to ν_2 are the 365-, 350-, and 340- cm^{-1} bands in a , c , and b polarizations, respectively. These are almost overlapped by the bands in the 300- cm^{-1} region, which are clearly due to external modes of the SiO_4^{4-}

TABLE II: Frequencies (cm^{-1}) of the Bands Observed in the Polarized Raman Spectrum of Mn_2SiO_4 at 14 K

Ag (bb)	(cc)	B _{1g} (ab)	B _{2g} (ac)	B _{3g} (bc)	Assignment
935 (56) ^a	933 (98)	934 (2)	933 (4)	933 (6)	ν_3
892 (2)	892 (2)	892 (2)		892 (59)	ν_3
839 (456)	840 (859)	840 (20)	840 (34)	840 (45)	ν_3
		820 (4)			ν_1
808 (1000)	808 (189)	809 (25)	808 (23)	809 (13)	ν_1
		588 (1)			ν_4
575 (2)	575 (4)	574 (1)	575 (2)		ν_4^b
			553 (1)	555 (9)	ν_4
		546 (3)			ν_4
515 (43)	515 (10)	515 (<1)		514 (<1)	ν_4
			401 (12)		ν_2
		393 (69)			ν_2
389 (35)	386 (9)			378 (7)	ν_2
	316 (2)	320 (<1)	318 (9)		e
308 (2)	306 (2)	307 (19)		304 (27)	$\nu_e(\text{B}_{1g}), \nu_e(\text{B}_{3g})$
291 (13)		288 (2)	288 (<1)		$\nu_e(\text{A}_g), \nu_e(\text{B}_{1g})$
278 (<1)	275 (1)	278 (<1)	274 (4)	276 (17)	$\nu_e(\text{B}_{2g}), \nu_e(\text{B}_{3g})$
		271 (2)			ν_e^c
256 (2)					ν_e^c
247 (10)	244 (74)	248 (1)	244 (2)	244 (4)	ν_e^c
	197 (<1)	203 (4)		223 (<1)	ν_e^c
			188 (2)		ν_e^c
169 (13)	167 (119)		168 (2)	167 (6)	ν_e^c
155 (2)		155 (60)	154 (2)	153 (2)	ν_e^c
139 (<1)	137 (2)	140 (2)	137 (<1)	137 (32)	ν_e^c
	124 (5)				ν_e^c
			119 (5)		ν_e^c

^a Relative intensities as measured peak heights for 488-nm excitation normalized to 1000. ^b See text. ^c ν_e = external mode.

TABLE III: Frequencies (cm^{-1}) of the Bands Observed in the Infrared Absorption and Reflectance Spectra of Mn_2SiO_4 ^a

Absorption (Mull, 77 K)	TE reflectance (300 K)			Assignment
	B _{1u} (c)	B _{2u} (b)	B _{3u} (a)	
960			~950	ν_3
946		945		ν_3
914			912	ν_3
~875(b)	875(b)			ν_3
862		860(b)		ν_3
818		816		ν_1
b			~815(b,vw)	ν_1
565			565	ν_4
508		512		ν_4
b			~490(b,vw)	ν_4
482	480			ν_4
459		454		ν_4
433	430			b
362(sh)			365	$\nu_2 + \nu_e^c$
350(b)	350			$\nu_2 + \nu_e$
340(vw)		340		$\nu_2 + \nu_e$
	317		320(sh)	ν_e
	310	299	306	ν_e
	300	292	297	ν_e
		276		ν_e
		242		ν_e
244	240			ν_e
190	187			ν_e
179		175	177	ν_e

^a b = broad, sh = shoulder, vw = very weak, ν_e = external mode. ^b See text. ^c Mixed mode, see text.

and Mn^{2+} sublattices. Thus, some of the bands observed in the 300- cm^{-1} region are probably due to mixed-modes of ν_2 and external phonons. In all, six of the external vibrations are expected below 320 cm^{-1} in B_{1u} and seven each in B_{2u} and B_{3u}, but only five bands are clearly identifiable in B_{1u} and B_{2u}, while only four can be identified in B_{3u} polarization in this region.

2. *Longitudinal Optical Modes.* It has been shown by Hargreave¹⁴ and by Decius, Frech, and Bruesch¹⁵ that LO modes polarized perpendicular to a crystal face can give rise to characteristic features in TM reflectance spectra measured at a nonnormal angle of incidence. In the case discussed by Hargreave, the feature resembles the reflection band of an undamped TO mode except that the band is reversed, and the high- and low-frequency asymptotes are equal. Similar features were observed in the TM reflectance measured at a 60° angle of incidence (Figure 4). An example is seen in the $E \parallel b$ spectrum in which the a axis is perpendicular to the bc face ($bc \perp a$). The band at ~950 cm^{-1} is similar to the feature described by Hargreave and indicates the frequency of a $\nu_3(\text{B}_{2u})$ LO mode near this value. Other such features may be obscured by strong reflection bands from TO modes as in the 60° $E \parallel c$, $ac \perp b$ spectrum, which exhibits a deep minimum at ~923 cm^{-1} . We believe that this minimum as well as other minima observed in the 60° reflection spectra correspond to the features described by Hargreave but are partly obscured by overlap with intense TO reflection bands. The position of these minima indicate the approximate frequencies of LO modes.

A second type of feature observed in the 60° TM reflection spectra corresponds to the reflection bands reported by De-

TABLE IV: Estimated Longitudinal Optical (LO) Mode Frequencies of Mn_2SiO_4

B_{1u} Components			B_{2u} Components			B_{3u} Components		
Mode	Frequency		Mode	Frequency		Mode	Frequency	
	TO	LO		TO	LO		TO	LO
ν_3	875	950	ν_3	945	960	ν_3	912	1000
ν_2	350	380	ν_3	860	930	ν_3	875	950
			ν_2	340	370	ν_4	565	580
						ν_2	306	320

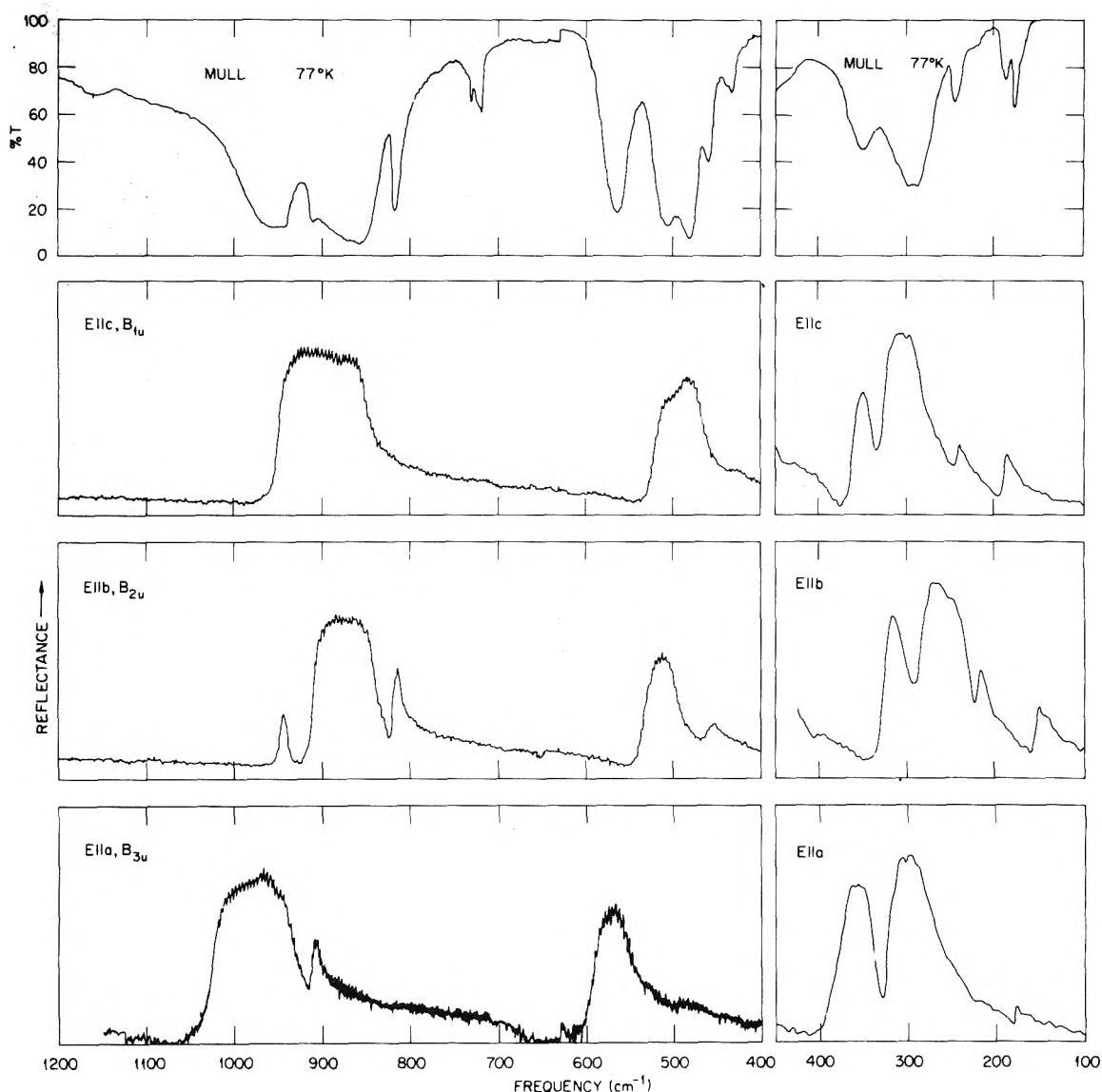


Figure 3. Absorption and TE reflectance infrared spectra of tephroite. (1) Absorption spectrum of hydrocarbon suspension of tephroite powder at 77 K spread on Csl or Si plates. (2,3,4) Room temperature reflectance spectra in *c*, *b*, and *a* polarizations, respectively.

cius, Frech, and Brüesch.¹⁵ In this case, the peak of the reflection band occurs between $\nu_L(LO)$ and ν_{LI} , where $\nu_{LI} > \nu_L$. The frequency of the LO mode is given approximately by the position of the base of the reflection band on the low-energy side. In Figure 4, the reflection band centered at $\sim 1050 \text{ cm}^{-1}$ in the $E \parallel b, bc \perp a$ spectrum is such a feature, and the associated LO mode frequency is $\sim 1000 \text{ cm}^{-1}$. Other similar reflection maxima can be seen in Fig. 4.

The LO mode frequencies estimated from the two types of

spectral features observed in the 60° TM reflectance spectra of Mn_2SiO_4 are collected in Table IV, along with the associated TO mode frequencies and assignments. The pattern or trend of TO–LO splitting of the Mn_2SiO_4 data is generally consistent with the results for Mg_2SiO_4 reported by Servoin and Piriou,^{2b} which were obtained from a Kramers–Kronig analysis of their reflection spectra. For example, the highest LO mode frequency of ν_3 and the largest TO–LO splitting in Mg_2SiO_4 occur with the B_{3u} components: $\nu_3(B_{3u}, LO) = 1081 \text{ cm}^{-1}$, $\nu_3(B_{3u},$

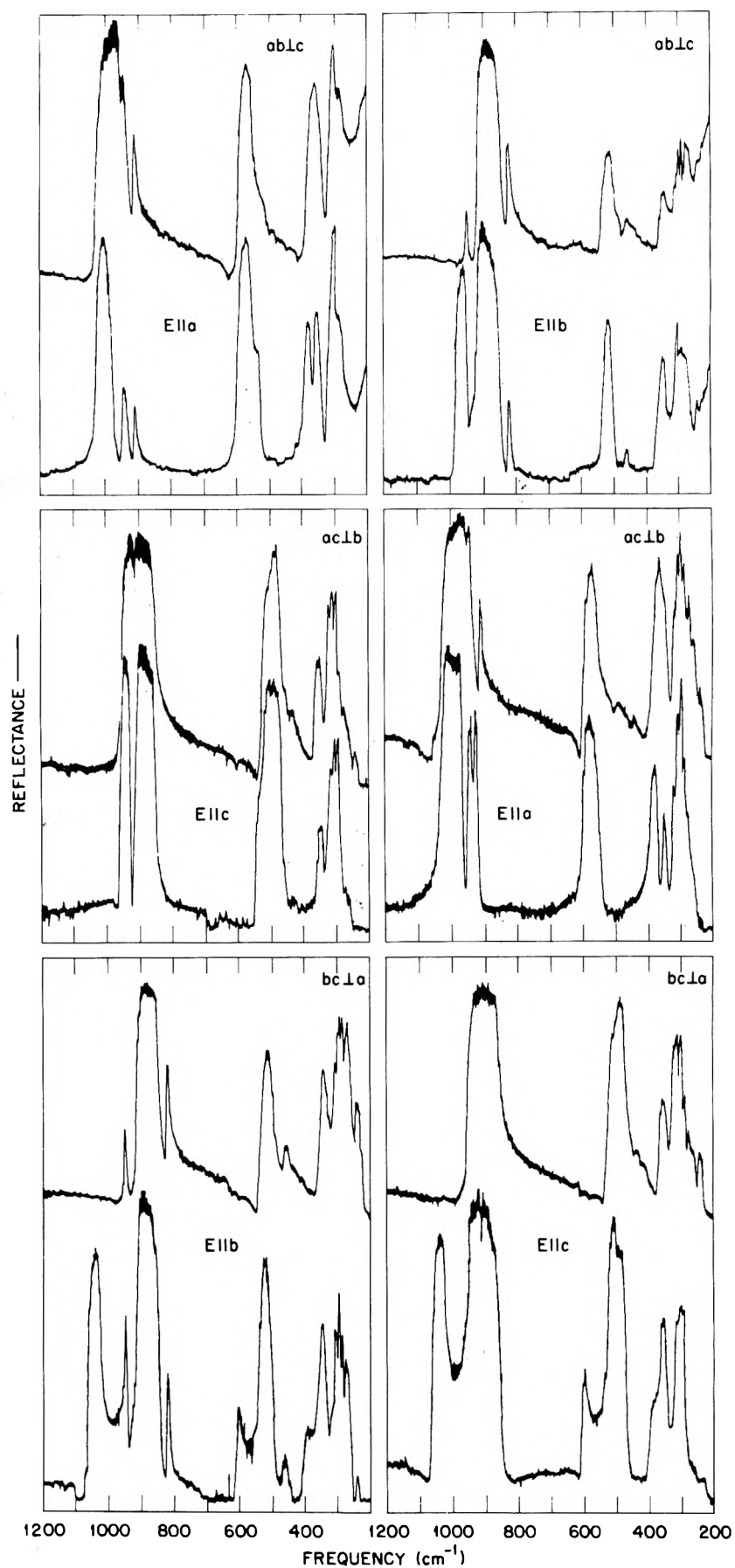


Figure 4. TM infrared reflectance spectra of tephroite: lower curves, 60° incidence angle; upper curves, 10° incidence angle. Polarization conditions and crystal faces are as noted.

TABLE V: Comparison of Assignments for the Internal Vibrations of Tephroite (Mn_2SiO_4) and Forsterite (Mg_2SiO_4)^a for Setting $Pbnm$ ^b

	Mn_2SiO_4			Mg_2SiO_4			Δ	$\langle \Delta \rangle$
	Freq, cm^{-1}	$\langle \nu \rangle$	$\langle \Delta_c \rangle$	Freq, cm^{-1}	$\langle \nu \rangle$	$\langle \Delta_c \rangle$		
ν_1	A_g	808		822			14	15
	B_{1g}	820	814	835	829		15	
	B_{2g}							
	B_{3g}							
				-3			-9	
ν_2	B_{1u}							
	B_{2u}	818	817	838	~838		20	22
	B_{3u}	815		838			23	
	A_g	935,839		960,854			25,15	
	B_{1g}	(), ()	(889)	972,863	908		(), ()	(22)
ν_3	B_{2g}	()		880			()	
	B_{3g}	892		917			25	
				(-22)			-25	
ν_4	B_{1u}	875		871			-4	
	B_{2u}	946,860	911	983,875	933		37,15	22
	B_{3u}	960,914		978,957 ^c			18,43	
	A_g	575,515		606,541			31,26	
	B_{1g}	588,546	(559)	626,577	587		38,31	28
ν_4	B_{2g}	(575)		583			8	
	B_{3g}	555		588			33	
				(59)			(36)	
ν_2	B_{1u}	480		531			51	
	B_{2u}	508,459	(500)	527, ()	(551)		19, ()	(40)
	B_{3u}	565,(490)		601,545			36,(55)	
	A_g	389		420			31	
	B_{1g}	393	390	428	423		35	33
ν_2	B_{2g}	401		436			35	
	B_{3g}	378		407			29	
				39			-79	
ν_2	B_{1u}	350		501			151	
	B_{2u}	340	351	506	502		166	151
	B_{3u}	362		498			136	

^a Reference 3. ^b $\Delta = \nu(\text{Mg}_2\text{SiO}_4) - \nu(\text{Mn}_2\text{SiO}_4)$, $\langle \nu \rangle$ = average of Raman or infrared active correlation field split components, $\langle \Delta_c \rangle = \langle \nu \rangle$ (Raman) - $\langle \nu \rangle$ (infrared), and $\langle \Delta \rangle = \langle \nu \rangle(\text{Mg}_2\text{SiO}_4) - \langle \nu \rangle(\text{Mn}_2\text{SiO}_4)$ for Raman or infrared. () = missing or doubtful assignment involved. ^c Assignment given in ref 2b.

TO) = 978 cm^{-1} , and $\Delta\nu_3(\text{LO-TO}) = 103 \text{ cm}^{-1}$ (Table IIc, ref 2b). Likewise the same holds for Mn_2SiO_4 where $\nu_2(\text{B}_3, \text{LO}) = \sim 1000 \text{ cm}^{-1}$, $\nu_3(\text{B}_{3u}, \text{TO}) = 912 \text{ cm}^{-1}$, and $\Delta\nu_3(\text{LO-TO}) = 88 \text{ cm}^{-1}$ (Table IV).

3. *Internal Mode Approximation.* The correlation field split components of ν_1 , ν_2 , ν_3 , and ν_4 in tephroite are compared with those for forsterite³ in Table V. This table also provides a convenient summary of assignments for the internal modes in both compounds. As expected, most of the tephroite fundamentals occur at lower frequencies than do those of forsterite. For most of the bands for which assignment is secure and the approximation of internal vibrations acceptable, the difference between the forsterite and tephroite frequencies is about $30 \pm 15 \text{ cm}^{-1}$. There are several notable exceptions. If the 877- cm^{-1} assignment suggested for one of the B_{3u} components of ν_3 by Devarajan and Funck³ is accepted, the difference between the frequencies of the corresponding components in the two crystals is 37 cm^{-1} , and tephroite has the larger frequency. Restoration of the 957- cm^{-1} assignment originally suggested by Servoin and Piriou^{2b} makes the frequency of this component of ν_3 greater in forsterite than in tephroite by 43 cm^{-1} . This is more consistent with the other cases in Table V than is the 877- cm^{-1} selection, and is compatible with the relative intensities in the infrared reflectance spectra of the two crystals. The 575- cm^{-1} assignment sug-

gested above for $\nu_4(\text{B}_{2g})$ in tephroite is uncertain, and the regularity of the other ν_4 frequency differences in Table V suggests that this component may have simply been missed in the Raman spectrum for the reasons discussed above.

The Raman-active components of ν_4 generally display the normal differences of about 30 cm^{-1} between forsterite and tephroite frequencies. In contrast, the infrared-active components of ν_4 in forsterite lie nearly 60 cm^{-1} above those in tephroite. Furthermore, the Raman-active components of ν_2 again differ by only about 30 cm^{-1} in the two compounds, while the infrared-active components of ν_2 differ by about five times as much, if the assignment of Devarajan and Funck³ is accepted. These results suggest that, in the infrared-active vibrations of tephroite and especially forsterite, the external vibrations of the metal ion sublattices mix somewhat with the ν_4 motions, and much more extensively with the ν_2 motions. In contrast, the motions of the C_i metal ion sublattice do not contribute to the Raman-active modes due to symmetry. The small and almost uniform frequency differences found for the Raman frequencies of corresponding vibrations of the two compounds suggest that most of the differences are due to the slightly different nonbonded atom-atom force constants that arise in lattice expansion when manganese is substituted for magnesium. Apparently, the metal ions on the C_s sites do not contribute very much relative motion to the Raman-active

vibrations, and the approximation of internal and external modes retains descriptive utility for these. These results can be understood by assuming that, for the crystal components of the Raman-active ν_2 and ν_4 bending vibrations, the C_s metal ions approximately follow the oxygen atom motions and thus do not affect the frequencies greatly, while in the infrared-active vibrations the motions of the metal ions oppose those of the oxygen atoms. In an ungerade motion, both metal ion sublattices are able to move against the bending motions of the SiO_4^{4-} ions, and the resulting vibration is a mixture of internal SiO_4^{4-} bending and external motion of the Mn^{2+} ions. Depending on the extent of mixing, the internal mode approximation will have more or less descriptive utility, and the frequencies will localize more or less in the vicinities expected for the internal modes. The more closely an internal mode frequency approaches a frequency of the metal ion sublattices, the greater will be the mixing, and the more greatly the frequency of the resulting vibration will depart from the approximate internal mode values expected. For this reason the infrared-active ν_2 vibrations are difficult to locate in tephroite, and the bands listed in Table II near 350 cm^{-1} are assigned to a mixture of internal and external modes. In the case of forsterite, the lighter magnesium ion sublattices vibrate at higher frequencies than the manganese ion sublattices in tephroite and therefore mix more extensively with the bending modes of the SiO_4^{4-} ions.

It is useful to remark that the infrared-active components of ν_2 that are mixed with metal ion sublattice vibrations should display metal ion isotopic substitutional sensitivity. The basis

for the assignment of the infrared-active vibrations of ν_2 in forsterite suggested by Devarajan and Funck³ and listed in Table V was the observation of Paques-Ledent and Tarte⁵ of a shift to lower frequencies of all the low-frequency bands in the infrared spectrum of powdered ^{26}Mg substituted forsterite relative to those of the natural material. The present interpretation makes it unnecessary to accept such high frequencies as those suggested by Devarajan and Funck for ν_2 , but it requires discarding the internal mode approximation in this region of the infrared spectra of the silicate olivines.

References and Notes

- (1) (a) Research sponsored by the U.S. Energy Research and Development Administration under contract with Union Carbide Corporation. (b) On leave from the Department of Chemistry, University of Massachusetts, Amherst, Mass. 01002. Ph.D. with Professor Richard C. Lord, 1955.
- (2) (a) V. Hohler and E. Funck, *Z. Naturforsch. B*, **28**, 125 (1973); (b) J. L. Servoin and B. Piriou, *Phys. Status Solidi b*, **55**, 677 (1973).
- (3) V. Devarajan and E. Funck, *J. Chem. Phys.*, **62**, 3406 (1975).
- (4) J. D. Birle, G. V. Gibbs, P. B. Moore, and J. V. Smith, *Am. Mineral.*, **53**, 807 (1968).
- (5) M. Th. Paques-Ledent and P. Tarte, *Spectrochim. Acta, Part A*, **29**, 1007 (1973).
- (6) MnO and SiO_2 were supplied by Johnson Matthey Chemicals, Ltd.
- (7) C. B. Finch, G. W. Clark, and O. C. Kopp, *J. Crystal Growth*, **29**, 269 (1975).
- (8) J. B. Bates and J. C. Pigg, *J. Chem. Phys.*, **62**, 4227 (1975).
- (9) J. W. Stout, *J. Chem. Phys.*, **31**, 709 (1959).
- (10) S. Koide and M. H. L. Pryce, *Phil. Mag.*, **3**, 607 (1958).
- (11) G. E. Shankle and J. B. Bates, *J. Chem. Phys.*, **64**, 2539 (1976).
- (12) R. W. G. Wyckoff, "Crystal Structures", Interscience, New York, N.Y., 1965, Vol. 3, p. 93.
- (13) "International Tables of X-Ray Crystallography", Vol. 1, 3rd ed., Kynock Press, Birmingham, 1969, p. 544.
- (14) M. M. Hargreave, *J. Phys. C: Solid State Phys.*, **174** (1971).
- (15) J. C. Decius, R. Frech, and P. Bruesch, *J. Chem. Phys.*, **58**, 4056 (1973).

Oxygen($^1\Sigma_g^+$) Energy Transfer Carbon Dioxide Laser^{1a}

Gale D. Downey and Dean W. Robinson*^{1b}

Department of Chemistry, The Johns Hopkins University, Baltimore, Maryland 21218 (Received January 29, 1976)

Publication costs assisted by the Energy Research and Development Administrations

Flash photolysis of mixtures of $\text{O}_2/\text{CO}_2/\text{O}_3$ in a laser cavity produces oscillation on the P(14)–P(20) lines of the $10.6\text{-}\mu$ band of CO_2 . All the experimental observations are consistent with the pumping scheme: $\text{O}_3 + h\nu \rightarrow \text{O}(^1\text{D}) + \text{O}_2(^1\Delta_g)$ (1); $\text{O}(^1\text{D}) + \text{O}_2(^3\Sigma_g^-) \rightarrow \text{O}(^3\text{P}) + \text{O}_2(^1\Sigma_g^+)$ (2); $\text{O}_2(^1\Sigma_g^+) + \text{CO}_2(000) \rightarrow \text{O}_2(^1\Delta_g) + \text{CO}_2(n, m, 1)$ $n = 1, m = 0; n = 0, m = 2^0, 2^2$ (3); $\text{CO}_2(n, m, 1) + \text{CO}_2(000) \rightarrow \text{CO}_2(n, m, 0) + \text{CO}_2(001)$ (4). The population inversion between the (001) and (100) vibrational levels of CO_2 is created by reaction 4, as only a fraction of the V–V energy exchange populates the lower laser level, while every V–V exchange populates the upper laser level. Computer modeling of this sequence of reactions with $k_4 = 3.3 \times 10^{-10}\text{ cm}^3\text{ molecule}^{-1}\text{ s}^{-1}$ reproduces both the observed pulse's profile and its onset delay after flash initiation.

Introduction

The discovery and analysis of chemically pumped CO_2 lasers has produced a wealth of information on the rates and types of collisional processes which excite and relax the upper and lower laser levels of CO_2 . Generally, the population in-

version between the (001) and (100) levels is created by a resonant V–V energy exchange between $\text{CO}_2(000)$ and a vibrationally excited diatomic molecule. To date N_2 ,² HF , DF , HCl ,³ OH , OD ,⁴ and CO ⁵ are the diatomics that have been found to pump CO_2 lasing by V–V energy transfer.

Very few chemical lasers are known where an E-V energy transfer pumps a vibrational population inversion. One line of the far-infrared, water vapor laser has been pumped directly by E-V energy transfer from O₂(¹Σ_g⁺) to H₂O.⁶ This reaction was found selectively to excite ν₃ of H₂O, while the O₂(¹Σ_g⁺) ν = 0 was preferentially quenched to O₂(¹Δ_g) ν = 1. However, no chemical CO₂ lasers, which are pumped by an E-V energy transfer process, have been reported.

CO₂ is known to quench O₂(¹Σ_g⁺) rapidly ($k_q = 2.3 \times 10^{-13}$ cm³ molecule⁻¹ s⁻¹).⁷ Near-infrared emission studies have shown that CO₂(101) and CO₂(02⁰1) states are produced by the quenching reaction.⁸ This indicates that O₂(¹Σ_g⁺) ν = 0 is preferentially quenched to O₂(¹Δ_g) ν = 1. To probe the specifics of this quenching reaction, gas mixtures of O₂, CO₂, and O₃ were flash photolyzed in a laser cavity and examined for lasing.

Experimental Section

The optically coupled flash lamp and laser cavity have been previously described.⁶ For these experiments the detector was a zinc-doped germanium photoconducting element which was mounted in a liquid helium dewar possessing a sodium chloride window. Pure gases were used directly from the cylinders without further purification. The method for preparing O₃ and the procedures for storing it and preparing gas mixtures have been previously described.⁶ The O₂/CO₂/O₃ mixtures ($P_T < 300$ Torr), which produced lasing upon flash photolysis, could be stored for several hours without decreasing the laser pulse's peak power.

Observations

Optimally, flash photolysis of 11.8 Torr of a 60/15/1 = O₂/CO₂/O₃ mixture leads to strong lasing on the P(16) line of the (001)-(100) band of CO₂. Figure 1 shows an oscilloscope trace of this line. Weaker laser emission, by a factor of 10, is observed for the P(14), P(18), and P(20) lines. Peak laser power is estimated to be a few hundred milliwatts. The onset delay after flash initiation is 18 μs for each of the observed laser lines, while the minimum pulse half-width of each is 60 μs.

Strong lasing is observed from the flash photolysis of O₂/CO₂/O₃ mixtures in a laser cavity: if the total pressure is greater than 5 Torr and less than 20 Torr, if the CO₂/O₃ ratio is between 10 and 20, and if the O₂/O₃ ratio is between 30 and 80. Decreasing or increasing either the total pressure, or the CO₂/O₃ ratio, or the O₂/O₃ ratio beyond these boundary limits results in a substantial reduction in the laser's peak power. Flash photolysis of either O₃/O₂ or O₃/CO₂ mixtures over a wide range of mixture ratios and total pressures produces no laser emission. Substitution of Ar for O₂ in the 60/15/1 = O₂/CO₂/O₃ mixture produces weak lasing whose peak power is one-tenth of that from the oxygen-containing mixture under identical conditions and whose onset delay after flash initiation is 25 μs.

Discussion

Since simple omission of O₂ from the O₂/CO₂/O₃ mixtures results in no infrared laser emission, O₂(³Σ_g⁻) must be a necessary reactant in the chemical pumping scheme which is initiated by O₃ photolysis. Only one rapid reaction of O₂(³Σ_g⁻) with the products of the near ultraviolet photolysis of O₃ is known: namely, the reaction

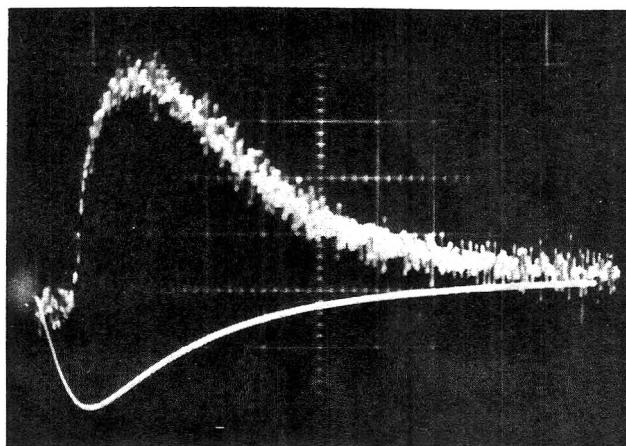
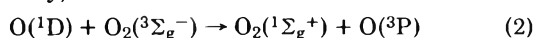
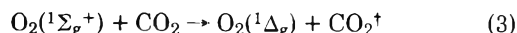
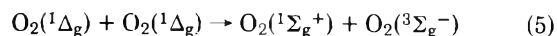


Figure 1. Laser emission observed on the P(16) line of the (001)-(100) band of CO₂ from flash photolysis of 11.8 Torr of a 60/15/1 = O₂/CO₂/O₃ mixture (upper trace shows laser emission, 1 division = 20 μs; lower trace shows flash profile, 1 division = 10 μs).

In the absence of polar molecules such as H₂O, NH₃, and CH₃OH, CO₂ is an effective quencher¹⁰ of O₂(¹Σ_g⁺). Several workers^{7,10,11} have measured the rate constant for reaction 3

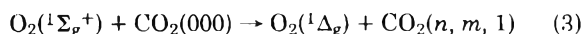
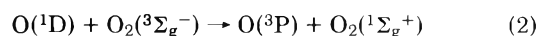
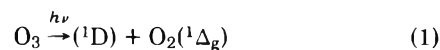


and found it to be 2.3×10^{-13} cm³ molecule⁻¹ s⁻¹, although, until recently, nothing was known about the details of this quenching process. In 1974 Ogryzlo and Thrush observed infrared emission near 3700 cm⁻¹ when CO₂ was added to discharged O₂ containing only O₂(¹Δ_g) and O₂(¹Σ_g⁺) as excited species. In their experiments the sole reaction producing O₂(¹Σ_g⁺) was



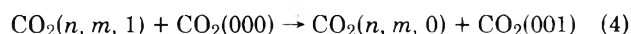
Due to the second-order dependence of the 3700-cm⁻¹ emission intensity on the O₂(¹Δ_g) concentration, they showed that quenching of O₂(¹Σ_g⁺), not O₂(¹Δ_g), was responsible for the observed chemiluminescence. The emission was assigned to the CO₂ combination bands, Δν₁ = Δν₃ = -1 and Δν₂ = -2, Δν₃ = -1. Since no emission near 5000 cm⁻¹ was detected, they postulated that only the (101), (02⁰1), and (02²1) levels were populated by reaction 3. This reaction is then a resonant V-V energy transfer if O₂(¹Σ_g⁺) ν = 0 is quenched to O₂(¹Δ_g) ν = 1, and not ν = 0.

Consistent with their observations and our experimental data, a pumping scheme for the P branch emission of the (001)-(100) band from the flash photolysis of O₂/CO₂/O₃ mixtures is



$$n = 1, m = 0$$

$$n = 0, m = 2^0, 2^2$$



where the population inversion between (001) and (100) is created by the V-V energy transfer occurring in reaction 4. In the above scheme only one species which is produced by the flash leads to excitation of CO₂; a plot of laser peak power as a function of flash energy should thus be linear. Figure 2 shows that over the accessible flash energy range, the laser peak

TABLE I: Reactions and Their Rate Constants which Were Used in the Computer Calculations

Reaction	k , $\text{cm}^3 \text{ molecule}^{-1} \text{ s}^{-1}$	Ref
(2) $\text{O}(^1\text{D}) + \text{O}_2(^3\Sigma_g^-) \rightarrow \text{O}(^3\text{P}) + \text{O}_2(^1\Sigma_g^+)$	7.00×10^{-11}	7
(3) $\text{O}_2(^1\Sigma_g^+) + \text{CO}_2 \rightarrow \text{O}_2(^1\Delta_g) + \text{CO}_2(n, m, 1)_{n=0, m=0, 2, 2}^{n=1, m=0, 0, 2}$	2.30×10^{-13}	7
(4) $\text{CO}_2(n, m, 1) + \text{CO}_2 \rightarrow \text{CO}_2(n, m, 0) + \text{CO}_2(001)$	3.30×10^{-10}	<i>a</i>
(7) $\text{O}(^1\text{D}) + \text{CO}_2 \rightarrow \text{O}(^3\text{P}) + \text{CO}_2$	2.10×10^{-10}	16
(8) $\text{O}(^1\text{D}) + \text{O}_3 \rightarrow \text{O} + \text{O} + \text{O}_2$	2.70×10^{-10}	16
(9) $\text{O}_2(^1\Sigma_g^+) + \text{O}_3 \rightarrow \text{O} + \text{O}_2 + \text{O}_2$	2.50×10^{-11}	17

^a See text.

TABLE II: Rate Constants for Relaxation of Excited Vibrational States of CO_2 which Were Used in the Computer Calculations

Reaction	M	k , $\text{cm}^3 \text{ molecule}^{-1} \text{ s}^{-1}$	Ref
(10) $\text{CO}_2(001) + \text{M} \rightarrow \text{CO}_2(100) + \text{M}$	O_3	1.18×10^{-12}	18
(11) $\text{CO}_2(001) + \text{M} \rightarrow \text{CO}_2(000) + \text{M}$	O_2	3.42×10^{-15}	19
	CO_2	1.13×10^{-14}	19
(12) $\text{CO}_2(100) + \text{M} \rightarrow \text{CO}_2(01^1_0) + \text{M}$	O_2^a	3.11×10^{-15}	20
(13) $\text{CO}_2(02^0_0) + \text{M} \rightarrow \text{CO}_2(01^1_0) + \text{M}$	O_2^a	3.11×10^{-15}	20
(14) $\text{CO}_2(100) + \text{M} \leftrightarrow \text{CO}_2(02^0_0) + \text{M}$	CO_2	3.11×10^{-11}	19
(15) $\text{CO}_2(02^0_0) + \text{M} \leftrightarrow \text{CO}_2(02^0_0) + \text{M}$	CO_2	1.86×10^{-11}	19
(16) $\text{CO}_2(02^2_0) + \text{M} \leftrightarrow \text{CO}_2(01^1_0) + \text{M}$	CO_2	1.12×10^{-10}	19
(17) $\text{CO}_2(01^1_0) + \text{M} \rightarrow \text{CO}_2(000) + \text{M}$	O_2^a	2.95×10^{-15}	19
	CO_2	6.21×10^{-15}	19

^a Values for k_{O_3} have not been reported. In the calculations $k_{\text{O}_3} = k_{\text{O}_2}$.

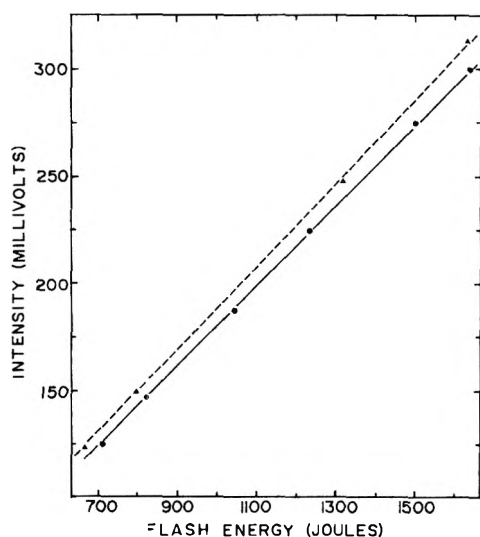


Figure 2. Plot of laser peak power as a function of flash energy for photolysis of 60/15/1 = $\text{O}_2/\text{CO}_2/\text{O}_3$ mixtures (\blacktriangle , $P_T = 11.8$ Torr; \bullet , $P_T = 15.9$ Torr).

power is a linear function of flash energy in agreement with the proposed pumping mechanism.

Confirmation of this pumping scheme was sought by computer modeling as described by Molina and Pimentel.¹² The prediction of the laser output from 11.8 Torr of a 60/15/1 = $\text{O}_2/\text{CO}_2/\text{O}_3$ mixture for the proposed energy transfer mechanism is shown in Figure 3. The experimentally found 18 μs pulse onset delay (17.5 μs calculated), peak power maximum at 35 μs (27 μs calculated), and slow decay in the first 100 μs after flash initiation are all reproduced by the calculations. The initial spikes are not observed experimentally; this is probably a result of the limiting bandwidth of the pulse amplifier.¹³

Due to the fact that lasing begins in the first 25 μs , only

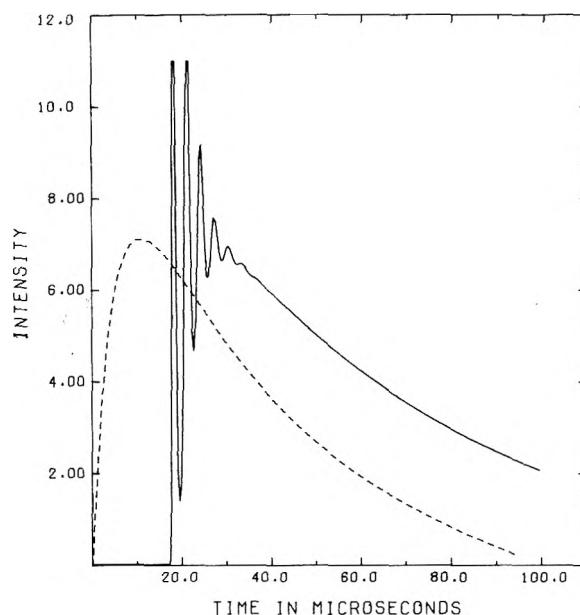
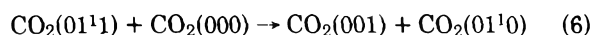


Figure 3. Calculated CO_2 laser emission from flash photolysis of 11.8 Torr of a 60/15/1 = $\text{O}_2/\text{CO}_2/\text{O}_3$ mixture (—, laser emission; - - -, flash profile; observed emission is shown in Figure 1).

those reactions which involve major species and for which $k \geq 10^{-16} \text{ cm}^3 \text{ molecule}^{-1} \text{ s}^{-1}$ were included in the calculations. Table I lists the rate constants of the pumping and competing reactions, while those of various CO_2 relaxation pathways are listed in Table II. Ninety-five percent of the O_3 initially present was assumed to be decomposed by the flash. Each vibrational manifold of CO_2 was assumed to be rotationally equilibrated ($T = 300$ K). The fact that the P(16) laser line is most intense supports this assumption. The rate constant for the excitation of CO_2 (k_3) was assumed to be that of the known quenching rate of $\text{O}_2(^1\Sigma_g^+)$ by CO_2 . Taking a smaller

value for k_3 would require an extremely selective excitation of (001) vs. (100) which seems unlikely. The fraction of k_4 which produces the lower laser level was set equal to 0.25, as reaction 3 populates four laser levels, (101, (02⁰1), and (02²1), but only one of these can relax by reaction 4 to the (100) level. Reproducing the observed 18 μs onset delay after flash initiation sets a lower limit on the value of k_4 to be 3.30×10^{-10} cm³ molecule⁻¹ s⁻¹. For the similar V-V resonant energy transfer reaction



a value of 1.65×10^{-10} cm³ molecule⁻¹ s⁻¹ has been determined¹⁴ for its rate constant, which is in good agreement with the lower limit found here for k_4 . Values of this order of magnitude have also been calculated¹⁵ for a number of other resonant CO₂ V-V energy transfer reactions.

Excitation of CO₂ to (201), (121), and (041) levels would produce a smaller net inversion between (001) and (100), as more of the excited levels could relax directly to the lower laser level. This in turn would cause the lower limit, which was found for k_4 in the calculations, to be significantly larger. This seems unlikely by comparison to calculated rate constants¹⁵ for similar resonant CO₂ V-V energy transfer reactions. Thus these chemical laser studies are consistent with the previously suggested hypothesis that reaction 3 populates only (101) and (021) levels, and O₂(¹Σ_g⁺) $v = 0$ is quenched predominately to O₂(¹Δ_g) $v = 1$.

The weak delayed lasing which is observed from mixtures in which Ar has been substituted for O₂ can probably be attributed to pumping of an (001) and (100) population inversion by E-V energy transfer from O(¹D). Then V-V relaxation of CO₂⁺ produces, by comparison to the O₂-containing mixtures, a smaller net population inversion between ν_3 and ν_1 . Searles and Airey⁴ found evidence for gain on the P(16) line using a tandem discharge CO₂ laser to investigate the flash photolysis of CO₂/O₃ mixtures. However, they could not achieve independent oscillation from photolyzed CO₂/O₃ mixtures and attributed this to the fact that the gain was insufficient to overcome cavity losses. As omission of Ar from the photolyzed Ar/CO₂/O₃ mixtures here also results in no laser emission, Ar must be required to achieve rotational equilibration to enhance the gain of the P(16) CO₂ laser line sufficiently to overcome cavity losses. Due to the large number of excited CO₂ vibrational states which could be produced by E-V energy transfer to CO₂ from O(¹D), no attempt to model the weak, observed lasing was made. However, k_7 (Table I) is three orders of magnitude larger than k_3 , yet the observed lasing from Ar/CO₂/O₃ mixtures has a longer onset delay after flash initiation. Thus E-V energy transfer from O(¹D) to CO₂

must be extremely inefficient in producing, by subsequent V-V relaxation, a population inversion between ν_3 and ν_1 .

Conclusion

For CO₂, this is the first example of laser pumping by an E-V energy transfer reaction and subsequent V-V relaxation processes. The chemical laser studies and computer prediction of the laser output are consistent with the previous interpretation that reaction 3 produces CO₂ in (100) and (021) levels and that O₂(¹Σ_g⁺) $v = 0$ is preferentially quenched to O₂(¹Δ_g) $v = 1$. A lower limit of 3.3×10^{-10} cm³ molecule⁻¹ s⁻¹ for k_4 was found in the calculations. This is in agreement with other experimentally found and/or calculated rate constants of similar V-V CO₂ resonant energy transfer reactions. Some evidence exists for E-V energy transfer pumping of the 10.6 μ band by O(¹D).

Flash photolysis of gas mixtures with an O₂/O₃ ratio greater than 30 appears to be a useful means of producing O₂(¹Σ_g⁺) to study the fate of its electronic excitation in quenching reactions whose rate constants are less than 1.0×10^{-13} cm³ molecule⁻¹ s⁻¹. Near-infrared lasing (~5 μ) from flash photolyzed mixtures of O₂/CO/O₃ has been observed in this laboratory and will be reported at a later date.

Acknowledgment. We wish to express our sincere thanks to Dr. T. Poehler of the Applied Physics Laboratory for supplying the Zn-doped Ge element which was used as a detector. We further acknowledge the financial support of this research by the Energy Research and Development Administration.

References and Notes

- (1) (a) Research supported by the Energy Research and Development Administration. (b) Ph.D. with Professor R. C. Lord, 1955.
- (2) (a) E. Bin-Nun and M. Rokni, *IEEE J. Quantum Electron.*, **10**, 89 (1974); (b) T. J. McGee and F. X. Powell, *ibid.*, **10**, 853 (1974).
- (3) C. E. Wiswall, D. P. Ames, and T. J. Menne, *IEEE J. Quantum Electron.*, **9**, 181 (1973).
- (4) S. K. Searles and J. R. Airey, *Appl. Phys. Lett.*, **22**, 513 (1973).
- (5) A. B. Peterson and C. Wittig, *Chem. Phys. Lett.*, **27**, 442 (1974).
- (6) G. D. Downey and D. W. Robinson, *J. Chem. Phys.*, **64**, 2854 (1976).
- (7) M. J. E. Gauthier and D. R. Snelling, *J. Photochem.*, **4**, 27 (1975).
- (8) E. A. Ogryzlo and B. A. Thrush, *Chem. Phys. Lett.*, **24**, 314 (1974).
- (9) D. R. Snelling, *Can. J. Chem.*, **52**, 257 (1974).
- (10) R. J. O'Brien, Jr., and G. H. Myers, *J. Chem. Phys.*, **53**, 3832 (1970).
- (11) S. V. Filseth, A. Zia, and K. H. Welge, *J. Chem. Phys.*, **52**, 5502 (1970).
- (12) M. J. Molina and G. C. Pimentel, *IEEE J. Quantum Electron.*, **9**, 64 (1973).
- (13) Such relaxation oscillations have been observed in the case of HF vibrational lasers using a low impedance InSb PEM detector (see ref 12).
- (14) I. Burak, Y. Noter, and A. Szoke, *IEEE J. Quantum Electron.*, **9**, 541 (1973).
- (15) R. D. Sharma and C. A. Brau, *J. Chem. Phys.*, **50**, 924 (1969).
- (16) R. F. Heidner, III, D. Husain, and J. R. Wiesenfeld, *J. Chem. Soc., Faraday Trans. 2*, **69**, 927 (1973).
- (17) R. Gilpin, H. I. Schiff, and K. H. Welge, *J. Chem. Phys.*, **55**, 1087 (1971).
- (18) T. A. Cool and J. R. Airey, *Chem. Phys. Lett.*, **20**, 67 (1973).
- (19) D. C. Tyte, *Adv. Quantum Electron.*, **1**, 129 (1970).
- (20) R. L. Taylor and S. Bitterman, *Rev. Mod. Phys.*, **41**, 26 (1969).

Spectroscopic Study of the Ozone–Ethylene Reaction. Matrix-Infrared Spectra of Three Isotopic Ethylene Ozonides

H. Kühne and Hs. H. Günthard*†

Laboratory for Physical Chemistry, Swiss Federal Institute of Technology, CH-8092 Zurich, Switzerland (Received March 2, 1976)

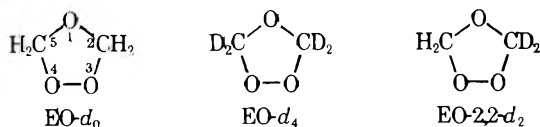
Publication costs assisted by the Swiss Federal Institute of Technology

Infrared and far-infrared spectra of three isotopic modifications of the secondary ethylene ozonide isolated in solid argon are reported. Assignments are given for the vibrational spectra based on both empirical arguments and normal coordinate analysis. A 30-parameter harmonic force field is reported and fairly detailed analysis of the Fermi resonance of the CH_2 stretching and bending modes is presented. Statistical thermodynamic functions of the normal species $^{12}\text{C}_2^{1}\text{H}_4^{16}\text{O}_3$ are tabulated.

1. Introduction

In a series of recent papers Kuczkowski et al.¹ showed, by analysis of the microwave spectra of secondary ozonides, that the mechanism proposed by Criegee for the reaction of ethylene and ozone in the liquid phase essentially correctly describes the products observed. The reaction of ozone with olefins has considerable practical importance in organic chemistry and in photochemical smog problems. Though by Kuczkowski's analysis of products little doubt is left about the latter steps of the ozonolysis reaction, only little is known about the reaction mechanism prior to formation of secondary ozonides. The scarcity of available data applies in particular to the homogeneous reaction in gas phase. A rather comprehensive discussion of possible steps in the gas phase mechanism has been presented by O'Neal and Blumstein,² which explains most of the reaction products so far observed in gas phase ozonolysis. Nevertheless, many of the complex intermediates postulated in the O'Neal mechanism have not been observed so far. This is evident from a paper of Pitts et al.³ on a photoionization mass spectrometric study of the gas reaction, in which for ethylene only small particles have been observed.

In this paper we wish to report results of a study of the matrix spectra of three isotopic secondary ozonides produced by liquid phase ozonolysis of ethylene:



This work forms a part of an extended study of this reaction in the gas phase by both infrared and microwave spectroscopy using linear reactor type experiments.⁴ Assignments of the spectra are given based both on empirical arguments and normal coordinate analysis; from the latter a harmonic force field with 14 diagonal and 16 off-diagonal elements are given. The analysis of the matrix infrared spectra confirms through an independent method the results obtained by Kuczkowski by microwave spectroscopy, thus giving further evidence for the essential correctness of the Criegee mechanism for solution ozonolysis.⁵ In agreement with predictions from the latter mechanism the production of $-d_0$, $-d_2$, and $-d_4$ secondary ozonide from ethylene-2,2- d_2 has been found. The spectra will prove to be important as basis for identification of secondary ozonides as a possible reaction product in the gas phase re-

action of ethylene with ozone. Finally statistical thermodynamic functions of the secondary ethylene ozonide are presented.

In forthcoming papers results on the gas phase reaction observed in linear reactor type experiments will be reported.

2. Experimental Section

2.1 Apparatus. Spectra reported in this work were taken with a Perkin-Elmer Model 325 spectrophotometer in the frequency range 4000–200 cm^{-1} . Deposition rates for production of matrix-isolated ozonides were measured by means of a small HeNe laser.⁶ Layer thickness growth rates of 50 $\mu\text{m}/\text{h}$ corresponding to 30 nmol of Ar/h were chosen. A cryostat of our own construction was used.⁷ Far-infrared matrix spectra in the range 400–130 cm^{-1} were taken with a Perkin-Elmer Model 301 spectrophotometer. For generation of matrices, deposition rates of 10 $\mu\text{m}/\text{h}$ of Argon were used.

2.2 Chemicals. The ozone was produced in a standard ozone generator (Fischer ozone-generator Model OZ III). Ethylene ozonide was prepared by passing an ozone flow through a 0.1 M solution of ethylene (CP Grade, Matheson) in methyl chloride at -78°C . A flow rate of approximately 1.5 g/h of ozone (ozone:oxygen \approx 5:100) was used for the reaction. Due to the explosive nature of ethylene ozonide not more than 5 mmol quantities were prepared. The ozonide was purified from the solvent by low temperature trap-to-trap distillation. The same procedure was used for the ozonolysis of $\text{D}_2\text{C}=\text{CD}_2$ and $\text{H}_2\text{C}=\text{CD}_2$.

Preparation of Ethylene- d_4 .⁸ As a first step 1,2-dibromoethane- d_4 was produced by photochemical addition of deuterium bromide to acetylene- d_2 . Deuterium bromide and acetylene- d_2 were transferred to a reaction flask in a mole ratio of 2:1, and irradiated with a mercury arc. Deuterium bromide was produced from PBr_5 and D_2O and C_2D_2 from pure calcium carbide and D_2O . Finally the 1,2-dibromoethane- d_4 was debrominated by refluxing with zinc dust to ethylene- d_4 in dioxane solution.⁹

Preparation of Dideuterioethylene-1,1- d_2 . The preparation of dideuterioethylene-1,1- d_2 was done by electrolysis of propionic-1,2,2- d_3 acid. A mixture containing 20% $\text{CH}_3\text{CD}_2\text{COOD}$ and 8% NaOD in D_2O was electrolyzed with platinum electrodes at a current density not greater than 0.084 A/cm².¹⁰ The ethylene was dried by passing through a trap at -80°C and collected at liquid nitrogen temperatures. The product contained some ethane and butane but was not purified further for the preparation of the ozonide.

Preparation of Propionic-1,2,2-d₃ Acid. In a sealed tube (stainless steel) a mixture of methylmalonic acid and D₂O (99.8%) in a ratio of 1:1 was heated over night at 55 °C. Then the solution was cooled to 0 °C and the water removed by freeze drying under vacuum. This exchange was repeated three times yielding a deuterium content of exchangeable hydrogen atoms of at least 95% as measured by NMR. Then as a last step the methylmalonic acid was decarboxylated by heating to 135 °C under vacuum. The product was finally purified by distillation.

3. Results

Matrix-infrared and far-infrared spectra of the isotopic secondary ethylene ozonides are shown in Figure 1. The conditions under which the spectra were taken are listed in the figure legend. Spectra taken with higher resolution in spectral regions relevant for later discussion are shown in Figure 2. In Tables I, II, and III observed infrared absorption frequencies of the three isotopic species are listed together with the assignment discussed in section 4.

4. Discussion

Discussion of the infrared spectra will be presented in the following order:

(i) *Assignment Based on Qualitative Arguments.* The data for the -d₂ species are derived from the spectrum of the ozonide obtained through ozonolysis of ethylene-1,1-d₂. This spectrum is shown to result from a mixture of the -d₀ and -d₄ secondary ozonides and an unknown compound. The latter is found to be identifiable in a consistent manner with ethylene-2,2-d₂ ozonide.

(ii) *Normal Coordinate Analysis (NCA) of the Spectra of the Three Isotopic Species.* Thereby the qualitative assignment is supported and an approximate harmonic force field is derived. Also the vibrational analysis is found to be consistent with C₂ symmetry of the r_s-r₀ structure as derived recently from microwave spectra.¹

(iii) *Fermi Resonances in the ν(CH) Region.*

4.1 *Assignment of Spectra.* The assignments given in Tables I, II, and III are based on the r₀-r_s structure with C₂ symmetry obtained from analysis of rotational spectra. The normal frequencies of the species -d₀ and -d₄ should be classified according to

$$11A \oplus 10B$$

where both types of normal modes should be infrared active. The heavy atom modes should be essentially the modes of the five-membered ring and classified according to 5A and 4B. Among these there are two lying modes to be expected, one A type puckering and one B type ring bending mode. The hydrogen stretching modes may be described as 2ν(CH)(a) ⊕ 2ν(CH)(b), whereas the remaining bending, wagging, twisting, and rocking group modes each contribute one A and one B mode. Since the two CH₂ groups have no nucleus in common direct coupling between their group modes may be assumed to be small.

The -d₂ species has C₁ symmetry, therefore all its normal modes will have the same symmetry A.

As a consequence of this situation a qualitative assignment may be made in a straightforward manner. Therefore, only relevant points will be discussed in detail.

Identification of the Spectrum of Ethylene-1,1-d₂ Ozonide. Comparison of the spectrum of the ozonide obtained by ozonolysis of ethylene-1,1-d₂ (cf. Figure 1c) with the spectra of the -d₀ and -d₄ species reveals the fact that all absorption

bands of the latter also occur in the former (Figure 1c). Besides the -d₀ and -d₄ bands there may be located a set of some 20 further bands, besides few very weak spurious bands. This set has been demonstrated to belong to one single species by comparison of spectra of ozonides obtained from ethylene samples of the following approximate isotopic composition (in molar fractions):

	C ₂ H ₄	C ₂ H ₃ D	CH ₂ CD ₂
Sample I	0.016	0.299	0.766
Sample II	0.003	0.095	0.902

In spite of the large content of the -d₁ species in particular in sample I, both samples yielded qualitatively the same spectrum. From this and the fact that both the -d₀ and the -d₄ spectrum are clearly recognizable, one may conclude that the -d₁ species does not lead to a noticeable contribution to the spectrum. The latter fact may be understood if the Criegee mechanism of olefin ozonolysis holds, which predicts six stereochemical isomers of the secondary ozonide -d₁ to be produced. Owing to the low concentration of each of these, they practically only contribute to the background of the spectrum. Therefore, the fact that only one further species has been detectable in the secondary ozonide of CH₂:CD₂ affords indirect support for the Criegee mechanism under the conditions of this work, i.e., ozonolysis in solution.

The absorption bands, as obtained by exclusion of the -d₀ and -d₄ bands from the spectrum Figure 1c, are collected in Table III and are attributed to ethylene ozonide (EO-2,2-d₂).

4.2 *Assignment. 1. ν(CH) Stretching Region.* According to Figure 2a one finds five bands in the ν(CH) region of the -d₀ species, whereas four bands are to be expected for either symmetries C₂, C_s, or C₁. Hence, C_{2v} symmetry may be excluded with high probability. Since each CH₂ group contributes one locally symmetric and one locally asymmetric mode and the two CH₂ groups may be assumed to be only slightly coupled in this molecule, one would expect two (A, B) doublets near 2970 and 2940 cm⁻¹. The two doublets observed at 2973, 2967 and 2900, 2894 cm⁻¹ may be identified with the ν₁₂(b), ν₁(a) and ν₂(a), ν₁₃(b) fundamentals, respectively, whereas the remaining band probably arises from a Fermi resonance ν(CH), 2δ(CH₂). The latter will be considered in more detail in section 4.4. From Figure 2b it is obvious that the ν(CH) region of the -d₂ species shows no CH stretching fundamentals other than those of the -d₀ modification, though the line width of the ν(CH) stretching bands of the former is definitely larger, hereby indicating slight differences in the band frequencies of -d₀ and -d₂. The ν(CD) stretching of the -d₄ modification (cf. Figure 2c) should show four fundamental bands, but is obviously complicated by Fermi resonance. Numerous bands in the 1150-900-cm⁻¹ region could give rise to Fermi resonance with ν(CD) fundamentals (cf. Table II), as will be discussed in detail below.

2. *1500-200-cm⁻¹ Region.* Whereas the CH₂ group bending (very weak) and twisting modes may in part be assigned rather directly (cf. Table I), assignment of fundamentals involving ring stretching-bending modes on a purely empirical basis appears rather uncertain. The choice given in Table I rests essentially on the results of the NCA and therefore will be discussed in section 4.3.

3. *Far-Infrared Region.* In the far-infrared matrix spectrum of the -d₀ species only one absorption band near 193 cm⁻¹ has been found. This frequency agrees reasonably with an estimate based on microwave spectra of vibrationally excited states reported by Kuczkowski.¹ From consideration of nuclear spin statistical weights in the intensity of those microwave lines

TABLE I: Infrared Absorption Frequencies of Ethylene Ozonide in an Argon Matrix

Assignment	Frequency, cm ⁻¹		Rel intensity	PED ^a
	Obsd	Calcd		
$\nu_1(\text{a})$	2973	2982	m	$\nu(\text{CH})(98)$
$\nu_2(\text{a})$	2894	2893	vs	FR: $\nu(\text{CH})(99)^b$
$\nu_3(\text{a})$		1482		$\delta(\text{CH}_2)(96)$
$\nu_4(\text{a})$	1387	1368	m	$\gamma_w(\text{CH}_2)(86)$
$\nu_5(\text{a})$	1196	1187	m	$\gamma_t(\text{CH}_2)(82)$
$\nu_6(\text{a})$	1129	1132	s	$\gamma_r(\text{CH}_2)(66)$
$\nu_7(\text{a})$	1078	1073	vs	$\nu(\text{C}_2\text{O}_3)(42)$, $\nu(\text{C}_2\text{O}_1)(29)^c$
$\nu_8(\text{a})$	952	959	vs	$\delta(\text{OCO})(43)$, $\nu(\text{OO})(26)$
$\nu_9(\text{a})$	808	808	s	$\nu(\text{OO})(39)$, $\nu(\text{C}_2\text{O}_3)(38)$
$\nu_{10}(\text{a})$	737	745	vw	$\nu(\text{C}_2\text{O}_1)(39)$, $\nu(\text{OO})(19)$, $\delta(\text{COC})(16)$
$\nu_{11}(\text{a})$	352	377	vw	Ring pucker
$\nu_{12}(\text{b})$	2967	2980	s	$\nu(\text{CH})(99)$
$\nu_{13}(\text{b})$	2900	2899	m	$\nu(\text{CH})(99)$
$\nu_{14}(\text{b})$	1483	1478	vw	$\delta(\text{CH}_2)(99)$
$\nu_{15}(\text{b})$	1346	1357	m	$\gamma_w(\text{CH}_2)(78)$
$\nu_{16}(\text{b})$	1202	1200	m	$\gamma_t(\text{CH}_2)(97)$
$\nu_{17}(\text{b})$	1143	1133	vw	$\gamma_r(\text{CH}_2)(92)$
$\nu_{18}(\text{b})$	1029	1025	s	$\delta(\text{OCO})(52)$, $\nu(\text{C}_2\text{O}_1)(25)$
$\nu_{19}(\text{b})$	926	927	w	$\nu(\text{C}_2\text{O}_3)(59)$, $\delta(\text{OOC})(26)$
$\nu_{20}(\text{b})$	698	712	m	$\nu(\text{C}_2\text{O}_1)(77)$, $\nu(\text{C}_2\text{O}_3)(17)$
$\nu_{21}(\text{b})$	193	193	m	Ring bending
	2889		w	FR: $2\nu_3$ and ν_2
	2716		w	$\nu_4 + \nu_{15} = 2733 \text{ cm}^{-1}$
	2020		w	$\nu_7 + \nu_8 = 2030 \text{ cm}^{-1}$
	1103		vw	$\nu_{19} + \nu_{21} = 1119 \text{ cm}^{-1}$
	1001		vw	$\nu_9 + \nu_{21} = 1001 \text{ cm}^{-1}$
	403		vw	FR: $2\nu_{21}$ and ν_{11}

^a Potential energy distribution. ^b Fermi resonance. ^c For numbering of atoms, cf. section 1.

TABLE II: Infrared Absorption Frequencies of Ethylene-d₄ Ozonide in an Argon Matrix

Assignment	Frequency, cm ⁻¹		Rel intensity	PED ^a
	Obsd	Calcd		
$\nu_1(\text{a})$	2249	2238	m	$\nu(\text{CD})(96)$
$\nu_2(\text{a})$	2118	2123	w	$\nu(\text{CD})(95)$
$\nu_3(\text{a})$	1160	1170	s	$\gamma_w(\text{CD}_2)(44)$, $\nu(\text{C}_2\text{O}_3)(23)$, $\nu(\text{C}_2\text{O}_1)(23)$
$\nu_4(\text{a})$	1135	1138	s	$\delta(\text{CD}_2)(59)$, $\nu(\text{C}_2\text{O}_1)(10)$, $\delta(\text{OCO})(10)$
$\nu_5(\text{a})$	1021	1028	s	$\nu(\text{C}_2\text{O}_1)(21)$, $\nu(\text{OO})(16)$, $\delta(\text{OCO})(12)$
$\nu_6(\text{a})$	972	970	m	$\nu(\text{C}_2\text{O}_3)(17)$, $\delta(\text{CD}_2)(17)$, $\delta(\text{OCO})(16)$
$\nu_7(\text{a})$	911	899	w	$\gamma_r(\text{CD}_2)(33)$, $\delta(\text{OCO})(25)$, $\nu(\text{OO})(24)$
$\nu_8(\text{a})$	851	852	m	$\gamma_t(\text{CD}_2)(76)$, $\nu(\text{OO})(10)$
$\nu_9(\text{a})$	759	749	s	$\nu(\text{OO})(42)$, $\gamma_r(17)$
$\nu_{10}(\text{a})$	672	641	m	$\nu(\text{C}_2\text{O}_1)(36)$, $\gamma_w(19)$, $\nu(\text{C}_2\text{O}_3)(17)$
$\nu_{11}(\text{a})$	338	339	vw	Ring pucker
$\nu_{12}(\text{b})$	2246	2233	w	$\nu(\text{CD})(97)$
$\nu_{13}(\text{b})$	2092	2111	w	$\nu(\text{CD})(97)$
$\nu_{14}(\text{b})$	1143	1164	s	$\gamma_w(\text{CD}_2)(45)$, $\nu(\text{C}_2\text{O}_3)(36)$
$\nu_{15}(\text{b})$	1059	1083	vs	$\delta(\text{CD}_2)(83)$
$\nu_{16}(\text{b})$	980	992	w	$\delta(\text{OCO})(46)$, $\nu(\text{C}_2\text{O}_1)(29)$
$\nu_{17}(\text{b})$	930	929	m	$\gamma_t(72)$
$\nu_{18}(\text{b})$	904	902	m	$\gamma_r(59)$, $\delta(\text{OOC})(12)$
$\nu_{19}(\text{b})$	830	832	w	$\gamma_r(45)$, $\nu(\text{C}_2\text{O}_3)(16)$
$\nu_{20}(\text{b})$	707	660	w	$\nu(\text{C}_2\text{O}_1)(62)$, $\nu(\text{C}_2\text{O}_3)(22)$
$\nu_{21}(\text{b})$		163		Ring bending
	2204		w	$\nu_{14} + \nu_{15} = 2202 \text{ cm}^{-1}$
	2181		w	$\nu_3 + \nu_5 = 2181 \text{ cm}^{-1}$
	2161		vw	$\nu_5 + \nu_{14} = 2164 \text{ cm}^{-1}$
	2132		vw	$\nu_3 + \nu_6 = 2132 \text{ cm}^{-1}$
	1122		vw	$\nu_6 + \nu_{21} (?)$
	1083		vw	$\nu_7 + \nu_{21} (?)$
	1074		w	$\nu_{18} + \nu_{21} (?)$

^a Potential energy distribution. ^b Fermi resonance.

TABLE III: Infrared Absorption Frequencies of Ethylene-2,2- d_2 Ozonide Produced from Ethylene- d_2 and Ozone in an Argon Matrix

Assignment	Frequency, cm^{-1}		Rel intensity	PED ^a	Remarks
	Obsd	Calcd			
ν_1	2973	2981	m	FR: ^b $\nu(\text{CH})(99)$	d_0d_2
	2967		s		d_0d_2
ν_2	2900	2891	m	$\nu(\text{CH})(99)$	d_0d_2
	2894		s		d_0d_2
ν_3	2240	2236	w	$\nu(\text{CD})(97)$	d_2
ν_4	2111	2117	m	$\nu(\text{CD})(97)$	d_2
ν_5		1480		$\delta(\text{CH}_2)(95)$	d_2
ν_6	1369	1363	w	$\gamma_w(\text{CH}_2)(75)$	d_2
ν_7	1199	1192	w	$\gamma_t(\text{CH}_2)(92)$	d_2
ν_8	1147	1167	s	$\gamma_w(\text{CD}_2)(42)$	d_2
ν_9	1132	1142	w	$\gamma_r(\text{CH}_2)(63)$	d_2
ν_{10}	1103	1117	s	$\delta(\text{CD}_2)(50), \gamma_r(15)$	d_2
ν_{11}	1068	1040	vs	$\nu(\text{C}_2\text{O}_1)(22), \nu(\text{C}_2\text{O}_3)(20),$ $\delta(\text{CD}_2)(18)$	
ν_{12}	986	998	m	$\delta(\text{O}_1\text{O}_2\text{O}_3)(34), \nu(\text{C}_5\text{O}_4)(25)$	d_2
ν_{13}	965	978	w	$\delta(\text{O}_1\text{C}_5\text{O}_4)(24), \gamma_r(\text{CD}_2)(16)$	d_2
ν_{14}	920	912	w	$\delta(\text{O}_3\text{O}_4\text{C}_5)(14), \gamma_r(\text{CD}_2)(13)$	d_2
ν_{15}	910	903	m	$\gamma_r(\text{CD}_2)(35)$	d_2
ν_{16}	847	858	m	$\gamma_t(\text{CD}_2)(71)$	d_2
ν_{17}	783	775	w	$\nu(\text{OO})(45)$	d_2
ν_{18}		716		$\nu(\text{C}_2\text{O}_1)(56), \nu(\text{C}_2\text{O}_3)(13)$	d_2
ν_{19}	683	655	w	$\nu(\text{C}_5\text{O}_1)(47), \nu(\text{C}_5\text{O}_4)(20)$	d_2
ν_{20}		359		Ring pucker	d_2
ν_{21}		177		Ring bending	d_2

^a Potential energy distribution. ^b Fermi resonance.

this author assigned the first excited state to symmetry species B. This assignment has been taken over in this work and will be supported by NCA.

4.3 Normal Coordinate Analysis (NCA). 1. Structural Data and Internal Coordinates. The following NCA is based on the r_s-r_0 structure of ethylene ozonide published by Kuczkowski¹ and shown in Figure 3.

The five-membered ring structure of the ozonides implies characteristic difficulties for a NCA, owing (i) to redundancies between the internal coordinates of the five-membered ring and (ii) to the fact that redundancies impede seriously transferability of force constants between molecules. In order to circumvent these difficulties the following procedure was chosen:

(i) Use of a redundant set of five stretching, five bond-bending, and five bond-torsion coordinates for the five-membered ring, for definition cf. Figure 3. s vectors for these coordinates were given by Wilson et al.¹¹ This set leads to six redundancies, but for most of the coordinates zeroth order estimates of force constants may be found in the literature.^{12,13}

(ii) For each of the CH_2 groups two stretching and one bending, wagging, twisting, and rocking coordinate were chosen, assuming local C_{2v} symmetry for the group. These six coordinates are linearly independent, and there are zeroth order values of the associated force constants available. Expressions for the vectors of the less common wagging, twisting, and rocking coordinates were constructed according to (referring to Figure 4)

$$\begin{aligned} \gamma_w &= 2^{-1}(R_{143}^{\text{II}} - R_{243} + R_{153} - R_{253}) \\ \gamma_t &= 2^{-3/2}(R_{143} - R_{243} - R_{153} + R_{253}) \\ \gamma_r &= 2^{-1}(R_{143} + R_{243} - R_{153} - R_{253}) \end{aligned} \quad (1)$$

where the R_{ikl}^{II} 's denote bending type coordinates of the valence angles spanned by nuclei i, k, l .

Table IV gives a list of symmetrized coordinates obtained from the 27 internal coordinates mentioned above. The representation of the covering group generated by the latter decomposes according to $15A \oplus 12B$, for the internal coordinates of the ring alone $9A \oplus 6B$. The redundancies among the latter decompose according to $4A \oplus 2B$. Referring to the structural parameters shown in Figure 3 and the definitions of the symmetry coordinates given in Table IV, the redundancies may be given in numerical form as

A block

$$\begin{pmatrix} S_{6A} \\ S_{8A} \\ S_{14A} \\ S_{15A} \end{pmatrix} = \begin{pmatrix} -0.0823 & 0.3440 & -0.3645 & -0.2676 & -0.4627 \\ 0.2254 & -0.4791 & 0.3594 & -0.8174 & -0.2754 \\ 0.1507 & 0.0547 & -0.2778 & -0.0255 & -0.4085 \\ 0.2596 & -0.1978 & -0.0751 & 0.4711 & -0.7554 \end{pmatrix} \begin{pmatrix} S_{1A} \\ S_{2A} \\ S_{3A} \\ S_{7A} \\ S_{13A} \end{pmatrix} \quad (2)$$

B block

$$\begin{pmatrix} S_{6B} \\ S_{12B} \end{pmatrix} = \begin{pmatrix} -0.8309 & -0.5798 & -0.6187 & -0.2863 \\ -0.2976 & -0.2077 & 0.4589 & -1.5356 \end{pmatrix} \begin{pmatrix} S_{1B} \\ S_{2B} \\ S_{5B} \\ S_{11B} \end{pmatrix} \quad (3)$$

Relations 2 and 3 allow expression of the harmonic potential energy function by independent coordinates solely. They further may serve in relating harmonic potential constants of five-membered rings expressed either in independent or redundant coordinates.

Since the data available at the present time do not allow determination of the most general harmonic force field (comprising 111 constants), it was a priori subject to restrictions. Most interaction constants between internal coordinates having no nucleus in common were put equal to zero. In particular no interaction constants between typical CH_2 group coordinates were admitted (cf. section 4.3(ii)). Normal coor-

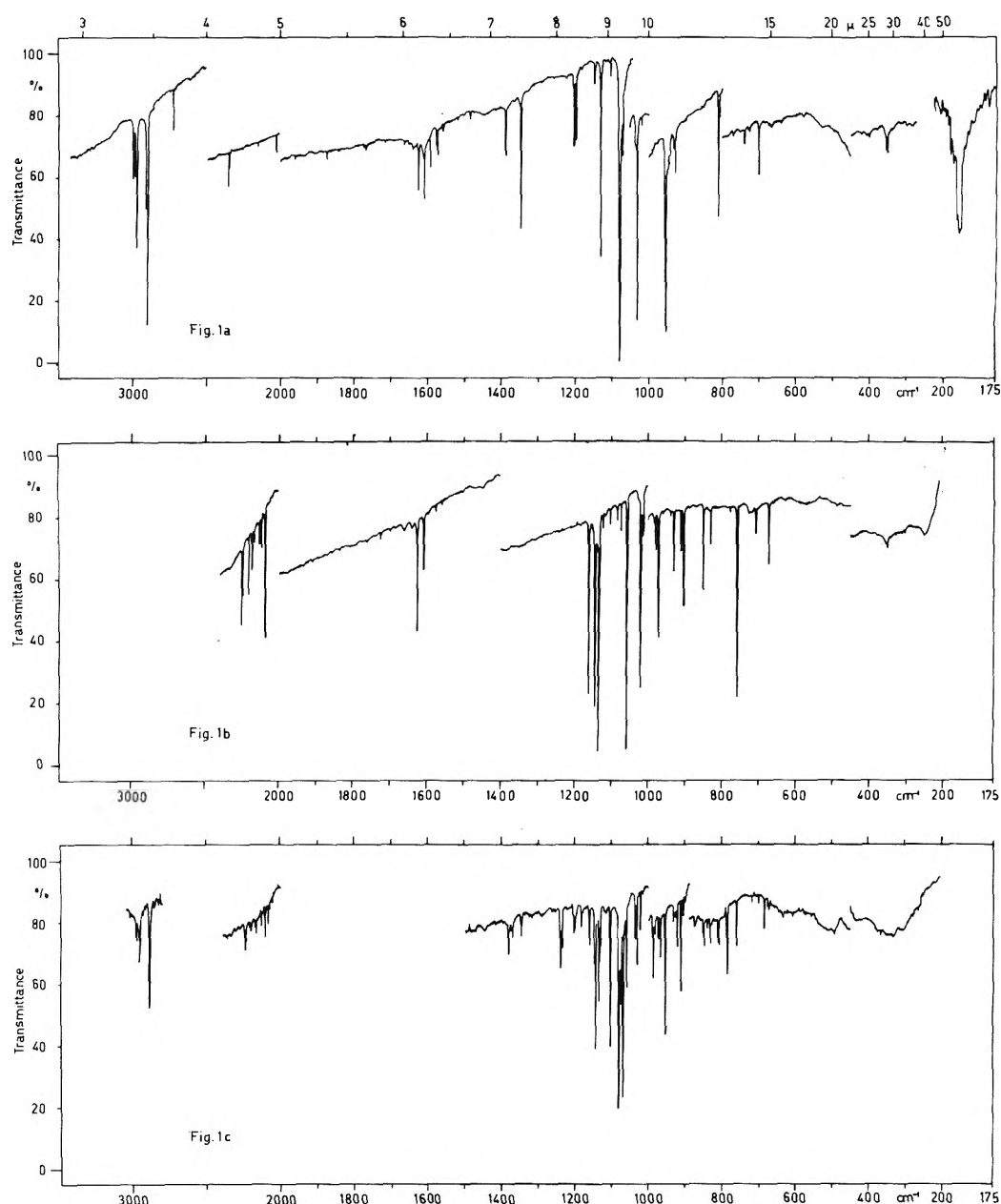


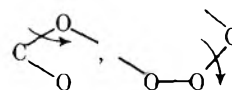
Figure 1. Infrared spectra of isotopic ethylene ozonides: (a) ethylene ozonide in an argon matrix $M/A \approx 350$; (b) ethylene- d_4 ozonide in an argon matrix $M/A \approx 350$; (c) ethylene ozonide produced from ethylene-1,1- d_2 and ozone in an argon matrix $M/A \approx 350$. 4000–200 cm^{-1} : Perkin-Elmer Model 325 spectrophotometer, slit program 4. <200 cm^{-1} : Perkin-Elmer Model 301 far-infrared spectrophotometer, spectral slit width 1–0.7 cm^{-1} .

dinate analysis was carried out by means of a computer program,¹⁴ allowing least-squares fitting of harmonic force constants. Force constants resulting from the fitting process not exceeding their root mean square value were discarded. The NCA yielded a set of 30 significant force constants based on 55 observed fundamentals; values are collected in Table IV. The following comments should be made:

(i) *Values of Force Constants.* Where comparison with other molecules is possible, ozonide force constants agree reasonably. This applies in particular to the bending, wagging, twisting, and rocking force constants of the CH_2 group, which turn out similar to those of paraffins.¹⁵ However, the $\text{O}_1\text{-C}_2$ force constant appears to be appreciably lower than, for instance, in tetrahydrofuran¹³ (4.7 vs. 5.5 mdyn/\AA).

For the typical ring force constants there exist few examples for comparison, in particular where the peroxide group incorporated in a five-membered ring is concerned.

In hydrogen peroxide, in which the dihedral angle amounts to approximately 112° , the O–O torsional force constant (for infinitesimal vibration) is approximately 0.037×10^{-11} erg/radian²,¹⁶ whereas for EO it lies near 0.2×10^{-11} erg/radian². It should be remembered that in the latter case for the dihedral angle a value of 50.2° has been found. Probably the much greater stiffness toward O–O torsion is related to the near cis conformation in the ozonide. In contrast to the O–O torsional force constant the remaining two pairs of ring torsional constants



were found to be much lower in value (cf. Table IV). This result is an immediate consequence of the assignment of the lowest mode as a B type vibration.

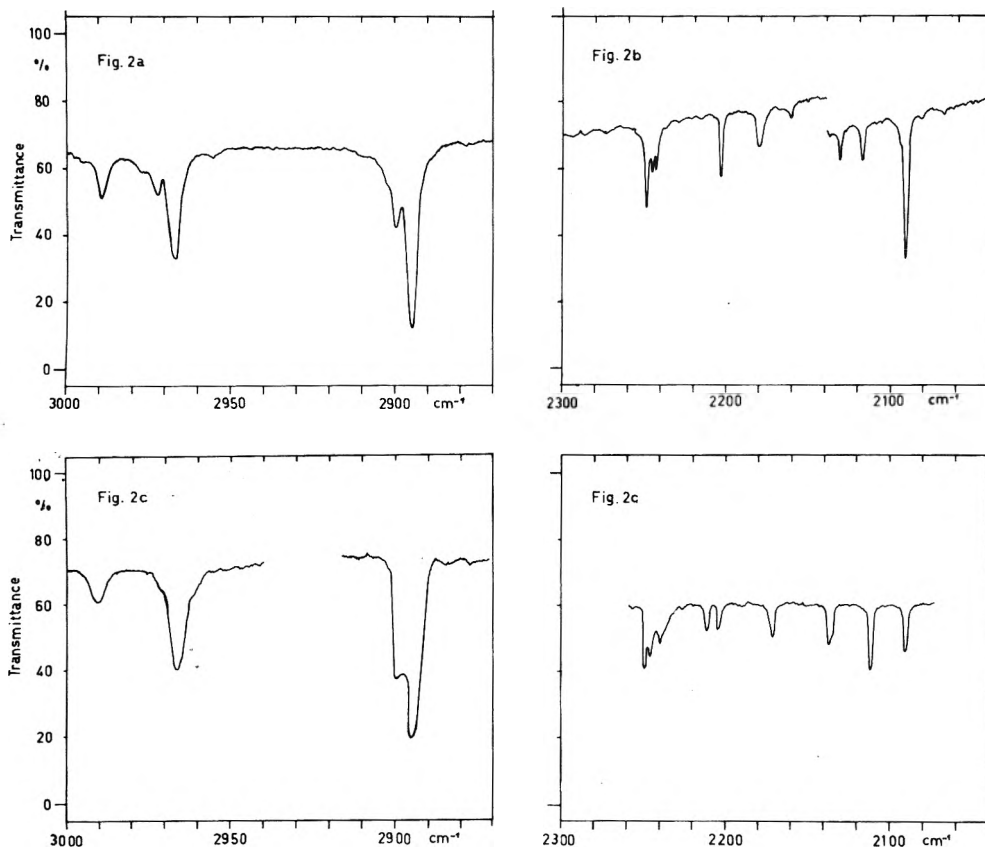


Figure 2. Matrix infrared spectra of secondary ethylene ozonides, $\nu(\text{CH})$ stretching region expanded: (a) EO-d_0 , (b) EO-d_4 , (c) EO-2,2-d_2 , slit program 3.

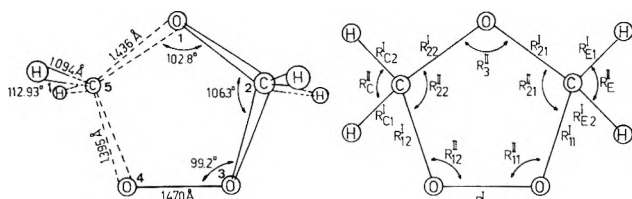


Figure 3. r_s-r_o structure and internal coordinates of ethylene ozonide. Dihedral angles and the corresponding bond-torsion coordinates for the five-member ring are defined as in ref 11: $(\text{O}_1\text{C}_2\text{O}_3\text{O}_4) = (\text{O}_1\text{C}_5\text{O}_4\text{O}_3) = 41.27^\circ$ (τ_{11}, τ_{12}); $(\text{C}_2\text{O}_1\text{C}_5\text{O}_4) = (\text{C}_5\text{O}_1\text{C}_2\text{O}_3) = -16.60^\circ$ (τ_{21}, τ_{22}); $(\text{C}_2\text{O}_3\text{O}_4\text{C}_5) = 50.24^\circ$ (τ_3).

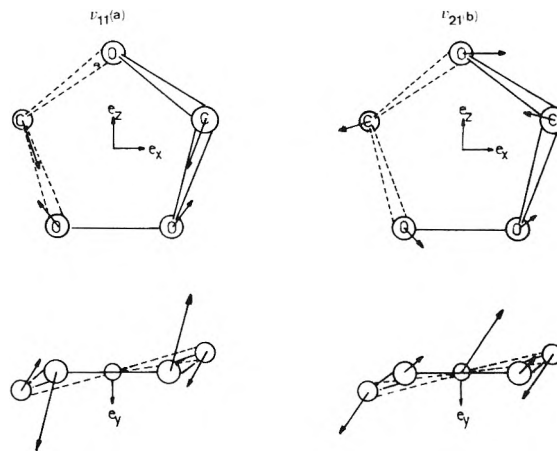


Figure 5. Ring puckering modes of ethylene ozonide.

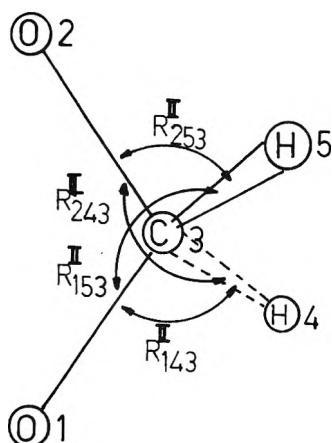


Figure 4. Definitions of CH_2 group internal coordinates.

(ii) Description of Normal Modes by Group Modes. As may be seen from the potential energy distribution (PED) given in Tables I, II, and III, some of the normal modes are approximately typical CH_2 group modes, e.g., CH stretching, CH_2 bending, wagging, twisting, and rocking modes of the EO-d_0 species. However, as is to be expected, the ring normal modes are complex mixtures of the 15 ring coordinates. The two low lying ring pucker type modes $\nu_{11}(\text{a})$ (352 cm^{-1}) and $\nu_{21}(\text{b})$ (193 cm^{-1}) among these are particularly interesting. As already has been mentioned above in connection with ring force constants, the fact that the A type mode is higher in frequency seems to be related with the high O-O torsional

TABLE IV: Symmetry Coordinates and Harmonic Force Constants of Ethylene Ozonide

Linear combination of internal coordinates ^a	Notation	Harmonic force constants ^b
$2^{-1/2}(R_{11}^I \pm R_{12}^I)$	S_{1A}, S_{1B}	4.652
$2^{-1/2}(R_{21}^I \pm R_{22}^I)$	S_{2A}, S_{2B}	4.701
R_3^I	S_{2A}	4.620
$1/2(R_{E1} + R_{E2} \pm R_{C1} \pm R_{C2})$	S_{4A}, S_{3B}	4.689
$1/2(R_{E1} - R_{E2} \pm R_{C1} \mp R_{C2})$	S_{5A}, S_{4B}	
$2^{-1/2}(R_{11}^{II} \pm R_{12}^{II})$	S_{6A}, S_{5B}	2.294
$2^{-1/2}(R_{21}^{II} \pm R_{22}^{II})$	S_{7A}, S_{6B}	2.949
R_3^{II}	S_{8A}	2.267
$2^{-1/2}(R_E^{II} \pm R_C^{II})$	S_{9A}, S_{7B}	0.739
$2^{-1/2}(\gamma_{w1} \pm \gamma_{w2})$	S_{10A}, S_{8B}	0.653
$2^{-1/2}(\gamma_{t1} \pm \gamma_{t2})$	S_{11A}, S_{9B}	1.334
$2^{-1/2}(\tau_{r1} \pm \tau_{r2})$	S_{12A}, S_{10B}	0.958
$2^{-1/2}(\tau_{11} \pm \tau_{12})$	S_{13A}, S_{11B}	0.071
$2^{-1/2}(\tau_{21} \pm \tau_{22})$	S_{14A}, S_{12B}	0.030
τ_3	S_{15A}	0.209
	S_{1A}, S_{2A}	1.804
	S_{1A}, S_{3A}	0.567
	S_{1A}, S_{6A}	0.165
	S_{1A}, S_{7A}	0.853
	S_{2A}, S_{7A}	1.673
	S_{2A}, S_{8A}	1.275
	S_{3A}, S_{6A}	1.773
	S_{3A}, S_{8A}	0.174
	$S_{9A}, S_{1A}; S_{9A}, S_{2A}$	-0.253
	$S_{11A}, S_{1A}; S_{11A}, S_{2A}$	-0.052
	$S_{12A}, S_{1A}; S_{12A}, S_{2A}$	-0.046
	S_{7A}, S_{8A}	0.477
	S_{7A}, S_{9A}	0.256
	R_{11}^{II}, R_{12}^{II}	0.921
	R_{11}^{II}, R_{21}^{II}	-0.668
	R_{21}^{II}, R_{22}^{II}	0.762

^a Internal coordinates refer to Figures 3 and 4. ^b Stretching force constants in 10^5 erg cm^{-2} ; bending force constants in 10^{-11} erg radian^{-2} ; stretching-bending force constants in 10^{-3} erg cm^{-1} radian^{-1} .

TABLE V: Levels Included in Fermi Resonance (Problem of the CH_2 Groups, cf. Table I)

Levels no.	Quantum no.					
	ν_1	ν_2	ν_3	ν_{12}	ν_{13}	ν_{14}
0	0	0	0	0	0	0
1	1	0	0	0	0	0
2	0	1	0	0	0	0
3	0	0	1	0	0	0
4	0	0	0	1	0	0
5	0	0	0	0	1	0
6	0	0	0	0	0	1
7	0	0	2	0	0	0
8	0	0	0	0	0	2

force constant and the low O-O torsional angle. The behavior of the two modes is best illustrated by Figure 5, in which the amplitudes of the Cartesian displacement vectors of the ring nuclei are reproduced.

4.4 *Fermi Resonances Associated with CH_2 Modes.* Numerous normal coordinate analyses of medium size molecules

TABLE VI: Fermi Resonance Matrix Elements, $\nu(\text{CH})$ and $\delta(\text{CH}_2)$ Levels

$$\begin{aligned}
 H_{00} &= \frac{3}{4}f_{EEEE}(\frac{1}{2}\gamma_3^{-2} + \frac{1}{2}\gamma_6^{-2} + \gamma_3^{-1}\gamma_6^{-1}) \\
 H_{11} &= H_{22} = H_{44} = H_{55} = H_{00} \\
 H_{33} &= \frac{1}{8}f_{EEEE}(5\gamma_3^{-2} + 3\gamma_6^{-2} + 3\gamma_3^{-1}\gamma_6^{-1}) \\
 H_{66} &= \frac{1}{8}f_{EEEE}(3\gamma_3^{-2} + 5\gamma_6^{-2} + 3\gamma_3^{-1}\gamma_6^{-1}) \\
 H_{77} &= \frac{3}{8}f_{EEEE}(13\gamma_3^{-2} + \gamma_6^{-2} + 10\gamma_3^{-1}\gamma_6^{-1}) \\
 H_{88} &= \frac{3}{8}f_{EEEE}(\gamma_3^{-2} + 13\gamma_6^{-2} - 10\gamma_3^{-1}\gamma_6^{-1}) \\
 H_{02} &= 2^{-3/2}f_{EIEE}(\gamma_3^{-1}\gamma_1^{-1/2} + \gamma_3^{-1}\gamma_6^{-1/2}) \\
 H_{03} &= \frac{3}{4}f_{EEE}(\gamma_3^{-3/2} + \gamma_3^{-1/2}\gamma_6^{-1}) \\
 &\quad + \frac{1}{8}f_{EIEE}\gamma_3^{-1/2}(\gamma_1^{-1} + \gamma_4^{-1} - \gamma_2^{-1} - \gamma_5^{-1}) \\
 H_{07} &= 3 \cdot 2^{-1/2}f_{EEEE}(2^{1/2}\gamma_3^{-2} + 2^{-1}\gamma_6^{-2} + 2^{1/2}\gamma_3^{-1}\gamma_6^{-1}) \\
 H_{08} &= 3 \cdot 2^{-1/2}f_{EEEE}(2^{-1}\gamma_3^{-2} + 2^{1/2}\gamma_6^{-2} + 2^{1/2}\gamma_3^{-1}\gamma_6^{-1}) \\
 H_{27} &= \frac{1}{2}f_{EIEE}\gamma_3^{-1}\gamma_1^{-1/2} \\
 H_{28} &= \frac{1}{2}f_{EIEE}\gamma_6^{-1}\gamma_1^{-1/2} \\
 H_{37} &= 3 \cdot 2^{-1/2}f_{EEE}(\gamma_3^{-1/2} + 2^{-1}\gamma_3^{-1/2}\gamma_6^{-1}) \\
 &\quad + 2^{-5/2}f_{EIEE}\gamma_3^{-1/2}(\gamma_1^{-1} - \gamma_2^{-1} + \gamma_4^{-1} + \gamma_5^{-1}) \\
 H_{38} &= 3 \cdot 2^{-3/2}f_{EEE}\gamma_4^{-1}\gamma_3^{-1/2}
 \end{aligned}$$

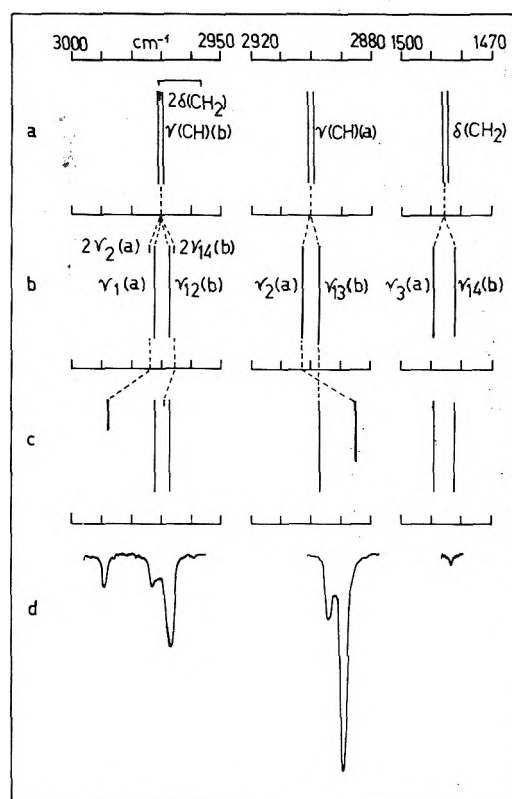


Figure 6. EO- d_0 Fermi resonance of $\nu(\text{CH})$ stretching and bending modes: (a) uncoupled CH_2 groups; (b) splitting by harmonic interaction; (c) splitting by Fermi resonance interaction; (d) experimental spectrum.

(8-11 nuclei) provide evidence for the assumption that most often interaction constants between internal coordinates may be considered negligibly small, if their s vectors have no nucleus in common. Expressed in a more direct way, this amounts to considering as significant only interaction constants between internal coordinates whose s vectors have at least one nucleus in common. If they have one bond in common most often the interaction constants appear to be indispensable. It appears tempting to transfer this concept of the (topologically) local nature of harmonic force fields to the anharmonic constants.

The EO molecule offers a favorable example for study of Fermi resonances associated with the stretching and bending modes of CH_2 groups. In this molecule the two CH_2 groups are

TABLE VII: Eigenvalues and Eigenvectors of Fermi Resonance, $\nu(\text{CH})$ Region

Zeroth order states	Zeroth order levels (assumed), cm^{-1}	Resulting states by FR	FR levels, cm^{-1}	Eigenvectors		
				α_i	β_i	γ_i
$\psi_2(Q_{a1})$	2903	$\bar{\psi}_1$	2885	0.908	-0.313	-0.278
$\psi_7(Q_{a3})$	2975	$\bar{\psi}_2$	2989	0.401	0.461	0.792
$\psi_8(Q_{b3})$	2965	$\bar{\psi}_3$	2969	0.119	0.830	0.544

TABLE VIII: Thermodynamic Functions of Ethylene Ozonide $^{12}\text{C}_2^{14}\text{H}_4^{16}\text{O}_3^{a-c}$ [J/(K mol)]

T, K	$-(g^0 - h_0^0)/T$	$(h^0 - h_0^0)/T$	s^0	c_p^0
298.15	232.860	46.002	278.862	68.599
300	233.145	46.142	279.287	68.982
400	247.528	54.447	301.975	89.565
500	260.632	63.341	323.972	107.717
600	272.954	72.019	344.973	122.576
700	284.673	80.131	364.804	134.621
800	295.867	87.578	383.445	144.482
900	306.580	94.369	400.949	152.649
1000	316.848	100.548	417.396	159.480
1250	340.754	113.701	454.455	172.272
1500	362.449	124.226	486.674	180.886

^a Ideal gaseous state. ^b Rigid rotor-harmonic oscillator approximation. ^c Recommended values of fundamental physical constants (NBS).

separated by one oxygen nucleus. One therefore might assume that Fermi resonances between $\delta(\text{CH}_2)$ combination tones and the $\nu(\text{CH})$ stretching fundamentals occur only within each CH_2 group. If this assumption is made, the part of the anharmonic potential function involving the CH_2 stretching and bending coordinates reads as (cf. Figure 4 and Table IV, omitting upper indices)

$$V_{\text{anh}} = f_{\text{EEE}}(R_E^3 + R_C^3) + f_{\text{E1E2E}}(R_{E1}R_{E2}R_E + R_{C1}R_{C2}R_C) + f_{\text{E1E}}(R_{E1}R_E^2 + R_{E2}R_E^2 + R_{C1}R_C^2 + R_{C2}R_C^2) + f_{\text{EEEE}}(R_E^4 + R_C^4) \quad (4)$$

In eq 4 it has again been assumed that the CH_2 groups have C_{2v} local symmetry. If for each CH_2 group locally symmetrized CH -stretching coordinates are introduced

$$\begin{pmatrix} L_{E_s} \\ L_{C_s} \\ L_{E_a} \\ L_{C_a} \end{pmatrix} = \frac{1}{\sqrt{2}} \begin{pmatrix} 1 & 1 & \cdot & \cdot \\ \cdot & \cdot & 1 & 1 \\ 1 & -1 & \cdot & \cdot \\ \cdot & \cdot & 1 & -1 \end{pmatrix} \begin{pmatrix} R_{E1} \\ R_{E2} \\ R_{C1} \\ R_{C2} \end{pmatrix} \quad (5)$$

and if, based on the results of the NCA, these coordinates are then symmetrized with respect to the covering group C_2 , one finds, considering the symmetrized coordinates as generalized normal coordinates:

$$\begin{pmatrix} Q_{a1} \\ Q_{a2} \\ Q_{b1} \\ Q_{b2} \\ Q_{a3} \\ Q_{b3} \end{pmatrix} = \begin{pmatrix} \frac{1}{2} & \frac{1}{2} & \frac{1}{2} & \frac{1}{2} & \cdot & \cdot \\ \frac{1}{2} & -\frac{1}{2} & \frac{1}{2} & -\frac{1}{2} & \cdot & \cdot \\ \frac{1}{2} & \frac{1}{2} & -\frac{1}{2} & -\frac{1}{2} & \cdot & \cdot \\ \frac{1}{2} & -\frac{1}{2} & -\frac{1}{2} & \frac{1}{2} & \cdot & \cdot \\ \cdot & \cdot & \cdot & \cdot & 2^{-1/2} & 2^{-1/2} \\ \cdot & \cdot & \cdot & \cdot & 2^{-1/2} & -2^{-1/2} \end{pmatrix} \begin{pmatrix} R_{E1} \\ R_{E2} \\ R_{C1} \\ R_{C2} \\ R_E \\ R_C \end{pmatrix} \quad (6)$$

the potential function (4) transforms into

$$V_{\text{anh}} = \frac{1}{\sqrt{2}} f_{\text{EEE}}(Q_{a3}^3 + 3Q_{a3}Q_{b3}^2) + \frac{1}{2\sqrt{2}} f_{\text{E1E2E}}(Q_{a1}^2Q_{a3} - Q_{a2}^2Q_{a3} + Q_{b1}^2Q_{a3} - Q_{b2}^2Q_{a3} + 2Q_{a1}Q_{b1}Q_{b3} - 2Q_{a2}Q_{b2}Q_{b3}) + f_{\text{E1EE}}(Q_{a3}^2Q_{a1} + Q_{b3}^2Q_{a1} + 2Q_{a3}Q_{b3}Q_{b1}) + f_{\text{EEEE}}(Q_{a3}^4 + 6Q_{a3}^2Q_{b3}^2 + Q_{b3}^4) \quad (7)$$

Using harmonic oscillator wave functions and the results from the normal coordinate analysis, one may directly set up a Fermi resonance eigenvalue problem with the energy matrix

$$H_{v\bar{v}} = (\psi_{v\bar{v}} | \hat{V}_{\text{anh}} | \psi_{v\bar{v}})$$

encompassing the levels listed in Table V:

A block

$$\begin{pmatrix} E_0 + H_{00} - \lambda & H_{01} & H_{03} & H_{07} & H_{06} \\ H_{01} & E_2 + H_{11} - \lambda & 0 & H_{27} & H_{26} \\ H_{03} & 0 & E_3 + H_{33} - \lambda & H_{37} & H_{36} \\ H_{07} & H_{27} & H_{37} & E_7 + H_{77} - \lambda & 0 \\ H_{06} & H_{26} & H_{36} & 0 & E_6 + H_{66} - \lambda \end{pmatrix} = 0 \quad (8)$$

B block

$$\begin{pmatrix} E_1 + H_{11} - \lambda & & & & \\ & E_4 + H_{11} - \lambda & & & \\ & & E_5 + H_{11} - \lambda & & \\ & & & E_6 + H_{11} - \lambda & \end{pmatrix} = 0 \quad (9)$$

where

$$E_0 = \frac{1}{2} \sum \bar{\nu}_k \\ E_i = \frac{1}{2} \sum \bar{\nu}_k + \bar{\nu}_i \quad i = 1, 2, 3, 4, 5, 6 \\ E_i = \frac{1}{2} \sum \bar{\nu}_k + 2\bar{\nu}_i \quad i = 7, 8 \quad (10)$$

The values $H_{0\bar{v}}$ are collected in Table VI, expressed in the conventional harmonic oscillator quantities $\gamma_i = \omega_i/\hbar$.¹¹ In

order to treat isotope effects in the anharmonic problem, it proved convenient to use the generalized normal coordinates given by eq 6 directly. In these coordinates the Hamiltonian of the harmonic problem assumes the form

$$\hat{H} = \sum \frac{1}{2} (\lambda_i^{(G)})^2 \hat{P}_i^2 + \lambda_i^{(F)2} \hat{Q}_i^2$$

i.e., the kinetic energy is in diagonal (not in unit) form. The eigenvalues ω_i of the normal oscillator problem in conventional normal coordinates are related to the eigenvalues of the generalized normal oscillators by

$$\omega_i = \lambda_i^{(G)} \cdot \lambda_i^{(F)}$$

therefore, $\gamma_i = \omega_i/h = (\lambda_i^{(G)}\lambda_i^{(F)})/h$. Obviously the various isotope species differ only in the quantities $\lambda_i^{(G)}$.

From eq 8 and 9 it is obvious that all zeroth order B type levels and one A type level experience the same shift H_{11} by the Fermi resonance interaction. For solution of the eigenvalue problem connecting the remaining five A type levels some simplification may be achieved by remarking that the ground state level ($V = 0$) and the first excited level of $\delta(\text{CH}_2)\nu_3(a)$ are widely separated from the other resonating levels. This reduces eq 8 to

$$\begin{vmatrix} \tilde{\nu}_2 + H_{11} - \lambda & H_{27} & H_{28} \\ H_{27} & 2\tilde{\nu}_7 + H_{77} - \lambda & 0 \\ H_{28} & 0 & 2\tilde{\nu}_8 + H_{88} - \lambda \end{vmatrix} = 0 \quad (8')$$

which has been solved either by iteration or direct diagonalization. By trial and error the interaction elements H_{27} and H_{28} were determined considering the diagonal elements as given by the observed fundamentals. The result of the analysis may be presented as follows:

(i) The observed pattern of absorption bands in the 3000- cm^{-1} region may be satisfactorily reproduced with respect to frequencies, if $H_{27} \approx H_{28} \approx 27.5 \text{ cm}^{-1}$.

(ii) Using this value one may interpret the interaction as shown in Figure 6. The uppermost part shows the normal mode pattern of two uncoupled CH_2 groups. In the middle part the splittings of the modes by harmonic interaction is reproduced, as obtained from the NCA. This splittings typically amount to $\approx 3 \text{ cm}^{-1}$ for the $\nu_1(a)$ $\nu_1 = 1$, $\nu_{12}(b)$ $\nu_{12} = 1$, $\nu_2(a)$ $\nu_2 = 1$, and $\nu_{13}(b)$ $\nu_{13} = 1$ levels, all associated with the stretching modes, and to $\approx 5 \text{ cm}^{-1}$ for the $\nu_3(a)$ $\nu_3 = 1$ and $\nu_{14}(b)$ $\nu_{14} = 1$ levels. The bottom part (Figure 6c, d) shows the band pattern produced by Fermi resonance, together with the observed spectrum. Obviously satisfactory agreement is achieved.

Qualitatively the Fermi resonance type interaction produces a shift of the $\nu = 1$ level of $\nu_2(a)$ by $\approx -18 \text{ cm}^{-1}$, whereas the $\nu = 2$ levels of $\nu_{14}(b)$ and $\nu_3(a)$ are shifted by $\approx +4$ and $\approx +14 \text{ cm}^{-1}$, respectively. These shifts are accompanied by remarkable intensity effects. As already pointed out B levels remain nearly unaffected.

The interpretation given above is further substantiated by qualitative consideration of intensities. Denoting the dipole moment expansion by

$$\mu(Q) = \mu(0) + \sum_s \left(\frac{\partial \mu}{\partial Q_s} \right)_0 Q_s + \sum_{s \leq s'} \left(\frac{\partial^2 \mu}{\partial Q_s \partial Q_{s'}} \right)_0 Q_s Q_{s'} + \dots \quad (11)$$

the intensity I of the transitions in which Fermi resonance levels are involved may be written as

$$I \propto |(\psi_0, \mu_z(Q) \bar{\psi}_i)|^2 \quad i = 1, 2, 3 \quad (12)$$

where

$$(\bar{\psi}_1 \bar{\psi}_2 \bar{\psi}_3) = (\psi_2(Q_{a1}) \psi_7(Q_{a3}) \psi_8(Q_{b3})) \begin{vmatrix} \alpha_1 & \alpha_2 & \alpha_3 \\ \beta_1 & \beta_2 & \beta_3 \\ \gamma_1 & \gamma_2 & \gamma_3 \end{vmatrix} \quad (13)$$

and the matrix of the coefficients of the resonating levels is given by the eigenvectors of eq 8. In Table VII a set of quantities relevant for intensity effects are collected. They show (i) the two overtones $2\nu_3(A)$ and $2\nu_{14}(A)$ may gather intensity only from the fundamental $\nu_2(a)$; (ii) $2\nu_3(A)$ may pick up 15–20% and $2\nu_{14}(A)$ at the most 2–4% of the intensity of $\nu_2(a)$. This behavior is qualitatively realized by the 3000- cm^{-1} band group of EO- d_0 , in which only five bands are detectable, namely, four fundamentals ($\nu(\text{CH})$) and one overtone ($2\delta(\text{CH}_2)$).

A further argument for the essential correctness of the interpretation given before is provided for by the $\nu(\text{CH})$ stretching region of the EO- d_2 species. Both the $-d_0$ and $-d_2$ species exhibit nearly identical spectra in the 3000- cm^{-1} region. In the case of EO- d_2 only Fermi resonance within one CH_2 group may contribute in this region. The Fermi resonance problem may be approximated by a 2×2 eigenvalue problem

$$\begin{vmatrix} \tilde{\nu}_5 + h_{11} - \lambda & h_{13} \\ h_{13} & 2\tilde{\nu}_8 + h_{33} - \lambda \end{vmatrix} = 0 \quad (14)$$

$\tilde{\nu}_5$ and $\tilde{\nu}_8$ denote the frequency of the locally symmetric $\nu(\text{CH})$ and of the $\delta(\text{CH}_2)$ mode. Furthermore, one has to consider the relation $h_{13} \approx \sqrt{2}H_{27}$. Equations 8' and 14 are based on the assumption that both the EO- d_0 and EO- d_2 species possess the same potential function (3). Solution of eq 14 is straightforward and yields nearly the same shifts as for EO- d_0 . This result explains the fact that the $\nu(\text{CH})$ regions of the two isotopes are practically identical.

As was mentioned in section 4.2 the $\nu(\text{CD})$ region of the EO- d_4 species is highly complex. At the present time there is little hope to successfully analyze the complex Fermi resonance which no doubt is responsible for the complexity of the 2200- cm^{-1} region.

5. Statistical Thermodynamic Functions

The available spectroscopic data allow calculation of the molar thermodynamic function of EO- d_0 in the ideal gaseous state in the harmonic oscillator rigid rotor approximation. Using principal moments of inertia given by Kuczkowski et al.:¹

$$I_a = 61.3035 \text{ u } \text{Å}^2$$

$$I_b = 62.4399 \text{ u } \text{Å}^2$$

$$I_c = 110.2300 \text{ u } \text{Å}^2$$

and the fundamentals given in Table I one finds the data collected in Table VIII.

Acknowledgment. We wish to thank the Swiss National Foundation (Projects No. 2.110.0-74 and No. 2.302.0-75) and Sandoz AG, Basle, for financial support. Furthermore, we wish to express our gratitude to the ETHZ Computing Center for generously granting computer time.

References and Notes

- † Research associate with Professor Richard C Lord, 1954.
- (1) C. W. Gillies and R. L. Kuczkowski, *J. Am. Chem. Soc.*, **94**, 6337, 7609 (1972); R. Latimer, R. L. Kuczkowski, and C. W. Gillies, *ibid.*, **94**, 348 (1972).
- (2) H. E. O'Neal and C. Blumstein, *Int. J. Chem. Kinet.*, **5**, 397 (1973).
- (3) R. Atkinson, B. J. Finlayson, and J. N. Pitts, Jr., *J. Am. Chem. Soc.*, **95**,

- 7592 (1973).
 (4) H. Kühne, S. Vaccani, T. K. Ha, A. Bauder, and Hs. H. Günthard, *Chem. Phys. Lett.*, **38**, 449 (1976).
 (5) R. Criegee and G. Weiner, *Justus Liebigs Ann. Chem.*, **546**, 9 (1949).
 (6) P. Groner, I. Stolkin, and Hs. H. Günthard, *J. Phys. E*, **6**, 122 (1973).
 (7) R. Werder, Thesis ETH, Zurich, No. 3970.
 (8) A. Murray, III, and D. L. Williams, "Organic Syntheses with Isotopes", Part II, pp 1433, 1474.
 (9) Reference 8, Part III, p 1425.
 (10) P. Hölemann and K. Clusius, *Berichte*, **70B**, 819 (1937).

- (11) E. Br. Wilson, Jr., J. C. Decius, and P. C. Cross, "Molecular Vibrations", McGraw-Hill, London, 1955.
 (12) K. B. Blick, J. W. DeHaan, and K. Niedensu, *Spectrochim. Acta, Part A*, **26**, 2319 (1970).
 (13) J. M. Eyster and K. W. Prohovsky, *Spectrochim. Acta, Part A*, **30**, 2041 (1974).
 (14) H. Hunziker, *J. Mol. Spectrosc.*, **17**, 131 (1965).
 (15) H. Primas and Hs. H. Günthard, *Helv. Chim. Acta*, **36**, 1659, 1791 (1953).
 (16) J. A. Lannon, F. D. Verderame, and R. W. Anderson, *J. Chem. Phys.*, **54**, 2212 (1971).

Infrared Frequencies of Amide, Urea, and Urethane Groups

C. G. Cannon¹

Research Department, ICI Fibres, Harrogate, Yorkshire, United Kingdom (Received February 14, 1975)

Publication costs assisted by ICI Fibres Limited

A possible interpretation is given with regard to the factors causing frequency shifts of certain characteristic amide bands appearing in related compounds.

The difference between the in-plane OCN group frequencies of the *N*-alkyl amide, *N,N'*-dialkyl urea, and *N*-alkyl urethane structures was briefly discussed in a previous paper where the spectra of polyamides, a polyurea, and a polyurethane were described.² In solid polymer films these structural groups are in comparable states of association and environment. The *N*-deuterio polymers have since been prepared and the amide II' frequencies identified.

The frequency differences are presented pictorially in Figure 1 where the four structures are arbitrarily positioned along the abscissa axis and the observed frequencies are plotted as ordinates. At first sight the frequency differences are puzzling. For example, in comparison with the amide I and II frequencies of the polyamide (CONH) those of the polyoxalamide (-NHCO-CONH-) are farther apart and those of the polyurea (-NHCONH-) closer together. In the polyurethane (-NHCO-O-) amide I is at a much higher frequency amide II is at roughly the same frequency as the polyamide. These shifts are rationalized if we consider that the extent of the π -p interaction between the C=O and the nitrogen lone pair electrons increases from left to right in the figure. The two full lines in the figure represent the hypothetical $\nu_{C=O}$ and ν_{C-N} frequencies of the OCN group assuming that no coupling of the type described by Fraser and Price³ exists. These are at approximately 1800 and 1280 cm^{-1} respectively in the absence of π -p interaction. If complete π -p conjugation occurred, and a symmetrical distribution of π electrons was realized in $^{-\delta}\text{O}=\text{C}=\text{N}^{+\delta}$, the two frequencies would be coincident at about 1550 cm^{-1} . The coupling and splitting of these two vibrations give the observed frequencies I and II' of the N deuterio groups (- - \odot - -, Figure 1). The further complication of coupling of II' with δ_{NH} to give II and III in the hydrogenated groups is thus responsible for their rather confused pattern of frequencies (- - \times - -, Figure 1). If this rationalization is accepted then we can conclude that the qualitative picture of increasing π -p conjugation through this series of structures is correct. This would imply, for example,

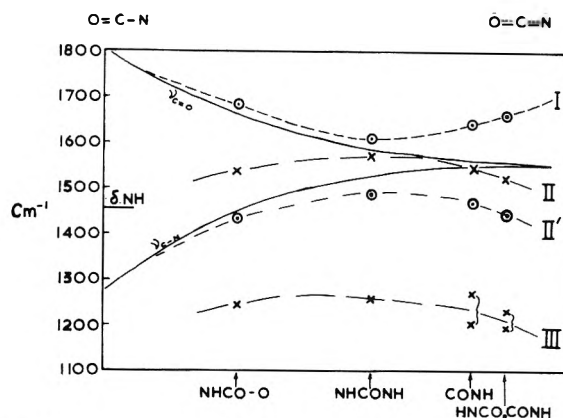


Figure 1.

decreasing basicity of the N atoms from urethane to oxalamide.

The pattern of frequency shifts of I and II' conforms exactly to that expected from vibrational coupling of two modes approaching each other in frequency. Do these frequencies cross over at the point of maximum mixing of vibrations? This usually occurs when the two modes are closest in frequency. The urea group has amide I and II' closest together but this point cannot correspond to the cross over because, were this so, the amide I frequency for the polyamide and polyoxalamide would then have more ν_{C-N} character than $\nu_{C=O}$. The calculations of Mizushima and his coworkers⁴ show that amide I has about 80% or more $\nu_{C=O}$ contribution. We must conclude therefore, that the $\nu_{C=O}$ and ν_{C-N} do not cross over and that the π -p interaction in the amide groups can never give a structure $^{-e}\text{O}-\text{C}=\text{N}^{+e}$.⁵ The limiting extent of interaction occurs in the $^{-\delta}\text{O}=\text{C}=\text{N}^{+\delta}$ structure with a symmetrical distribution of π electrons for which $\nu_{C=O} \approx \nu_{C-N}$.

Of course this whole analysis, however convincingly presented, rests on the arbitrary position of the four structural

groups along the abscissa axis. However, no other order could be found which gave a rational pattern fitting all the conditions.

Acknowledgment. Thanks are due to Dr. B. C. Stace for preparing the deuterated polymers and recording their spectra.

References and Notes

- (1) Postgraduate Research Associate with Richard C. Lord, 1953.
- (2) C. G. Cannon, *Spectrochim. Acta*, **16**, 302 (1960).
- (3) R. D. B. Fraser and W. C. Price, *Nature (London)*, **170**, 490 (1952).
- (4) S. Mizushima et al., *J. Chem. Phys.*, **24**, 408 (1956); **29**, 611 (1958).
- (5) Unless O protonation occurs in a proton donor medium when the 1669-cm^{-1} band is indeed $\nu_{\text{C}=\text{N}}$; Stewart and L. J. Muenster, *Can. J. Chem.*, **39**, 401 (1961).

Vibrational Spectra and Force Field of Tricarbonyl(trimethylenemethane)iron- h_6 and - d_6 ^{1a,b}

Dennis H. Finseth, Claude Sourisseau, and Foil A. Miller*^{1c}

Department of Chemistry, University of Pittsburgh, Pittsburgh, Pennsylvania 15260 (Received January 26, 1976)

Complete vibrational spectra are presented for tricarbonyl(trimethylenemethane)iron, $[(\text{H}_2\text{C})_3\text{C}]\text{Fe}(\text{CO})_3$, and for its perdeutero derivative. The latter has been made for the first time. The data include Raman spectra for the gas, liquid, and solid and infrared spectra for the gas and solid. A vibrational assignment has been made for 49 of the 50 active modes (25 in each molecule). All but 8 or 10 of these are certain. From the assignments a force field has been deduced which (a) reproduces the observed frequencies of both isotopic molecules with an average error of less than 1%, and (b) provides descriptions of the normal modes. From selected frequencies and force constants the following conclusions are drawn about the bonding. (1) All the C-H stretches are above 3000 cm^{-1} , indicating that the methylene carbons are unsaturated. (2) The C-C average stretching frequency, force constant, and bond distance all indicate that these bonds are unsaturated. (3) The iron-ligand stretching and tilting force constants are relatively large and indicate strong metal-ligand bonding. It appears that a model with bonds between iron and the three C-C π orbitals is better than one with a bond along the iron-central carbon line. These data, assignments, and force constants differ somewhat from earlier work on the hydrogenic compound. Some comments are made on the reliability and significance of force constants.

Introduction

Trimethylenemethane, $\text{C}(\text{CH}_2)_3$, is of considerable interest because of its unusual valence. In the free state it is a reactive diradical,^{2a} but it can be stabilized by formation of its tricarbonyliron complex to give tricarbonyl(trimethylenemethane)iron, $[(\text{H}_2\text{C})_3\text{C}]\text{Fe}(\text{CO})_3$. For brevity, the hydrogen version of the complex will hereafter be called h_6 and the deuterium version d_6 . Tricarbonyl(trimethylenemethane)iron was first prepared by Emerson et al. in 1966,^{2b} and was found to be fairly stable. The deuterated molecule has not been reported heretofore.

The structure of the complex, obtained by electron diffraction,³ is shown in Figure 1. Note that the CC_3 portion is nonplanar with the outer carbons displaced toward the iron atom. The angle Fe-C-C is 76.4° . The central carbon is 0.34 \AA out of the plane of the three methylene carbons in the direction away from the iron atom. The Fe-central C distance is 1.938 \AA whereas the Fe-outer C distance is 2.123 \AA . In addition, the plane of each CH_2 group is tilted about 14.4° relative to the extension of the corresponding C-C line, the tilt being away from the iron atom. There has also been an x-ray diffraction study of a related compound in which one hydrogen atom has been replaced by a phenyl group, with very similar results.⁴ Proton and ^{13}C NMR spectra indicate that

the six methylene protons are equivalent and the three methylene carbons are equivalent, or else are exchanging rapidly.^{2b} An early, very low resolution photoelectron spectrum was interpreted as giving ionization potentials for the orbitals in the hydrocarbon portion of the complex.⁵

It seemed to us that the vibrational spectrum would be useful and interesting, so a study of the infrared and Raman spectra of h_6 was undertaken.⁶ We hoped to make a complete vibrational assignment, and through that to answer some questions concerning the bonding. For example, do the C-C bonds behave spectroscopically more like single or double bonds? Also, one can imagine two extreme models for the bonding between iron and trimethylenemethane. In one case the bonding is directed from the iron to the central carbon atom; in the other case it is directed from the iron to the three methylene carbons or C-C bonds. The actual situation is probably intermediate, but just where is it between these two extremes?

During the course of the work a paper on the same subject by Andrews and Davidson appeared.⁷ This was followed by another by Andrews, Davidson, and Duce dealing with the force constants.⁸ These papers will be referred to hereafter as AD and ADD, respectively. Our work is considerably more extensive. It differs from that of AD and ADD in the following ways. (1) We have made the first preparation of d_6 , and report

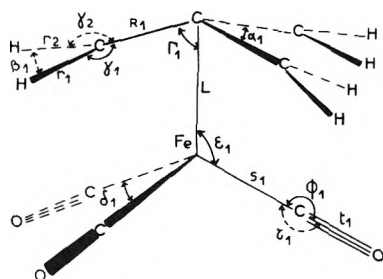
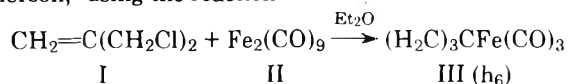


Figure 1. Structure of tricarbonyl(trimethylenemethane)iron and internal coordinates.

data for it too. These added results are very useful in the vibrational assignments and the force constant calculations; they provide important constraints. (2) We have obtained gas phase infrared and Raman data for both molecules. AD had only liquid state results. The gas phase data simplify the choice of some of the fundamentals, and remove the effects of intermolecular interactions. (3) We give values for two low fundamentals which AD left unassigned, and we differ with them on three other assignments. (4) Our calculated valence force constants differ from theirs in almost every case.

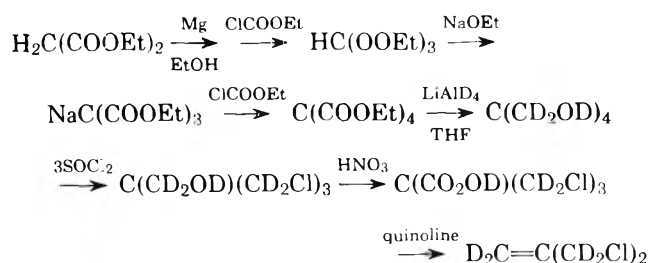
Experimental Section

A. *Preparation of h_6* . The method was that of Ehrlich and Emerson,⁹ using the reaction



I was obtained from Aldrich Chemical Co. and was used without further purification. II was purified immediately before use by washing with aqueous HCl, water, ethanol, and ether in the recommended manner.¹⁰ Because of the small scale of our preparation (0.5 g of I), III was not purified by distillation as was done by Ehrlich and Emerson. Instead the reaction mixture was vacuum-pumped at -22°C , and then chromatographed through neutral alumina (Wolem) with pentane for the solvent. This yielded a pale yellow liquid which was recrystallized from pentane at -78°C to yield the pure product. III is a pale yellow solid, mp 29°C , which is volatile and sublimates readily at room temperature. The vapor has a remarkable tendency to dissolve in stopcock grease. The product was further identified by its mass spectrum, the sample being introduced directly into the spectrometer as a gas.

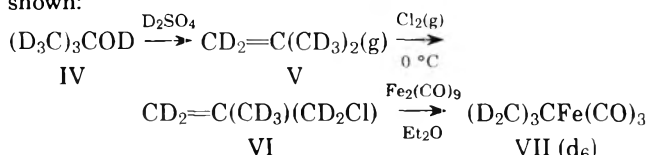
B. *Preparation of d_6* . To prepare d_6 by the same reaction used for h_6 , one would have to start with $\text{CD}_2=\text{C}(\text{CD}_2\text{Cl})_2$. Since it is not commercially available, the problem becomes one of obtaining it. Two methods were tried. The first was unsuccessful, but will be outlined because it seems reasonable on paper, and it may be helpful to describe our experience. The proposed reaction sequence was as follows:



This route allows one to deuterate with LiAlD_4 , which is

usually very efficient. There is very little chance of unwanted H-D exchange. Every step in the reaction sequence has been reported previously with the one exception of the reduction of $\text{C}(\text{COOEt})_4$ to $\text{C}(\text{CD}_2\text{OD})_4$.¹¹⁻¹⁴ We have done this reduction several times, but found that the separation of the product from the reaction mixture is very difficult. As a result, the $\text{C}(\text{CD}_2\text{OD})_4$ was not isolated in reasonable yield, and the method was abandoned.

The second, and successful, method involved the use of isobutylene- d_8 as an intermediate.¹⁵ The entire route to d_6 is shown:



In the first step 10 g of *tert*-butyl- d_9 alcohol- d (99.5% d) from Bio Rad Laboratories and 0.6 ml of D_2SO_4 (99% d) from Stohler Isotope Chemicals were used. About 6 g of isobutylene- d_8 was obtained, and its purity was checked by infrared spectroscopy. The spectrum was in complete agreement with that reported by Pathak and Fletcher, who prepared a sample with 99.5% deuterium.¹⁶ In the second step chlorine and isobutylene reacted in the gas phase in an 0.8-mm i.d. Pyrex capillary tube immersed in an ice bath.¹⁷ Following the advice of Reeve et al.,^{18,19} we adjusted the flow ratio of isobutylene to chlorine to approximately 1.3:1.0, and collected the product in a tower filled with crushed ice. The organic layer was extracted with several portions of di-*n*-butyl ether and carefully fractionated. The yield was about 4 g of methallyl- d_7 chloride (VI), bp $72-73^\circ\text{C}$ at 760 Torr. This sample contained a small amount of $\text{ClDC}=\text{C}(\text{CD}_3)_2$ as reported in the literature,¹⁸ but it was not removed. For the final reaction, the procedure of Ehrlich and Emerson was used.⁹ Because of the small scale of the preparation, the purification was done chromatographically as for h_6 . After recrystallization from *n*-pentane at -78°C , and evacuating to eliminate traces of iron pentacarbonyl, about 100 mg of product was obtained.

It is also possible to convert VI to $\text{CD}_2=\text{C}(\text{CD}_2\text{Cl})_2$ (VIII) by a liquid phase chlorination at 40°C .^{20,21} VIII could then be used in the same procedure as was employed to make h_6 . However the chlorination is reported to give only 34% of the desired product,^{20,21} so we chose to omit this step and proceed directly from VI to VII.

C. *Infrared Procedures*. Infrared spectra were obtained from 33 to 4000 cm^{-1} with Beckman IR-11 and IR-12 spectrophotometers. The frequency calibration was checked at or near the time the sample spectra were recorded.²² For the gas phase spectra a 10-cm cell was used. This proved inadequate to reveal any absorption below 370 cm^{-1} . Our 10-m cell was not used because there was too little well-purified sample at that time (10-20 mg) to risk losing it by adsorption on the metal walls and by solution in the stopcock grease. Solid phase spectra ($\sim 100\text{ K}$) were obtained with a cold cell of conventional design.²³ The sample was condensed from a jet of vapor onto a plate cooled with liquid nitrogen, and then annealed by repeated warming and cooling. Annealing had only a small effect on the spectrum.

D. *Raman Procedures*. Raman spectra were obtained with a Spex Ramalog unit which has been described elsewhere.²⁴ Excitation was from either the 488.0- or 514.5-nm lines from a Spectra Physics Model 164 argon ion laser. The frequency calibration was checked near the times the spectra were run.

Gas phase Raman spectra were obtained with a small heated gas cell designed here which allows the use of tem-

peratures from 25 to approximately 260 °C without the problem of condensation.²⁵ The principle is to have an attached liquid reservoir held at a lower temperature than the gas cell. The vapor pressure can be adjusted by controlling the temperature of the liquid reservoir, keeping that always the coolest portion of the system. The part of the cell containing the vapor to be examined is maintained a few degrees warmer to avoid condensation. The cell is constructed of Pyrex, with optically flat Pyrex windows to transmit the laser beam and with a side-arm liquid reservoir. It is filled by vacuum transfer and sealed, allowing it to be pressurized above 1 atm if desired. The cell is then completely enclosed in a two-section aluminum heating block. One section surrounds the liquid sample reservoir and the other the gas cell. The latter section has small ports at 90° for admitting the exciting radiation and observing the Raman scattering. The heating block is insulated, and the two sections are separated by a thin asbestos sheet. The two sections are heated separately by small cartridge heaters so that they can be maintained at different temperatures which are monitored continuously by thermocouples. In this work the sample reservoir was held at about 75 °C and the vapor at about 90 °C. This gave a vapor pressure of about 50 Torr. The laser power was 300–800 mW (measured at the laser). Under these conditions there was very little difficulty due to sample decomposition. The cell worked well, and satisfactory spectra were obtained for both compounds.

Liquid and solid samples were sealed in 1-mm i.d. thin-walled melting point capillaries. To keep the samples liquid, the sample compartment was held at approximately 30 °C with a heating tape. Solid state spectra were run in a variable temperature cold cell described previously,²⁶ using several temperatures between 25 and –100 °C. Changing the temperature had very little effect on the appearance of the spectra.

Experimental Results

Survey spectra are shown in Figures 2–5. The measured frequencies for h_6 (including the results of AD) are given in Table I, and for d_6 in Table II. Our infrared frequencies are believed to be accurate to $\pm 1 \text{ cm}^{-1}$ and the Raman ones to $\pm 2 \text{ cm}^{-1}$ unless a band is marked as broad, shoulder, or approximate.

The agreement between AD's results and ours for the Raman spectrum of liquid h_6 is quite good. Nowhere else are the measurements duplicated, for AD have no data for gas or solid, nor for d_6 , and we have no infrared results for liquid h_6 .

Vibrational Analysis

A. Aids in the Assignments. The symmetry was assumed to be C_{3v} as indicated by the electron diffraction study.³ We found the spectra to be completely compatible with it. The 45 normal modes are classified under C_{3v} as $10a_1 + 5a_2 + 15e$. They are summarized, together with the selection rules and our assignments, in Table III. The assignments of AD for h_6 are also included for comparison. As usual the schematic descriptions are a convenience but in many cases are not literally correct.

It was hoped that the gas phase infrared band contours would be helpful in interpreting the spectra. The P–R separation for the a_1 modes was calculated in the manner described by Seth-Paul and Dijkstra.²⁷ The structural parameters deduced from the electron diffraction study gave the following values for the principal moments of inertia: for h_6 , $I_A = 515.5$ and $I_B (=I_C) = 527.0 \text{ amu } \text{Å}^2$; for d_6 , $I_A = 543.3$ and $I_B (=I_C) = 551.8 \text{ amu } \text{Å}^2$. Thus both molecules are prolate tops, but are also almost spherical tops by accident. These values lead to

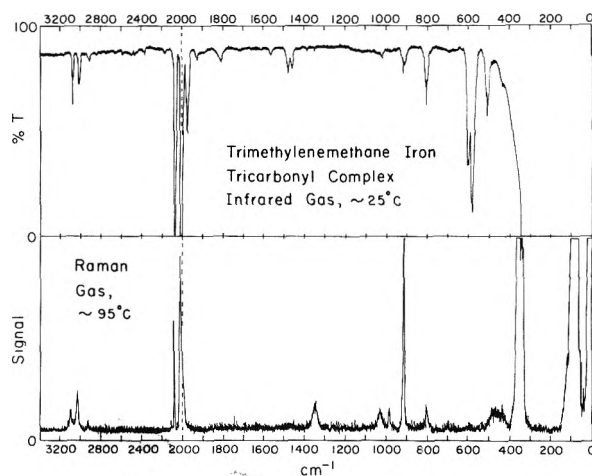


Figure 2. Infrared and Raman spectra of gaseous tricarbonyl(trimethylenemethane)iron (h_6).

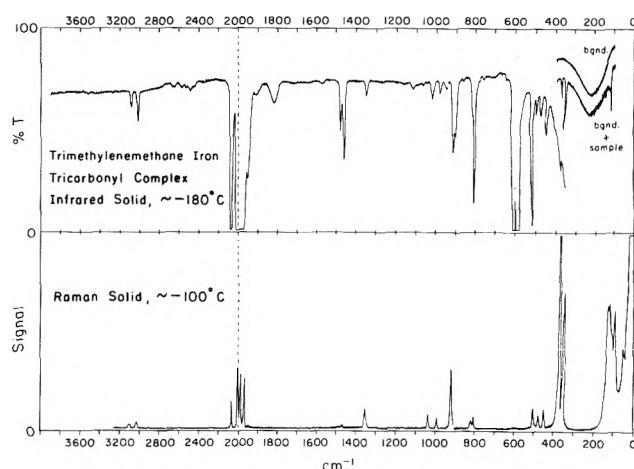


Figure 3. Infrared and Raman spectra of solid tricarbonyl(trimethylenemethane)iron (h_6).

a calculated P–R separation for the a_1 bands of 13.3 cm^{-1} for h_6 and 13.0 cm^{-1} for d_6 . These calculated values are apparently a little too high. Many bands were found to have P–R separations of 11 or 12 cm^{-1} , but almost none with 13 cm^{-1} . For e modes the P–R separations will vary unpredictably because of Coriolis interactions, but a value considerably different from 13 cm^{-1} indicates an e mode. Examples are 582, 603, and 3022 in h_6 and 1374 in d_6 .

The Raman depolarization ratio provided an independent criterion which sometimes contradicted the band contour evidence. Thus the following bands were depolarized (suggesting species e) but had parallel type contours and P–R separations (suggesting a_1): in h_6 , 2010 and 3086 cm^{-1} ; in d_6 , 549, 613, 1975, 2010, and 2328 cm^{-1} . In these cases we judged the Raman evidence to be decisive because the contours of the e modes can be similar to those for a_1 .

Another useful tool is the Teller–Redlich product rule.²⁸ Using the moments of inertia given earlier, and a molecular weight of 193.97 g/mol for h_6 and 200.01 g/mol for d_6 , one calculates a theoretical product rule ratio of 2.785 for species a_1 and 7.699 for species e . (We prefer to use the inverse of Herzberg's expression to make the ratios >1 .)

We wish to emphasize how helpful it was in making the assignments to have (a) data for both h_6 and d_6 , and (b) complete Raman and infrared gas phase data for both mole-

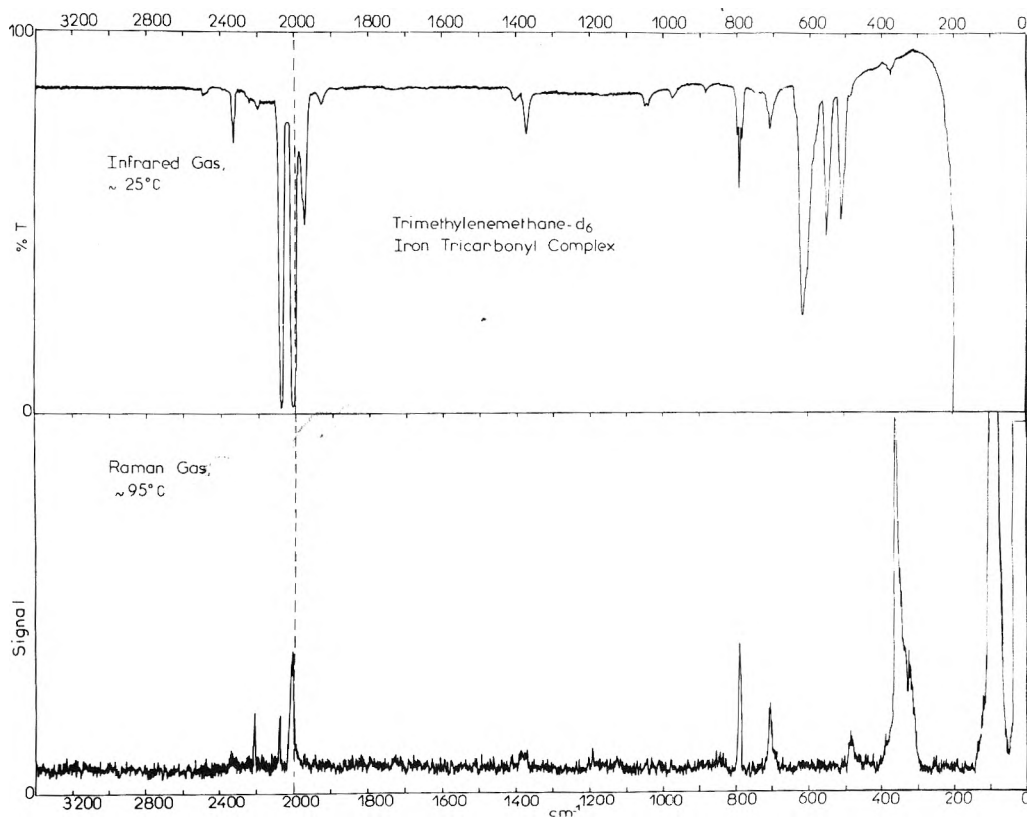


Figure 4. Infrared and Raman spectra of gaseous perdeuteriotricarbonyl(trimethylenemethane)iron (d_6).

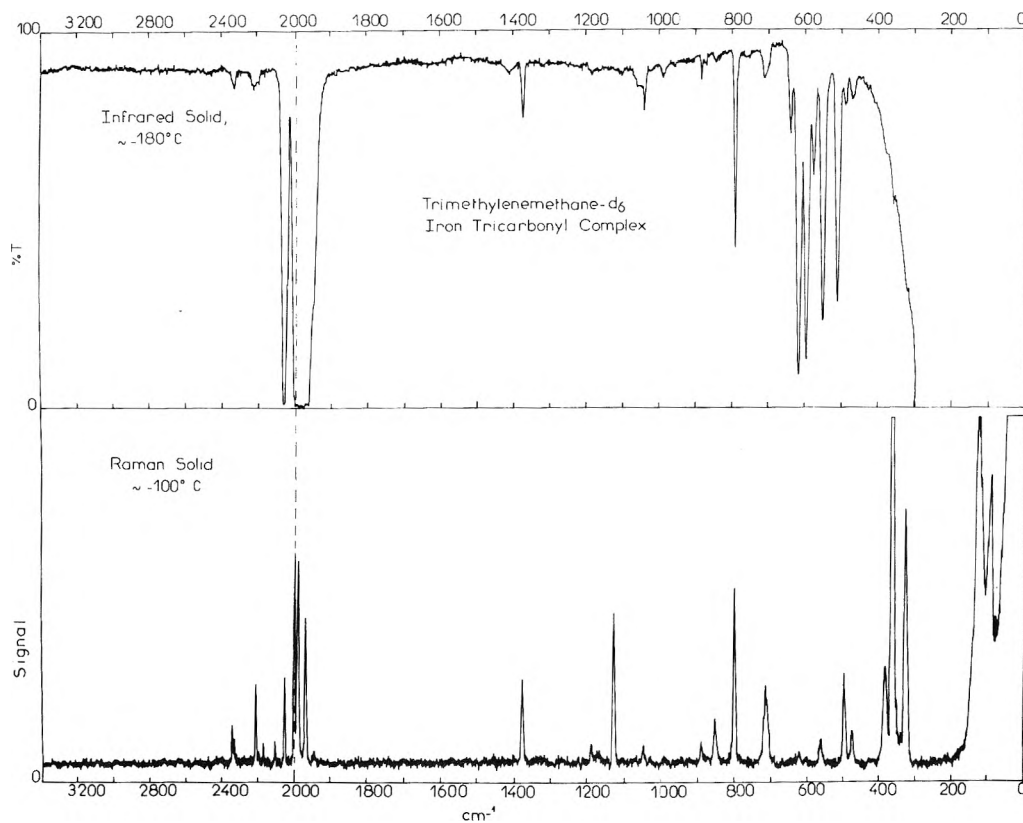


Figure 5. Infrared and Raman spectra of solid perdeuteriotricarbonyl(trimethylenemethane)iron (d_6).

TABLE I: Infrared and Raman Spectra of Tricarbonyl(trimethylenemethane)iron (h_6)^a

Liquid										Gas					
Solid					AD ^b										
Infrared		Raman		This work, Raman		Infrared		Raman		Infrared		Raman		Assignment	
cm ⁻¹	Inten ^c	cm ⁻¹	Inten ^c	cm ⁻¹	Inten ^c	cm ⁻¹	Inten ^c	cm ⁻¹	Inten ^c	cm ⁻¹	Inten ^c	cm ⁻¹	Inten ^c	cm ⁻¹	ρ
130	w	~144	~3, sh	130	3, sh	350	v	95	s, b	~130	sh	88	80, vb	0.74	Real ? ν ₃₀
350	v	351	45	~172	2, sh	350	v	352	m	350	18, sh	350	18, sh	0.63	ν ₁₀ 2 × 88 = 176
356	w	375	100	371	w	371	w	373	s	437	w	369	100	0.01	ν ₉
438	w	442	7	440	m	438	m	441	m	487	v	438	1		ν ₂₇
		470	6	468	3	471	w	471	m	487	v	470	2		ν ₂₆
		492	7	492	3	493	m	493	m	505	v	488	1		ν ₈
515	m			510	1, sh	510	s			512	m				ν ₂₅
579	s			582	v	579	s	582	v	582	s				ν ₂₄
602	m			605	v	603	s	605	v	606	s		<1		ν ₇
				727	w	727	w	726	w						?
				748	w	748	w								?
804	m	804	4	802	6	800	m	803	m	796	m	802	2	0.02	ν ₆
818	v, sh	816	3	814	1	814	sh	815	sh	808		820	<1		ν ₂₃
908	m			900	m	900	m			900	v	820	<1		ν ₂₂ ?
918	m	916	19	918	24	916	m	920	s	910	m	917	25	0.01	ν ₅
950	v			989	3	1023	w	989	m	922					?
989	w	1030	4	1030	4	1103	w, b	1026	m	1020	v, b	987	1	0.08	ν ₄
1028	w			1157	v	1157	v			1028	v	1028	1	0.77	ν ₂₁
				1262	v	1262	v			1242	v, b				?
1350	w	1350	7	1350	8	1347	w	1349	m	1349	v	1348	2	0.70	ν ₂₀
1460	m	1480	1	1460	1	1387	w			1459	m				ν ₁₉
1478	m	1480	1	1480	1	1456	m			1478	m	1480	<1		ν ₃
				1474	m	1474	m			1550	v				1459 + 350 = 1809
										1805	m				

Year	Assignment	Frequency (cm ⁻¹)	Intensity	Other	Relative Intensity	Assignment	Frequency (cm ⁻¹)	Intensity	Other	Relative Intensity	Assignment		
1908	vw; b	1927	w										
1949	w, sh	1970	m	1981	1989	s	2010	dp	?	2011	14	0.81	
		1974 or											2 × 987 =
		1975											
1979	vs	2004	vvs	2010	vs	s	2062	p	?	2075	10	0.02	
		2015											
		2070											
2059	vs	2074	vs	2074	s	m	2916	dp	?	2075	10	0.02	
		2079											
3013	vw	2920	vw	2913	w	dp	2976	w	?	2075	10	0.02	
		3020											
		3024											
3082	vw	3080	m	3086	m	w	3086	dp	?	2075	10	0.02	
		3091											

^a w, m, s = weak, medium, strong; v = very; b = broad; sh = shoulder; ~ = approximately; p = polarized; dp = depolarized; || = parallel; ⊥ = perpendicular; ρ = depolarization ratio. For depolarized lines, ρ = 0.75 ± 0.06. ^b Reference 7. ^c Relative peak intensities on a scale of 0-100, uncorrected for instrument response.

cules. The former put valuable constraints on both the assignments and the force constant calculations, and indicated something about the form of the normal modes. The gas phase data in the infrared provided band contour evidence, and in the Raman spectrum clarified some of the choices. They also removed all doubts about the effects of intermolecular interactions, although it turned out that these were generally very small.

Finally, it was some help to use analogy with similar modes for the allyl radical, HC(CH₂)₂,²⁹ and guanidinium ion, C(NH₂)₃⁺.³⁰ These are the most closely analogous systems for which data are available.

In discussing the assignments we shall use gas phase frequencies unless they are not available.

B. C-H Stretches. If a carbon atom is unsaturated, its C-H stretches invariably occur above 3000 cm⁻¹; if it is saturated, they occur (with a few exceptions) below 3000 cm⁻¹.³¹ Thus the numerical value may provide valuable information on the nature of the methylene carbons in h₆.

AD observed no polarized Raman band in the C-H stretching region of liquid h₆, and we agree for this state. AD therefore assigned ν₁ to a weak infrared band at 2976 cm⁻¹ which has no Raman counterpart. However in the gas phase Raman spectrum there is a band at 3024 cm⁻¹ which is strongly polarized, and which we assign to ν₁. The gas phase infrared band near here, with maxima at 3020 and 3024 cm⁻¹, has neither the contour nor the 13-cm⁻¹ P-R separation expected for an a₁ band, so we assign it to ν₁₇, the CH₂ symmetric stretch of species e. Presumably in the liquid the a₁ and e modes overlap so badly that only a single depolarized band is observed. In the gas the Q branch of the a₁ Raman mode stands out clearly, and it is possible to show with certainty that the band is polarized. The CH₂ antisymmetric stretch of species e (ν₁₆) is obviously 3086 cm⁻¹. It is higher than the two symmetric stretches as expected.

All three of the active C-H stretches of h₆ are above 3000 cm⁻¹, so we conclude that the spectroscopic behavior of the methylene carbon is consistent with that of an unsaturated carbon atom. This is compatible with the C-C bond distance of 1.437 Å.³ The C-C stretching frequency and force constant will later be shown to be consistent with this evidence.

In d₆ the band at 2210 cm⁻¹ is polarized in both gas and liquid Raman spectra and is clearly ν₁. The higher e mode, ν₁₆, is obviously 2328 cm⁻¹. There is no good candidate for the second e mode (ν₁₇), but the weak infrared gas bands at 2193 and 2237 cm⁻¹ can be postulated as due to Fermi resonance of ν₁₇ with the sum 1374 + 844 = 2218. This indicates that unperturbed ν₁₇ would have been about 2215 cm⁻¹. If this is correct, ν₁₇ and ν₁ are very close together in both d₆ and h₆.

C. C=O Stretches. The next lower fundamentals are the carbonyl stretches. The a₁ mode (ν₂) is certainly 2074 cm⁻¹ in both h₆ and d₆, and the e mode (ν₁₈) is just as clearly 2010 cm⁻¹ in both compounds. These are normal values.^{32a}

D. Other a₁ Modes. There are eight remaining a₁ fundamentals. The following Raman bands of h₆ and d₆ show at least some evidence of being polarized. They are arranged to show possible correlations between the two molecules, i.e., the h₆ frequencies are always higher than corresponding d₆ ones.

h₆: ---, ---, 987, 916, 802, ---, 488, ---, 369, 350?, 172?
 d₆: 1184, 1165, 881, 790, 708, 594, 482, 377?, 355, 321?, 94?

In h₆ there are two CH₂ scissorings (ν₃ and ν₁₉) which must be near 1460 cm⁻¹. Bands are observed at 1478 and 1459 cm⁻¹, but both are too weak in the Raman effect for depolarization measurements, and infrared contours are not helpful. The two

TABLE II: Infrared and Raman Spectra of Tricarbonyl(trimethylenemethane)iron- d_6 ^a

Solid				Liquid			Gas					Assignment	
Infrared		Raman		Raman			Infrared			Raman			
cm ⁻¹	Inten	cm ⁻¹	Inten ^b	cm ⁻¹	Inten ^b	ρ	cm ⁻¹	Inten	Type	cm ⁻¹	Inten	ρ	
		49	sh	49	8								Real ?
		91	{ 43	94	81	0.60				86	100	0.82	ν_{30}
		100	{ sh										
		116	38	104	70	0.70				~128	sh		ν_{29}
		126	{ 52	130	sh								ν_{10}
		143	{ sh										
327	w	324	44	321	43	0.71				321	16	0.70	ν_{28}
										341	{ sh		
358	m	360	100	358	100	0.13				355	{ 65	0.04	ν_9
378	w	380	{ 18	377	20	0.60	377	w		377	7	0.65	ν_{27}
		395	{ 1										
469	m	471	5	467	4	0.86				461	3	0.78	ν_{26}
489	m	492	14	486	9	0.36				482	10	0.16	ν_8
							483	vw					
511	s						501	{					
							507	s	?				ν_{25}
							513	{					
							542	{					
551	s	555	4	550	2	0.83	549	s	?				ν_{24}
							553	{					
578	m						577	w					482 + 104 = 586
596	s	594	1	594	2	0.38	599	sh		594	1		ν_7
													550 + 49 = 599
							607	{					
618	s	615	2	615	2	0.84	613	s	?				ν_{23}
							618	{					
641	m												2 × 327 = 654
711	m	708	13	707	16	0.25	708	m	?	707	16	0.09	ν_6
							785	{					
791	s	792	29	791	38	0.14	790	m		790	27	0.03	ν_5
							796	{					
843	m	846	9	843	8	0.83				844	4	0.76	ν_{22}
870	{ vw												
883	{ w	882	5	881	4	0.50	881	vw					ν_4
988	w						974	vw					881 + 104 = 985
1022	vw	1024	1										
1040	m	1043	3	1043	2	0.88	1040	w					ν_{20}
1049	w												
1103	vw												
1162	vw	1163	2	1165	1	0.65							615 + 550 = 1165
1185	vw	1187	4	1185	7	0.21				1184	4	0.10	ν_3
1373	m	1375	16	1374	9	0.81	1374	m	⊥	1375	6	0.73	ν_{19}
1409	vw						1401	w					
							1926	w					
1950	sh	1943	1				1969	{					
		1968	24				1975	s					
1981	vs	1988	31	1981	21	0.81	1981	{					1374 + 613 = 1987
							2003	{					or ¹³ CO deriv
		2001	33	2000	sh		2010	vs		2010	21	0.81	ν_{18}
							2014	{					
							2068	{					
2058	vs	2055	14	2061	9	0.20	2074	vs		2075	14	0.05	ν_2
							2079	{					
2188	w						2193	vw					ν_{17} in FR
2220	w	2212	14	2208	15	0.21				2210	15	0.14	ν_1
2232	vw						2237	w					ν_{17} in FR
							2322	{					
2327	w	2330	4	2333	6	0.82	2328	m		2329	5	0.73	ν_{16}
							2333	{					
2338	w	2340	6	2338	sh								
2490	vw						2492	vw					

^a w, m, s = weak, medium, strong; v = very; sh = shoulder; || = parallel; ⊥ = perpendicular; ρ = depolarization ratio. For depolarized lines, $\rho = 0.75 \pm 0.08$. ^b Relative peak intensities on a scale of 0–100, uncorrected for instrument response. FR = Fermi resonance. See text.

could result from Fermi resonance between the species e CH₂ scissoring and the sum $1028 + 438 = 1466$ cm⁻¹. However, it is more likely that they are the two fundamentals. We assign 1478 cm⁻¹ to ν_3 because it appears in the Raman spectrum of

the gas and therefore probably has a relatively strong Q branch. The 1459 -cm⁻¹ band is assigned to ν_{19} , but these two could be interchanged.

Returning to the list of polarized bands, we note that the

TABLE III: Observed and Calculated (cm^{-1}) Fundamental Vibrations and Potential Energy Distributions of Tricarbonyl(trimethylenemethane)iron- h_6 and - d_6

C_{3v} species and activity No.	Schematic descript	This work						h_6		d_6	
		AD^a		$h_6(\text{gas})$	$d_6(\text{gas})$	$\bar{\nu}(h_6)/\bar{\nu}(d_6)$	Calcd	PED b,c	Calcd	PED b,c	
		$h_6(\text{liq})$	$h_6(\text{liq})$								
a_1	CH_2 str, sym	2976	3024	3024	2210	1.37	3024	1(99)	2212	1(97)	
$R(\rho)$	$\text{C}\equiv\text{O}$ str	2061	2074	2077	2074	1.00	2077	2(98)	2077	2(98)	
$ir(\parallel)$	CH_2 scissors	1474	1478	1490	1184	1.25	1490	3(89)	1184	3(58), 5(37)	
	CH_2 wag	989	987	988	881	1.12	988	4(89)	873	4(52), 6(56)	
	$\text{C}-\text{C}$ str	918	916	918	790	1.16	918	4(18), 5(85), 6(25), 9(17)	802	3(45), 5(39), 6(48), 9(45)	
	CC_3 deformation	802	802	799	707	1.13	799	6(80), 9(62)	712	4(37), 9(26)	
	$\text{Fe}-\text{C}-\text{O}$ deformation	604	603?	608	594?	1.02	608	7(36), 8(22), 10(19)	589	7(39), 8(18), 10(19)	
	$\text{Fe}-\text{CO}$ str	440	488	485	482	1.01	485	7(38), 8(44)	481	7(32), 8(52)	
	$\text{Fe}-\text{C}(\text{CH}_2)_3$ str	372	369	367	355	1.04	367	8(27), 9(37)	345	6(15), 8(20), 9(34)	
a_2	$\text{Fe}(\text{CO})_3$ deformation		130?	129	128?	1.02	129	7(23), 10(74)	127	7(23), 10(74)	
	CH_2 str, antisym			3094			3094	11(100)	2305	11(99)	
	CH_2 twist										
	CH_2 rock			795			795	12(100)	607	12(99)	
	$\text{Fe}-\text{C}-\text{O}$ deformation			450			450	13(100)	450	13(100)	
	Torsion			35			35	14(100)	32	14(99)	
e	CH_2 str, antisym	3086	3086	3098	2328	1.33	3098	15(99)	2316	15(98)	
$R(\text{dp})$	CH_2 str, sym	3019	3022	3022	[2215] ^d	1.36	3022	16(99)	2209	16(96)	
$ir(\perp)$	$\text{C}\equiv\text{O}$ str	1994	2010	2010	2010	1.00	2010	17(99)	2010	17(99)	
	CH_2 scissors	1456	1459	1472	1040	1.40	1472	18(72), 19(30)	1028	18(94)	
	$\text{C}-\text{C}$ str	1348	1348	1338	1374	0.98	1338	18(30), 19(46)	1369	19(75)	
	CH_2 wag	1025	1028	1030	844	1.22	1030	20(94)	845	20(86)	
	CH_2 twist	900	900?								
	CH_2 rock	815	821	819	613	1.34	819	21(77)	675	19(16), 21(60), 25(21)	
	$\text{Fe}-\text{C}-\text{O}$ deformation	581	582	582	549	1.06	582	24(64)	577	24(66)	
	$\text{Fe}-\text{C}-\text{O}$ deformation	510	512	513	507	1.01	513	22(69), 23(16)	513	22(70), 23(16)	
	$\text{Fe}-\text{CO}$ str	493	470	468	461	1.02	468	22(20), 23(54), 24(18)	468	22(20), 23(54), 24(20)	
	CC_3 deformation	471	438	445	377	1.16	445	25(75), 26(22)	376	21(22), 25(48), 26(37)	
	$\text{Fe}-\text{C}(\text{CH}_2)_3$ tilt	351	350	356	321	1.09	356	26(63)	308	25(22), 26(43)	
	$\text{Fe}(\text{CO})_3$ deformation		104 ^e	104	104 ^e	1.00	104	27(80)	104	23(16), 27(81)	
	$\text{OC}-\text{Fe}-\text{C}(\text{CH}_2)_3$ deformation	95	88	96	86	1.02	96	28(90)	93	28(92)	

Av error = 0.5%

Av error = 0.9%

^a Reference 7. ^b (PED) $_{ij} = 100(L_{ij})^2 F_{ij}/\lambda_j$. Contributions < 15% are not given. ^c Numbers 1, 2, . . . refer to the symmetry coordinates given in Table IV. ^d Estimated from Fermi resonance pair. See text. ^e Liquid value.

d_6 frequency at 1165 cm^{-1} can be explained as a sum tone ($615 + 550 = 1165$). This allows us to pair up the following a_1 fundamentals in h_6 and d_6 : 1478 and 1184, 987 and 881, 916 and 790, 802 and 708, 488 and 482, and 369 and 355 cm^{-1} .

Frequencies are still needed for two more fundamentals. We believe that one of these modes is the Fe-C-O deformation. In iron carbonyls these occur between 450 and 750 cm^{-1} as strong bands in the infrared and relatively weak bands in the Raman spectrum. We also expect this mode to exhibit a very small shift on deuteration. In h_6 three bands meet these requirements: 603, 582, and 512 cm^{-1} . Only the latter has the expected infrared contour. Its counterpart in d_6 is clearly 507 cm^{-1} . Thus, $512\text{--}507\text{ cm}^{-1}$ is one possible choice, although there is no Raman polarization evidence to support it. On the other hand, 594 cm^{-1} in d_6 is definitely polarized. Its counterpart in h_6 is 603 cm^{-1} . This was too weak for us to obtain a depolarization ratio, but AD call it questionably polarized. Unfortunately its infrared contour is not that of an a_1 mode. Thus the $603\text{--}594\text{ cm}^{-1}$ choice also has problems. We arbitrarily choose to assign the $603\text{--}594\text{ cm}^{-1}$ pair as ν_7 and $512\text{--}507\text{ cm}^{-1}$ as ν_{25} , but these could well be interchanged.

The lowest a_1 fundamental is expected to be the symmetric Fe(CO)₃ deformation in the vicinity of 100 cm^{-1} .^{32b} It is assigned to 135 cm^{-1} in $\text{C}_4\text{H}_4\text{Fe}(\text{CO})_3$ ³³ and to 136 cm^{-1} in $\text{C}_6\text{H}_6\text{Cr}(\text{CO})_3$.³⁴ In the gas phase Raman spectrum of h_6 there is an intense, broad band extending from about 70 to 140 cm^{-1} . It is centered near 88 cm^{-1} with a weak shoulder at 130 cm^{-1} . Similar features are observed for d_6 at 86 and 128 cm^{-1} . The main bands are depolarized. We think they are e modes, overlain by excited state transitions. The lowest a_1 mode is assigned to the weak shoulders at 130 and 128 cm^{-1} on the basis of the similarity to frequencies in related molecules and of the lack of any better alternative.

The observed product rule ratio for the above assignments is 2.73 compared to a theoretical value of 2.78. This is very satisfactory agreement, but is not a critical test for the two dubious pairs of assignments.

The values of the individual isotopic ratios $\nu(h_6)/\nu(d_6)$ are included in Table III. They show that many of the modes are neither mainly hydrogenic (ratio about 1.35) nor mainly skeletal (ratio 1.00–1.04), but are badly mixed. Examples are ν_3 through ν_6 . Clearly, the names given to them are inadequate.

E. a_2 Modes. None of the five a_2 modes, which are inactive in both infrared and Raman spectra, were identified experimentally. Calculated values were obtained from force constants given later.

F. e Modes. There are 15 e fundamentals. The three highest have already been discussed. Candidates for the next few are as follows:

$$h_6: 1459, 1348, 1028, 900, 821\text{ cm}^{-1}$$

$$d_6: 1374, 1040, 844, 641, 613\text{ cm}^{-1}$$

The CH₂ scissors in h_6 is assigned to 1459 for the reason given earlier. A drop by $\sqrt{2}$ would place it at 1031 cm^{-1} in d_6 . There is a suitable band at 1040 cm^{-1} . The next lower depolarized band in h_6 is 1348 cm^{-1} . We believe that this is the C-C stretch, and that it is 1374 cm^{-1} in d_6 . It is uncommon to have a frequency increase on going from a lighter to a heavier isotopic molecule. We think it is due, in this case, to first-order interaction with the CH₂ scissoring at 1459 cm^{-1} in h_6 ; this forces the C-C stretch down a little to 1348 cm^{-1} . In d_6 the scissoring has been removed from this region, and the C-C stretch is free to move back up toward its unperturbed position. If one lists the e frequencies in numerical order in each molecule, he would associate 1459 and 1348 cm^{-1} in h_6 with

1374 and 1040 cm^{-1} , respectively, in d_6 . If the listing is by descriptive name, the association is 1459 cm^{-1} with 1040 cm^{-1} (CH₂ and CD₂ scissoring), and 1348 cm^{-1} with 1374 cm^{-1} (C-C stretch). We use the latter in Table III. Obviously the assignment of the C-C stretch is very important if one is to use the spectral data to say something about the strength of the C-C bonds. We feel that the increase of frequency on deuterium substitution is strong support for the assignment to the C-C stretch.

The next lower obvious candidates for e fundamentals in h_6 are 1028 and 821 cm^{-1} . We believe that in d_6 these drop to 844 and 613 cm^{-1} , respectively. One more hydrogenic mode still has to be located, but it is a problem and will be temporarily deferred.

The seven remaining lower e modes are assigned as follows:

$$h_6: 582, 512, 470, 438, 350, 104, 88\text{ cm}^{-1}$$

$$d_6: 549, 507, 461, 377, 321, 104, 86\text{ cm}^{-1}$$

The 350 cm^{-1} band is reported as polarized in the gas, but we believe this is because it overlaps the very strong, highly polarized band at 369 cm^{-1} . Therefore we have no reluctance about assigning 350 cm^{-1} to an e mode. As mentioned earlier, the Raman spectra of both molecules show a broad, intense, flat-topped scattering profile extending from about 70 to 140 cm^{-1} with hints of three maxima. They cannot be better resolved even in the gas with narrow slits. We believe that this is the superposition of several hot bands on a fundamental. In the liquid spectra there are maxima at 104 and 95 cm^{-1} for h_6 and 104 and 94 cm^{-1} for d_6 . These were used for the normal coordinate calculations, but the gas phase values for the lower pair are 88 and 86 cm^{-1} . There is also a band at 48 cm^{-1} in h_6 and 49 cm^{-1} in d_6 which might be the lowest e fundamental, but we are not certain that they are really Raman bands. There are troublesome instrumental ghosts in this region.

All seven of these vibrations are skeletal modes, and all have relatively small isotope shifts except one, $438\text{--}377\text{ cm}^{-1}$ (Table III). For it the isotope ratio is 1.16. We assign this pair to the CC₃ deformation, and assume that there is mixing with the CH₂ wag (1028 and 844 cm^{-1}) which accounts for the unexpectedly large ratio. The shift for the wag is unexpectedly small (1.22 cm^{-1}), and the product of the two ratios is 1.42 which is about what is expected. The interaction seems reasonable on mechanical and intuitive grounds. This idea is not supported by the potential energy distribution (PED), however. It shows that the mixing is mainly with the Fe-C(CH₂)₃ tilt (see later).

We return now to the problem of the missing hydrogenic mode. In h_6 it will be somewhere between 1350 and 600 cm^{-1} . The only reasonable unused band is 900 cm^{-1} . In d_6 it will be somewhere between 1300 and 420 cm^{-1} , and the only obvious possibilities are 1165 (p), 974, 641, and 577 cm^{-1} . At this point the product rule can be used, since values have been assigned to all e modes except this one (ν_{22}). If we assume that the observed τ value will be about 4% lower than the theoretical one to allow for anharmonicity, or about 7.40, and if all the other assignments are correct, then the isotopic ratio for ν_{22} will be about 1.30. Calculated values for the missing partner are shown in parentheses:

$$h_6: (1515), (1266), 900, (833), (750)\text{ cm}^{-1}$$

$$d_6: 1165, 974, (692), 641, 577\text{ cm}^{-1}$$

There is nothing reasonable near any of these calculated values, nor can a good case be made for one of these bands being overlain by another fundamental. The only possible pair

is 1242–974 cm^{-1} , but both are very weak and unconvincing. If one pairs 900 and 641 cm^{-1} , their ratio is 1.404, and $\tau_{\text{obsd}} = 8.07$, which is far too large.

In lieu of any better alternative, we assign 900 cm^{-1} to ν_{22} for h_6 , and leave it unassigned for d_6 . This is as far as we can go with the assignments.

G. *Comments.* It is rather remarkable that values can be suggested for 49 of the 50 active modes, and that all but 8–10 of these seem to be reliable. The questionable ones are, in our opinion, the following: (a) 900 cm^{-1} for ν_{22} ; (b) 130 and 128 cm^{-1} for ν_{10} ; (c) possibly the values for ν_7 (603 and 594 cm^{-1}) should be interchanged with those for ν_{25} (512 and 507 cm^{-1}); (d) perhaps the values for ν_{29} (104 and 104 cm^{-1}) should be replaced by 48 and 49 cm^{-1} . Changes (c) and (d) will have a negligible effect on the calculated product rule ratio.

Furthermore, all but two of the 49 frequencies are for the gas phase, which is unusual for a solid compound. This is not very important, however, because the shifts of frequency due to phase changes are relatively small.

Another unusual feature is that because there are several low-frequency fundamentals, most of the molecules are not in the ground state. If it is assumed that all the modes below 500 cm^{-1} are properly assigned and are harmonic, it is easily found that less than 0.3% of the molecules are in the ground state at 300 K.³⁵ Most of the observed bands are therefore really hot bands of the type $(\nu_a + \nu_b) - \nu_a$.

H. *Comparison with the Assignments of AD.* The assignments of AD for h_6 are included in Table III for ready comparison. AD give no values for ν_{10} and ν_{29} . We differ from them on the assignments for ν_1 , ν_8 , ν_{26} , and ν_{27} . The case of ν_1 has already been discussed. We found 488 cm^{-1} to be definitely polarized and 438 cm^{-1} not, which was the converse of AD's finding and accounts for the difference in ν_8 , ν_{26} , and ν_{27} . Possibly they thought 438 cm^{-1} is polarized because it is adjacent to the very strong, highly polarized Raman band at 369 cm^{-1} .

I. *Comments on the Bonding.* Although it is usually hazardous to use frequencies alone to obtain information about the nature of bonds, we believe two things can be safely concluded in the present case. First, from the fact that all the C–H stretches are above 3000 cm^{-1} , it is quite certain that the C–C bonds have considerable unsaturation. Second, this is supported by the C–C stretching frequencies. The a_1 stretch is either 987, 916, or 802 cm^{-1} in h_6 , and it is apparently mixed with a hydrogenic mode in either h_6 or d_6 (or both). The e mode is almost certainly 1374 cm^{-1} (d_6 value, where it seems to be isolated). The average of $2 \times 1374 + 302$ (the lowest a_1 possibility) is 1183 cm^{-1} . This is considerably higher than saturated C–C bond stretches. Examples of the latter are 995 cm^{-1} in ethane, and 1054 and 870 cm^{-1} in propane (average = 962 cm^{-1}). This result would be expected for an isolated trimethylenemethane radical where the C–C bond order is presumably 1.33. It is significant that the unsaturation still remains in the $\text{Fe}(\text{CO})_3$ complex.

We cannot go farther than this without calculating the force constants.

Normal Coordinate Analysis

The normal coordinate analysis by ADD⁸ appeared while our work was in progress, but it seemed desirable to proceed because (a) some of our assignments differ from theirs and (b) we have data for d_6 , which puts additional constraints on the force field. It turns out that there is very little agreement between our force constants and theirs.

A. *Internal Coordinates and Symmetry Coordinates.* The

method was the usual Wilson GF matrix procedure. The molecular dimensions were those reported in the electron diffraction study,³ except that the angle between each C–C bond and the line bisecting the HCH angle was assumed to be zero. (Reported values are $14.4 \pm 5.1^\circ$.)

A valence force field was employed. Figure 1 illustrates the internal coordinates that were used. In addition to those shown, there were three w_i coordinates for the wagging motions of the CH_2 groups ($i = 1, 2, 3$), and a T coordinate for the torsion around the Fe–C bond. This makes a total of 47 internal coordinates. Torsional coordinates for the CH_2 twists have not been included because it is difficult to obtain the corresponding symmetry coordinates since the trimethylenemethane portion is not planar. Also, only one internal coordinate (L) has been used to represent the Fe–C(CH_2)₃ stretch. There are two reasons for this. First, the Fe–C distance is significantly shorter than the Fe–CH₂ distances (1.938 Å vs. 2.123 Å). Second, the force constant is simple to interpret. A calculation by Hyams on one Fe–(C₅H₅) unit³⁶ suggests that for our case the use of all four Fe–C bond vectors would be most satisfactory, but it would lead to complicated expressions for the symmetry coordinates, and the resulting force constant would be difficult to interpret.

Table IV gives the symmetry coordinates in terms of the internal coordinates. Note that because the CH_2 twists are omitted ($1a_2 + 1e$ mode), there are 28 rather than 30 symmetry coordinates. Unfortunately, the numbering of the symmetry coordinates (S_1, S_2, \dots, S_{28}) does not parallel the numbering of the normal modes ($\nu_1, \nu_2, \dots, \nu_{30}$) beyond number 11 because of the missing CH_2 twists. One must watch out for this in using the PED's later. We have not assumed tetrahedral bond angles around the iron atom as did ADD. The measured angles, $\epsilon = 118.4^\circ$ and $\delta = 99.2^\circ$, make this a dubious approximation.

B. *Calculated Force Field.* The computer programs used for these calculations were those described by Snyder and Schachtschneider³⁷ plus another used at the CNRS laboratory for the perturbations of the force constants. The latter program allows one to find relations between correlated force constants so that all constants can vary while searching for the best fit.

The course of the calculations was as follows. Initially each half of the molecule, $(\text{H}_2\text{C})_3\text{C}-\text{X}$ and $\text{Y}-\text{Fe}(\text{CO})_3$, was treated separately. Preliminary values for the diagonal force constants were chosen by analogy with other systems; no off-diagonal terms were included in the F matrices initially. For the trimethylenemethane part there is very little pertinent information in the literature, but for the iron tricarbonyl part the results of many calculations are available. The most important are those by Jones and coworkers on $\text{Cr}(\text{CO})_6$, $\text{Mo}(\text{CO})_6$, and $\text{W}(\text{CO})_6$,³⁸ and on $\text{Fe}(\text{CO})_5$.³⁹ The values of the diagonal force constants were allowed to vary to obtain the best agreement between observed and calculated frequencies. Then selected interaction terms were included and optimized by the same criterion. Next, the two halves were combined to give the whole molecule, and again the values of the force constants were adjusted to achieve the best fit with the experimental frequencies. Significant changes in several of the constants were required at this stage. This is consistent with the electron diffraction results, which indicate a high barrier to torsion around the Fe–C(CH_2)₃ bond, and therefore imply considerable interaction between the two halves.

The final set of symmetry force constants is given in Table V. Any constant not listed there was fixed at zero. The frequencies calculated from them are included in Table III

TABLE IV: Symmetry Coordinates of Tricarbonyl(trimethylenemethane)iron

	A_1^a	
$S_1 = 1/\sqrt{6}(r_1 + r_2 + r_3 + r_4 + r_5 + r_6)$	$\nu_s \text{ CH}_2$	
$S_2 = 1/\sqrt{3}(t_1 + t_2 + t_3)$	$\nu \text{ C}\equiv\text{O}$	
$S_3 = 1/3\sqrt{2}(2\beta_1 + 2\beta_2 + 2\beta_3 - \gamma_1 - \gamma_2 - \gamma_3 - \gamma_4 - \gamma_5 - \gamma_6)$	$\delta \text{ CH}_2$	
$S_4 = 1/\sqrt{3}(w_1 + w_2 + w_3)$	Wag CH_2	
$S_5 = 1/\sqrt{3}(R_1 + R_2 + R_3)$	$\nu_s \text{ C}-\text{C}_3$	
$S_6 = Y(\alpha_1 + \alpha_2 + \alpha_3) + X(\Gamma_1 + \Gamma_2 + \Gamma_3)$	$\delta_s \text{ C}-\text{C}_3$	
$S_7 = 1/\sqrt{3}(\phi_1 + \phi_2 + \phi_3)$	$\delta \text{ Fe}-\text{C}-\text{O}$	
$S_8 = 1/\sqrt{3}(S_1 + S_2 + S_3)$	$\nu_s \text{ Fe}-(\text{CO})_3$	
$S_9 = L$	$\nu \text{ C}(\text{CH}_2)_3-\text{Fe}$	
$S_{10} = V(\delta_1 + \delta_2 + \delta_3) - W(\epsilon_1 + \epsilon_2 + \epsilon_3)$	$\delta \text{ CO}-\text{Fe}-\text{CO}$	
Red 1 = $X(\alpha_1 + \alpha_2 + \alpha_3) - Y(\Gamma_1 + \Gamma_2 + \Gamma_3) = 0$	Redundancy	
Red 2 = $1/3(\beta_1 + \beta_2 + \beta_3 + \gamma_1 + \gamma_2 + \gamma_3 + \gamma_4 + \gamma_5 + \gamma_6) = 0$	Redundancy	
Red 3 = $W(\delta_1 + \delta_2 + \delta_3) + V(\epsilon_1 + \epsilon_2 + \epsilon_3) = 0$	Redundancy	
	A_2	
$S_{11} = 1/\sqrt{6}(r_1 - r_2 + r_3 - r_4 + r_5 - r_6)$	$\nu_a \text{ CH}_2$	
$S_{12} = 1/\sqrt{6}(\gamma_1 - \gamma_2 + \gamma_3 - \gamma_4 + \gamma_5 - \gamma_6)$	rock CH_2	
$S_{13} = 1/\sqrt{3}(\tau_1 + \tau_2 + \tau_3)$	$\delta' \text{ Fe}-\text{C}-\text{O}$	
$S_{14} = T$	$\text{C}(\text{CH}_2)_3-\text{Fe}(\text{CO})_3$ torsion	
	E_a	
$S_{15} = 1/2\sqrt{3}(2r_1 - 2r_2 - r_3 + r_4 - r_5 + r_6)$	$\nu_a \text{ CH}_2$	
$S_{16} = 1/2(r_3 + r_4 - r_5 - r_6)$	$\nu_s \text{ CH}_2$	
$S_{17} = 1/\sqrt{2}(t_2 - t_3)$	$\nu \text{ C}\equiv\text{O}$	
$S_{18} = 1/2\sqrt{3}(\beta_2 - \beta_3 - \gamma_3 - \gamma_4 + \gamma_5 + \gamma_6)$	$\delta \text{ CH}_2$	
$S_{19} = 1/\sqrt{2}(R_2 - R_3)$	$\nu_a \text{ C}-\text{C}_3$	
$S_{20} = 1/\sqrt{2}(w_2 - w_3)$	Wag CH_2	
$S_{21} = 1/2\sqrt{3}(2\gamma_1 - 2\gamma_2 - \gamma_3 + \gamma_4 - \gamma_5 + \gamma_6)$	Rock CH_2	
$S_{22} = 1/\sqrt{6}(2\tau_1 - \tau_2 - \tau_3)$	$\delta' \text{ Fe}-\text{C}-\text{O}$	
$S_{23} = 1/\sqrt{2}(S_2 - S_3)$	$\nu_a \text{ Fe}-(\text{CO})_3$	
$S_{24} = 1/\sqrt{2}(\phi_2 - \phi_3)$	$\delta \text{ Fe}-\text{C}-\text{O}$	
$S_{25} = 1/\sqrt{2}(\alpha_2 - \alpha_3)$	$\delta_a \text{ C}-\text{C}_3$	
$S_{26} = 1/\sqrt{2}(\Gamma_2 - \Gamma_3)$	Tilt $\text{Fe}-\text{C}(\text{CH}_2)_3$	
$S_{27} = 1/\sqrt{2}(\delta_2 - \delta_3)$	$\delta \text{ CO}-\text{Fe}-\text{CO}$	
$S_{28} = 1/\sqrt{2}(\epsilon_2 - \epsilon_3)$	$\delta \text{ C}(\text{CH}_2)_3-\text{Fe}-\text{CO}$	
Red 4 = $1/3\sqrt{2}(2\beta_1 - \beta_2 - \beta_3 + 2\gamma_1 + 2\gamma_2 - \gamma_3 - \gamma_4 - \gamma_5 - \gamma_6) = 0$	Redundancy	
	E_b	
$S'_{15} = 1/2(r_3 - r_4 - r_5 + r_6)$	$\nu_a \text{ CH}_2$	
$S'_{16} = 1/2\sqrt{3}(2r_1 + 2r_2 - r_3 - r_4 - r_5 - r_6)$	$\nu_s \text{ CH}_2$	
$S'_{17} = 1/\sqrt{3}(2t_1 - t_2 - t_3)$	$\nu \text{ C}\equiv\text{O}$	
$S'_{18} = 1/6(4\beta_1 - 2\beta_2 - 2\beta_3 - 2\gamma_1 - 2\gamma_2 + \gamma_3 + \gamma_4 + \gamma_5 + \gamma_6)$	$\delta \text{ CH}_2$	
$S'_{19} = 1/\sqrt{6}(2R_1 - R_2 - R_3)$	$\nu_a \text{ CC}_3$	
$S'_{20} = 1/\sqrt{6}(2w_1 - w_2 - w_3)$	Wag CH_2	
$S'_{21} = 1/2(\gamma_3 - \gamma_4 - \gamma_5 + \gamma_6)$	Rock CH_2	
$S'_{22} = 1/\sqrt{2}(\tau_2 - \tau_3)$	$\delta' \text{ Fe}-\text{C}-\text{O}$	
$S'_{23} = 1/\sqrt{6}(2S_1 - S_2 - S_3)$	$\nu_a \text{ Fe}-(\text{CO})_3$	
$S'_{24} = 1/\sqrt{6}(2\phi_1 - \phi_2 - \phi_3)$	$\delta \text{ Fe}-\text{C}-\text{O}$	
$S'_{25} = 1/\sqrt{6}(2\alpha_1 - \alpha_2 - \alpha_3)$	$\delta_a \text{ C}-\text{C}_3$	
$S'_{26} = 1/\sqrt{6}(2\Gamma_1 - \Gamma_2 - \Gamma_3)$	Tilt $\text{Fe}-\text{C}(\text{CH}_2)_3$	
$S'_{27} = 1/\sqrt{6}(2\delta_1 - \delta_2 - \delta_3)$	$\delta \text{ CO}-\text{Fe}-\text{CO}$	
$S'_{28} = 1/\sqrt{6}(2\epsilon_1 - \epsilon_2 - \epsilon_3)$	$\delta \text{ C}(\text{CH}_2)_3-\text{Fe}-\text{CO}$	
Red' 4 = $1/\sqrt{6}(\beta_2 - \beta_3 + \gamma_3 + \gamma_4 - \gamma_5 - \gamma_6) = 0$	Redundancy	

^a In A_1 species the coefficients (X, Y) and (V, W) come from the fact that there are not tetrahedral angles around C and Fe atoms respectively: in the first case: $X = 1/\sqrt{c_1}$ and $Y = -b_1/\sqrt{c_1}$ with $b_1 = -\sqrt{3} \cos \Gamma / \cos(\alpha/2)$, $c_1 = 3(b_1^2 + 1)$; in the second case: $V = b_2/\sqrt{c_2}$ and $W = 1/\sqrt{c_2}$ with $b_2 = -\sqrt{3} \cos \epsilon / \cos(\delta/2)$ and $c_2 = 3(b_2^2 + 1)$.

where they can be compared with the observed ones. Values were not obtained for the two CH_2 twist modes, but are given for four of the five forbidden a_2 fundamentals.

1. *Forms of the Normal Modes (PED's)*. Table III also contains the diagonal elements of the potential energy distribution, which provide a more precise description of the normal vibrations than the schematic names in the earlier part of Table III. In fact this is one of the most valuable results of a normal coordinate calculation. Several of the modes warrant comment.

In h_6 , ν_3 and ν_4 are fairly pure CH_2 scissors and wag, respectively. In d_6 the CD_2 scissors is mixed with the $\text{C}-\text{C}_3$

stretch, and the CD_2 wag is mixed with the CC_3 deformation. This explains the anomalous isotope ratio for ν_3 and ν_4 . Similar considerations apply to the remaining fundamentals. Mode 5 is the most badly mixed of the entire group. Although it is called a $\text{C}-\text{C}$ stretch, we see now that this is an inadequate description.

In species e the assignments for ν_{20} ("C-C degenerate stretch") give an isotope shift less than 1.0. It was suggested earlier that this is due to interaction between the CH_2 scissors and the $\text{C}-\text{C}$ stretch in h_6 , pushing the latter down. In d_6 the CD_2 scissors has dropped to 1040 cm^{-1} , and the $\text{C}-\text{C}$ stretch is back at its unperturbed position. This suggestion is sup-

TABLE V: Force Constants for Tricarbonyl(trimethylenemethane)iron in Symmetry Coordinate Representation

Symmetry species	Description ^b	Values ^a		
A_1	F_{11}	$\nu_s CH_2$	5.132	
	F_{22}	$\nu C\equiv O$	17.072	
	F_{33}	δCH_2	0.462	
	F_{44}	$w CH_2$	0.325	
	F_{55}	$\nu_s CC_3$	6.688	
	F_{66}	$\delta_s CC_3$	2.378	
	F_{77}	$\phi Fe-C\equiv O$	0.603	
	F_{88}	$\nu_s Fe-(CO)_3$	3.084	
	F_{99}	$\nu TMM-Fe$	3.703	
	F_{1010}	$\delta CO-Fe-CO$	0.604	
	F_{28}	$\nu C\equiv O, \nu_s Fe-(CO)_3$	0.600	
	F_{35}	$\delta CH_2, \nu_s CC_3$	-0.189	
	F_{36}	$\delta CH_2, \delta_s CC_3$	-0.277	
	F_{46}	$w CH_2, \delta_s CC_3$	-0.195	
	F_{49}	$w CH_2, \nu TMM-Fe$	0.107	
	F_{56}	$\nu_s CC_3, \delta_s CC_3$	1.113	
	F_{69}	$\delta_s CC_3, \nu TMM-Fe$	1.115	
	A_2	F_{1111}	$\nu_a CH_2$	5.076
		F_{1212}	$r CH_2$	0.367
F_{1313}		$\tau Fe-C\equiv O$	0.552	
F_{1414}		Torsion	0.007	
E	F_{1515}	$\nu_a CH_2$	5.076	
	F_{1616}	$\nu_s CH_2$	5.132	
	F_{1717}	$\nu C\equiv O$	16.227	
	F_{1818}	δCH_2	0.462	
	F_{1919}	$\nu_a CC_3$	4.865	
	F_{2020}	$w CH_2$	0.341	
	F_{2121}	$r CH_2$	0.367	
	F_{2222}	$\phi Fe-C\equiv O$	0.644	
	F_{2323}	$\tau Fe-C\equiv O$	0.552	
	F_{2424}	$\nu_a Fe-(CO)_3$	3.084	
	F_{2525}	$\delta_a CC_3$	1.257	
	F_{2626}	Tilt TMM-Fe	2.529	
	F_{2727}	$\delta CO-Fe-CO$	0.535	
	F_{2828}	Def TMM-Fe(CO) ₃	0.306	
	F_{1724}	$\nu C\equiv O, \nu_a Fe-(CO)_3$	0.822	
	F_{1819}	$\delta CH_2, \nu_a CC_3$	-0.189	
	F_{1825}	$\delta CH_2, \delta_a CC_3$	0.083	
	F_{1925}	$\nu_a CC_3, \delta_a CC_3$	-0.068	
	F_{2025}	$w CH_2, \delta_a CC_3$	0.108	
	F_{2526}	$\delta_a CC_3, \text{tilting}$	0.413	

^a Stretching principal constants and stretch-stretch interactions in mdyn/Å, bending principal constants and bend-bend interactions in mdyn Å/radian², stretch-bend interactions in mdyn/radian. ^b TMM = trimethylenemethane.

ported by the PED's, which show that in h_6 , ν_{19} and ν_{20} are indeed mixtures of the CH_2 scissors and the C-C stretch whereas in d_6 they are relatively pure modes.

Finally, ν_{27} has a large isotope shift for a mode described schematically as a CC_3 deformation, and it was suggested that it is mixed with the CH_2 wag. This is not verified by the PED's. Instead, the mixing is mainly with the $Fe-C(CH_2)_3$ tilt.

2. *Force Constants for the $-C(CH_2)_3$ Part.* The symmetry force constants given in Table V are functions of the valence force constants, and in some cases there are enough equations to allow the latter to be evaluated. This is important because these are the constants which one hopes can be transferred or compared between molecules. Our results are given in Table VI. From the values of F_{11} and F_{1515} the C-H stretching force constant in internal coordinate representation is found to be 5.10 mdyn/Å. This value is between that expected for a C-H

bond (4.9 ± 0.1) and a $=C-H$ bond (5.3 ± 0.1), and is consistent with a carbon hybridization which is intermediate between sp^3 and sp^2 .

The value of the carbon-carbon stretching force constant calculated from F_{55} and F_{1919} is 5.47 mdyn/Å. This is intermediate between C-C (typically 4.5-5.0) and C=C (typically 9.5-9.9). Interestingly, it agrees quite well with the value of 5.55 mdyn/Å obtained from Gordy's relation when a bond order of 1.33 is assumed.⁴⁰ Finally, it is near the value of the C-C stretching constant for the allyl radical, $H\dot{C}(CH_2)_2$, of 5.40 mdyn/Å.⁴¹ These considerations all indicate that the C-C bonds are intermediate between single and double bonds.

3. *Force Constants for the $-Fe(CO)_3$ Part.* Most of these constants have been transferred with little change from the hexa- and pentacarbonyls (Table VI). However, the value for the $C\equiv O$ stretch is lower than those in the reference compounds and that for the $Fe-CO$ stretch is higher. This can be interpreted by assuming that the trimethylenemethane ligand is a stronger electron donor than a $C\equiv O$ group. Its presence causes an increase in electron density in the $Fe-CO$ bond and in the $CO \pi^*$ antibonding orbital.⁴² The values of the bending constants are rather similar to those for the reference carbonyl compounds.

4. *Force Constants for the Iron-Ligand Bond(s).* Our values for the trimethylenemethane-iron stretching and tilting force constants are 3.70 mdyn/Å and 2.53 mdyn Å/radian², respectively. The latter when reduced to the dimension of a stretching constant has the value $F_T = 0.91$ mdyn/Å. The large value of 3.70 mdyn/Å for the stretch indicates strong bonding, but it also indicates that the model assumed when defining the internal coordinates is not realistic, i.e., that the metal-ligand bond is between the iron and the central carbon atom of $C(CH_2)_3$. A better model is to assume π type bonding between the iron atom and each C-C of the ligand. The symmetrized force constant $F_L = 3.70/3 = 1.23$ mdyn/Å now corresponds to a totally symmetric vibration, and the reduced tilting force constant $F_T = 0.91$ mdyn/Å refers to a nonsymmetric stretching vibration. The former value is similar to the symmetrized constant for Cr-ligand bonds in dibenzenechromium of 1.48⁴³ and for Fe-ligand bonds in ferrocene of 1.40 mdyn/Å.³⁶ Thus, it seems that the magnitude of a single π type interaction in all these complexes is 1.2-1.5 mdyn/Å.

C. *Comparison with ADD's Force Constants.* ADD carried out a similar calculation for h_6 , and their valence force constants are included in Table VI. It will be noted that many of them differ considerably from ours. There are several reasons for this which will now be described briefly.

1. *Vibrational Assignments.* The differences between our assignments and those used by ADD are shown in Table III, and are summarized as follows:

ADD: a_1 : 2976, 2061, 440, - - -; e: 1994, 493, - - -, 95 cm^{-1}

This work: a_1 3024, 2074, 488, 130; e: 2010, 438, 104, 88 cm^{-1}

They are significant for two a_1 and three e modes. In all other cases we agree within a few cm^{-1} .

2. *Internal Coordinates and Symmetry Coordinates.* ADD defined their internal coordinates in their Figure 1.⁴⁵ They assumed each C- CH_2 group to be planar, as we did also, although they do not mention it.

We disagree with them on the definitions for S_3 and S_{13} in species a_1 (the CH_2 scissoring and a redundancy). Neither of their two symmetry coordinates leads to a zero value as a redundancy should. In the e symmetry blocks ADD have not given the corresponding redundancies, but in any case there

TABLE VI: Valence Force Constants for $(\text{H}_2\text{C})_3\text{CFe}(\text{CO})_3$, $\text{M}(\text{CO})_6$ and $\text{Fe}(\text{CO})_5$

Coordinate	This work	$(\text{H}_2\text{C})_3\text{CFe}(\text{CO})_3$		$\text{M}(\text{CO})_6^c$	$\text{Fe}(\text{CO})_5^{b,d}$
		Value	Symbol		
ADD ^a					
Stretching ^e					
C≡O	16.51	16.18	f_u	17.22 to 17.33	16.47, 17.43
C-H	5.10	5.36	f_s		
C-C	5.47	4.41	f_r		
Fe-ligand	3.70	2.83	f_R		
Fe-CO	3.08	3.04	f_t	1.96 to 2.36	2.57, 2.64
Bending ^f					
Fe-C-CH ₂ (tilt)	~2.53	3.27	f_π		
C-C-C	~2.00	1.41 ^g	f_α		
C-C-H	~0.37	0.77	f_β		
CH ₂ wag	0.34	0.29	f_γ		
H-C-H	0.46	0.36	f_δ		
OC-Fe-CO	~0.56	0.98	f_θ	0.50, 0.60	~0.46
Fe-C-O (in σ_v plane)	0.63	0.62	f_η	0.48	0.50
Fe-C-O (1 σ_v plane)	0.55	0.82	f_ϵ		0.40
OC-Fe-ligand	~0.31	0.31	f_ϕ		
CH ₂ twist		0.16	f_τ		
Stretch-Stretch Interactions ^e					
C≡O, C≡O	0.28	0.36	f_{uu}	0.22	0.13
Fe-CO, Fe-CO	0.0			-0.02, +0.05	-0.08
Fe-CO, C≡O	0.75	0.70 ^h	f_{tu}	0.69, 0.84	0.68, 0.76
Fe-CO, C≡O ⁱ	-0.074			-0.08	-0.12
Fe-CO, Fe-ligand	0.0	0.57	f_{Rt}		
Bend-Bend Interactions ^f					
Fe-C-O, Fe-C-O	-0.014		$(f_{\eta\eta})$	-0.02	-0.05
Fe-C-O, Fe-C-O	0.0		$(f_{\epsilon\epsilon})$	0.01	-0.02
OC-Fe-CO, OC-Fe-CO	~0.023		$(f_{\theta\theta})$	0.06, 0.09	
Stretch-Bend Interaction ^j					
Fe-CO, Fe-C-O	0.0	-0.09	$f_{t\eta}$	-0.04	
(plus others)					

^a Reference 8. ^b Several values because of the unlike C≡O groups. ^c Reference 38. ^d Reference 39. ^e mdyne/Å. ^f mdyne Å/radian. ^g 1.27 in ADD text. ^h Constrained. ⁱ Nonadjacent bonds. ^j mdyne/rad.

is a small error in their definition of S_{34a} ; the term $+2\beta_1$ should be included.

In species a_1 the definitions of ADD's symmetry coordinates S_6 (ν CC₃) and S_{10} (δ OC-Fe-CO) are incorrect because the angles around the central carbon atom and the iron atom are not tetrahedral. As a result their redundancies S_{11} and S_{12} are also wrong.

3. *Final Force Field.* A 31-parameter valence force field has been proposed by ADD to reproduce 23 different experimental frequencies. Six of the interaction constants had to be constrained to fixed values to obtain a good fit. We adjusted the values of 37 *symmetrized* force constants (17 in a_1 and 20 in e) to reproduce 48 experimental frequencies. Internal valence force constants were then obtained from the symmetrized ones. Most of them differ significantly from the values given by ADD.

The differences in the principal valence force constants are summarized in Table VI. For the metal-ligand constant our value is 3.70 mdyne/Å, compared to 2.83 mdyne/Å of ADD. This is a very large difference for what one hopes will be one of the most informative constants. ADD concluded that the C-C stretching constant is comparable to that for a C-C single bond, and take this as evidence for a substantial interaction of the π electrons of the CC₃ skeleton with the iron atom. It seems to us, in view of the C-C bond distance of 1.437 Å, that this bond has a very significant amount of double bond character. This should be indicated by the force constant. It is by our value (5.47 mdyne/Å) but not by that of ADD (4.41 mdyne/Å). On the other hand, ADD find that all the force

constants for the CH₂ groups are quite similar to those for an sp²-hybridized carbon atom. There seems to be an inconsistency; how can an sp² carbon be compatible with the C-C single bonds that they propose?

In the ADD paper the CCC deformation constant (their f_α) has a value of 1.27 mdyne Å/radian⁻² in the text and 1.41 in the table. However it is not worthwhile to discuss the exact value because the corresponding symmetry coordinate was ill-conditioned. The same problem occurs with their f_ϕ , f_θ , and f_π .

Finally, we differ with most of the interaction constants deduced by ADD. For example, it seems that their constants $f_{rs} = -0.75$ and $f_{rs}' = +0.39$ mdyne/Å are too large in magnitude. These are interactions between C-C and C-H stretches, and it is well established that such interactions are generally small. We have been able to neglect them in our force field.

4. *PED's.* It is very difficult to compare ADD's potential energy distributions with ours because theirs are given in terms of valence force coordinates and ours are in terms of symmetry coordinates. For example, they describe the 1478-cm⁻¹ mode of h₆ as 46% H-C-H deformation and 49% C-C-H deformation. We describe it as 89% CH₂ scissors. The correlation is much more complicated in some other cases, but it is clear that we disagree seriously on the forms of about half the vibrations.

D. *How Significant are the Force Constants?* Two different valence force fields are now available for tricarbonyl(trimethylenemethane)iron, that of ADD and ours. Both reproduce the starting frequencies well, but the individual force

constants differ considerably as shown in Table VI. Is either set right? What is their significance? This is worth a few comments.

We believe that most force constants which have been derived from large symmetry blocks should be regarded with skepticism. There are several sources of uncertainty. First, a few of the assignments are probably wrong. Second, assumptions are invariably made about some of the interaction constants. Third, it is known that the refinement procedure can converge on different sets of answers for the symmetry force constants depending upon the initial values that are assumed. The different sets will reproduce the frequencies equally well, and sometimes there are two or more sets which seem equally reasonable. It is then almost impossible to tell which is "right". One is seldom aware of the existence of these other sets. For all these reasons one should use great caution in drawing conclusions from the numerical values of valence force constants. We have a healthy skepticism in the present case, and have tried to use the numbers with care.

Conclusion

Complete vibrational data have been presented for both tricarbonyl(trimethylenemethane)iron- h_6 and - d_6 , including infrared and Raman results for the gas phase. These data have led to a vibrational assignment which differs in some respects with previous work, and which is much more firmly established. From the assignments a force field has been deduced which (a) reproduces the observed frequencies of both h_6 and d_6 with an average error of less than 1%, and (b) provides descriptions of the normal modes.

Another goal of this work was to attempt to clarify the description of the bonding in this molecule. The observation of the C-H stretches above 3000 cm^{-1} , as well as the agreement of the calculated C-C force constant with that estimated for a bond order of 1.33, indicate that the terminal carbons of the ligand should be described as having appreciable sp^2 character.

Our data also indicate that trimethylenemethane is behaving as a strong ligand. The observed lowering of the $C\equiv O$ stretching force constant when compared with $Fe(CO)_5$ indicates that the ligand is making a substantial bonding contribution through π donation. The strength of the metal-ligand bond is also indicated by the large value of both the metal-ligand stretching force constant and the ligand tilting force constant. In particular, the large tilting force constant suggests to us that the bonding description of this molecule in terms of a single bond between iron and the central carbon of the ligand is a misleading oversimplification.

In order to get a better understanding of the bonding in this molecule and of the variation of force constants in the series $Fe(CO)_5$, $C_4H_4Fe(CO)_3$, and $(H_2C)_3CFe(CO)_3$, one of us (C.S.) plans to investigate the electronic structure of these complexes by a semiempirical approach (CNDO/2). Such a calculation has been performed on $Fe(CO)_5$ ⁴⁶ and seems promising for h_6 .

NOTE ADDED IN PROOF: The referee has pointed out that in $Fe(CO)_5$ the two Fe-C distances are near 1.82 \AA and the corresponding valence stretching force constant is ca. 2.6 mdyn/\AA . The Fe-C(CH₂)₃ distance is much larger, 1.938 \AA , so a stretching force constant of 3.7 mdyn/\AA is unreasonable. This supports the π interaction postulated in section B4. He also noted that the $C\equiv O$ stretching force constants given in Table VI for reference compounds have been obtained from frequencies corrected for anharmonicity. If observed frequencies are used the force constants are smaller by 0.5 mdyn/\AA . (L. H. Jones, "Inorganic Vibrational Spectroscopy",

Marcel Dekker, New York, N.Y., 1941, p 156.) We should have used these lower values for comparison. This weakens the evidence that $C(CH_2)_3$ is a stronger electron donor than CO (section B3 and Conclusion).

Acknowledgments. We are grateful to Dr. E. C. Tuazon for aid with the computations. This work was supported by the National Science Foundation under Grant No. GP-33186. C.S. is most appreciative to O.T.A.N. (NATO) for a stipend while at the University of Pittsburgh.

References and Notes

- (1) (a) Dedicated to Professor Richard C. Lord on his 65th birthday and retirement. (b) Taken in part from a thesis submitted by D. H. Finseth for the degree of Doctor of Philosophy at the University of Pittsburgh, 1973. (c) Ph.D. Degree with Professor Richard C. Lord, Johns Hopkins University, 1942.
- (2) (a) P. Dowd, *Acc. Chem. Res.*, **5**, 242 (1972); (b) G. F. Emerson, K. Ehrlich, W. P. Giering, and P. C. Lauterbur, *J. Am. Chem. Soc.*, **88**, 3172 (1966).
- (3) A. Almenningen, A. Haaland, and K. Wahl, *Acta Chem. Scand.*, **23**, 1145 (1969).
- (4) M. R. Churchill and K. Gold, *Inorg. Chem.*, **8**, 401 (1969).
- (5) M. J. S. Dewar and S. D. Worley, *J. Chem. Phys.*, **51**, 1672 (1969).
- (6) D. H. Finseth, Ph.D. Thesis, University of Pittsburgh, 1973; *Diss. Abstr. Int. B* **34**, 4896 (1974).
- (7) D. C. Andrews and G. Davidson, *J. Organomet. Chem.*, **43**, 393 (1972).
- (8) D. C. Andrews, G. Davidson, and D. A. Duce, *J. Organomet. Chem.*, **97**, 95 (1975).
- (9) K. Ehrlich and G. F. Emerson, *J. Am. Chem. Soc.*, **94**, 2464 (1972).
- (10) E. H. Braye and W. Hübel, *Inorg. Syn.*, **8**, 178 (1966).
- (11) H. Lund and A. Voigt, *Org. Syn.*, **17**, 86 (1937).
- (12) (a) R. Scholl and W. Egerer, *Justus Liebigs Ann. Chem.*, **397**, 301 (1913), especially 361 ff. (b) K. Michael, *J. Prakt. Chem.*, (2) **37**, 477 (1888).
- (13) H. J. Backer and J. Lolkema, *Recl. Trav. Chim. Pays-Bas*, **58**, 23 (1939).
- (14) A. Mooradian and J. B. Cloke, *J. Am. Chem. Soc.*, **67**, 942 (1945).
- (15) G. B. Kistiakowsky, J. R. Ruhoff, H. A. Smith, and W. E. Vaughan, *J. Am. Chem. Soc.*, **57**, 876 (1935).
- (16) C. M. Pathak and W. H. Fletcher, *J. Mol. Spectrosc.*, **31**, 32 (1969).
- (17) J. Burgin, W. Engs, H. P. A. Groll, and G. Hearne, *Ind. Eng. Chem.*, **31**, 1413 (1939).
- (18) W. Reeve and D. H. Chambers, *J. Am. Chem. Soc.*, **73**, 4499 (1951).
- (19) W. Reeve, D. H. Chambers, and C. Prickett, *J. Am. Chem. Soc.*, **74**, 5369 (1952).
- (20) J. T. Gragson, K. W. Greenlee, J. H. Derfer, and C. E. Boord, *J. Am. Chem. Soc.*, **75**, 3344 (1953).
- (21) B. C. Anderson, *J. Org. Chem.*, **27**, 2720 (1962).
- (22) IUPAC, "Tables of Wavenumbers for the Calibration of Infrared Spectrometers", Butterworths, London 1961; or *Pure Appl. Chem.*, **1**, 537 (1961); **33**, 613 (1973).
- (23) R. C. Lord, R. S. McDonald, and F. A. Miller, *J. Opt. Soc. Am.*, **42**, 149 (1952).
- (24) F. A. Miller, B. M. Harney, and J. Tyrrell, *Spectrochim. Acta, Part A*, **27**, 1003 (1971).
- (25) D. H. Finseth, to be submitted for publication. See also ref 6.
- (26) F. A. Miller and B. M. Harney, *Appl. Spectrosc.*, **24**, 291 (1970).
- (27) W. A. Seth-Paul and G. Dijkstra, *Spectrochim. Acta, Part A*, **23**, 2861 (1967).
- (28) G. Herzberg, "Infrared and Raman Spectra", Van Nostrand, New York, N.Y., 1945, p 231.
- (29) C. Sourisseau and B. Pasquier, *Can. J. Spectrosc.*, **18**, 91 (1973).
- (30) C. L. Angell, N. Sheppard, A. Yamaguchi, T. Shimanouchi, T. Miyazawa, and S. Mizushima, *Trans. Faraday Soc.*, **53**, 589 (1957).
- (31) L. J. Bellamy, "The Infrared Spectra of Complex Molecules", 3d ed, Chapman and Hall, London, 1975, especially p 50.
- (32) D. M. Adams, "Metal-Ligand and Related Vibrations", Edward Arnold, London, 1967: (a) pp 97-107, 150-153; (b) pp 120-121.
- (33) D. C. Andrews and G. Davidson, *J. Organomet. Chem.*, **36**, 349 (1972).
- (34) I. J. Hyams and E. R. Lippincott, *Spectrochim. Acta, Part A*, **28**, 1741 (1972).
- (35) $N_0/N(\text{total}) = 1/Q$. For the latter, see ref 28, p 503.
- (36) I. J. Hyams, *Chem. Phys. Lett.*, **15**, 88 (1972).
- (37) (a) J. H. Schachtschneider and R. G. Snyder, *Spectrochim. Acta*, **19**, 117 (1963); (b) Shell Development Co. Technical Reports No. 231/64 (1964), and No. 57/65 (1965).
- (38) L. H. Jones, R. S. McDowell, and M. Goldblatt, *Inorg. Chem.*, **8**, 2349 (1969).
- (39) L. H. Jones, R. S. McDowell, M. Goldblatt, and B. I. Swanson, *J. Chem. Phys.*, **57**, 2050 (1972).
- (40) W. Gordy, *J. Chem. Phys.*, **14**, 305 (1946).
- (41) C. Sourisseau, unpublished results.
- (42) F. A. Cotton and G. Wilkinson, "Advanced Inorganic Chemistry", 3d ed, Wiley, New York, N.Y., 1972, pp 684-688.
- (43) S. J. Cyvin, J. Brunvoll, and L. Schäfer, *J. Chem. Phys.*, **54**, 1517 (1971).
- (44) D. C. Andrews and G. Davidson, *J. Organomet. Chem.*, **76**, 373 (1974), especially p 374.
- (45) In the lower right corner of their figure the designation δ_1 for OC-Fe-CO angle should be changed to θ , in order to be consistent with their equations defining the symmetry coordinates, and to avoid duplication with the δ_1 used in designating the HCH angle (upper left of ADD's Figure 1).
- (46) A. Serafini, J. M. Savariault, P. Cassoux, and J. F. Labarre, *Theor. Chim. Acta*, **36**, 241 (1975).

Vibrational Spectra and Assignments for Tetrachloro- and Tetraiodoallene^{1a,b}

A. Monroe Snider, Jr., Paul F. Krause, and Foil A. Miller*^{1c}

Department of Chemistry, University of Pittsburgh, Pittsburgh, Pennsylvania 15260 (Received December 22, 1975)

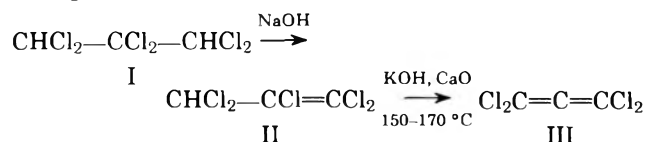
Infrared and Raman spectra were obtained for solid $\text{Cl}_2\text{C}=\text{C}=\text{CCl}_2$ and $\text{I}_2\text{C}=\text{C}=\text{CI}_2$. A complete vibrational assignment is presented for each compound, except for one mode of C_3I_4 . The observed spectra are completely compatible with D_{2d} symmetry. The values of the fundamentals are as follows for the solids: C_3Cl_4 a_1 : 1312, 425, 252; b_1 : 91(?); b_2 : 1977, 651, 221; e : 859, 305, 202, 141 cm^{-1} ; C_3I_4 a_1 : 1226, 179, 98; b_1 : —; b_2 : 1912, 424, 200; e : 682, 275, 133, 84(?) cm^{-1} .

I. Introduction

This work is part of a study in our laboratory of various perhalo allenes and butatrienes. Although tetrafluoro-, tetrachloro-, tetrabromo-, and tetraiodoallene have all been prepared, there has been no study of their vibrational spectra.^{2a} Only infrared survey spectra, obtained for characterization purposes, are available. This alone made the study of these allenes seem worthwhile. In addition it was thought that a knowledge of their fundamentals would be helpful in interpreting the spectra of the corresponding butatrienes. Because all four of these compounds are unstable, they are not easy to work with. We report here our results for tetrachloro- and tetraiodoallene.

II. Tetrachloroallene

A. *Experimental*. 1. *Preparation of the Sample*. The following reactions were used:



Compound I was obtained from K & K Laboratories. The first reaction has been described by Prins^{2b} and the second by Pilgram and Korte,^{2c} who were the first to isolate III. For the second step it was necessary to remove the water normally present in reagent grade KOH by preheating it in vacuo until its melting point exceeded 200 °C. The grinding of the dry KOH, the mixing of it with CaO, and the loading of the pyrolysis tube were done in a glove box in order to maintain dryness. III was collected in a trap maintained at -78 °C.

Tetrachloroallene is a white solid. When warmed to about 10 °C, it melts and dimerizes spontaneously to form another solid which melts at 93 °C.^{2c} Both the monomer and the dimer have considerable vapor pressure below their melting points.

2. *Spectroscopic Procedures*. Because of the low stability of tetrachloroallene, infrared and Raman spectra were obtained only on the polycrystalline solid at about 100 K. An exception was one fairly strong Raman band observed in CCl_4 solution.

The infrared spectrum was measured from 35 to 4000 cm^{-1} with Beckman IR-11 and IR-12 spectrophotometers. The spectral slit width was less than 2 cm^{-1} throughout the entire range. A low temperature cell of conventional design, equipped with KBr or polyethylene windows, was used.³

The Raman spectrum was obtained with a Spex Ramalog unit which has been described elsewhere.⁴ Briefly, it uses a 90° illumination-to-viewing arrangement, a Spex 1401 double

monochromator with two 1200 line/mm gratings blazed at 500 nm, and an ITT FW 130 detector with S-20 spectral response. Excitation was with 488.0-nm radiation from a Spectra Physics Model 164 Ar⁺ laser.

Because of the low stability of tetrachloroallene, it was studied only at low temperature and in the solid state. Consequently no depolarization ratios were obtained, with the exception of the one band at 252 cm^{-1} which was also measured in solution. The Raman cold cell was a modified version of the infrared one. The usual infrared cell frame, which is attached to the refrigerant reservoir and hangs in vacuo, was replaced by a stainless steel wedge with a mirror finish. The sample was deposited from a vapor jet onto a face of the liquid-nitrogen-cooled wedge which is tilted 15° relative to the incoming vertical laser beam.

Infrared wavenumbers are believed to be accurate to ±1 cm^{-1} and Raman ones to ±2 cm^{-1} except for the one band marked "circa".

3. *Results*. The observed infrared and Raman wavenumbers of tetrachloroallene are given in Table I. Additional bands at 164 and 390 cm^{-1} in both infrared and Raman spectra were identified as impurities by their variation in intensity in different samples. Similar evidence suggests that an impurity band overlaps the sample band at 203 cm^{-1} .

B. *Discussion of the Results*. 1. *General Comments*. It is unfortunate that Raman depolarization ratios and infrared vapor phase band contours are not available. Consequently band assignments are based only on selection rules, group frequencies, and analogy with similar molecules.

Tetrachloroallene is expected to have D_{2d} symmetry, with one CCl_2 twisted 90° relative to the other, by analogy with allene.⁵ The number of fundamental vibrations in each symmetry species, and their spectroscopic activity, is given in Table II. Table III compares our assignments for tetrachloro- and tetraiodoallene with those for analogous bands of tetrachloro- and tetraiodoethylene.

2. *Species a_1* . These three fundamentals are only Raman active. The $\text{C}=\text{C}=\text{C}$ symmetric stretch is expected around 1100 cm^{-1} . (It is 1073 cm^{-1} in allene,⁵ 1095–1075 cm^{-1} in chloro-, bromo-, and iodoallene,⁶ and has similar values in several other derivatives.⁶) There are two possible candidates in perchloroallene, 866 and 1312 cm^{-1} . Unhappily, each is about 200 cm^{-1} from the expected position, with no apparent reason for a displacement such as there is in allene- d_4 .⁵ The 866- cm^{-1} band is appreciably more intense. On the other hand, it can be explained as a sum tone, whereas 1312 cm^{-1} cannot. Since the corresponding band in tetraiodoallene is certainly at 1226 cm^{-1} , 1312 cm^{-1} rather than 866 cm^{-1} is adopted for ν_1 .

TABLE I. Observed Infrared and Raman Bands of Polycrystalline $\text{Cl}_2\text{C}=\text{C}=\text{CCl}_2$ at ca. 100 K

Infrared		Raman		Assignment
cm^{-1}	Intensity ^a	cm^{-1}	Intensity ^b	
89	vw, sp			Lattice mode
		91	1000	ν_4 (torsion)?
93	vw, sp			Lattice mode
100	vw, sp			Lattice mode
140	w	ca. 143	790	ν_{11}
202	m	204	?	ν_{10} + impurity (see text)
221	vs	222	10	ν_7
253	w	252	40	ν_3
305	w	305	15	ν_9
427	vw	425	70	ν_2
		464	5	221 + 253 = 474
		515	10	221 + 305 = 526
651	s	652	5	ν_6
859	vs			ν_8
		866	10	221 + 651 = 872
		1312	2	ν_1
1977	vs			ν_5
		2178	5	1312 + 866 = 2178

^a w, m, s = weak, medium, strong; v = very; sp = sharp. ^b Relative peak intensities on a scale of 0–1000, uncorrected for instrument response. ^c CCl_4 solution.

TABLE II: Fundamental Vibrations of $\text{X}_2\text{C}=\text{C}=\text{CX}_2$ (D_{2d} Symmetry)

Species	Activity	No.	Schematic description	Assignment, cm^{-1}	
				$\text{Cl}_2\text{C}=\text{C}=\text{CCl}_1$	$\text{I}_2\text{C}=\text{C}=\text{Cl}_2$
a_1	R(p), -	1	C=C=C sym stretch	1312	1226
		2	CX_2 sym stretch	425	179
		3	CX_2 scissors	252	98
h_1	R, -	4	Torsion	91?	?
b_2	R, ir	5	C=C=C antisym stretch	1977	1912
		6	CX_2 sym stretch	651	424
		7	CX_2 scissors	221 or 202	200
e	R, ir	8	CX_2 antisym stretch	859	682
		9	CX_2 wag and rock	305	280, 270
		10	CX_2 wag and rock	202 or 221	137, 130
		11	C=C=C bend	141	84?

TABLE III: Comparison of the Fundamentals (in cm^{-1}) for Tetrachloroethylene and Tetrachloroallene, Tetraiodoethylene and Tetraiodoallene

Schematic description	C_2Cl_4^a	C_3Cl_4	C_2I_4^b	C_3I_4
CX_2 antisym str	1000	859	780	682
CX_2 antisym str	908		638	
CX_2 sym str, in phase	447	425	183	179
CX_2 sym str, out of phase	777	651	525	424
CX_2 scissoring, in phase	237	252	106	98
CX_2 scissoring, out of phase	310	221	129	200
CX_2 wag	288	305	218	275
CX_2 wag	512		423	
		and		and
CX_2 rock	347	202	148	133
CX_2 rock	176		94	
Torsion	110	91?	53?	

^a Reference 7. ^b Reference 11.

For the CCl_2 symmetric stretch (ν_2) there are four possible candidates: 886, 515, 464, and 425 cm^{-1} . The last one, 425 cm^{-1} , is selected because it is by far the most intense of the four. It is similar to the wave-number of the corresponding

mode in tetrachloroethylene, 447 cm^{-1} (ref 7 and Table III). The fact that it also appears as a very weak band in the infrared spectrum could well be due to a lowering of symmetry in the solid state, and is not regarded as a serious obstacle to the assignment.

The lowest a_1 mode is a CCl_2 scissors (ν_3). The polarized band at 252 cm^{-1} is the obvious choice. It too appears weakly in the infrared spectrum, and the same reason given above is suggested for this. In C_2Cl_4 the analogous wavenumber is 237 cm^{-1} .⁷

3. *Species* b_1 . The only mode in this species is the torsion, and the only candidate which fits the selection rules is 91 cm^{-1} . This is the strongest band in the entire Raman spectrum. Torsional bands are usually weak in the Raman effect; that is certainly the case in allene and allene- d_4 .⁵ However in our molecule the mode involves motions of highly polarizable chlorine atoms, so it could be intense. The torsion in allene is 865 cm^{-1} , in tetrachloroethylene about 110 cm^{-1} .⁷ Therefore 91 cm^{-1} seems reasonable for the torsion. This value for the solid is probably considerably higher than the vapor wave-number would be.⁸ Another possibility is that 91 cm^{-1} is a lattice mode. This could be tested by seeing whether the Raman band is still present in solution, but unfortunately a

TABLE IV: Observed Infrared and Raman Bands of $I_2C=C=CI_2$

Infrared			Raman			Assignment
Nujol Mull cm ⁻¹	KBr disk		Solid		CH ₃ OH solution cm ⁻¹	
	cm ⁻¹	Intensity ^a	cm ⁻¹	Intensity ^b		
	Not studied		84	720		ν_{11} ?
	130	m	98	29	94	ν_3
	137	vw	130	490	112	} ν_{10}
	202	w	137	83, sh		
	269	m	179	1000	173, p	ν_2
	277	m	199	33	187	ν_7
	422	ms	261	9, sh		$2 \times 130 = 260$
			271	44		} ν_9
			283	61		
			426	190		ν_6
			439	130		$2 \times 130 + 179 = 439$
			447	1, sh		$2 \times 84 + 271 = 439$
			466	9		$179 + 271 = 450$
			560	9		$199 + 271 = 470$
	608	w	611	16		$2 \times 283 = 566$
681	682	s	682	270		$2 \times 130 + 98 = 620$
693	693	m	695	4, sh		ν_8
	700	w, sh	705	1, sh		$271 + 426 = 697$
	718	m				$283 + 426 = 709$
		721	m	722	6	
			846	10		$2 \times 426 = 852$
			872	17		$2 \times 429 = 878$
			1226	100		ν_1
	1910	s	1914	14		ν_5

^a w, m, s = weak, medium, strong; v = very; sh = shoulder; p = polarized. ^b Relative peak intensities on a scale of 0–1000, uncorrected for instrument response.

doublets to the wag and rock modes: 280 and 270 cm⁻¹ to ν_9 and 137 and 130 cm⁻¹ to ν_{10} . (The e mode at 682 cm⁻¹ may also be split, but the weaker component at 694 cm⁻¹ can be explained as a sum tone (see Table IV)).

The singlet at 200 cm⁻¹ must be due to ν_7 , the Cl₂ scissors. It is too high for the only other possibility, ν_{11} , which is 141 cm⁻¹ in C₃Cl₄ and is certainly lower in C₃I₄. For ν_{11} , the C=C=C bend, 84 cm⁻¹ is a good candidate. Both it and its counterpart in C₃Cl₄ (141 cm⁻¹) are very intense. It must be admitted, though, that it is not known whether 84 cm⁻¹ is due to ν_{11} , to the torsion, or to a lattice mode.

3. *Remaining Bands.* Eleven other bands were observed that cannot be used as fundamentals. All of them can be assigned reasonably as sum tones as shown in Table IV.

IV. Conclusions for Both Molecules

The spectra of both tetrachloro- and tetraiodoallene can be interpreted very satisfactorily on the basis of D_{2d} symmetry. A little consideration convinces one that no other reasonable symmetry would be acceptable.

The antisymmetric C=C=C stretch drops only 3.3% on going from tetrachloro- to tetraiodoallene. The symmetric stretch drops just twice as much, or 6.6%. This is compatible with one's qualitative ideas about these modes. In the antisymmetric stretch the central carbon atom has most of the amplitude, and the C-X bonds are scarcely affected by the vibration. In the symmetric stretch the outer carbon atoms have most of the amplitude, and the C-X bonds are com-

pressed a little when the C=C ones are lengthened. Hence this mode is more sensitive to the nature of X.

Acknowledgments. Dr. G. L. Carlson of Mellon Institute, Carnegie-Mellon University, very kindly made the Digilab instrument available to us. This work was supported by the National Science Foundation under Grant No. GP-40836.

References and Notes

- (1) (a) Dedicated to Professor Richard C. Lord on his 65th birthday and retirement. (b) The portion on tetrachloroallene is from a thesis submitted by A. Monroe Snider, Jr., in partial fulfillment of the requirements for the degree of Doctor of Philosophy at the University of Pittsburgh, 1974. (c) Ph.D. degree with Professor Richard C. Lord, Johns Hopkins University, 1942.
- (2) (a) We have just learned that a paper on tetrafluoroallene by J. R. Durig, Y. S. Li, J. D. Witt, A. P. Zens, and P. D. Ellis is being submitted to *Spectrochim. Acta*. (b) H. J. Prins, *Recl. Trav. Chim. Pays-Bas*, **68**, 901 (1949); (c) K. Pilgrim and F. Korte, *Tetrahedron Lett.*, No. **19**, 883 (1962).
- (3) R. C. Lord, R. S. McDonald, and F. A. Miller, *J. Opt. Soc. Am.*, **42**, 149 (1952).
- (4) F. A. Miller, B. M. Harney, and J. Tyrrell, *Spectrochim. Acta, Part A*, **27**, 1003 (1971).
- (5) R. C. Lord and P. Venkateswarlu, *J. Chem. Phys.*, **20**, 1237 (1952).
- (6) F. R. Dollish, W. G. Fateley, and F. F. Bentley, "Characteristic Raman Frequencies of Organic Compounds", Wiley, New York, N.Y., 1974, p. 143.
- (7) T. Shimanouchi, "Tables of Molecular Vibrational Frequencies", Consolidated Vol. 1, U.S. Government Printing Office, Washington, D.C., (1972), No. C13.48:39.
- (8) W. G. Fateley, I. Matsubara, and R. E. Witkowski, *Spectrochim. Acta*, **20**, 1461 (1964).
- (9) R. Forneris and D. Bassi, *J. Mol. Spectrosc.*, **26**, 220 (1968).
- (10) E. J. Fluorine and W. D. Jones, *Spectrochim. Acta, Part A*, **25**, 653 (1969).
- (11) R. Forneris and M. Uehara, *J. Mol. Struct.*, **5**, 441 (1970).
- (12) J. R. Durig, Y. S. Li, C. C. Tong, A. P. Zens, and P. D. Ellis, *J. Am. Chem. Soc.*, **96**, 3805 (1974).
- (13) F. Kai and S. Seki, *Chem. Pharm. Bull.*, **14**, 1122 (1966).
- (14) W. Kiefer and H. J. Bernstein, *Appl. Spectrosc.*, **25**, 609 (1971).

Inorganic Chemistry

the publication that covers the syntheses, properties, quantitative structure studies, reaction thermodynamics and kinetics of new and old inorganic compounds

Every monthly issue of Inorganic Chemistry includes approximately 50 papers of original research by many of the world's leading inorganic chemists—never-before published information to keep you current on the latest developments in both experimental and theoretical fundamental studies in the field.

Inorganic Chemistry is essential to active chemists in this rapidly developing science... use the coupon below to enter your subscription now. Just complete the information and send it back today.

Inorganic Chemistry
American Chemical Society
1155 Sixteenth Street, N.W.
Washington, D.C. 20036

1976

Yes, I would like to receive INORGANIC CHEMISTRY at the one-year rate checked below:

	U.S.	Foreign and Canada	Latin America
ACS Member Personal-Use One-Year Rate	<input type="checkbox"/> \$24.00	<input type="checkbox"/> \$30.50	<input type="checkbox"/> \$29.75
Nonmember	<input type="checkbox"/> \$96.00	<input type="checkbox"/> \$102.50	<input type="checkbox"/> \$101.75
Bill me <input type="checkbox"/>	Bill company <input type="checkbox"/>	Payment enclosed <input type="checkbox"/>	

Name _____

Street _____ Home
Business

City _____ State _____ Zip _____

Journal subscriptions start January '76

RADIONUCLIDES IN THE ENVIRONMENT

ADVANCES IN CHEMISTRY SERIES NO. 93

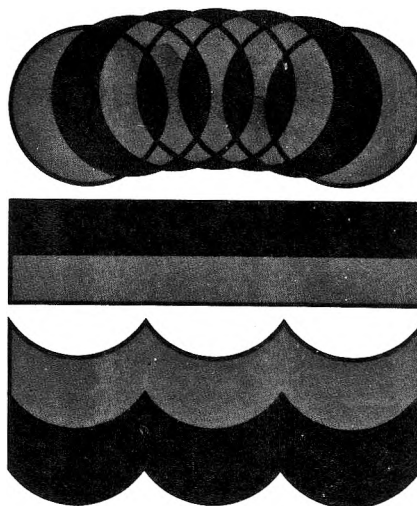
Twenty-eight papers from a symposium sponsored by the Division of Nuclear Chemistry and Technology, chaired by E. C. Freiling.

Pollution . . . a growing concern . . . a concept not generally associated with radionuclides. The successful control of this hazardous waste product of nuclear energy is essential to the continued use and development of nuclear power. Critical to this problem is an understanding of the processes by which radionuclides are produced, dispersed, and retained in the environment.

The papers in this volume discuss and evaluate the properties and problems relating to radionuclides, including

- mechanisms of release, absorption, uptake, transport
- behavior, measurement and characterization, specific weapons tests
- specific activity, public health aspects, fallout
- new methods and equipment

522 pages with index Clothbound (1968) \$15.00
Set of L.C. cards with library orders upon request.



Other books in the ADVANCES IN CHEMISTRY SERIES OF related interest include:

No. 89 Isotope Effects in Chemical Processes. Methods of separating isotopes and labeled molecules—chemical exchange, electromigration, photochemical processes, and distillation—are examined, along with factors that suit a process to isotope separation—single stage fractionation, exchange rate, and reflux. 278 pages cloth (1969) \$13.00

No. 82 Radiation Chemistry—II. Thirty-six papers and 17 abstracts on radiation chemistry in gases, solids, and organic liquids. Includes three plenary lectures. 558 pages cloth (1968) \$16.00

No. 81 Radiation Chemistry—I. Forty-one papers and 17 abstracts on radiation chemistry in aqueous media, biology, and dosimetry. From the international conference at Argonne National Laboratory. 616 pages cloth (1968) \$16.00. No. 81 and 82 ordered together \$30.00

No. 72 Mass Spectrometry in Inorganic Chemistry. A basic tool for chemical manipulations, the mass spectrometer is a conventional monitor for any stage in a research problem to help establish what is going on. 21 Research reports. 329 pages cloth (1968) \$12.00

No. 68 The Mössbauer Effect and Its Application in Chemistry. Ten papers that will familiarize chemists with Mössbauer spectroscopy as an analytical tool for studying chemical bonding, crystal structure, electron density, magnetism, and other properties. 178 pages cloth (1967) \$8.00

No. 66 Irradiation of Polymers. Eighteen papers survey radiation mechanics in polymers, the chemical nature of reactive species produced, crosslinking and scission, homopolymerization, graft copolymerization, and the effects of ultraviolet light radiation. 275 pages cloth (1967) \$10.00

No. 58 Ion-Molecule Reactions in the Gas Phase. Eighteen papers survey spectrometric and other methods for producing and studying ion-molecule reactions such as pulsed sources for studying thermal ions, reactions in flames and electrical discharges. 336 pages cloth (1966) \$10.50

No. 50 Solvated Electron. Reviews of theory, structure, reactions of solvated and hydrated electrons; detailed papers on electrical transport properties, photochemistry, theory of electron transfer reactions, structure of solvated electrons, hydrated electron research. 304 pages cloth (1965) \$10.50

Postpaid in U. S. and Canada; plus 30 cents elsewhere.

Order from:

**SPECIAL ISSUES SALES
AMERICAN CHEMICAL SOCIETY
1155 SIXTEENTH ST., N.W.
WASHINGTON, D. C. 20036**

PHYSICAL PHENOMENA

spectroscopy,
thermodynamics,
reaction kinetics,
and other areas
of experimental
and theoretical
physical chemistry
are covered
completely in

THE JOURNAL OF PHYSICAL CHEMISTRY

The biweekly JOURNAL OF PHYSICAL CHEMISTRY includes over 25 papers an issue of original research by many of the world's leading physical chemists. Articles, communications, and symposia cover new concepts, techniques, and interpretations. A "must" for those working in the field or interested in it, the JOURNAL OF PHYSICAL CHEMISTRY is essential for keeping current on this fast moving discipline. Complete and mail the coupon now to start your subscription to this important publication.

The Journal of Physical Chemistry
American Chemical Society
1155 Sixteenth Street, N.W.
Washington, D.C. 20036

1976

Yes, I would like to receive the JOURNAL OF PHYSICAL CHEMISTRY at the one-year rate checked below:

	<i>U.S.</i>	<i>Canada**</i>	<i>Latin America**</i>	<i>Other Nations**</i>
ACS Member One-Year Rate*	<input type="checkbox"/> \$24.00	<input type="checkbox"/> \$30.25	<input type="checkbox"/> \$29.75	<input type="checkbox"/> \$30.25
Nonmember	<input type="checkbox"/> \$96.00	<input type="checkbox"/> \$102.25	<input type="checkbox"/> \$101.75	<input type="checkbox"/> \$102.25

Bill me Bill company Payment enclosed

Air freight rates available on request.

Name _____

Street _____

Home
Business

City _____

State _____

Zip _____

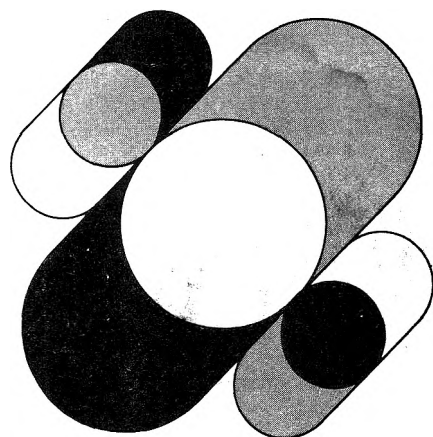
Journal subscriptions start January '76

*NOTE: Subscriptions at ACS member rates are for personal use only. **Payment must be made in U.S. currency, by international money order, UNESCO coupons, U.S. bank draft, or order through your book dealer.

Nonequilibrium Systems In Natural Water Chemistry

ADVANCES IN CHEMISTRY
SERIES No. 106

Thirteen papers from a symposium by the Division of Water, Air, and Waste Chemistry of the American Chemical Society, chaired by J. D. Hem.



Which is more important: efficient exploitation of our natural resources or a stable ecosystem? What is the relationship between a wide variety of life forms and a healthy environment? What do geology and groundwater flow patterns have to do with the chemical composition of water? How may one predict when a lake will reach equilibrium or tell how long it has supported life?

This volume features:

- principles of water pollution control
- methods of analysis for dissolved chemicals
- mathematical models
- discussion of stratified lakes
- chemical processes in a carbonate aquifer
- decomposition and racemization of amino acids

342 pages with index Cloth (1971) \$11.00
Postpaid in U.S. and Canada; plus 40 cents elsewhere.
Set of L.C. cards with library orders upon request.

Other books in the ADVANCES IN CHEMISTRY SERIES on water chemistry include:

No. 105 Anaerobic Biological Treatment Processes

Nine papers survey the state of the art of this natural process for waste treatment, with three papers on methane fermentation, others on process control and design. Considers volatile acid formation, toxicity, synergism, antagonism, pH control, heavy metals, light metal cations.
196 pages with index Cloth (1971) \$9.00

No. 79 Adsorption from Aqueous Solution

Fifteen papers discuss thermodynamic and kinetic aspects of adsorption phenomena and the results of studies on a variety of adsorbate-adsorbent systems.
212 pages with index Cloth (1968) \$10.00

No. 73 Trace Inorganics in Water

Research reports; analytical developments including atomic absorption, flame emission, and neutron activation; and broad reviews, such as effects of trace inorganics on the ice-water system and the role of hydrous manganese and iron oxides on fixing metals in soils and sediments.
396 pages with index Cloth (1968) \$12.50

No. 67 Equilibrium Concepts in Natural Water Systems

Sixteen papers represent the collaboration of aquatic chemists, analytical chemists, geologists, oceanographers, limnologists, and sanitary engineers, working with simplified models to produce fruitful generalizations and valuable insights into the factors that control the chemistry of natural systems.
344 pages with index Cloth (1967) \$11.00

No. 38 Saline Water Conversion—II

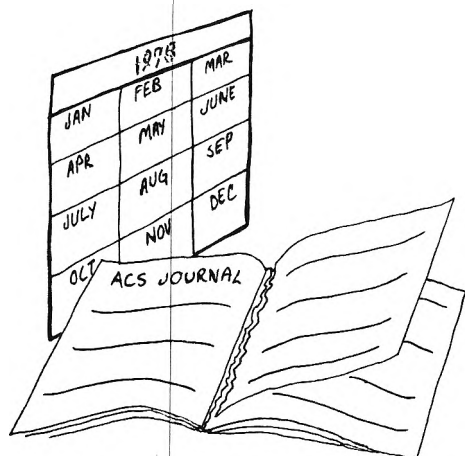
Fourteen papers from two symposia; includes recovery of minerals from sea water, minimizing scale formation, wiped thinfilm distillation, diffusion still, solar flash evaporation, osmosis, electro dialysis (3 paper), research in Israel, hydrate process.
199 pages Paper (1963) \$8.00

No. 27 Saline Water Conversion

Thermodynamics of desalting, solvent extraction, freezing, centrifugal phase barrier recompression distillation, multi-stage flash evaporation, ion exchange, osmosis, and electrochemical demineralization.
246 pages Paper (1960) \$9.00

Order from: **Special Issues Sales, American Chemical Society**
1155 Sixteenth St., N.W., Washington, D.C. 20036

TIMELY TEARSHEETS



Here's an opportunity to choose any article you wish which has been published during the past 12 months in any one of the American Chemical Society journals.*

The price for this service is very modest—just \$2.50 for the first copy and \$1.25 for each additional copy.

Also, if you wish, you may select articles which have appeared in earlier non-current ACS journal issues, but these will be photocopies rather than tearsheets and an additional 50¢ is required per article.

All you have to do is fill in the order forms below, *include your payment*, mail now, and we'll do the rest.

1. Give complete details for each article. Sorry, we cannot provide a search service.
2. **PRINT** or **TYPE** all information, including label.
3. Make check or money order payable to the AMERICAN CHEMICAL SOCIETY, and mail to: ACS, Business Operations, Books and Journals Division, 1155 16th Street, N.W., Washington, D.C. 20036.

Name _____

Address _____

City _____

State/Zip _____

AMERICAN CHEMICAL SOCIETY JOURNALS TIMELY TEARSHEETS Order Form

The following article(s) came to my attention in a recent issue of one of the ACS journals. I would like to order the number of tearsheets of each article indicated in the box(es).

ACS Journal _____

Title _____

Author(s) _____

Issue Date _____ Page(s) _____

ACS Journal _____

Title _____

Author(s) _____

Issue Date _____ Page(s) _____

ACS Journal _____

Title _____

Author(s) _____

Issue Date _____ Page(s) _____

\$2.50 for the first tearsheet.

\$1.25 for each additional tearsheet ordered at the same time.

\$ _____
Total Enclosed

These prices do not apply to articles from Chemical Reviews and Journal of Physical and Chemical Reference Data. For information regarding cost of these copies, contact the Books and Journals Division, ACS.

* Copyright restrictions prevent us from providing copies from other than ACS journals

Platinum Group Metals and Compounds

ADVANCES IN CHEMISTRY SERIES
NO. 98



Eleven papers from a symposium by the Division of Inorganic Chemistry of the American Chemical Society chaired by U. V. Rao.

What new complexes of the platinum group metals have been synthesized? Here is a collection of papers presenting data on chalcogenides, oxides, nitrido and hydrido complexes, as well as the catalytic properties of these metals and their alloys. Information is included on

- synthesis
- structure
- magnetic susceptibility
- double bond migration

The platinum group metals are considered from the viewpoints of both industry and research. Their magnetic and thermodynamic properties are explored, as well as recent chemistry of σ - and π -bonded complexes. Crystal structure is discussed by several authors, with data presented in the form of

- x-ray scattering data
- absorption spectra
- crystal spectra
- infrared spectra
- Mossbauer spectra
- vibrational spectra

165 pages with index. Cloth bound (1971) \$9.00 Postpaid in U.S. and Canada; plus 35 cents elsewhere.

Set of L. C. cards with library orders upon request.

Other books in the ADVANCES IN CHEMISTRY SERIES of interest to inorganic chemists include:

No. 89 Isotope Effects in Chemical Processes
278 pages Cloth bound (1969) \$13.00

No. 82 Radiation Chemistry — II
558 pages Cloth bound (1968) \$16.00

No. 81 Radiation Chemistry — I
616 pages Cloth bound (1968) \$16.00

No. 81 and No. 82 ordered together \$30.00

No. 78 Literature of Chemical Technology
732 pages Cloth bound (1968) \$17.50

No. 73 Trace Inorganics in Water
396 pages Cloth bound (1968) \$12.50

No. 72 Mass Spectrometry in Inorganic Chemistry
329 pages Cloth bound (1968) \$12.00

Order from:
Special Issues Sales
American Chemical Society
1155 16th St., N. W.
Washington, D. C. 20036

30.9.2519